Pyrolytic gasification:

Energy, char, and phosphorus recovery from sewage sludge

By Marc Heitmann

The Department of Civil and Environmental Engineering

Imperial College London

A thesis submitted in partial fulfilment of the requirements of Imperial College London for the award of Doctor of Philosophy

May 2021

Declaration

I hereby declare that the work presented in this thesis has not been submitted for any other degree or professional qualification, and that it is the result of my own independent work. As such all the views expressed in the thesis are mine and not necessarily those of any supervisors, funders or participants that have been involved and/or engaged in this process‘

The copyright of this thesis rests with the author and is made available under a Creative Commons Attribution Non-Commercial No Derivatives licence. Researchers are free to copy, distribute or transmit the thesis on the condition that they attribute it, that they do not use it for commercial purposes and that they do not alter, transform, or build upon it. For any reuse or redistribution, researchers must make clear to others the licence terms of this work.

Marc Heitmann

06.08.2021

Abstract

Sewage sludge is an energy and nutrient rich resource, typically treated by anaerobic digestion and recycled to agriculture in the UK. Sludge provides soil with organic matter and essential nutrients which contribute to crop growth and offsets inorganic fertiliser use. However, this model has limitations:

- Sludge mineralisation releases CO_2 and energy that could be recovered.
- The sludge land bank is constrained.
- Sludge contains emerging contaminants.

Pyrolysis has the potential to convert sludge into; energy-rich volatiles and char whose formation sequesters carbon and potentially facilitates nutrient recovery and manufacturing high-value products. A laboratory pyrolysis plant was designed and built to enable investigation into practical application of pyrolysis in a representative manner. Key process and energy findings were:

- Accumulation of carbon and soot-tar composites must be managed to avoid blockages.
- Energy-rich gas was formed (LHV = 15.6-19.7 MJ m^{-3}), which comprised hydrocarbons, hydrogen, carbon oxides and other components.
- Conversion efficiency maximised at 800ºC, with 59% conversion of sludge (HHV) to gas (LHV).

Sludge char retained one-third of sludge carbon by weight, including graphitic and heterocyclic structures which influences char surface chemistry. Sludge char is a Class-B candidate for soil carbon sequestration and analysis suggests it sequesters more than biosolids recycling. Char phosphate extraction with mineral acids is >90% effective, however co-extraction of iron and aluminium complicates phosphate valorisation. Char land application provides a circular-materials approach to phosphate recycling, assuming bespoke permits are obtained. Char contains heavy metals but is not expected to be ecotoxic because of their chemical form (e.g. sulphides). Solvent extraction is required to confirm organic contaminants do not pose a risk.

Several regulatory challenges (e.g. End-of-waste) have been identified that inhibit fuel-gas valorisation and char disposal or recycling. These may inhibit widespread adoption of pyrolysis and further development of novel processes that improve process reliability and product valorisation.

Publications associated with this research

Presentation at the 24th European Biosolids Conference, Manchester , 19-20th November 2019.

Acknowledgements

This research project was funded by Thames Water and The Engineering and Physical Sciences Research Council, and this financial support is gratefully acknowledged. I would like to thank my supervisor Dr. Geoff Fowler whose guidance, support and encouragement throughout this challenging project has been unrivalled. I would also like to thank Dr. Ángel Nievas Pino for his technical support in the Roger Perry laboratory.

Dr. Fowler, Dr. Nievas Pino, Ajax Equipment, and Sean McCabe of APAC Automation all contributed time to the successful design and assembly of the laboratory-scale plant and its successful functioning is a testament to our efforts.

I would also like to thank Aurelien Perrault for his encouragement throughout the project. I would also like to thank the operational team at Crossness STW for helping me get sludge.

Finally, I am very grateful to my parents for their support. Thank you for always encouraging and looking out for me.

Table of contents

Content

Declaration **2**

Abstract **3**

Publications associated with this research **4**

Acknowledgements **5**

Table of contents **6**

List of figures **12**

List of tables **16**

List of abbreviations **20**

Chapter 1: Introduction **23**

1.1 Background 23

1.1.1 Sludge treatment processes 23

1.1.2 Greenhouse gas emissions 30

1.2 Process outputs 30

1.2.1 Biosolids 30

1.2.2 Ash 33

1.2.3 Char 34

Chapter 2: Literature Review **35**

2.1 Introduction 35

2.2 Advanced Thermal Conversion 35

2.2.1 Pyrolysis 35

2.2.2 Gasification 45

2.2.3 Hydrothermal carbonisation 48

2.2.4 Thames Water: Proposed ATC process 49

2.3 ATC Outputs 51

2.3.1 Gas 51

2.3.2 Tar and other gaseous contaminants 54

2.3.3 Pyrogenic carbon 61

2.4 Waste Regulation 72

2.4.1 Biosolids 73
2.4.2 Biochar 74
2.4.3 Manufactured gas 79
2.4.4 Combustion products 83
Chapter 3: Research aims and objectives 85
3.1 Research Aims 85
3.2 Objectives 85
Chapter 4: Methods 86
4.1 Sludge preparation 86
4.2 Material characterisation 87
4.2.1 Dry solids and loss on ignition 87
4.2.1 Bulk Density 87
4.2.2 Ultimate analysis 87
4.2.3 Thermogravimetric analysis 87
4.2.4 Bomb calorimetry 90
4.2.5 Combustion testing 90
4.2.6 XPS 90
4.2.7 Inorganic analysis 91
4.2.8 Gas chromatography (GC) 92
4.3 Lab-scale pyrolysis 95
4.3.1 Mass balances 95
4.3.2 Slow batch pyrolysis 95
4.3.3 Pyrolytic gasification plant 97
4.4 Extraction experiments 99
Chapter 5: Design, construction, and operation of a laboratory scale pyrolytic gasification plant 101
5.1 Laboratory Scale Pyrolysis 101
5.1.1 Feed Hopper 102
5.1.2 Hot-zones 103
5.1.3 Drives and electrics 104
5.1.4 Heating 105

5.1.5 Pipework 105
5.1.6 Frame 107
5.2 Operational Experiences 108
5.2.1 Leaks 108
5.2.2 Reactor carbon stability 109
5.3 Laboratory-scale pyrolysis limitations 116
Chapter 6: Sludge characterisation 118
6.1 Fuel characteristics 118
6.1.1 Proximate analysis 120
6.1.2 Ultimate analysis 123
6.2 Elemental composition 125
6.2.1 Alkaline earth metals 125
6.2.2 Iron and aluminium 126
6.2.3 Potentially valuable elements 126
Potentially toxic elements 126
6.3 Summary 127
Chapter 7: Laboratory-scale pyrolysis 128
7.1 Mass yields 128
7.1.1 Batch-fed slow pyrolysis 128
7.1.2 Continuously fed pyrolytic gasification 130
7.1.3 Mass yields: A comparison of batch and continuous pyrolysis 132
7.2 Gas 134
7.2.1 Gas composition 135
7.2.2 Fuel-gas flammability 144
7.3 Overall energy balance 145
7.3.1 Parasitic load 147
7.3.2 Estimated net electrical energy output 149
7.4 Elemental mass balance 150
7.4.1 Elemental mass balance: Char 150
7.4.2 Elemental mass balance: Liquids 156

7.5 Non-isothermal pyrolysis and tar formation 160
7.6 Regulatory compliance 164
7.6.1 Hydrogen sulphide (H_2S): End-of-waste compliance 168
7.6.2 End-of-waste compliance: Total aromatic hydrocarbons 171
Chapter 8: Char characterisation 173
8.1 Elemental characterisation 173
8.1.1 Aqua-regia digestion 173
8.1.2 X-ray diffraction 174
8.1.3 X-ray photoelectron spectroscopy (XPS) 174
8.1.4 Ultimate analysis 186
8.1.5 Char aromaticity and stability 187
8.2 Sewage sludge char: hazardous waste assessment 193
8.2.1 Explosive (HP1) 194
8.2.2 Flammability (HP2) 195
8.2.3 Produces toxic gases in contact with water, air, or acid (HP12) 195
8.2.4 Inorganic hazards 197
8.2.5 Leaching tests (Landfill) 208
8.2.6 Active waste testing (Landfill) 209
Chapter 9: Char disposal and value recovery options 210
9.1 Pyrogenic carbon sequestration 210
9.1.1 Biosolids carbon 211
9.1.2 Char carbon 213
9.1.3 Carbon value 214
9.2 Phosphorus 215
9.2.1 Background 215
9.3 Phosphorus recovery from Biosolids 223
9.3.1 Direct land application 224
9.3.3 Phosphorus extraction 235
9.3.4 SSC leachate 260
Chapter 10: Crossness STW: Site energy 263

10.1 Crossness STW: Energy 263
10.1.1 Crossness STW: Present performance data 263
10.1.2 Energy flow diagrams 266
10.1.3 Summary 274
Chapter 11: Discussion, Conclusions & Future Work 275
11.1 Discussion 275
11.1.1 Introduction 275
11.1.2 Feedstock 275
11.1.3 Sludge pyrolysis 275
11.1.4 Char 276
11.1.6 Pyrolysis: Energy 282
11.1.7 STW: Site energy balance 284
11.1.8 Pyrolysis: Gas treatment 285
11.1.9 Pyrolysis: Regulatory challenges 287
11.2 Contributions to knowledge 289
11.3 Conclusions 290
11.3.1 Process 290
11.3.2 Char 291
11.4 Future Work 292
References 293
Chapter 12: Appendices 326
12.1 Appendix 1 - Health and safety considerations 326
12.1.1 Motor control panel 326
12.1.2 Heating Equipment 327
12.1.3 Mechanical Equipment 327
12.1.4 Flammable gases and materials 327
12.1.5 Chemical safety 328
12.2 Appendix 2 – Mass balance results 329
12.2.1 Slow batch-pyrolysis (Py-B) 329
12.2.2 Continuously-fed pyrolytic gasification 329

12.3 Appendix 3 – Carbon Values 330
12.4 Appendix 4 – P extraction 330
12.5 Appendix 5 – Energy balance assumptions 331
12.6 Appendix 6: Raw sludge pyrolysis 332

List of figures

Figure 1-1 – Typical THP configuration, showing (i) sludge flow (ii) the main energy inputs and outputs and (iii) integration with other system assets (e.g. digesters, steam boilers and CHP). Based on a diagram published by Williams & Burrows (2016) 24
Figure 1-2 – Gross energy flows for (a) conventional THP (b) SAS-only THP and (c) iTHP based on a throughput of 1kg DS hour^{-1}. Produced using data and assumptions available in Mills (2015). Material energy contents are based on their lower heating value (LHV). 26
Figure 1-3 - Gross energy flows for incineration based on a throughput of 1kg DS hour^{-1}. Produced using data and assumptions available in Mills (2015). Material energy contents are based on their lower heating value (LHV). 27
Figure 1-4 – Gross energy flows for THP ATC based on a throughput of 1kg DS hour^{-1}. Produced using data and assumptions available in Mills (2015). Material energy contents are based on their lower heating value (LHV). 28
Figure 2-1 – Decommissioned Lurgi fluidised bed incinerator at Crossness STW showing the air injectors that fluidised inert sand and sewage sludge and an injector rod used to inject water to control bed temperature and prevent clinker forming. 39
Figure 2-2: Sewage sludge pyrolysis process, based on digram published by Pyreg GmbH (Eliquo, 2021) 41
Figure 2-3: British Gas slagging coal gasification system, showing tar and soot recirculation 46
Figure 2-4: U-GAS fluidised bed gasifier (NETL, 2020) 48
Figure 2-5: Proposed tar and contaminant removal at Crossness STW 50
Figure 2-6: Gas engine that may be used for combined heat and power production from fuel-gas or syngas (MWM Energy, 2019) 52
Figure 2-7: Tar compounds formed at different temperatures from biomass (Elliott, 1988) 55
Figure 2-8 - The structure of MeIQx (left) and pyrimidine (right) 63
Figure 2-9 – The Waste Hierarchy (DEFRA, 2011) 73
Figure 4-1: Thermogravimetric analysis of graphite in air at a heating rate of 5^{o}C min^{-1} and air flow rate of 50ml min^{-1}. The reference lines highlight the temperature in which 50% of the graphite has been oxidised (T_{50}) 89
Figure 4-2 – Experimental setup for slow batch pyrolysis (Py-B) 96
Figure 4-3 – Pyrolysis liquids condensate train 98
Figure 5-1: Simplified drawing of laboratory-scale pyrolysis plant 101
Figure 5-2: Simplified drawing of the laboratory-scale pyrolysis plant feed-hopper. 102
Figure 5-3: Simplified drawing of the hot zones, showing furnaces 1-3, conveyors A-B, and the inlets and outlets. 103
Figure 5-4: Expansion joints: Facilitating vertical, horizontal, and differential expansion (e.g. twisting). Drawing not to scale. 106

Figure 5-5: Loading and shear force diagrams for the pyrolysis rig. The y-axis is the force in newtons and the x-axis is the length across the beam. S1 and S2 indicate where the beams were supported. Individual point loads are also shown. 107
Figure 5-6: Assembly of the pyrolysis rig, showing use of an overhead crane to position sections of the pipework into place. 108
Figure 5-7: Carbon deposits within furnace 1 (left) and the expansion bellow inlet (right). The expansion bellow is attached to the outlet of furnace 1 and exhausts the hot-gases. 110
Figure 5-8: Carbon deposits on the outlet flange of furnace 1, the internal diameter of the pipe was fully bridged with a thin friable porous layer of carbon that did not block gas-flow. 110
Figure 5-9 – Soot structures recovered from inside furnace 1 (F1) showing the porous shiny black carbon that faced outwards into F1 and the silvery carbon that adhered to inside wall of furnace 1, the silvery-colour is highly indicative of graphitisation. These samples were highly friable. 111
Figure 5-10: Soot structures recovered from the inside of the expansion bellow inlet and flange face of furnace 1 (F1). The carbon was typically thicker, less friable and harder than the carbon recovered from inside F1 it also had a slightly tarry odour. 112
Figure 5-11 – Long-term pitch-drop experiment at Trinity College Dublin (Webb, 2014) (Johnston, 2013) 113
Figure 5-12 – Ascension pipework layout for the proposed ATC reactor at Crossness STW 114
Figure 5-13: Retort ascension pipes (Meade, 1921) typically one side would be connected to 115
Figure 6-1: Proximate analysis of XS-6, showing the sample weight (%) and temperature (°C) when 50% of the materials volatiles had been volatilised. When cooled from 950°C to 600°C, the sample weight appeared to increase because of the buoyancy effect – therefore FC carbon content was calculated from the weight of the sample before & after ashing at 600°C. 120
Figure 7-1: A comparison of the mass yields generated during Py-B and Py-G. The error bars show the minimum and maximum for each test condition. 132
Figure 7-2: Total and component gas volume produced during Py-G. The component volumes for hydrogen sulphide and nitrogen gas are not shown 137
Figure 7-3: The relationship between liquid yield and hydrogen production with confidence 140
Figure 7-4: Gaseous sulphur emissions calculated by elemental mass balance expressed as hydrogen sulphide (H_2S) between 600-1000°C. Alongside the mass yield of S fractionated between the char, liquid and gas fractions. 142
Figure 7-5: Measured energy content of char, condensable liquids and fuel-gas. Alongside the total energy recovery compared to the XS-6 feedstock. 145
Figure 7-6: Power consumption for Furnace 2 during isothermal Py-C at a constant feed rate of 2.6 kg hr^{-1} and a dwell (t) of 120s. 147
Figure 7-7: Yield of carbon, hydrogen, nitrogen and sulphur in sewage sludge char between 500-1000°C during isothermal Py-G 150

Figure 7-8: Yield of carbon, hydrogen, nitrogen and sulphur in pyrolysis liquids between 500-1000ºC during isothermal Py-G. _____ 156
Figure 7-9: : Influence of initial thermal decomposition in furnace 2 and thermal cracking in furnace 1 on liquid yields for XS-9 sludge at 700, 850 and 1000ºC _____ 161
Figure 8-1: XPS survey scan spectra for SSC-700, covering a binding energy range between 0-1350 eV (0.5 eV step-size). _____ 174
Figure 8-2: High resolution XPS scan of C 1s orbital (70 scans, 400um, CAE 20.0, 0.1 eV) showing raw data and the deconvoluted peaks generated in CasaXPS using voigt line shapes 176
Figure 8-3: High resolution XPS scan of N 1s orbital (70 scans, 400um, CAE 20.0, 0.1 eV) showing raw data and the deconvoluted peaks generated in CasaXPS using voigt line shapes 178
Figure 8-4: Structure of pyridine and pyrrole molecules which XPS analysis suggests are present within sewage sludge chars condensed aromatic structure as surface functional groups ____ 179
Figure 8-5: High resolution XPS scan of S 1s orbital (200 scans, 400um, CAE 20.0, 0.1 eV) showing raw data and the deconvoluted peaks generated in CasaXPS using Voigt line shapes _____ 180
Figure 8-6: High resolution XPS scan of P 2p orbital (70 scans, 400um, CAE 20.0, 0.1 eV) showing raw data and deconvoluted peaks generated by CasaXPS using Voigt line shapes _ 182
Figure 8-7: High resolution XPS scan of Ca 2p (70 scans, 400um, CAE 20.0, 0.1 eV) _____ 184
Figure 8-8: High resolution XPS scan of Zn 1s (200 scans, 400um, CAE 20.0, 0.1 eV) showing characteristic Zn $2p_{3/2}$ and Zn $2p_{1/2}$ peaks at 1022.35eV and 1045.38eV respectively _____ 185
Figure 9-1: The global production of phopshate fertilisers in 2016. Based on estimated P_2O_5 content for SP, TSP, MAP and DAP of 22%, 46%, 52% and 46% respectively (Yara, 2018) 216
Figure 9-2: Reuse option for sludge phosphorus _____ 223
Figure 9-3: The pH dependent speciation of sulphide in aqueous solutions _____ 227
Figure 9-4: P availability for sludge, char, and ash in 2% formic acid _____ 229
Figure 9-5: Sewage sludge char (<5mm) produced at 1000ºC and a dwell-time of 120 seconds. Photograph taken with a Canon G9X with flash please note that when observed with the human eye the char generally appears more black. The silver coloured lump (bottom left) is highly carbonised, low density, fixed carbon thought to originate from tar, these exited the reactor from time to time. _____ 233
Figure 9-6: Sewage sludge char (<5mm) produced at 700ºC and a dwell-time of 120 seconds. . Photograph taken with a Canon G9X with flash please note that when observed with the human eye the char generally appears more black. _____ 234
Figure 9-7: HCl leaching: Extraction efficiency distributions for P and other elements (n = 40) _____ 238
Figure 9-8: The effect of various factors tested at two levels (1 and -1) with centre point (0) on mean P extraction for hydrochloric acid (HCl) leached char _____ 239
Figure 9-9: Phosphate: The relative effect of extraction parameters _____ 240

Figure 9-10: P extraction with HCl: Two-way interaction plot for extraction factors. The y-axis shows P_{EE} and the x-axis shows each factors values at levels -1, 0 and 1. The greyed-out plots are non-significant two-interactions that were excluded from the model. 241
Figure 9-11: Zinc extraction: Pareto chart of standardised effects generated in Minitab (2021) using factorial regression with backwards elimination (α = 0.003). Factors with a standardised effect of >3.26 are statistically significant at a 0.3% significant level. 243
Figure 9-12: H_2SO_4 leaching: Extraction efficiency distributions for P and other elements (n = 40) 244
Figure 9-13: The effect of various factors tested at two levels (1 and -1) with centre point (0) on mean phosphate extraction for sulphuric acid leached char 245
Figure 9-14: Phosphate extraction: The relative effect of extraction parameters 246
Figure 9-15: P extraction with H_2SO_4: Two-way interaction plot for extraction factors. The y-axis shows P_{EE} and the x-axis shows each factors values at levels -1, 0 and 1. The greyed-out plots are non-significant two-interactions that were excluded from the HCl model 247
Figure 9-16: Zinc extraction: Pareto chart of standardised effects generated in Minitab (2021) using factorial regression with backwards elimination (α = 0.05). Factors with a standardised effect of >2.05 are statistically significant at a 5% significance level. 249
Figure 9-17: HNO_3 leaching: Extraction efficiency distributions for P and other elements (n = 40) 250
Figure 9-18: The effect of various factors tested at two levels (1 and -1) with centre point (0) on mean P_{EE} for HNO_3 leached char 251
Figure 9-19: Phosphate extraction: Pareto chart of standardised effects generated in Minitab (2021) using factorial regression with backwards elimination (α = 0.003). Factors with a standardised effect of >3.26 are statistically significant at a 0.3% significant level. 252
Figure 9-20: Zinc extraction: Pareto chart of standardised effects generated in Minitab (2021) using factorial regression with backwards elimination (α = 0.05). Factors with a standardised effect of >2.05 are statistically significant at a 5% significance level. 254
Figure 9-21: Lead extraction: Pareto chart of standardised effects generated in Minitab (2021) using factorial regression with backwards elimination (α = 0.05). Factors with a standardised effect of >2.05 are statistically significant at a 5% significance level. 255
Figure 9-22: Copper extraction: Pareto chart of standardised effects generated in Minitab (2021) using factorial regression with backwards elimination (α = 0.05). Factors with a standardised effect of >2.048 are statistically significant at a 5% significance level. 255
Figure 9-23: Phosphate and metal ion solubility in SSC H_2SO_4 leachate solution neutralised with NaOH between pH 1-7 (Lee, 2019) 260
Figure 9-24: Phosphate and metal ion solubility in SSC HNO_3 leachate solution neutralised with NH_4OH between pH 2-9 261

Figure 10-1: Gross energy flows of THP-MAD for 1kg DS^{-1} hr^{-1} based on data obtained from Crossness STW and assumptions from Mills (2015) and personal communication (2021). Units based on feed-rate of 1kg DS $hour^{-1}$. 267
Figure 10-2: Gross energy flows of THP-pyrolysis at 850°C for A) XS-6 and B) XS-9 biosolids. Based on data obtained from Crossness STW, laboratory-scale pyrolysis and assumptions from Mills (2015) and personal communication (2021). Units based on feed-rate of 1kg DS $hour^{-1}$. 270
Figure 10-3: Gross energy flows of THP-pyrolysis at 850°C for XS-6 biosolids. Based on data obtained from Crossness STW, laboratory-scale pyrolysis and assumptions from Mills (2015) and personal communication (2021). Units based on feed-rate of 1 kg DS $hour^{-1}$. 272
Figure 12-1- Gross energy flows for standalone pyrolysis at 850°C. Based on data obtained from Crossness STW, laboratory-scale pyrolysis and assumptions from Mills (2015). Units based on feed-rate of 1kg DS $hour^{-1}$. 333

List of tables

Table 2-1: Coal pyrolysis gas treatment by-products 42
Table 2-2: The properties of common ATC gases 51
Table 2-3: Tar categorisation by analytical groups (Anis & Zainal, 2011) 54
Table 2-4: Predominant structures in coke oven tars (Mcneil, 1975) 54
Table 2-5: Maximum addition of sludge heavy metals to soils 73
Table 2-6 - International biochar initiative product testing guidelines for biochar (IBI, 2015) and EBC standards (EBC, 2012-2022). 75
Table 2-7 - Processing requirements for PGM production 76
Table 2-8 - CMC level requirements for N-PGM re-use in agriculture (Huygens et al, 2019) 77
Table 2-9: PFC level requirement for fertilisers (Regulation (EU) 2019/1009) 78
Table 2-10: Emission limit values for waste incineration plants 79
Table 2-11 - National grid specifications for natural gas (Environment Agency, 2016) 80
Table 2-12 - Sampled natural gas sulphur and BTEX (Environment Agency, 2016) 81
Table 2-13 - Specification for biomethane for injection into the UK gas-grid and for use in appliances (Environment Agency, 2013) 82
Table 2-14 - Environment Agency regulatory position: "Syngas" EoW status[1] 82
Table 2-15 - Engine ELVs under medium combustion plant directive for new plants 83
Table 2-16: Incineration ELVs under medium combustion plant directive for new plants 83
Table 2-17: Engine emission limits for biogas combustion at sewage treatment works 83
Table 4-1: Slow batch pyrolyis (Py-B) experimental conditions 96
Table 4-2: Resolution (V) fractional-factorial experimental design. Generated in Minitab (v18.1) for the SSC extraction experiments with H_2SO_4, HCl and HNO_3 100

Table 5-1: Gear motor technical summary 104
Table 5-2: The composition of 310 and 316L stainless steel 105
Table 5-3: Thermal stability of carbon deposits in air, sampled from within reactor 1 and the inlet of the expansion bellow which vents gases out of furnace 1. 113
Table 6-1: Fuel characteristics of Crossness STW raw and digested sewage sludge..... 118
Table 6-2: Typical sludge composition (Gialacone, 2018)[1] 119
Table 6-3: Average proximate analysis results for Crossness sludge samples..... 121
Table 6-4: Proximate analysis of pure macromolecules (Krueger, 2021)[1]..... 122
Table 6-5: Ultimate analysis of Crossness sludge (Dry Wt %)..... 123
Table 6-6: Ultimate analysis of Crossness sludge and comparator materials[1] (DAF Wt %) 123
Table 6-7: Molar ratios of Crossness sludge and comparator materials[1] 124
Table 6-8: Elemental analysis of XS-B and XS-6..... 125
Table 7-1: Batch pyrolysis of XS: Mass Yields 128
Table 7-2: Results of one-way ANOVA and Tukey testing for Py-B mass yield data 128
Table 7-3: Mass yields during isothermal pyrolysis (Py-G)[1] 130
Table 7-4: Statistical testing of Py-G mass yield data..... 130
Table 7-5: Mean fuel-gas composition (XS-6 sludge) 135
Table 7-6: Mean fuel gas composition, lower heating value and specific gas production for XS-6 135
Table 7-7: The higher and lower heating values for the measured gases..... 136
Table 7-8: Fuel-gas components lower- and upper- explosion limits (Yaws & Braker, 2001) 144
Table 7-9: Higher heating value (HHV) of the SSC and condensable liquids 146
Table 7-10: Parasitic load of F2 when feeding dried sludge at a feed-rate of 2.6 kg hr^{-1} 148
Table 7-11: Energy conversion during lab-scale sewage sludge pyrolysis[1]..... 149
Table 7-12: Char carbon yields for Py-B and Py-G 151
Table 7-13: Char hydrogen yields for Py-B and Py-G 152
Table 7-14: Py-B and Py-G char nitrogen yields 153
Table 7-15: Py-B and Py-G char sulphur yields..... 155
Table 7-16: Ultimate analysis of Py-G liquids..... 157
Table 7-17: Molar ratios Py-G liquids 159
Table 7-18: The C:H ratio and boiling points of select hydrocarbons and Py-G products 159
Table 7-19: Experimental conditions 160
Table 7-20: End-of-waste requirements for “syngas” 164
Table 7-21: Estimated SO_2 emissions for natural gas, biomethane and syngas based on their harmonised MCPD emission limits values (ELV) for different fuels and oxidation methods.. 165
Table 7-22: Permitted syngas H_2S concentration if regulated to achieve the same harmonsied SO_2 emissions as comparable fuels and processes. 167
Table 7-23: Chemical usage: Conversion of H_2S to Na_2SO_4 for fuel-gas at 800º & 1000ºC 168

Table 8-1: The elemental composition of XS-6 and iso-SSC produced between 500-1000ºC with a dwell-time of 120 seconds (mg kg^{-1}) 173
Table 8-2: Ultimate analysis of SSC produced from XS-6 during Py-G 186
Table 8-3: Ultimate analysis of SSC produced from XS-B during Py-B 186
Table 8-4: Ultimate analysis of SSC produced from XS-Raw during Py-G 187
Table 8-5: The double-bond equivalence, aromaticity index and molar ratios of various chars 189
Table 8-6: R_{50} summary information showing pyrolysis material, pyrolysis dwell (t), Q_3, R_{50} and carbon sequestration class. 192
Table 8-7: Sewage sludge char: Minimum ignition temperature for dust explosions 194
Table 8-8: HP12 classification of sulphide compounds 196
Table 8-9: Worst case compounds as outlined in WM3 197
Table 8-10: SSC inorganic hazardous waste assessment (worst-case) 198
Table 8-11: SSC inorganic hazardous waste assessment: Most likely scenario[1] 205
Table 8-12: EN 12457-3 & NEN 7371 leaching tests for SSC-800 208
Table 9-1: Estimated carbon value of digested sludge and SSC, and the long-term retention of this carbon value in soil (expressed as CO_2e per tonne digested sludge) 214
Table 9-2: Recycling of biosolids to land: Main benefits and limitations 224
Table 9-3: Heavy metals: Char application rates 225
Table 9-4: Crop nutrient requirments and SSC application rates to meet these requirements for selected crops based on total element concentration.[1] 226
Table 9-5: Direct application of char to land: Exceedance of Strubias regulations for PFC 1 . 229
Table 9-6: Mean P availability in 2% formic acid with one-way ANOVA and Tukey testing. 230
Table 9-7: MSc Project: Preliminary screening experiment of SSC extractants (Koulouri, 2018) 235
Table 9-8: Factors for P extraction experimentation 236
Table 9-9: The optimal combination of experimental factors for P_{EE} according to model 2 during constraint and non-constraint of factorial levels 242
Table 9-10: Response optimisation for P and Zn 244
Table 9-11: The optimal combination of experimental factors for P_{EE} according to the H_2SO_4 model when factorial levels are unconstrained or constrained to the lowest performing levels for each factor 248
Table 9-12: Response optimisation for P and Zn 249
Table 9-13: The optimal combination of experimental factors for P extraction during constraint and non-constraint of factorial levels 253
Table 9-14: Response optimisation for P and Zn 256
Table 9-15: The pK_{sp} constants for selected Cu, Zn and Pb compounds (Dean, 1999) 258
Table 9-16: Approximate solubility of metal sulphides in non-oxidising acids 258

Table 10-1: Daily data obtained from Crossness STW between 01.01.2019 and 06.08.2020 .. 263
Table 10-2: Annualised mass & energy balance of Crossness STW between 01.01.2019 and 06.08.2020 264
Table 10-3: Energy content of XS-6 fuel-gas and liquids 271
Table 10-4: Gross and net conversion efficiencies for different sludge treament configurations based on the HHV of Crossness sludge[1] 274
Table 12-1: Health & Safety control measures for the motor control panel. 326
Table 12-2: Health & Safety control measures for the heating equipment 327
Table 12-3: Batch pyrolysis of Crossness Sludge (supplementary data for Table 7-1) 329
Table 12-4: Mass yields during isothermal pyrolysis (supplementary data for Table 7-3)..... 329
Table 12-5: P-extraction summary statistics 330
Table 12-6: Main process assumptions for Crossness STW energy balances..... 331
Table 12-7: Key results for XS-raw isothermal pyrolysis at 850^{o}C [120s dwell (t)] 332

List of abbreviations

AEM	Alkaline Earth Metals
AICc	Modified Akaike Information Criteria
AMF	Arbuscular mycorrhizal fungi
ATC	Advanced thermal conversion
ATEX	Explosive Atmosphere
ATP	Adenosine triphosphate
B.P	Boiling point
BAT	Best available technologies
BSPP	British standard parallel pipe
BTEX	Benzene, Xylene, Ethylbenzene & Xylene
CAGR	Compound annual growth rate
CAPEX	Capital expenditure
CfD	Contracts for difference
CHP	Combined heat and power
CLP	Classification labelling and packaging regulations
CMC	Component material category
CPF	Carbon price floor
CV	Calorific value
DAF	Dry ash-free
DAP	Diammonium phosphate
DBE	Double bond equivalence
DCP	Dicalcium Phosphate
DS	Dry solids
EBC	European Biochar Certificate
ECE	Electrical conversion efficiency
EE	Extraction efficiency
ELV	Emission limit value
EoW	End of waste
ETS	Emissions trading scheme
EWC	European waste catalogues
FC	Fixed Carbon
FOG	Fat, oil, greases
FPR	Fertilising products regulations
GC	Gas chromatography
GCE	Gross conversion efficiency
GHS	Globally harmonised system
GSM	Gas safety management regulations
HAP	Hydroxyapatite
HAA	Heterocyclic aromatic amines
HCl	Hydrogen chloride
HCN	Hydrogen cyanide
HF	Hydrogen Fluoride
HHV_{DAF}	higher heating value on a dry ash-free basis

HHT	Highest heating temperature
HHV	Higher heating Value
HP	Hazardous property
ICP-OES	Inductively coupled plasma
IED	Industrial Emissions Directive
ITD	Initial thermal decomposition
iTHP	intermediate thermal hydrolysis
IUPAC	International union of pure and applied chemistry
LEL	Lower explosion limit
LFL	Lower flammability limit
LHV	Lower heating value
LOI	Loss on ignition
MAD	Mesophilic anaerobic digestion
MAP	Mono-ammonium phosphate
MCPD	Medium combustion plant
MRT	Mean residence time
NCE	Net conversion efficiency
NEN	Royal Netherlands Standardization Institute
NMR	Nuclear magnetic resonance
NVZ	Nitrate vulnerable zone
OPEX	Operating expenditure
Ortho-P	Ortho-phosphate
OSHA	Occupational safety and health administration
PAH	Polycyclic aromatic hydrocarbon
Py-C	Pyrolytic carbon
PCB	Polychlorinated biphenyls
PCM	Pyrogenic carbonaceous materials
PCDD/F	Polychlorinated dibenzo-p-dioxins
PFAS	Per- and polyfluoroalkyl substances
PFC	Product function category
PFOA	Perfluorooctanoic Acid
PFOS	Perfluorooctanesulfonic acid
PGM	Pyrolysis and gasification materials
Poly-P	Poly-phosphate
POX	Partial oxidation
PRESS	Predicted sum of squares
PS	Primary Sludge
PTE	Potentially toxic element
PTFE	Polytetrafluoroethylene
PVA	Polyvinyl alcohol
Py-B	Slow batch-fed pyrolysis
Py-C	Pyrogenic carbon
Py-G	Pyrolytic gasification

ROCs	Renewable obligation certificates
RP	Rock Phosphate
SAS	Surplus activated sludge
SBA	Sludge-based adsorbent
SOFC	Solid oxide fuel cell
SOM	Soil organic matter
SP	Super Phosphate
SGP	Specific gas production
SS	Sewage sludge
SSA	Sewage sludge ash
SSC	Sewage sludge char
STRUBIAS	Struvite, biochar, ash
STW	Sewage treatment works
Syngas	Synthesis gas
TCD	Thermal conductivity detector
tds	Tons dry solids
THC	Total hydrocarbons
THP	Thermal hydrolysis
TOC	Total organic carbon
TSP	Triple super phosphate
TWh	Terawatt-hour
UFL	Upper flammability limit
USGS	US Geological Survey
VOC	Volatile organic carbon
Vol	Volume
VS	Volatile solids
VSD	Volatile solids destruction
WFD	Waste framework directive
XPS	X-ray photoelectron spectroscopy
XRD	X-ray diffraction
XS	Crossness sewage sludge

Chapter 1: Introduction

1.1 Background

1.1.1 Sludge treatment processes

Each year the UK produces approximately 1.7 million tonnes dried solid (tds) of sewage sludge (Mills, 2015) although estimates do vary, for example: Ofwat (2015) and Eurostat (2020) state an annual production of 1.4 mdt (Eng. & Wal. Only) and 1.1 mdt respectively. UK sewage sludge contains an energy content of approximately 7.5 TWh, however, only 10% is converted to electrical energy (Mills, 2015). The main methods of treating sludge and converting it into useable energy include anaerobic digestion and thermal conversion. There are also a variety of process configurations, including pre-treatments that influence the overall energy conversion and process efficiency on sewage treatment works.

1.1.1.1 Digestion Processes

Approximately, 80% of the UK's sludge is treated by mesophilic anaerobic digestion (MAD). The solid waste, digestate, is then dewatered and recycled to agriculture as a soil amendment and fertiliser because of its high concentration of C, N and P (Ofwat, 2015). The biogas produced is typically combusted in otto-cycle spark ignition combined heat and power (CHP) gas engines with the electricity produced predominantly used on site to offset site electricity imports. Engine heat is recovered and used to pre-heat sludge prior to digestion. However, for conventional digestion sites there is an excess of high-grade heat and most of this energy is wasted. The main advantages of digestion include:

- Sludge stabilisation and destruction of pathogens which facilitate its beneficial re-use in agriculture.
- Low parasitic energy and low gas-cleaning requirements.
- Electricity production.

Value can also be attained from biogas by upgrading it to biomethane and injecting it into the gas-grid and this is supported by the renewable heat incentive. Until recently this was not commonly practiced in the UK, however the transition from Renewable Obligation Certificates (ROCs) to Contracts for Difference (CfD) has led to increased uptake because of the deflationary effect of CfDs on electricity subsidies. In addition, water companies have pledged to achieve net-zero carbon emissions by 2030 and biomethane is viewed as a more efficient way to convert the gas into energy. For example, the 'Boiler Plus' legislation requires new domestic boilers to achieve at least 92% efficiency (BEIS, 2017). It should also be cautioned that bio-methane injection may not be compatible in long-term if UK domestic heating was electrified (e.g. heat pumps) or converted to hydrogen.

Despite its advantages digestion alone has limitations; valuable energy is not recovered, the sludge land bank is constrained and transporting sludge from large urban sewage treatment works to agricultural land is costly and contributes to air pollution and traffic. To overcome these challenges, the industry is adopting different process streams that aim to increase net energy conversion, reduce overall treatment costs, and reduce waste volumes.

Since 2000, the UK water industry has invested heavily in a MAD pre-treatment called thermal hydrolysis (THP) to help achieve these goals.

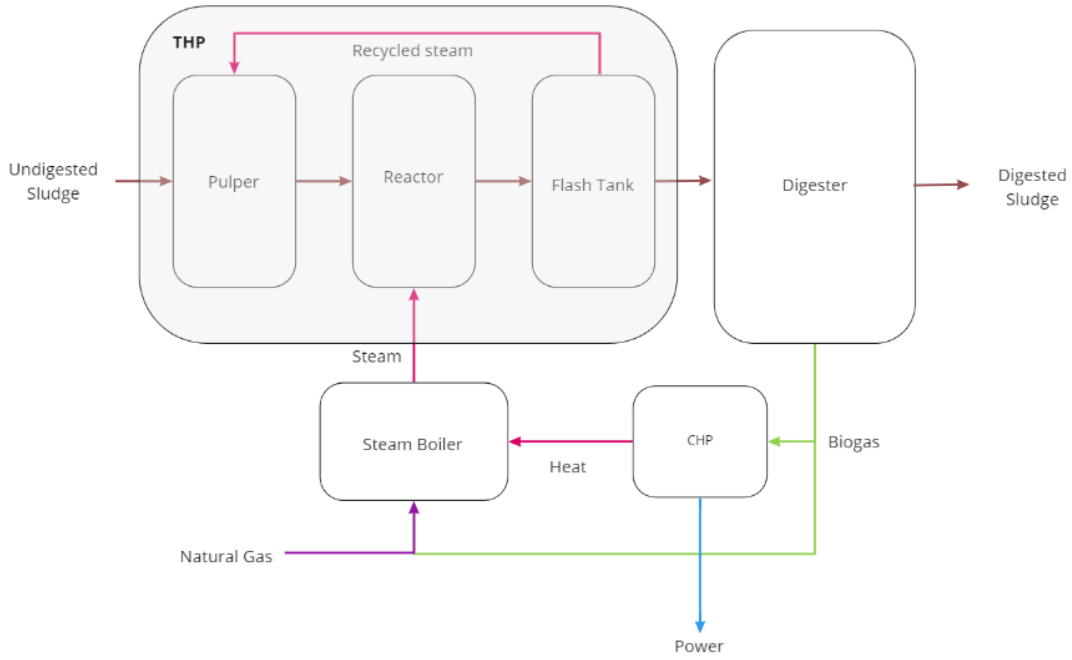


Figure 1-1 – Typical THP configuration, showing (i) sludge flow (ii) the main energy inputs and outputs and (iii) integration with other system assets (e.g. digesters, steam boilers and CHP). Based on a diagram published by Williams & Burrows (2016)

The THP process (figure 1-1) comprises three reactors: the pulper, which mixes and pre-heats sludge with recycled steam; the reactor, which heats sludge to $\leq$170°C and $\leq$6 bar pressure using steam produced in a boiler; the flash tank, where sludge is rapidly de-pressurised (a "steam explosion") and steam is recycled to the pulper (Williams & Burrows, 2016).

The main advantage of THP-MAD is its ability to rupture the cell walls of surplus activated sludge (SAS). THP facilitates:

- Increased SAS volatile solids destruction (VSD) from 20% to 50% (Shana et al., 2013);
- Higher digester loading rates (Pook et al., 2013);
- Increased sludge dewaterability (Mills, 2015) (Shana et al., 2013);

Cumulatively, up to a three-fold reduction in digestor volume requirement is achievable per TDS (Mills, 2015). This is supported by Rus et al (2013) who suggested the optimum organic loading rate for conventional digestion is 1.5-2.5 kg VS/m^3/d whilst Pook et al., (2013) recommended up to 8 kg VS/m^3/d for THP-MAD. This has allowed THP-MAD sites to import additional sludge from sites without digestion facilities, thus decreasing the amount of sludge that would conventionally be limed. THP sludge is also classified as a Class A biosolid and can be recycled to land with fewer restrictions than sludge treated solely by MAD. THP-MAD has a significant disadvantage, the process requires approximately 0.95kg steam kg DS^{-1}. Steam can be produced from high-grade CHP heat in a waste boiler, however additional fuel is required to bridge the overall heat balance.

This deficit is typically met by diverting biogas to a THP boiler or consuming natural gas. Mills (2015) assumed the latter because of favourable biogas subsidies. Although this may become less common because of changes in subsidies and the high emission factor of natural gas - 0.20297 kg CO_2e kWh (LHV) compared to biogas – 0.00022 kg CO_2e (LHV) (BEIS[c], 2021). Although, both fuels release CO_2, so reducing the parasitic use of biogas may also be beneficial.

Different configurations allow THP to be operated without biogas diversion or support fuels. SAS-only THP only hydrolyses SAS prior to digestion, therefore all the steam required for THP can be generated from high-grade CHP heat. As a result, the NCE of SAS-only THP is higher than conventional THP. This comes at a cost to throughput and cake dewaterability: <45% for conventional THP and <38% for SAS-only THP and digester volume requirements (Mills, 2015). In addition, SAS-only THP sites require secondary series-digestion to achieve a Class A pathogen count (Mills, 2015) (Shana et al., 2013) although presumably alternative technologies such as pasteurisation could be used. Regardless, these increase SAS-only CAPEX, and the process has only been adopted at Long Reach STW (to knowledge).

Intermediate THP (iTHP) is a two-stage digestion process, developed by Achame Shana of Thames Water (WWT, 2016) and has been tested at pilot-scale by Thames Water innovation (Rus et al., 2017) (Rus et al., 2015). Sludge is digested to decrease its volume and remove easily digestible material; the residual material is then thermally hydrolysed and re-digested. This reduces the size and steam requirement of the THP step. Intermediate THP has to date the highest gross and net electrical conversion of any digestion configuration. However, its complex and requires relatively high CAPEX (Rus et al., 2015) (Mills, 2015).

Figures 1-2 (a-c) show that THP and SAS-only THP suit post-digestion drying due to the large quantity of unused heat, sludge drying presents several opportunities for the water industry:

- Reduced tankering costs, for land recycling;
- Production of solid fuel for incineration;
- Production of solid fuel for advanced energy recovery (AER) (Mills, 2015).

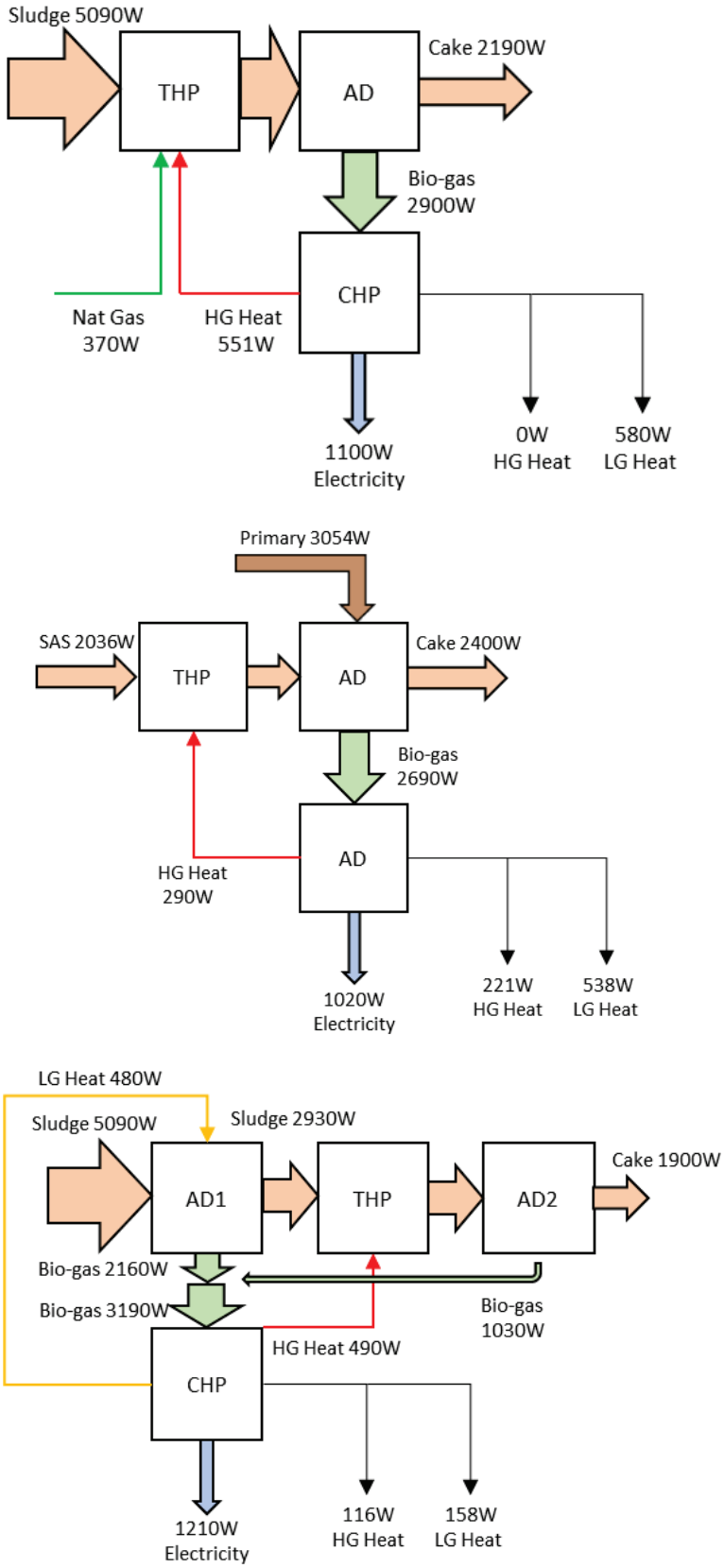


Figure 1-2 – Gross energy flows for (a) conventional THP (b) SAS-only THP and (c) iTHP based on a throughput of 1kg DS hour^{-1}. Produced using data and assumptions available in Mills (2015). Material energy contents are based on their lower heating value (LHV).

1.1.1.2 Thermal Processes

Thames Water operate a single incineration site, Beckton STW. At Beckton, sludge is dewatered and then incinerated in a Lurgi fluidised bed incinerator (FBC). The output of the process is high-grade heat, which is converted to steam in a boiler and electricity in a steam turbine. Until recently, the raw-cake at Beckton STW was dewatered with plate presses, which achieved an average DS% of approximately 25% (Personal communication, 2021). Due to the low DS, the process relied heavily on natural gas consumption to maintain bed temperature above 850ºC required for dioxin elimination. However, within recent years, the plate presses have been replaced by Bucher presses and the site now achieves a DS of approximately 35.1% (Thames Water, 2019) meaning the process is typically auto-thermal (e.g. no support fuel required). The process energy flows for a typical autothermal fluidised bed incinerator are shown in figure 1-3 (Mills, 2015).

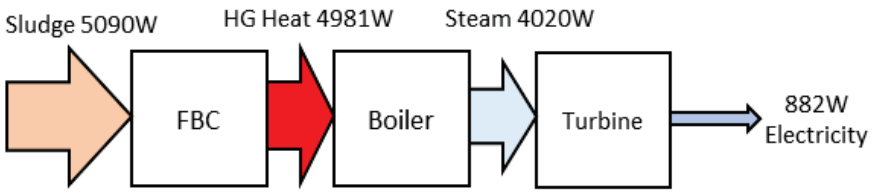


Figure 1-3 - Gross energy flows for incineration based on a throughput of 1kg DS hour^{-1}. Produced using data and assumptions available in Mills (2015). Material energy contents are based on their lower heating value (LHV).

There are several reasons why the UK water industry is not investing in new incineration facilitates, for example:

- High costs for both CAPEX and OPEX (Mills, 2015) (Palmer et al., 2013);
- The operational challenges and costs associated with the following: dioxin and furan formation; clinker formation; and corrosion.
- It converts sludge C, N and S into the pollutants CO_2, NO_x and SO_x which could otherwise be beneficially recycled in agriculture.
- The high parasitic load because of the requirement to maintain a fluidised bed and the low electrical efficiency of steam turbines (typically, ~8.2%) (BEIS[b], 2021) unless conducted at utility scale (Takaishi et al., 2008).
- Viable alternatives (e.g. digestion and land-recycling)

Advanced thermal conversion technologies (ATC) are the main alternative to incineration and include technologies such as pyrolysis and gasification. No ATC processes are currently being operated by the water industry in the UK (to knowledge). Although, Yorkshire Water operated an industrial-scale gasifier for 10,000 hours that processed both wood-chips and sludge as a trial in 2017 (Yorkshire Water, 2019) (Atkins Ltd., 2019) .

Like incineration, ATC processes could treat raw sludge instead of digestion-based processes. However, the UK water-industry already has extensive digestion assets and has invested heavily in THP over the last couple of decades. Mills (2015) suggested ATC could be used post MAD to produce additional energy from sludge, eliminate the requirement for THP support fuels and provide the water industry with an alternative to pathway to biosolid recycling to land. The facilitation of ATC post THP-MAD is possible due to innovations within the industry, for example:

- The adoption of THP and piston presses, which has increased biosolids DS% from approximately 20-25% DS to <45% (Mills, 2015) and <42% (Macedo et al., 2015).
- The development of low-temperature dryers, which could utilise the low-grade heat typically underutilised by THP-MAD (Mills, 2015).

Overall, Mills (2015) suggested the sequential combination of THP, MAD, and pyrolysis (figure 1-4) now offer the most efficient overall energy recovery configuration for sludge treatment based on economic and environmental criteria.

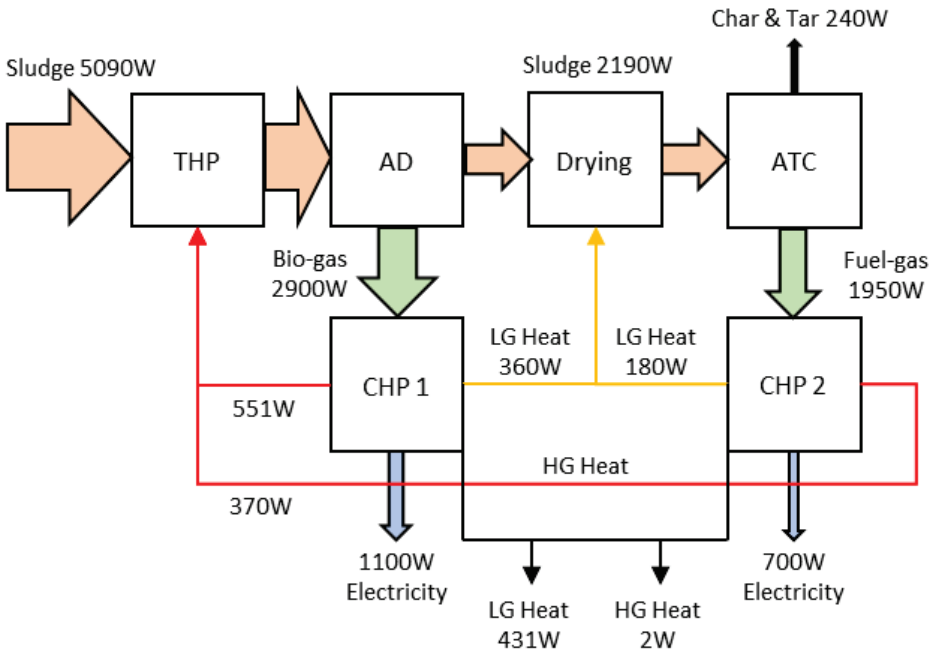


Figure 1-4 – Gross energy flows for THP ATC based on a throughput of 1kg DS hour^{-1}. Produced using data and assumptions available in Mills (2015). Material energy contents are based on their lower heating value (LHV).

Further evidence is required to validate Mills (2015) assumptions. For example, an assumption was made that ATC will convert 89% of sludge energy into fuel-gas. The evidence base for this assumption is unclear and is not consistent with previous findings.

For example, Gao et al., (2020) reports conversion of 55% during sludge gasification and between 41-62% for a range of co-gasification processes. Zhang et al., (2014) conducted high temperature pyrolysis (1000-1400ºC) of sludge and found a maximum sludge to gas energy conversion of 72.6%. Total tar elimination was achieved at 1300ºC however, carbon was retained in the char at all temperatures tested. These finding are expected since pyrolysis promotes carbon stabilisation through carbonisation reactions. Further energy could be recovered through char/tar gasification; however, this was not considered by Mills (2015). Figure 1-4 shows that THP-pyrolysis has no spare high-grade heat capacity, therefore if energy conversion is <89% the process will require a support fuel to maintain full functionality of the THP. Although If high-grade heat availability was constrained, rather than use a support fuel, some primary sludge could simply be diverted directly to the digesters or pyrolysis unit.

In addition, Mills (2015) assumed THP-digested sludge will achieve a cake DS of <45% when dewatered with a Bucher Press. Bucher Unipektin manufacture hydraulic filter presses for the fruit juice industry, recently these were adopted by the UK wastewater industry. Mills (2015) assumed these presses could achieve up to 45% when dewatering THP-digested sludge based on short-term trials conducted at Oxford and Chertsey STW (Fountain et al., 2013). Subsequent full-scale operation at Oxford STW suggests Bucher presses have achieved between 38-42% DS (Macedo et al., 2015) whilst Crossness STW only achieves a DS% of around 30.9%. Rus (2017) found that lower sludge dewaterability corresponds with higher quantities of soluble P, higher ratios of monovalent to divalent ions and higher quantities of extra polymeric substances. Figure 1-4 shows that there is a large surplus of low-grade heat expected for THP-ATC, therefore the process is more sensitive to high-grade heat deficits than low-grade heat deficits.

Given the sensitivity of THP-ATC to high-grade heat availability, other configurations may be more suitable from an energy and cost perspective. In addition, there are several configurations not considered by Mills. For example:

- Standalone ATC that converts raw sludge into fuel-gas.
- SAS-only THP followed by ATC, because the former would significantly reduce the high-grade heat requirements of the THP (this could be operated with/without digestion).
- Digestion ATC without THP pre-treatment
- The co-treatment of sludge and other wastes generated on sewage treatment works including: FOG (fat, oil, and greases) and screenings.
- The use of alternative energy conversion technologies, for example steam turbines or fuel-cells.

1.1.2 Greenhouse gas emissions

In 2019, the UK government made a legally binding commitment to reach net zero emissions by 2050. To support this the UK water industry plans to achieve net-zero operational emissions by 2030. From 2011 to 2019, the industries net emissions have reduced by 45% to 2.4 $MtCO_2$ (Water UK, 2020). Much of this progress however has been achieved because of grid-decarbonisation. For example, the emissions factor for grid electricity has decreased from 0.452 to 0.256 kg CO_2e kWh^{-1} (a 43% reduction) (BEIS, 2012) (BEIS, 2020), over this time period whilst overall consumption of grid electricity has remained relatively static (Water UK, 2020). Significant net emissions reductions (>0.5Mt CO_2e) have also been achieved by purchasing "green electricity" backed by power purchasing agreements or the renewable energy guarantees of origin scheme (Water UK, 2020). Over-reliance on green electricity imports carries a risk, for example prices may increase to unsustainable levels as companies across the UK seek to decrease their reported carbon emissions. In 2019, importing grid electricity and burning fossil fuels accounted for more than 1Mt CO_2e for UK wastewater treatment (Water UK, 2020). The UK water industry must make a concerted effort to increase the overall efficiency of their wastewater treatment system and decrease fossil-based energy consumption. The treatment of sewage sludge and the production of renewable fuels (e.g. biogas, syngas, and hydrogen) provides an opportunity for the industry to achieve this.

1.2 Process outputs

Sludge treatment technologies convert sludge into one of three solid by-products:

- Biosolids: Covers sludge treated by several technologies including anaerobic or aerobic digestion, composting or liming. Most biosolids in the UK are produced through anaerobic digestion therefore, only anaerobic digestates will be discussed.
- Ash: The direct combustion of sludge converts the carbon content of the sludge into carbon dioxide, water vapour and heat. Dependent on the temperature the solids are exposed to, the residual inorganics form either ash or slag.
- Char: Pyrolysis is the thermal decomposition of organic matter (e.g. sludge) in an oxygen deprived atmosphere, the process forms gas, tar (or "bio-oil") and char. Sludge char is a porous material comprising condensed carbon and ash.

1.2.1 Biosolids

MAD converts sludge into "biosolids" which are suitable for application on to agricultural soils. In 2010, approximately 1.1 million tds^{-1} of sludge was recycled to agricultural land in the UK (Ofwat, 2015). According to Smith (2009) the opinion of the European Commission is that the use of sludge on agricultural soils is the best environmental option provided it does not pose any threat to the environment, animal, and human health. Biosolids provide soil with organic matter and a range of essential macro- and micro-nutrients which contribute to crop growth and offset

the input of inorganic fertilisers. The benefits and some concerns associated with biosolid applications to agricultural lands will be discussed in the following sub-sections.

1.2.1.1 Biosolids: Organic matter

Soil organic matter (SOM) is an important indicator of soil health, and plays an important role in soil water retention, nutrient turnover, soil microbiology, aeration, and resistance to erosion. Soil organic matter is a complex mixture of carbon-based substances including: (i) living biomass, such as plant and animal tissues and microorganisms; (ii) decaying biomass; and (iii) humus, which comprises alkali soluble organic acids (molecular weight 2000-300,000 Da) such as humic and fulvic acids and alkali insoluble organics such as organo-clay complexes (Weil & Brady 2008). Although it varies, SOM typically contains about half carbon by dry weight (Weil & Brady, 2008). The environment agency (EA) estimate that the UK soils store 10 billion tonnes of carbon, however, most arable UK soils may have already lost 40-60% of their carbon (Guo and Gifford, 2002). Long-term trials conducted at Rothamsted show biosolid amended soils have increased SOM contents (Chambers et al., 2007) and improved physical characteristics such as soil water capacity, soil texture, soil strength and trafficability. The application of biosolids to land has been suggested as a possible method for soil-C sequestration. This is discussed in depth, in section 9.3.

1.2.1.2 Biosolids: Inorganic content

Biosolids contain a range of useful macro-nutrients (N, P, S and Ca) and micronutrients (Mn, Fe, Zn, Cu) which when added to soils can help increase the fertility of soils. For example, Nicholson et al., (2018) found that the long-term (20 years) addition of biosolids to land increased total soil N, S, and extractable P by 20%, 30% and 48% respectively compared to inorganically fertilised control samples. In comparison to fields amended with inorganic fertilisers, biosolid amended fields produce crops such as grass with superior nutritional qualities due to the wide range of macro- and micro-nutrients present (Chambers et al., 2007). The increased retention of nutrients in the soil is likely due to increased SOM and improved soil structure and water retention.

However, the level of nutrients applied through biosolid addition tend not to match crop demand, for example: P is over-supplied leading to eutrophication or build-ups of P after consecutive years of application, whilst K is under supplied (AHDB, 2020). Biosolid-N is mostly present as organic proteins or amino-acids which are not immediately plant available and are instead released gradually over-time. Weil and Brady (2008) state that 1.5-3.5% of the total organic nitrogen contents of a soil are mineralised into plant available forms annually. This gradual release of nitrogen has benefits; however, it does not necessarily replace inputs of inorganic N fertilisers because farmers try to regulate N-inputs to match specific plant growth stages.

Sludge contains several potentially toxic elements (PTEs) including Zn, Cu and Ni alongside the toxic element Pb. The application rate of these metals is controlled by the Sludge (Use in Agriculture) Regulations (1989).

1.2.1.3 Biosolids: Emerging contaminants

Traditionally, the main environmental concerns associated with the land application of biosolids have been pathogen kill and heavy metals content. Together these have been successfully managed through adherence to the "Sludge (Use In Agriculture) Regulation 1989", the safe sludge matrix, participation in the biosolid assurance scheme and regular testing (Assured biosolids Ltd, 2020). However, there are a vast range of emerging contaminants, amongst others, these include (Diaz-Cruz et al., 2009):

- Microplastics
- Nano Particles
- Sex hormones (e.g. Oestrogens)
- Pharmaceuticals
- Illicit drugs
- Flame retardants
- Perfluorinated compounds
- Surfactants
- Antibiotics

Generally, these compounds accumulate in sludge because of their low polarity and resist biological degradation because of inherent stability/non-reactivity (e.g. perfluorinated compound) or metabolic pathway restrictions. In addition, few have a point source because of their widespread use in society. Identification and quantification of these compounds is challenging due to sample matrix complexity and analytical limitations; however, advances are making analysis quicker and easier. If these compounds become greater environmental concerns, the long-term viability of sludge to land may be questionable since some of these substances are human and environmental health hazards.

1.2.1.4 Biosolids: Other challenges

Aside from issues with biological, inorganic, and organic contaminants in sludge there are several issues that could affect the long-term viability of sludge to recycling to land. For example:

- Nitrate vulnerable zones (NVZ): 55% of the England is classified as an NVZ which means there is a N field limit of 250 kg ha yr^{-1} (S.I. 2015) for organic manures. Roughly, this corresponds to a biosolids application rate of up to 8.3t ha^{-1} year (Powlson et al., 2012). If NVZs were expanded to cover more of the UK or the NVZ field limit was reduced, this would decrease the quantity of biosolids that could be recycled to agricultural land.

- The Landfill Directive (1999/31/EC) requires EU member states to reduce biodegradable municipal waste landfilling by 65% (Zglobisz et al., 2010). To divert bio-degradable

waste, the full landfill tax is applied at £94.15 t^{-1} (in 2019) to waste with a loss on ignition (at 440°C) of over 10%. This has led to explosive growth in anaerobic digestion and composting, for example: between 2008 and 2017 the energy produced by MAD in the United Kingdom increased from 3.6 TWh to 15.8 TWh (Sönnichsen, 2020). As digestate production increases, sludge will increasingly compete for access to the UK land bank.

- Maintaining a positive perception of biosolids applications to land with consumers, land-owners and farmers may become more challenging in the future, especially when influential media outlets describe sludge as "the most pollutant-rich manmade substance on earth" (Perkins, 2019). Tenant sheep-farmer Turpin (2021) also suggests that odour generated by biosolid applications can be unpopular with both residents and landlords and in the past a landlord had stopped Turpin (2021) applying sludge because of these concerns. The likelihood of these situations arising could increase in the future because of the diversification of economic activities in rural localities.

Biosolids application accounts for just 3% (by volume) of "manures" added to UK agricultural land (Ofwat, 2015), therefore diversion of biosolids from agricultural soils may not have a major impact on farmers.

1.2.2 Ash

When sludge is incinerated, it is converted into heat and CO_2, the remaining material is ash. Most gasification processes also fully convert sludge into gas and ash. Raw sludge contains approximately 13-35% ash by weight (Mills, 2015) whilst biosolids contain approximately 30-50% ash by weight (Schnell et al., 2020). In 2010, 260,000 tds of raw sludge were disposed by incineration in the UK (Ofwat, 2015). Based on an ash content of 13-35% this equates to 34,000-91,000 tonnes of sewage sludge ash (SSA) generation per year. Unlike the UK, the quantity of sludge being disposed by incineration is increasing in some countries (e.g. Germany) and is often co-combusted in cement kilns, coal power stations or waste incinerators although this may decrease because of the requirement to recover P from sludge ash.

SSA contains a multitude of useful macro- and micro- nutrients; however, it is not recycled directly to agriculture because of its heavy metal content and the potential presence of PAHs and dioxins. In soil metal oxides would likely form hydroxides, which have relatively low solubility, however the regulatory emphasis is currently based on total concentrations rather than availability. However, the physical structure of ash (fine powder) may contribute to greater heavy metal availability. Sludge ash contains calcium, lead, zinc, and copper oxide in concentrations that exceed the threshold value for hazardous waste as outlined in Directive 2008/98/EC otherwise known as the waste framework directive (European parliament and council, 2008). Most sludge ash in the UK is disposed of in hazardous landfills and attracts the full landfill tax of £94.15 t^{-1}.

To reduce landfill fees, carbonate encapsulation can be conducted to reduce the surface area of the material (Carbon8, 2020). Alternatively, the material can be blended into cement products. However, whilst sludge ash exhibits slight pozzolanic activity, it typically reduces the compressive strength of resulting mortars and increases heavy metal leaching compared to standard blends (Cyr et al., 2007). Rather than simply dispose of SSA many researchers are working towards recovering its P content in agronomically useful forms, however the materials heavy metal content is problematic and increases recovery costs.

As previously mentioned, the UK water industry is moving away from incineration due to its technical challenges, high CAPEX, high OPEX and high release of carbon dioxide. Therefore, SSA will not be discussed further.

1.2.3 Char

Char is a non-volatile carbon-based material that is produced when organic materials are heated in an oxygen deficient atmosphere (e.g. pyrolysis). Currently char is not being produced in meaningful quantities from sludge. However, several options exist to recover value from char, these include:

- Pyrogenic carbon sequestration
- Soil amendment (e.g. biochar)
- Phosphorus recovery
- Precious metal recovery
- Adsorbent production
- Carbon black replacement in tyres
- Energy recovery
- Contaminated land management

Some of these will be discussed in more detail in the following chapters.

Chapter 2: Literature Review

2.1 Introduction

There is a recognition within the Water Industry that a sustainable, effective, and economically viable means of treating wastewater sludge is required. The most promising technology which has the greatest potential to meet these requirements is a group of processes generically described as "Advanced Thermal Conversion". The main focus of the research in this thesis is the application of ATC to Sludge.

2.2 Advanced Thermal Conversion

In the waste industry, pyrolysis, gasification, and hydrothermal carbonisation are considered "advanced thermal conversion technologies" (ATC).

2.2.1 Pyrolysis

Pyrolysis is the thermal decomposition of organic matter in an oxygen deprived atmosphere. During pyrolysis, the material being heated undergoes: dehydrogenation, devolatilisation, carbonisation, polymerisation and a complex range of free-radical driven reactions that cause a proportion of the carbon present to form a condensed covalently bonded aromatic structure (e.g. fixed carbon). Pyrolysis and carbonisation are used interchangeably within the literature, carbonisation specifically refers to the process of concentrating carbon within the solid residues, usually by pyrolysis in an inert atmosphere (Fitzer et al., 1995). The carbon that does not form char and instead volatilises typically forms a range of compounds including syngas (CO, H_2), hydrocarbon gases, volatile organic carbon (VOCs), bio-oils, tars, pitches, and soot (McNeil, 1975) (Mohan et al., 2006). The yield of these products depends on the pyrolytic condition, namely temperature and volatile residence times. The ash content of the material is typically retained alongside the char.

Pyrolysis or carbonisation are typically deployed when the solid by-product is valued, for example: to produce coke from coal, activated carbon from coal or woody biomass, charcoal (or biochar) from woody biomass and carbon black from hydrocarbons. Gas-phase pyrolysis or thermal cracking is used by the oil industry to upgrade gas-oil and heavy naphtha into alkenes (e.g., ethylene) although fluid catalytic cracking is more common nowadays (Sadrameli, 2015).

There are three main types of pyrolysis referred to in the literature for the processing of solid materials:

- Slow pyrolysis, also called carbonisation: The process conditions used enhance the yield of char and typically include slow heating rates, lower operating temperatures, and longer vapour residence times. By heating the material slowly and enhancing vapour residence times, volatile compounds are carbonised and condense to form secondary char (Garcia-Nunez et al., 2017).

Increased solid residence times also promote carbonisation, consequently: H, O, N, S, Cl, and other elements are removed from the char over-time. Typically coke, biochar and charcoal are produced using batch-fed slow pyrolysis processes, whilst activated carbon is produced using a continuous slow pyrolysis process.

- Fast Pyrolysis: This favours oil production and occurs under moderate temperatures and very short vapour residence times (<2s). Moderate temperatures ensure adequate separation of the feedstock volatiles, whilst the short residence time minimises secondary cracking reactions (Garcia-Nunez et al., 2017). The aim of the process is to maximise oil yield.
- Pyrolytic gasification (PyG) - This favours gas production and occurs under moderate-high temperatures and moderate-high vapour residence times (Bridgewater, 2012) (Akhtar et al., 2018). The high temperature and vapour residence times used decompose primary bio-oils into additional gas and aromatic compounds such as VOCs and tar. Historically, both batch and continuously fed pyrolytic gasification of coal was conducted to produce town-gas, organic chemicals, and coke from coal.

2.2.1.1 Historical perspective: Pyrolysis reactors

Pyrolysis has a long industrial history, the process was widely adopted to produce town gas, organic chemicals (benzoles, tars, organic acids), inorganic chemicals (ammonia, sulphuric acid) and chars (coke and charcoal) from coal and wood. The first company to manufacture gas from coal was the London-based "Gas Light and Coke Company" founded by Frederick Winsor (1763-1830). The main market for coal-gas was for street lighting, cooking, and heating. To maximise gas yields D-shaped horizontal retorts were only partially filled this facilitated extended gas residence times which increased gas yield, at the expense of tar quality. Lewes (1912) states that tars produced from lightly charged horizontal retorts were "so choked with naphthalene and free carbon as to be almost valueless". One of the main operational challenge was the avoidance of carbon crusts, which accumulated in the gas outlet, although this was resolved by blasting the carbon with air and steam (Meade, 1921).

After the electricity supply act in 1926, the focus of the process was to generate value from both the gas and tar. Many operators packed horizontal retorts tightly with coal to minimise gas residence times, decreasing secondary cracking reaction and maintaining the quality of the tar produced. Tar valorisation helped drive the beginnings of the chemical processing industry. The first continuously fed vertical coal retorts entered commercial operation in 1906 at Bournemouth gasworks. Vertical retorts were favoured at many medium and large sites because of their reduced footprint and labour costs. They typically had a capacity of 1-5-4.5 tons each and were roughly 25 feet in length and tapered to the top to aid the downward flow of coal (BP, 1965).

Coal was fed continuously by gravity into the top of the retort, as it moved downwards, it carbonised, forming coke which was then removed mechanically by a screw or periodically discharged by gravity. To further increase gas yields operators injected steam into the bottom of the reactor to partially gasify the coke (via the water-gas reaction) prior to discharge (BP, 1965). Vertical retorts were typically heated externally through the combustion of producer gas in vertical or horizontal flues between the rows of the retorts (BP, 1965). Producer gas was generated by passing saturated air through the red-hot coke produced. Due to the exothermic nature of this partial oxidation reaction, the coke could provide producer gas to the process on a continuous basis. The coke was then fully quenched in water to suppress dust generation and generate additional water-gas. A typical coal carbonisation plant consumed heat equivalent to 35-50% of the thermal value of the gas produced. Vertical retorts caused the lowest degree of atmospheric pollution and had high thermal efficiency, especially if producer-gas was made in situ from the hot-coke (BP, 1965).

Several factors undermined the economics of gas-works, these included:

- Increased production costs because of increases in the price of coal and increased regulation;
- Damage to the industries infrastructure and loss of skilled workforce because of World War 1 and 2;
- The development of the modern petrochemicals industry.

To reduce costs, many processes began to co-pyrolyse coal and produce process heating with low-value by-products from the petrochemicals industry (BP, 1965). In addition, complete gasification processes such as the Lurgi process were developed to convert the coke and tar produced during pyrolysis into additional heat and gas within the reactors itself (Thomas, 2014). Several high-pressure gasification processes were built during the 1960s including a plant in Scotland and the West Midlands, which produced gas and dry-ash (Thomas, 2014). In addition, the British Gas Lurgi slagging gasifiers were developed in the 1970s, however the process was never adopted commercially in the UK. In 1965, North Sea gas was discovered off the coast of Grimsby. Less than two years later the gas council announced the move from coal-gas to natural gas and every gas appliance in the UK was retrofitted (British Gas, 2021). This signified the end of the gas-making industry in the UK. Today coke ovens comprise long rectangular boxes constructed of refractory material which are lined up in batteries (Thomas, 2014). The technology has not developed significantly since the 1930s. Coke ovens still operate in the UK to produce metallurgical coke for blast furnaces and smokeless fuels. In 2018, the UK produced 63% of its coke requirements mainly at Port Talbot and Scunthorpe, however, both coke production and demand have fallen significantly since 2000 because of the decline of the UK steel industry. For example, the UK's only dedicated coke plant, “Monckton Coke and chemicals” closed in December 2014 whilst Redcar steelworks ceased production in September 2015.

2.2.1.2 Modern perspective: Pyrolysis reactors

Several designs for pyrolysis reactors exist, including: fluidised beds, screw-augers, cyclonic, ablative, rotating cone, entrained flow, and fixed bed reactors. According to Campuzano et al. (2019) there are three pyrolysis reactor designs that currently have high market attractiveness and technology strength, these include: bubbling fluidised bed, circulating fluidised bed and screw auger systems. Screw auger systems typically comprise single or twin augers within stainless-steel casing; these systems have several advantages over fluidised beds including:

- Lower cost of construction and maintenance.
- Flexible control of feed-rates and dwell times.
- Greater scalability (including modular and skid mounted systems). For example, Campuzano et al., (2019) states that for fluidised beds providing the enthalpy for pyrolysis through heat transfer alone becomes increasingly difficult as the reactors are scaled-up. Fluidised beds have been successfully implemented at scale for incineration (Figure 2-1) and gasification.
- Char separation by gravity.
- Low attrition
- No requirement for an inert sweeping gas, which is energetically demanding and complex.
- Higher gas retention times which facilitate thermal cracking of tar to gas.
- Direct heating of the screw itself through joule heating leading to high thermal transfer between heater and material.
- Adjustable mixing and bed thickness across the length of the screw through changes in flight parameters.

Fluidised beds are widely adopted for gasification and incineration reactors, the bed typically comprises an inert or catalytic material that is suspended alongside the fuel by air injected from below (Figure 2-1). Fluidisation facilitates uniform particle mixing and temperatures across the bed. Without fluidisation, incinerators and to a lesser extent gasifiers are prone to dioxin formation because of incomplete combustion occurring below 850^{o}C. However, maintaining continuous fluidisation is energetically demanding and increases both the capital and operating expenditures of these technologies. Since dioxins are not expected to form during pyrolysis, and pyrolysis does not generate process heat from combusting fuel within the reactor, fluidisation does not appear to be a suitable technology for pyrolysis. Unless the bed material helps decompose contaminants produced during pyrolysis. The scalability of fluidised beds is also an issue (Campuzano et al., 2019). Thus, for a continuously-fed pyrolysis processes mechanical feeders such as screw-augers or gravity-feeders offer design advantages.

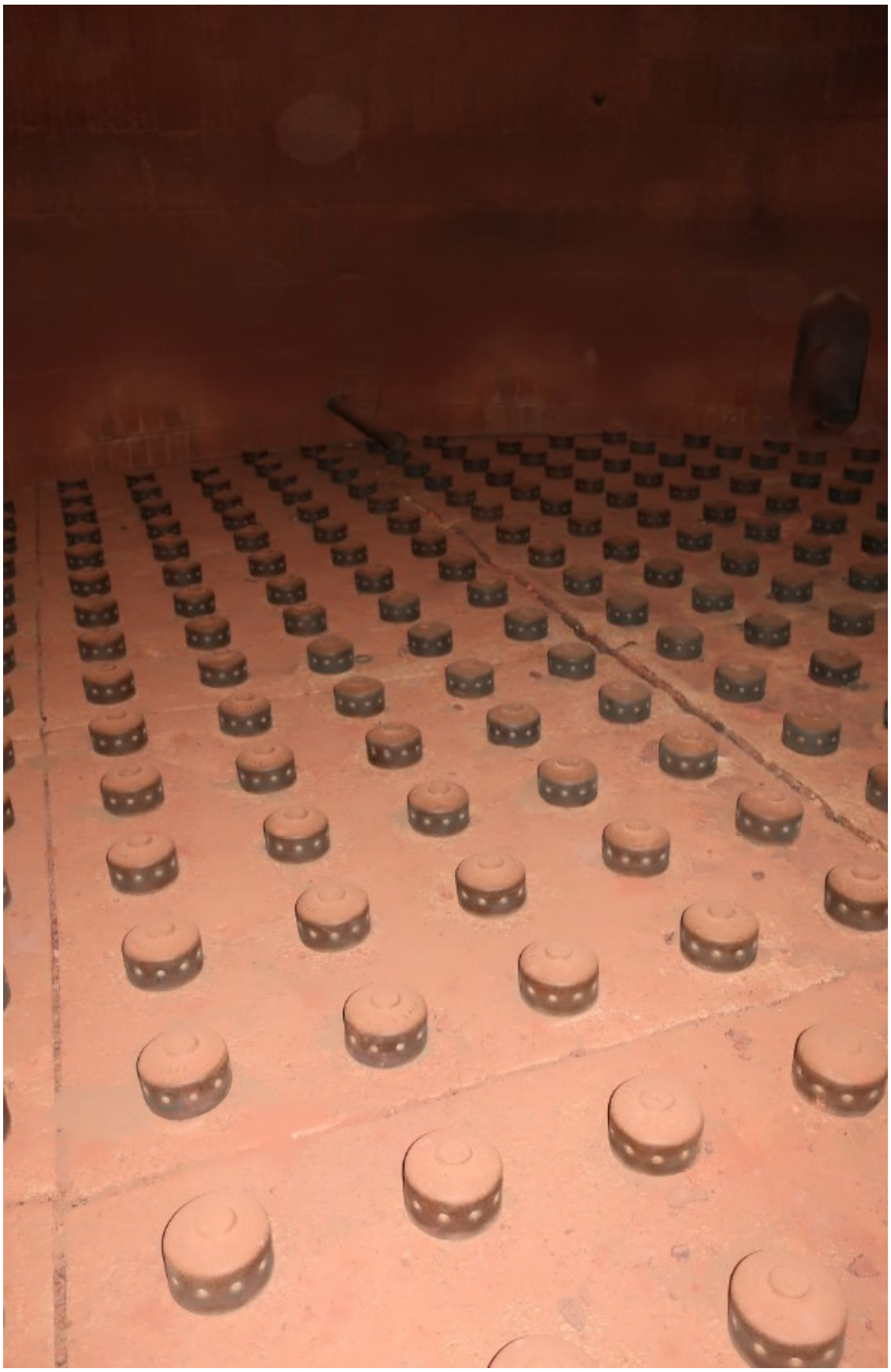


Figure 2-1 – Decommissioned Lurgi fluidised bed incinerator at Crossness STW showing the air injectors that fluidised inert sand and sewage sludge and an injector rod used to inject water to control bed temperature and prevent clinker forming.

The material within a pyrolyser can be heated indirectly through electric heaters or the combustion of primary fuels such as fuel or producer-gas. External heaters have scalability issues because of conductive heat transfer limitations through the reactor casing (Campuzano et al., 2019). Whilst there are conductive limitations, the conversion of primary fuel-sources to high-grade heat via combustion is a highly efficient process. For example, Mills (2015) suggested fluidised bed incinerators convert 97.9% of sludge energy into high-grade heat whilst the typical conversion efficiency of a gas boiler to heat is approximately 88-90%. External heating through the combustion of generated fuels was always the favoured method of the gas industry and is implemented by several modern processes, for example: Pyreg GmbH (Figure 2-2), Carbon Gold, Cynar PLC, and Anergy Ltd.

Almost all "biochar" produced from lignocellulosic materials such as crop residues in the literature is produced under slow-pyrolysis conditions in double walled kilns. For example, Carbon Gold (2015) have designed a small-scale slow-pyrolysis system (patent: WO2014/155058) to produce biochar from biomass. The system includes two double-walled kilns and a combustor. To initiate heating, the combustor is fed with fuel (wood-chips) and the heat produced is circulated to one of the kilns. As the kiln heats up, volatiles are released from the biomass and these are combusted supplying further heating to the kiln. Once the kiln reaches approximately 500^{o}C any further heat produced is recirculated to the drying kiln. According to Carbon Gold, the system can process feedstocks with a dried solids content of 40% and higher. Systems like this are commonly implemented across the world to produce biochar from biomass, however they are not designed to produce enough excess heat for electricity production.

Pyreg GmbH have developed an externally heated screw-auger fed pyrolysis process that heats sewage sludge (<65% DS) up to 500-750^{o}C through pyrolysis alone, the char and volatiles are then partially gasified with a carefully controlled air-steam ratio to provide further heating. The volatiles released are immediately combusted at 1000^{o}C (to minimise NO_x) and all the heat produced by the process is recirculated to provide system heating. Pyreg (2021) claim their process is auto-thermal (i.e. does not require an external heating source) and the excess heat can dry the feedstock prior to pyrolysis. A simplified process flow diagram of the Pyreg system is presented in figure 2-2.

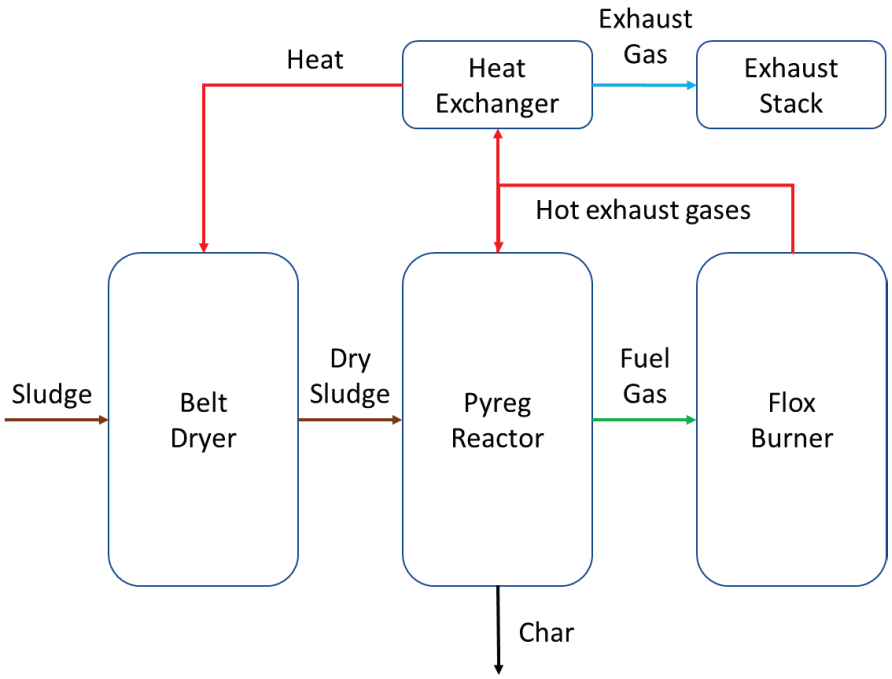


Figure 2-2: Sewage sludge pyrolysis process, based on digram published by Pyreg GmbH (Eliquo, 2021)

The system developed by Pyreg (Figure 2-2) and Carbon Gold have several aspects in common:

- Both processes combust all the volatiles generated to provide system heating, however, neither process appears to produce enough excess heat to produce electricity via a steam turbine. Therefore, these technologies are waste treatment and minimisation technologies.
- Both operate at relatively low temperatures, approximately 500ºC and <750ºC, respectively.

Although the Pyreg process is auto-thermal, it injects sub-stoichiometric air into the backend of the reactor (e.g. gasification) this will cause partial oxidation (POX) reactions which release heat and consume char carbon, volatiles, and gas.

Clinipower Ltd. (previously Compact Power) also combine pyrolysis and gasification within one process stream at their clinical waste treatment plant in: Avonmouth, UK. The system utilises pyrolysis to produce volatiles from clinical waste. The char is then processed in a separate reactor and undergoes simultaneous gasification and partial oxidation to produce syngas and ash at 1000ºC. Therefore, the operation is almost identical to a traditional coal pyrolysis plant heated through the production of producer gas. The pyrolysis gas is then blended with synthetic gas and combusted at 1250ºC to produce steam for energy generation or waste sterilisation (Clinipower, 2020) (Compact Power, n.d.). This process stream is attractive for Clinipower, because:

- Issues associated with tar condensation are avoided and the generation of harmful by-products are avoided.
- Lower pyrolysis temperatures can be used because extensive tar cracking is unnecessary.
- The company have large requirements for heat/steam.

If char recycling is uneconomical or additional energy generation is required, char gasification may be a viable method of producing additional energy and could be conducted in a secondary vessel as demonstrated in the Clinipower process. One of the main issues with pyrolysis is the complex range of contaminants in the gas produced. No modern commercial pyrolysis processes appear to have resolved these issues, consequently companies such as Scanship AS, Pyreg GmbH, Clinipower Ltd and others have all developed oxidisers to combust the generated gas and eliminate its contaminants. EPi Ltd. were the only company identified that claim their fuel-gas can be cleaned and is then suitable for conversion in a gas engine (EBRI, 2015).

Due to the high temperatures used and the corrosive atmosphere within the reactor, the casing material is typically constructed from 316L/310 stainless steels or refractory materials. These materials are relatively poor conductors and the internal casing typically cokes up, leading to an additional insulating layer. Due to the inefficiency of heating the process externally, electric heaters are not typically suitable. The main method of providing process heat within the reactor are electric resistance heaters. Several screw conveying processes (e.g. Scanship) use Spirajoule™, a patented process whereby low voltage current is passed through a shaftless screw auger to heat the screw itself (ETIA, 2020). This process is called joule or ohmic heating, however it requires large currents. Alternatively, conventional insulated electrical heating elements can be placed within the reactor although these may be less compatible with screw conveyors, this is the favoured approach of Environmental Power Limited (EPi) (EBRI, 2015).

2.2.1.3 Historical perspective: Pyrolysis gas treatment

The main product of coal pyrolysis was town-gas which was used for lighting, cooking, heating, and power production in engines. These historic pyrolysis processes could operate without oxidising the volatiles produced. However, coal gas required extensive cleaning prior to its use. Cleaning coal gas produced valuable by-products and waste by-products, which are summarised in table 2-1.

Table 2-1: Coal pyrolysis gas treatment by-products

Product	Inorganic	Organic
Potentially valuable	Elemental sulphur Sulphuric acid Ammonia Liquor Ammonium salts	Tar Benzole
Wastes	Ferrocyanates Thiocyanates	Carbon disulphide

At Beckton Gasworks in East London the disposal of ferrocyanates led to the formation of large spoils heaps, nicknamed the "Beckton Alps". A dry ski-slope was even built on the site and operated until 1991. From a modern perspective, ATC technologies need to avoid or minimise the generation of waste by-products if they are to be sustainable. Therefore, it's useful to understand how coal gas was treated historically. McNeil (1975) describes the two main processes used to produce clean town gas, recover tar, and produce chemicals from coal pyrolysis.

(i) Direct Process

Step 1 - Tar Removal: Three processes were used to remove vapour-phase tar from coal gas, these included: (i) a collecting main; (ii) an atmospheric cooler; and (iii) a tar extractor. Processes (i) and (ii) high dew-point vapours such as heavy tars. The collecting main was flushed and sealed with recirculated tar to prevent blockages and the hot-gas was sprayed with cooler tar to encourage condensation prior to entering the atmospheric cooler. Exhausters or gas pumps were used to actively pull the gas through the gas treatment process. In the tar extractor, the gas was sprayed with a high velocity mix of cold-tar and liquor, causing the tar particles to condense (McNeil, 1975). Throughout these processes, the gas was kept above the dew-point for benzoles and water. In the UK, the gases were typically cooled to just above the dew-point in the collecting main and atmospheric cooler, so that they entered the tar separator at 85-90^{o}C and the saturator at 65-70^{o}C (McNeil, 1975).

Step 2 - Ammonia removal: The gas entered the saturator, a large cylindrical vessel with a conical bottom made of stainless steel. It contained a hot mixture of ammonium sulphate and free sulphuric acid through which the gas was bubbled. The ammonia was absorbed, and crystals of ammonia sulphate formed and accumulated at the base of the saturator (McNeil, 1975). The adsorption of ammonia released heat, which was enough to maintain the temperature of the gas above the dew point of water.

Ammonia sulphate was sucked from the base of the saturator as a slurry and crystallized in the crystallising tank, the mother liquid was then returned to the saturator. Before return, the mother liquid was treated to recover pyridine bases (McNeil, 1975). Organic bases such as pyridine are likely to be preferentially removed by an acid scrubber.

Step 3 - Naphthalene and water removal: The gas was cooled to 40^{o}C in an unpacked tower with a water spray. This condensed both water and naphthalene, which formed a solid and was recovered.

Step 4 - Benzole removal: The cooled gas entered the benzole absorbing towers where they were counter-currently scrubbed in hydrocarbon oils which distil in the range 230-270^{o}C. The towers were packed with metal or ceramic rings to enhance benzole condensation. The oil-benzole mixture was separated, and the oil was recirculated.

Step 5 - Acid gas removal: Hydrogen sulphide and hydrogen cyanide were removed by passing the gas through porous beds of hydrated iron oxide. The media was manufactured from natural bog-ore or wood shavings impregnated with iron oxide. Hydrogen sulphide reacted to form elemental sulphur and hydrogen cyanide formed thiocyanates and ferrocyanides. Some installations roasted the loaded media to form sulphur dioxide, which was then manufactured into sulphuric acid via the contact process. Wet-scrubbing with sodium carbonate was also used however, it typically could not remove hydrogen sulphide to sufficiently low quantities and was followed by oxide boxes (McNeil, 1975).

(ii) Indirect process

The indirect process was introduced to avoid contamination of the precipitated ammonium sulphate with tar and ammonium salts such as thiocyanate. The main difference was that tar treatment was more extensive. The gas was cooled to 80-95^{o}C in the collecting main by spraying it with ammoniacal liquor. This caused the less volatile components to condense as tar or ammonium salts. In the primary and secondary cooler, the gas was cooled to 30-40^{o}C by directly spraying it with cold weak ammoniacal liquor and indirectly through contact with cold steel tubes, in which water was circulated.

McNeil (1975) states that a highly entrained tar-fog could not be removed by condensation alone and had to be removed by an electrostatic precipitator. Tar becomes entrained due to its small droplet size, modern processes within the oil refining industry typically use demisters to remove fine droplets this involves scrubbing the gas and passing it through a high-surface area, low porosity filter such as pall rings to promote coalescence.

The gas was then scrubbed in series for ammonia, benzole and acid gases. The condensed tars and ammoniacal liquors were separated by gravity. The ammoniacal liquors consist of free ammonia salts such as bicarbonate, carbonates, sulphides, and cyanides, which could be decomposed by boiling and fixed ammonia salts such as chlorides, thiocyanates, ferrocyanates (McNeil, 1975).

2.2.2 Gasification

Gasification is the thermochemical conversion of organic materials (e.g. sludge) into calorific gases through the addition of heat, sub-stoichiometric oxygen, and mild oxidisers (steam, CO_2). A variety of reactions can occur within a gasification process, including combustion, gasification, and reforming reactions. For example:

Combustion

- Partial oxidation: $2C_{(s)} + O_{2(g)} = 2CO_{(g)}$ (ΔH_{298}: -111 kJ mol^{-1})
- Combustion: $CO_{(g)} + 0.5O_{2(g)} = CO_{2(g)}$ (ΔH_{298}: -283 kJ mol^{-1})
- Combustion: $H_{2(g)} + 0.5O_{2(g)} = H_2O_{(g)}$ (ΔH_{298}: -242 kJ mol^{-1})

Gasification

- Water-gas reaction: $C_{(s)} + H_2O_{(g)} = CO_{(g)} + H_{2(g)}$ (ΔH_{298}: +131 kJ mol^{-1})
- Boudouard reaction: $C_{(s)} + CO_{2(g)} = 2CO_{(g)}$ (ΔH_{298}: +172 kJ mol^{-1})

Reforming

- Water-gas shift reaction: $CO_{(g)} + H_2O_{(g)} = H_{2(g)} + CO_{2(g)}$ (ΔH_{298} −41 kJ mol^{-1})
- Steam reforming (e.g. CH_4): $CH_{4(g)} + H_2O_{(g)} = CO_{2(g)} + 3H_{2(g)}$ (ΔH_{298} +206 kJ mol^{-1})

The partial oxidation (POX) reaction between carbon and oxygen is used to supply most of the heat required for the gasification process. When air is used to supply oxygen, the resulting gas is called producer gas (CO, N_2). The endothermic water-gas reaction is also important and converts C into syngas (CO, H_2, N_2). Most gasification processes inject both steam and air in a pre-defined ratio to provide a surplus of heat to sustain the process and convert the feedstock into gas. These reactions were also used to produce heat from red-hot coke for coal pyrolysis. Within gasification and pyrolysis processes, steam reforming reactions are also important and convert gaseous hydrocarbons, VOCs, and tars into additional syngas.

A variety of reforming reactions can also be conducted within gasification processes, including the water-gas shift reaction and methanation, these are typically conducted over catalysts and are used to produce hydrogen and synthetic methane, respectively. Because of scalability and the H_2S rich atmosphere expected during sewage sludge pyrolysis or gasification, it is unlikely these reactions will be used.

The elimination of organic process contaminants such as tar, with a combination of POX, the water-gas reaction and the steam-reforming reaction is one of the main advantages of gasification processes because the gas-treatment requirements are simplified. To a lesser extent these reactions can also occur within a pyrolysis reactor, since the pyrolysis can produce reactants such as steam and CO_2 whilst other reactants such as oxygen may be present in small amounts.

Gasification reactors typically produces syngas, suitable either for direct energy conversion or chemicals production. For example, Yorkshire Water have operated a sludge and woodchip gasifier which is used to produce heat and electricity. However, there are not many projects currently conducting gasification at sewage treatment works scale. The coal and petrochemicals industries operate many gasifiers, these are almost always used to produce value added products or to produce reactants as part of a larger process stream. For example:

- The Dakota Gasification Company produces approximately 4.8 million m^3 of synthetic methane per day with a calorific value of approximately 36 MJ m^{-3} through catalytic syngas methanation (Dakota Gas, n.d).
- The South African company Sasol convert syngas into chemicals (e.g. methanol) and liquid fuels (e.g. diesel) (Van Dyk et al., 2006).
- Grey hydrogen is produced by reforming methane and using the water-gas shift reaction to convert any CO produced into H_2. Grey hydrogen is produced for sale and for hydrogenation reactions in refining processes.

There are two main categories of gasifiers, including fixed bed and fluidised bed systems.

(1) Fixed bed updraft:

The simplest type of gasifier, the feedstock is fed at the top of the reactor whilst air is injected at the bottom and moves concurrently.

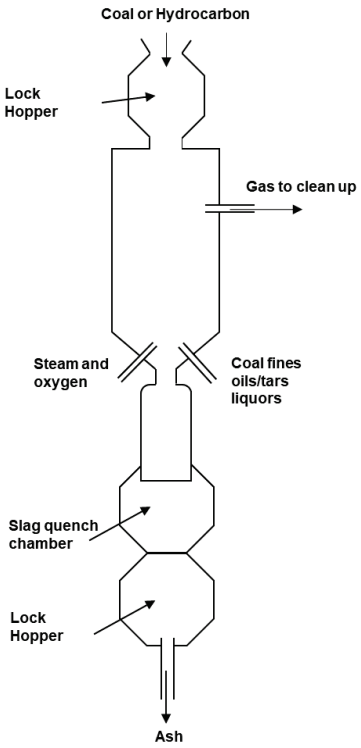


Figure 2-3: British Gas slagging coal gasification system, showing tar and soot recirculation (NETL, n.d)

Updraft gasifiers can typically process a wide range of feedstocks (Bhasker et al., 2011), however, they are prone to tar accumulation and the gas requires cleaning prior to processing in a gas engine (Akhtar et al., 2018). Figure 2-3 present a British Gas updraft coal gasification reactor; it utilises pyrolytic conditions to convert feedstock volatiles into fuel-gas and tar. Inherent of updraft systems, the tar-laden gas exits the reactor at relatively low temperature (450^{o}C) however, British Gas reactors condense the tar and reinject it into the bottom of the reactor. Here tars and char undergo simultaneous endothermic steam gasification and exothermic partial oxidation/combustion reactions at approximately 2000^{o}C (NETL, n.d). The temperature achieved is carefully controlled by adjusting the ratio of steam to oxygen. The system uses oxygen rather than air, to avoid dilution of the gas with nitrogen. Coal gasifiers operate under auto-thermal conditions, and high proportions of the feedstock energy content are converted into useable energy (e.g. gas and heat). Although attractive from an energy and gas cleaning perspective, this design may not be suitable for sludge processing because of its lower CV and high ash content.

(2) Fixed bed downdraft

The feedstock is fed at the top of the reactor, and passes through a pyrolysis zone to produce gas, char, and tar. These products then pass into a combustion zone alongside injected air (or oxygen) and move co-currently through the combustion zone into a gasification zone. Here, gas and volatiles pass through a hot-char bed and exit at the bottom of the reactor. By passing the gas through both a combustion zone and hot char bed, tar conversion is very high, and the process forms a relatively clean syngas. The disadvantage is that the process has relatively low energy efficiency and can only process dense feedstocks. Although not specifically mentioned in the literature, the ATC technology that has been operated at Lower Brighouse STW by Yorkshire Water and Enertec Green appears to be a grateless downdraft gasifier. The system briquettes dried sludge and woodchips (3:7) and produces high-quality syngas, which requires limited cleaning prior to conversion in gas engines (Yorkshire Water, 2019).

(3) Fluidised bed gasifiers

In these processes a gasifying agent (e.g. air and steam) is injected into the bottom of the reactor and suspends an inert bed material (e.g. silica). Typically, the feedstock enters near the bottom of the reactor to maximise contact with the bed material. Figure 2-4 details one example of this type of system, the U-GAS^{TM} gasifier developed by the gas technology institute and designed to process coal, pet-coke, biomass, and industrial wastes. Both the bed and feedstock are fluidised, however as ash is formed it amalgamates into bigger particles and drops out of the bed by gravity.

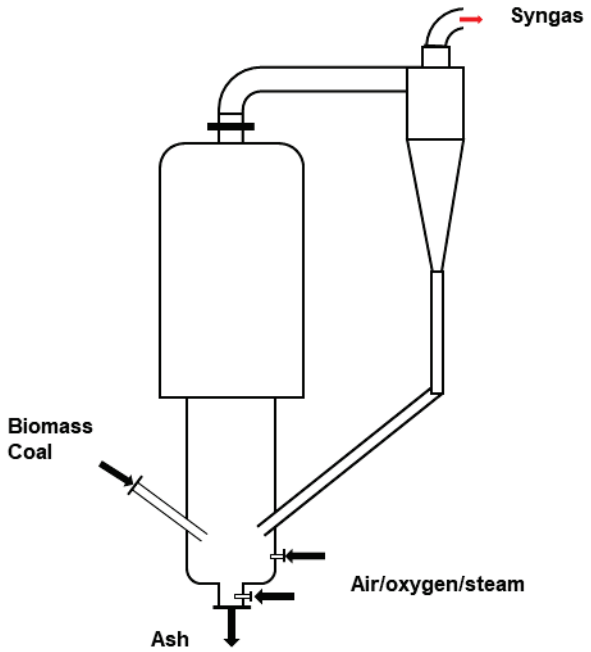


Figure 2-4: U-GAS fluidised bed gasifier (NETL, 2020)

2.2.3 Hydrothermal carbonisation

When pyrolysis is conducted in the presence of subcritical liquid water, the process is redefined as hydrothermal carbonisation. It transforms wet biomass into a carbon rich solid product called hydrochar. The process operates at elevated pressure 10-60 bar, elevated temperature (180-260^{o}C) and extended dwell times (5-240 minutes). Hydrothermal liquification and hydrothermal gasification occur at higher temperatures and pressures and produce greater quantities of bio-oil and syngas, respectively. Some of the key advantages of hydrothermal processes include (Nasrollahzadeh., 2021)

- Low operational temperatures used;
- Wet feedstock processed;
- Avoided air pollution;

- The retention of polar groups (e.g. oxygenated groups) at the surface of the material.

At present, the technology readiness level of hydrothermal processes for sludge are low and the operational and capital costs are expected to be high (Munir et al., 2018). However, CPL industries recently developed a hydrothermal carbonisation process at commercial scale in Immingham – United Kingdom, to produce solid fuel from biomass (Bioenergy International, 2017). Hydrothermal processes are not the focus of this research and will not discussed further.

2.2.4 Thames Water: Proposed ATC process

Thames Water have been interested in constructing a demonstration-scale pyrolytic gasification reactor at Crossness STW, the full specification cannot be discussed because of commercial sensitivities. The proposed process does not use a screw-auger nor a fluidised bed feeding system. Although it shares many of the advantages of the screw system. The retort is rectangular, electrically heated within and constructed of refractory material.

The process comprises a single furnace with multiple heating zones. The reactor does not require a sweeping gas although the feed is purged with nitrogen before entry into the reactor.

Based on the literature reviewed above, the performance of the reactor is expected to be most similar to the lightly charged horizontal retorts developed by the gas-industry in the 19th century (e.g. maximises tar conversion). The fundamental difference is that the reactor will be heated from within, will be fed continuously fed and exhausters will not be used to move the gas through the process. The coupling of high temperatures and long volatile residence times has been designed to maximise conversion of tar to gas. Generated fuel-gas will be converted to electrical power in spark-ignition gas engines, prior to conversion the gas will be extensively cleaned. The gas-cleaning stream includes a multitude of steps including:

- Separation of entrained solids with a cyclone;
- Separation of gas-phase tar aerosols using a quench and scrubber. These processes recirculate an inert cooled oil to promote condensation and combine demister technology to promote vapour coalesce and condensation;
- Scrubbers to remove acid gases and ammonia;
- Reaction vessels to oxidise cyanides;
- Activated carbon filters to capture residual hydrogen sulphide and VOCs.

These processes share many features of those used by the coal-gas industry suggesting the same contaminants are expected to be produced. This may be problematic because a market demand for these products no longer exists. Figure 2-5 shows the proposed series of gas clean-up steps for a demonstration-scale plant at Crossness STW.

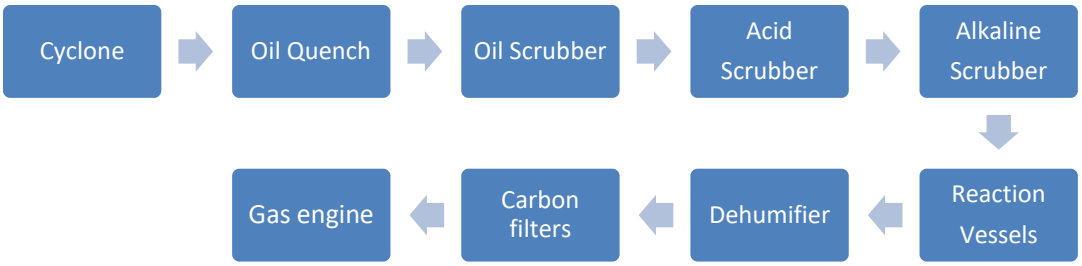


Figure 2-5: Proposed tar and contaminant removal at Crossness STW

The cyclone aims to remove soot from the fuel-gas stream, and separately remove tars within the oil quench and scrubber. This approach may be problematic because cyclones are capable of removing finely entrained vapour (>10 microns), subsequent tar deposition could lead to blockages. The exits of coal retorts frequently suffered from carbon build-ups (Lewes, 1912) and the proposed approach could suffer from the same issues.

The solution used by the coal-gas industry to remove these deposits was gasification however this would need to be accounted for in the design of the exit pipes and cyclone. Using demisting technology such as vane-packing and random packing is likely to be effective at removing entrained vapour, however, unless these can be periodically cleaned, they are likely to block, which could lead to plant closure.

Tar induced blockages are one of the leading causes of pyrolysis plant failure, in addition tar deposition downstream of the reactor can also cause issues with contamination, attrition and choking of downstream equipment such as exit pipes, heat exchangers and gas engines (Odongo, 2015) (Li & Suzuki, 2009). Standard scrubbing technology will then remove both ammonia and acids gases such as H_2S and HCN. The latter will be oxidised to form non-toxic products such as nitrogen gas and cyanates using a suitable oxidising agent. Ancillary activated carbon filters will also be used to sweeten the gas to the required specifications.

Overall, the design of the gas-treatment stream is similar to the processes used during coal-gas treatment. However, there are some significant deviations for tar treatment which based on past-experience within the coal-gas industry may lead to adverse outcomes. What is striking about the proposed process is its heavy reliance on the performance of ancillary gas-treatment technologies. This suggests that modern pyrolysis processes have not addressed gas-phase contaminants and their performance may be affected in a similar way to processes developed in the early 20th century.

Alternatively, full-oxidation of the fuel-gas and contaminants may be preferable, which is the approach taken by ATC companies such as Pyreg, Scanship and Clinipower. Mills (2015) suggested pyrolysis could produce fuel-gas suitable for conversion in a gas engine. However, because of the complex range of contaminants produced by pyrolysis, and the complex nature of the treatment steps previously required for treatment by the coal-gas industry, it is not clear whether the efficacy and economics associated with gas cleaning at sewage treatment works scale will be viable.

2.3 ATC Outputs

2.3.1 Gas

ATC processes typically produce gas consisting of saturated hydrocarbons (e.g. CH_4), unsaturated hydrocarbons (e.g. C_2H_4), synthesis gas (CO, H_2) and non-calorific gases such as CO_2 and N_2. This mixture is commonly referred to as fuel-gas, or when produced from coal, town-gas. Gasification processes typically produce synthesis gas (syngas). However, since air is injected into the process to supply oxygen for POX reactions, the syngas produced is diluted with nitrogen. Gas composition influences gas properties such as the heating value, density, lower/upper flammability range, flame speed and adiabatic flame temperature and auto-ignition temperature. The properties of common gases produced by ATC process are shown in table 2-2. Hydrogen has an extremely low density, therefore when generated within an ATC reactor it occupies a large volume and dependent on the design may increase reactor pressure or decrease the volatile retention time. Table 2-2 shows that the flammability range of syngas and acetylene are much wider than saturated hydrocarbon gases such as natural- or bio-gas therefore additional safety considerations must be considered when operating an ATC process. Hydrogen has a high laminar flame speed which can influence the kinetics of combustion within spark-ignition engines, for example, when blended with natural gas: Biffiger & Soltic (2015) found it improved combustion stability and Shudo et al., (2000) found it can lower hydrocarbon and CO emissions.

Table 2-2: The properties of common ATC gases

Gas	Unit	H_2	CO	CH_4	C_2H_6	C_2H_4	C_2H_2
HHV[1]	MJ Nm^{-3}	12.769	12.622	39.781	69.693	63	58.059
LHV[1]	MJ Nm^{-3}	10.788	12.622	35.814	63.748	59.036	56.078
Density	kg Nm^{-3} (STP)	0.08988	1.250	0.716	1.282	1.260	1.170
Flame speed[2]	Index	100	18	14	17	30	n/a
Autoignition Temperature[4]	°C	500	609	600	515	450	305
Flammability range[3]	% vol	4-75	12.5-74.0	4.4-17	3-12.4	2.7-36.0	2.6-100

[1] Higher and lower heating values (HHV, LHV) values from national renewable energy laboratory as reported by Waldheim & Nilsson (2001)

[2]Weaver flame speed index: Laminar flame speed, indexed to H_2 (=100). Data obtained from BP (1965).

[3]Data obtained from Matheson Tri-gas (2021)

[4]Data obtained from HSE (2015)

However, its presence can also cause ignition of the fuel-mixture before top-dead centre is reached (e.g. pre-ignition) which increases unspent fuel carryover. Therefore, gas composition influences energy recovery, process design and process safety. Because of the reducing conditions within pyrolysis reactors, volatilised N, S, O and Cl typically produce N_2, H_2S, CO/CO_2 and HCl, respectively. Although other products can also be formed, for example: NH_3, HCN, SO_2, COS and CS_2. Processes that immediately oxidise the gas in a combustor such as Pyreg (Figure 2-2) do not need to remove these contaminants prior to combustion, however products of combustion such as NO_x and SO_x are typically scrubbed to minimise pollution. If the gases are oxidised within a gas engine (Figure 2-6) or solid-oxide fuel-cells (SOFC) these contaminants must be removed prior to conversion.

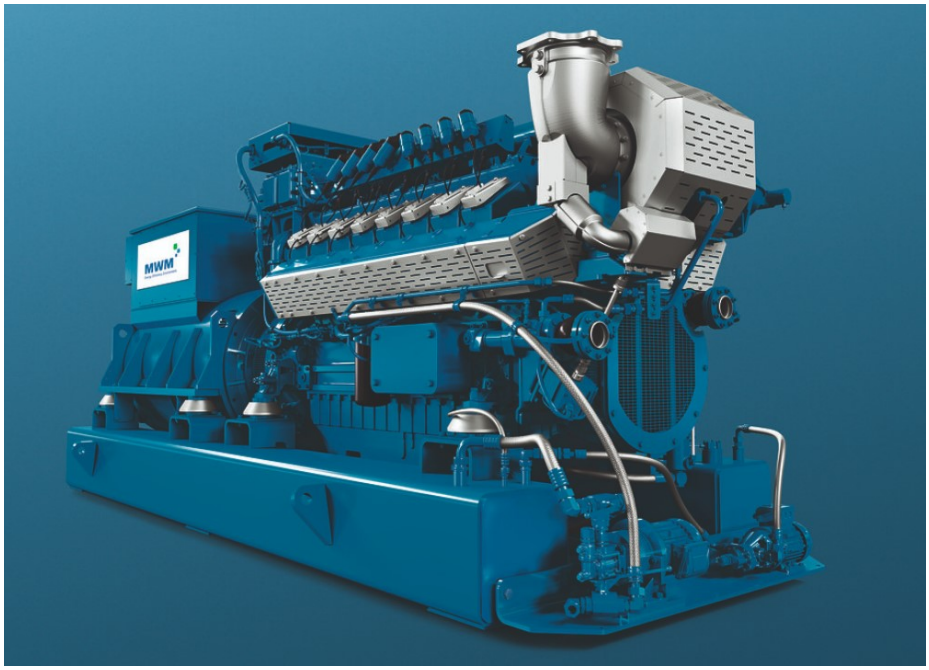


Figure 2-6: Gas engine that may be used for combined heat and power production from fuel-gas or syngas (MWM Energy, 2019)

The gases produced by pyrolysis are primarily influenced by the feedstock, the heating rate and highest heating temperature. For example, torrefaction or mild pyrolysis is typically conducted at 200-300^{o}C. At this temperature, macromolecules decompose because of depolymerisation. The main gases produced by this process are typically CO, CO_2, and steam, although small quantities of H_2 and hydrocarbons are also generated (Tumuluru et al., 2011) (Chen et al., 2018).

As macromolecules depolymerise, they form lower-molecular-weight fragments that volatilise with increased temperatures, a process called devolatilisation. Primary volatiles produced from biomass are referred to as bio-oils and are fragments of their original macromolecule. Bio-oil structures are typically unstable at high temperatures and undergo dehydrogenation, cracking, aromatisation, and reforming reactions. The reaction mechanisms for these processes are often complex and are driven by the formation of free-radicals.

The structure of the original macromolecule has a large bearing on the products formed. The main components within lipids are tri-glycerides which consist of long aliphatic hydrocarbon chains attached to a glycerol group. Under rigorous thermal cracking conditions aliphatic hydrocarbon chains generally crack into smaller alkanes or alkenes, the most stable of which include methane and ethylene respectively, although these may further decompose into soot and hydrogen (BP, 1965). Condensation reactions also occur and a minority of the hydrocarbons form aromatics such as benzene and naphthalene whilst others polymerise forming multi-ring aromatics and carbon.

According to Shen et al. (2013) CO and CO_2 are the main carbon species formed during the thermal cracking of cellulose, with CO_2 dominant at low temperatures and CO dominant at high temperatures due to secondary tar decomposition. Hajalgol et al. (1982) investigated the pyrolysis of cellulose under medium to rapid heating rates (100-15000^oC sec^{-1}) between 300-1000^oC. The results show that most weight loss occurs between 500-700^oC, with 94% conversion of cellulose to volatiles by 750^oC. The char yield decreases from 6% at 750^oC to 3% by 800^oC, however above 900^oC it increases slightly to 4% due to carbon deposition. The tar yield peaks at 700^oC at 60% wt. however it gradually declines with increased temperatures to between 40-45% at 1000^oC. By far the most dominant gas formed is carbon monoxide, accounting for approximately 7% and 23% of the overall mass yield at 700^oC and 1000^oC respectively. Water-vapour is the second most dominant species, increasing linearly between 350-700^oC, and plateauing at approximately 6-10% of overall mass yields between 700-1000^oC. Between 600-900^oC small quantities of CH_4, H_2 and CO_2 are generated forming up to 3% of the mass yield each, except H_2, which generates just over 1%. The domination of cellulose pyrolysis gas by CO and water vapour is unsurprising given the high concentration C-O bonds present in sugar monomers.

Amino-acids are composed of an amino ($-NH_2$), carboxyl (-COOH) and side chain groups that are specific to each amino acid. The side chains may contain a variety of structures including sulphur bridges, aliphatic hydrocarbon chains, and unsaturated aromatics like phenol, benzene, and pyrrole. Due to the variety of structures present in the side chains, a wide array of volatile compounds may be formed including: hydrocarbons, carbon oxides, H_2S and tar compounds. In addition, the amino-group likely forms N_2, NH_3 and HCN.

The heating rate has a large influence on the gases formed, for example: during slow pyrolysis dehydration, devolatilisation and cracking reactions may occur separately from one another. Whilst under rapid heating rates, these reactions occur simultaneously meaning more reactants are present increasing the chances of side reactions occurring.

2.3.2 Tar and other gaseous contaminants

2.3.2.1 Tars

Tar is a complex mixture of organic compounds, the literature tends to categorise the substances produced based on analytical groups, structure, polarity, boiling point, and decomposition conditions (e.g. temperature and time). For example, Anis & Zainal (2011) characterised tar by its analytical groups during GC analysis.

Table 2-3: Tar categorisation by analytical groups (Anis & Zainal, 2011)

Class	Properties	Representative compounds
1. GC-undetectable (e.g. non-volatile tars)	Very heavy tars, may not be detectable by GC.	
2. Heterocyclic	Water soluble.	- Pyridine
3. Light monoaromatic	Do not pose a problem regarding condensability and solubility.	- Toluene - Ethylbenzene
4. Light polyaromatic (2-3 rings)	Condense at low temperature even at low concentrations.	- Naphthalene - Indene
5. Heavy polyaromatic (4-7 rings)	Condense at high temperature at low concentrations	- Fluoranthene - Pyrene

Extensive literature exists on the structural composition of industrially produced coal tars, due to the long history of chemical production from coal tars. The predominant structures of tar from coke ovens are summarised in Table 2-4 (McNeil, 1975).

The quantity and composition of tar produced depends on feedstock properties and process parameters, including temperature, gas residence time, particle size distribution, and atmospheric composition (Dumfort et al., 2015). McNeil (1975) explains that the chemistry of coke oven tars and vertical retort tars (e.g. gas manufacturing tars) is significantly different. For example, vertical retorts produce large quantities of non-aromatic hydrocarbons such as branched paraffin chains; hydroxy substituted aromatic hydrocarbons; and tars with methyl groups.

Table 2-4: Predominant structures in coke oven tars (Mcneil, 1975)

Boiling range	Tar	Major components	Ring structure
0-150°C	0.8%	BTEX	Single 6 membered rings (e.g. VOCs)
150-200°C	3%	Indene, hydrinene, coumarone	Fused 6,5-rings
200-250°C	12%	Naphthalene, methyl-naphthalene	Fused 6,6-rings
250-300°C	8%	Acenaphthene, Fluorene, Diphenylene oxide	Fused 6,6,5-rings
300-350°C	15%	Anthracene, phenanthrene, carbazole	Fused 6,6, 6- & Fused 6,6,5- rings
Pitch crystalloids	32%	Benzfluorenes, brazan, pyrene, chrysene, coronene.	Larger rings

McNeil (1975) explains that the dehydrogenation of saturated or partially saturated rings to fully aromatic rings can occur at relatively low temperatures however it occurs rapidly at high temperatures. The removal of alkyl side-chains larger than ethyl groups occurs similarly. In contrast, the removal of OH- groups from phenolic compounds, the conversion of alkanes to smaller molecules and the demethylation of methyl and polymethyl aromatic compounds occurs at higher temperatures and often not to completion. As temperatures increase, the production of high molecular-weight compounds increases due to polymerisation and condensation reactions. Figure 2-7 shows the tar compounds formed at each temperature during wood gasification (Elliott, 1988), however, the products formed vary with retention time (Houben, 2004).



Figure 2-7: Tar compounds formed at different temperatures from biomass (Elliott, 1988)

Marsh et al. (2004) used the model fuel catechol (ortho-dihydroxybenzene) to investigate the production of PAHs by pyrolysis using HPLC-UV and GC/FID at temperatures between 700-1000°C and residence times of 0.4-1.0s. Eight structural categories of PAH were found including benzene, benzenoid PAH, indene benzalogues, fluoranthene benzalogues, cyclopenta-fused PAH, ethynyl-substituted aromatics (HC≡C-R), akyl-substituted aromatics and vinyl-substituted aromatics. The results corroborate with Elliott (1998) that above 800°C there is a large increase in aromatics, however above 950°C, the concentration for all components decreases.

Evidence from the literature suggests thermal non-catalytic decomposition of tar molecules occurs at temperatures between 700-1250°C, which leads to the formation of lighter gases, refractory tars, and steam (Dumfort et al., 2015). The mechanism for tar destruction at high temperatures is the formation of radicals. Other than high temperature, radicals can also be produced by gasification reactions or a plasma and electromagnetic radiation (e.g. microwaves or UV radiation) (Vreugdenhil and Zwart, 2009). Tars produced from biomass pyrolysis and coal generally have lower thermal cracking temperatures than polynuclear aromatic hydrocarbons (PAHs) such as naphthalene and phenanthrene, because of heteroatoms (e.g. N and O) and pendant groups such as hydroxyl and methyl groups which increase reactivity and facilitate decomposition. Oxygen-containing phenolic compounds are converted between 700-850°C whilst non-oxygen containing aromatic compounds crack between 850°-1200°C (Vreugdenhil & Zwart, 2009).

Jess (1996) investigated the mechanisms and kinetics of aromatic hydrocarbon cracking, using toluene, benzene, and naphthalene in the presence of hydrogen and steam. The results corroborated with March et al., (2004) for benzene decomposition although degradation occurred to a lesser degree, whilst the presence of hydrogen increase toluene conversion. The main product of naphthalene conversion was soot, although pyrene and fluoranthene (soot precursors) are also formed to a lesser extent. The main cracking products of naphthalene were benzene, methane, and ethane. Vreugdenhil & Zwart (2009) states polynuclear aromatic hydrocarbons with 3-rings and higher also favour soot formation, with some using soot as an intermediary break down product. However, the reactivity of soot is low, requiring high temperatures and long residence times to gasify into H_2 and CO_2.

Benzene, a lighter aromatic produces less soot and instead favours direct conversion to methane and ethane, amongst other minor products. Further conversion of light hydrocarbons required temperatures above 1200°C, however, this was within the constraints of the experimental set-up which had a very short overall retention time (2s). The minor products formed from benzene cracking included biphenyl, acenaphthene, pyrene and others. Toluene conversion occurred at lower temperatures than naphthalene and benzene and was entirely decomposed to methane and benzene at 950°C with a retention time of 1s. Jess (1996) states that at 1200°C the retention time required to achieve 95% conversion was <0.1s for toluene, 1s for naphthalene, and 5s for benzene, whilst Houben (2004) found that at 1150°C a gas residence time of 4s was required to achieve 98% naphthalene conversion. Jess (1996) found steam had little or no influence on the reaction rates. Milne et al., (1998) suggests steam addition enhances decomposition of primary tars leading to less tertiary tars overall. Zhang et al. (2014) conducted high temperature pyrolysis (1000-1400°C) of sludge and found a maximum energy conversion rate of 72.6%. Total tar elimination was achieved at 1300°C. As expected, carbon was retained in the char at all temperatures tested.

2.3.2.2 Sulphur

During pyrolysis feedstock S is fractionated between the solid, liquid, and gaseous components and forms several compounds. The main S gas produced during pyrolysis and gasification is hydrogen sulphide (Garcia-Labiano, 1995). Other gases can also be formed, including sulphur dioxides (SO_2), carbon disulphide (CS_2) and carbonyl sulphide (COS) albeit in lower concentrations. Luo et al. (2014) states that COS and CS_2 are formed in reactions (i-iii) presented below. The formation of both gases is suppressed in the presence of hydrogen or water vapour. CS_2 also forms because of a direct reaction between H_2S and C (Owen et al., 1953) and in the past has been associated with high temperatures, extended gas residence times and char-gas contact.

(i) $CO + H_2S = H_2 + COS$

(ii) $CO_2 + H_2S = COS + H_2O$

(iii) $H_2S + COS = CS_2 + H_2O$

Organosulphur tar compounds can be formed during coal pyrolysis (700-1000ºC), for example: thiophene, benzothiophenes and dibenzothiophene (Machado et al., 2011). The compounds formed are likely to heterocyclic and may contain both N and S in the ring structure (e.g. Thiazole).

A proportion of feedstock-S will be retained within the solids, possibly in reduced forms such as pyrite however heterocyclic rings and surface S functional groups may also be present in char carbon structure. The quantity of S retained as sulphides is likely to be influenced by atmospheric concentrations of steam, whilst removal of organically bound S is likely to be more difficult and may be reduced by increasing the extent of carbonisation (e.g. increased temperature or longer dwell-times).

Dewil et al.,(2008) investigated the distribution and speciation of sulphur compounds during successive steps on a sewage treatment works. Initially, sludge primarily contained sulphates however due to the oxygen limiting conditions during thickening, storage and anaerobic digestion S was reduced to sulphides and was retained with the sludge. During pyrolysis, sulphides are less likely to volatilise because they are already in a stable reduced form. This means that digested sludge may retain more S in the char and produce less H_2S than raw sludge, although this requires further investigation. However, sulphates are generally more soluble than sulphides (Dean, 1999), dewatering the sludge during its initial aerobic state could also be an effective method for reducing sludge sulphur content prior to pyrolysis.

2.3.2.3 Nitrogen

During pyrolysis, feedstock N is fractionated between the solid, liquid, and gaseous components and forms a variety of structures and compounds. In the literature, there is a variety of data on N fractionation during pyrolysis, including data from: the coal-gas industry which operated large-scale industrial processes; lab/pilot-scale pyrolysis of coal and biomass materials and very small-scale processes that pyrolyse pure compounds to investigate degradation mechanisms.

Meade (1921) published “Modern Gasworks Practice” a comprehensive reference book for gasworks engineers. The fate of N during high temperature coal carbonisation is discussed it includes several different coals, reactor designs (e.g. continuous vertical & coke ovens) and conditions (steamed and non-steamed). To summarise, it reported that: 43.3-72.2% of N was retained in coke, 1.63-8.9% in tar, 6.82-37.1% as N_2, 9.4-22.5% as NH_3 and 0.47-1.56% as HCN. The objectives of the coal-gas industry were to remove N from coke, ensure volatile N formed NH_3 (to sell as fertiliser) and avoid HCN formation, which had to be treated at cost and created waste disposal issues. The data presented by Meade (1921) shows that the industry was not successful at removing N from the coke, which suggests, in coal at least, N forms stable non-volatile structures. In contrast, the industry was more successful at minimising HCN formation, although NH_3 yields were not high because significant quantities of gas were converted to N_2. In

reality, the properties of fuel-gas were the primary objectives and N was a secondary consideration.

The dwell-time or "charge" during coal carbonisation was typically 6-12 hours. Most NH_3 was produced during the initial decomposition (Meade, 1921). Afterwards, the coke undergoes carbonisation whereby the amount of non-carbon constituents is slowly removed. Meade (1921) explains that HCN formation occurred at the end of a charge and was associated with the decomposition of "synthetically produced ammonia". Meade (1921) states that HCN "makes no appearance in the retort below temperatures of 870°C to 925°C. An experiment reported by Meade (1921) found that at 750°C only 4% of NH_3 had been converted to HCN, whilst at 980°C this had increased to almost 25%. The reaction of ammonia with hot-coke to form hydrogen cyanide is thermodynamically unfavourable below 1000°C (Sherwood & Maak, 1962) therefore the mechanism proposed by Meade (1921) is unlikely to be correct.

Tian et al. (2007) investigated the conversion of fuel-N into HCN and NH_3 during ATC of coal and biomass. The main route for HCN formation was the thermal cracking of N-volatiles, whilst small quantities were also formed during char decomposition. Thermal cracking increases with increased temperature, thus HCN formation is concentrated when temperatures were highest. During pyrolysis, N compounds form heterocyclic aromatics in both the tar and char ring structures, such as Pyrrole (C_4H_5N), pyridine (C_5H_5N) and pyridazine ($C_4H_4N_2$).

The thermal cracking of these compounds has been studied in small-scale experiments to investigate decomposition mechanisms. For example: Houser et al. (1980) pyrolysed pyridine between 900-1000°C and found that HCN was the main product and was formed through a complex sequence of reactions. Likewise, Mackie (1991) pyrolysed pyrrole between 927-1427°C and found the major products at low temperatures were pyrrole isomers, HCN and propyne whilst at elevated temperatures acetylene, cyanoacetylene and hydrogen became major products.

Hansson et al. (2004) investigated the formation of isocyanic acid, HCN and NH_3 during the pyrolysis of protein-rich model nitrogen compounds between 700-1000°C. The results corroborate with the findings of Meade (1921), HCN was not detectable when the experiment was conducted at 700°C and 800°C but had significant concentrations at 900-1000°C. Hansson et al. (2004) also found that materials with small particle sizes had higher HCN/NH_3 ratios and postulated this was because of higher heating rates. They further suggested NH_3 formation primarily occurs during char formation, since proteins that did not form char (leucine and poly-L-proline) produced much higher HCN/NH_3 ratios. HCN formation mainly occurred when cyclic amides were cracked. To support this, Hansson et al. (2004) cites literature by Leichtnam et al. (2000) who found HCN formation was sensitive to temperature and gas residence time, whilst ammonia was not sensitive to either.

Meade (1921) reports several innovations that were associated with increased NH_3 yields, these include: (i) addition of lime or iron oxide to the coal prior to carbonisation (ii) addition of H_2 to the hot coke (iii) addition of water vapour to the hot coke (iv) limiting gas residence times (v) using horizontal kilns to minimise gas-coke interactions (vi) minimising reactor oxygen content. Both lime and iron oxide are well known tar cracking catalysts. During sewage sludge pyrolysis, organic N compounds will probably be exposed to inorganic ash compounds, char carbon and gases in the atmosphere such as water vapour and hydrogen. For example: Xiao et al. (2019) states that red-mud a by-product of the aluminium industry and a substance rich in iron oxide and calcium oxide can: (i) enhance N retention in char because of the formation of metal-N complexes (FexN and CaCxNy) and (ii) enhance decomposition of NH_3 and CHN to N_2 during sewage sludge pyrolysis. Likewise, Meade (1921) presented a study where gas was: (i) actively drawn out of the reactor, thus minimising secondary reactions; (ii) exposed to radiant heat and (iii) passed through hot coke. The experimental conditions yielded 22.5%, 17.2% and 9.4% of feedstock N as NH_3 respectively (Meade, 1921). Meade did not state which gases formed; however it is suspected that reduced NH_3 yields occurred because of greater decomposition to N_2 (see below - Rahinov et al., 2003).

Paterson et al. (2005) tested the HCN concentration of sewage sludge fuel-gas produced in a pressurised spouted-bed gasifier. However, the gasifier was not packed with a bedding material, rather as the experiment proceeded an SSC bed developed.

The following conditions were tested: (i) 820-930^{o}C in a dry empty reactor; (ii) 930^{o}C packed with an SSC bed (iii) with steam added to the fluidising gas between 770-980^{o}C. In an empty reactor, the volume of HCN increased with temperature from 2000ppv at 820^{o}C to 3600ppv at 930^{o}C. When a bed of SSC was added to the reactor at 930^{o}C, the concentration of HCN decreased from 3100ppv to 580ppv. The addition of the steam increased the quantity of HCN to 5870-9480ppv between 770-940^{o}C and led to concentrations of 2740-3910ppv between 970-980^{o}C. It was hypothesised that steam addition increased the removal of N from the fuel, however, no N balance was conducted to confirm this. In addition, Paterson et al. (2005) states that HCN yield were much lower (50ppm) under the same conditions when tested by the British Coal Corp at pilot-scale although this data is unpublished.

The difference may be because of the varying gas residence times, just 1s at laboratory scale but 6s at pilot-scale. Paterson et al. (2005) suggest NH_3 undergoes rapid decomposition to N_2 during gasification. In a gasifier, NHi radicals typically react with free oxygen to form NO, the NO then reacts with another NHi radical forming nitrogen gas (Higman & Van Der Burgt, 2008). Meade (1921) reports that most N during coal carbonisation formed N_2 rather than NH_3 or CHN. Dean et al. (1984) investigated the kinetics of ammonia decomposition in ammonia-rich flames and found (NHi + NHi) reactions dominate under oxygen deficient conditions.

First, an amidogen radical, ˙NH_2, is formed from the dissociation of ammonia (Rahinov et al., 2003):

(i) $NH_3 + M = ˙NH_2 + ˙H + M$

(ii) $NH_3 + ˙H = ˙NH_2 + H_2$

Davidson et al. (1990) provides a comprehensive list of N free-radical reactions that occur following the formation amidogen. The precursor radicals for N_2 formation include ˙NNH, ˙NH and ˙N. A potential route for N_2 formation is shown below:

(iii) $˙NH_2 + ˙NH_2 = ·N_2H_4$

(iv) $˙N_2H_2 + M = ˙NNH + ˙H + M$

(v) $˙NNH + M = N_2 + ˙H + M$

Rahinov et al. (2003) explain that in the presence of oxygen active species such as OH are formed which promote amidogen radical formation, for example:

(vi) $NH_3 + OH = ˙NH_2 + H_2O$.

Both water vapour and hydrogen have been reported to preserve atmospheric NH_3 concentrations, this may be explained by the reverse of reactions (i), (ii) and (vi). Interestingly, Meade (1921) states that moisture addition concurrently decomposed H_2S into SO_2. During sludge pyrolysis recovering fuel-N as NH_3 is attractive because the agronomic value of the sludge-N would be retained. However, from an operational and cost perspective, it may be best to maximise conversion to N_2, at least at small-scale because retention as NH_3/CHN requires the consumption of chemicals during gas treatment.

Feedstock-N is also retained within the char during pyrolysis, Paneque et al., (2017) found peptide-like N found in sewage sludge formed heterocyclic aromatic-N during heat treatment and the efficiency differed depending on treatment technology. It is suggested that these forms of organic carbon may act as a slow-release N fertiliser, however chemical form will affect their fertilisation capability. Rosa & Knicker (2011) conducted a 72-hour incubation study of N-enriched pyrogenic organic material produced at 350ºC. During bioassay, 10% of the nitrogen added to the soil was incorporated into new biomass and NMR analysis suggested that “at least some” of this N derived from the degradation of pyrrole-type structures. Rosa & Knicker (2011) concluded that these results confirm a relatively low recalcitrance of N-rich pyrogenic material and suggest it could act a slow-release fertiliser. Wang et al., (2012) suggested low-temperature sewage sludge contained hydrolysable forms of organic-N with fertiliser potential, however the proportion of hydrolysable-N decreased with increased temperature as N progressively formed aromatic structures.

Biochar, produced through pyrolysis of organic matter, is negatively charged (Munera-Echeverri et al., 2018) and biochar has been shown to adsorb positively charged-ions (e.g. NH_4^+) (Clough et al., 2013) meaning it could reduce N-leaching from agriculture. Janu et al., (2021) states hydroxyl- aldehyde- and ketone-groups are the most important for adsorption of polar compounds. However, at 600°C there is a partial and at 750°C a complete loss of biochar surface functional groups. Most biochars are produced from lignocellulosic biomass which are rich in oxygen. For animal by-products (e.g. manure, sewage sludge) the retention of nitrogen likely plays an important role in the materials capacity for charged ions and its ability to exchange these ions within soil.

2.3.3 Pyrogenic carbon

2.3.3.1 Pyrogenic carbon: Terminology

Pyrogenic carbon (Py-C): A hypernym for a vast range of solid carbonaceous substances referred to in the literature including: coke, petcoke, soot, carbon black, acetylene black, lampblack, char, biochar, charcoal, activated carbon, black carbon any many others. Py-C is the solid residue formed when organic materials are heated under pyrolytic (oxygen deficient) conditions. This process is called carbonisation and results in an increased content of elemental carbon with condensed polycyclic structures. The structures formed are typically amorphous although crystalline structures or a mixture of the two may be formed.

Pyrolytic carbon (PC) is a subset of Py-C, the international union of pure and applied chemistry (IUPAC) (Fitzer et al., 1995) state that it is "carbon material deposited from gaseous hydrocarbon compounds on suitable underlying substrates at temperatures ranging from 1000-2500K" (727-2227°C). Carbon black is a form of manufactured PC produced under controlled conditions for commercial use and is >97% elemental carbon arranged as aciniform particulates.

Carbon black typically contains less than 1% ash and less than 1% solvent extractable fractions; however, the latter strongly adheres to carbon surfaces and is not released by biological fluids (Watson & Valberg, 2001). Soot also contains elemental C (~60%), however it has a greater proportion of impurities such as ash, extractable organic compounds, and charred feedstock (Medalia et al., 1983). Pott (1775) first reported the carcinogenic nature of soot, which is because of the materials polycyclic aromatic hydrocarbon (PAH) content such as benz[a]anthracene, benzo[c]phenanthrene, benzo[a]pyrene, dibenz[a,h]anthracene, chrysene, and indeno[1,2,3-cd]pyrene (IARC, 2012). Carbon black is possibly carcinogen to humans (Group 2B) based on sufficient evidence in experimental animals (IARC, 2010). However, only one epidemiological study from British process workers in the 1960s shows strong evidence that carbon black exposure is a lung carcinogen however exposure rates were high, up to 20 mg m^3 in the air for some workers.

Char is another subset of Py-C and refers to the solid decomposition product of natural or synthetic organic materials. It is produced from solid feedstocks, although some solid compounds

may pass through a fluid stage prior to charring, for example, sugar (Fitzer et al., 1995). Biochar and charcoal are forms of char. Biochar is produced from natural biomass such as lignocellulosic material or manure and is manufactured for use as a soil amendment. Charcoal is produced from lignocellulosic materials; however, it is typically manufactured for use as a smokeless fuel. Sewage sludge is a form of biomass, although it may contain synthetic pollutants. Once carbonised, it will be categorised as char because of its uncertain end-of-use status.

Coke and petcoke are both produced by the fossil fuel industry, the former is carbonised coal and is primarily manufactured for use as a reducing agent during steel-making or as an anode. Historically, it was also produced by coal gasworks. Petcoke is a by-product of fluid catalytic cracking units used in the oil refining industry and used as a fuel or to produce: anodes, graphite, and silicon carbide. Both coke and petcoke are gasified to produce syngas for energy, fuel, or chemicals production.

2.3.3.2 Pyrogenic C: Char Organics

Like soot, the organic properties of char range considerably, however this is because the manufacturing parameters such as feedstock, reactor-type, heating-rate, highest heating temperature and dwell-time are not consistent. As stated above, carbon black and soot are characterised by their content of extractable, and fixed, organic carbon. Both fractions contain aromatic compounds, however the former (e.g. PAHs) are expected to be carcinogenic whilst the latter are expected to be in a fixed elemental form with reduced bioavailability and increased long-term stability (McBeath et al., 2014).

Chars have also been found to contain both extractable and fixed carbon. For example, Keiluweit et al. (2012) found extractable polycyclic aromatic hydrocarbon (PAH) concentrations in char peaked when pyrolysed at a highest heating temperature (HHT) of 400-500^{o}C with concentrations declining at both lower and higher temperatures. However, temperatures above 500^{o}C led to the formation of high-molecular-weight PAHs, some of which are toxic, such as benzo[a]pyrene. Keiluweit et al. (2012) concluded that chars produced above 600^{o}C may be more suitable for agronomic uses due to significantly reduced levels of extractable PAHs. The presence of extractable PAHs in char is problematic if applied to agriculture because Wang et al. (2018) found that vegetable root exudates enhance PAH release from char and the consumption of these vegetable may elevate incremental lifetime cancer risk. Wang et al. (2019) conducted a synthesis study of extractable PAH concentrations in char reported in the literature and found the concentration ranged from 12-355,295 μg kg^{-1} with concentrations increasing with increased temperature until 800^{o}C and decreasing at higher temperatures. According to Wang et al. (2019) PAHs were dominated by 2-3 rings, followed by 4-ring and 4-6 rings.

Sludge contains a variety of heteroatoms including N, S and O, which when heated under pyrolytic conditions will probably form heterocyclic aromatic compounds and condensed heterocyclic structures within the char. Extractable heterocyclics may present human health

hazards, however many of these compounds have been less extensively studied than PAHs. For example, N-heterocyclic and S-heterocyclic compounds are present within bitumen emissions and the International Agency for Research on Cancer has classified several of these compounds as possible carcinogens (Group 2B), including: Carbazole and Dibenz[a,h]acridine whilst many other compounds that have been identified in bitumen have not been classified due to lack of evidence (Group 3) (IARC, 2013).

Heterocyclic aromatic amines (HAAs) refer to any chemical with one heterocyclic ring and an amine group (John & Beedanagari, 2014). Two classes of HAAs exist, differentiated by their formation temperature, these include thermic HAAs (150-300^{o}C) and pyrolytic HAAs (>300^{o}C).

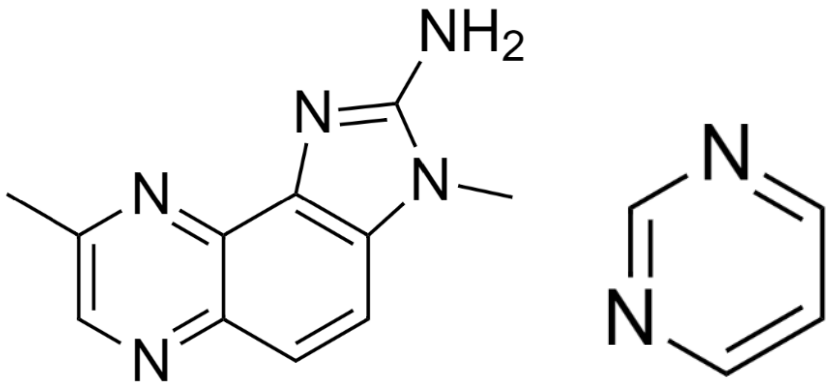


Figure 2-8 - The structure of MeIQx (left) and pyrimidine (right)

In recent years, epidemiological surveys have demonstrated that HAAs are the leading factor in breast, stomach, colon, pancreatic, prostate, and other cancers (Barzegar et al, 2019). Figure 2-8 illustrates the structures of the carcinogenic HAA compound 2-Amino-3,8-dimethylimidazo[4,5-f]quinoxaline (or MeIQx) and the N-heterocyclic diazine - pyrimidine. Pyrimidine is a base pair found in DNA, the carcinogenic mechanism of HAAs and other aromatics, such as PAHs is because of their structural similarity to these compounds. DNA can form pi-pi interactions with HAAs and PAHs ultimately leading to cancer and mutations. Unlike PAHs, heterocyclic compounds range from being slightly polar to polar, which increases their solubility in water and thus likelihood of human exposure. Heterocyclic aromatics have also been found to be ecotoxic to sensitive receptor species such as D. magna and D subspicatus, and like PAHs require regulation (Brendal et al., 2018). During pyrolysis, macromolecules within sludge may decompose into volatile HAAs (e.g. MeIQx), which may undergo further decomposition into heterocyclic compounds (e.g. pyrimidine) and PAHs (e.g. benzene). SSC must be sufficiently pyrolysed so that extractable organics have either volatilised or formed condensed aromatic structures that are no longer bio-available.

Several authors have measured the aromaticity and aromatic condensation of chars using NMR spectrometry. The aromaticity is the proportion of compounds in an aromatic form, whilst

aromatic condensation is the extent of aromatisation, with increased condensation the ring-size of the aromatic structures increases which vastly increases their stability and decreases bioavailability. The aromaticity of chars increases to >85% by 350°C (McBeath et al., 2011) and by 500°C the maximum aromaticity of a material is reached. In contrast, condensation increases more slowly above 400°C reaching a maximum value above 1000°C (Wiedemeier et al., 2015).

McBeath et al. (2014) conducted NMR spectroscopy (^{13}C) of chars produced between 350-600°C. Aromaticity and aromatic condensation increased with increased production temperature regardless of the feedstock source. However, the absolute value of these measures was dependent on the feedstock used. For example, feedstocks with higher lignin contents produced char with greater aromaticity and greater aromatic condensation. McBeath et al. (2014) estimated the mean residence time (MRT) of the char produced in the environment from the NMR output: "$-\Delta\delta$". For most chars produced at HHTs of 500°C and 600°C the MRTs expected were over 460 and 1400 years. Lu et al. (2016) investigated the organics of lignocellulosic chars produced between 400-800°C using NMR spectroscopy (^{13}C). At 400-600°C the ring sizes identified ranged from 4-52 rings, however, at 800°C 4-ring PAHs were eliminated and ring sizes below 19 were substantially decreased. At 800°C, most PAHs present ranged between 30-169 rings.

In summary:

- Pyrolysis produces polycyclic compounds such as PAHs, HAAs and other heterocyclics that are likely to be carcinogenic, mutagenic, and toxic. There is a risk these could be retained within the char.
- The concentration of extractable polycyclic compounds from chars increases with temperature, until a threshold temperature is reached, and then declines. This decline may be because of condensation into non-bioavailable forms, volatilisation, or thermal decomposition.
- Aromatisation of pyrolysis feedstocks occurs at relatively low temperature (<500°C); however, the extent of condensation and subsequent ring-sizes increases slowly with increased temperatures.
- Simple techniques such as the molar ratios of H:C can assess the extent of Py-C condensation in chars.

2.3.3.3 Pyrogenic Carbon: Char Inorganics

Sludge is expected to contain large proportions of inorganic elements, in particular: silicates, alkali-earth metals, iron and phosphorus. Elemental carbon, CO and H_2 are all highly effective reducing agents. When sludge inorganics are heated in the presence of C, CO and H_2 they may be reduced into their elemental forms. The thermodynamics of metal oxide and sulphide reducibility was explored by Ellingham (1944). An updated metal oxide Ellingham diagram is available from Tegg (2019) using data obtained from Reed (1971) and Colters (1985).

If an elements ΔG^o_f is lower than a corresponding metal oxide, thermodynamically it can reduce that oxide into its elemental form, although this ignores the kinetics of the reaction. Carbon is unique, when forming carbon monoxide its entropy increases therefore its (ΔG^o_f) decreases with increasing temperature. This means that with increasing temperature, carbon in the char will become an increasingly effective reducing agent, potentially leading to the formation of elemental metals and the consumption of Py-C and possibly other carbon sources.

The presence of inorganic elements in sludge may lead to the consumption of Py-C in char reducing carbon yield and perhaps retarding the growth of condensed aromatic structures. Although reduction by H_2 and CO may provide alternative kinetically favourable reduction pathways. The consumption of condensed aromatic carbon by oxidation reactions is used to produce highly porous, high-surface-area chars. For example, R. von Ostrejko produced steam activated wood char in early 1901 (Bandosz, 2006). Carbon oxidation through metal reduction may also improve the porosity of char, although this method is not typically used to produce activated carbon. The boiling points (b.p.) of elemental metals is typically lower than their compounds, for example: ZnO (b.p. = 2360ºC) compared to elemental Zn (b.p. =912ºC).

2.3.3.4 Char: Potential uses

2.3.3.4.1 Fuel

Historically hot-coke was gasified with saturated air. The manufactured producer-gas was immediately combusted to provide system heating for the coal-pyrolysis process. Clinipower Ltd. currently uses a similar approach for clinical waste char, however the gas produced is combusted alongside the pyrolysis gas to produce high-grade heat, which is converted to steam in a boiler for energy production or waste sterilisation purposes. The air-blast used for coke producer-gas plants is typically continuous and saturated with steam at 50ºC to control the temperature of the coke bed undergoing partial oxidation which helps prevent clinker formation. If the process is operated at high pressures (10-30 atmospheres), a proportion of the syngas produced forms methane through Sabatier synthesis (BP, 1965).

Based on an atmospheric pressure process, each kilogram of carbon gasified can yield approximately 2.3 kg of CO with a total energy content of 23.5MJ. However, this is based on 100% conversion of C to CO. In reality, the efficiency of the process will be reduced because of CO_2 formation and non-oxidised char carbon in the ash. The energy content of carbon is 32.8 MJ

kg^{-1}. Assuming a 100% conversion to CO occurs, the maximum efficiency of char gasification is approximately 71.6%. If SSC was gasified, the gas produced could produce steam for thermal hydrolysis or heat for drying prior to pyrolysis.

Alternatively, SSC could be combusted in cement kilns, coal power stations or waste incineration processes.

2.3.3.4.2 Pyrogenic carbon sequestration

Due to formation of condensed aromatic carbon, the mean residence time (MRT) of carbon in biochar may extend to millennia. Sludge could be converted into char using pyrolytic gasification. The high-heating rates and high temperatures used may reduce the char carbon yield, however high temperature is associated with increased condensation and stability (Lu et al., 2016) (McBeath et al., 2014). In the short-term, pyrolysis of organic matter likely releases additional carbon into the atmosphere however in the long-run the recalcitrance of the char produced may sequester additional carbon. For example, NMR studies suggest char carbon may have MRTs of between 460-1400 years (McBeath et al., 2014). This will be explored in more detail in section 9.3.

2.3.3.4.3 Reducing agent

Carbonised materials such as coke are typically used for iron oxide reduction in blast furnaces during steel manufacture. SSC could be used for this purpose; however, it is unlikely to be suitable because of its high ash content and potential presence of sulphur and nitrogen. This was discounted as a viable disposal route and will not be explored in any more detail.

2.3.3.4.4 Biochar

The Amazon basin mostly comprises highly weathered Oxisol and Ultisol soils, which are dominated by Fe and Al oxide clays. These soils have low-levels of fertility and have little capacity to hold nutrients. Amongst this landscape however there are small patches (averaging 20 Ha) of highly fertile soils called Terra-Preta de Índio (Portuguese for Amazonian black-earth) which were anthropogenically formed over thousands of years by pre-Columbian Amazonian people (Glaser, 2006). The unique facet of these soils is their high concentration of char, nutrients and fertility compared to surrounding soils. The formation of Terra-Preta soils is thought to be due to ancient farmers incorporating charred biomass alongside mineral rich materials such as human excreta, composts, aquatic biomass and ash from wood and animal bones. The discovery of these soils was the basis of later work on biochar as a potential soil amendment both in the tropics and temperate regions.

Biochar addition to soil has been found to:

- Improve crop yields (Hammond et al., 2013);
- Increase the pool of exchangeable plant available nutrients due to physical sorption in biochar pores and retention on negatively charged surface functional groups (e.g. cation exchange capacity) (Agegnehu et al., 2017);
- Improve water-holding capacity due to biochars porosity and surface functionalities (Agegnehu et al., 2017);
- Improve soil structure and aeration due to increased aggregation and decreased bulk density (Burrell et al., 2016);
- Alter the population and diversity of soil microbiology such as bacteria and fungi because of changes in nutrient availability, alterations in soil signalling dynamics and diversification of soil habits (Warnock et al., 2007);
- Increase soil pH and total nutrient concentrations, particularly for high-ash biochars such as manures;
- Reduce the bioavailability of heavy metals (Rodrigues-Vila et al., 2017) and organic contaminants such as PAHs (Gomez-Eyles et al., 2011);
- Sequester carbon.

Biochar addition is not ubiquitously positive and careful consideration of production conditions, application rates, application method and soil properties must be considered. Biochar production and resale from "virgin" wastes such as untreated plant, wood and vegetables is already permitted in the UK and regulated as a low-risk activity. However, the production of biochar is limited to small-scale processes with throughputs limited to 50kg per hour. Several companies operate in this sector in the UK including: Carbon Gold, Oxford Biochar, Earth Vida, Soil Fixer, Earthly biochar, Courage Copse Creatives, and many others. Carbon Gold dope their biochar with Trichoderma, mycorrhizal fungi, seaweed, and wormcasts presumably to aid in the formation of soil aggregates and root-fungi symbiosis. These companies biochars are sold on their own or blended with compost. Meyer et al. (2017) reports that several European countries permit the use of charred materials in agriculture. For example: Germany allows charcoal produced from chemically untreated wood; Switzerland allows EBC certified biochar produced from woody materials and Italy allows biochar produced from traceable biomass of vegetal origin from the agro-forestry sector if it complies with a range of minimum criteria. Further, in 2020 the EU began allowing biochar ("pyrolysis product made from a wide variety of organic materials of plant origin ") to be applied to agricultural soils (including organic production). In Annex II of regulation (EU) 2021/1165, it states the biochar: must be produced from "plant material"; contain ≤4mg PAHs kg dry matter and must comply with the relevant limits for contaminants set in regulation (EU) 2019/1009.

Land application of sewage sludge char is an attractive option since agriculture is already the largest disposal route for biosolids in the UK. In addition, SSC is expected to contain large quantities of phosphorus and other micronutrients (Kleemann, 2015). The main barriers to SSC land application are likely to be:

- The materials regulatory status (section 8.2);
- The presence of organic contaminants in the feedstock whose fate during pyrolysis may not be fully understood;
- The presence of extractable organic contaminants in the biochar, for example PAHs and heterocyclics (section 8.2.5);
- The heavy metal content of the char and its extractability (section 8.2.6).

2.3.3.4.5 Adsorbent production

In the early 18th century charcoal was used to decolourise sugar (Harris, 1942) and by 1901 R. von Ostrejko developed activated carbon (AC) which was produced by activating carbon with high temperature steam to improve its properties (Bandosz, 2006). The IUPAC definition of AC: "a porous carbon material, a char which has been subjected to reaction with gases, sometimes with the addition of chemicals, e.g. $ZnCl_2$, before, during or after carbonisation in order to increase its adsorptive properties" (Fitzer et al., 1995).

The main methods used to improve the adsorptive capacity of carbon materials include:

- Physical activation
- Chemical activation
- Ash removal

Physical activation involves heating pyrogenic carbon to between 800-1100^{o}C and partially gasifying it with an oxidant such as steam, carbon dioxide and air. Chemical activation involves mixing carbonaceous materials (e.g. wood/coal/char) with chemical agent and carbonising the material. Both processes increase the porosity of the material by removing pore-blocking carbon deposits and tarry residues (Smith et al., 2009). Chemical activation also influences the process of carbonisation, for example many commonly used agents such as $ZnCl_2$ and H_3PO_4 promote dehydration (Makeswari and Santhi, 2013). Typically, the inorganic ash within activated carbon is removed by acid washing the material, this may also be conducted to recover the chemical activation agent and alter the surface chemistry of the material.

There are two main types of adsorption: physical adsorption in which adsorbates are held within the material's internal pores by weak electrostatic Van der Waals forces; and chemi-sorption in which adsorbates are held by chemical bonds (Carrier et al., 2012). Adsorption isotherms are used to represent the equilibrium states of an adsorption system for an adsorbate and can be used for determining adsorption at a given temperature. The pollution capacity of an adsorbent can be

measured by the following properties: Brunauer Emmett and Teller (BET) surface area, total pore volume, micropore volume, mesopore volume and surface chemistry (Pullket, 2015; Smith et al., 2009).

The IUPAC categories pore sizes as follows (Wing, 1991):

- Micropores (below 2nm)
- Mesopores (2-50nm)
- Macropores (>50nm)

Micro and meso pores provide a large proportion of the total surface areas and are important for adsorbing small inorganic and large organic molecules, respectively. Whilst meso and macro pores provide connectivity, allowing adsorbates to access surface area and adsorption sites (Gee, 1997). The dominant pore size in coconut shell activated carbons is micropores whilst coal has a more balanced mix of meso and micro pores, although this depends on production methods.

For specific applications activated carbon may also be impregnated with a chemical that directly reacts with a target adsorbate. For H_2S removal, carbon is often impregnated with sodium or potassium hydroxides that undergo oxidation reactions with sulphur, converting it to its elemental state. Over time the caustic is depleted, the pores become blocked, and the material is landfilled rather than regenerated. Activated carbon may also be impregnated with iron oxides, these aide H_2S removal through catalytic oxidation reactions (Abatzoglou & Boivin, 2009).

In 2015, the global market size for activated carbon (AC) was $3.0 billion and was forecast to reach $5.2 billion by 2022, with a compound annual growth rate (CAGR) of over 12% (Roskill, 2017). Currently, the fastest major growth market is powdered activated carbon for mercury control with a CAGR of 14.5%, US industry consumes 150,000 metric tonnes per year for this purpose. If China were to implement standards equivalent to mercury and air toxics standards regulations, world demand for powdered activated carbon could double. Powdered- and granular activated carbon are used for different applications and have different business models. Powdered activated carbons are single use and are typically used for gas adsorption in applications such as flue gas desulphurisation and mercury scrubbing. Granular activated carbons can be used multiple times because adsorbates can be desorbed from the material by regeneration, they are commonly used in the water industry for micro-pollutant control and in the mining industry for recovering gold from ore leachates. Until recently, Thames Water operated a regeneration facility at Kempton Park in West London. Activated carbons are typically disposed of by incineration or landfill, however sometimes disposal to land may be suitable.

Activated carbon production is based on coal, coconut shells and wood charcoal; shortages of raw materials are commonplace and price increases may negatively affect growth projections. The largest manufacturer of activated carbon globally is Calgon Carbon (Roskill, 2017). Given the raw material shortages experienced by the activated carbon industry and the potential market

growth opportunities, the production of sludge based activated carbons (SBA) is an attractive option. The value of activated carbons varies massively, depending on its properties and applications, general use coal based granular activated carbon is valued at \$1500 t^{-1}, whilst coconut shell based activated carbon used for gold recovery are valued at \$3500-5500 t^{-1} and activated carbons for nuclear applications are valued at >\$15000 t^{-1}. The average export value from the world's biggest producer, China, has increased from \$533 t^{-1} in 2003 to \$1431 p t^{-1} in 2012 (Roskill, 2017).

Several researchers have manufactured activated carbon from sewage sludge, referred to as sludge-based adsorbents (SBAs) (Smith et al., 2009) (Devi & Saroha, 2017) . The production of SBAs could alleviate some of the material shortages experienced by the activated carbon industry, maximise sludge valorisation and lower the cost of adsorbents to end-users. Pullket (2015) conducted extensive experimentation investigating the manufacture of SBAs for bisphenol A adsorption. Bisphenol A is a precursor molecule used in the manufacture of certain plastics such as polycarbonates and epoxy resins. Bisphenol A is a xenoestrogen and can cause disruptions to the endocrine system of humans and other organisms. Pullket (2015) found:

- Physical activation with steam was less effective at producing SBAs, the optimal BET surface area achieved for raw and digested sludge was 263 m^2 g^{-1} and 165 m^2 g^{-1}. Whilst the optimum bisphenol A adsorption achieved was 87 mg g^{-1} and 55 mg g^{-1}, respectively.
- K_2CO_3, KOH, $ZnCl_2$, $FeCl_3$ and H_3PO_4 were effective chemical activating agents for raw and digested sludge, achieving BET surface areas for digested sludge of 1476, 1106, 1036, 761 and 672 m^2 g^{-1}. Raw sludge produced higher BET surface areas, up to 1979 m^2 g^{-1}, when activated with K_2CO_3.
- SBAs produced from raw sludge were more effective than those made from digested sludge. For example, K_2CO_3 activated SBAs from raw and digested sludge could adsorb 714 mg g^{-1} and 580 mg g^{-1} of bisphenol A.

A major downside of chemical activation is the generation of additional emissions, for example chemical agents such as $FeCl_3$ and $ZnCl_2$ would be expected to form additional HCl whilst Pullket (2015) found K in K_2CO_3/KOH was reduced into its elemental form and volatilised. Metallic K would likely re-condense later in the gas process stream and because of its pyrophoric properties may pose a fire-risk. Based on Tegg (2019), the reduction of potassium oxide with carbon (e.g. carbothermic reduction) is thermodynamically favourable at 800ºC and above, therefore K volatilisation could be minimised by avoiding excessive temperatures. Interestingly, Pullket (2015) found that the surface areas of SBAs activated with K_2CO_3/KOH vastly improved at temperatures of 750ºC and above. The carbothermic reduction of K may have been involved in the enhancement of SBA surface area by consuming C, this mechanism was not explored by Pullket (2015).

If SBAs were produced as powdered activated carbon this may create a secondary waste disposal issues since they are single use. This issue would be compounded if the material is less effective than the corresponding activated carbon and requires more regular replenishment. Marques et al. (2011) found that although granular activated carbons can be produced from sludge, the material exhibits a low attrition resistance in operation. Smith et al. (2012) investigated the production of attrition resistant granular activated carbons from steam activated SBAs. The SBAs were mixed with an organic binder, pelletised, and then carbonised in a rotary furnace. They concluded that polyvinyl alcohol (PVA) was the most effective binder and obtained a ball pan hardness (a measure of attrition resistance) competitive to that of commercially available ACs.

Based on the work conducted by Pullket (2015) and Smith et al. (2012) a two-step carbonisation process may be required to produce sludge-based granular activated carbons. The water industry typically utilises these to remove organic micro-pollutants from water prior to chlorination and H_2S and siloxanes prior to biogas combustion. Because of the potential heavy metal content in SSC and organic contaminants, the latter may be a more suitable application for SBAs. Dependent on their application, spent SBA's may be suitable for land application, energy recovery or landfilling.

2.4 Waste Regulation

Directive 2008/98/EC on waste otherwise known as the Waste Framework Directive (WFD) (EC, 2008) provides a legal framework for treating waste in the European Union, the main features of the legislation include:

(i) The definition of 'waste' as 'any substance or object which the holder discards or intends or is required to discard;

(ii) The definition of a 'by-product' as a 'substance or object, resulting from a production process, the primary aim of which is not the production of that item'. Further, several conditions are required for a substance to be considered a by-product rather than a waste including:

- Further use of the substance or object is certain;
- The substance can be used without any further processing;
- Production of the substance is integral to the process;
- Further use is lawful.

(iii) The definition of 'hazardous waste' as waste that displays hazardous properties. A full list of hazardous properties is presented in section 8.2.

(iv) The introduction of 'End-of-Waste' status, whereby a waste ceases to be a waste after it has undergone a recovery operation and complies with specific criteria, including:

- The substance is commonly used for specific purposes;
- A market or demand exists for the substance;
- The substance fulfils the technical requirements for the specific purpose and meets the existing legislation and standards applicable to products;
- The use of the substance will not lead to adverse human or environmental health impacts.

(v) The waste hierarchy (figure 2-9) – This ranks waste management options according to which options are best for the environment (DEFRA, 2011), the most and least preferable options are prevention and disposal respectively. Anaerobic digestion and ATC technologies are typically regarded as methods of energy or "other recovery", whilst incineration or landfilling would be regarded as disposal.

(vi) The 'polluter pays principle' whereby the generator of waste bears the costs of managing it and preventing damage to human and environmental health.

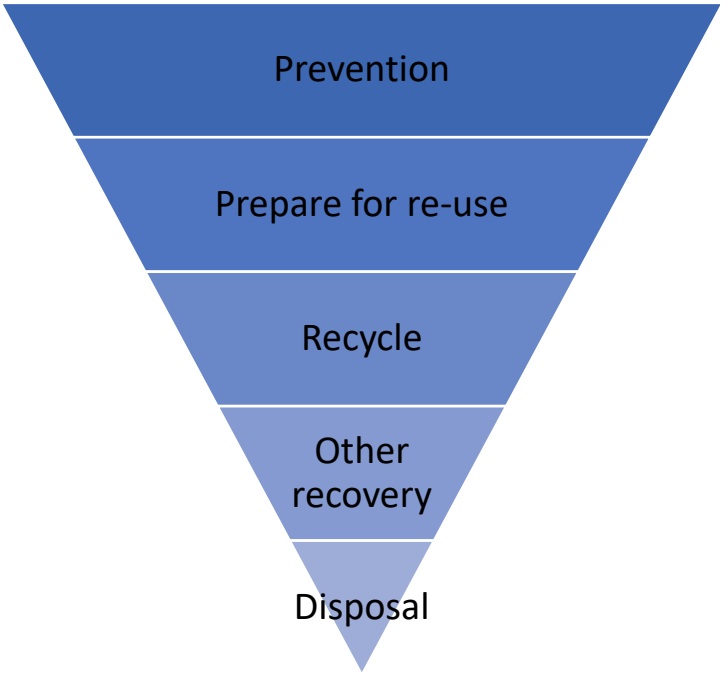


Figure 2-9 – The Waste Hierarchy (DEFRA, 2011)

2.4.1 Biosolids

Untreated sludge is considered a waste product, however the 'Sludge (Use in Agriculture) Regulations (1989)' facilitate the use of treated sludge in agriculture. These regulations outline several restrictions for applying sludge, for example, the permitted land-use after application. Table 2-5 summarises the maximum annual rate of addition and the soil limits for heavy metals in sludge-amended soils.

Table 2-5: Maximum addition of sludge heavy metals to soils

Element	Max addition rate	Soil limit according to pH of soil			
	kg Ha^{-1} yr^{-1}	5.0-5.5	5.5-6.0	6.0-7.0	>7.0
Zinc	15	200	250	300	450
Copper	7.5	80	100	135	200
Nickel	3	50	60	75	110
Lead	15	300			
Cadmium	15	3			
Mercury	0.1	1			

In addition to these regulatory requirements, the UK water industry adheres to the Biosolids Assurance Scheme which aims "to provide food chain and consumer reassurance that BAS Certified Biosolids can be safely and sustainably recycled to agricultural land" and "combines legislative requirements and best practice" (Assured Biosolids Ltd., 2021).

Also, it adheres to the ADAS Safe Sludge Matrix which is an agreement made between Water UK and the British Retail Consortium and provides limits on what time of year sludge can be applied and to which crop, in order to limit pathogen risks (Gale, 2005).

By facilitating an outlet for waste sludge, these regulations promote the biological treatment and land application over thermal treatments. The main thermal process used for sludge treatment and disposal is currently incineration, but this is now declining in the UK. Sludge incineration ash contains useful elements (e.g. P) however, the material is landfilled as hazardous waste rather than recycled to land. The reason for this is related to concerns over the concentration and leachability of heavy metal compounds. In addition, many of the beneficial elements including: C, N and S form gaseous emissions (e.g. CO_2, NO_x, SO_x) and are lost to the atmosphere during combustion.

2.4.2 Biochar

Biochar is used as a soil amendment with the intention to improve soil functions and to reduce emissions from biomass that would otherwise naturally degrade to greenhouse gases. The beneficial properties of biochar include enhanced: crop yields, soil nutrient retention, soil moisture retention, soil carbon content and increased biological activity (Lehmann & Joseph, 2015). The IBI (2015) released a "standardized product definition and product testing guidelines for biochar that is used in soil", the requirements are summarised in table 2-6. This certification has no legal basis although it could provide the basis for future regulations when pyrolysis operators look for sludge char outlets.

Likewise, the European biochar certificate (EBC) "was developed to limit the risks of biochar usages to the best of our scientific knowledge and to help the users and producers of biochar to prevent or at least to reduce any hazard for the health and for the environment while producing and using biochar" (EBC, 2022). The scheme is a voluntary industry standard in Europe, although it is obligatory for all biochar sold for agriculture in Switzerland, whilst several countries have aligned their biochar regulation with this standard. The EBC (2012-2022) standards include a "positive list of permissible biomasses for the production of biochar" this includes plant biomass from: (1) agricultural farms; (2) forestry and wood processing; (3) landscape management; (4) recycling economy (e.g. wastepaper and un-/treated wood waste); (5) kitchen & canteen waste; (6) food processing residues; (7) water maintenance & vegetal marine biomass; (8) textiles and (9) non-animal digestates.

The standards state that if biochar producers are interested in certifying sewage sludge char "an official application should be sent to EBC". "The EBC scientific committee would review the application in detail and could then introduce a separate EBC class for sewage sludge pyrolysates".

EBC standards also includes certification classes which limit the use of the material to certain applications, these include: EBC-urban, EBC-consumer materials, EBC-basic material, EBC-agro, EBC-agro organic and EBC-feed. For a specific biochar, its material origin, concentration of contaminants and properties dictate which classification class it is suitable for. The requirements for IBI and EBC (-agro, -agro organic and -basic material) biochar are summarised in table 2-6.

Table 2-6 - International biochar initiative product testing guidelines for biochar (IBI, 2015) and EBC standards (EBC, 2012-2022).

Parameter	Unit	IBI Criteria	EBC Criteria		
			-agro	-agro organic	-basic material
Organic carbon (C_{org})	% (Dry wt.)	Class 1: ≥ 60% Class 2: ≥ 30% Class 3: ≥ 10%	n/a		
H: C_{org}	Molar ratio	0.7	<0.7		
O/C_{org}		n/a	<0.4		
Germination Inhibition	-	Pass/Fail	n/a		
PCDD/Fs	ng kg^{-1}	17	20		
PCBs	mg kg^{-1} (Dry Wt.)	0.2-1	0.2		
16 EPA PAH		6-300	4 (±2)	6.0 (+2.2)	n/a
Polychlorinated Biphenyls		0.2-1			
Arsenic		13-100	13	13	15
Cadmium		1.4-39	0.7	1.5	5
Chromium		93-1200	70	90	250
Cobalt		34-100	n/a		
Copper		143-6000	70	100	250
Lead		121-300	45	150	250
Mercury		1-17	0.4	1	1
Molybdenum		5-75	n/a		
Nickel		47-420	25	50	250
Selenium		2-200	n/a		
Zinc		416-7400	200	400	750

The STRUBIAS (struvite, biochar, and ash) working group aims to support the European Commission in assessing the suitability of STRUBIAS materials for inclusion in The Fertilising Products Regulations (FPR) (EU) 2019/1009 (Huygens et al., 2019). The working group expanded STRUBIAS materials to include any material from a thermochemical process (e.g. hydrochar or slags) and expanded struvite to include any precipitated salts.

The FPR regulation outline the legal framework for fertilised products from biogenic wastes and other secondary raw materials. Annex II of the FPR outlines component material category (CMC), at present there are 11 CMCs, for example CMC 5 refers to "digestate other than fresh crop digestate". Each CMC outlines rules specific to that material. At present, there are not any CMC's specific to STRUBIAS materials. Huygens et al. (2019) suggests new CMCs should cover STRUBIAS materials, these include CMC's for: (i) "Precipitated phosphate salts & derivatives", (ii) "Thermal oxidation materials & derivatives" and (iii) Pyrolysis and gasification materials (PGM). Annex I of the FPR outlines product function categories (PFC's), these outline the beneficial affects certain CMSs provide. Huygens et al. (2019) suggests PGM's may provide the following functions: PFC 1 (fertiliser), PFC 3 (soil improver), PFC 4 (growing medium) and PFC 6 (non-microbial plant bio-stimulant).

Huygens et al. (2019) states that under the precautionary principle and the broad-range of emerging contaminants in human-derived waste streams it is justified to exclude human-derived waste streams from the positive input material list (e.g. The CMC for PGMs) to ensure human and environmental health. According to Huygens et al. (2019) there is insufficient scientific evidence that has examined the influence of ATC technologies on organic contaminants. The contaminants of concern in sludge chars include PAHs, PCBs, PCDD/Fs, phthalates (e.g. DEHP), surfactants (LAS & NPE), personal care products, pharmaceuticals, endocrine disruptors (e.g. sulphonamides) and polymers (Huygens et al., 2019). Amendments to the regulations and guidance could be made once robust and extensive techno-scientific evidence is available to underpin the safe use of PGMs derived from sludge. Table 2-7 summarises the processing requirements for char produced by pyrolysis (and related technologies) (Huygens et al., 2019). The processing requirements for char production are minimal, because of large difference between various char producing technologies (e.g. pyrolysis and hydrothermal carbonisation).

Table 2-7 - Processing requirements for PGM production

Parameter	Processing requirements
Minimum temperature	180^{o}C (for 2 seconds)
Additives	<25% (Wt.) of final product – Can only be added to assist pyrolysis, not to enhance the properties of the PGM
Post-processing	Allowance for agglomeration, granulometry adjustment and washing or rewetting (to improve chemical/physical stability).

The suitability of PGMs for agricultural re-use are based on the materials properties, at CMC level (Table 2-8) and PFC level (Table 2-9). The quantity of carbon in the PGM dictates whether the material is considered a carbon-rich PGM (C-PGM) or nutrient rich (N-PGM), this influences the limit concentrations for some metals. (Huygens et al., 2019). Sludge char will likely be considered a N-PGM due to the high concentration of inorganic elements.

Table 2-8 - CMC level requirements for N-PGM re-use in agriculture (Huygens et al, 2019)

Parameter	Unit	Specification
Total Carbon	% Wt	≥ 50 (C-PGM) < 50 (N-PGM)
H:C_{org}	Molar ratio	<0.7 (DAF where Char C_{org} <50%)
Phosphate (if >3% Wt.)	% Solubility	>25 in water >30 in neutral ammonium citrate >35 in 2% formic acid
Chloride	% Wt	3
Manganese	% Wt.	>3.5 Labelling required
Arsenic	mg kg^{-1}	31 (UK SGV: 20)
Barium		1335
Beryllium		54
Cobalt		101
Chromium		243 (UK SGV: 130)
Molybdenum		52
Antimony		12 (UK SGV: 35)
Selenium		108 (UK SGV: 35)
Thallium		2
Vanadium		377
PAHs		6 (16 US EPA congeners)
D1-PCB		0.2 (PCBs: 28, 52, 101, 153, 180)
PCDD/F	ng kg^{-1}	20 (Toxicity equivalents)

Nutrient-rich PGM materials such as SSC contain substantial quantities of total phosphorus, however, these may not be in a plant available form. Continuous application of non-plant available forms of P can lead to a build-up of phosphorus over-time and is not considered sustainable. This is also a historical issue for conventional phosphate fertiliser application, whereby application rates were historically excessive and plant available forms of phosphorus (e.g. ammonium phosphate) were converted in soils into non-available forms (e.g. iron/aluminium phosphate). Huygens et al. (2019) suggested PGMs could have PFC 1, 3, 4 and/or 6, table 2-9 summarises the PFC level requirements for fertilisers under regulation (EU) 2019/1009.

Table 2-9: PFC level requirement for fertilisers (Regulation (EU) 2019/1009)

Parameter	Unit	PFC 1[1]	PFC 3[2]	PFC 4[3]	PF6[4]
Single Nutrient declared	% Wt	P_2O_5: >2 K_2O: >2 Total N: >2.5 (>1 Org N)	-	-	-
Multiple nutrients declared	% Wt	P_2O_5: >2 K_2O: >2 Total N: >2 (>0.5 Org N) Sum: >8	-	-	-
C_{org}	% Wt	>7.5	-	-	-
Cadmium	mg kg^{-1}	3 (If < 5% P_2O_5) 60 (If > 5% P_2O_5)	1.5	1.5	1.5
Nickel		50	100	50	50
Copper		600	300	200	600
Zinc		1500	800	500	1500
Lead		120	120	120	120
Inorganic arsenic		40	40	40	40
Chromium (VI)		2	2	2	2
Mercury		1	1	1	1

[1]PFC 1: Solid organo-mineral material

[2]PFC 3: Inorganic soil improver

[3]PFC 4: Growing medium

[4]PFC 5: Plant bio-stimulant

The FBR 2019/2019 regulations state that for "recovered wastes" such as "biochar" a market demand for their use as fertilising products has been identified. Therefore, if "biochar" complies with the requirements in this regulation it should cease to be a waste (directive 2008/98/EC) and can access the internal market. Pyreg, a manufacturer of pyrolysis equipment, claims that sewage sludge char produced by their process has been successfully registered as an inorganic phosphate fertiliser (PYREGphos) in Sweden and is available throughout the EU (Pyreg, n.d). However, the regulatory framework for this is unclear.

2.4.3 Manufactured gas

The Industrial Emissions Directive (IED) 2010 is the main EU instrument regulating pollutant emissions from industrial processes. The aim of the IED is to promote the application of best available technologies (BAT) to minimise the generation of harmful emissions and protect human and environmental health (EC, 2020). According to the IED (2010) a waste incineration plant is defined as:

"any stationary or mobile technical unit and equipment dedicated to the thermal treatment of waste, with or without recovery of the combustion heat generated, through the incineration by oxidation of waste as well as other thermal treatment processes, such as pyrolysis, gasification or plasma process, if the substances resulting from the treatment are subsequently incinerated".

Fuel gas or syngas produced from ATC processes is considered waste therefore subsequent oxidation of the gas through incineration or combustion within an engine is considered waste incineration. Consequently, ATC processes must comply with the requirements for waste incineration (table 2-10).

Table 2-10: Emission limit values for waste incineration plants

Substance	Daily ELV mg Nm^{-3}	Half-hourly ELV mg Nm^{-3}	Other ELV mg Nm^{-3}
Total dust	10	30	-
Gaseous and vaporous organic substances (expressed as TOC)	10	20	-
HCl	10	60	-
HF	1	4	-
SO_2	50	200	-
NO & NO_2 (expressed as $NO_{2)}$	200	400	-
CO	50	100	-
Dioxins & Furans [1] (expressed as TEQ)	-	-	0.1 ng Nm^{-3}
Heavy metal (Cd, Tl)[1]	-	-	Total: 0.05
Heavy metals (Other)[1]	-	-	Total: 0.5
Mercury[1]	-	-	0.05

[1]Heavy metals, dioxins and furans need to be analysed twice per year
[2]Limit at 273.15k, 101.1 kPa, moisture corrected gas containing 11% oxygen

The requirement to comply with waste incineration guidelines may pose an unfair regulatory burden for pyrolysis processes. For ATC processes utilising gas engines the fuel-gas must be cleaned prior to combustion to remove contaminants such as dust, VOCs, HCl, HF, H_2S and metals. Therefore, post-combustion these contaminants are not expected to be present. Whilst dioxins are less likely to form during pyrolysis because no free oxygen is present within the reactor. In addition, processes that immediately combust pyrolysis volatiles typically conduct

combustion at 1000-1250ºC, far above the temperature to eliminate dioxins. Whilst the adiabatic flame temperature within a standard otto-cycle spark ignition engine is even greater. Therefore: the control of emissions; monitoring of emissions; required operating conditions; and reporting requirements outlined for waste incinerators in chapter IV of the IED may be inappropriate for ATC systems. This issue extends to the solid by-products, for example, the IED requires incineration processes to produce ash with less than 3% TOC or 5% LOI.

The title for chapter IV of the IED is "Special provisions for waste incineration plants and waste co-incineration plants" it outlines the requirements for waste incinerators. Article 42 (chapter IV) of the IED states 'this chapter shall not apply to gasification or pyrolysis plants, if the gases' are 'purified to such an extent they are no longer a waste' and cause 'emissions no higher than'… 'burning natural gas'.

To avoid regulatory burden, ATC systems could aim to clean the gas produced to natural gas specifications in order to achieve end-of-waste status and bypass the requirements of chapter IV of the IED. Nevertheless, the gas would still need to meet to the emission limit values (ELV) outlined in the MCPD for natural gas combustion within an engine.

The Environment Agency has published material comparator reports, in which waste materials can be benchmarked against to assess their suitability for end-of-waste status. The comparator report for natural gas includes the specifications of natural gas as outlined in the gas safety (management) regulation 1996 (Table 2-11).

Table 2-11 - National grid specifications for natural gas (Environment Agency, 2016)

Parameter	Unit	Limit
Hydrogen Sulfide (H_2S)	mg m^{-3}	≤5
Total Sulphur	mg m^{-3}	≤50
Organo-halides	mg m^{-3}	≤1.5
Hydrocarbon Dew Point	°C (<85 bar)	≤ -2
Wobbe Index (real gross dry)	MJ m^{-3}	47.20 to 51.41
Soot Index	-	≤0.60
Incomplete combustion factor	-	<0.48

In addition, the material compactor report also includes (Table 2-12):

- The results of nine natural gas samples taken by the regulator from one "gas shipper" over three days. The results in table 2-12 exclude data for VOCs and metals, however these are available in the material comparator report (Environment Agency, 2016).
- The results for 119 natural gas samples taken by the national grid over a two-day period.

The values presented by the Environment Agency (2016) in table 2-11 originate from the Gas Safety (Management) regulations (GSM) 1996. These were written to ensure the safe management of gas flow through pipelines, primarily for domestic use. Parameters such as hydrocarbon dew point, Wobbe index, soot index and incomplete combustion factor are specifically related to safe transportation in pipelines and use within homes. Therefore, these parameters are less relevant to industrial use in a gas-engine. The limit value for hydrogen sulphide (Table 2-11) is based on human health considerations, since the occupational exposure standard for H_2S exposure in the UK are set at 5ppm (8 hour - time weighted average) and 10ppm (short-term exposure limit) (Costigan, 2003).

In air, 5 mg Nm^3 of H_2S approximately corresponds to 4.4ppm. For engines, H_2S is corrosive in the presence of free water, forming sulphuric acid and damaging engine components such as piston rings and spark plugs. However, for landfill gas engine manufacturers Jenbacher and Deutz recommend total sulphur of <2000 and <2200 mg Nm^3 respectively whilst Deutz specifies <0.15% v/v H_2S (Environment Agency, 2010). This highlights the difference between engine requirements (~2000 mg H_2S Nm^3) and human health requirements (5 mg Nm^3).The limit value for total sulphur in accordance with GSM (1996) is 50 mg m^{-3} (Table 2-11) whilst the samples reported by the Environment Agency (2016) contained a maximum of 0.57 mg kg^{-1} total sulphur (Table 2-12). A separate limit for total sulphur is required because natural gas may contain other sulphur gases such as SO_2, COS, CS_2 and mercaptans. Mercaptans are added to natural gas to odorize the gas and help detect leaks, the Occupational Safety and Health Administration (OSHA) exposure limit for mercaptans is 10ppm in air. It is not clear whether the sample data presented by the Environment Agency (2016) was taken from odorized natural gas or not. The scientific basis for total sulphur in natural gas is unclear.

Table 2-12 - Sampled natural gas sulphur and BTEX (Environment Agency, 2016)

Parameter	Unit	Limit	Source
Hydrogen Sulfide	mg m^3	<0.4	National Grid (119 samples)
Total Sulphur		<0.57	
Total Sulphur		<0.5	Environment Agency (9 samples)
Hydrogen sulphide		Not measured	
Benzene		<1.9	
Toluene		<0.575	
Ethylbenzene		<0.410	
o-Xylene		<0.380	

The Environmental Agency released an end-of-waste criteria for the production and use of biomethane from landfill gas and anaerobic digestion. The specifications are summarised in table 2-13. For biomethane to attain EOW status, the limit values for hydrogen sulphide and halogenated hydrocarbons (Table 2-13) are the same as the GSM regulations (1996) for natural gas. For H_2S, this is far above the quantity (<0.4 mg kg-1) found in natural gas according to the

Environment Agency (2016). Likewise, the limit for aromatics (expressed as Xylene) is 100 mg m^{-3} which also far exceeds the concentrations found in natural gas.

Table 2-13 - Specification for biomethane for injection into the UK gas-grid and for use in appliances (Environment Agency, 2013)

Parameter	Unit	Limit
Total Sulphur	mg m^{-3}	30
Hydrogen Sulphide (H_2S)		5
Ammonia (NH_3)		20
Hydrogen chloride (HCl)		1.5
Hydrogen fluoride (HF)		5
Total halogenated hydrocarbons		1.5
Total aromatic hydrocarbons expressed as Xylene		100
Arsenic (As)		0.1

The Environment Agency released a preliminary regulatory statement for Syngas EoW status, the gas must meet CV adjusted limits, as specified in table 2-14 (Personal Communication, 2020).

Table 2-14 - Environment Agency regulatory position: "Syngas" EoW status[1]

Parameter	Unit	Limit	CV adjusted limit	Basis of limit
Total sulphur	mg m^{-3}	0.57	0.27	119 natural gas samples (Environment Agency, 2016)
Hydrogen sulphide		0.4	0.19	
Total halogenated hydrocarbons		0.07	0.03	Analysis of 9 natural gas samples (Environment Agency, 2016)
Heavy metals total		0.16	0.07	
Total aromatic hydrocarbons expressed as Xylene		2.6	1.21	
HF		5	2.33	Limits from Biomethane Quality Protocol
HCl		1.5	0.70	

[1] Personal communication (2020)

[2] Natural gas LHV, 35.06 (Personal communication, 2020) and fuel-gas LHV, 16.34 (Mills, 2015).

For syngas, the limit values for total sulphur, hydrogen sulphide, total halogenated hydrocarbons, heavy metals, and total aromatic hydrocarbons are based on the small number of natural gas samples taken from North Sea gas (Table 2-12) and then adjusted for CV.

This approach means the limit values are much stricter for "syngas" compared to "biomethane". For example, a "syngas" with a LHV of 16.34 MJ m^{-3} (Mills, 2015), would need to achieve a H_2S concentration over 26 times less than biomethane whilst its total aromatic hydrocarbon would need to be over 82 times lower. This approach will likely inhibit investment into ATC processes not operated as incinerators.

2.4.4 Combustion products

The medium combustion plant directive regulates pollutant emissions from the combustion of fuels in plants between 1-50 MW thermal. Rather than apply fair competition across all technologies, however, the ELVs are technology specific. This has been conducted because blanket standards may be unattainable for certain industries or applications. Unfortunately, it does not create a consistent regulatory environment. Regardless of whether or not fuel-gas achieves EOW status, it will also need to comply with MCPD regulations. Tables 2-15 and 2-16 outline the post-combustion MCPD emission limits for new MCPD plants. If fuel-gas achieves EOW status it will be treated the same as natural gas and will need to comply with the relevant ELVs for NOx as outlined in table 2-15 and 2-16. If not, it will probably need to comply with the ELVs for other gaseous fuels.

Table 2-16: Incineration ELVs under medium combustion plant directive for new plants

	Pollutant	Unit	Solid biomass	Natural Gas	Other gaseous fuels
Oxidation (other than engines or turbines[2])	SO_2	mg m^{-3}	200	-	35 (100 for biogas)[1]
	NO_x		300	100	200
	Dust		20	-	-

[1]For existing incinerators the limit is 170 mg kg^{-1} for biogas

[2] Limit at 273.15k, 101.1 kPa, dry-gas containing 3-11% oxygen, fuel specific.

Table 2-15 - Engine ELVs under medium combustion plant directive for new plants

	Pollutant	Unit	Liquid-fuels	Natural gas	Other gaseous fuels[1]
Engine	SO_2	mg m^{-3}	120	-	15 (40 for biogas)[2,3]
	NO_x		190	95	190
	Dust		10	-	-

[1] Limit at 273.15k, 101.1 kPa, dry-gas containing 15% oxygen

[2] Limit at 273.15k, 101.1 kPa, dry-gas containing 5% oxygen

[3] For existing engines the limit is 60 mg m^{-3} for biogas

The statutory guidance "SR2009 No 4" explains the regulatory framework for combusting biogas in new medium combustion plant engines (<5MW) at sewage treatment works (Environment Agency[a], 2018). This activity is regulated in accordance with the medium combustion plant directive (MCPD) and the specified generator regulations (tranche B, without secondary abatement). Secondary abatement are measures post-combustion to control pollutants (e.g. selective catalytic reduction). The emissions limits for biogas engines are summarised in table 2-17.

Table 2-17: Engine emission limits for biogas combustion at sewage treatment works

Parameter	Limit (mg m^{-3})[1]
NO_x (expressed as NO_2)	500
SO_2	107
CO	1400

[1]Limit at 273.15k, 101.1 kPa, moisture corrected gas containing 5% oxygen

The aim of concentration limits for fuels and emission limits for combustion processes is to protect human or environmental health. This aim should not be influenced by the technology used to process waste. The Environment Agencies regulatory position for "Syngas" EOW status is inconsistent and disadvantageous compared to other regulations. However, the fuel concentration limits and ELVs presented in tables 2-10 to 2-17 are difficult to compare as presented in the IED and MCPD because they compare pre- and post-combustion product. In addition, the regulations present the contaminant concentrations at technology specific oxygen concentrations. To improve comparability, the H_2S values were converted into SO_2 values and the oxygen contents for the limit values was harmonised at 0%. This was calculated using the following formula, as specified in part 7 of the IED:

$$E_S = \frac{21 - O_s}{21 - O_M} \times E_M$$

E_s = Calculated emission concentration at the standard percentage oxygen concentration

E_M = Measured emission concentration

O_s = Standard oxygen concentration

O_M = Measured oxygen concentration

To make an accurate comparison, the gas composition of biogas, syngas and natural gas must be known. Later in this Thesis (section 7.6), the concentration of H_2S was calculated based on observations during laboratory lab-scale pyrolysis. The proceeding information has highlighted the challenges around building and implementing an advanced thermal treatment system based upon a pyrolysis and gasification process. The subsequent chapters of this Thesis will report a detailed study which addresses some of these issues and offers a way forward to bring pyrolysis and gasification to a point where it can be used at a commercial scale and become the best technology for managing the sewage sludge arising from treating wastewater treatment produced by modern society.

Chapter 3: Research aims and objectives

3.1 Research Aims

Agricultural recycling is the primary route for sludge disposal in the United Kingdom, however this practice is threatened by a range of factors. Sludge could also be disposed of by incineration however this method is expensive, inefficient and releases large quantities of carbon dioxide. Advanced thermal conversion technologies such as pyrolysis and gasification are now being considered by the industry. The aim of this project was to explore the potential of pyrolysis in a manner representative of pyrolytic gasification concepts being considered by the industry. Pyrolytic gasification has not yet been adopted by the industry and there is scarcity of information on process outputs (including safety data) required for design and commissioning. This research will allow the technical feasibility and potential for pyrolysis to dispose of digested sludge and produce valuable by-products such as fuel-gas and char to be explored. Another aim is to characterise the products formed, explore their reuse value, and gain an understanding of the relationship between pyrolysis operating conditions and product characteristics. Since the technology is not currently used for sludge treatment, another aim was to explore how the process and the products formed fit into the current regulatory sphere which currently centres around treatment by digestion or incineration.

3.2 Objectives

a) What are the outputs from the pyrolysis of digested sludge?

- Design, assemble and operate a representative pyrolytic-gasification process.
- Quantify the mass yields obtained during pyrolysis and benchmark this against carbonisation, the technology generally explored in the literature for char production.
- Quantify the gas species produced during pyrolysis and explore the relationship between operating conditions and gas speciation. Identify the optimal conditions for energy recovery.
- Characterise the sewage sludge char produced and explore how this will influence the products regulatory status, disposal, and subsequent reuse value.
- Assess the environmental impact of char production, its utilisation within the environment and the viability of reuse options with a focus on P recovery.

b) What are the main challenges associated with sludge pyrolysis? How does pyrolysis fit into the wider sludge treatment process?

- Determine the pyrolysis conditions that minimise tar yield and other process contaminants and explore the operational issues associated with these contaminants both within the reactor and during subsequent gas clean-up.

- Investigate the potential of implementing pyrolysis at a representative advanced digestion site (e.g. Crossness STW) and explore how the technology will influence overall site energy flows and performance.

Chapter 4: Methods

4.1 Sludge preparation

Crossness Sewage Treatment Works is located in the Borough of Bexley in Southeast London and serves a population equivalent of approximately two-million people. It produces approximately 48,000 tonnes dried solids of raw sludge each year which is a blend of approximately 60% indigenous primary sludge and 40% SAS. Blended thickened raw sludge is thermally hydrolysed in a two stream Cambi B12 THP system and then undergoes mesophilic anaerobic digestion. Digested sludge is dewatered with a piston press and stored in a cake barn before being exported to agriculture. Crossness is a representative example of a large urban sludge treatment centre and was selected on this basis. In addition, Crossness does not import primary sludge and therefore operates and produces a relatively consistent cake. Its proximity within a densely populated residential district of London also makes the site a prime candidate for advanced thermal treatment because this would limit vehicle movements into and out of the site and relieve pressure on the constrained landbank in the region.

Class A, thermally hydrolysed, digested sludge was sampled from the cake barns at Crossness STW. Raw blended sludge was sampled from the digester feed. Since the sludge had been sterilised by thermal hydrolysis, it was not autoclaved prior to use. The sludge was sampled and characterised on three occasions during the first week of August 2017-2020. The sample sizes were relatively large and comprised 180-240L of freshly dewatered sludge (~30% dried solids). Operations conduct daily loss-on-ignition analysis of Crossness cake; the sampled sludge was tested for loss-on-ignition (Table 6-1), and this was cross referenced with operational data to ensure the sample was representative. The materials were dried at 105ºC in a laboratory oven and dried until constant weight. Dried sludge had a granular texture, the particle size typically exceeded >10mm, however the design specification for the feed-screw was <6mm. Therefore, the material was disintegrated by hand and sieved to a particle size of <5.6mm. Some aggregates could not be broken up by hand, therefore these were disintegrated in a food processor. An effort was made to minimise the quantity of dust generated during food processing, by minimising operation speed and only using it when required. Approximately 40L of dried homogenised feedstock was prepared and stored in a sealed plastic barrel until further use. This barrel was partially-filled which allowed sample harmonisation before sub-sampling through repeated inversion and gentle mixing.

4.2 Material characterisation

To obtain representative sub-samples, solid materials (e.g. char produced at a specific temperature) were mixed through inversion and gentle mixing. A random sub-sample was then taken and further sub-sampled for each replicate through coning and quartering (Campos & Campos, 2017).

4.2.1 Dry solids and loss on ignition

The dry solids (DS%) were calculated in triplicate using a method presented by Rowell (1994). Approximately 10g of material was weighed in a crucible, this was heated in an oven at 105°C until constant weight. The crucible was cooled in a desiccator and the dry weight was recorded (Rowell, 1994). DS (%) is determined:

$$Dried\ solids = \ DS\ (\%) = \frac{Wet\ weight}{Dry\ weight} \cdot 100$$

Loss on ignition (LOI) was calculated in triplicate using a method presented by Rowell (1994). Once DS (%) had been measured, the crucible was placed in a furnace and ignited at 550°C until constant weight. The crucible was then cooled in a desiccator and its weight was recorded. LOI (%) is determined:

$$Loss\ on\ ignition\ = \ LOI\ (\%) = \frac{(Dry\ weight) - (Ignited\ weight)}{(Dry\ weight)} \cdot 100$$

4.2.1 Bulk Density

The dry bulk density of sewage sludge (sieved <5.6mm) and SSC-700 (as received & milled) were measured in accordance with ASTM D2854-09. This involved measuring the volume packed by free fall from a vibrating feeder into a 500ml graduated cylinder and determining the mass of the volume.

4.2.2 Ultimate analysis

Ultimate analysis measures the total concentrations of carbon, hydrogen, nitrogen, and sulphur (CHNS) and was determined by MEDAC Ltd (Surrey, UK) using an elemental analyser in triplicate. This involves combusting the material and quantifying the gases formed by GC-TCD (Accuracy ±0.3%). The oxygen content was measured by difference:

$$Oxygen\ (\%\ Wt) = \ 100\% - C\ (\%) - H\ (\%) - N\ (\%) - S(\%) - Ash\ (\%)$$

4.2.3 Thermogravimetric analysis

Thermogravimetric analysis (TGA) differential scanning calorimetry (DSC) was conducted using a “Polymer Laboratories - STA 1500 thermal analyser”. Approximately 15mg of finely ground

sample was loaded into a quartz crucible and heated under controlled conditions, in either nitrogen or air. During heating, the analyser monitored: (i) the weight of the loaded crucible over time (ii) the temperature of the loaded crucible and a control. The flow rate of gas was set at 50ml min^{-1}. Each sample was measured in triplicate, however for some runs additional replicates were taken and were included within the analysis.

4.2.3.1 Proximate analysis

Proximate analysis was used to determine the gravimetric fraction of a materials moisture (% H_2O), volatile solids (% VS), fixed carbon (% FC), and ash content (% ash), under ASTM D7582. Each sample was measured in triplicate, however for some runs additional replicates were taken and were included within the analysis. The sample was heated (20°C min^{-1}) in a nitrogen atmosphere (50 ml min^{-1}) and held at 105°C for 20 minutes, followed by 950°C for 20 minutes. The material was cooled from 950°C to 600°C, the gas was changed from nitrogen to air and the sample was oxidised for 45 minutes. The extended residence time was required to ensure the carbon was fully oxidised. For pyrolytic carbon materials recovered from the furnace, a modified method was used whereby the material were oxidised at 800°C. Where:

- M (S) = Initial specimen mass
- M (105) = Specimen mass after being held at 105°C isothermal
- M (N_2) = Specimen mass at 600°C isothermal in N_2

$$\% H_2O = \left(\frac{(M\ (s) - M(105)}{M\ (S)}\right) \cdot 100$$

$$\% VS = \left(\frac{(M\ (105) - M\ (N_2)}{M\ (S)}\right) \cdot 100$$

$$\% FC = \left(\frac{(M(N_2) - M\ (Air)}{M\ (S)}\right) \cdot 100$$

$$\% Ash = \left(\frac{M\ (Air)}{M\ (S)}\right) \cdot 100$$

4.2.3.2 The recalcitrance index (R_{50})

The recalcitrance index (R_{50}) measures the thermal stability of materials compared to a graphite control (Harvey et al., 2012) and indicates their long-term C-sequestration potential. It is calculated using the following equation:

$$R_{50}\ (x) = \frac{T_{50}\ (x)}{T_{50}\ (graphite)}$$

T_{50} refers to the corresponding temperature when 50% of a sample or graphite have been oxidised in air during thermogravimetric analysis. The powdered graphite control and each sample were measured in triplicate. Figure 4-1 illustrates the measured T_{50} for one of the graphite standards used in this study. The average T_{50} for graphite was 802.5°C.

The R_{50} index can assess the carbon sequestration potential of materials, for example:

- Class A = $R_{50} \geq 0.70$
- Class B = $0.50 \geq R_{50} < 0.70$
- Class C = $R_{50} < 0.50$

For samples, the weight loss zone between (i) $375 < Q_2 < 475$°C and $475 < Q_3 < 600$°C indicate recalcitrant organic matter and poly-condensed aromatics (Santin et al., 2017) and are referred to as Q_2 and Q_3.

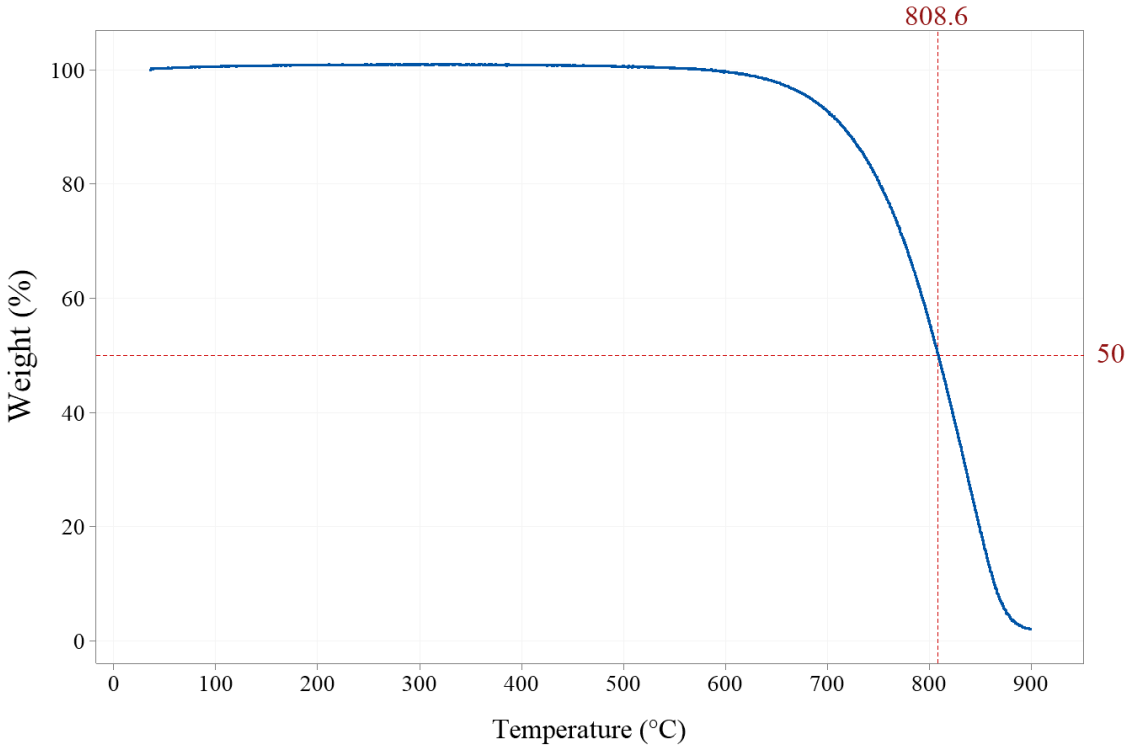


Figure 4-1: Thermogravimetric analysis of graphite in air at a heating rate of 5°C min^{-1} and air flow rate of 50ml min^{-1}. The reference lines highlight the temperature in which 50% of the graphite has been oxidised (T_{50})

4.2.4 Bomb calorimetry

The higher heating value (HHV) of sludge, char and pyrolysis liquids were determined using a Parr 6100 bomb calorimeter (Parr, Illinois) using the standard method ASTM D5865M-19. Prior to sample analysis, the bomb was standardised with benzoic acid which has a HHV of 26.454 MJ kg^{-1}. The samples were then ignited at approximately 25^{o}C in pure oxygen at 30.4 bar. Two ml of water was added to the bomb to capture acidic gases. Char was difficult to ignite, therefore benzoic acid tablets were added to the sample pan to aid ignition. The software automatically corrected the sample HHV, for a given weight of samples and benzoic acid. Each sample was conducted in triplicate.

4.2.5 Combustion testing

4.2.5.1 Char: Ignition temperature

The minimum (dust cloud) ignition temperature (MIT) and layer ignition temperature (LIT) are important process safety parameters and are in the design of industrial processes to prevent the probability of dust explosions (Danzi et al., 2015). SSC-850 obtained from multiple runs was homogenised by mixing and a sample was taken at random. MIT and LIT were determined for this sample by DEKRA Process Safety (Southampton, UK) in accordance with ASTM E1491 and E2021, respectively. For MIT, a dust cloud is dispersed through a heated Godbert-Greenwald tube furnace with air until a flame propagates. For LIT, a 5mm dust layer is heated on a hot plate, ignition occurs when a flame propagates, or the material undergoes a temperature rise of more than 250K above the hot plate temperature.

4.2.5.2 Gas: Lower and upper flammability level

The limits of flammability (LOF) are defined by the UFL and LFL and represent the range of concentrations in which a gas or mixture is flammable. A single 60L fuel-gas mixture was made up by FTI Ltd (Surrey, UK) and sent to DEKRA process safety (Southampton, UK) and tested for UFL and LFL under ASTM E681. Test gas is added to a spherical glass reaction vessel with air in the desire concentration, it is then homogenised and ignited through high-voltage spark ignition (15kV). If outward flame propagation occurs, the gas mixture is flammable.

4.2.6 XPS

X-ray photoelectron spectroscopy (XPS) is an analytical technique for analysing the surface chemistry (≤10nm) of a material. XPS uses low energy X-rays to photoexcite core electrons, this causes them to be emitted and their kinetic energy is measured. The kinetic energy of an electron depends on the photon energy and binding energy of the electron. The binding energy of an electron depends on its respective element, chemical form, and orbital (Lee et al., 2017). Finely milled SSC-700 was analysed with a Thermo Fisher K-Alpha+ spectrophotometer with a monochromatic Al-Kα X-ray source. A Survey spectra in the range 0-1350eV (pass energy = 200eV) was collected, followed by high resolution measurements of Zn (2p), Si (2p), S (2p), P (2p), O(1s), N(1s), Mg (1s), Fe (2p), Cu (2p), Ca (2p), C (1s), Al (2p) core electrons. Spectra were

shifted to the carbon maximum at 284.7 eV and deconvolution was performed with a Voigt line shape, with Shirley background removal in Avantage (v. 5.948) and Casa XPS (v. 2.3).

XPS can quantify the atomic concentration of elements/bonds at the surface of the materials (≤10nm).The underlying assumption for quantitative XPS is that the number of electrons recorded is proportional to the number of atoms in a given state (Casa Software Ltd., 2008).

4.2.7 Inorganic analysis

4.2.7.1 Aqua-regia extractable inorganic elements

The material was ground to <250µm and homogenised so a representative sample could be attained. The sample was dried in an oven at 105ºC until constant weight. Dry samples (~500mg) were weighed into acid washed (10% Nitric Acid) digestion tubes and the samples were ashed at 550ºC for 24 hours. Once cool, concentrated nitric acid (HNO_3) and hydrochloric acid (HCl) were dispensed directly into the digestion tubes in a 1:3 ratio to make aqua regia. A modified USGS (2019) digestion method was used (method 36). Briefly, the digestion tubes were placed into a water bath and digested at 70ºC for 4 hours. The digestion tubes were then removed from the water bath, cooled, filtered to 0.45µm and quantitatively transferred into volumetric flasks. Aliquots were taken from these volumetric flasks and these were analysed directly by ICP-OES (PerkinElmer Avio 500) or diluted prior to analysis. Samples were analysed for P and 23 elements. Analysis of rare earth metal and precious was also conducted. Parallel digestions were conducted using concentrated aqua-regia or nitric acid. However, except Erbium, none of these metals were present within detectable concentrations. The concentration of the elements within the extracts was compared against a 5-point calibration with regression (>0.999) and quantified.

Quality control methods were used for all ICP experiments:

- Samples were tested in triplicate.
- A method blank was used, this was taken through all the steps within the analytical procedure and its concentration was deducted from the sample concentrations.
- Samples were spiked with standard prior to digestion and the recovery rate of the MES was measured. A recovery rate of 95-105% was deemed acceptable. Any lower and the measurement was repeated, or the digestion rerun.
- Detector drift was identified by periodically re-analysing the standard during a run. Issues related to the torch and injector rod which required periodic cleaning through sonication in dilute acid. An internal standard was not used.

Aqua-regia digestion cannot dissolve silicates, these require HF digestion, however this was not conducted due to handling and toxicity issues.

4.2.7.2 Hazardous waste: Leaching tests

EN 12457-2 is used to assess the suitability of hazardous waste materials for landfilling, see the Landfill (England and Wales) (Amendment) Regulations (2005) for more information. It

measures the water leachable inorganic elements within waste materials. NEN 7371 is a Dutch method used for end-of-waste risk assessments (Environmental Agency, 2014) and consists of leaching materials at pH 4 and 7 and is supposed to replicate the worst-case scenario for leaching in the environment (Environment Agency, 2005).

EN 12457-2 requires large sample sizes (<2kg) in a liquid:solid (L:S) ratio of 10:1 whilst NEN 7371 requires high L:S ratios of 50:1. To avoid excessive samples size and excessive dilution a modified methodology was used for both methods, whereby 20g of dry Py-G SSC produced at 800ºC (SSC-800) was mixed with 200ml of RO water (L:S = 10) and shaken at 20rpm in an end-over-end shaker for 24 hours. For EN 12457-2, char and solution were quantitatively transferred to a vacuum filter assembly, filtered (0.45 µm), acidified to 1M HNO_3 to matrix match the standard, and were analysed by ICP-OES. For NEN 7371, the solution was filtered, and its pH determined with a pH meter (Fisher brand Hydrus 500), which was calibrated with a buffer at pH 4, 7 and 9. An automatic pipette was then used to adjust the pH to either pH4 or pH7 with 0.2M NA. The samples were then shaken for 3 hours at 20rpm, quantitatively transferred to a vacuum filtration assembly, filtered, and analysed by ICP-OES. For EN 12457-2, the dry sample was sieved to <4mm, for NEN 7371 the sample was ground with a pestle and mortar and sieved to <125um prior to extraction.

4.2.7.3 Formic acid (2%): Leaching test

The extraction of char phosphorus with 2% formic has been shown to be the most sensitive indicator of P availability in char (Wang et al., 2012) and is an accepted method in the Strubias regulation for assessing the agronomic suitability of char. SSC samples produced at a set temperature were mixed and samples were sub-sampled at random. Approximately 0.5g of this homogenised biochar was mixed with 50ml of 2% formic acid, the mixture was shaken in an end-to-end shaker for 3 hours. The mixture was then; quantitatively transferred to vacuum filtration assembly, filtered to 0.45µm, and quantitatively transferred to a volumetric flask. Serial dilutions were conducted, and the samples were analysed by ICP-OES.

4.2.8 Gas chromatography (GC)

The gas mass fractions were quantified using a Perkin Elmer Clarus 500 gas chromatograph with a thermal conductivity detector (TCD). TCD detectors have two cells and work by measuring the difference in thermal conductivity between the helium cell and sample cell. A Supelco Carboxen 1010 (30m, 0.53mm, 30 µm) column was used for gas separation. This column contains carbon molecular sieves and may separate hydrogen (H_2), carbon oxides (CO, CO_2), light hydrocarbons (C1-C3), oxygen (O_2), and nitrogen (N_2). Helium was used as a gas carrier.

Gas was sampled from the pyrolysis rig in Tedlar bags. Gas tight Hamilton syringes were used to extract between (30-300uL) of gas and inject it into the GC injector. Prior to injection, both the injector and TCD detector were preheated to 230ºC whilst the oven was heated to 35ºC. The oven temperature was held isothermally at 35ºC for 9 minutes and then ramped at a heating rate of 10ºC

min^{-1} to 240ºC. The oven temperature was then held isothermally for a further 6.5 minutes to ensure full elution of the injected gas.

A carrier gas velocity of 25cm s^{-1} was used, meaning carrier gas flow rates were variable throughout the run. The reference and detector gas flow rates were set to 30ml min^{-1}, and the detector was operated in positive mode with a 5.0mV offset.

Long GC run-times (<90 minutes) were used during method development to identify the number of gases present. Nine peaks were found to be present, and these gases eluted in the following order: H_2, O_2, N_2, CO, CH_4, CO_2, C_2H_2, C_2H_4, C_2H_6. Calibration gases were acquired from FTI (Ltd.) and were used to periodically calibrate the GC prior to analysis.

For TCD detectors, H_2 is not typically quantified when a helium carrier gas is used because both gases have similar thermal conductivities (0.18 and 0.15 W mK^{-1} respectively), and the detector response may not be high enough. When tested, the detector response for H_2 was lower than other gases, however given its high concentration it produced large enough peaks and could be calibrated and quantified with reasonable accuracy ($R^2 > 0.995$). The only limitation was that larger volumes of gas had to be injected into the GC, which meant for some samples, H_2 and other gases had to be quantified using multiple injections for a given tedlar bag sample.

4.2.8.1 GC data analysis

Raw data was exported from the GC and analysed in MATLAB using interactive peak fitter software (ipf.m) developed by O'Haver (2018). All the peaks were best fit with an exponentially decaying Gaussian line shape, because of a slight positive skew, which is normal for chromatography data. Most of the peaks were fit with an error <1%. Once fit, the area of the fitted curve was determined, and the output was compared against the calibration to determine "gas mass". Calculating the gas composition from these gases however would not have been accurate because the pyrolysis reactor was purged with nitrogen. This meant that the quantity of N_2 produced during pyrolysis could not be quantified. In addition, the detector did not identify H_2S. To counteract this, several calculations were conducted:

1. The concentration of the analysed gases (wt wt^{-1}) was calculated based on the measured mass of gas (x) and the cumulative masses of the measured gases. For example:

$$(x)\ (\%\ wt) = \frac{\text{Gas wt } (x)}{\sum_{wt}[H_2, CO, CO_2, CH_4,\ C_2H_2, C_2H_4, C_2H_6]}$$

Where (x) is one of the measured gases (e.g. H_2)

2. For each experimental run, the mass of feedstock used, and the mass of both the char and liquids were recorded. Therefore, the mass yield of gas was calculated by difference:

$$Total\ Gas\ (wt) = Total\ Feedstock\ (wt) - \sum_{total\ wt} [char, liquids]$$

3. The N and S concentration within the feedstock, char and liquids was measured by ultimate analysis. Therefore, the mass yield of N and S within these fractions were determined and the mass yield of N and S within the gas were calculated by difference:

$$Gas(x)\ wt = Feedstock(x)\ wt - \sum_{wt} [char(x)\ wt\ , liquids(x)\ wt]$$

Where (x) is the mass yield of N or S

4. Previous research suggests N and S will mostly form N_2 and H_2S, respectively. Therefore, an assumption was made that all gas-phase N and S formed these compounds. In reality, other compounds will form, particularly for N. The mass of gas phase N_2 and H_2S was subtracted from the overall gas mass yield to give the adjusted gas (wt).

$$Adjusted\ gas\ (wt) = Total\ Gas\ (wt) - \sum_{wt} [H_2S\ , N_2]$$

$$Adjusted\ (x)\ (\%\ wt) = (x)\ (\%\ wt) \cdot \text{Adjusted gas (wt)}$$

Where (x) is one of the measured gases (e.g. H_2)

5. The concentration of the measured gases was multiplied by the adjusted gas weight. The output is the N/S adjusted weight for each gas.

6. The adjusted weights for the measured gases (e.g. H_2, CO, CO_2, CH_4, C_2H_2, C_2H_4, C_2H_6) and the weights for N_2 and H_2S were then used to calculate the concentrations of the gases. These calculations provided the concentration (% wt wt^{-1}) of H_2, CO, CO_2, CH_4, C_2H_2, C_2H_4, C_2H_6 adjusted for fuel-gas N_2 and H_2S content. The volumetric concentrations were calculated assuming standard temperature and pressure (0^oC, 1 bar).

$$Concentration\ (x) = \frac{Adjusted(x)\ wt}{Total\ gas\ wt}$$

Where (x) is one of the gases present

4.3 Lab-scale pyrolysis

4.3.1 Mass balances

During pyrolysis, sewage sludge is decomposed into gas, condensable liquids, and char. The overall mass balance for the process was therefore calculated as:

$$Total\ Feedstock\ (wt) = \sum_{total\ wt} [char, liquids, gas]$$

For the condensable liquids, the whole of the condensation train had to be weighed prior to and after pyrolysis. This included all the borosilicate traps, condensers, and connecting joints. After an experimental run, traps were cleaned with acetone and the condenser and connecting joints were fired in a furnace at 600ºC to ash or evaporate any liquids present. Therefore, spares of all the condensers and connecting joints were readied so that the condensation stream could be rapidly reconstructed following a run. Therefore:

$$Total\ liquids\ (wt) = \ Condensate\ train\ (Dirty\ Wt) - Condensate\ train\ (Clean\ Wt)$$

The gas mass fraction was measured by difference:

$$Total\ Gas\ (wt) = Total\ Feedstock\ (wt) - \sum_{total\ wt} [char, liquids]$$

4.3.2 Slow batch pyrolysis

Slow batch pyrolysis (Py-B) was conducted within a Carbolite 11/600 laboratory-scale rotary furnace (Carbolite, UK). The furnace is insulated with vacuum formed calcium silicate with embedded heating elements and a heated length of 53cm. A central void provides space for a thermocouple and quartz reactor (with a fluted internal surface, to aid mixing). The quartz reactor (1L capacity) was weighed, loaded with approximately 300g of dried sample, reweighed, and placed within the rotary furnace. The furnaces thermocouple was embedded within the void space and the desired heating rate and highest heating temperature are set using a controller. When operational, the rotary furnace was continuously purged with N_2 gas, which flowed into the reactor through an injection arm. The gas flow-rate was adjusted with a flow meter and was always operated at 10ml min^{-1}. The outlet arm of the quartz reactor was placed within a borosilicate condensate trap and sealed with a nitrile gasket and grease. The condensate trap comprised a single-stage 2L borosilicate vessel and lid. To aid distillation, a quick fit Vigreux column was placed atop the lid. The volatiles rapidly condensed within the trap because of the low temperatures in which they were generated, and the gases were vented to the fume cupboard.

Because of devolatilisation reactions occurring at low temperatures (predominately <500°C), the condensable liquids were removed with relatively high efficiency however some entrained vapours escaped with the gas. An illustration of the process is shown in figure 4-2.

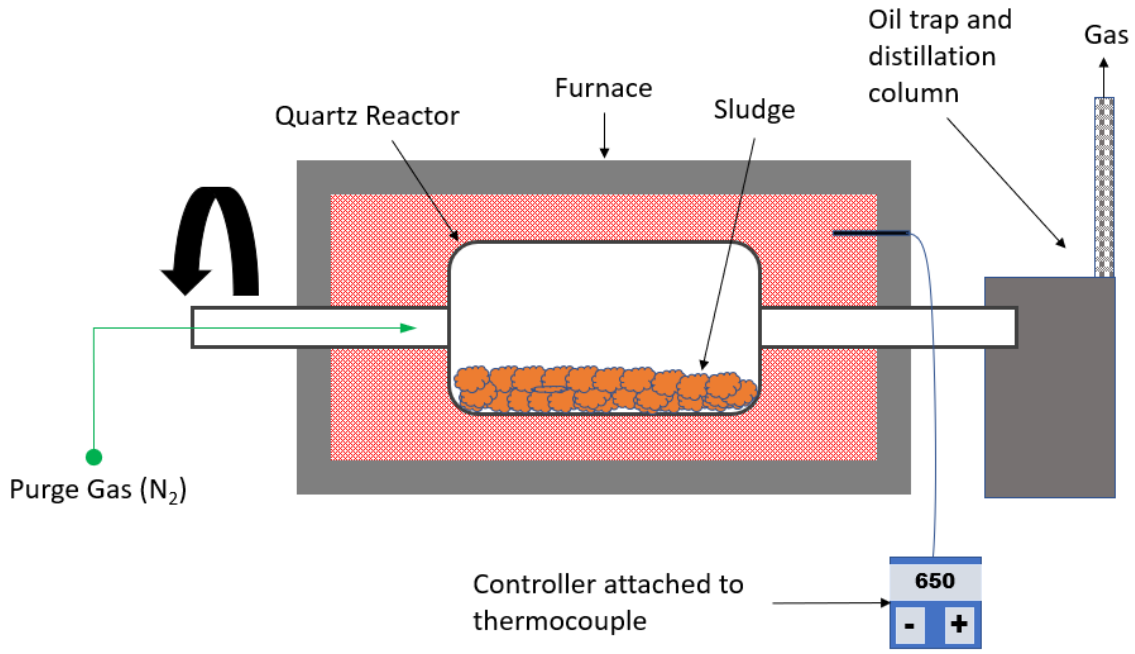


Figure 4-2 – Experimental setup for slow batch pyrolysis (Py-B)

Once fully assembled, the quartz reactor was rotated at a speed of 10rpm, and the furnace was heated at 10°C min^{-1} to its desired highest heating temperature (HHT) with an overall dwell (t) of 90 minutes. The experimental conditions used are summarised in table 4-1.

Table 4-1: Slow batch pyrolysis (Py-B) experimental conditions

HHT (°C)	Ramp (t)	Hold (t)	Dwell (t)
450	43	47	90
500	48	42	90
550	53	37	90
600	58	32	90
650	63	27	90
700	68	22	90
750	73	17	90
800	78	12	90
850	83	7	90
900	88	2	90

4.3.3 Pyrolytic gasification plant

Pyrolytic gasification (Py-G) was conducted within a bespoke reactor that was designed and constructed during this PhD project (Chapter 5). A standard operating procedure (SOP) was written for the safe operation of the machine, which involves very specific steps that will not be fully detailed within this thesis. However, further health and safety information is provided in appendix 1.

The reactor was pre-heated under a continuous nitrogen purge to the target temperature (600-1000ºC) and held isothermally for two hours, to ensure the mid-sections between furnaces 2/3 and furnace 1 reached thermal equilibrium. Meanwhile conveyors A and B were switched on to ensure any residual char or soot had been removed from reactors 2 and 3. Any collected residues were discarded.

A pre-weighed quantity of feedstock was loaded into the empty feed hopper and the lid secured with a nitrile gasket, grease, and clamps. The clean condensate train was weighed, assembled within the fume cupboard, and attached to the gas outlet with quick-fit connections. The char trap was placed onto the char outlet, sealed, and secured. The feedstock was then continuously fed into the process until gas production ceased and the fuel had been exhausted. The process was then left under a nitrogen purge until the gas within the condensers had been fully purged and the exhaust gas was clear, this typically took 30 minutes. The conveyors were also left operating to ensure all the char had been removed. The char outlet valve was closed, the trap removed, and the content of char within was weighed. The condensation stream was then disconnected, and the assembly was weighed so that the weight of the condensed liquids could be calculated in accordance with section 4.3. The mass yield of gas was calculated by difference.

For the mass balance, it was essential to achieve high recoveries of the condensable liquids stream. The condensation stream consisted of three steps:

1. Gas entered a spherical borosilicate trap; the shape of the trap encouraged the gas to spread outward across the walls and deposit condensable liquids such as tars. The gas left the trap via a Liebig condenser, which was cooled with recirculated water supplied by a chiller outside of the fume cupboard.

2. Gas entered a finger trap which was jacketed and filled with dry-ice.

3. Gas entered a trap through a Graham condenser, which was cooled to 4ºC with chilled water supplied by an external chilled. The gas was vented at the bottom of the trap to discourage gas stratification. The gas moved upwards out of the trap and a valved sampling point was used to collect gas in a Tedlar bag. The gas then moved through a Vigreux and Cynder column, which were used to encourage volatile-solid contact which encouraged condensation. The gas was then vented to the fume cupboard below 35ºC.

Inside the Cynder columns there were hollow borosilicate balls, which had to be lifted by the gas pressure prior to venting. This meant that the pressure within the traps constantly cycled between atmospheric and a slight positive pressure, which further slowed gas velocity through the condensation stream. In reality, the column vented the gas in continuous pulses as the balls rapidly lifted up and downwards. Notice that the trap also had a Cynder column, however, this was slightly longer, which meant more pressure was required to lift the balls. Negligible quantities of gas escaped from this column because the preferential pathway was through the shorter Cynder column. However, it acted as a failsafe in case of a tar blockage downstream.

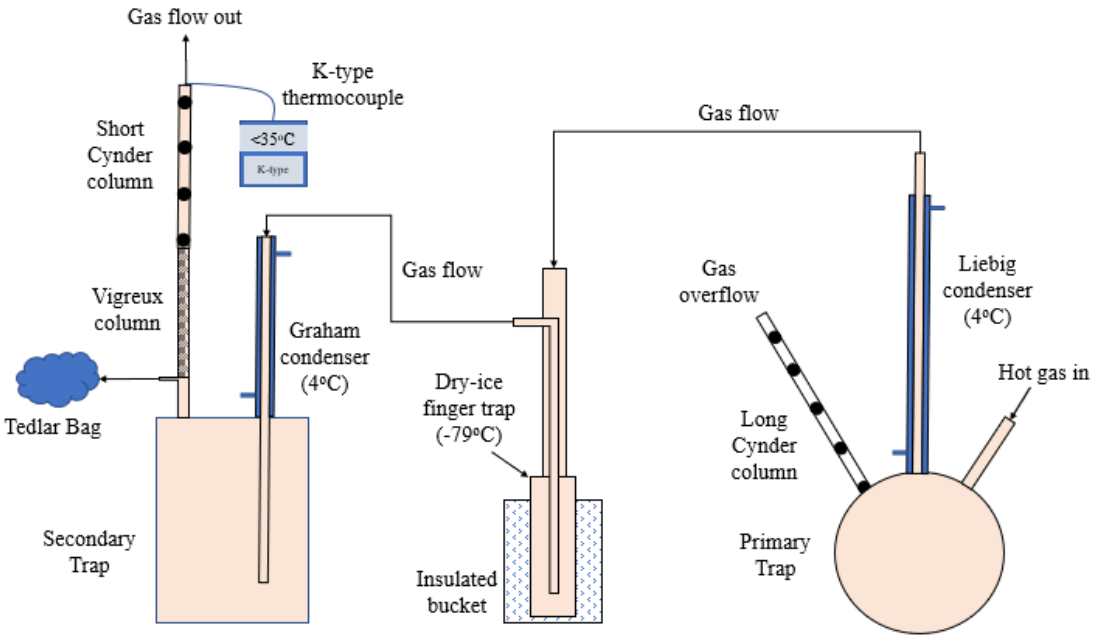


Figure 4-3 – Pyrolysis liquids condensate train

Dried sludge fed into the Py-G reactor immediately generated gas which displaced the nitrogen gas within the condensate train. After 10 minutes of pyrolysis gas feeding into the condensate train a valve was opened between the second trap and 1 litre Tedlar bag. Because of the slight positive pressure within the traps, the Tedlar bag rapidly inflated (5-10 seconds). Once inflated, the valve was shut, sealing the gas within the Tedlar bag. It was then immediately sampled with a gas syringe and analysed by GC-TCD.

4.3.3.1 Pyrolytic gasification: Parasitic load

Furnace 2 was attached to an extension lead, whereby the live wire was looped and separate from the neutral and earth. The insulated live was clamped with an ampmeter (Kewtech KT200 digital AC clamp meter) and its current was measured. The furnace was fed under isothermal conditions for 30 minutes before a reading was observed. The amps were then measured for 10 minutes. Unfortunately, a data collector was not available, therefore the reader was filmed, and the individual frames had to be manually recorded to work out the total current consumed. Furnace 2 power consumption was then calculated, based on the following equation:

$$Power\ (Watts) = Current\ (Amps) \times Voltage\ (V)$$

Supply voltage: 230V

4.4 Extraction experiments

Phosphorus (P) fertiliser production is currently conducted by acid leaching phosphate minerals with sulphuric acid (H_2SO_4) or nitric acid (HNO_3) to directly produce phosphate salts or produce phosphoric acid (H_3PO_4), which can then be upgraded to phosphate salts. Acid leaching experiments for H_3PO_4 production were investigated with H_2SO_4, HNO_3, and hydrochloric acid (HCl).

4.4.1.1 Experimental design

The fractional-factorial design was generated in Minitab 19 to investigate the influence of five extraction factors, including: acid contact time, extraction temperature, acid concentration, particle size and the stoichiometric ratio, on the extraction of elements from SSC for each acid. For each factor, two experimental levels (-1, 1) were investigated with a mid-point (0), except particle size, where a mid-point was not used. The design had a resolution of "V" which meant that no main effects or 2-factor interactions were aliased with one another. The design required each experimental condition to be run in duplicate across two experimental blocks, meaning 40 runs were conducted for each acid. The experimental factors, the levels tested and the combination of experimental factor levels for each run are summarised in table 4-2.

4.4.1.1 Experimental procedure

SSC produced at 800ºC was homogenised and sub-samples were taken by corning and quartering. Half of the sub-samples were milled with a pestle and mortar and sieved to a <500µm particle size, the other half was sieved to 5mm and required no particle size reduction. Char samples were loaded into centrifuge tubes with 30ml of extractant and a variable quantity of SSC. The sample weights for each experimental run depended on the stoichiometric ratio, acid concentration and char phosphorus content. The P in SSC was assumed to be present as hydroxyapatite (HAP) - $Ca_{10}(PO_4)_6(OH)_2$. Based on this, it required 3.3 moles of acid normality [N] to produce each mole of H_3PO_4.

Experimental runs that were tested with elevated stoichiometric ratios, required lower sample weights. Conversely, runs that required elevated acid concentrations required higher sample weights. The char-acid solutions were placed in a water bath (Grant OLS Aqua pro) and shaken at the desired temperature and shaking speed. The solution was then centrifuged (Thermo Scientific Heraeus Megafuge 16) at 4000 for 10 minutes. The solution was then quantitatively transferred to a volumetric flask and filtered to 0.45µm prior to analysis by ICP-OES for P and 23 other elements. The extraction efficiency for each element was calculated by dividing the recovered elemental mass by the aqua-regia extractable elemental mass.

Table 4-2: Resolution (V) fractional-factorial experimental design. Generated in Minitab (v18.1) for the SSC extraction experiments with H_2SO_4, HCl and HNO_3

Factors	Units	Coded Symbol	Low level (-1)	Centre point (0)	High level (+1)
Contact-time	Hours	A	2	13	24
Temperature	°C	B	20	30	40
Acid concentration	[N]	C	0.2	1.1	2
Particle-size	mm (max)	D	<0.5mm	-	<5mm
Stoichiometric ratio	ratio	E	1	1.25	1.50
Block design	A	B	C	D	E
1	-1	-1	-1	-1	1
2	1	-1	-1	-1	-1
3	-1	1	-1	-1	-1
4	1	1	-1	-1	1
5	-1	-1	1	-1	-1
6	1	-1	1	-1	1
7	-1	1	1	-1	1
8	1	1	1	-1	-1
9	-1	-1	-1	1	-1
10	1	-1	-1	1	1
11	-1	1	-1	1	1
12	1	1	-1	1	-1
13	-1	-1	1	1	1
14	1	-1	1	1	-1
15	-1	1	1	1	-1
16	1	1	1	1	1
17	0	0	0	0	-1
18	0	0	0	0	1
19	0	0	0	0	-1
20	0	0	0	0	1

Chapter 5: Design, construction, and operation of a laboratory scale pyrolytic gasification plant

This chapter and sub-sections describe; the rationale for build a laboratory scale pyrolysis rig, an explanation of its mechanical principles and the design considerations taken.

5.1 Laboratory Scale Pyrolysis

To investigate continuously-fed sludge pyrolysis a laboratory scale pyrolysis plant was designed, assembled, and operated. The plant was designed with guidance and feedback from project stakeholders and replicates to an extent the design features of the proposed demonstration-scale pyrolysis plant at Crossness STW. The project stakeholders involved in the design include: bulk handling specialists, Ajax Equipment Ltd and Utility Company, Thames Water Utilities Ltd. Other suppliers used include: furnace manufactures, Carbolite-Gero Ltd; frame manufacturer, KJN Aluminium Profiles Ltd; drive manufacturer, SEW Eurodrive GmbH & Co KG; automation specialist, APAC Automation Ltd; Vibration Control specialists, Mason UK Ltd; electricians, JD Electrical Services, and others. Figure 5-1 shows the system design:

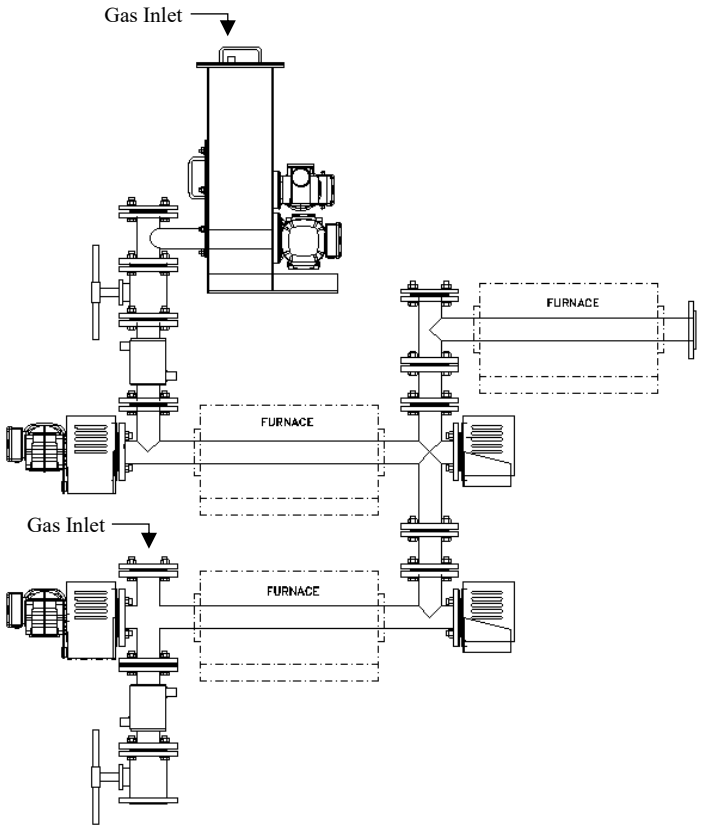


Figure 5-1: Simplified drawing of laboratory-scale pyrolysis plant

5.1.1 Feed Hopper

The capacity of the pyrolysis plant feed hopper is 40L or 22.4kg of dried sewage sludge. The feed hopper has a removable lid, to facilitate re-filling during gas production the feed hopper can be isolated from Conveyor A with a gas tight ball valve. A ¼ inch BSPP gas inlet in the feed hopper and feed pipe allows continuous purging of the feed hopper during operation, preventing build-up of pyrolysis gas in the hopper during operation. The feed hopper is bolted directly to the aluminium frame and coupled to conveyor A via 316L stainless steel piping and a flanged nitrile rubber expansion bellow (supplied by FLEXEJ Ltd.) to prevent axial, lateral, and angular strain between the feed hopper and the hot zones. The feed hopper contains a feed screw, designed to deliver dried sewage sludge (<6mm) with a bulk density of approximately 560 kg m^{-3} at a rate of upto 10 kg hr^{-1} and an agitator to prevent the material bridging the feed screw and causing blockages (see figure 5-2). The agitator and the screw are driven by 415v 3ph helical-worm gear motors at a frequency of between 5-60 Hz. Each motor has a dedicated Movitrac B frequency inverter which controls output speed and is interfaced with a FBG11A keypad or using MOVITOOLS Motion Studio (via Ethernet). Dried sewage sludge driven by the feed screw drops into Conveyor A under gravity.

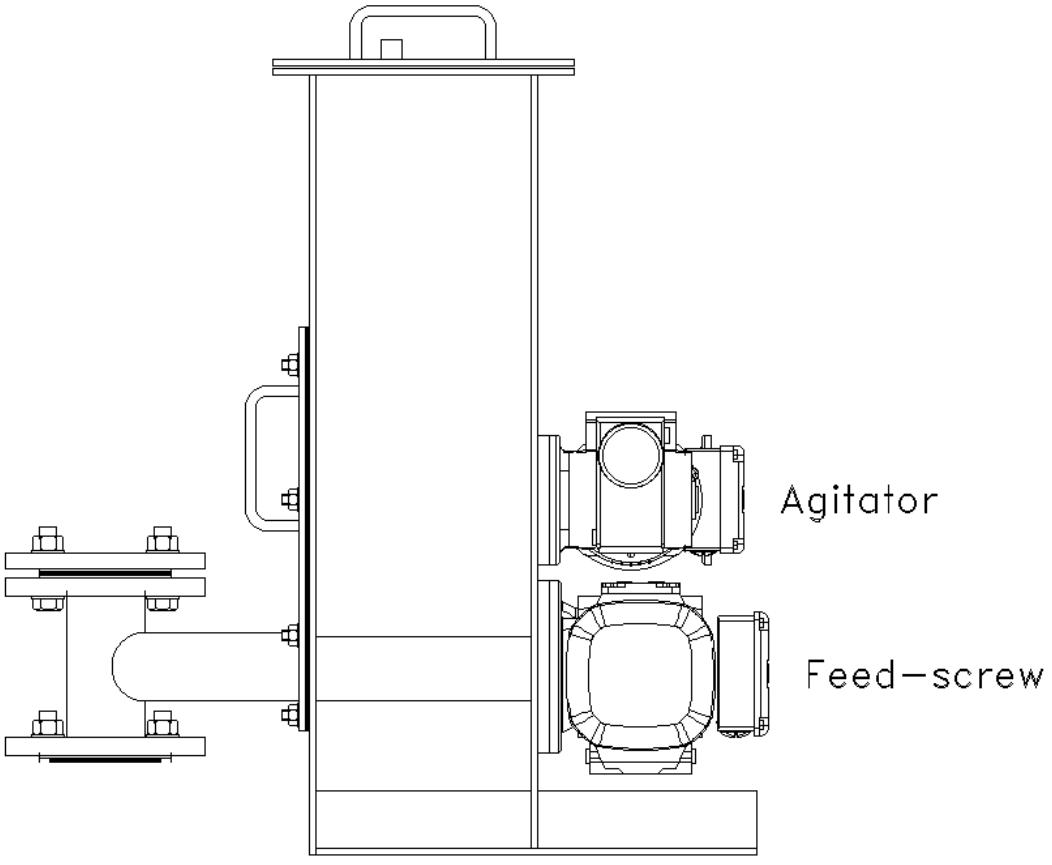


Figure 5-2: Simplified drawing of the laboratory-scale pyrolysis plant feed-hopper.

5.1.2 Hot-zones

Dried sewage sludge entering Conveyor A is transported through furnace 2 where initial thermal decomposition occurs. Solids comprising char, inorganic compounds and a small quantity of condensed tars move onto conveyor B via gravity whereby further thermal decomposition occurs, these are then ejected (via gravity) and are collected in a borosilicate trap. A nitrile gasket, grease and clips were used to interface the steel outlet flange and glass trap. To prevent leaks, it is important the trap is correctly centred. To prevent ignition, the char trap is thoroughly purged with nitrogen prior to operation, and the char is left to cool before the trap is removed from the rig and exposed to oxygen.

Hot gases and volatiles tars are transported from furnace 2/3 to 1 by pressure gradients. The hot-gases exited furnace 1 via a stainless (316L) expansion bellow and stainless (316L) pipe all of the pipework was directed downwards towards the traps to minimise potential blockages. The expansion bellow and elbow joint between the bellow and pipe were insulated with basalt wraps to prevent excessive heat losses. The gas passed through a borosilicate trap and condenser assembly where the tars condensed, and the gases were vented into an ATEX rated fume cupboard at <50ºC and are quickly diluted to below <0.3% v/v. The thresholds stated are below the auto-ignition temperature and lower explosion limit (LEL) for all major gases produced. The temperature within the borosilicate trap and at the gas outlet to the fume cupboard was monitored with a K-Type thermocouple and a dual channel thermometer.

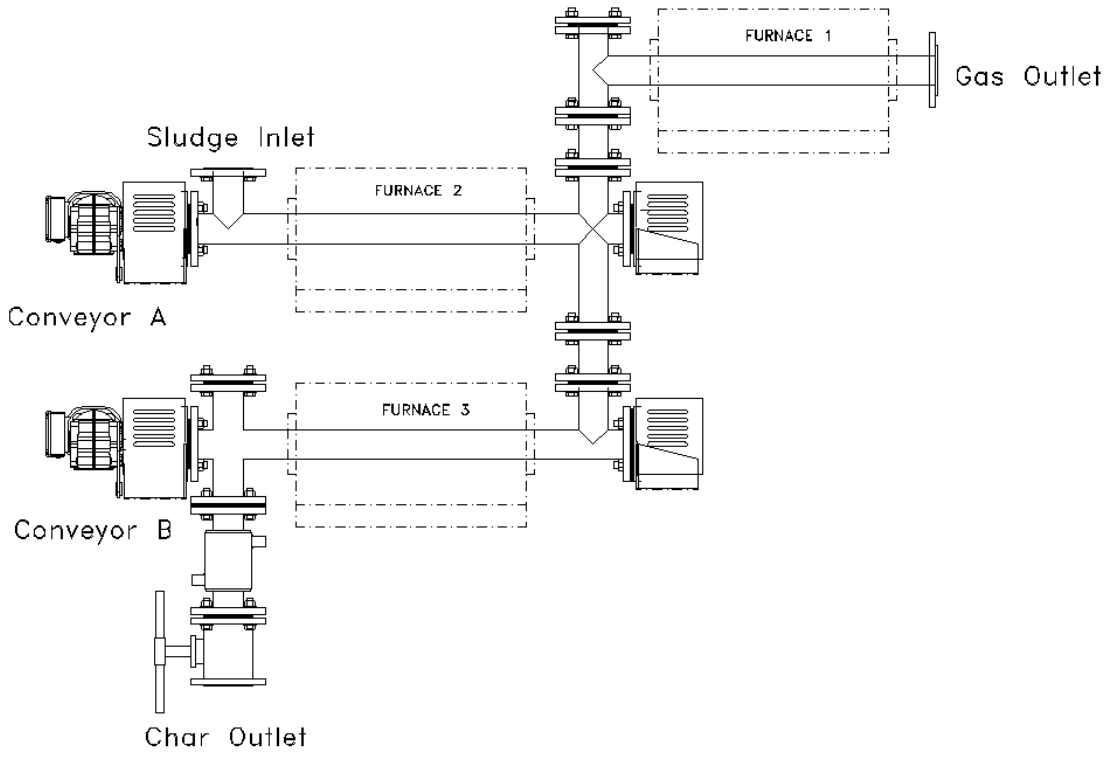


Figure 5-3: Simplified drawing of the hot zones, showing furnaces 1-3, conveyors A-B, and the inlets and outlets.

All of the furnaces have built-in controllers whilst Conveyors A-B have dedicated gear motors, frequency inverters and controllers (operated between 5-60 Hz). Nitrogen purge gas and gasification reactants (carbon dioxide or steam) are fed through a 1/4" BSPP inlet counter-current to the incoming char (figure 5-3).

5.1.3 Drives and electrics

The gear motors, frequency inverters and controllers were supplied by Sew-Eurodrive GmbH & Co KG, table 5-1 summarises the parameters, full technical specification are available online.

Table 5-1: Gear motor technical summary

Drive	Supply	Power	Location	Serial No.[1]
1	415v 3ph	120W	Agitator	30.7649148302.0001.18
2		180W	Feed Screw	30.7649148301.0001.18
3		250W	Conveyor A	30.7649148303.0001.18
4		250W	Conveyor B	30.7649148304.0001.18

[1]See "productid.sew-eurodrive.com" for full technical specifications.

The motor control panel has the following components: 4 x Frequency Inverters, 4 x Adjustable 0.8A electrical overloads, 1 x Electrical Isolator, 1 x 6A circuit breaker, 1 x 32A Plug and supply cable (3ph, 415v). The electrical components were supplied by RS components and were installed by APAC Automation and JD Electrical services. To prevent the motors drawing excessive current and overheating (e.g. in the event a blockage), the adjustable overloads were set to just above the current required under normal loading. Frequency inverters are incompatible with residual current devices, due to high earth leakage (approximately 11.5 mA per inverter). To reduce the risk of electrocution, equipotential bonding conductors were installed onto the frame of the rig and surrounding metal work, including: high level pipework, the fume cupboards, air ducts, light fixtures, and cable trays. The MCPD components are IP2X rated, to prevent ingress of solid particles (>12.5mm) and are "finger-safe", however an enclosure was constructed from acrylic to provide further protection.

To prevent heat transfer from the hot-zones to the gear motors, the shaft length was increased and minimal contact between the screw-shaft and gear shaft was maintained. The screw shaft is sealed with Pilot Pack 8511 packing (temperature rating – 700ºC). The packing can be tightened by adjusting the tension on a gland packer, in accordance with the SOP.

5.1.4 Heating

Three HZS 12/450 (220-240v, 1ph) split-tube furnaces, 3 x Pairs of slave controllers and 3 x digital over-temperature protection were supplied by Carbolite Gero Ltd. Each furnace had a heated length of 45cm with free radiating wire elements embedded within vacuum formed calcium silicate insulation. Each furnace contained three heating zones with individual thermocouples, although they were set isothermally, the end-zones drew additional current to account for additional heat loss and provide a constant temperature. The furnaces have a maximum operating temperature of 1200°C; however, they were not operated above 1000°C and the over-temperature was set to 1005°C.

5.1.5 Pipework

The hot-zone pipework and conveyor screws (figure 5-3) are constructed from 310 stainless steel whilst the feed hopper, water-cooled chutes, ball valves, gas outlet hose and outlet pipework were constructed of 316L stainless steel. Both 310 and 316L stainless steel grades are suitable for high temperature applications (up to 1135°C and 870°C respectively). Both alloys have elevated concentrations of nickel and chromium (see table 5-2), the former increases ductility, high temperature strength and resistance to carburisation and nitridation.

Table 5-2: The composition of 310 and 316L stainless steel

Element	310 Stainless steel[1] Wt%	316L Stainless steel[2] Wt%
Carbon	<0.25	<0.03
Chromium	25	16-18
Nickel	20	10-14
Molybdenum	n/a	2-3
Manganese	<2	<2
Silicon	<1.5	<1
Phosphorus	<0.045	<0.045
Sulphur	<0.03	<0.03

[1]Austral Wright Metal (2008)

[2]AZoM (2004)

The feed-hopper and char-outlet have gas-tight 316L ball valves with PTFE seals (temperature rating – 180°C). The integrity of these valves is safety critical since they allow the machine to be quickly isolated if a leak occurs. To protect the valves from excessive heat, water-cooled jacketed chutes were installed and the temperature is controlled at 20°C. The flanged connections were sealed with high temperature 'Klinger Milam PSS' mica gaskets (temperature rating – 900°C) in the hot zones and nitrile rubber gaskets in the cold zones (e.g. feed-hopper and char outlet). Due to thermal cycling the bolts were periodically re-tightened to minimise the risk of leaks.

To reduce heat losses and to provide personal protection the pipework outside of the furnaces was insulated with both basalt fibre (temperature rating - 982ºC) and glass fibre (temperature rating – 648ºC) exhaust wraps (supplied by Nimbus Motorsports Ltd).

5.1.5.1 Pipework Supports

The feed-hopper is directly bolted to the aluminium frame and physically isolated from expansionary forces in the hot-zones by an Elaflex nitrile flanged expansion bellow (temperature rating – 90ºC). The allowable static range of movement for the expansion bellow is 50mm axial, 30mm lateral and 30º angular (FlexEJ, 2019). For the hot zones linear thermal expansion and twisting (a result of differential expansion) had to be accounted for, as a result the pipework was hung from spring loaded roller hangers in three locations. The configuration at each location is shown in figure 5-4.

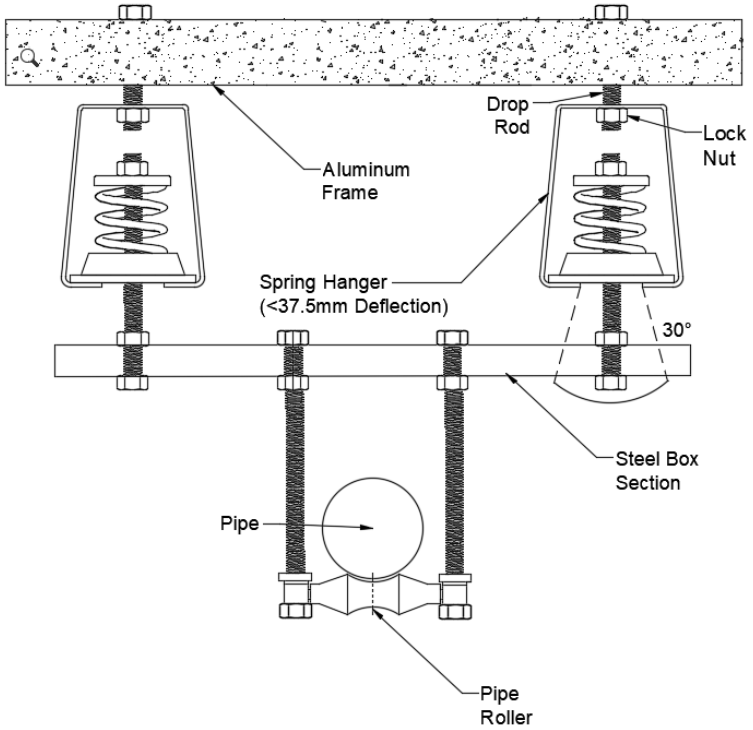


Figure 5-4: Expansion joints: Facilitating vertical, horizontal, and differential expansion (e.g. twisting). Drawing not to scale.

Unlike the pipework, the furnaces were supported by the frame. So, the pipework was free to move within the furnaces, however the calcium silicate plugs on the ends of the furnaces were cut to approximately the same diameter as the pipe, so as to restrict vertical movement to within several millimetres. Before operating the furnaces, the pipework was levelled by adjusting the bolts on the drop rods.

In order to calculate the size of the springs required, the loads on the supports and frame needed to be considered. The loading and shear force diagrams for the rig are shown below (Figure 5-5). The largest load on an individual support (e.g. 2 springs) was approximately 1kN, as a result

springs were chosen with an overall deflection range of 37.5mm (at 20N/mm). The combination of partially deflected spring hangers and pipe roller hangers allows for both horizontal and vertical expansion.

The drop rod on the spring was also free to swing ±15° in any direction, which helps accommodate differential expansion and associated twisting. The springs were supplied by Mason Industries Inc. whilst the cast-iron pipe rollers were supplied by Globe Pipe Products Inc.

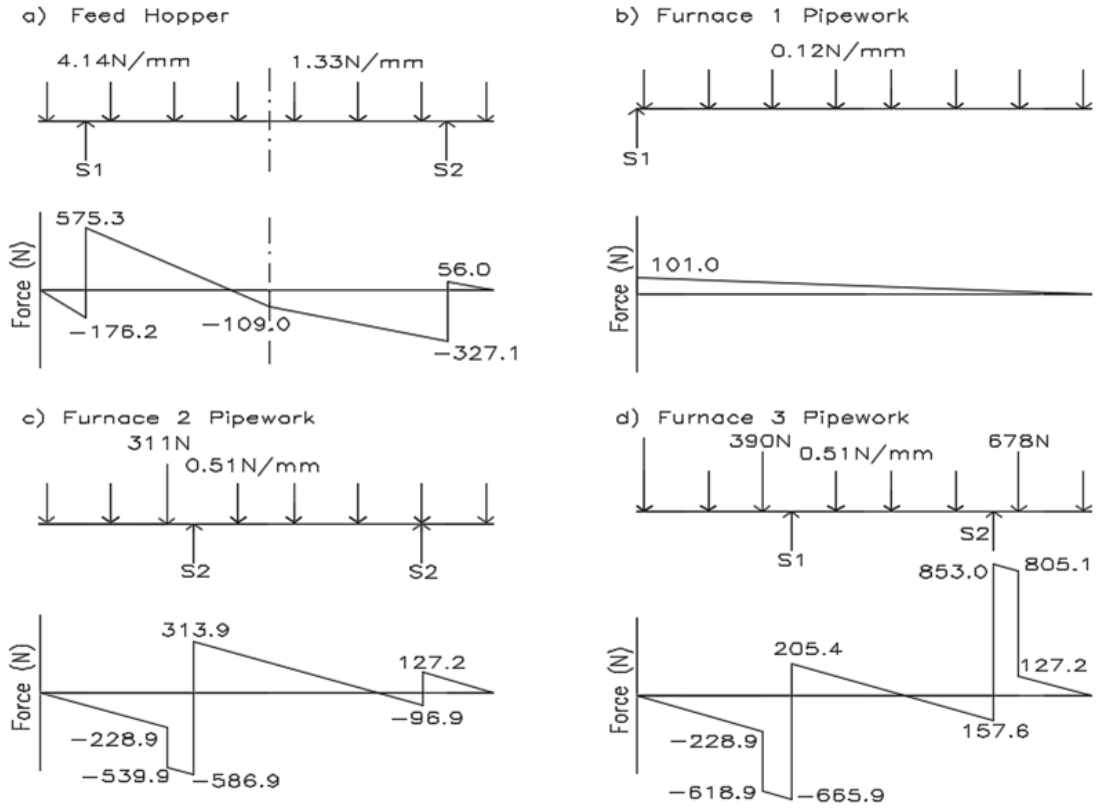


Figure 5-5: Loading and shear force diagrams for the pyrolysis rig. The y-axis is the force in newtons and the x-axis is the length across the beam. S1 and S2 indicate where the beams were supported. Individual point loads are also shown.

The hot-gas and volatile tar was transferred from furnace 1 to a borosilicate trap by a 316L pipe. To prevent the transfer of expansionary forces and possible breakages at the steel-borosilicate interface a flexible stainless steel hose was placed between the outlet of furnace 3 and the stainless pipe. Both sides of the flexible pipe were fixed so that movement was isolated to the hose itself rather than being passed through the steel-borosilace interface.

5.1.6 Frame

The frame was manufactured by KJN Automation Ltd based on the provided specifications. The frame is constructed from extruded aluminium profile, the furnaces rest on sheet aluminium and the frame itself is mounted on lockable castors that allow the rig to be moved. The columns run the full height of the frame, therefore the frame had to be fully constructed before the pipework

and furnaces could be moved into position. Individual parts of the pipework were lifted into position using an overhead crane (see figure 5-6) the furnaces were then slotted around the pipework. On reflection, a modular design for the frame where each level was fully constructed (frame + pipework + furnace) prior to the construction of the next would have been easier to assemble.



Figure 5-6: Assembly of the pyrolysis rig, showing use of an overhead crane to position sections of the pipework into place.

5.2 Operational Experiences

5.2.1 Leaks

Extensive testing over two years of operation showed that gas leaks mainly occurred from the removable lid on the feed hopper and the gland packer bolts and shaft packing on conveyor A. If the reactor is not purged during operation, backflow of carbon monoxide can occur. To avoid this, adequate purging should always be conducted during gas production. To minimise leakage, the following should be noted:

- The feed-hopper lid gasket is prone to creep relaxation. Care should be taken to fasten the lid with even torque and if signs of gasket stretching occur, it should be replaced.
- The shaft-packing should be routinely tightened under AJAX instructions.
- The bolt holes used to tighten the shaft-packing were not drilled blind during manufacture. Therefore, leakage from the reactor via the packing bolts is theoretically possible. To mitigate this, the holes were plugged with grease and the bolts were checked for leaks with soapy-water every-time the reactor was run.
- A rapid response CO or H_2S monitor should be worn at all times, and the operator should not leave the reactor when it is feeding sludge. If leaks occur, it's imperative to stop the machine feeding to prevent further gas generation.

Generally, leaks were not an issue, however there was some down-time, especially in 2020, caused by a blockage in the outlet of the expansion bellow. The blockage was difficult to locate,

however it consisted of a large clump of bitumen-like material which had to be chiselled out of the bellow outlet.

5.2.2 Reactor carbon stability

Carbon was deposited within furnace 1, on the flange face-plate between furnace 1 and the expansion bellow, and within the inlet and outlet of the expansion bellow. Figure 5-7 and figure 5-9 show that carbon was deposited within furnace 1 (F1). The carbon within this zone ranged from dull fine grey/black powder to shiny deposits of porous black carbon, which appeared to be the fixed carbon structure left behind when deposited tar had been carbonised.

Figure 5-8 shows the outlet flange of furnace 1, which was located approximately 15-20cm outside of F1. The pipework in this area was relatively well insulated compared to other pipe-work however, it was an area of intense heat loss. Figure 5-8 shows that the internal diameter of the F1 outlet pipework was entirely bridged with carbon, this bridge comprised a thin friable porous deposit of dull grey/black carbon that did not block gas-flow. Figure 5-8 also shows that on the cooler flange face between the outlet hole and the raised rim where the gasket is placed, there is a layer of shiny black carbon. The properties of this carbon were different to the carbon recovered from the internal diameter of the pipework.

The deposit was not-friable; it was hard and had a slight aroma of tars which suggests it is a composite material formed from soot and condensed tars.

Figure 5-7 shows carbon that was deposited within the inlet of the expansion bellow, this material consisted of fine dull grey/black powder and had no smell. The blockage that occurred within the expansion bellow occurred at the outlet, however, its appearance was entirely different. It comprised a hard, slightly spongy, bitumen-like material that smelled strongly of tars. Like the hard deposit formed on the flange face in furnace 1, this material is thought to be a soot-tar composite. The deposit was difficult to dislodge and upon removing it with a hammer and chisel did not break-up due to its spongy texture. Unfortunately, a picture of this material was not collected.

The outlet of the expansion bellow was connected to a long horizontal stainless-steel pipe, this pipe was angled slightly downwards to aid in the drainage of any condensed tars. The pipe was bent at a right angle and entered a borosilicate glass trap vertically. Occasionally, the morning after running the machine, a large drop of thick, highly viscous, pitch-like material had formed and was dripping into the first trap. Although a picture of this phenomena was not taken, it resembled the coal pitch in figure 5-11 and the tar recovered from trap 1. It should be noted that none of the outlet pipes other than the expansion bellow outlet ever suffered from blockages or an excessive build-up of pitchy-tars.

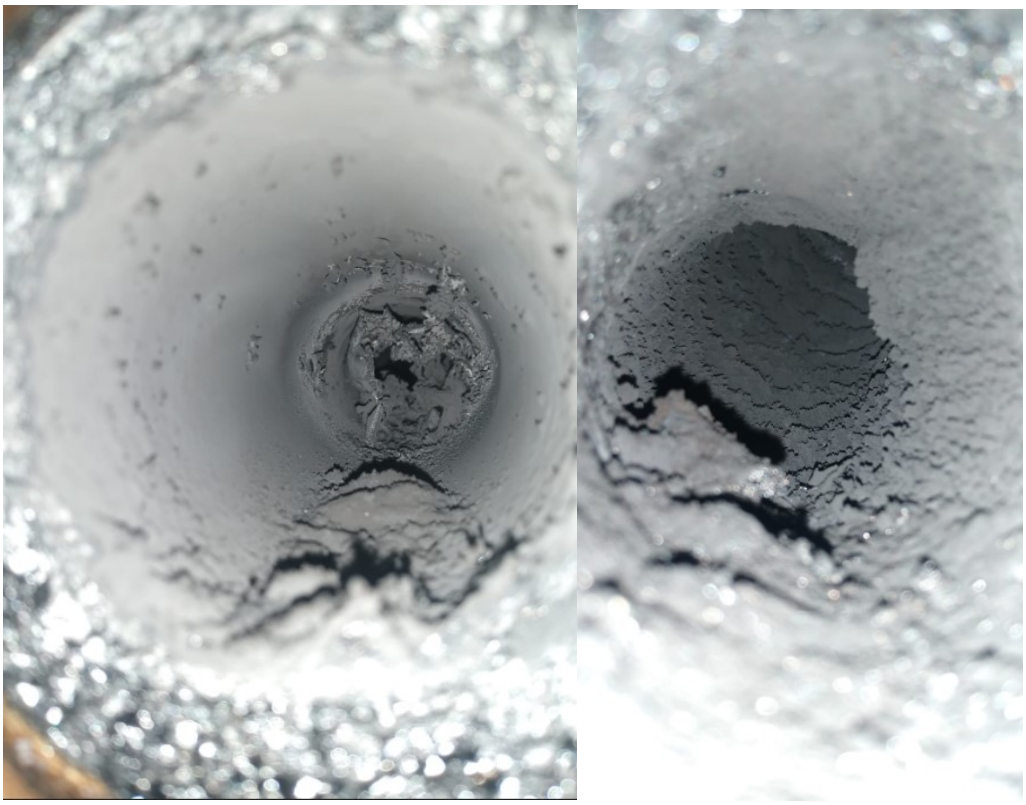


Figure 5-7: Carbon deposits within furnace 1 (left) and the expansion bellow inlet (right). The expansion bellow is attached to the outlet of furnace 1 and exhausts the hot-gases.

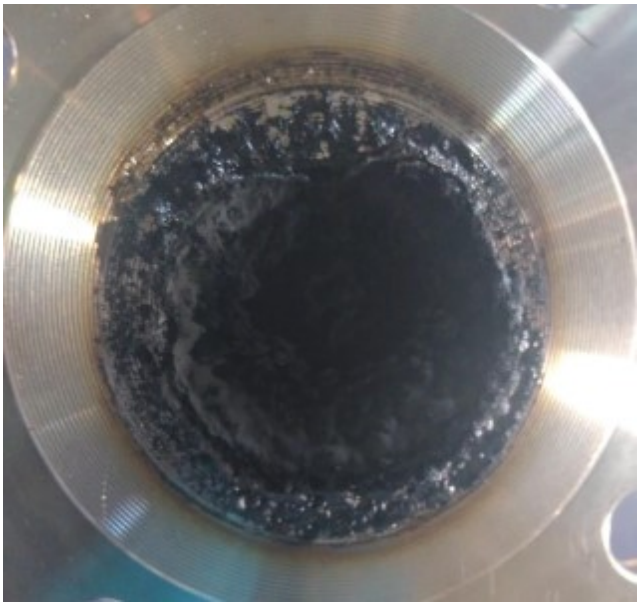


Figure 5-8: Carbon deposits on the outlet flange of furnace 1, the internal diameter of the pipe was fully bridged with a thin friable porous layer of carbon that did not block gas-flow.



Figure 5-9 – Soot structures recovered from inside furnace 1 (F1) showing the porous shiny black carbon that faced outwards into F1 and the silvery carbon that adhered to inside wall of furnace 1, the silvery-colour is highly indicative of graphitisation. These samples were highly friable.



Figure 5-10: Soot structures recovered from the inside of the expansion bellow inlet and flange face of furnace 1 (F1). The carbon was typically thicker, less friable and harder than the carbon recovered from inside F1 it also had a slightly tarry odour.



Figure 5-11 – Long-term pitch-drop experiment at Trinity College Dublin (Webb, 2014) (Johnston, 2013)

Carbon deposits were a common problem in the outlets of coal carbonisation retorts and required routine removal. Initially this was conducted manually, however Lewes (1912) suggested that baking the retorts with air and steam was effective at removing the deposits. Samples of these carbon deposits were heated in a thermogravimetric analyser in air at a heating-rate of 5°C between 20-800°C. Table 5-3 summarises the temperature required to decompose 50%, 80% and 95% of the material (e.g. T_{50}, T_{80}, T_{95}).

Table 5-3: Thermal stability of carbon deposits in air, sampled from within reactor 1 and the inlet of the expansion bellow which vents gases out of furnace 1.

Material	T_{50}	T_{80}	T_{95}	Loss on ignition (at 800°C)
Expansion bellow inlet-carbon	519°C	560°C	603°C	96%
Furnace 1 Internal-carbon	556°C	606°C	724°C	96%

Table 5-3 suggests that commercial pyrolysis reactors processing sewage sludge could rapidly remove the majority of carbon deposits from within the reactor and gas ascension pipes by heating the material to approximately 556ºC in air. However, to rapidly remove 95% of the carbon deposited temperatures up to approximately 724ºC may be required. A routine maintenance protocol is recommended whereby feeding is halted and air (and possibly steam) is injected into the reactor to burn-off deposited carbon. Alternatively, the gas could be continuously reformed to eliminate soot and vapour-phase tars from the gas. The carbon deposits appear to transition from: (i) soot, to (ii) soot-tar composites, to (iii) pitch-like tertiary tars. This is likely because soot was immediately deposited by gravity whilst tertiary tars condensed out more as the gas cooled. These materials have the potential to cause issues within the reactor, such as blockages however given the hardness of the soot-tar composite materials, an effort should be made to prevent tars and soot condensing together.

To prevent operational issues, manufactures of sewage sludge pyrolysis equipment need to carefully design the layout of outlet pipes and control the temperatures within them. Figure 5-12 shows the fuel-gas ascension pipework layout for the proposed ATC reactor at Crossness STW.

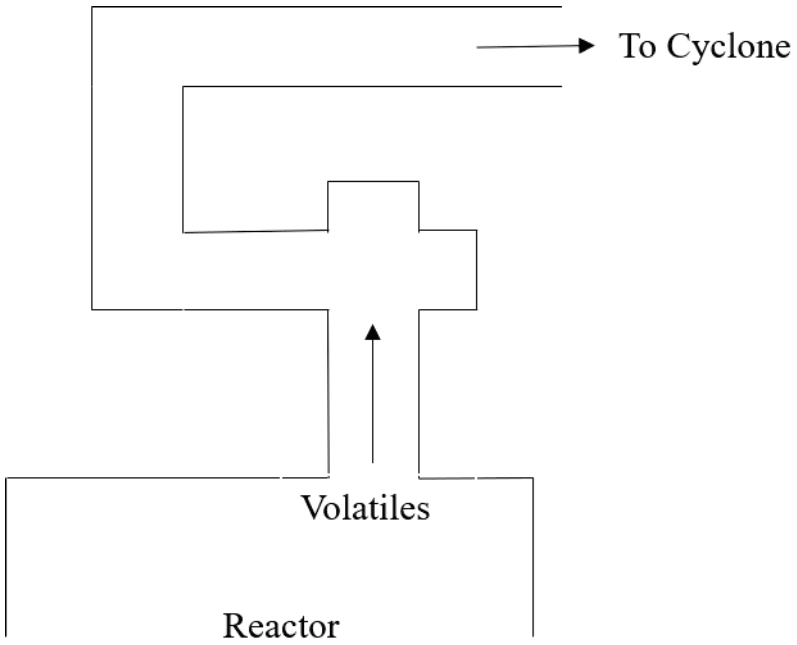


Figure 5-12 – Ascension pipework layout for the proposed ATC reactor at Crossness STW

There is a short gas ascension pipe, which comprises a stainless-steel tee piece with two of its flanges blanked off. The gas exits from the side of the tee-piece and then moves horizontally where there is an expansion bellow to isolate lateral and vertical movement.

The expansion bellow is connected to further pipework that twists with a 180º turn and transports the gas to a cyclone via a long section of horizontal piping. The proposed pipe layout has several deviations from the designs used successfully by the coal-gas industry (Meade, 1921) and coal-gas chemical works industry (Mcneil, 1975). These deviations include:

- Using horizontal pipe-sections which are prone to vapour deposition.
- The use of three 90º turns which occur relatively sharply.
- Difficult access to the internal pipework if there are maintenance issues.

Meade (1921) explains that the choking of gas ascension pipes was a common issue for poorly managed gas-works. Another issue was the carry-over of soot and coal-dust from the reactor into the tar-collecting main, which caused the tar to thicken and cause issues. These challenges appear to be similar to those observed for sludge.

Meade (1921) recommends:

- Pipework should be kept clean to prevent the proliferation of soot/tar deposits.
- The diameter and length of the ascension pipe should be sized to prevent gas passing through them too rapidly. This was important to prevent soot and coal-dust carry-over.
- Variations in the pipes "sectional area, and sudden changes of direction of the gas in its passage must be avoided". When the direction of gas-flow needs to be changed, the change "must be effected as gradually and smoothly as possible, so as to avoid mechanical deposition of the tarry vapours and suspended particles".

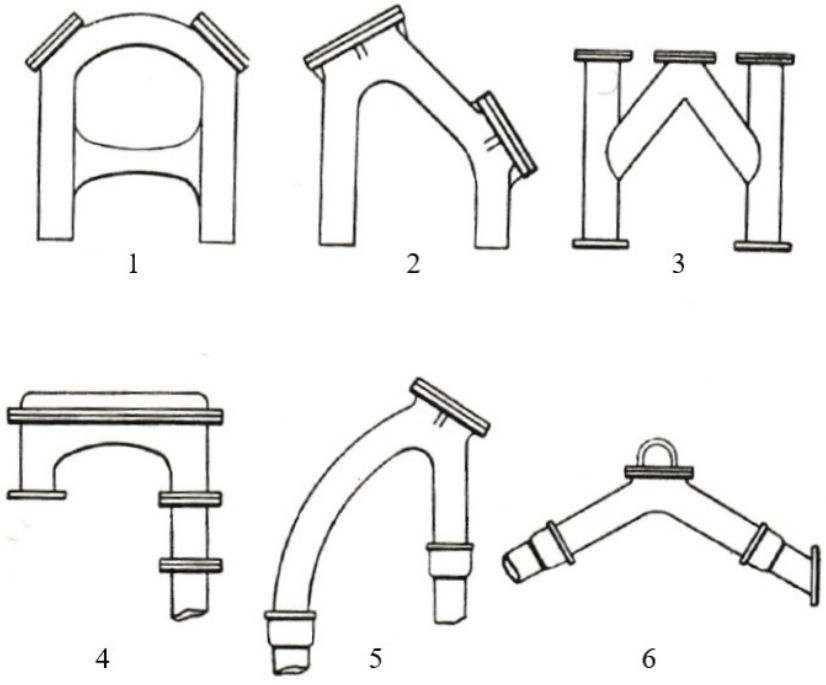


Figure 5-13: Retort ascension pipes (Meade, 1921) typically one side would be connected to the retort and the other would be connected to the tar collecting main

Meade (1921) presented common bridging pipes which were used to change the direction of gas-flow between the ascension pipe and the tar collecting main (Figure 5-13). He notes that: (i) layout 1 was common on small gas-works; (ii) layout 3 should be avoided because the angles are far too sharp (iii) layout 5 (the Bournemouth type) was recommended for the ease of access afforded from a single flange during maintenance (iv) layout 6 was typically used for vertical retorts. Note:

- None of the designs have horizontal sections
- None exceed 180^{o} between the reactor and first gas-cleaning asset and all of them have access flanges.
- Many bridge-pipes used sockets rather than flanged connections although the rationale for this is not entirely clear but could be due to expansion joints being less well developed at the time.

Given that soot-bridges and soot-tar composites formed such a short distance away from the exit of furnace 1 in the laboratory-scale reactor, it is of vital importance for full-scale installations that the pipework minimises potential issue associated with tar. Compared to pyrolysis, issues with soot and tar deposition are less likely to occur for gasification reactors because these contaminants are largely oxidised forming heat and gas (Figure 2-4). For pyrolysis, an alternative approach to these issues is to gasify the soot and reform the vapour-phase tars prior to them leaving the reactor or in a dedicated secondary zone (Stein, 2016).

5.3 Laboratory-scale pyrolysis limitations

The laboratory-scale pyrolytic gasification plant as described in section 5.1 had limitations and was not fully representative of commercial processes. For example:

- The stainless-steel pipework was heated by external electric furnaces however because of scalability issues this is not the typical approach of electrically heated commercial-scale plants which use internal heating. The internal pipework may have formed deposits of carbon which will have influenced heat transfer through the pipework.
- The stainless-steel pipework may have undergone attrition because of friction with the conveyed solids. This may have influenced the concentrations of Ni and Cr within the char. The commercial-scale plant considered by Thames Water is constructed from refractory materials.
- The laboratory-scale plant included three heating zones which were individually controlled by separate furnaces, between these zones there were lengths of insulated pipework. Commercial plants typically use a single-zone for the heated length of the char although multi-stage processes can be used for secondary thermal cracking and/or reforming of the hot gas and volatiles. The unheated lengths may have provided an opportunity for organic liquids to prematurely condense which may have affected the values obtained for the mass yields. Improvements to the plant could be made by

providing trace heat lagging to these sections to ensure a completely uniform temperature distribution. Despite these issues, deposition of liquids within the reactor was limited, however premature liquid condensation was observed downstream of reactor 1 prior to the condensers. The commercial-scale plant considered by Thames used a single-reactor with multiple heating zones, however it was not technically feasible to replicate this approach at laboratory-scale

- Vapour condensation has limitations without the use of an electrostatic precipitator and or demisting equipment to promote coalescence. This may have affected the mass yields, although the majority of liquids present within the fuel-gas are expected to have condensed.

Chapter 6: Sludge characterisation

The mean properties of XS (XS mean) and, where necessary, the individual sample batches will be presented. The samples include: (i) XS-B which was used for batch pyrolysis in section 7.1.1, (ii) XS-6 which was used for continuous pyrolysis in section 7.1.1 and (iii) XS-9 which was used in section 7.6. raw blended digester feed (XS-Raw) was also sampled alongside XS-9 and is denoted XS-Raw.

6.1 Fuel characteristics

The XS had a mean DS content of 28.8% (±0.4) which is below the 2018-2019 site average for XS of 30.3% as published by Thames Water (2019). It is also below other THP Bucher Press sites such as Oxford STW (34.4%) and far below the assumption of Mills (2015) of THP bucher achieving 45% DS. Lower DS will increase the heat required for drying and will influence the process energy balance. In the laboratory, the sludge was dried until constant weight, sieved to a consistent particle size (<5.6mm) and stored in a barrel until further use. The stored sludge had an average DS content of 97.0% and this varied little across samples.

The water industry typically refers to loss on ignition (LOI) as volatile solids (VS), and VS is used as a proxy for sludge organic content (Suez, 2021). The average VS content of XS was 70.6% although this varied across samples from 67.4% for XS-6 to 72.6% for XS-B. Raw sludge (XS-Raw) was sampled with XS-9 in August 2020 and is blended primary and secondary sludge taken from the digester feed. It contained a VS content of 85.2%. Despite the VS of digested sludge varying up to 5.3%, the HHV of the material was extremely consistent between samples with an average of 17.8 MJ kg^{-1}. The mismatch between VS and HHV consistency is indicative of variations in XS macromolecule content. The estimated LHV calculated from ultimate analysis data using a method by Cooper et al. (1999) was less stable and more closely resembled HHV on a dry ash-free basis (HHV_{DAF}).

Table 6-1: Fuel characteristics of Crossness STW raw and digested sewage sludge

Sludge	Feed DS	Loss on ignition[2]	HHV[3]	HHV_{DAF}[4]	Est. LHV
Unit	% Wt.	% Wt.	MJ kg^{-1}	MJ kg^{-1}	MJ kg^{-1}
XS Mean[1]	97.0 (±0.3)	70.6 (±1.7)	17.8 (0.00)	25.1 (±0.4)	14.9
XS-B	97.6 (±0.1)	72.7 (±0.6)	17.9 (±0.2)	24.6	15.2
XS-6	96.5 (±0.2)	67.4 (±0.5)	17.9 (±0.0)	26.0	13.7
XS-9	96.8 (±0.2)	71.7 (±0.1)	17.8 (±0.1)	24.8	15.9
XS-Raw	96.8 (±0.3)	85.2 (±0.1)	20.5 (±0.2)	24.2	19.1

[1]XS mean = mean (XS-B, XS-6, and XS-9); [2]Loss on ignition at 550°C; [3]HHV as measured by bomb calorimetry; [4]Calculated from mean HHV and VS content.

On average, XS HHV_{DAF} was 25.1 MJ kg^{-1}, however XS-B and XS-9 both contained a slightly lower HHV_{DAF} of 24.6 and 24.8 MJ kg^{-1} respectively whilst XS-6 contained a HHV_{DAF} of 26.0 MJ kg^{-1}. This suggests some differences in sludge macromolecule content. Table 6-2 summarises the typical macromolecule content of raw primary and secondary sludge at three Thames Water sites, their relative digestibility and average energy content (Gialacone, 2018).

Table 6-2: Typical sludge composition (Gialacone, 2018)[1]

Components	Primary %Wt	SAS %Wt	Higher heating value MJ kg^{-1}	Digestibility[4] %Wt
Fibre	28.3-46.5	2.8-9.2	Lignin-22.2-28.5[3] Cellulose-17.5[3] Hemicellulose-17.5[3]	Lignin-15% Cellulose-80% Not Reported
Protein	24.0-39.8	60.7-68.5	18.2[2]	20-25%
Lipids	11.5-14.3	7.5-10.4	38.9[2]	60-65%
Sugars	4.4-7.7	5.4-8.4	15.6-16.5[2]	Not reported
Starch	2.8-7.0	6.2-9.3	17.3[2]	

[1]Average composition of sludge from Maple Lodge, Reading and Slough STW (Gialacone, 2018)

[2] HHV as reported by Yao (2014)

[3] HHV as reported by Demirbas (2017)

[4]Digestability during mesophilic anaerobic digestion (Giacalone, 2018).

The data presented in table 6-2 shows that primary sludge and surplus activated sludge (SAS) typically contain very different macromolecules profiles. The variations in HHV_{DAF} for XS may be due to variations in primary sludge to SAS ratio, which will decrease if excess N in sewage liquors is loaded onto the aeration lanes. Also, primary sludge imported from satellite sites (that lack digestors and the activated sludge process) could also affect this ratio and have been known to decrease the performance of primary settlement. Seasonal or random variations could also explain the changes in the HHV_{DAF}. Unlike the sludge presented in table 6-2, XS was thermally hydrolysed prior to digestion. Prior to digestion, macromolecules such as protein are hydrolysed forming smaller molecules such as amino acids that are then assimilated into bacterial cells. Hydrolysis is often the rate-limiting step of digestion, Mills (2015) investigated the impact of THP on the breakdown of macromolecules and found carbohydrates and protein were broken down and solubilised, but lipids were not. Barber (2016) corroborates, stating: “it is well understood” that THP is suited to carbohydrates and protein and has “little influence on lipids, which explains why it is more suited to activated, rather than primary sludge”.

Table 6-1 shows that the HHV_{DAF} of XS-raw was approximately 1.8 MJ kg^{-1} (~9.5%) lower than XS-9. This suggests that energy sparse macromolecules such as sugar, starch and cellulose are preferentially digested at Crossness STW which is consistent with the results presented in table 6-2.

6.1.1 Proximate analysis

Figure 6-1 shows the output of proximate analysis (ASTM D7582) for a XS-6 sample. It demonstrates that most sewage sludge mass volatilises whilst a small amount forms FC. Figure 6-1 also shows that 50% of the material's volatile content had volatilised at 386°C whilst 85% had volatilised at 568°C. Further weight loss then occurs between 568-950°C, albeit more gradually. After cooling the material to 600°C (in accordance with ASTM D7582), the FC content of the material was oxidised, which caused further weight loss.

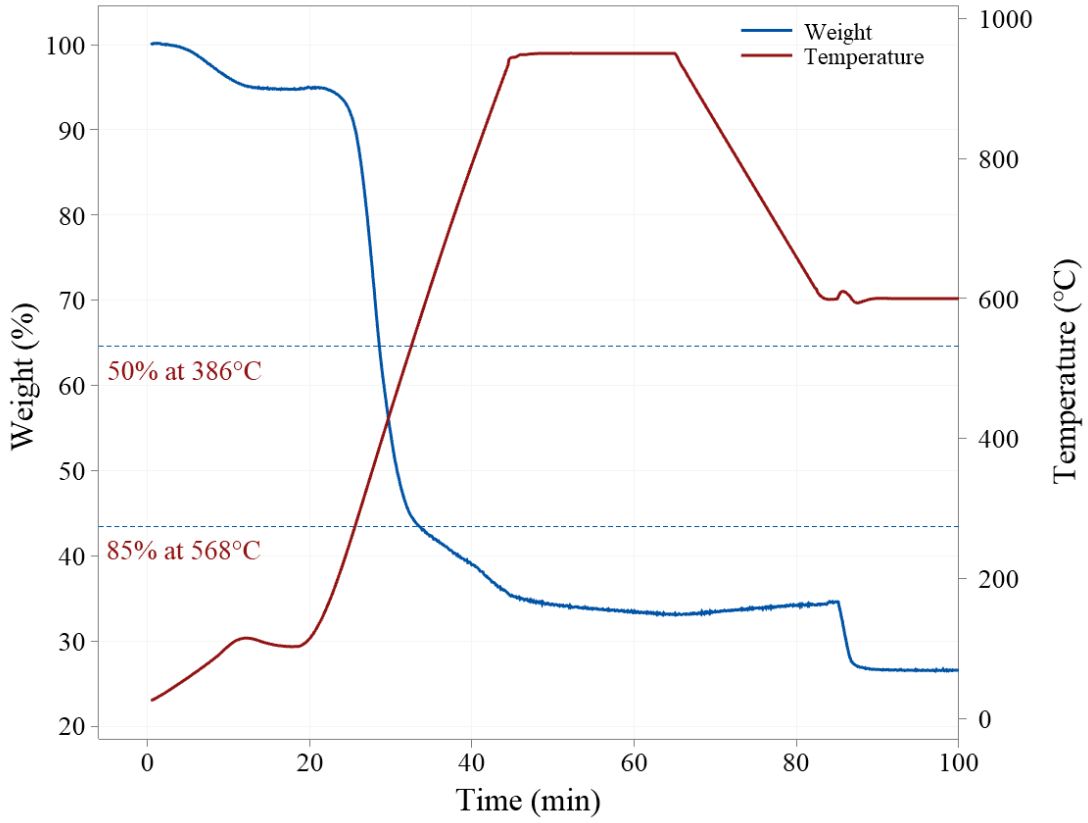


Figure 6-1: Proximate analysis of XS-6, showing the sample weight (%) and temperature (°C) when 50% of the materials volatiles had been volatilised. When cooled from 950°C to 600°C, the sample weight appeared to increase because of the buoyancy effect – therefore FC carbon content was calculated from the weight of the sample before & after ashing at 600°C.

The average proximate analysis results obtained from digested sludge samples (XS-B, XS-6), raw blended sludge (XS-raw) and raw SAS (XS-SAS) are summarised in table 6-3. This table also shows: the char yield during proximate analysis and its FC content, and the results of proximate analysis illustrated on a DAF basis. XS-mean is the average of XS-B and XS-6 and shows that digested sludge formed: 29.0% ash, 7.4% FC and 63.6% volatiles. Thus, during proximate analysis XS produced a char yield of 36.4% with a FC content of approximately 20.3%. The remaining 63.6% of XS Wt formed volatiles, which in practice may include gas, tar, VOCs, and water vapour (produced during dehydration reactions). By comparing the samples on a DAF basis it's easier to compare the tendency of sludge organics to form char and volatiles.

On a DAF basis XS-mean formed 89.7% volatiles and 10.3% fixed carbon however there was some variation amongst samples XS-B and XS-6.

Table 6-3: Average proximate analysis results for Crossness sludge samples

Sludge	Proximate analysis (Dry Wt. %)	Char properties (Dry Wt. %)	Proximate analysis (DAF Wt%)
XS-mean[1]	Ash: 29.0 (±0.7) FC: 7.3 (±0.5) Vol: 63.6 (±1.1)	Char yield: 36.4 Char FC content: 20.2	FC_{DAF} = 10.4 Vol_{DAF} = 89.7
XS-B	Ash: 27.5 (±0.3) FC: 6.8 (±0.9) Vol: 65.8 (±1.2)	Char yield: 34.3 Char FC content: 19.8	FC_{DAF} = 9.3 Vol_{DAF} = 90.7
XS-6	Ash: 30.6 (±0.3) FC: 7.9 (±0.1) Vol: 61.5 (±0.2)	Char Yield: 38.5 Char FC content: 20.5	FC_{DAF} = 11.4 Vol_{DAF} = 88.6
XS-Raw	Ash: 14.7 (±0.2) FC: 6.4 (±1.2) Vol: 78.9 (±1.0)	Char Yield: 21.1 Char FC content: 30.2	FC_{DAF} = 7.5 Vol_{DAF} = 92.5
XS-SAS	Ash: 21.4 (±0.2) FC: 8.1 (±0.1) Vol: 70.5 (±0.3)	Char Yield: 29.5 Char FC content: 27.5	FC_{DAF} = 10.3 Vol_{DAF} = 89.7

[1]XS mean is the mean of XS-B and XS-6

XS-raw and XS-SAS were anticipated to produce a greater proportion of volatiles because the materials had not yet been stabilised by digestion. XS-raw produced higher volatiles, however XS-SAS was almost identical to XS-mean. SAS largely comprises proteins which are quite recalcitrant during the digestion process, therefore SAS and digested sludge may behave similarly during pyrolysis with both materials containing high protein concentrations according to Gialacone (2018). XS-Raw was expected to produce a greater proportion of FC compared to XS-SAS, due to the potential presence of lignin within this material. However, SAS formed a greater proportion of FC, which suggests that its protein content contributes to the FC content of sludge char. Approximately, XS-raw contained 60% primary sludge and 40% SAS.

Proximate analysis is typically used for materials with low N contents (e.g. coal and lignocellulosic materials), therefore fixed "carbon" is an accurate description of the non-volatile organics. If proteins contribute to FC content, significant quantities of N may be present in the chars covalently bonded organic framework altering its properties and stability.

The "char properties" column in table 6-3 shows the properties of char produced from Crossness sludge during proximate analysis. XS-Raw/SAS produced a char with a FC content of 27.5-30.2% whilst for XS-B and XS-6 it was 19.8-20.5%. The higher quantity of organics in char produced from raw sludge suggests the material will be better suited to adsorbent production. This corroborates with the finding of Pullket (2015), who investigated sludge based adsorbent production from raw and digested sludge.

The conditions used during proximate analysis are partially representative of slow pyrolysis systems, for example both systems use low heating rate and long dwell times. In contrast, continuously fed systems will have: (i) higher heating rates (ii) shorter dwell times (iii) less tar-char polymerisation (vi) more high temperature char-volatile interactions.

Table 6-3 highlights the suitability of sludge for conversion to gas via pyrolysis. Competing technologies such as gasification are typically used when feedstock organics form a greater proportion of FC which can only be converted to gas with the addition of gasifying agents (e.g. steam and O_2). Speight (2011) compared the proximate analyses for 38 materials, the ratio of volatiles to FC for biomass ranged between 1.6-7.0, with a median of 4.4 whilst for coal the ratio was 0.6. In contrast, the average ratio for XS was 8.7 and for XS-Raw 12.4. Another reason gasification is used is to minimise tar in the fuel-gas.

The tendency for certain macromolecules to form different quantities of FC and volatiles is of interest and could be used to model the gas yield from sludges with different compositions. Krueger (2020) conducted proximate analysis on lignocellulosic material, protein, oil and starch, the results are summarised in table 6-4.

Table 6-4: Proximate analysis of pure macromolecules (Krueger, 2021)[1]

Compound	Vol_{DAF}	FC_{DAF}	Vol:FC
Unit	%Wt	%Wt	ratio
Hemicellulose	83	17	4.9
Cellulose	90	10	9.0
Lignin	55	45	1.2
Protein[2]	81	19	4.3
Oil[3]	100	0	-
Starch[4]	86	14	6.1

[1]Permission obtained from Krueger for redistribution, [2]Bovine serum albumin, [3]Sunflower oil, [4]Potato starch

Table 6-4 shows that lignin yields the most fixed carbon, with 45% of its weight forming fixed carbon. Lignin and other fibres such as cellulose and hemicellulose are predominately found in primary sludge (table 6-2) therefore increased PS:SAS ratio in sludge may increase char yield. This could be achieved by increased primary sludge imports from non-digestion sites or improving site primary settlement.

Other macromolecules also formed fixed carbon, with protein forming 19%, the second largest amount after lignin. Both primary sludge and SAS contain large quantities of protein which is poorly digestible (Table 6-2) therefore protein likely contributes significantly to char formation during sewage sludge pyrolysis. Table 6-4 shows that oil produced no char, therefore water companies could dispose of fats, oils, and greases (FOG) by pyrolysis to maximise gas yields and energy content.

6.1.2 Ultimate analysis

Table 6-5 summarises the results of ultimate analysis for XS-B, XS-6, XS-9, XS-Raw on a dry-weight basis. XS-mean is the mean of XS-B, XS-6, and XS-9. XS-Raw and XS-9 were sampled together in 2020 and represent the elemental concentrations before and after MAD. The oxygen content can be calculated by difference, which is the method used for coals according to BS ISO 17247:2013. This method is used for numerous biomass samples in the literature (Bakshi et al., 2020), however it has serious shortcomings for samples containing high concentrations of ash, in particular those with high levels of carbonates, alkali metals and AEMs. In addition, during ashing some of the oxygen present within the material has been shown to form secondary carbonates (Bakshi et al., 2020). Therefore, table 6-5, 6-6 and 6-7 simply present this non-quantified fraction of the feedstock as "other", although to a large extent this will consist of organic oxygen.

Table 6-5: Ultimate analysis of Crossness sludge (Dry Wt %)

Feedstock	Carbon	Hydrogen	Nitrogen	Sulphur	Chlorine	Ash[1]	Other
XS-mean	37.0%	5.1%	5.2%	2.1%	-	29.4%	21.1%
XS-B	37.6%	5.2%	6.0%	2.3%	0.32%	27.3%	21.2%
XS-6	34.7%	4.7%	4.6%	2.2%	-	32.6%	21.2%
XS-9	38.7%	5.5%	5.0%	1.7%	-	28.3%	20.8%
XS-Raw	46.3%	6.4%	5.2%	1.7%	-	14.8%	25.6%

[1]As measured by loss on ignition (LOI) at 550°C

Table 6-6 summarises the results of ultimate analysis for XS-B, XS-6, XS-9, XS-Raw, wood and coal on a dry ash-free basis. Understanding the fate of these elements during thermal conversion is important for predicting the quantity and properties of the products formed.

Table 6-6: Ultimate analysis of Crossness sludge and comparator materials[1] (DAF Wt %)

Feedstock	Carbon	Hydrogen	Nitrogen	Sulphur	Chlorine	Other[2]
XS-mean	52.4	7.3	7.4	3.0	0.4	31.4
XS-B	51.7	7.2	8.3	3.2	0.4	29.1
XS-6	51.5	6.9	6.9	3.2	-	31.4
XS-9	54.0	7.7	7.0	2.4	-	28.9
XS-Raw	54.4	7.5	6.1	2.0	-	30.0
Wood[4,6]	50.9	6.1	0.2	0.0	-	42.8
Coal[5,6]	84.2	5.6	1.3	3.5	-	5.5

[1]Dry-ash free data calculated from LOI ash content, [2]Other measured by difference, [3]Chlorine only measured for XS-B, [4]Wood category mean (Speight, 2011) [5]Pittsburgh Seam (Speight, 2011) [6]On a dry wt% basis the wood and coal contained 1.8% and 10.3% ash (Speight, 2011).

For wood, coal, and sludge, the "other" contents were 42.8%, 5.5% and 28.9-31.1% respectively, hence constituting one of the main differences between these materials. This is suggestive that sludge contains less oxygen than wood, but much higher oxygen than coal, although without full quantification of the oxygen content it is hard to draw a conclusion.

All the macromolecules in sludge contain oxygen, however carbohydrates such as cellulose, starch and sugars are particularly oxygen rich. After digestion, the "other" content of sludge decreases, which is likely because cellulose and sugars (O rich macromolecules) are preferentially digested. During pyrolysis, oxygen likely forms carbon oxide gases (CO, CO_2) and oxygenated tar compounds such as phenolic compounds or organic acids. Pyrolysis bio-oil from lignocellulosic feedstocks typically have high oxygen contents and is extremely corrosive (Brady et al., 2017), which limits their integration into traditional petrochemical processes.

Another major difference is that sludge contains much higher concentrations of N compared to wood or coal. This is because of the material's high concentration of proteins, which is concentrated during digestion because of its relative recalcitrance to digestion. Other materials containing nitrogen such as coal and melamine have been pyrolysed in the literature and have been shown to produce condensed structures within pyrogenic carbon, heterocyclic tars, and gases such as N_2, HCN and NH_3 (Meade, 1921) (Atiania et al., 2020).

Digested sludge may contain more S than blended raw sludge because Crossness STW and other digestion sites dose sludge with ferric chloride to minimise H_2S formation, hence concentrating S during digestion. Both S and Cl typically form acidic gases such as H_2S and HCl which need to be removed prior to gas conversion in an engine.

The data in table 6-6 is illustrated in table 6-7 as the molar ratios: H:C, C:Other, C:N and C:S and compared against the typical values for wood and coal. Illustrating the data this way makes it easier to compare the relative amounts of these elements within sludge and comparator materials such as coal and wood.

Table 6-7: Molar ratios of Crossness sludge and comparator materials[1]

Feedstock	H:C	C:Other	C:N	C:S
XS-mean	1.64	2.30	8.75	46.2
XS-B	1.66	2.36	7.29	42.9
XS-6	1.60	2.27	9.49	45.9
XS-9	1.70	2.48	9.02	60.5
XS-Raw	1.64	2.41	10.3	72.3
Wood[2]	1.43	1.59	292	6674
Coal[3]	0.79	20.5	73.4	65.0

[1]Other calculated by difference for sludge, for wood and coal , [2]Wood category mean (Speight, 2011)
[3]Pittsburgh Seam (Speight, 2011)

6.2 Elemental composition

XS-B biosolids (sampled - 2017) and XS-6 biosolids (sampled - 2019) were ashed at 550ºC, digested with concentrated aqua-regia and analysed by ICP-OES (see section 4.2.7.1). Table 6-8 summarises the mean elemental composition of these sludges. Tables 6-5 and 6-8 show that sludge contains a variety of useful soil macronutrients (Ca, N, S, P, Mg and K) and micronutrients (Fe, Cl, Zn, Cu, Mn, and Ni) although these elements are not present in balanced quantities. For example, K is undersupplied, whilst micronutrients such as P, Fe, Cu and Zn may be over-supplied if recycled to land.

Table 6-8: Elemental analysis of XS-B and XS-6

Element	XS-B Mean	XS-B SD	XS-6 Mean	XS-6 SD
Unit	mg kg^{-1}	mg kg^{-1}	mg kg^{-1}	mg kg^{-1}
Calcium (Ca)	39450	3827	46512	3744
Phosphorus (P)	26140	1756	26008	308
Iron (Fe)	24596	2022	24584	354
Aluminium (Al)	6787	453	7032	124
Magnesium (Mg)	4615	504	5457	427
Potassium (K)	1398	139	1594	100
Sodium (Na)	1204	723	1447	122
Zinc (Zn)	820	89	800	11
Manganese (Mn)	506	45	461	23
Copper (Cu)	441	68	408	17
Barium (Ba)	200	18	215	8
Erbium (Er)	175	22	183	5
Lead (Pb)	162	34	123	20
Strontium (Sr)	108	12	140	16
Nickel (Ni)	39	3	41	1

Below experimental detection limit (30 mg kg^{-1}): Ag, As, B, Bi, Cd, Cr, Co, Ga, In, Li, Tl, Sc, Y, La, Ce, Pr, Nd, Sm, Eu, Gd, Tb, Dy, Ho, Tm, Yb, Lu, Ru, Rh, Pd, Os, Ir, Pt and Au.

For quantification, the lowest experimental detection limit was 30 mg kg^{-1} using 2g digestions because a linear calibration could not be achieved below a standard concentration of 0.1 mg kg^{-1}

6.2.1 Alkaline earth metals

XS contains large quantities of AEMs, such as Ca, Mg and trace levels of Sr and Ba (Table 6-8). This is explained by the water hardness in East London, which is classified as hard to very hard. During drying, AEMs precipitate forming carbonates. Carbonates decompose at elevated temperatures forming metal oxides and carbon dioxide. For example, calcium carbonate decomposes between 700-800ºC in a nitrogen atmosphere (Jiang et al., 2019). Metal oxides are expected to participate in tar cracking reactions whilst the CO_2 released during carbonate decomposition is a gasifying agent and may react with char or tar to form CO in the Boudouard reaction. Alkali metals such as Na and K are found in relatively low concentrations compared to AEM, because they have higher solubilities and likely fractionate in wastewater rather than sludge.

6.2.2 Iron and aluminium

XS contains relatively high quantities of iron and aluminium. Iron as ferric chloride ($FeCl_3$) is dosed at Crossness STW for several reasons. For example:

- To promote flocculation: Sludge is typically negatively charged (approximately 30 mV), anionic synthetic polymers in combination with cations (Fe^{3+}), are dosed to neutralise the surface charge and promote flocculation and settling during primary settlement (Subramanian et al., 2010).
- To precipitate phosphate: Anaerobic digestion releases the anion phosphate ($PO4^{3-}$) from sludge, therefore cations are dosed prior to digestion to reduce the concentration of $PO4^{3-}$ in the dewatering liquor post-digestion to meet the legal phosphorus effluent requirements of <1.0 mg P L^{-1} (Mulder et al., 2017). The iron-phosphate mineral formed is fractionated within the sludge.
- To suppress hydrogen sulphide in the biogas, which causes odours issues and safety issues for operators working on site.

The high concentration of iron in sludge is likely a result of ferric dosing on site, however, iron likely forms stable compounds such as FeS and $FePO_4$ and may not influence the pyrolysis of sludge. Aluminium can also be used as a flocculant on sewage treatment works.

6.2.3 Potentially valuable elements

XS contains significant quantities of phosphorus (P), a valuable element primarily used as an agricultural fertiliser. During pyrolysis, P is not expected to form volatile therefore, it could be recovered from the char post-pyrolysis (section 9.4.2)

An array of precious and rare earth elements (REE) was also tested, however, these were not found in detectable quantities except for Erbium. The relatively high concentration suggests either a geological presence or a significant point source within the catchment. Erbium is a rare-earth element used for optics, lighting, medical, nuclear and lasers. Erbium is a critical raw material with one of the highest supply risks of any metal. The main global supplier of erbium is China (86%) with all the EUs supplies imported from abroad (EC, 2020).

Potentially toxic elements

Sludge contained detectable concentrations of zinc, copper, lead, and nickel and their presence may lead to toxicity issues (section 8.2). For biosolids application, this risk is controlled by limiting the metal application rates and testing the metal concentrations within soils to ensure they are not overloaded with toxic elements.

6.3 Summary

Chapter 6 presents the basic characteristics of the Crossness sludge used within the project; the results highlight that:

- Digested sludge HHV was 18 MJ kg^{-1}, however its HHV_{DAF} varied between 24.6-26.0 MJ kg^{-1} which could be due to variation in sludge macromolecule content.
- On a DAF basis, carbonisation converts approximately 90% of sludge mass into volatiles. These volatilise at relatively low temperatures, for example figure 6-1 showed 50% of XS-6 volatile loss occurred at 386ºC whilst 85% occurred at 568ºC.
- On a DAF basis sludge contains an equivalent concentration of C to wood, however it contains far greater N and S than either wood or coal. The products these elements form pose unique operational challenges for sludge pyrolysis.
- Sludge has a high ash content which mostly comprises AEMs, iron, and phosphorus. However, it also contains Erbium, a relatively valuable REE and a range of PTEs, including Zn, Cu, Pb and Ni.

Chapter 7: Laboratory-scale pyrolysis

7.1 Mass yields

7.1.1 Batch-fed slow pyrolysis

Batch-fed slow pyrolysis (Py-B) of sludge was investigated at laboratory scale. For methodology and full experimental details, refer to Chapter 4. Table 7-1 summarises the mass yields of XS during Py-B with standard error (SE) shown in brackets, for these experiments the furnace temperature was the only independent variable investigated.

Table 7-1: Batch pyrolysis of XS: Mass Yields

T °C	Char Yield %wt (SE[1])	Liquids Yield %wt (SE[1])	Gas Yield[2] %wt (SE[1])
450	57.1% (±0.5)	20.1% (±0.5)	22.8% (±0.6)
500	51.0% (±0.6)	23.1% (±0.2)	25.9% (±0.5)
550	51.0% (±0.3)	24.7% (±0.5)	24.3% (±0.5)
600	46.4% (±0.2)	23.0% (±0.3)	30.6% (±0.3)
650	48.9% (±0.6)	20.2% (±0.9)	30.8% (±0.9)
700	46.5% (±0.3)	22.8% (±0.1)	30.8% (±0.3)
750	45.0% (±0.5)	23.0% (±0.5)	32.0% (±0.6)
800	40.1% (±0.9)	23.1% (±0.1)	36.8% (±0.7)
850	42.0% (±0.6)	21.6% (±0.2)	36.4% (±0.6)
900	43.5% (±0.8)	20.3% (±0.5)	36.1% (±0.8)

Char, liquid, and gas (n=3)

[2]Gas yields calculated by difference from runs 1-3 (see Appendix 2 – Table 12-3)

The data presented in table 7-1 was tested for normality and equal variances using an Anderson-Darling test and Bartletts test in Minitab 19. Each level is normally distributed, and each category measured (e.g. char, liquid, and gas) had equal variances. A one-way analysis of variance

Table 7-2: Results of one-way ANOVA and Tukey testing for Py-B mass yield data

Char			Liquids			Gas		
T (°C)	$\bar{x}$ (%)	Tukey group	T (°C)	$\bar{x}$ (%)	Tukey group	T (°C)	$\bar{x}$ (%)	Tukey group
450	57.1	A	550	24.7	A	800	36.8	A
550	51.0	B	500	23.1	A B	850	36.4	A
500	51.0	B	800	23.1	A B	900	36.1	A
650	48.9	B C	750	23.0	A B	750	32.0	B
700	46.5	C D	600	23.0	A B	650	30.8	B
600	46.4	C D	700	22.8	A B	700	30.8	B
750	45.0	D E	850	21.6	B C	600	30.6	B
900	43.5	E F	900	20.3	C	500	26.0	C
850	42.0	F G	650	20.2	C	550	24.3	C D
800	40.1	G	450	20.1	C	450	22.8	D
ANOVA: *P = 0.000*			ANOVA: *P = 0.000*			ANOVA: *P = 0.000*		

(ANOVA) and post hoc Tukey test were conducted to test for significant differences between the experimental levels: 450-900ºC the results of which are summarised in table 7-2.

All tests were conducted at a significance level of two-sigma ($\alpha = 0.05$). Because of the small sample sizes (3), the statistical power of these tests was relatively low, therefore the results are indicative rather than definitive.

7.1.1.1 Py-B: Char

Most char weight losses occurred at ≤450ºC (Table 7-1), this corroborates with proximate analysis, which showed peak XS weight loss occurred between 350-400ºC. There appear to be three main temperature zones associated with further reductions in char yield, these zones include: (i) 450-500ºC (ii) 550-600ºC (iii) 750-800ºC. The data is variable and some exceptions to these observations occurred, for example, the char yield appears to increase between 600-650ºC and >800ºC. However, these data points correspond with lower-than-expected tar yields, suggesting material heterogeneity or an alternative confounding variable.

7.1.1.2 Py-B: Liquids

Liquid yields are relatively consistent between 450-900ºC suggesting liquid formation mostly occurs during primary devolatilisation. Low liquid yields were obtained at 450, 650, 850 and 900ºC. At 450ºC the material is undergoing rapid devolatilisation therefore the significant increase in liquid yield between 450-500ºC is likely to be due to conversion of sludge to primary bio-oils. The other low liquid yield may be because of material heterogeneity since these temperatures also produced higher than expected char yields (see above).

7.1.1.3 Py-B: Gas

Between 450-550ºC gas yields are relatively low (22.8-26.0%). A significant increase occurs between 550-600ºC and yields remain constant up to 700ºC. Gas yields increase slightly between 700-750ºC and a large statistically significant increase occurs between 750-800ºC. The gas yields between 800-900ºC are similar despite the differences in char and tar yields for these temperatures.

7.1.2 Continuously fed pyrolytic gasification

Continuously fed pyrolytic gasification (Py-G) of sludge was investigated at laboratory scale. For methodology and full experimental details, refer to chapter 4.3.3. The Py-G reactor contained three zones: furnace 1-3 (figure 5-3). Table 7-3 summarises the mass yields obtained when these zones were operated isothermally with the reactor's minimum retention time (120s) and feed-rate (2.6 kg hr^{-1}).

Table 7-3: Mass yields during isothermal pyrolysis (Py-G)[1]

T	Char Yield	SE	Liquid Yield	SE	Gas Yield[1]	SE
°C	%wt	%wt	%wt	%wt	%wt	%Wt
500	79.5	±0.7	-	-	-	-
550	61.9	±0.7	-	-	-	-
600	52.4	±0.8	18.6	±0.3	28.5	±0.5
650	47.7	±0.4	18.4	±0.3	33.2	±0.4
700	43.2	±0.4	16.6	±0.2	40.5	±0.6
750	43.6	±0.7	13.3	±0.5	42.8	±1.0
800	46.0	±0.4	8.1	±0.1	47.7	±0.4
850	45.5	±0.3	7.5	±0.1	47.5	±0.1
900	44.9	±0.7	7.2	±0.1	48.5	±0.9
950	45.9	±0.2	6.2	±0.2	48.2	±0.4
1000	45.9	±0.2	3.7	±0.2	50.4	±0.1

[1] Char (n=5) and liquid/gas (n=3).

[2]Gas yields calculated by difference from runs 1-3 (see Appendix 2 – Table 12-4)

The data presented in table 7-3 was statistically tested for normality using an Anderson-Darling test ($\alpha = 0.05$) and for equal variances using a Bartletts test ($\alpha = 0.05$) in Minitab 19. The results suggest each level is normally distributed ($P > 0.05$) and each category measured (e.g. char, liquid, and gas) have equal variances ($P > 0.05$). A one-way analysis of variance ($\alpha = 0.05$) and post hoc Tukey test ($\alpha = 0.05$) were conducted to test for significant difference for the levels between 600-1000°C. The results are summarised in table 7-4.

Table 7-4: Statistical testing of Py-G mass yield data

Char							Liquid							Gas						
T	$\bar{x}$	Tukey					T	$\bar{x}$	Tukey					T	$\bar{x}$	Tukey				
(°C)	(%)	Group					(°C)	(%)	Group					(°C)	(%)	Group				
600	52.4	A					600	18.6	A					1000	50.4	A				
650	47.7		B				650	18.4	A					900	48.5	A	B			
800	46.0		B	C			700	16.6		B				950	48.2	A	B			
950	45.9		B	C	D		750	13.3			C			800	47.7	A	B			
1000	45.9		B	C	D		800	8.1				D		850	47.5	A	B			
850	45.5		B	C	D	E	850	7.5				D		750	42.8			C		
900	44.9			C	D	E	900	7.2				D	E	700	40.5			C		
750	43.6				D	E	950	6.2					E	650	33.2				D	
700	43.2					E	1000	3.7					F	600	28.5					E
ANOVA		*P = 0.000*					ANOVA		*P = 0.000*					ANOVA		*P = 0.000*				

It should be noted that due to the small number of sample replicates (n =3-5), the statistical power of all these tests is relatively low, therefore the results are indicative rather than definitive.

7.1.2.1 Continuous pyrolysis: Char

Under the conditions tested, char produced below 600ºC visibly off-gassed upon leaving the reactor, therefore there was thermal lag between the highest heating temperature of the material and temperature of the furnace. The results <600ºC were omitted from the statistical analysis because they are clearly significantly different from the rest of the data. It is important that during full-scale pyrolysis, char is properly stabilised prior to exiting the reactor to prevent potential fire or explosion risks outside of the reactor. In addition, tar-laden char may be sticky, causing material handling and potential toxicity issues.

The char yield decreased between 500-700ºC from a high of almost 79.5% Wt. to a low of 43.2% Wt. at 700ºC this is because of greater dehydration and devolatilisation occurring in the sludge. This is also demonstrated statistically since char produced at 600ºC, 650ºC and 700ºC do not share the same Tukey groupings. At 700-750ºC the char yield stabilises and appears to increase slightly between 700-1000ºC although there is only a statistically significant difference between: [700ºC]– [800ºC, 950ºC, 1000ºC] and [750ºC]-[800ºC]. This result was unexpected since SSC contains significant quantities of calcium carbonate which would begin to decompose between 750-800ºC and continue to decompose at higher temperatures thus reducing char weight. In addition, some metals may volatilise at higher temperature, for example: mercury (357ºC), potassium (765.5ºC), sodium (880ºC) and zinc (907ºC) (ILO, 2021). The increased char yield may be due to metal oxide (CaO, ZnO and CuO) sulphidation (Jagtap & Wheelock, 1996), soot deposition from tar cracking, random error, or an alternative unknown reaction.

7.1.2.2 Continuous pyrolysis: Liquids

Under the conditions tested, liquid yields decreased with increasing temperature. At low temperatures (600-650ºC) the liquid yield (18.4-18.6% Wt) was at its highest, although slightly lower than that observed during Py-B (20.1-24.7% Wt). A statistically significant decline then occurs between 650-800ºC with each 50ºC increment occupying a different Tukey grouping. The largest decline in liquid yield occurred between 750ºC (13.1% Wt) and 800ºC (8.1% Wt). From 800ºC to 950ºC there are small decreases in liquid yield with increasing temperature, this cumulates in a statistically significant reduction between 950-1000ºC. Because of experimental constraints, the condensed liquids in the trap were not separated, individually identified and quantified. However, a small aqueous phase was visibly present, and its presence decreased with increasing pyrolysis temperature, suggesting that, alongside cracking reactions, steam reforming may be a mechanism for tar reduction. The experimental set-up is discussed in section 4.3.3 and present in figure 4-3.

7.1.2.3 Continuous pyrolysis: Gas

Under the conditions tested, the gas yield increased with pyrolysis temperature from a minimum of 28.5% at 600°C to a maximum of 50.3% at 1000°C. At low temperatures (600-700°C) there is a rapid increase in gas production with each experimental temperature level occupying a different Tukey grouping, indicating significant changes. At 650°C and below, the generated gas appears to be due to further char devolatilisation because liquid yields are stable at these temperatures and the char is undergoing rapid weight-loss. Between 650-700°C a transition begins with both char and tar yields declining to form additional gas. Above 700°C, increases in gas production are due to tar cracking and decomposition. Most gas production is concentrated within two temperatures zones above 700°C, these include: (i) 750-800°C and (ii) 950-1000°C.

7.1.3 Mass yields: A comparison of batch and continuous pyrolysis

A comparison of mass yields for Py-B and Py-G is presented in figure 7-1.

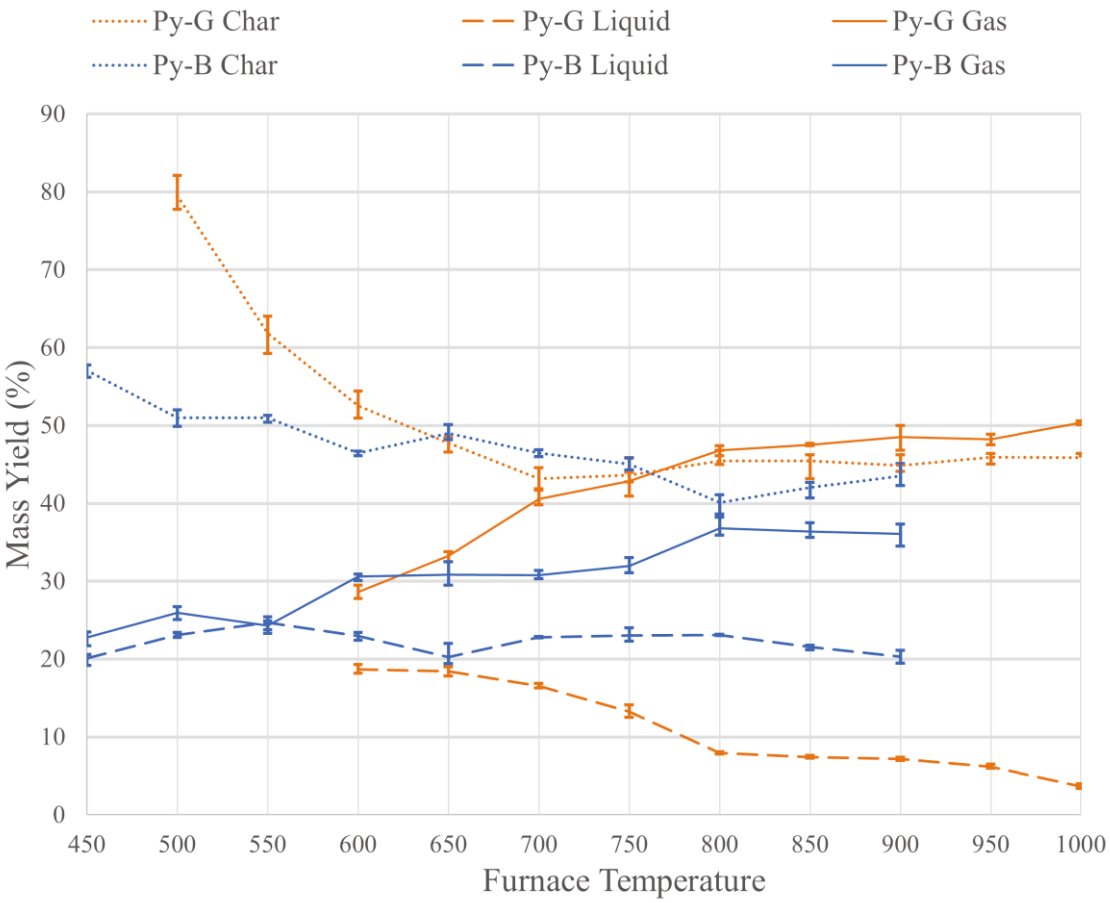


Figure 7-1: A comparison of the mass yields generated during Py-B and Py-G. The error bars show the minimum and maximum for each test condition.

Figure 7-1 illustrates the effect of dwell-time and heating-rate on char yield, for example whilst Py-G char is undergoing rapid devolatilisation between 500-700°C the yield of Py-B char decreases only slightly. However, both materials continue to decompose with increased

temperature suggesting extended dwell-times cannot stabilise char until critical temperatures are reached. For Py-G this occurs at approximately 700ºC, however, for Py-B decomposition does not stop occurring until 800ºC.

This is interesting because many slow-pyrolysis processes produce biochar for soil application (e.g. Carbon Gold), however these processes may not reach the higher temperatures or sufficiently long dwell-times required to fully stabilise the material. Therefore, there may be residual organics in these chars which may be less stable and breakdown over-time, potentially releasing contaminants into the soil.

Figure 7-1 also highlights that both Py-B and Py-G display significant increases in gas yield between 700-800ºC. For Py-G, the gas yield increases from 40.5 to 47.7%, a relative increase of 16%. Likewise, Py-B gas yields increase from 30.8% to 36.8%, a relative increase of 20%. In both cases, the increased gas yield mostly occurs between 750-800ºC, for Py-B this is driven by declines in the char yield whilst for Py-G its driven by declines in the liquid yield.

There are several potential explanations, these include:

- Organic compounds that volatilise and form tar during Py-G, instead carbonise during Py-B forming secondary char. However, between 700-800ºC threshold temperatures are reached, causing the decomposition of bonds common in both Py-G liquid and Py-B char. Since these bonds are less stable, it suggests they are heterocyclic. If Py-B char contains less stable organic structures this has implications for C-sequestration potential. This warrants further investigation because most biochars applied in the environment (e.g. soils) are produced via slow-pyrolysis.
- Calcium carbonate decomposition is expected to occur between 750-800ºC, for example, Li et al. (2017) found that the peak weight loss occurred at 792ºC during thermogravimetric analysis. During Py-G, there may be kinetic limitations for calcium carbonate decomposition because of the short dwell times (120s) used. For Py-B, calcium carbonate decomposition may be more extensive, hence this could explain the large reduction in char yield between 750-800º.

Evidence presented in Figure 8-2 and section 8.2.4.1. suggest carbonates in Py-G char at 700ºC were minimal which could be because of reaction between $CaCO_3$ and SiO_2 to form wollastonite at relatively low temperatures. Therefore, the first explanation is more likely.

7.2 Gas

Pyrolysis gas was sampled in a Tedlar bag and analysed using Gas Chromatography (GC) with a Carboxen 1010 column and thermal conductivity detector (TCD) (chapter 4.2.8). Based on previous literature and initial method development the following gases were quantified: hydrogen (H_2), carbon monoxide (CO), methane (CH_4), carbon dioxide (CO_2), acetylene (C_2H_2), ethylene (C_2H_4) and ethane (C_2H_6). Nitrogen (N_2) and Oxygen (O_2) were initially quantified by GC-TCD, however the results obtained were excluded because (i) N_2 was used as a purging gas which made quantification of feedstock-derived N_2 inaccurate and (ii) the Carboxen 1010 column could not achieve baseline resolution of O_2 and N_2 therefore quantification of either gas was inaccurate. For S, GC-TCD could not identify H_2S at the concentrations present in fuel-gas.

On a DAF basis, N & S accounted for 6.9% and 3.2% of feedstock (XS-6) mass (Table 6-6) therefore it is important to understand their fate during pyrolysis. Gas-phase N and S mass was indirectly quantified through the elemental mass balance. To calculate the volume of N_2 and H_2S produced, all gas-phase N and S was assumed to be present as N_2 and H_2S and the volumes were estimated in accordance with Avogadro's Law. In reality, N may also form significant quantities of HCN and NH_3. For each mole of N present, N_2, HCN and NH_3 weigh 28.01, 54.05 and 17.031 grams respectively therefore the assumption that all N forms N_2 will likely overestimate the dilatory effect of N gases if HCN is present in large concentration but underestimate it, if NH_3 is present is large concentrations. The assumption that most gaseous-S is present as H_2S is more realistic. The coal carbonisation and gasification industries have previously found most gaseous S forms H_2S although a minority of it may be present as COS, mercaptan-S, thiophenes and CS_2 (Higman & Van der Burgt, 2008).

7.2.1 Gas composition

Table 7-5 summarises the gas composition obtained when XS-6 sludge was pyrolysed isothermally between 600-1000°C. An assumption was made that all gas-phase N and S formed N_2 and H_2S.

Table 7-5: Mean fuel-gas composition (XS-6 sludge)

T	H_2	CO	CH_4	CO_2	C_2H_2	C_2H_4	C_2H_6	N_2[1]	H_2S[1]
°C	vol%	vol%	vol%	vol%	vol%	vol%	vol%	vol%	vol%
600	16.9	19.2	17.3	28.6	0.0	6.0	4.3	5.8	1.9
650	15.0	19.4	15.4	33.2	0.0	5.7	3.6	5.9	1.9
700	20.8	17.8	18.0	26.1	0.0	7.6	3.8	4.6	1.3
750	24.2	19.5	19.4	20.6	0.0	7.8	2.9	4.3	1.2
800	30.9	19.9	19.6	13.2	1.2	8.3	1.6	4.3	1.0
850	31.6	20.8	18.5	12.2	2.5	7.6	1.0	4.8	1.0
900	30.1	26.7	18.0	9.9	3.2	5.5	0.4	5.1	1.0
950	30.1	29.1	16.1	9.5	5.7	2.7	0.1	5.6	1.2
1000	38.7	28.5	13.2	6.6	4.9	1.9	0.0	5.1	1.2

[1]All gas-phase N and S assumed to be present as N_2 and H_2S, gas-phase N/S calculated from mass balance data.

Table 7-6 summarises the fuel-gas energy concentration and energy content alongside feedstock energy conversion and specific gas production (SPG) when XS-6 sludge was pyrolysed isothermally between 600-1000°C. All of the values in

Table 7-6: Mean fuel gas composition, lower heating value and specific gas production for XS-6

T	LHV	HHV	SGP	Fuel gas[1]	Conversion[2]
(°C)	MJ m^{-3}	MJ m^{-3}	m^3 tds^{-1}	MJ tds^{-1}	%
600	17.2	18.2	242	4059	22.7
650	15.6	16.6	268	4071	22.7
700	18.1	19.4	367	6541	36.5
750	18.7	20.2	420	7763	43.4
800	19.7	21.5	539	10510	58.7
850	19.4	21.3	540	10337	58.1
900	18.6	20.6	554	10184	56.9
950	17.8	19.9	547	9589	53.6
1000	16.7	18.7	648	10611	59.3

[1]Fuel-gas LHV MJ tds^{-1} calculated from hydrocarbons, CO and H_2. The energy content of H_2S was excluded because Thames Water are expected to remove this component prior to energy conversion.

[2]Energy conversion from feedstock HHV to fuel-gas LHV (Excluding H_2S). Feedstock HHV measured by bomb calorimetry as 17,900 MJ tds^{-1}.

Table 7-5 and 7-6 show:

- The energy density (LHV) of the fuel-gas increased between 600-800ºC from 15.6 MJ m^{-3} at 650ºC to 19.7 MJ m^{-3} at 800ºC due to the increased concentration of hydrocarbon gases. Although fuel-gas LHV may be underestimated at low temperatures because of the presence of less stable higher order hydrocarbons that were not measured.
- Fuel-gas LHV declines between 800-1000ºC to a low of 16.7 MJ m^{-3} due to increased concentrations of syngas (H_2, CO) and decreased hydrocarbon concentrations
- The SPG increases with increased temperature, particularly between 650-800ºC and 950-1000ºC. These regions coincide with decreases in the mass yield of tar.
- The percentage energy conversion from feedstock (HHV) to fuel-gas (LHV) increases up to 800ºC from a low of 22.7% between 600-650ºC to 58.7% at 800ºC. It then declines between 800-950ºC as hydrocarbon volumes decline. From 950ºC to 1000ºC SPG spikes due to tar conversion to syngas. This reduces fuel-gas LHV however overall energy conversion peaks at an experimental high of 59.3%.

The HHV is higher than the LHV because it includes the energy obtained from condensing combustion water vapour. Eurostat (2019) have adopted the methodology of using the LHV for energy balance calculations because it represents the energy "that can actually be used". Mills (2015) also used the LHV for energy balance calculations therefore the same approach will be used in this work. The HHVs and LHVs of the measured gases are presented for reference in table 7-7.

Table 7-7: The higher and lower heating values for the measured gases

Gas	Higher heating value (HHV) (MJ m^{-3})[1]	Lower heating value (LHV) (MJ m^{-3})[1]
Hydrogen (H_2)	12.77	10.79
Carbon monoxide (CO)	12.62	12.62
Methane (CH_4)	39.78	35.81
Acetylene (C_2H_2)	58.06	56.08
Ethylene (C_2H_4)	63.00	59.04
Ethane (C_2H_6)	69.69	63.75

[1]HHV and LHV values obtained from Waldheim and Nilsson (2001)

Figure 7-2 illustrates the specific gas production and component gas volumes (excl. N_2 & H_2S) produced during sewage sludge pyrolysis between 600-1000°C.

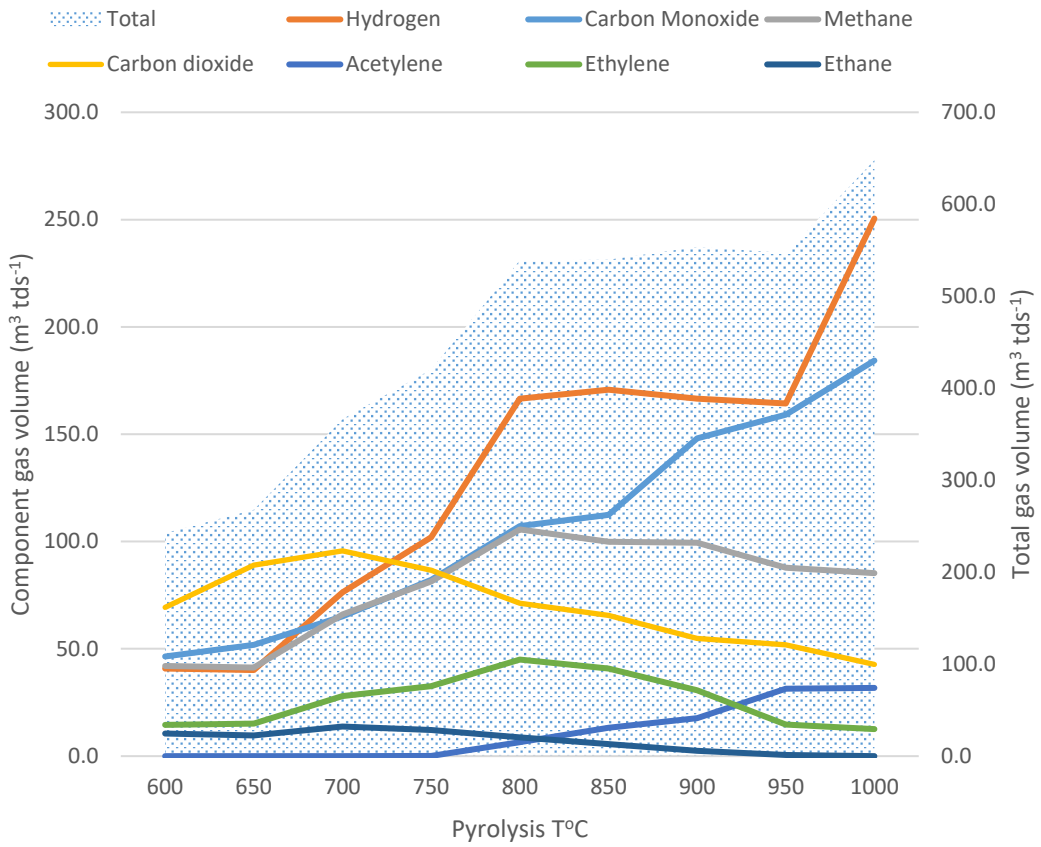


Figure 7-2: Total and component gas volume produced during Py-G. The component volumes for hydrogen sulphide and nitrogen gas are not shown

Figure 7-2 shows:

- The total gas volume undergoes large increases between 650-800°C and 950-1000°C. From 650-800°C: H_2, CO and hydrocarbons all increase simultaneously. Although, ethane peaks at 700°C and likely decomposes into ethylene and acetylene. Above 950°C, only H_2 and CO volumes increase, acetylene is stable, and other hydrocarbons all decrease.
- The total gas volume plateaus between 800-950°C, however: CO volume increases strongly in this region, hydrocarbon and carbon dioxide volumes decrease (except acetylene) and H_2 volume plateaus. The increased volume of CO and decreased hydrocarbon content without corresponding increases in H_2 is strongly indicative of the exothermic water-gas shift reaction, which is favoured by reactants at high temperatures.

The results presented in figure 7-2 will be discussed by splitting them into their respective compound's classes, these include hydrogen, carbon oxides and hydrocarbons.

7.2.1.1 Hydrogen

Macromolecules first decompose due to dehydration and depolymerisation reactions (Mamvura & Danha, 2020) (Cho et al., 2015). These reactions are typical of torrefaction, a low temperature process (<300°C), which predominately forms bio-oil, water vapour and carbon oxides. Therefore, at 600-650°C, Py-G only produced small volumes of H_2 which may be due to secondary decomposition of the bio-oils produced and their initial decomposition into unsaturated tar compounds. The gas results corroborate with figure 7-8 (discussed later in section 7.4.2) which show that at 600°C, 32.2% of feedstock H is fractionated in the condensable liquids fraction and this declines only slightly between 600-650°C.

From 650-800°C, the volume of H_2 produced increased rapidly from 41 m^3 tds^{-1} to 167 m^3 tds^{-1} this corresponds with a decrease in the yield of hydrogen in the condensable liquids (Figure 7-8). During initial volatilisation, bio-oil structures are expected to retain similar structural units to the parent macromolecules. However, as these molecules temperature increases, cyclisation or cracking reaction occur. For example, amino-acids undergo cyclisation to form unstable piperazines, which then undergo dehydration to N-heterocyclics (Leng et al., 2020). Whilst linear aliphatic compounds such as fatty acids and residual side chains are expected to undergo cracking reactions to form smaller hydrocarbon units. These processes are expected to release H_2, H_2O and other gases such as CO and hydrocarbons. Figure 7-2 shows that relatively stable hydrocarbons such as ethane decomposes above 700°C, the decomposition of ethane and other hydrocarbon gases will release methane, alkenes, alkynes and H_2. From 800-850°C, the volume of H_2 stabilises suggesting bio-oils and secondary tar compounds have formed thermally labile unsaturated aromatic forms. The volume of H_2 then decreases slightly from 171 m^3 tds^{-1} at 850°C to 159 m^3 at 950°C. Decreased H_2 volumes occur despite:

- The liquid yield decreased from 7.5% to 6.2% between 850-950°C (Table 7-3)
- The liquid hydrogen yield decreased from 10.3% to 7.5% of feedstock hydrogen content between 900-950°C (Figure 7-8)
- Methane, ethane, and ethylene all underwent large declines between 800-950°C (Figure 7-2).

Due to Le Chateliers principles, the Water Gas Shift reaction is expected to be favoured at higher temperatures. This corroborates with laboratory notes that observed an increased aqueous phase in the condensable liquids between 800-900°C and the molar ratios of the condensable liquids (Table 7-17), which show elevated H:C ratios in the condensed liquids between 800-900°C.

This also indicates that steam reforming reactions are not significantly active during pyrolysis until at least 950°C which has large implication for the design of ATC processes that aim to produce minimal tar yields.

From 950-1000ºC, the volume of H_2 produced increased over 57% from 159 to 250 m^3 tds^{-1}. This corresponds with large declines in the yield of condensable liquids from 6.2% to 3.7% (Table 7-3) and large reductions in the molar H:C ratio of condensable liquids from 1.1 to 0.55. (Table 7-17). All the following mechanisms likely contribute to the large increase in H_2 observed between 950-1000ºC:

- Thermal cracking - Above 950ºC the H:C ratio of the condensable liquid fraction halves and the C:N ratio doubles. This suggests that heterocyclic compounds such as pyrrole and pyridine are rapidly decomposed in this temperature range, leading to the generation of H_2.
- Steam reforming - Above 950ºC the condensed liquids did not contain an observable aqueous fraction and the tar remaining became highly viscous. This suggests that the water vapour present in the gas was consumed through steam reforming reactions, which may occur for both volatile tars and gaseous hydrocarbons (e.g. methane). The volume of methane and ethylene both decrease slightly between 900-1000ºC (Figure 7-2) however, the yield of condensable liquids decreased more, which suggests volatile reforming may be the dominant mechanism.
- N_2 formation - From 600-1000ºC the yield of nitrogen fractionated in the char and condensable liquids decrease and it is expected to form N_2 and the intermediate compounds NH_3 and HCN. At 1000ºC, the conversion of NH_3 and HCN to N_2 may be more extensive. At standard temperature and pressure gas occupies 22.4 L mol^{-1}. If one mole of NH_3 was decomposed, it would form half a mole of N_2 and one and a half moles of H_2 therefore the overall volume of the gas would double. From 950-1000ºC, the gas volume increased markedly and H_2 was released disproportionally compared to CO, this could suggest that NH_3 is converted to $0.5N_2$ and $1.5H_2$ at these temperatures.

Regression analysis was conducted in Minitab 19 to test the statistical significance ($\alpha = 0.05$) of the relationship between hydrogen production and liquid yield. The relationship is significant ($P < 0.001$) and is best fitted with the equation:

- $(y) = 0.03629(x)^2 - 1.937(x) + 27.70$ [where (x) = % liquid yield, (y) = kg H_2 tds^{-1}].

The model suggests 93.9% of hydrogen production can be explained by liquid yield variations (e.g. adjusted $R^2 = 93.4\%$). There is a 95% chance the line of best fits true-value lies between the upper and lower bands of the confidence interval. The prediction interval ($\alpha = 0.05$) shows the range in which 95% of y-values will be found for a given x-value (Figure 7-3). Given the relatively low sample size (n = 27), the range is relatively wide, so it would be prudent to gather further data to improve the predictability of the response variable.

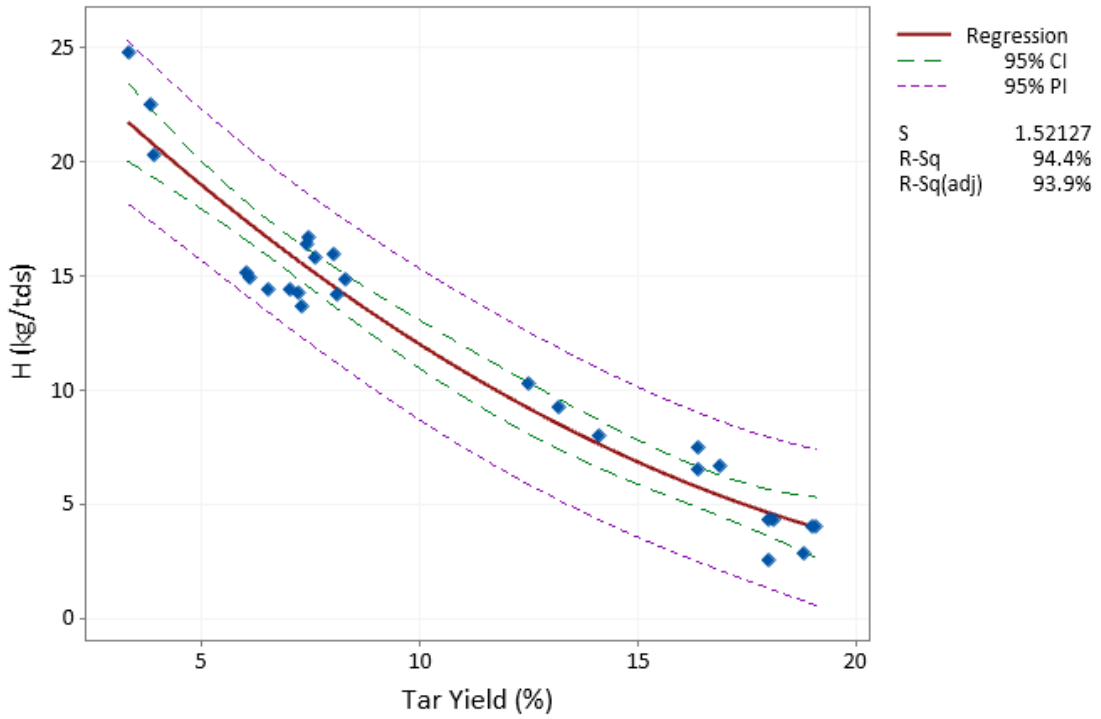


Figure 7-3: The relationship between liquid yield and hydrogen production with confidence intervals (CI) and prediction intervals (PI) ($\alpha = 0.05$)

7.2.1.2 Carbon oxides

Low temperature pyrolysis or torrefaction processes typically produce gas with high concentrations of CO_2. Likewise, Py-G produced disproportionally high volumes of CO_2 at low temperatures with the volume produced peaking early at 650-700°C (89-96 m^3 tds^{-1}). When feedstock enters the furnace, the macromolecules will undergo thermal lag as endothermic decomposition reactions occur. Therefore, whilst the char may reach the HHT of the furnace before it exits the reactor, the primary volatiles may decompose far below this temperature and form CO_2. The volume produced declines sharply between 750-800°C from 87 to 71 m^3 tds^{-1} despite the overall volume of gas increasing 119 m^3 tds^{-1} over this range. It then declines with increasing temperature to a low of 43 m^3 tds^{-1} at 1000°C. Carbon dioxide is formed due to:

(i) The decarboxylation of proteins and fatty-acids, the former is expected to be a major component of digested sludge

(ii) The water-gas shift reaction, which thermodynamically favours the formation of CO_2 and H_2 <517°C; and CO and H_2O >517°C (Ellingham, 1944).

Increased furnace temperatures equate to an increase in heating rates therefore, the rapidly decomposing sludge spends less time at the low temperatures that favour CO_2 formation. However, as temperatures increase, gas production also increases, decreasing the residence time of the gas.

Carbon, hydrogen, and carbon monoxide all act as reducing agents during metal oxide reduction:

- $CO + MO = CO_2 + M$;
- $H_2 + MO = H_2O + M$;
- $C + 2MO = CO_2 + M$.

The reactions above are thermodynamically favourable reduction pathways compared to: $C + MO = CO + M$ until approximately 672ºC, 749ºC and 872ºC respectively (Ellingham, 1944). However, the generation of CO and CO_2 through inorganic reduction is expected to be a very minor source of these gases overall.

From 600-800ºC, the volume of CO produced per tds increased from 46m^3 to 107m^3 tds^{-1}. This represents a +131% increase, which is much less than hydrogen (+308%) but similar to methane (+152%) and C_2's (+141%). From 800 to 950ºC the volume of CO generated increases by 48% to 159m^3 tds^{-1} with much of this increase (36 m^3) occurring sharply between 850-900ºC. However, over this temperature range hydrogen volume plateaus (+1.2%) whilst methane, C_2's and liquid yield all decrease. At other temperatures, 650-750ºC, 750-800ºC and 950-1000ºC, decreases in liquid yield have been associated with increases in both CO and H_2.

The increase in CO without corresponding increases in H_2 can be explained by two potential mechanisms:

- The Boudouard reaction;
- Water-gas shift reaction

The Boudouard reaction could be responsible if it consumed char or soot however char-C yields are stable between 700-1000ºC. Also, the Boudouard reaction would not explain why H_2 yields plateau despite hydrocarbon yields decreasing.

When CO increases sharply between 850-900ºC there is a simultaneous drop in CO_2 volume. Therefore, it is likely that between 800-950ºC the reverse water-gas shift reaction consumes generated H_2 and CO_2 and forms CO and water vapour. The quantity of water produced at each pyrolysis temperature was not measured, however water was visibly present at all pyrolysis temperatures except 1000ºC in the condensed liquids. From 950-1000ºC, CO volume increases to a maximum value of 184m^3 tds^{-1}, but this occurs concurrently with a large increase in hydrogen. The concurrent increase of CO and H_2 suggests the action of a steam reforming or gasification mechanism however this may also include hydrocarbon reforming and ammonia decomposition reactions because H_2 volume increases far outweigh the volume of CO generated.

7.2.1.3 Hydrocarbons

From 600-650ºC, total hydrocarbons (THC) are stable at 66-67m^3 tds^{-1} however THC rapidly increases between 650-800ºC to an experimental high of 166 m^3 tds^{-1}. THC then declines with increased temperature reaching 130 m^3 tds^{-1} by 1000ºC. The decline in THC is mostly due to

reductions in ethane and ethylene. Ethane volume (14 m^3 tds^{-1}) peaks at 700°C and rapidly declines above 750°C being practically eliminated by 950-1000°C. Ethylene volume (45 m^3 tds^{-1}) peaks at 800°C and rapidly declines above 850°C. By 1000°C, its volume had undergone a 72% reduction from its peak to a low of 14.1m^3 tds^{-1} at 1000°C. Methane volume (106 m^3 tds^{-1}) also peaks at 800°C; however, it declines to a lesser extent, to a low of 95.3m^3 tds^{-1} at 1000°C. Or a 19% reduction between 800-1000°C. Acetylene is a hydrocarbon and tar cracking product and was first detected at 750°C. It undergoes strong growth with increasing temperature until 950-1000°C where it plateaus at 31-32 m^3 tds^{-1}. The strong growth in H_2 production between 950-1000°C may be because of the steam reforming of hydrocarbons since these compounds have relatively high H:C ratios.

7.2.1.4 Hydrogen sulphide

Figure 7-4 shows the estimated volume of hydrogen sulphide produced during sewage sludge pyrolysis between 600-1000°C.

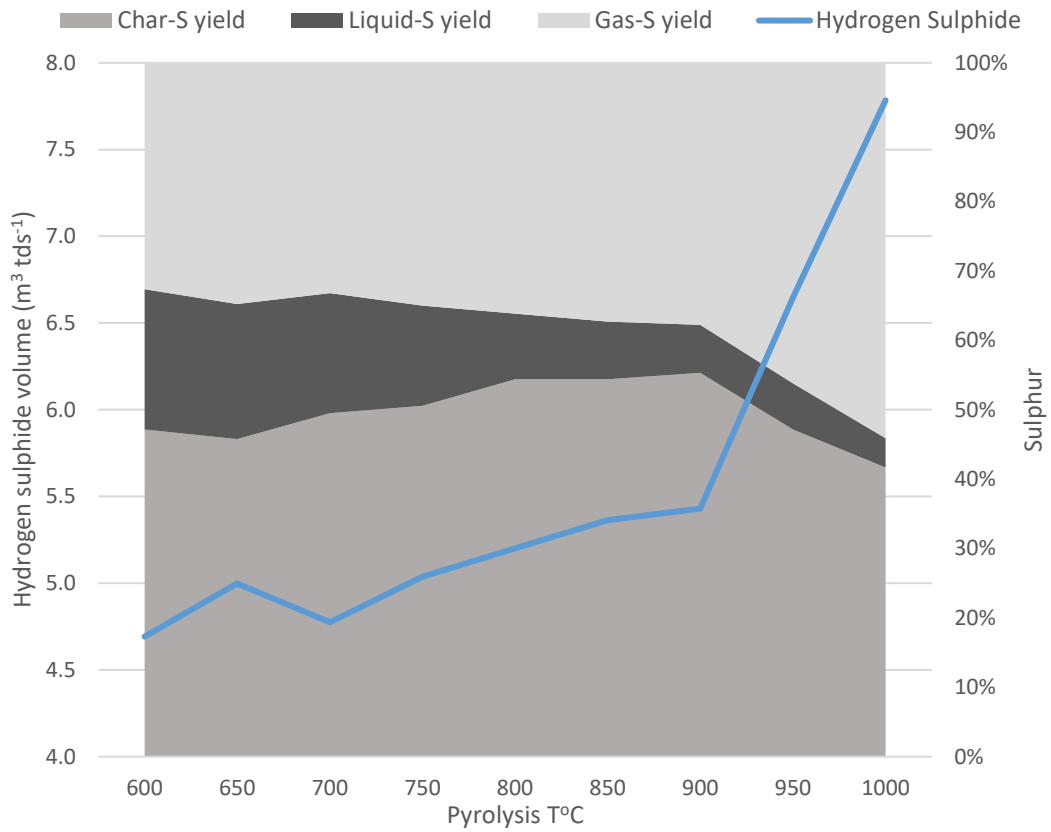


Figure 7-4: Gaseous sulphur emissions calculated by elemental mass balance expressed as hydrogen sulphide (H_2S) between 600-1000°C. Alongside the mass yield of S fractionated between the char, liquid and gas fractions.

H_2S production at 600-650°C is 4.7-5.0 m^3 tds^{-1} which represents up to 64% of peak H_2S production. This is associated with the decomposition of sludge macromolecules and conversion of bio-oils into aromatic tar compounds.

It also corroborates with Meade (1921), who reported that the bulk of H_2S formation occurred during the initial low-temperature stages of coal carbonisation. From 650-900°C, the liquid-S yield decreases from 19.5% to 6.9% of feedstock-S however H_2S yield increases only slightly to 5.4 m^3 tds^{-1}. From 650-900°C, char-S yield increased from 45.8% to 55.3% of feedstock-S. Therefore, ≤900°C SSC appears to act as a buffer preventing generation of additional H_2S. From 900-1000°C the quantity of sulphur retained within the SSC rapidly declines causing a spike in the estimated volume of H_2S to 7.8 m^3 tds^{-1}.

Table 7-17 shows that the C:S molar ratio of pyrolysis liquids is relatively stable between 600-700°C ranging between 82-84. However, from 700-800°C this ratio drops to an experimental low of 48 meaning the liquids become more saturated with sulphur compounds.

This is likely due to the formation and retention of thermally recalcitrant unsaturated heterocyclic sulphur compounds such as thiophenes, thiopyrans and thioazines. Above 800°C, the C:S ratio of the liquids increases again to a maximum value of 84 at 1000°C. From 650-900°C, the char-S yield increased at the apparent expense of liquid-S yield. This suggests that with increased temperature sulphur radicals preferentially react with condensing char aromatics which is likely due to favourable reaction kinetics and decreased tar availability. Alternatively, sulphide radicals may react with metal oxides and carbonates, forming group 2 sulphides, pyrites, and heavy metal sulphides.

Above 900°C, there are two likely mechanisms for the increase in gaseous sulphur species:

1. Decomposition of metal sulphates in SSC

XPS analysis showed that SSC-700 contained a significant content of metal sulphates (See Chapter 8.1.3.2, Fig 8-4), which is likely dominated by calcium sulphate ($CaSO_4$). $CaSO_4$ is thermally recalcitrant decomposing at approximately 1140°C in nitrogen (Yan et al., 2015). Yet, carbothermal reduction of $CaSO_4$ with CO proceeds at lower temperatures (~900°C) (Oh & Wheelock, 1990):

- $CaSO_4 + 4CO \rightarrow CaS + 4CO_2$ (>900°C)
- $CaSO_4 + CO \rightarrow CaO + CO_2 + SO_2$ (>997°C)

Above 900°C, the following solid-solid reaction between calcium sulphide and sulphate can also occur (Davies et al., 1994):

- $CaS + 3CaSO_4 \rightarrow 4CaO + 4SO_2$ (>900°C)

2. Decomposition of heterocyclic sulphur

From 900-950°C, char-S yield decreased from 55.3% to 47.1% and then further declined to 41.7% of feedstock-S at 1000°C. In contrast, liquid-S yields are stable between 900-950°C at 6.9% and 6.7% respectively and then decrease substantially to 4.2% at 1000°C.

This suggests that above 900ºC the remaining heterocyclic sulphur compounds in tar do not decompose until 1000ºC. Therefore, the decrease in char-S yields between 900-950ºC is less likely to be because of its heterocyclic structures decomposing.

Both mechanisms are likely contributors to increased sulphur emissions. Sulphate decomposition occurring between 900-1000ºC and producing mostly CaS and SO_2 rather than H_2S. Heterocyclic sulphur decomposition occurring predominately above 950ºC, a temperature associated with reforming reactions.

7.2.2 Fuel-gas flammability

The flammability of a gas or a mixture is influenced by several factors including: autoignition temperature, flammability limits, minimum ignition energy and others. The limits of flammability (LOF) are defined by the upper- and lower flammability limits (UFL & LFL) and represent the range of concentrations in which the gas or mixture is flammable (Coward & Jones, 1952). Table 7-8 illustrates the flammability limits for a range of gases that may be produced during pyrolysis:

Table 7-8: Fuel-gas components lower- and upper- explosion limits (Yaws & Braker, 2001)

Gas % Vol	LFL % vol vol^{-1}	UFL % vol vol^{-1}
Hydrogen	4.0	75.0
Carbon monoxide	12.5	74.0
Methane	5.0	15.0
Acetylene	2.5	100.0
Ethylene	3.8	36.0
Ethane	3.0	12.4
Ammonia	15.0	28.0
Hydrogen Cyanide	5.6	40.0
Hydrogen Sulfide	4.0	44.0
Carbonyl sulfide	12.0	29.0
Fuel-gas mixture[1]	7.5[2]	41.0[2]

[1] 32.7% H_2, 27.9% CO, 17.3% CH_4, 8.7 CO_2, 5.8% C_2H_2, 2.9% C_2H_4 and 4.8% N_2

[2]Tested by DEKRA Process Safety (Southampton, UK) in accordance with ASTM E681.

Table 7-5 showed that fuel-gas acetylene concentrations peaked at 5.7% at 950ºC. Since acetylenes UFL is 100%, it is potentially flammable at any concentration above 2.5% vol and could therefore pose a flammability and explosion risk when piped from the reactor through gas cleaning processes to the engine. The flammability limits of mixtures are different from the individual gases present (Chakrabarty et al., 2016). Le Chatelier (1891) first proposed a method of predicting gas flammability limits for mixtures which is still widely used, however the assumption used for LFL are not valid for the UFL (Mashuga & Crowl, 2000). Testing remains the more reliable method for attaining the UFL of gas mixtures.

Based on a H_2S-free fuel-gas sample produced at 950°C, a fuel-gas mixture was made up by FTI Ltd. (Sussex, UK) and its flammability limits were tested by DEKRA Process Safety (Southampton, UK). The mixtures LOF ranged between 7.5-41.0%. The UFL was lower than expected given its concentration of H_2, CO and acetylene. This suggests that the gas does not pose a safety risk when transported in pipelines or through gas cleaning systems. At the time of testing, this fuel-gas mixture had the highest concentration of acetylene observed, which is why this composition was selected.

Fuel-gas had not yet been produced at 1000°C, which although has less acetylene contains much higher hydrogen. Therefore, the LOF of fuel-gas produced at 1000°C may be slightly wider than the fuel-gas mixture tested.

7.3 Overall energy balance

The total energy content of fuel-gas, condensable liquids, and char for XS-6 are presented in figure 7-5. Total SSC (HHV) reduced from 1595 kWh tds^{-1} at 600°C to 1299 kWh tds^{-1} at 700°C, SSC (HHV). It then stabilised between 700-1000°C, ranging between 1262-1287 kWh tds^{-1}. Total liquid (HHV) rapidly declined between 600-800°C from 1664 to 509 kWh tds^{-1}. It then undergoes a further decline from 471 to 312 kWh tds^{-1} between 950-1000°C. Figure 7-5 also presents the total energy content of the measured char, liquids, and gas as a percentage of feedstock energy.

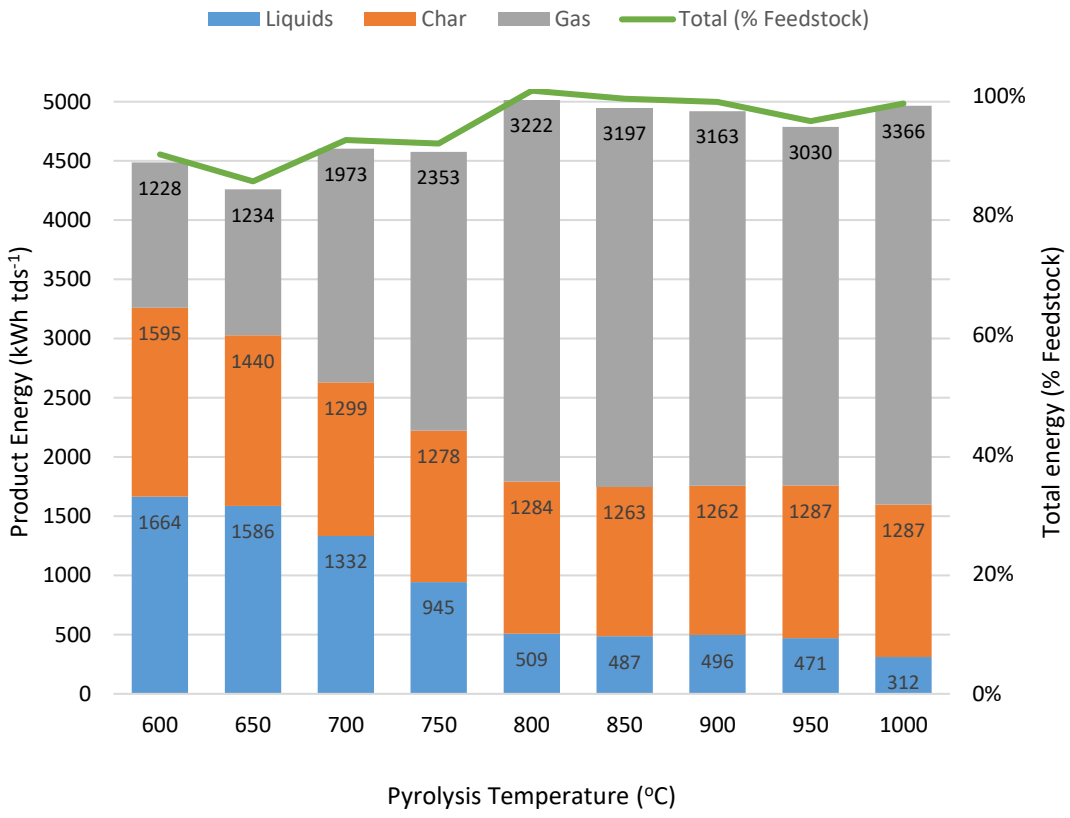


Figure 7-5: Measured energy content of char, condensable liquids and fuel-gas. Alongside the total energy recovery compared to the XS-6 feedstock.

It is indicative of the accuracy of the mass balance and measured energy values for the gas, liquids, and char. From 600-750ºC, only 86-93% of the feedstock's energy content was recovered. This is likely due to an underestimate in the liquid yield because of condensation in the outlet pipes. At low temperatures a greater proportion of NH_3 and C_3+ hydrocarbons are also expected to be present within the gas, therefore gas (HHV) may be slightly underestimated. From 800-1000ºC, the recovered energy content appeared more stable, ranging from 96.3 to 100.9% of feedstock energy. To improve the accuracy of the energy balance, measurement of NH_3 and CHN would have been helpful. Sample heterogeneity will have also contributed to imbalances.

The HHV of the SSC and condensable liquids were measured by bomb calorimetry, the results are presented in table 7-9. From 600-1000ºC, SSC (HHV) only underwent a slight reduction in energy content from 10.9 to 9.7 MJ kg^{-1} which shows that the material is largely stabilised at 600ºC. SSC (HHV) primarily drops between 700-800ºC and 900-1000ºC which is likely due to losses of N and S, rather than organic C or H.

From 600-700ºC, liquids (HHV) were high, 28.9-32.2 MJ kg^{-1}, which is reflected in the material high organic content. The high HHV is almost certainly due to the presence of fatty acid bio-oils within the liquids fraction. Note that from 600-650ºC, the fuel-gas contains little energy, but this rapidly increases between 700-800ºC because of hydrocarbon formation. These hydrocarbon gases are likely the result of fatty acids decomposing into fuel-gas. By 800ºC, the HHV of the liquids dropped to just 22.5 MJ kg^{-1}, it then gradually increased between 800-900ºC to 24.8 MJ kg^{-1}. From 900-1000ºC, the HHV of the fuel-gas increased rapidly which is likely due to the carbonisation of the tar and the elimination of its moisture content. At 1000ºC, the liquids had a HHV of 30.6 MJ kg^{-1}.

There was difficulty recovering a representative sample of the liquids because the consistency within the different traps was slightly different. A silicon kitchen spatula was used to wipe almost all the condensed liquids from the traps, it was then homogenised and tested by bomb calorimetry.

Table 7-9: Higher heating value (HHV) of the SSC and condensable liquids

Temperature (ºC)	Char HHV (MJ kg^{-1})	Condensable liquids (MJ kg^{-1})
600	10.9	32.2
650	10.9	31.0
700	10.8	28.9
750	10.5	25.6
800	10.1	22.5
850	10.0	23.5
900	10.1	24.8
950	9.9	27.4
1000	9.7	30.6

7.3.1 Parasitic load

The "current load" of furnace 2 (F2) was measured whilst pyrolyzing sewage sludge between 600-1000ºC in 100ºC intervals. The current was converted to power by the following equation:

$$Power\ (Watts) = Current\ (Amps) \times Voltage\ (V)$$

For further details on methodology see chapter 4.3.3.1. The values obtained were then plotted to generate a calibration curve of average power consumption during sewage sludge pyrolysis (Figure 7-6).

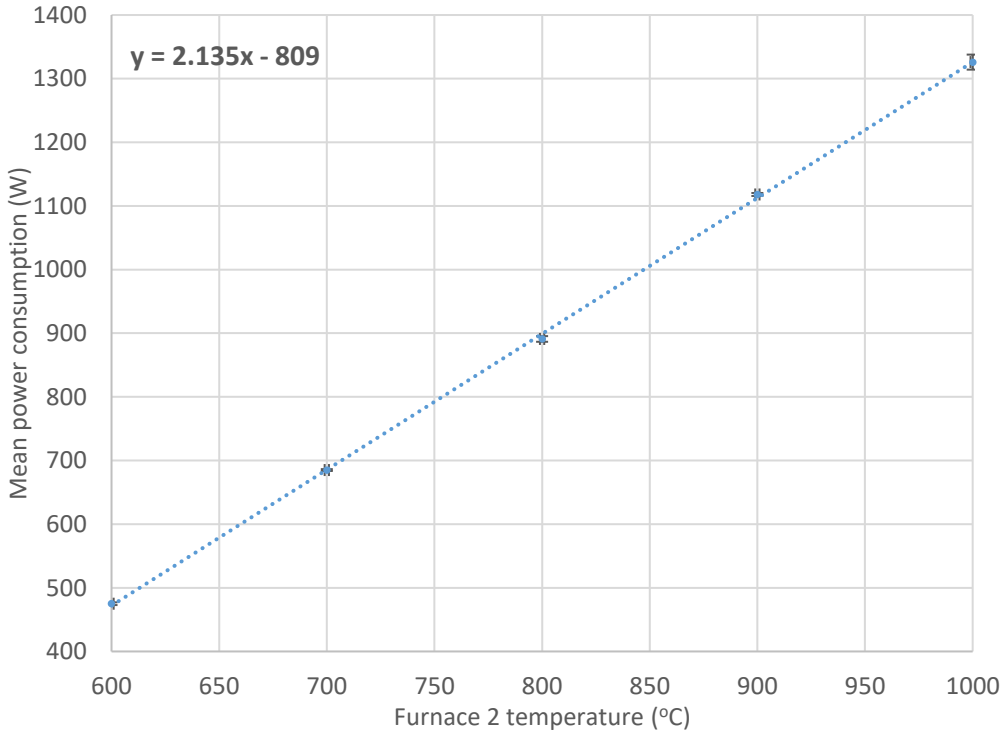


Figure 7-6: Power consumption for Furnace 2 during isothermal Py-C at a constant feed rate of 2.6 kg hr^{-1} and a dwell (t) of 120s.

Figure 7-6 illustrates there is a linear relationship (R2 = 0.9998) between F2 power consumption and furnace temperature with the equation: Y = 2.1349(x) - 809.01

This equation was then used to estimate F2 power consumption values between 600-1000ºC in 50ºC intervals. The energy consumption per tds was then calculated based on the machine's average feed-rate (2.6 kg ds hr^{-1}) the results are summarised in Table 7-10.

Table 7-10: Parasitic load of F2 when feeding dried sludge at a feed-rate of 2.6 kg hr^{-1}

Temperature	F2 power[1]	Parasitic Load
°C	Wh	kWh tds^{-1}
600	472	182
650	579	223
700	685	264
750	792	305
800	899	346
850	1006	387
900	1112	428
950	1219	469
1000	1326	510

[1]Estimated F2 power consumption at a feed-rate of 2.6 kg hr^{-1} (see figure 7-6)

To fully characterise the parasitic load of the lab-scale pyrolysis process, the electrical consumption of all furnaces and motors should have been conducted. However, the parasitic load of F2 alone was considered representative because it provides the energy to drive most endothermic pyrolysis reactions and is most similar to the layout of the proposed commercial process. In addition, the motors used 3-phase power which could not be measured using the ammeter available and are expected to have a minor electrical consumption compared to the thermal heating process steps of the apparatus.

The parasitic loads of a commercial pyrolysis and gasification process are reported by Mills (2015). Based on a throughput of 1.35 tds hr^{-1} of digested sludge the processes consumed 0.58 MW_e and 0.49 MW_e, respectively. Alternatively, this can be expressed as 363 W kg DS^{-1} and 430 W kg DS^{-1}. The exact operating conditions of the pyrolysis process reported by Mills (2015) are not disclosed, however the process used temperatures (>800°C) and retention times (>60 seconds). The value for pyrolysis reported by Mills (2015) was similar to the values obtained at laboratory-scale at 900°C.

7.3.2 Estimated net electrical energy output

The gross conversion efficiency (GCE) is the estimated quantity of electricity that could be generated from fuel-gas if it were combusted in a gas engine with an electrical conversion efficiency (ECE) of 40% and a parasitic load of 5%. The net conversion efficiency (NCE) is the electricity that could be generated minus any parasitic loads. Based on the measured fuel-gas energy content (table 7-6), measured parasitic load (Table 7-10), XS-6 energy content of 4972 kWh tds^{-1}, and estimated engine efficiency. The net conversion efficiency of lab-scale pyrolysis was calculated between 600-1000°C. The results are presented in table 7-11.

Table 7-11: Energy conversion during lab-scale sewage sludge pyrolysis[1]

T	Fuel gas[1]	GCE[2]		NCE[3]		Parasitic Load	
°C	kWh tds^{-1}	kWh tds^{-1}	% (XS-6)	kWh tds^{-1}	% (XS-6)	kWh tds^{-1}	%[3] (XS-6)
600	1127	428	8.6	246	5.0	182	42.5%
650	1131	430	8.6	207	4.2	223	51.9%
700	1817	690	13.9	426	8.6	264	38.2%
750	2156	819	16.5	514	10.3	305	37.2%
800	2920	1109	22.3	763	15.4	346	31.2%
850	2871	1091	21.9	704	14.2	387	35.5%
900	2829	1075	21.6	647	13.0	428	39.8%
950	2664	1012	20.4	543	10.9	469	46.3%
1000	2947	1120	22.5	610	12.3	510	45.5%

[1]Fuel-gas (LHV) - results based on isothermal Py-G of XS-6;

[2]Results based on conversion of fuel-gas (LHV) to electricity in a spark ignition gas engine with an ECE of 40% and a parasitic load of 5%;

[3]NCE = GCE minus parasitic load;

[4]Parasitic load as a percentage GCE

Table 7-11 demonstrates that GCE peaks at both 800°C and 1000°C with these temperatures achieving GCE of more than 22.3%. In comparison, NCE peaks at 800°C with 15.4% conversion of feedstock energy to net electricity. For lab-scale pyrolysis, energy recovery from fuel-gas was maximised at 800°C because:

- The parasitic load was relatively low at approximately 346 kWh tds^{-1} or 31.4% of GCE;
- Fuel-gas energy content was high because both methane and ethylene volumes peaked at 800°C before declining with increasing temperature;
- Fuel-gas H_2S concentrations were at their lowest recorded (approx. 15,600 mg m^{-3}) meaning the gas would require less extensive cleaning prior to conversion in a gas-engine.

There are two zones of liquid-yield reduction: the first occurs up to 800°C the latter from 1000°C. At 800°C, the operator benefits from the first zone in liquids reduction however the liquids yield is still 8.2% which is relatively high.

7.4 Elemental mass balance

This section will detail the mass balance of CHNS between the feedstock and products during sludge pyrolysis.

7.4.1 Elemental mass balance: Char

The yield of C, H, N and S in sewage sludge char as a percentage of the quantity in sewage sludge prior to pyrolysis is shown in figure 7-7 during Py-G, under isothermal temperatures between 500-1000°C. The results are discussed by element in the following sections.

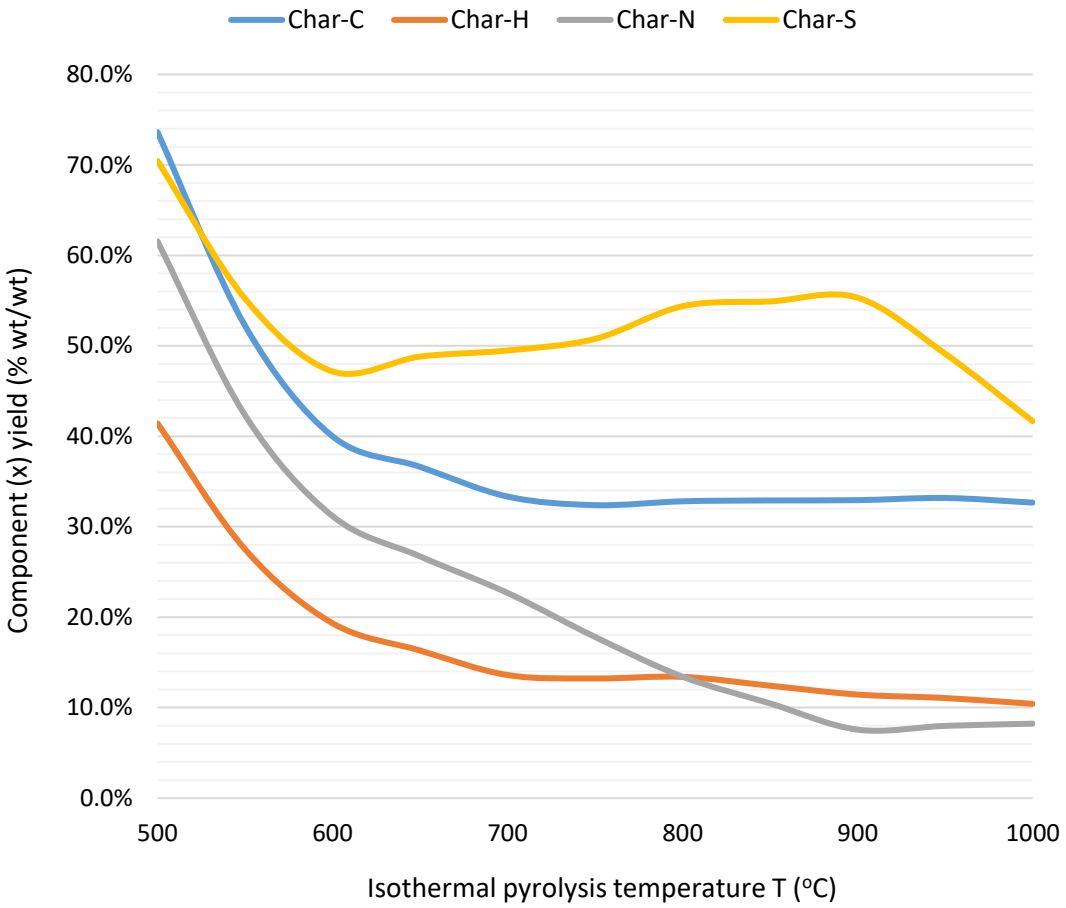


Figure 7-7: Yield of carbon, hydrogen, nitrogen and sulphur in sewage sludge char between 500-1000°C during isothermal Py-G

7.4.1.1 Elemental mass balance: Char carbon

Figure 7-7 shows that between 500-700°C the quantity of C in the char rapidly decreases, which is thought to be due to the loss of volatiles from the residual solids. From 700-1000°C, the char C yield is stable with a maximum value of 33.3% at 700°C and a low of 32.4% at 750°C. The results show that once C stabilises within char it is thermally stable and does not degrade with increased temperature. It suggests that the conditions at ≥700°C (120s retention time) were sufficient to stabilise carbon for biochar applications. It also shows that during the decomposition of tars or

hydrocarbons secondary carbon such as soot is not deposited on the char rather it remains in the gas or is deposited in the reactor as a fine particulates.

Last, the implication is that an increased temperature between 700-1000ºC has no effect on the conversion of C to char. Therefore, if one was to optimise char C retention by adjusting the initial temperature of decomposition, temperatures below 700ºC should be used. Table 7-12 compares the char-C yield during Py-B and Py-G.

Table 7-12: Char carbon yields for Py-B and Py-G

Pyrolysis T ºC	Py-B	Py-G
	Char carbon yield (%)[1]	
500ºC	42.3	73.6
550ºC	41.8	50.1
600ºC	38.1	40.0
650ºC	39.7	36.6
700ºC	39.1	33.3
750ºC	38.1	32.8
800ºC	32.4	32.8
850ºC	36.5	32.7
900ºC	36.7	32.9
950ºC	-	33.2
1000ºC	-	32.7
Non-isothermal Pyrolysis[2]	-	37.6[1]

[1]Char C as a percentage of total feedstock (XS-6 or XS-B) carbon

[2]Result obtained during non-isothermal Py-G where F2 was operated at 600ºC for 600s and F3 was operated at 800ºC for 45s

During Py-B, sludge was heated slowly at 10ºC min^{-1}, whilst for Py-G the furnace was at the required temperature, hence the sludge heating rate would be high, and the material would have reached the furnace temperature in a time-frame of seconds to minutes. At higher temperatures, the temperature gradient between sludge and furnace is steeper, therefore the material likely reaches the furnace temperature more quickly. Slow heating rates are typically associated with increased char-C yields because a greater proportion of C can polymerise into the char ring structure.

From 500-600ºC, char-C yields are lower for Py-B than Py-G this is strongly indicative that Py-G char is insufficiently pyrolysed and still contains volatiles. The SSC produced between 500-600ºC was tested by thermogravimetric analysis and contained low temperature volatiles. Also, when Py-G SSC produced at 500 or 550ºC was leached with methanol it discoloured the solvent, suggesting the material still contained non-condensed organic compounds. Py-G char yields stabilised between 700-1000ºC at approximately 32-33% whilst Py-B char yields stabilise at 38-39% between 600-750ºC and 36% at 850-900ºC. This shows that slow heating-rates can increase

char-C retention by up to 7% between 600-750ºC and 3% between 850-900ºC. This is not a particularly large difference and the increase between 600-750ºC is likely driven by the retention of less stable ring structures.

For example, Py-B C, H, N simultaneously undergo a yield reduction in SSC at temperatures >750ºC which suggests that heterocyclic ring structures breakdown because of carbonisation. In contrast, Py-G SSC C is stable between 700-1000ºC suggesting the increased heating rates during Py-G retard the formation of these stable condensed structures.

To test the theory that Py-G C yield could be increased by operating the reactor at temperatures below 700ºC and thus lower heating rates, non-isothermal pyrolysis was conducted. Furnaces 2 was operated at 400ºC, 500ºC, 600ºC and 700ºC for 600s and furnace 3 was operated at 800ºC for 45 seconds. The SSC that was first stabilised at 500ºC and 600ºC showed an elevated quantity of fixed carbon, with the latter producing the highest quantity of fixed carbon. The SSC produced non-isothermally at 600ºC followed by ramping period to 800ºC was analysed by ultimate analysis and the results shown in table 7-12 show that the material retained similar quantities of C to Py-B SSC.

7.4.1.2 Elemental mass balance: Char hydrogen

Table 7-13 compares the char-H yields during Py-B and Py-G.

Table 7-13: Char hydrogen yields for Py-B and Py-G

Pyrolysis T ºC	Py-B	Py-G
	Char hydrogen yield (%)[1]	
500ºC	22.1	41.4
550ºC	20	25.2
600ºC	15.6	19.3
650ºC	15.3	16.3
700ºC	12.9	13.5
750ºC	11.4	13.2
800ºC	9.9	13.4
850ºC	7.9	12.1
900ºC	7.9	11.4
950ºC	-	11.2
1000ºC	-	10.4
F2: 600ºC F3: 800ºC	-	12.8[2]

[1]Char H as a percentage of total feedstock (XS-6 or XS-B) hydrogen

[2]Result obtained during non-isothermal Py-G where F2 was operated at 600ºC for 600s and F3 was operated at 800ºC for 45s

At 500ºC, Py-G char-H yields are just 41.4%, the lowest of the 4 elements in figure 7-13. This result was expected since dehydration reactions are the first to occur at low-temperatures and typically produce water vapour. From 500-600ºC, Py-G char was insufficiently pyrolysed

therefore char-H yields were far higher than corresponding Py-B values. However, Py-B char-H also remains elevated at ≤550ºC suggesting these temperatures are incapable of stabilising the SSC.

From 650-700ºC, the char-H yield for Py-B and Py-G narrows to within 1% suggesting Py-G char and furnace temperature had equilibrated and that temperature was the primary factor driving hydrogen removal and char-H retention ≤700ºC. At these temperatures, H removal is strongly associated with the loss of volatiles, therefore it also suggests that both processes have removed the majority of volatiles. From 700-850ºC, Py-B char-H yields drop from 11.4% to 7.9%, this loss is associated with the process of carbonisation rather than volatile loss. It also mirrors a small drop in char-C yields and may be associated with the decomposition of less stable structures that polymerise into the ring structure due to the slower heating rate. From 700-800ºC Py-G char-H yields stabilise between 13.2-13.6% before declining with increased temperature to 10.4% at 1000ºC. The extent of char-H retention is important because the literature suggests there is a strong relationship between long-term char-C stability and the molar ratio of H:C. This will be discussed in more detail in section 8.1.5.

7.4.1.3 Elemental mass balance: Char nitrogen

Py-G char was insufficient pyrolysed between 500-600ºC consequently char-N rapidly declines across this temperature range as volatiles are increasingly removed. For Py-G, yields of char, char-C and char-H all stabilised ≥700ºC however, table 7-14 shows that char-N follows a different trend. From 600-900ºC char-N declines at a constant rate to a minima of just 7.6%. The char-N then remains relatively stable, increasing slightly to 8.23% at 1000ºC. Table 7-14 also

Table 7-14: Py-B and Py-G char nitrogen yields

Pyrolysis T ºC	Py-B	Py-G
	Char nitrogen yield (%)[1]	
500	57.1	61.6
550	47.8	41.5
600	41.6	31.2
650	41.3	26.0
700	38.2	22.7
750	33.6	18.1
800	23.8	13.4
850	17.4	10.5
900	18.3	7.6
950	-	8.0
1000	-	8.2
F2: 600ºC F3: 800ºC	-	22.0[2]

[1]Char N as a percentage of total feedstock (XS-B or XS-6) nitrogen

[2]Result obtained during non-isothermal Py-G where F2 was operated at 600ºC for 600s and F3 was operated at 800ºC for 45s

compares the char-N yield during Py-B and Py-G. In both cases char-N decreases with increasing temperature however, Py-B produces higher char-N yields.

The structure of char is composed of a covalent network of polycyclic carbon (McBeath et al., 2014), whilst researchers have shown that N also forms condensed heterocyclic ring structures such a pyrollic-N, pyridinic-N and graphitic-N in char (Ayiania et al., 2020) (Haghighi et al., 2020). The retention of N within SSC suggests both polycyclic and heterocyclic ring structures are present. In addition, N may be present as surface functional groups (e.g. cyanogen's) and within the ash fractions as reduced inorganic nitrides.

Table 7-14 shows that heating rates appear to be an important factor regulating Char-N retention. For Py-G, the rapid heating rates may fragment proteins into smaller volatile heterocyclic tar compounds therefore char-N is minimised. When heated slowly, organic N such as amino-acids proline, histidine and tryptophan likely polymerise into the covalent char ring-structure. When Py-G was conducted in two stages: (i) 600ºC for 10 minutes followed by (ii) 800ºC for 45 seconds, the char-N yield was 22%. In comparison, Py-B yielded a similar result of 23.8%, whilst isothermal Py-G yielded 13.8% char-N. This suggests that the slow heating rates used during Py-B are unnecessary to stabilise additional N in the char if this is desired.

The difference between Py-B and Py-G char-N retention peaks at 750ºC at 15.8% it then declines to 10.4% by 800ºC. Interestingly, this decline corresponds with peak tar decomposition during Py-G, which suggests Py-B char-N and Py-G tar-N could have common parent compounds or have similar structures. This observation suggests that there may be advantages in managing the fate of the nitrogen in the sludge through modifying the reactor design to promote or inhibit char-N by adjusting the heating rates. For example, the resistivity of an electrically heated screw could be modified across its length to create an initial low-temperature zone to stabilise N followed by a high temperature zone to promote char-gas interactions.

7.4.1.4 Elemental mass balance: Char sulphur

Figure 7-7 shows that the Char-S yield decreased rapidly between 500-650°C from 70.4% to 45.8%, however unlike other elements the char-S yield then increased with increased temperature to 55.3% at 900°C. At temperatures above 900°C, the S yield decreases and reaches an experimental low of 41.7% at 1000°C. Table 7-15 compares the char-S yield during Py-B and Py-G.

Table 7-15: Py-B and Py-G char sulphur yields

Pyrolysis T °C	Py-B	Py-G
	Char sulphur yield (%)	
500	-	70.4
550	24.6	55.2
600	-	47.2
650	-	45.8
700	23.2	49.5
750	-	50.6
800	-	54.4
850	19.0	54.4
900	-	55.3
950	-	47.1
1000	-	41.7
F2: 600°C F3: 800°C	-	43.3

[1]Char S as a percentage of total feedstock (XS-6 or XS-B) sulphur

[2]Result obtained during non-isothermal Py-G where F2 was operated at 600°C for 600s and F3 was operated at 800°C for 45s

Unlike CHN, for Py-B, char-S was only measured at three temperatures 550°C, 700°C and 850°C. Despite fewer data points, it can be seen that under Py-B conditions, char yielded much lower char-S than Py-G. This suggests that heating rate is more important than the highest heating temperature for char-S retention. Although, the highest heating temperature influences the char-S yield because it decreases between 550-850°C for Py-B and undergoes changes during Py-G (table 7-15). Char-S may be present as: metal sulphides, metal sulphates, and organo-sulphur ring structures that resemble heterocyclic compounds such as thiophene (Ren et al., 2020).

7.4.2 Elemental mass balance: Liquids

The CHNS yield in pyrolysis liquids as a percentage of feedstock CHNS is presented in figure 7-8 during isothermal Py-G. The pyrolysis liquids include any condensed tar, moisture, or volatile organic compounds.

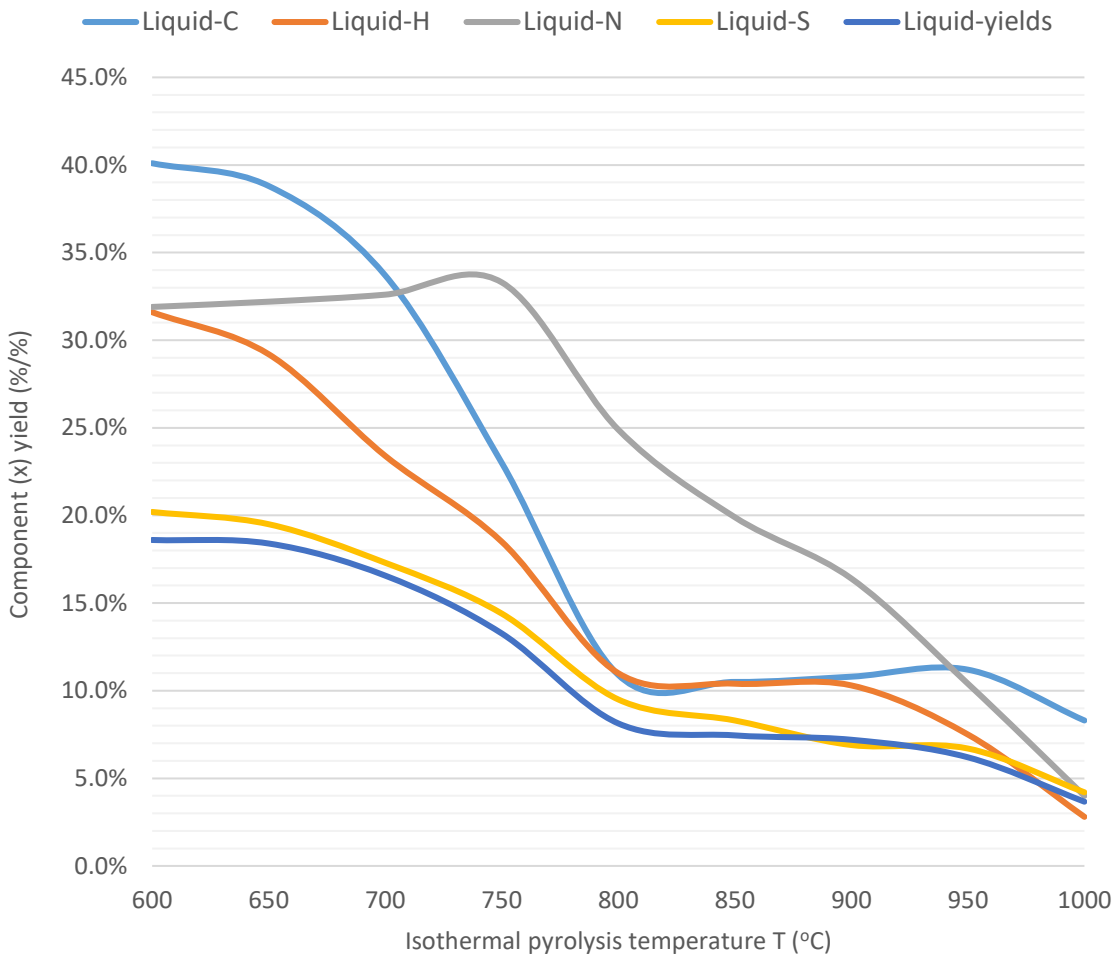


Figure 7-8: Yield of carbon, hydrogen, nitrogen and sulphur in pyrolysis liquids between 500-1000°C during isothermal Py-G.

Figure 7-8 shows that as the mass yield of Py-G liquids decreased with increased temperature, the yield of feedstock C, H, N and S in the liquids also decreased. From 600-750°C, only the yield of N increased in the liquids fraction, with C and H both undergoing disproportionally large reductions whilst S decreased proportionally compared to tar reduction. Consequently, the elemental composition of the tar changed considerably (Table 7-16). From 750-800°C, a large decline in tar yield occurred and the yield of N decreased for the first time from 33.3% to 24.9%. However, H/C decreased too, leading to further increases in liquid-N concentration to an experimental high of 14.1%.

Table 7-16: Ultimate analysis of Py-G liquids

T (°C)	C Wt. %	H Wt. %	N Wt. %	S Wt. %	O Wt. %	Other (Ash) Wt. %
600	74.9	7.9	7.9	2.4	-	6.9
650	73.2	7.4	8.1	2.3	-	9.0
700	70.7	6.6	9.1	2.3	-	11.3
750	60.1	6.5	11.6	2.4	-	19.4
800	46.5	6.3	14.1	2.6	-	30.6
850	48.8	6.5	12.3	2.5	28.2	(1.7)
900	52.1	6.7	10.5	2.1	-	28.6
950	62.9	5.6	7.8	2.4	-	21.4
1000	78.7	3.6	5.0	2.5	6.2	(4.0)

[1]Only Py-G liquids at 850°C & 1000°C were measured for ash content by LOI at 550°C. The oxygen content was then measured by difference. Other is the sum of oxygen and ash.

As carbohydrates, proteins, fatty acids, and lignocellulosic materials in sludge decompose, a wide variety of compounds are expected to be formed, including saturated aliphatic, aromatic, and branched organic compounds. As the pyrolysis temperature increased from 600 to 800°C many of these compounds are expected to decompose into the gas phase or form stable unsaturated aromatic structures. This helps explain why liquid C and H yields rapidly decreased within this temperature range. The simultaneous loss of C and H from the liquid fraction led to large increase in hydrocarbon gases from 116m^3 tds^{-1} at 700°C to 180m^3 tds^{-1} at 800°C, with fuel gas LHV and net energy balance both peak at 800°C (as discussed previously).

The recalcitrance of N between 600-750°C suggests this element is mostly present in a stable form, such as the ring structure of heterocyclic compounds (e.g. pyridine). From 800°C to 950°C the mass yield of C (7.5-11.2%) and H (7.5-11.0%) stabilised however liquid-N yield continued to decrease from 24.9% at 800°C to just 10.4% at 950°C. Large losses of N without corresponding losses of C suggest: (i) Tars carbonise rather than decompose ejecting less stable N from their ring structures; and/or (ii) N is lost as HCN, which then decomposes into N_2 and soot, with soot accumulating in the liquids fraction and contributing to Liquid-C because of the experimental design.

Table 7-16 demonstrates that the concentration of "other" elements in the liquids fraction peaks at 800°C, at 30.6 Wt.%, and undergoes meaningful reductions from 28.6% Wt. at 900°C to 21.4% Wt. at 950°C and then 10.2% Wt. at 1000°C. This "other" component is expected to predominately consist of O, however, compounds containing low boiling elements may be reduced through carbothermic reduction, volatilise, and then condense alongside the organics. For example, liquids at 850°C and 1000°C were tested by LOI (at 550°C) and were shown to contain 1.7% and 4.0% ash respectively. The compounds containing oxygen within the condensable liquids are likely to include water and organic compounds such as phenolics, furans and pyrans.

Liquids produced at ≤950ºC formed crystal-like precipitates when stored at room temperature, which could be separated from the residual tar due to their relatively low solubility in acetone and high solubility in water. This supports the theory that phenolic compounds are present within the condensable liquids, which has previously been reported for coal carbonisation liquids (Mcneil, 1975). Phenol is not currently classified as a carcinogen (ATSDR, 2008); however some studies suggest phenol acts as a tumour promoter (Babich & Davis, 1981). Likewise, furans

From 900-950ºC, the concentration of "other" compounds in the liquids decreased, which is likely due to phenolic or heterocyclic-O organics decomposing into CO rather the steam reforming reactions. Steam reforming reactions generate H_2 however no increase in volume occurs between 900-950ºC (Figure 7-2). From 950-1000ºC there was another decrease in the concentration of "other" in liquids, a sharp increase in H_2 volumes (figure 7-2) and a loss of the observable aqueous fraction with the condensed liquids which is strong evidence for steam reforming reactions occurring. As discussed in section 2.3.3.3, water vapour in the gas may inhibit decomposition of NH_3 into N_2 because of stabilisation of the amidogen radical and the generation of hydroxyl radicals.

From 950-1000ºC, the liquid yields of C, H, N and S all decreased by the following amounts: 2.9%, 4.7%, 2.4% and 6.4% respectively (Figure 7-7). Whilst the composition of the liquids also changed with the percentage of H and N reaching experimental lows, and C a high of 78.7% (Table 7-16). At 1000ºC several physical changes in the Py-G products were observed:

(i) The colour of the fuel-gas exhausted into the gas traps darkened from an orangey brown colour to a dark black-brown colour.

(ii) The viscosity of the tar markedly increased sticking to the glass trap walls rather than slowly running down and collecting at the bottom of the trap.

These changes may be due to increased concentrations of carbon within the condensable liquids and polymerisation of the carbon into soot and tertiary tars. The behaviour of liquid-S has not been discussed; however, its concentration remains relatively stable at all temperatures tested (Table 7-16), meaning its concentration correlates strongly with liquid yield. The reasons for this are unclear, although the implication is that S behaviour is biased towards forming heterocyclic organic species which are thermally stable and readily condensed.

Table 7-17 compares the molar ratio of elements in the liquids fraction. The data highlights the changing composition of Py-G liquids, in particular: (i) the increased H:C ratio between 700-850ºC which is associated with increased water vapour formation, followed by its rapid decline between 900-1000ºC. (ii) The increased concentration of heteroatoms between 600-800ºC followed by their relative decline between 800-1000ºC. The H:C ratio of 0.55 at 1000ºC is low, for comparison table 7-18 summarises the H:C ratios of select hydrocarbons and their boiling points.

Table 7-17: Molar ratios Py-G liquids

T (ºC)	H:C	C:N	C:S
600	1.3	11.1	83
650	1.2	10.5	84
700	1.1	9.1	82
750	1.3	6	67
800	1.6	3.8	48
850	1.6	4.6	52
900	1.5	5.8	66
950	1.1	9.4	70
1000	0.55	18.4	84

In benzene, each carbon atom is bonded to one hydrogen atom. Compounds with higher molecular weights, but lower H:C ratios, increasingly form covalent, multiple ring structures, where C is bonded only to C. This increases the stability of the compounds and decreases properties such as volatility and biodegradability. Compounds with large covalent ring-structures tend to form from aromatic pre-cursors through polymerisation. Soot and char are just large agglomerations of aromatic molecules with extensive amorphous ring structures formed through polymerisation. The low H:C ratio of tar produced at 1000ºC suggests its molecules have undergone polymerisation, which is characteristic of refractory tars and soots produced during high temperature thermal cracking (Milne et al., 1998). Although high temperatures (≥1000ºC) reduced the overall tar-yield, the liquid residues formed may be more problematic than the lighter aromatics because of their tendency to readily condense on inner surfaces, even at elevated temperatures, and their formation ultimately increase the chances of blockages within the reactor system (see figures 5-8 to 5-12).

Table 7-18: The C:H ratio and boiling points of select hydrocarbons and Py-G products

Compound	Boiling Point	H:C Ratio
Benzene (C_6H_6)	80.1ºC	1.00
Anthracene ($C_{14}H_{10}$)	340ºC	0.71
Pyrene ($C_{16}H_{10}$)	404ºC	0.63
Anthanthrene ($C_{22}H_{12}$)	547ºC	0.55
Py-G condensables (1000ºC)	n/a	0.55
Py-G Char (1000ºC)	n/a	0.51

7.5 Non-isothermal pyrolysis and tar formation

So far, chapter 7 has explored the mass & energy yields obtained during isothermal pyrolysis, for example, when furnaces 1-3 are operated at the same temperature. However, a dichotomy exists between the ideal highest heating temperature (HHT) for char and the gaseous volatiles. For example, above 700ºC the total C yields in the char were stable suggesting gas production from char decomposition has ceased, whilst large quantities of gas were generated due to tar decomposition between 700-850ºC and 950-1000ºC. Also, heating the volatiles to ≥950ºC increased gas yields and minimised tar yields. Whilst heating SSC to ≥950ºC decomposed its content of S, leading to a spike in emissions that need to be removed with additional cost affects upon the process operation.

Tar is a system contaminant, a pollutant and currently has no commercial value therefore its conversion to fuel-gas is highly preferable. This section will explore the effectiveness of tar reduction through thermal cracking during non-isothermal pyrolysis. Figure 5-3 demonstrated the design of the lab-scale reactor which includes three heating zones:

- In furnace 2 (F2) primary tars evolve from the char and undergo gas-solid reactions which may have a strong influence on tar yields. This process will be referred to initial thermal decomposition (ITD).
- In furnace 1 (F1) gaseous volatiles are decomposed in the absence of char. This process will be referred to as thermal cracking.
- In furnace 3 (F3) partial of fully devolatilised SSC enters the furnace and undergoes further stabilisation in the relative absence of gaseous volatile. This is expected to be less relevant to overall tar yields.

Many pyrolysis systems operate isothermally; however, it could be beneficial to operate multiple heating zones to minimise tar yield and parasitic load. To assess the relative effectiveness of initial thermal decomposition and thermal cracking on tar yields, the temperature of F1 and F2 were operated at 700ºC, 850ºC and 1000ºC in accordance with Table 7-19.

Table 7-19: Experimental conditions

Experimental label	F1 (ºC)	F2 and F3 (ºC)
Iso-700	700	700
Iso-850	850	850
Iso-1000	1000	1000
ITD-850	700	850
ITD-1000	700	1000
TC-850	850	700
TC-1000	1000	700
ITD-1000 (850)	850	1000
TC-1000 (850)	1000	850

A new batch of sludge was also used (e.g. XS-9), which unlike the sludge used in chapter 7 (XS-6) was visibly more fibrous and crumbled easily into pellets once dry. The properties of XS-9 are summarised in table 6-1, in summary:

- The organic content of XS-9 was higher than XS-6, with a LOI (% Wt) and C (% Wt) content 4.3% and 4.0% higher, respectively.
- XS-9 HHV was similar to XS-6, however on a DAF basis the organics in XS-9 were less energy dense containing 1.2 MJ kg^{-1} less energy. XS-9 was sampled when the SGP at Crossness STW was suppressed (§10.1.1). This is reflected in the materials higher C:N, suggesting a lower concentration of proteins.

When pyrolysed, XS-9 produced substantially higher gas yields, less char, and equivalent quantities of condensable liquids compared to XS-6. For example, at 850ºC isothermal XS-6 and XS-9 produced gas yields of 47.5% and 55.8% and char yields of 45.5% and 36.7% respectively. However, the condensable liquid yield was almost identical at 7.5% and 7.6% respectively. Despite the differences in sludge characteristics compared to Section 7.0, the effect of non-isothermal conditions was investigated. Figure 7-9 illustrates the relative effect of initial thermal decomposition and thermal cracking on XS-9 liquid yields.

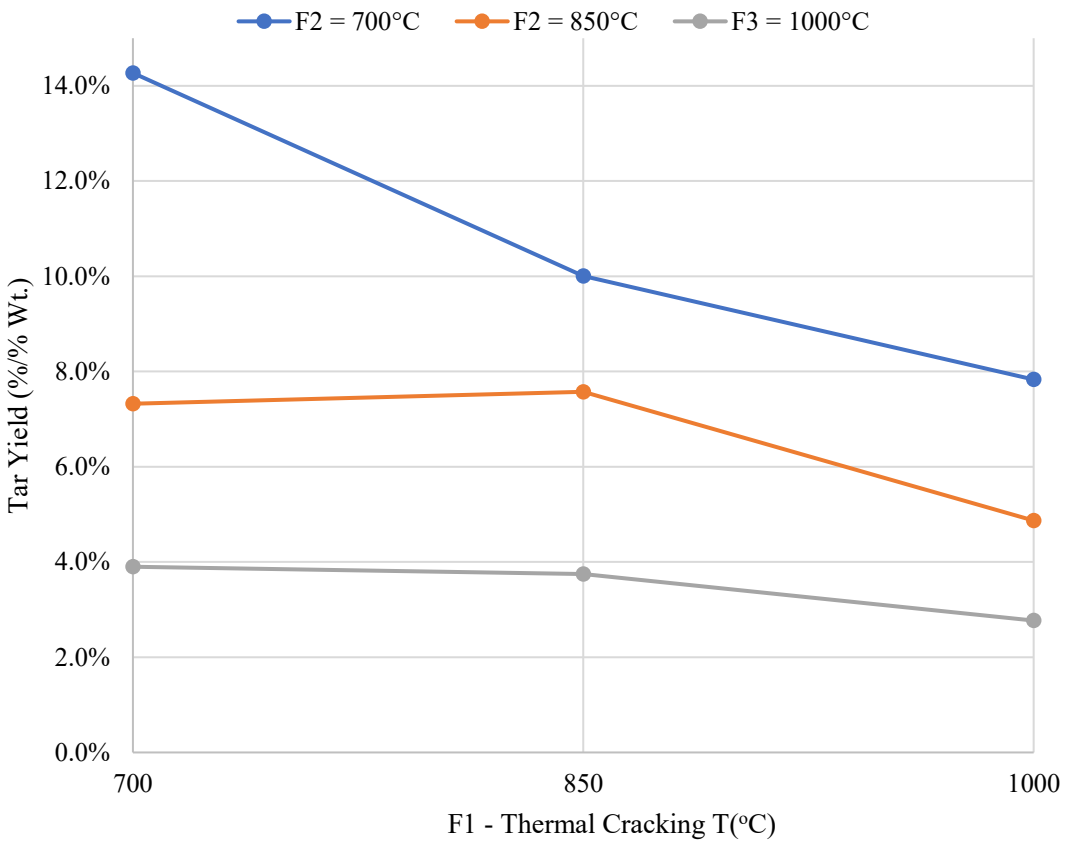


Figure 7-9: : Influence of initial thermal decomposition in furnace 2 and thermal cracking in furnace 1 on liquid yields for XS-9 sludge at 700, 850 and 1000ºC

Each series shows the liquid yield (% wt.) obtained for a set initial thermal decomposition temperature when thermal cracking is varied between 700-1000ºC in 150ºC increments. It shows that increasing the temperature of both these values lowers liquid yield, however, initial thermal decomposition has a disproportionate influence. Also, both temperatures work synergistically since the lowest liquid yield of 2.8% was obtained when both were set to the maximum of 1000ºC.

1. Initial thermal decomposition temperature = 700ºC

For iso-700ºC the average liquid yield was 14.3%, which is slightly lower than the results for XS-6 presented in table 7-3, when liquid yield was 16.6%. This difference could be due to differences in sludge composition. With an increased cracking temperature (850ºC & 1000ºC), the liquids obtained continued to decrease to 10% and 7.8% respectively.

2. Initial thermal decomposition temperature = 850ºC

When the temperature of thermal decomposition was increased from 700ºC to 850ºC, the liquid yield across all cracking temperatures decreased. At 850ºC the liquid yield was 7.3%, which is significantly lower than the yields obtained when the decomposition temperature was 700ºC. This result illustrated the disproportionate influence on liquid yield of the decomposition temperature compared to the thermal cracking temperature.

When the cracking temperature was increased from 700 to 850ºC the liquid yield obtained remained approximately constant at 7.6%, however a further increase to 1000ºC caused a reduction to 4.9%. The lack of liquid yield reduction between 700-850ºC is different from the results obtained for the decomposition at 700ºC. A possible explanation is that for decomposition at 700ºC, the fuel-gas contained a significant proportion of labile organic compounds such as bio-oils, which are decomposed when the cracking temperature is increased from 700ºC to 850ºC. However, when thermal decomposition occurs at 850ºC, these labile compounds have already been decomposed and are not present when F1 is operated at 850ºC. A further increase in cracking temperature to 1000ºC decreased overall liquid yields.

3. Initial thermal decomposition temperature = 1000ºC

When the decomposition temperature was increased from 850ºC to 1000ºC, the liquid yield, regardless of cracking temperature, was lower than the results obtained for decomposition at 700ºC and 850ºC. The liquid was stable when the cracking temperature was increased from 700ºC to 850ºC suggesting labile organic had already been eliminated. When the process was operated at iso-1000ºC, a further reduction in tar yield was observed from 3.8% to just 2.8%.

These results support the theory that bio-oils, derived from the sludge organics (fats, oils, carbohydrates, and proteins), are largely converted into thermally recalcitrant heterocyclic compounds between 700-850ºC. For example, high temperature cracking was only effective at reducing liquid yields between 700-850ºC when decomposition was conducted at 700ºC and recalcitrant compounds had not yet formed. When decomposition was conducted at 1000ºC, increasing the cracking temperature had no effect upto 850ºC, which suggests the heterocyclics are stable at 850ºC and the labile structures had already been eliminated. This corroborates with the elemental mass balance for liquids (table 7-16), which showed that the C:N and C:S ratio for pyrolysis liquids mostly increased at ≥900ºC.

When the temperature of cracking was increased from 850ºC to 1000ºC, the liquid-yields for all thermal decomposition series decreased. Interestingly, when cracking was increased to 1000ºC for decomposition at 700ºC and 850ºC the liquid yield reduction was proportional. It is suspected that between 700-850ºC the primary mechanism for decomposition is pyrolytic since the condensable liquids contained an aqueous fraction. However, at 1000ºC the aqueous fraction is eliminated therefore, the method of decomposition could be steam reforming. The proportional decrease may be because of both conditions producing equitable quantities of steam during pyrolysis which can only reform stoichiometric quantities of heterocyclic tars. Although it may also be because of kinetic constraints.

7.6 Regulatory compliance

The regulatory limits for syngas EOW status were presented in table 2-14, whilst the regulatory limits for combustion processes such as incinerators and engines were presented in section 2.4.4. To operate an ATC process in the UK, there are two options to ensure regulatory compliance:

(i) Classify the process as a waste incineration process and comply with waste incineration ELVs (Table 2-10). In addition, comply with the MCPD ELVs for "other gaseous fuels" for either incineration (Table 2-15) or engines (Table 2-16). The plant must be operated as a waste incinerator and conduct all the testing required for a waste incineration process.

(ii) Achieve EOW status for the fuel-gas and comply with the MCPD ELVs for other gaseous fuels for incineration or engines.

The conversion of fuel-gas to combined heat and power within engines is desirable because of the relatively high ECE compared to a steam turbine. Therefore, cleaning the gas to the highest possible standards and achieving EOW status may be viewed as desirable. Table 2-14 presented the Environment Agencies regulatory position on syngas EOW; however, these values were not adjusted for fuel-gas LHV (Personal communication, 2020). Table 7-20 presents the LHV-adjusted EOW requirements for "syngas" produced at 800°C and 1000°C alongside the requirements for biomethane (Environment Agency, 2013).

Table 7-20: End-of-waste requirements for "syngas"

Parameter	Unit	Fuel-gas (800°C)	Fuel-gas (1000°C)	Biomethane
Total sulphur	mg m^{-3}	0.32	0.27	30
Hydrogen sulphide		0.22	0.19	5
Total halogenated hydrocarbons		0.039	0.033	1.5
Heavy metals total		0.089	0.075	$(0.1)^3$
Total aromatic hydrocarbons expressed as Xylene		1.45	1.22	100
HF		2.78	2.34	5
HCl		0.83	0.70	1.5

[1]Natural gas, fuel-gas (800°C) and fuel-gas (1000°C) LHV of 35.06, 19.5 and 16.4 respectively

The EOW requirements for fuel-gas are far stricter than biomethane despite the limits being set in accordance with the same comparator material. Regulations are applied to protect human and environmental health. For natural gas and biomethane the GSM regulations and EOW requirements are based on gas safety in pipelines and public exposure. Syngas will be combusted in an engine on an industrial site, therefore natural gas is not a suitable comparator material.

For clean syngas of known specifications, the best comparator materials and applications are likely to be: (i) biogas combustion on STW (ii) waste incineration, since ATC processes represent an alternative to these processes.

Tables 2-15 to 2-17 summarised the MCPD ELV requirements for a variety of materials and processes. However, these ELVs are difficult to compare with syngas EOW requirements because the ELVs monitor post-combustion products (e.g. SO_2). In addition, the ELVs in the MCPD are presented at different concentrations of oxygen. A comparison of SO_2 emissions was conducted for all the regulatory limits. To aide comparison, all the regulatory limits have been converted to SO_2, harmonised to 0% oxygen (using the equation in 2.3.4) and are presented on a dry-basis where H_2S has been converted to SO_2 and diluent N_2 has been added on a stoichiometric basis.

Table 7-21: Estimated SO_2 emissions for natural gas, biomethane and syngas based on their harmonised MCPD emission limits values (ELV) for different fuels and oxidation methods

Parameter	Refer to #	H_2S Limit mg m^{-3}	SO_2 ELV[2] mg m^{-3} (dry)	Harmonised SO_2[3] mg m^{-3} (dry)
UK Natural gas	2-11	0.4	-	0.14
GSM		5	-	1.71[5]
Biomethane EOW	2-13	5	-	1.71[6]
Syngas-800°C EOW[7]	2-14	0.22	-	0.14[4]
Syngas-1000°C EOW	2-14	0.19	-	0.15[5]
Biogas engine	2-15	-	40 (15% O_2)	142
Other gas engine	2-15	-	15 (15% O_2)	53
Biogas engine STW (SR2009 No 4)	2-17	-	107 (5% O_2)	141
IED Incineration	2-10	-	50 (11% O_2)	106
Biogas incineration	2-16	-	100 (3% O_2)	117
Other gas incineration	2-16	-	35 (3% O_2)	41
Biomass incineration	2-16	-	200 (6% O_2)	281

[1]Refer to table number (#) for more information

[2]Standardised oxygen concentration in brackets

[3]Harmonised sulphur dioxide limit at 273.15k, 101.1 kPa, dry-gas containing 0% oxygen), fuels adjusted for N_2.

[4]Natural Gas: 92.5% CH_4, 0.8% CO_2, 3.0% C_2H_6, 3.7% N_2 (Illustrative purposes only)

[4]Fuelgas-800°C: 31.2% H_2, 20.1% CO, 19.8% CH_4, 13.3% CO_2, 1.2% C_2H_2, 8.4% C_2H_4, 1.6% C_2H_6, 4.3% N_2

[5]Fuelgas-1000°C: 39.1% H_2, 28.8% CO, 13.3% CH_4, 6.7% CO_2, 5.0% C_2H_2, 1.9% C_2H_4, 0% C_2H_6, 5.2% N_2

[6]Biomethane: 97.9% CH_4, 2.1% N_2 (Illustrative purposes only)

Table 7-21 illustrates that when compared on a harmonised basis, the SO_2 requirements for syngas EOW status are >12x stricter than comparable limits for natural gas and biomethane. Compared to biogas combustion on a STW the harmonised SO_2 limits are >1000x stricter and compared to IED incineration the limits are >750x stricter.

Therefore, there is a strong incentive to operate ATC processes as waste incineration plants, which typically means incinerating all the volatiles and running a steam-turbine cycle which has lower ECE (BEIS[b], 2021), and is less scalable than a gas engine.

Table 7-21 demonstrates that the harmonised SO_2 requirements for biogas combustion within engines or incineration processes is applied less stringently than the corresponding requirements for the combustion of "other gas". It also shows that biomass incineration plants can release far higher harmonised SO_2 emissions than corresponding technologies. This demonstrates that the MCPD regulations may not promote fair competition. Stricter ELVs increase the cost and technical complexity of delivering processes. More specifically, the regulations:

- Promote the use of biogas over "other gases";
- Promote biomass incineration, this is likely to promote the conversion of combined cycle coal power stations to biomass (e.g. Drax);

The H_2S concentration limit for syngas is based on the material comparator report for natural gas. This is problematic because:

- Currently syngas will not be injected into the gas grid, therefore it does not pose a health risk to the public.
- The limit value selected is based on a small set of natural gas samples, rather than relevant regulations (GSM).
- The approach taken is different to biomethane, despite both materials using natural gas a material comparator.

The approach of basing ELVs on SO_2 concentration in dry-gas is opposed to decarbonised ATC technologies. This is because once combusted, H_2 produces water vapour rather than the flue gas diluent CO_2. Therefore, ATC technologies will produce inflated SO_2 concentrations when measured in dry-gas. Several researchers, companies and government agencies have expressed interest in using ATC technologies and reforming to produce hydrogen or synthetic methane for conversion to power or blended gas-grid injection (Kew Projects Ltd., 2019) (Ecofys, 2018) (Prasertcharoensuk et al., 2019) (Eleonora et al, 2021). For H_2 production, any emission limit based on dry-gases may be unsuitable.

Table 7-22 summarises the allowable H_2S concentrations in syngas if the environmental regulator based its limit on the harmonised SO_2 emissions of relevant comparators. For example, fuel-gas produced at 800°C containing 223mg H_2S m^{-3} would comply with the harmonised SO_2 limits for biogas combustion on STW.

Table 7-22: Permitted syngas H_2S concentration if regulated to achieve the same harmonsied SO_2 emissions as comparable fuels and processes.

Fuel-gas 800°C[1] mg H_2S m^{-3}	SO_2 Emissions[3] mg SO_2 m^{-3}	Fuel-gas 1000°C[2] mg H_2S m^{-3}	SO_2 emissions[3] mg SO_2 m^{-3}	Comparator
0.22	0.14	0.19	0.15	Syngas EOW
2.69	1.71	2.19	1.71	Biomethane EOW
83.6	52.9	67.8	52.9	Other gas engine
167	106	136	106	IED Incineration
223	141	181	141	Biogas engines STW[4]

[1]Fuelgas-800°C: 31.2% H_2, 20.1% CO, 19.8% CH_4, 13.3% CO_2, 1.2% C_2H_2, 8.4% C_2H_4, 1.6% C_2H_6, 4.3% N_2

[2]Fuelgas-1000°C: 39.1% H_2, 28.8% CO, 13.3% CH_4, 6.7% CO_2, 5.0% C_2H_2, 1.9% C_2H_4, 0% C_2H_6, 5.2% N_2

[3]SO_2 emissions 273.15k, 101.1 kPa, dry-gas containing 0% oxygen, fuels adjusted for N_2

[4]SR2009 No.4 (see table 2-17)

Table 7-21 and 7-22 demonstrate that the syngas EOW requirements are lower than comparative regulations and would produce far less SO_2 than other waste to energy processes. The concentration of H_2S in syngas has been limited because a statement in the IED that syngas must produce emissions "no higher than natural gas". This may deter investment into these facilities, despite their potential to produce low carbon energy. An amendment could be made to the syngas EOW requirements that if processed on an industrial site for power generation it must produce emissions no higher than comparative fuels or waste to energy processes.

7.6.1 Hydrogen sulphide (H_2S): End-of-waste compliance

Thames Water have proposed acid gas elimination in a single stage caustic (NaOH) scrubber followed by a hypochlorite (NaCNO) scrubber. The following reactions will occur in the caustic scrubber:

1. $H_2S + NaOH = NaHS + H_2O$
2. $NaHS + NaOH = Na_2S + H_2O$
3. $HCN + NaOH = NaCN + H_2O$
4. $HCl + NaOH = NaCl + H_2O$
5. $SO_2 + 2NaOH \rightarrow Na_2SO_3 + H_2O$

Due to the presence of cyanides, the products formed in the caustic scrubber and any remaining acids gases will then be scrubbed in sodium hypochlorite (NaOCl). This will convert Na_2S into fully stabilised Na_2SO_4 and detoxify cyanides by converting them into cyanates (NaCNO) or N_2. The mains reactions are:

6. $Na_2S + 4NaOCl \rightarrow Na_2SO_4 + 4NaCl$
7. $NaCN + NaOCl \rightarrow NaCNO + NaCl$

At 800°C and 1000°C, 36.2% and 54.1% of feedstock S is present within the gas stream which equates to 7.9 kg S tds^{-1} and 11.8 kg S tds^{-1}. Sulphur gas speciation is unknown, assuming 100% conversion to H_2S this equates to 15,602 and 19,432 mg H_2S m^{-3} therefore to achieve EOW status a 99.999% reduction in H_2S concentration is required to meet syngas EOW. Table 7-23 summarises the potential chemical consumption during H_2S treatment, assuming all S gas is present as H_2S.

Table 7-23: Chemical usage: Conversion of H_2S to Na_2SO_4 for fuel-gas at 800° & 1000°C

Reactant	Reaction	Fuel-gas 800°C Reactant (kg tds^{-1})	Fuel-gas 1000°C Reactant (kg tds^{-1})
H_2S	-	8.4[1]	12.6[1]
NaOH	$H_2S \rightarrow NaHS$	9.85	14.8
NaOH	$NaHS \rightarrow Na_2S$	9.85	14.8
NaClO	$Na_2S \rightarrow Na_2SO_4$	73.3	110

[1]Estimate from mass balance

Table 7-23 shows that 8.4 kg H_2S may be produced for each tonne of sludge pyrolysed and would require almost 20kg of NaOH and 73kg of NaClO to fully convert from H_2S to Na_2SO_4. Additional NaOH will also be required for reactions 3 and 4, whilst additional NaClO will be required for reaction 7. Note, that SO_2 will also be present within the gas and reaction 5 shows that this will not require NaClO.

Caustic scrubbing is technically challenging in the presence of CO_2 and the following non-target reactions can occur:

8. CO2 + NaOH = $NaHCO_3$ (Non-target reaction)
9. $NaHCO_3$ + NaOH = Na_2CO_3 + H_2O (Non-target reaction)

The speciation of carbon dioxide and carbonates is pH dependent and can be predicted from pKa values. Above pH 8-8.5 carbon dioxide is speciated as the bicarbonate ion (HCO_3^-) and above pH 10.5 the carbonate ion (CO_3^-) is dominant (Trimeric Corp. n.d). To minimise carbonate precipitation special short-contact time caustic scrubbers are likely required for fuel-gas treatment. These work on the principle that carbonate precipitation is slower than sulphide precipitation. Trimeric (n.d.) state that gases with CO_2:H_2S ratios of <5 are typically cleaned in short-contact time scrubbers, with high ratios negatively influencing the scrubbing efficiency due to increased carbonate formation. At 700ºC the CO_2:H_2S ratio of fuel-gas peaks at 20, reducing with increased temperature to 13.7 at 800ºC and 5.5 at 1000ºC. Therefore fuel-gas exceeds the typical threshold even for specially designed short-contact time scrubbers. Achieving extremely low H_2S concentrations (0.19-0.22 mg m^{-3}) for a gas containing high concentrations of CO_2 will likely lead to reaction 8 and 9 consuming excessive quantities of CO_2 regardless of whether or not specially designed short-contact time scrubbers are used.

Wet-scrubbing fuel-gas produced from sludge is likely to be problematic because of the potential presence of heterocyclic compounds, which are expected to be at least partially polar due to the presence of electronegative elements (e.g. N, S). A general-rule of solubility is that like dissolves like. Since water is polar is may dissolve heterocyclic tars during scrubbing contaminating both the scrubbing liquors and the precipitated salts. Polarity is measured by the relative permittivity (ε) and dipole moment (D), laboratory observation suggest pyrolysis tar was:

- Slightly soluble in polar solvents, e.g. H_2O (ε = 80.1, D = 1.85).
- Completely soluble in partially polar aprotic solvents, e.g. DCM (ε = 9.14, D = 1.60)
- Mostly soluble in partially polar protic solvents, e.g. MeOH (ε = 33.0, D = 1.70)
- Insoluble in non-polar solvents, e.g. hexane (ε = 1,90, D = 0)

Values for (ε) and (D) obtained from Dean (1999)

At 1000ºC, tar was almost insoluble in all the solvents tested which is consistent with the increase in C:S and C:N ratios of the liquids at this temperature (see table 7-17) and condensation of the tar compounds into high-molecular-weight molecules. Alone scrubber contamination with heterocyclic compounds is an issue, however the use of NaClO could lead to the formation of chlorinated heterocyclic compounds which are expected to be particularly problematic and toxic. Heterocyclic tar deposition in wet scrubbing liquors was previously reported by McNeil (1975) during coal carbonisation. This could only be resolved by using an electrostatic precipitator to ensure entrained tars were completely removed prior to conducting wet-scrubbing. To avoid scrubber liquor and salt contamination, it is advisable to use an electrostatic precipitator, increase gas temperatures to 1000ºC or eliminate tars.

Conversion of H_2S to Na_2SO_4 using NaOH and NaClO is typically only applied in industry for emergency flare-gas scrubbing (Dupont, n.d.) or for odour control. This technology was proposed because of its high removal efficiency and its ability to remove and detoxify HCN. However, the process is expected to consume excessive quantities of chemicals, accumulate contaminants, and produce secondary chlorinated heterocyclic contaminants. Prior to constructing a full-scale process, utilities must:

- Ensure tars are fully removal prior to conducting wet scrubbing.
- Investigate full eliminated of HCN prior to conducting H_2S scrubbing.
- Investigate alternative methods of gas desulphurisation.
- Challenge the syngas EOW requirements.

Eliminating of HCN prior to conducting H_2S removal would mean that NaClO is no longer required, vastly reducing chemical consumption, and eliminating the risk of forming chlorinated organic contaminants. The process could then be optimised to conduct reaction 1 and produce high quality NaHS, which could be marketed to suitable end-users (e.g. paper mill manufactures). However, this would likely require multi-stage short-contact time caustic scrubbers (Trimeric, n.d.). The formation of NaHS over NaS_2 would half caustic requirements. The downside of this process would be decreased H_2S removal.

Hot fuel-gas desulphurisation may be viable alternative to scrubbing or a suitable method of minimising the H_2S concentration of the gas. This process is already conducted for coal gasification processes using metal oxides, suitable sorbents may include:

- ZnO-based sorbents have one of the highest equilibrium constant for sulphidation and can yield sub ppm concentration of H_2S in syngas (Rosso et al., 2003). They can also be used at a wide range of temperatures from 250-700ºC (Liu et al., 2018) (Rosso et al., 2003) and can be regenerated in air at >600ºC with limited sulphate formation (Jagtap & Wheelock, 1996) and then reused multiple times albeit with some loss of efficiency (Feng

et al., 2016). The carbothermal reduction of ZnO by CO, H_2 or tar may lead to volatilisation and losses of the sorbent overtime.

- CaO-based sorbents are inexpensive and effective in the temperature range between 800-1200ºC (Jagtap & Wheelock, 1996). In addition, CaO will not be reduced and is non-volatile (Ellingham, 1944). Therefore, CaO could be used within the reactor itself, previous research has shown that alkali-metals are effective tar cracking catalysts (Vassilatos et al., 1992). Because of sulphate formation, regeneration of CaO must be conducted above 1400ºC although cyclic oxidative reductive processes between 950-1100ºC have been developed (Japtap & Wheelock, 1996).

Post-scrubbing, polishing the fuel-gas to EOW requirements with impregnated activated carbon filters may be an option. Higgins & Hewins ltd. (n.d.) state that H_2S removal with activated carbon media costs £5-6.75 per kg H_2S removed. This is far more expensive than caustic scrubbing, therefore caustic scrubbing must be conducted efficiently to minimise activated carbon consumption. Impregnated H_2S filters are seldom re-activated and are typically landfilled after-use.

7.6.2 End-of-waste compliance: Total aromatic hydrocarbons

Pyrolysis at 800ºC and 1000ºC produced fuel-gas with 150,860 mg m^{-3} and 56,601 mg m^{-3} of condensable liquids respectively, this will primarily consist of aromatic compound and soot. However, the EOW requirement for "syngas" is just 1.22-1.45 mg m^{-3}. Bulk-tar removal is straightforward, however ensuring condensation occurs in the correct location without blocking the process will be challenging. Figures 5-8 to 5-12 demonstrated that pyrolysis produced soot and pitch-like tars that blocked the process at laboratory-scale. Prior to constructing a full-scale process, the proposed design could be altered:

- The ascension pipework must contain minimal bends to avoid tar deposition. In addition, the pipework must facilitate POX and steam gasification so that periodic cleaning of carbon deposits within the pipework and cyclone can be conducted (table 5-3).
- Bulk tar-removal could be conducted in a reactor not containing any vane-packing or random packing to avoid blockages. Any vessel containing packing material should only be used for entrained tar and/-or VOC removal.

The other main process challenge is the removal of highly entrained tar aerosols, which were observed at laboratory-scale. Demisters may be effective, alternatively Mcneil (1975) states the coal-industry used electrostatic precipitation.

Aside from improved removal efficiency, further work is required to minimise tar yields. Gasification processes typically produce less tar because POX and steam gasification convert tar vapours into syngas. For example, De Andres (2016) conducted sewage sludge gasification between 750-850ºC using non-catalytic and catalytic gasification, the tar yields obtained were:

- 0.71-4.09% during non-catalytic gasification.
- 0.58-3.49% during olivine catalysed gasification
- 0.49-2.94% during alumina catalysed gasification
- 0.40-2.58% during dolomite catalysed gasification

These values compare favourable to the yields obtained during sludge pyrolysis, 8.1 & 3.7% at 800 and 1000ºC. Rather than gasify sewage sludge, the hot fuel-gas could be immediately reformed at high temperatures through POX and steam-reforming reactions. POX could raise the temperature of the gas without consuming additional electricity although a proportion of the fuel-gas and tars would be oxidised thus lowering calorific gas yields. Compared to gasification this process would advantageous because the char would be retained, and only limited quantities of air would be added into the process limiting nitrogen dilution. Alternatively, the hot-tar could be condensed and then recirculated into the process for reforming within the reactor, like a British Gas gasifier (Figure 2-3). The laboratory-scale reactor was modified to facilitate POX and steam reforming reactions, however due to time constrains and the disruption caused by Covid-19 the experimental work was not conducted.

Chapter 8: Char characterisation

8.1 Elemental characterisation

8.1.1 Aqua-regia digestion

Sewage sludge char was ashed at 500ºC until constant weight was attained, the ash was then dissolved in concentrated aqua regia and analysed by ICP-OES (see section 4.2.7.1). Table 8-1 summarises the elemental contents of sewage sludge chars produced at temperatures between 500-1000ºC from XS-6 sludge. Between 500-700ºC, the concentration of inorganic elements increases, this corresponds with the loss of organic volatiles and other elements (N, S, and H) which concentrate residual elements in the char. Above 700ºC, the elemental concentrations in SSC were relatively stable although there is a slight upwards trend which could be due to changes in the H, N and S content of the char produced.

No evidence of preferential element loss was observed, even among the elements with low boiling points (e.g. K (760ºC), Na (884ºC) and Zn (907ºC) although, Hg (357ºC) and Se (700ºC) were not analysed and As (613ºC) was not present in a detectable concentration. All elements displayed a tendency to concentrate between 1-5-2.0x at 500-600ºC and 2.1-2.4x over 700-1000ºC which is approximately proportional to the materials weight loss during pyrolysis. The elements which were detected and pyrolysed above their boiling points included K, Na and Zn their apparent non-volatility suggests they are mostly present in non-elemental forms (e.g. sulphides) that have higher boiling points.

Table 8-1: The elemental composition of XS-6 and iso-SSC produced between 500-1000ºC with a dwell-time of 120 seconds (mg kg^{-1})

Element	XS-6	500	600	700	800	900	1000
Ca	46512	72100	92782	98605	99770	100721	109766
P	26008	40619	52680	55870	56497	56625	56903
Fe	24584	38562	49299	52464	53050	53532	53909
Al	7032	11106	14343	15207	15275	15519	15692
Mg	5457	8610	10952	11725	11821	11933	12893
K	1594	2482	3200	3414	3417	3449	3713
Na	1447	2282	2925	3097	3143	3188	3439
Zn	800	1256	1614	1711	1736	1752	1734
Mn	461	721	935	993	993	1012	961
Cu	408	633	829	877	892	897	859
Ba	215	337	435	459	461	468	488
Er	183	285	367	393	395	397	412
Pb	123	191	250	266	265	269	260
Sr	140	219	281	300	300	303	343
Ni	41	45	46	52	53	50	57

Proximate analysis of the expansion bellow carbon (section 4.2.3.1) suggested small quantities of inorganic ash were present therefore either ash entrainment in the off-gases or volatilisation of some elements during pyrolysis occurs, however this was not a significant effect identified in the results generated. Pilot/full-scale plants typically use a cyclone and scrubbers to remove condensables from the fuel-gas, any volatile elements will likely be deposited there, including mercury.

8.1.2 X-ray diffraction

Milled SSC-700 was analysed by x-ray diffraction using a Bruker D2 in the Royal School of Mines (Imperial College London). The results showed that calcium was likely present as calcite ($CaCO_3$). Other than calcite, XRD could not identify any other minerals, this may be due to the non-crystalline amorphous nature of char minerals and the carbon present.

8.1.3 X-ray photoelectron spectroscopy (XPS)

Milled SSC-700 was analysed by XPS using a Thermo Fisher K-Alpha+ in the Royal School of Mines (London) (see section 4.2.6). For SSC, the speciation of N, S and heavy metals was of particular interest. Although the detection limit for XPS is typically (0.1-1%) therefore the detection of Cu (0.09%) and Pb (0.04%) (Table 8-1) was not possible. The survey spectra for SSC-700 is shown in figure 8-1, some of the characteristic elemental regions have been highlighted alongside their respective peaks.

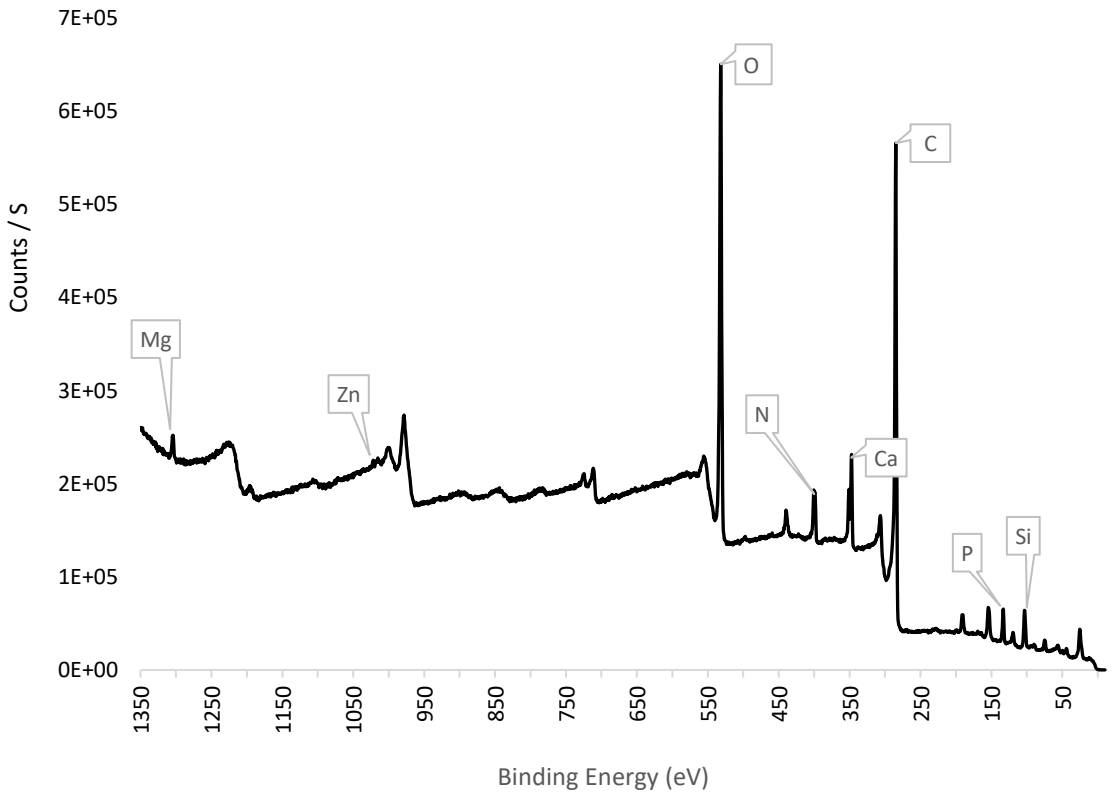


Figure 8-1: XPS survey scan spectra for SSC-700, covering a binding energy range between 0-1350 eV (0.5 eV step-size).

The largest survey peak for SSC-700 occurred at a binding energy of 529.09eV a value characteristic of the bonds formed by O. During pyrolysis, O associated with organic compounds are volatilised therefore the oxygen peak is likely to be associated with inorganic components which may include metal oxides, metal carbonates, alumina, and silicates whose binding energy ranges from 529-532.9eV. Heterocyclic oxygen groups may also be present within the condensed ring-structure however due to oxygens greater electronegativity compared to nitrogen or sulphur these may be less stable than N/S, for example FTIR analysis during carbonisation showed that by 700ºC most of organic oxygen and carbonate groups within biochar had been eliminated (Rodriguez-Vila et al., 2017). The stability of aromatic structures is related to their resonance energy which for their compounds decreases in the following order: benzene (33-36 kcal mol^{-1}) > thiophene (29 kcal mol^{-1}) > pyridine (23-28 kcal mol^{-1}) > pyrrole (21-22 kcal mol^{-1}) > furan (16 kcal mol^{-1}) (Louden & Parise, 2015). Bruinsma et al., (1988) suggested resonance energy per H atom predicts the stability of benzene and various heterocyclic compounds better than resonance energy alone because empirically the thermal stability of thiophene even exceeds benzene during pyrolysis.

Acid extractions of ashed SSC show that a large proportion of char is acid insoluble which is representative of mineral matter such as silicates. Several peaks were identified in the survey scan, which, when compared against the NIST XPS database, suggest the presence of mineral matter, for example:

- Silicon dioxide (103.4eV, 154.4eV)
- Aluminosilicates (50.4eV, 75.1eV, 119.9eV)

Analysis in CasaXPS showed that the O survey peak actually ranged between 527.09-545.00eV, with peak tailing at higher binding energies. This is likely because of individual peaks overlapping. The second largest survey peak for SSC-700 was obtained at 285.19eV, a value characteristic of the bonds formed by C. During pyrolysis, the non-volatile C retained within the char will form condensed aromatic structures likely dominated by sp^2 hybridised C (~284eV), although surface groups containing C-H, C-O, C-N and C-NH_2 bonds may also be present. SSC processed below 800ºC was expected to contain calcium carbonate. A non-resolved peak was identified at 351.4eV, which corresponds well with the value reported in the NIST EPS database (351.2eV) for calcium carbonate ($CaCO_3$). Analysis in CasaXPS showed that the carbon survey peak ranged between 281.25-298eV with peak tailing at higher binding energies. Again, this is likely due to individual peaks overlapping.

One challenge associated with XPS analysis, particularly of heterogenous substances like SSC, is that the binding energy of an element's electrons may be similar for a range of its compounds. This means that the peaks of individual compounds often overlap and can only be separated by deconvoluting the broad peak.

The full width half maximum is a useful measurement for determining whether the peak in a spectrum refers to one peak or multiple over-lapping peaks. In addition, XPS peaks typically have a Voigt or Doniach-Sunjic line shape, which software such as CasaXPS use to aide peak identification, fitting, and deconvolution. These line shapes are simply probability distributions. Deconvoluting and fitting the peaks can be prone to errors (Major et al., 2020) particularly when several compounds closely overlap which for SSC was the case for both C and O

8.1.3.1 XPS analysis: Carbon

Figure 8-1 showed that there is a peak at binding energy 285.19eV, a value characteristic of the bonds formed by carbon. A high resolution XPS-spectra was generated to analyse this binding energy region further, the output is illustrated in figure 8-2.

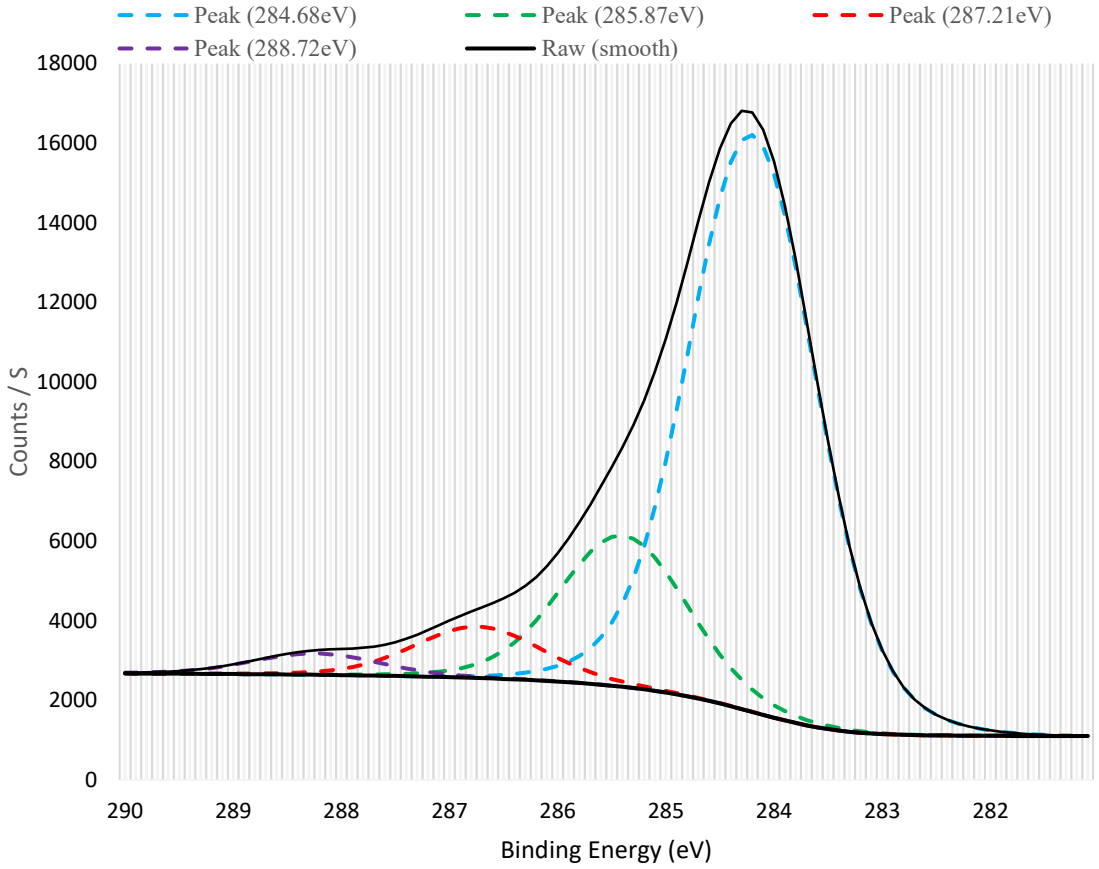


Figure 8-2: High resolution XPS scan of C 1s orbital (70 scans, 400um, CAE 20.0, 0.1 eV) showing raw data and the deconvoluted peaks generated in CasaXPS using voigt line shapes

Deconvolution was conducted in CasaXPS using a Voigt line shape, the results show a dominant peak at 284.68eV with atomic percentage (% at.) of 36.89% and three smaller peaks at 285.87eV, 287.21eV, and 288.87eV. Blyth et al., (2000) suggests graphite has a sp_2 peak at 384.4eV whilst Ayiania et al. (2020) suggests graphitic carbon ranges between 284.3-284.8eV which corresponds well with the main peak. The second largest peak may correspond to 2sp ethers (R-O-R) or Csp3 graphitic N which ranges between 285.9-286.5 or Csp2 electrons bonded to N in pyridinic or pyrrolic structures which typically range between 284.8-285.5eV (Ayiania et al., 2020).

Figure 8-3 identified pyridinic-N and pyrrolic-N within SSC, however, the output of the analysis suggested these had a combined of 5.93% at. whilst the peak at 285.87eV was 9.68% at. This suggests that alone these groups are not present in high enough concentrations to explain the peak at 285.87eV. Therefore, it may be constituted of several structural groups, which cannot be deconvoluted due to overlapping peaks and sample complexity.

Ayiania et al., (2020) assigned peaks between 286.5-287.6 eV to pyridone (C=O/N-) and carbonyl groups (C=O) therefore the peak at 287.1eV (3.29% at.) may correspond to these structures. Zhang et al., (2019) suggested that above 650ºC carboxylic and phenolic groups are eliminated from grass-derived biochar, carbonyl groups are eliminated between 650-800ºC and quinone becomes dominant at 800ºC. Therefore, if C=O structures are present, they may be present as carbonyls or quinones. The peak at 288.72eV (1.37 % at.) is indicative of metal carbonates, which is likely dominated by $CaCO_3$.

Based on the atomic concentrations for peaks 248.68eV, 285.87eV, 287.21eV and 288.72eV of 36.89%, 9.68%, 3.29% and 1.37% respectively the quantity of carbon present at the surface of SSC (≤10nm) within each of these peaks was estimated:

- The peak at 248.68eV was assigned to graphitic carbon, its atomic concentration suggests that 72% of C within SSC-700 was present as graphitic carbon or approximately 193,000 mg C kg^{-1} based on the total C concentration of 26.8% as determined by ultimate analysis.
- The peak at 285.87eV was assigned to ether structures which are likely in condensed heterocyclic forms (e.g. furans/pyrans) and condensed forms of N, including heterocyclic-N and graphitic-N. This peaks atomic concentration suggests 18.9% of C within SSC-700 was bound in these forms or 50,600 mg C kg^{-1} based on the total C concentration.
- The peak at 287.21eV was assigned to condensed pyridone or carbonyl groups. This peaks atomic concentration suggests 6.4% of C within SSC-700 was bound in these forms or 17,211 mg C kg^{-1} based on the total C concentration.
- The peak at 288.72eV was assigned to metal carbonates, this peaks atomic concentration suggests 2.7% of SSC-700 carbon was present as carbonates. Based on a correction for SSC-700 total carbon (%) and assuming all carbonates were present as calcium carbonate this equates to a calcium carbonate concentration of 5.97%.

The low concentration of carbonates within SSC-700 was an interesting finding and suggests that much of the Ca present within sludge may be predominately fractionated in other forms such as phosphate or sulphates. It has been reported that sulphates are the dominant form of S within secondary sludge (Dewil et al., 2008) and figure 8-5 suggest metal sulphates are the dominant form of S within SSC-700.

Since sulphates are not expected to form during pyrolysis, these results suggest that contrary to the findings of Dewil et al., (2008) sulphates are not mostly converted into sulphides during digestion and are not converted to sulphides or SO_2 during Py-G at 700°C.

8.1.3.2 XPS analysis: Nitrogen

Figure 8-1 shows that there is peak at binding energy 399.87eV, a value which is characteristic of the bonds formed by N. A high resolution XPS-spectra was generated to analyse this binding energy region further, the output is illustrated in figure 8-3.

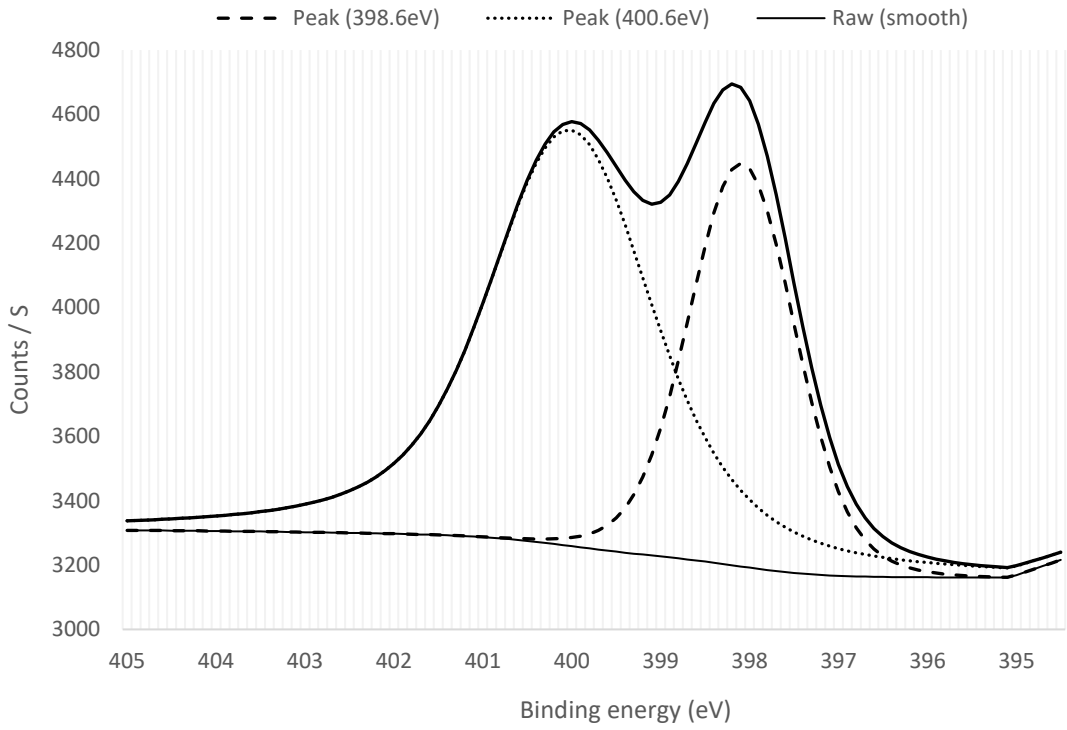


Figure 8-3: High resolution XPS scan of N 1s orbital (70 scans, 400um, CAE 20.0, 0.1 eV) showing raw data and the deconvoluted peaks generated in CasaXPS using voigt line shapes

The line-shape suggests two overlapping peaks. Deconvolution was conducted in CasaXPS using a Voigt line shape, the results show the peaks at 398.6eV and 400.6eV. These values are indicative of pyridine and pyrrole groups, which the literature suggests corresponds to 1s binding energies of 398.7 and 400.7eV respectively (Jansen and van Bekkum, 1995). The region at 398.7eV may alternatively correspond to nitride compounds.

The structure of pyridine and pyrrole molecules are illustrated in figure 8-4, these structures will not be present as molecules but as part of the condensed aromatic ring structure of SSC. Pyridine and pyrrole nitrogen contain a lone pair of electrons. For pyridine the lone pair are perpendicular to the carbon p-orbitals, therefore they are available for donation whilst for pyrrole the lone pair lie on the same plane as the C atom therefore, they participate in ring resonance and are not available for donation (Louden & Parise, 2015). Since char is likely to contain both pyridine and pyrrole surface functional groups, it is likely that SSC will act as a weak base.

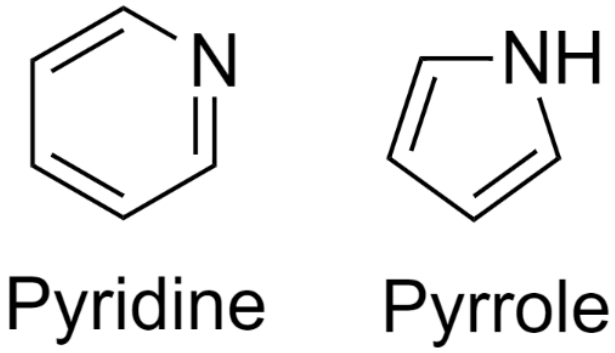


Figure 8-4: Structure of pyridine and pyrrole molecules which XPS analysis suggests are present within sewage sludge chars condensed aromatic structure as surface functional groups

In section 2.3.3.2, HAAs are described as potent mutagenic and carcinogenic compounds. However, this toxicity does not translate to the condensed forms of these compounds. For example, whilst PAHs are toxic, the same does not apply to the graphitic forms of carbon found in activated carbon. In recent years nitrogen-doped chars have been proposed for an array of uses, including: medicinal applications such as cell imaging and drug delivery (Park et al., 2020), phosphate adsorption (Mood et al., 2020), heavy-metal adsorption (Rodriguez-Vila et al., 2018) (Rajapaksha et al., 2016), phenol adsorption (Li et al., 2019) and VOC adsorption (Su et al., 2020)

Table 7-14 showed that Py-B and non-isothermal Py-G produced SSC that contained more nitrogen than isothermal Py-G char. Slow heating rates may promote polymerisation of the amine group within sludge proteins into condensed aromatic forms. The structure of these condensed forms may resemble pyridine, pyrrole, or graphitic nitrogen. Table 7-14 showed that increased pyrolysis (T) decreased the retention of nitrogen in SSC, this suggests that the relative stability of these surface groups varies. However, for Py-G, char-N stopped decreasing above 900^{o}C suggesting only the most stable forms remained in the char. The relative stability of ring structures may be dependent on their ring structure and position within the condensed structure.

8.1.3.3 XPS analysis: Sulphur

A peak was identified at 164.63eV a value characteristic of the bonds formed by S. A high resolution XPS-spectra was generated to analyse this binding energy region further, the output is illustrated in figure 8-5.

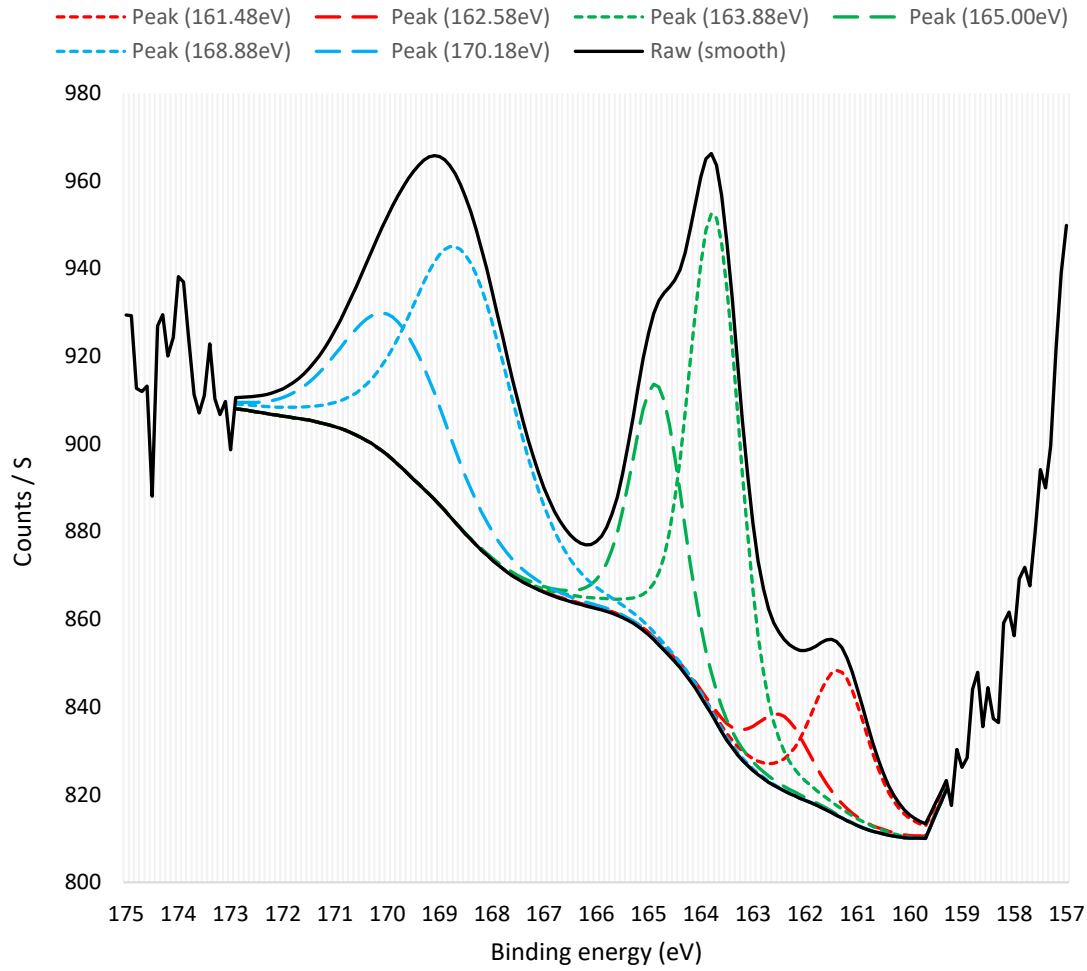


Figure 8-5: High resolution XPS scan of S 1s orbital (200 scans, 400um, CAE 20.0, 0.1 eV) showing raw data and the deconvoluted peaks generated in CasaXPS using Voigt line shapes

Deconvolution in CasaXPS suggest there are up to six S peaks present in the spectrum, although these are paired and relate to the $2p_{3/2}$ and 2p electrons for each form of S present. For example, the peaks at 170.18eV and 168.88eV are indicative of the $2p_{3/2}$ and 2p electrons for sulphate compounds such as $CaSO_4$ and $BaSO_4$. Thermogravimetric analysis of $CaSO_4$ decomposition in CO suggests decomposition begins at 780ºC and peaks at 865ºC (Kuusik et al., 1985). Therefore, if $CaSO_4$ is present in sludge, it would be unlikely to decompose at the temperatures used to produce SSC-700. The large quantity of sulphate compounds present relative to sulphides was not expected because of the oxygen deficient conditions used during both pyrolysis and anaerobic digestion.

The small peaks at 161.48eV and 162.58eV correspond to the $2p_{3/2}$ and 2p values for metal sulphides. A range of sulphide compounds may be present however, the sample is too heterogeneous to definitively distinguish which compounds are present at sulphides and which are not. The values of the peaks at 163.88eV and 165.00eV correspond to a range of organic S compounds presented by Lindberg et al. (1970) and Tang et al (2018). If organic sulphur structures are retained within SSC, the structures present are likely to heterocyclic, such as thiophenes (164.5eV). The peaks within this range are relatively large compared to those for sulphides, which suggests that a significant proportion of S may be bound covalently within the char matrix. Like pyridine, thiophene contains a lone pair of electrons perpendicular to carbons p-orbitals, therefore, they will also be available for donation outside of the ring system (Louden & Parise, 2015). Prevoteau et al. (2016) suggest that the electron donating capacity of biochar is dramatically underestimated and influences soil microbial redox reactions. Given the potential presence of condensed heterocyclic structures within SSC, the same underestimation may apply.

Based on the atomic concentrations for the $2p_{3/2}$ peaks at 170.18eV (sulphates), 161.48eV (sulphides), 163.88eV (organic sulphur – e.g. thiophene) of 0.21%, 0.07% and 0.20% respectively, approximately:

- 43.8% of the S within SSC-700 is expected to be present as metal sulphates (~10,994 mg S kg SSC-700^{-1})
- 14.6% of the S within SSC-700 is expected to be present as metal sulphides (~3,665 mg mg S kg SSC-700^{-1})
- 41.6% of the S within SSC-700 is expected to be present as organic S (e.g. condensed thiophene structures) (~10,422 mg S kg SSC-700^{-1})

8.1.3.4 XPS analysis: Silicates

Two major peaks for silicon's sp3 orbitals were identified at 104.16eV and 102.69eV with an atomic concentration of 0.8% at and 4.03% at respectively. The binding energies and atomic concentrations suggest that 16.6% of the Si present at the surface (≤10nm) of SSC is present at silicates (SiO_2) whilst the majority is present as aluminosilicates minerals, which may include kaolin or feldspars. The aqua-regia extractable fraction of SSC-700 equalled 24.5% of SSC Wt. (Table 8-1) whilst the elemental concentrations of C, H, N and S equalled 33.2% of SSC Wt. (Table 8-2). A majority of the remaining weight is thought to be composed of these silicate and aluminosilicate minerals. The presence of these minerals may influence the physical properties of the SSC, for example, its behaviour in soils or its attrition resistance.

8.1.3.5 XPS analysis: Phosphorus

Figure 8-1 shows that a peak was identified at 133.75eV, a value characteristic of 2p phosphate electrons. A high resolution XPS-spectra was generated to analyse this binding energy region further, the output is illustrated in figure 8-6.

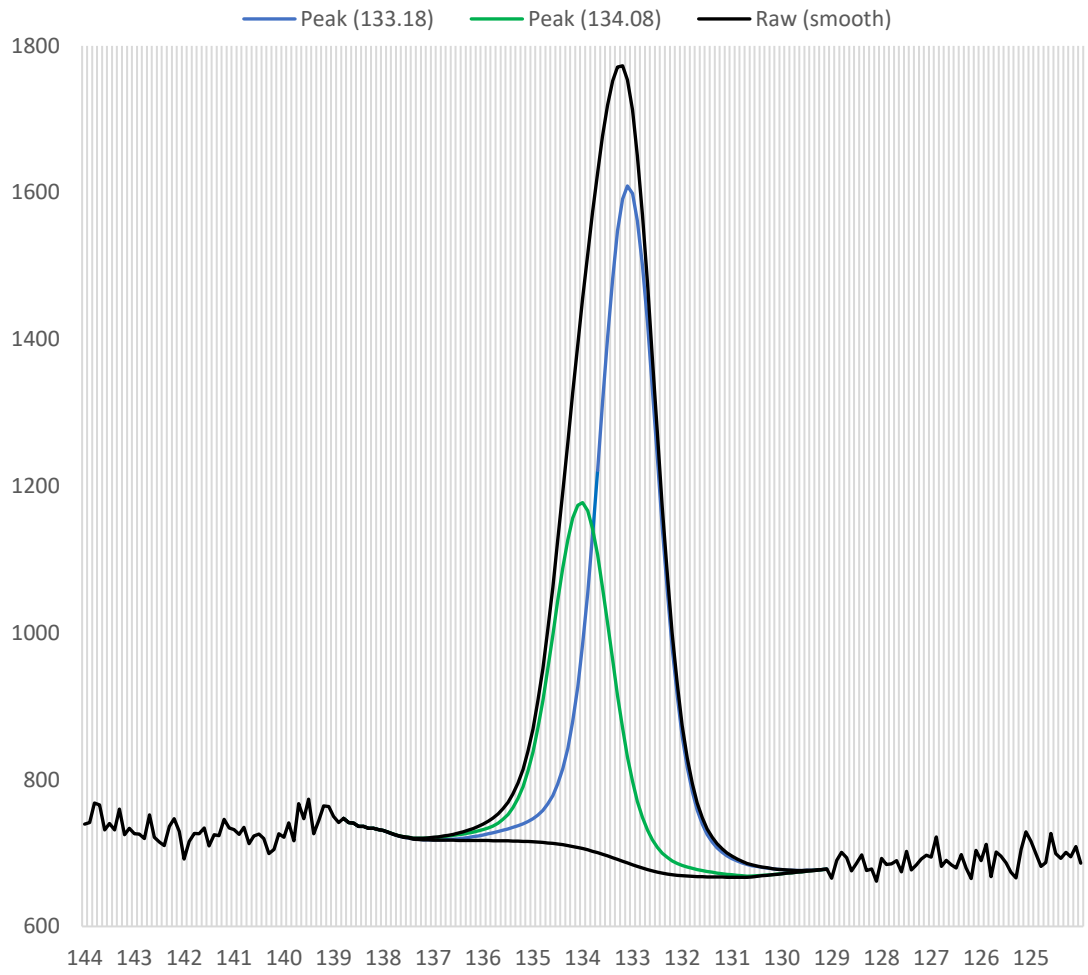


Figure 8-6: High resolution XPS scan of P 2p orbital (70 scans, 400um, CAE 20.0, 0.1 eV) showing raw data and deconvoluted peaks generated by CasaXPS using Voigt line shapes

High resolution XPS produced a spectra that peaked at 133.28eV however, the peak tailed so deconvolution was conducted in CasaXPS assuming Voigt line shapes. The two peaks identified were at 133.18eV and 134.08eV and likely refer to phosphates 2p and $2p_{3/2}$ electrons. The 2p peak at 133.18eV showed good fit with values in the NIST database for calcium phosphate hydroxide (133.00-133.20eV) although the $2p_{3/2}$ peak at 134.08eV was slightly higher than values for this compound (133.80eV). Binding energy values for ferric phosphate (133.70-133.75) and aluminium phosphate (133.9-134.60eV) are also reported in the NIST database.

Evidence in the literature suggests that the carbothermic reduction of sewage sludge ash can generate phosphorus oxide radicals. For example, Matinde et al. (2008) heated sewage sludge ash with powdered graphite at 10K min^{-1} in an argon atmosphere. The results suggest that phosphorus oxide radicals (PO/PO_2) were formed at temperatures from 700K (427°C), peaking at 1073K (800°C). Above 1273K (1000°C), elemental phosphorus (P_2) was detected rather than oxides, with P_2 increasing with increased temperature up to 1700K (1426°C). In addition, thermogravimetric analysis conducted by Matinde et al. (2008) suggested SSA and graphite powder underwent gradual weight loss between 923-1323K (650-1050°C) followed by significant weight loss above 1323K which could be due to P loss by radical formation.

Table 8-1 showed that SSC P did not undergo weight reductions between 600-1000°C, rather the P concentration increased slightly and relatively as the concentration of other elements volatilised. These finding contradict the finding by Matinde (2008) however, there are important distinctions between the studies. Ash and graphite do not contain organic forms of phosphate, nor do they contain volatiles which would simultaneously form radicals. The ash was heated slowly using long dwell times, in contrast to the "fast" pyrolytic gasification used in this study.

Since pyrolytic gasification generates an atmosphere rich in hydrogen, phosphorus oxide radicals could react with hydrogen forming toxic phosphine gas, which may re-react with inorganic matter in the SSC forming metal phosphides. However, metal phosphides have a characteristic binding energy peak at ~128.5eV and figure 8-6 suggests these are not present within SSC-700. Since pyrolytic gasification simultaneously releases a range of radicals, phosphorus oxides could also undergo radical-radical reactions forming unusual compounds such as phosphorus pentanitride and phosphorus pentasulphide. The NIST database suggests these compounds have binding energies of 134.0eV and 134.20eV respectively, which align with the peak at 134.08 so their presence cannot be completely discounted. However, no evidence of preferential phosphorus loss was identified (Table 8-1) during this experiment, however this warrants future investigation.

Unlike SSA, sludge contains organic adenosine triphosphate (ATP) which may behave differently to mineral phosphate during carbothermal reduction. For example, Robinson et al. (2017) suggests slow-pyrolysis fractionates ATP into mineral forms (e.g. calcium phosphate, iron phosphate and magnesium polyphosphate). However, under the more reductive atmosphere present with a pyrolytic gasifier, the resulting fractionation of phosphate compounds may be different. Ellingham (1944) illustrates that phosphorus pentoxide can undergo carbothermal reduction with CO and C at approximately 750°C and 800°C.

8.1.3.6 XPS analysis: Calcium

Figure 8-1 shows that two peaks were identified at approximately 347.62eV and 350.52eV, values characteristic of the bonds formed by calcium. A high resolution XPS-spectra was generated to analyse the binding energy region further, the output is illustrated in figure 8-7.

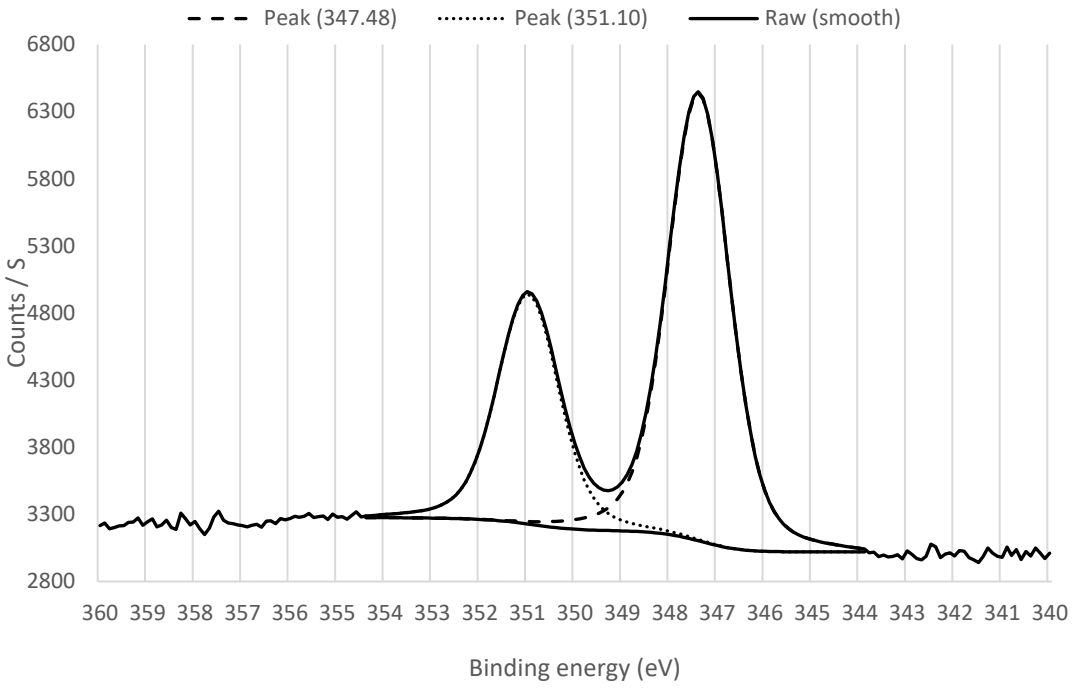


Figure 8-7: High resolution XPS scan of Ca 2p (70 scans, 400um, CAE 20.0, 0.1 eV)

Deconvolution of the high-resolution spectra was conducted in CasaXPS and suggested two peaks are present at 351.10eV and 347.48eV. The NIST database suggests calcium carbonate has a $2p_{1/2}$ and $2p_{3/2}$ peak at 351.1-351.2eV and 346.70-347.70 which provides a good match for the data shown in figure 8-7. The $2p_{3/2}$ peak also provides a close match for calcium phosphate (347.00-347.80eV) and calcium oxide (347.00-347.30eV), these may also contribute to the peak.

8.1.3.7 XPS analysis: Zinc and Copper

Figure 8-1 shows that a peak was identified at 1022.44eV a value characteristic of the bonds formed by Zn. A high resolution XPS-spectra was generated to analyse this binding energy region further, the output is illustrated in figure 8-8.

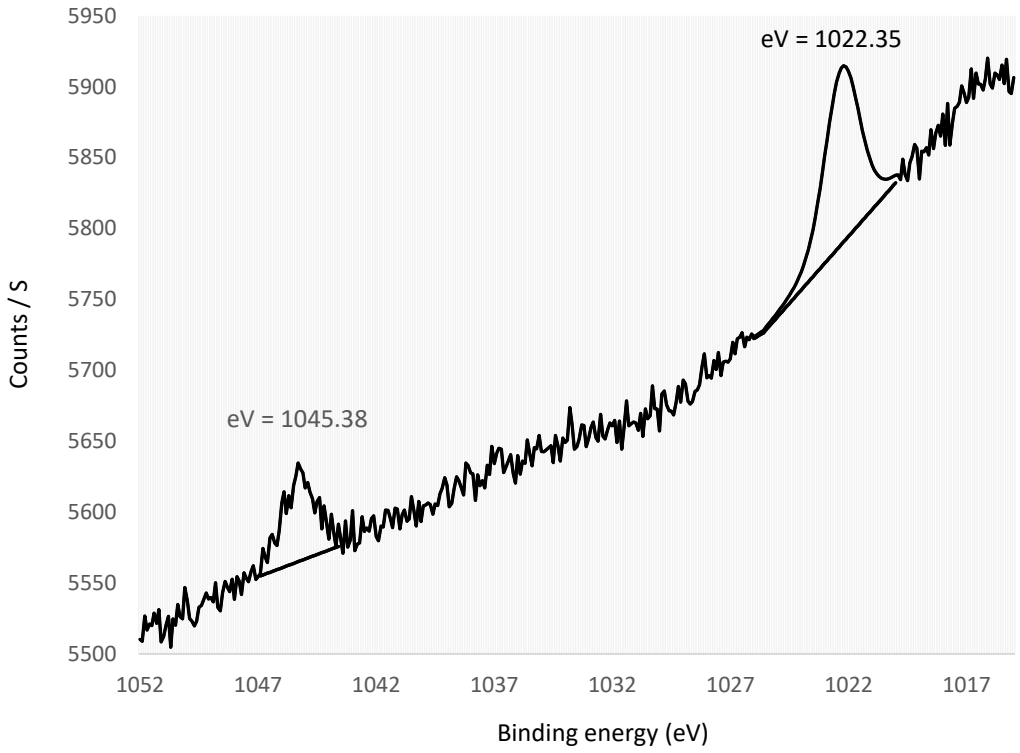


Figure 8-8: High resolution XPS scan of Zn 1s (200 scans, 400um, CAE 20.0, 0.1 eV) showing characteristic Zn $2p_{3/2}$ and Zn $2p_{1/2}$ peaks at 1022.35eV and 1045.38eV respectively

Figure 8-8 shows that XPS analysis of SSC-700 generated two peaks for Zn, 1022.35eV and 1045.38eV, characteristic of this metals $2p_{3/2}$ and $2p_{1/2}$ orbitals and the values approximately correlate with values reported in the literature. The chemistry of the system suggests ZnO will undergo sulphidation in the presence of H_2S however speciation of the Zn could not be conducted. For example, Rodriguez et al. (2018) states that the identification of ZnS is especially difficult in the presence of $Zn(OH)_2$ and ZnO because the binding energies of these compounds are very close together and even overlap. Typically, the Zn $2p_{3/2}$ binding energies for these different Zn compounds are found at 1022.0-1022.5, 1021.7 and 1021.5-1022.5, respectively. Based on these values, the peak identified at 1022.35eV provides the closest match for either ZnS or ZnO.

A small peak for Cu 2p orbitals was identified at 932.8eV, this region has previously been associated with Cu_2O (932.5eV), Cu_2S (932.5eV) and Cu-Cu (932.63eV) bond positions and is slightly shifted from the positions for CuO (933.6eV) and CuS (932.2eV) (Krylova & Andruevisius, 2009) which suggests Cu is present in its reduced forms, e.g. Cu (I) or Cu (0).

8.1.4 Ultimate analysis

Isothermal Py-G was used to produce char from XS-6 between 500-1000°C, it was analysed for CHN and S by ultimate analysis and the ash content by proximate analysis. The "other" content may include organic oxygen, chlorine, or be due to measurement error. The results are summarised in table 8-2.

Table 8-2: Ultimate analysis of SSC produced from XS-6 during Py-G

Dry Wt %.	C	H	N	S	Ash	Other[1]
XS-6	34.7	4.67	4.63	2.19	32.6	21.2
500	32.2	2.43	3.58	1.94	54.7	5.15
550	28.1	1.90	3.10	1.96	62.1	2.85
600	26.5	1.72	2.75	1.97	66.0	1.07
650	26.6	1.60	2.52	2.10	67.1	0
700	26.8	1.46	2.43	2.51	68.0	0
750	26.1	1.42	1.92	2.54	69.1	0
800	24.8	1.36	1.35	2.59	71.0	0
850	25.0	1.24	1.07	2.62	70.9	0
900	25.5	1.19	0.78	2.70	70.4	0
950	25.1	1.14	0.81	2.25	70.2	0.51
1000	24.7	1.06	0.83	1.99	69.6	1.79
F2: 600[2] F3: 800	28.6	1.31	2.23	2.08	66.5	0

[1]Other calculated by difference

[2]Result obtained during non-isothermal Py-G where F2 was operated at 600°C for 600s and F3 was operated at 800°C for 45s

Py-B was also used to produce char from XS-6 between 450-900°C, samples were analysed for CHN, S and Cl by ultimate analysis and ash content by proximate analysis, the results are summarised in table 8-3.

Table 8-3: Ultimate analysis of SSC produced from XS-B during Py-B

Dry Wt %.	C	H	N	S	Cl	Ash	Other[1]
XS-B	37.6	5.24	6.02	2.34	0.32	27.3	21.5
450	34.3	2.83	4.71	-	-	47.2	-
500	31.2	2.27	4.42	-	-	56.3	-
550	30.9	2.05	4.40	1.13	0.39	58.2	3.0
600	30.9	1.76	4.22	-	-	52.2	-
650	30.5	1.64	3.97	-	-	56.5	-
700	31.6	1.45	3.87	1.17	0.42	61.4	0.1
750	31.8	1.33	3.51	-	-	61.9	-
800	30.4	1.29	2.79	-	-	62.3	-
850	32.7	0.99	1.95	1.06	0.43	61.6	1.2
900	31.7	0.95	1.98	-	-	65.1	-

[1]Other calculated by difference

Isothermal Py-G was used to produce char from XS-Raw at 850ºC, the sample was analysed for CHN and S by ultimate analysis, ash content by proximate analysis and oxygen by difference. The results are summarised in table 8-4.

The values for C and N in table 8-2 are lower than those in table 8-3, suggesting Py-B retains more C and N than Py-G. Both these elements are expected to be predominantly associated with the organic fraction of SSC and likely benefit from lower heating rates which promotes polymerisation. Interestingly, when non-isothermal Py-G was conducted with decreased heating rates, a similar quantity of C and N were retained within SSC to Py-B, despite the overall dwell (t) being much shorter (Table 8-2).

Both inorganic and organic forms of S are expected to be retained within the SSC (figure 8.5), however S retention is higher during Py-G than Py-B (or non-isothermal Py-G) which suggests that high-temperature interactions help retain S within the char. For Py-B, S retention declines slightly with increased temperature, however there is not much change with increased temperature between 550-850ºC. For Py-G, S retention clearly increases between 600-900ºC and then declines thereafter. This could be due to steam gasification reactions removing inorganically bound sulphides or carbonisation of the SSC leading to removal of heterocyclic bound S. Py-G of raw sludge produces SSC with more C and N than digested sludge however S retention is lower.

Table 8-4: Ultimate analysis of SSC produced from XS-Raw during Py-G

Dry Wt %	C	H	N	S	Ash	O[1]
XS-Raw	46.3	6.36	5.23	1.71	14.8	25.6
Raw-850	31.4	1.2	1.5	2.2	66.0	-2.30

8.1.5 Char aromaticity and stability

Pyrogenic sequestration of biomass carbon is attractive because bio-degradable carbon that would otherwise decompose is converted into an unreactive char “pyrogenic carbon” (Py-C). The mean residence time of char carbon in the environment is not fully understood, however it is expected to range from hundreds to thousands of years (Mcbeath et al., 2014). Directly assessing the long-term fate of char-C in the environment is difficult. Several metrics have been developed to characterise the aromaticity and stability of char organics. These may be useful for understanding its properties.

8.1.5.1 Char aromatics

8.1.5.1.1 Aromatic fraction (fa)

The stoichiometry of saturated species can be represented as: "C_2H_{C+2}" and based on this the hydrogen deficiency (Z) of a molecule or substance can be estimated by equation (i) where "C" and "H" are the number of moles of these elements (Lehmann and Joseph, 2015):

$$\text{(i) } Z = -2C + H$$

The double bond equivalence (DBE) of a molecule or substance is defined as the number of double bonds plus the number of rings (Lehmann and Joseph, 2015) and can be estimated using equation (ii):

$$\text{(ii) } DBE = \frac{-z}{2} + \frac{N}{2} + 1$$

The DBE can be normalised to estimate the aromatic fraction (fa) in accordance with equation (iii) where "N" equals moles of nitrogen:

$$\text{(ii) } f_a = \frac{-z}{2} + \frac{n}{2} + 2$$

The f_a of benzene is 0.67 any hydrocarbon with a higher f_a is generally considered a condensed hydrocarbon although there are some cases of heterocyclic compounds breaking this rule (Koch and Dittmar, 2006). Unfortunately, DBE only measures C-C double bonds in pure hydrocarbons and does not account for carbonyl unsaturations (C=O) nor N-C π-bonds, which would reduce the potential number of C-C bonds at a given DBE. In addition, N-C π-bonds require an additional H atom to fill the spare N valence, thus influencing the H:C ratio of the ring structure (Koch and Dittmar, 2006).

8.1.5.1.2 Aromatic Index (AI)

Koch and Dittmar (2006) proposed the AI for high resolution mass-spec data, the index potentially serves as an alternative to DBE for assessing the aromaticity of organic materials containing C, H, O, N, S and P. AI is calculated from DBE_{AI} and C_{AI} in the following steps:

$$\text{(i) } DBE_{A1} = 1 + \frac{1}{2}(2(C - O - N - S - P) - (H - N - P) + N + P)$$

$$\text{[or] } DBE_{A1} = 1 + C - O - S - (\frac{1}{2}H)$$

DBE_{AI} is an estimate of the minimum number of C-C double bonds plus rings in a common molecular structure containing heteroatoms.

The next step is to calculate C_{AI}, this is used to normalise AI in the same way Fa was normalised by dividing by carbon. AI is then calculated by dividing DBE_{AI} by C_{AI}.

(ii) $C_{A1} = C - O - N - S - P$

(iii) $AI = \frac{DBE_{AI}}{C_{AI}}$

It was assumed that SSC does not contain organic P. In addition, the "other" fraction presented in table 8-2 was assumed to be equal to organic oxygen.

8.1.5.1.3 Char aromatics and molar ratios summary

The double-bond equivalence, aromatic index, and molar ratios for XS-6 and its char produced under isothermal conditions between 500-1000°C and non-isothermal conditions are summarised in table 8-5 alongside the values for XS-raw and its char produced under isothermal conditions at 850°C.

Table 8-5: The double-bond equivalence, aromaticity index and molar ratios of various chars

Sample[4]	f_a[1]	AI[2]	Molar H:C	Molar C:N	Molar C:S
XS-6	0.54	0.15	1.60	8.7	42.3
Iso-500[3]	0.89	1.02	0.90	10.5	44.3
Iso-550	0.98	1.15	0.81	10.6	38.3
Iso-600	1.02	1.18	0.77	11.2	35.9
Iso-650	1.05	1.20	0.72	12.3	33.8
Iso-700	1.08	1.23	0.65	12.9	28.5
Iso-750	1.10	1.22	0.65	15.9	27.4
Iso-800	1.13	1.22	0.65	21.4	25.6
Iso-850	1.16	1.24	0.59	27.2	25.5
Iso-900	1.18	1.23	0.56	38.1	25.2
Iso-950	1.19	1.26	0.54	36.1	29.8
Iso-1000	1.21	1.29	0.51	34.7	33.1
F2: 600°C[5] F3: 800°C	1.11	1.24	0.55	15.0	36.7
XS-Raw	0.44	0.01	1.65	10.4	72.7
Iso-850 (Raw)[4]	1.13	1.21	0.46	24.4	38.1

[1]Where $f_a > 0.7$ aromatic structures are present in hydrocarbons;

[2]Where AI > 0.67 aromatic structures are present in natural organic matter;

[3]All SSC were produced form XS-6 sludge except "SSC-850 (Raw)" which was produced from XS-Raw;

[4]All samples pyrolysed for 120 seconds, except where stated.

[5] Non-isothermal pyrolysis at 600°C for 600 seconds followed by 800°C for 60 seconds.

The threshold value for identifying condensed aromatic structures for f_a and AI is >0.7 and >0.67 respectively (Lehmann and Joseph, 2015), all chars attained these values, but sludge did not. The fa increased with increasing temperature, whilst AI increased up to 700°C and then plateaued between 700-900°C before increasing again at temperatures above 900°C.

In contrast, the H:C ratio increases up to 700ºC, plateaus between 700-800ºC and then decreases above 800ºC. Total C, N and S was used for these calculations however, inorganic forms of S were present (Figure 8-5), and carbonates may be present. Although the lack of carbon decomposition between 700-1000ºC suggests that carbonates may be decomposed <700ºC possibly due to a reaction with H_2S which is released at low temperatures.

Evidence in the literature suggests simple measures such as H:C of pyrogenic materials correlates with ring-size measured during NMR studies (Mcbeath et al., 2014) (Lu et al., 2016). Xiao et al. (2016) proposed a model that linked the H:C ratio to the number of aromatic rings present within char, however this is unlikely to be accurate for SSC because XPS analysis suggests it contains pyrrole which contains a N-H bonds. In addition, heterocyclics such as N, S and O are present within the ring structures in place of C increasing the H:C ratio (section 8.1.3)

The C:N ratio of Py-G SSC is relatively stable between 500-700ºC, marginally increasing from 10.5 to 12.9, which is only elevated from the source material XS-6 (8.7). Above 700ºC, the C:N ratio increases, suggesting higher temperatures eliminate N from the ring structure. However, the C:N ratio peaks at 900ºC at 38.1 and decreases to 34.7 by 1000ºC. Interestingly, the C:N ratio of non-isothermal char pyrolysed at 600ºC and then 800ºC was 15.0 which is approximately half-way between the C:N ratio of iso-600 and iso-800. This suggests decreased heating rates increase the retention of aromatic amine condensation. The C:S ratio of sludge appears to increase with increased temperature up 900ºC and is higher for Py-G than Py-B or non-isothermal pyrolysis (due to higher heating rates) which is due to organic and inorganic S retention (Figure 8-5).

The inclusion of N and S within the SSC ring structure also makes $H:C_{org}$ values in the literature redundant. For example, Lehmann & Joseph (2015) suggested biochars with a $H:C_{org}$ ratio of <0.4, would, when applied to soil, have a mean residence time of over 1000 years. An issue with the data collected in this research, however, is that the quantity of inorganic carbon has not been measured.

8.1.5.2 Char stability

The long-term stability of sewage sludge char in the environment is important for determining the materials suitability for pyrogenic carbon sequestration. Py-C is ubiquitous in the environment and widely distributed in soils, ice, sediments, and the atmosphere often due to incomplete combustion which can be both anthropogenic and "natural" in origin. For example, Doerr et al. (2018) suggests vegetation fires produce up to 116-385 Tg Py-C yr^{-1} globally. As explored in section 2.2.3, the long-term stability of Py-C varies from lightly charred plant materials to highly condensed soot and microcrystalline graphite. Laboratory studies can determine carbon mineralisation rates, although only over short time-frames and conditions that are not representative of the conditions in the environment (e.g. the soil). For example, Cross and Sohi (2012) developed an accelerated aging test using H_2O_2 (an oxidising agent) which may provide further evidence of carbon stability but is not necessarily representative of soil conditions.

Consequently, there is not a universally recognised rate-constant for Py-C stability in the environment (Bird et al., 2015).

Harvey et al. (2012) suggested an index-based approach to assessing the recalcitrance and soil carbon sequestration potential of engineered chars. The index assumes that chars of increasingly higher environmental recalcitrance will require much greater energy inputs to oxidise/mineralise (Harvey et al., 2012). For example, a char dominated by C=C bonds and other aromatic structures will have greater thermochemical stability than a material dominated by C-C bonds. The recalcitrance index (R_{50}) proposed by Harvey (2012) is calculated by the following equation, where T_{50} are the temperature values corresponding to 50% oxidation/volatilisation of char (x) and graphite during thermogravimetric analysis:

$$R_{50}\,(x) = \frac{T_{50}\,(x)}{T_{50}\,(graphite)}$$

The R_{50} index can assess the carbon sequestration potential of char (x), for example:

- Class A = $R_{50} \geq 0.70$
- Class B = $0.50 \geq R_{50} < 0.70$
- Class C = $R_{50} < 0.50$

According to Harvey et al. (2012), Class A chars would have a comparable carbon sequestration potential to soot/graphite, Class C to uncharred biomass whilst Class B would have an intermediate recalcitrance to degradation. When conducting R_{50} analysis, the decomposition of organics between 475-600ºC is referred to as Q_3 which is often used as an indicator of highly recalcitrant organics which have "proved to be more resistant to microbial degradation" over the long-term (Santin et al., 2017); although the scientific basis for this is relatively limited (Campo and Merino, 2016).

The R_{50} and Q_3 indexes of XS-6 sewage sludge and XS-6 SSC are presented in table 8-6. The results show that XS-6 and SSC produced between 400-500ºC with a dwell (t) of 120s had an R_{50} index below 0.50 therefore were classified as Class C sequestration agents (e.g. limited sequestration potential). All char produced at 600ºC and above had a class B sequestration classification. The amount of Q_3 carbon appeared to be relatively stable between 600-800ºC and markedly increased at 900ºC and above. The results for R_{50} and Q_3 for SSC produced under extended dwell-times were like those obtained at short dwell-times, suggesting temperature rather than dwell-time was the most important factor for determining carbon stability. The Q_3 result obtained at 900ºC for extended dwell-times was much lower than that obtained under short dwell-times this was credited to possible sample heterogeneity.

Table 8-6: R_{50} summary information showing pyrolysis material, pyrolysis dwell (t), Q_3, R_{50} and carbon sequestration class.

Material	Dwell (t) (sec)	Q_3[1] (DAF) (%)	R_{50}[2]	Sequestration Class[2]
Graphite[3]	n/a	1.3	1	A
XS-6	0	13.9	0.48	C
SSC-400	120s	9.0	0.48	C
SSC-500	120s	13.7	0.48	C
SSC-600	120s	27.8	0.55	B
SSC-700	120s	20.7	0.55	B
SSC-800	120s	26.3	0.56	B
SSC-900	120s	64.2	0.60	B
SSC-700	1200s	27.8	0.55	B
SSC-800	1200s	31.6	0.58	B
SSC-900	1200s	45.4	0.59	B

[1]Percentage weight-loss between 475-600ºC in oxygen at a heating rate of 10ºC (dry ash-free)
[2]R_{50} index and carbon sequestration class in accordance with Harvey et al (2012)
[3]T_{50} for powdered graphite was 802.5ºC

The R_{50} values presented in table 8-6 are comparable, and perhaps slightly higher than the values presented for lignocellulosic biomass pyrolysis. For example, Harvey et al. (2012) presents the indexes of a variety of lignocellulosic materials, when pyrolysed at 600ºC and above, these materials had R_{50}'s of between 0.52-0.61; whilst lignocellulosic biochars pyrolysed between 200-600ºC had R_{50} values of between 0.37-0.59 (Harvey et al., 2012). Santin et al., (2017) reports Q3 values of between 11-51% for charred materials produced between 350-950ºC and increased temperatures were associated with higher Q3 values. Because of the thermal oxidative method used to assess char stability, SSC may be slightly disadvantaged compared to lignocellulosic materials because SSC contains inorganic groups such as sulphides which may contribute to weight loss at low temperatures, lowering their R_{50} indexes.

The increased thermal stability of SSC when produced at 900ºC and above was unexpected however, it may be related to the quantity of char-N. For example, figure 7-7 showed that char-N continuously decreased between 600-900ºC and then stabilised between 900-1000ºC. This is likely due to the conversion of heterocyclic-N, such as pyrrole and pyridine into graphitic-N. This requires further investigation before any conclusions are drawn. However, if the retention of C-N bonds in char organics reduces the long-term stability of the carbon in the environment, this has important ramifications for the pyrolysis process and conditions used. For example, fast heating-rates and highest heating temperatures of approximately 900ºC and above may be favourable.

8.2 Sewage sludge char: hazardous waste assessment

The Waste Framework Directive (European parliament and council, 2008) defines waste as a substance or object which the holder discards, or intends to discard, or is required to discard. Different types of waste are assigned a European Waste Catalogue (EWC) code, which is based on material types the process or activity producing them. For SSC the code is either 19 01 17 (hazardous) or the mirror code 19 01 18 (non-hazardous). Where: 19 shows the material is from waste and water treatment, 01 shows the material origin was from incineration or pyrolysis and 17/18 separates it as hazardous or non-hazardous. Annex III of the WFD lists the properties of waste that render it hazardous or not. The potential hazard properties (HP) include:

- Explosive (HP1)
- Oxidising (HP2)
- Flammable (HP3)
- Irritant (HP4)
- Specific target organ toxicity/aspiration toxicity (SPOT) (HP5)
- Acute toxicity (HP6)
- Carcinogenic (HP7)
- Corrosive (HP8)
- Infectious (HP9)
- Toxic for reproduction (HP10)
- Mutagenic (HP11)
- Produces toxic gases in contact with water, air, or acid (HP12)
- Sensitising (HP13)
- Ecotoxic (HP14)
- Capable of exhibiting a hazardous property listed above not directly displayed by the original waste material (HP15)
- Persistent organic pollutant (HP16)

Several of the hazardous properties listed are not thought to be applicable to sewage sludge char and can be immediately discounted (HP2 and HP9). Technical guidance for waste classification is provided in the WM3 report (Environment Agency[b], 2018). The globally harmonised system

of classification and labelling of chemicals (GHS) is used to generate a hazard statement for each compound within the waste.

The concentration of the compound is then compared against guideline values in WM3 to determine whether the material has a composition which results in an HP assignment or not. It is the responsibility of the waste generator to accurately determine, through analytical means or by knowledge, the composition of the waste. When a producer knows the concentration of elements present but not the compounds present, the worst-case (most hazardous) compound must be assumed for each element.

8.2.1 Explosive (HP1)

In accordance with WM3, SSC is not expected to be explosive (HP1). However, there are other relevant legislation, for example the Dangerous Substances and Explosive Atmosphere Regulations (2002) (DSEAR) (HSE, 2002) and the explosive atmosphere's directive 99/92/EC (ATEX) that requires an assessment to be conducted. DSEAR states "a dust explosion involves the rapid combustion of dust particles that release energy and usually occurs when dust is dispersed in air". The low temperature industrial dryers proposed by Mills (2015) extrude the sludge and then dry the material on belts, this process produces a loose pellet, rather than a powder which is typical of high temperature dryers. It may be useful to conduct granulometric work to confirm whether dust formation is limited on low-temperature belts.

The feedstock used during this project was mostly granular (<5.6mm), during pyrolysis the SSC retains its structure although small quantities of dust are also generated which may be because of secondary carbon deposition. SSC dust could cause an explosion, if it accumulates on hot surface or is dispersed within air, although this is unlikely due to the material predominately retaining its granular structure. Coarse isothermal SSC produced at 850ºC was sent to DEKRA Process safety (Southampton UK), the material was hand-milled by DEKRA, and the dust formed was 81.1% <63µm and 99.98% <200 µm. The dust was then tested for its minimum ignition temperature (MIT) as a cloud and layer and its volume resistivity. The results are presented in Table 8-7 and show the dust cloud and layer MIT for SSC-850 were 680ºC and 360ºC respectively whilst its volume resistivity was 3.9 x 10^4.

Table 8-7: Sewage sludge char: Minimum ignition temperature for dust explosions

Test	Value
Minimum Ignition Temperature as a cloud[1]	680ºC
Minimum Ignition Temperature as a layer[2]	360ºC
Powder volume resistivity	3.9 x 10^4 Ωm (RH: 25%)

[1]ASTM E1491
[2]ASTM E2021

The results show SSC can produce an explosive atmosphere, although this applies to the accumulation of dust, not the granular material. SSC dust also has a resistivity of > 1 x 10^3 therefore it is classified as a Group IIIB combustible non-conductive dust.

8.2.2 Flammability (HP2)

SSC contains condensed elemental C, materials that contain this element such as charcoal or activated carbon are typically classified as "Flammable solid. 2" or H228, therefore this is likely to apply to SSC. Sewage sludge char is inherently flammable because it contains carbon, however the elemental mass balance suggests above 700ºC the materials volatile content has been removed. Whilst thermogravimetric analysis and Py-B suggest devolatilisation is largely complete at approximately 568ºC and 600ºC, respectively. So, whilst the material may be flammable, it may be difficult to ignite the material and sustain a flame because of the lack of volatiles. SSC, like activated carbon and other carbonaceous materials, will likely be classified as H228 (HP2).

At 700ºC, SSC contained approximately 3,665mg of metal sulphides per kilogram. In the presence of air and moisture some forms of metal sulphide undergo an exothermic oxidation reaction which causes self- heating of the material. For example: pyrite can cause self-heating in coals (Arisoy and Beamish, 2015) although pyrite is not classified as self-heating; K_2S and MgS are classified as H252 (Self-heating in large quantities; may catch fire); and Na_2S is classified as H251 (Self-heating; may catch fire). Fe(III) chloride is dosed at many STW's for chemical P removal and to suppress H_2S emissions during digestion, therefore it is likely that Fe(II) sulphide minerals will be present within SSC. The potential presence of alkali and ferrous sulphides within SSC means further testing is required to assess whether the material is self-heating.

8.2.3 Produces toxic gases in contact with water, air, or acid (HP12)

The definition of HP12 is a substance that "produces toxic gases in contact with water, air or acid", there are three hazard codes associated with HP12:

- EUH029 – Contact with water liberates toxic gas
- EUH031 – Contact with acids liberates toxic gas (e.g. H_2S)
- EUH032 – Contact with acids liberates very-toxic gas (e.g. HCN)

WM3 suggests calculating the limiting concentration of the substance from the expected stoichiometric ratio between the substance and water or acid. Table C12.2 of the WM3 protocol provides concentration limits for several sulphide compounds which range between 0.3-0.8%. For SSC, the concentration of individual sulphide compounds is not known however at 700ºC SSC contained 2.5% S (or 0.78 moles of S per kg SSC-900) which is far higher than the sulphide compound concentration limits. Since 1 mole of an ideal gas at STP occupies 22.4 litres, 1kg of SSC-700 could theoretically yield almost 17.5 litres of H_2S. For SSC, total S is not suitable metric to calculate potential H_2S formation because, alongside metal sulphide, the material also contains

metal sulphates and organic sulphur (Figure 8-5), neither of which would produce H_2S when mixed with an acid.

Based on the sulphide concentration outlined in section 8.1.3.3 the conversion of total SSC-700 sulphides into H_2S would generate approximately 2.6L H_2S kg^{-1}. The WM3 protocol provides concentration limits for specific AEM and alkali metal sulphides (Table 8-8). Because of sample complexity, the qualification and quantification of individual sulphide compounds within SSC has not been assessed. However, all of those present within Table 8-8 may be present. The WM3 concentration limits (Wt.%) were back-calculated to the volume of H_2S generated from these compounds.

Table 8-8: HP12 classification of sulphide compounds

Compound	Harmonised classification	Other Reach and CLP notifications	HP12 Classification	WM3 concentration limit
MgS	H252, H302, H311, H314, H400	-	Not stated, but likely to be EUH031	-
CaS	H315, H319, H335, H400	H302, H332, H317	EUH031 (Releases toxic gas H_2S upon contact with acid)[1]	0.3% Wt.
BaS	H332, H302, H400	H301, H314, H290, H318		0.8% Wt.
K_2S	-	H252, H314, H400		0.5% Wt.
Na_2S	H301, H314, H400	H318, H251, H290, H311		0.4% Wt.
ZnS	Not Classified	Not Classified	Not Classified	-
CuS		H413		-
Cu_2S		Not classified		-
FeS				-

[1]Hazard statements from Table 3.2 Annex VI of CLP regulations (Hennebert et al, 2016), ECHA (2020) and Pubchem.gov online search.

The results show that the concentration limits equate to between 0.09-0.11L H_2S kg^{-1}. The WM3 protocol does not provide a standard test method to assess HP12 in waste. Although it states that the test method for emission of flammable gas provided in section 2.12. of the European Chemical Agency's guidance on the application of the CLP should be used which consists of mixing waste with 1M HCl if suspected of being an EUH031/EUH032 substance. Hennebert et al. (2016) proposed a standard test for the assessment of HP12 in hazardous waste classification based on the analysis of 49 wastes.

In summary:

- One kilogram of waste should be mixed with 10L of water or 2.5M HNO_3 depending on whether EUH029 or EUH031/EUH032 is assessed.
- If gas emissions exceed 0.1L of gas per kilogram of waste over a 5-minute period, a qualitative assessment of the gases should be conducted.

- If one gas is toxic, either a WM3 worst case approach or specific test method (e.g. GC) should be used to estimate the quantity emitted.

The European chemicals agency does not classify all sulphide compounds as EUH031, presumably because some metal sulphides have very low solubility product constants, and when mixed with dilute acids (1-2.5N) may react slowly (e.g. Fe/Zn/Cu/Pb sulphides). This would explain why the test proposed by Hennebert et al. (2016) uses relatively intense extracting conditions but is time-limited to 5 minutes. Table 7-15 shows that the Py-G char-S yield increased between 650-900ºC, both $MgCO_3$ and $CaCO_3$ are expected to decompose within this temperature range and increasingly form metal sulphides. In addition, thermogravimetric analysis of $CaSO_4$ decomposition in CO suggests decomposition to CaS begins at 780ºC and peaks at 865ºC (Kuusik et al., 1985). Both AEM and alkali metal sulphides are expected to rapidly decompose when mixed with acids, therefore from the perspective of avoiding EUH031 risks, it may be beneficial to minimise the decomposition of carbonates and sulphates within SSC.

To conclude, the total concentration of metal sulphides within SSC-700 suggests the material could generate upto to 2.6L H_2S kg^{-1}, and this is expected to increase up to a HHT of 900ºC. This value far exceeds the H_2S limit of 0.1L kg^{-1}, based on a conservative approach, the material should be classified as EUH031. However, testing must be conducted to assess the rate of H_2S generation because, at moderate temperatures, limited quantities of AEM sulphides may have formed and the material may not be classified as EUH031.

8.2.4 Inorganic hazards

Many of the remaining hazardous properties relate to the inorganic elements within SSC. These can be determined through analytical means or knowledge, where there are uncertainties the worst-case scenario for each element must be used. The worst-case compounds for several elements are presented in table 8-9 alongside their hazard statements and hazardous properties.

Table 8-9: Worst case compounds as outlined in WM3

Compound	Hazard Statements	Hazardous properties (HP)
Arsenic trioxide (As_2O_3)	350, 300, 314, 400, 410	6, 7, 8, 14
Calcium Oxide (CaO)	302, 314, 315, 318, 335	6, 8, 4, 5
Chromium VI (Cr (VI))	271, 301, 330, 311, 314, 334, 317,340, 350, 361f, 335, 372, 400, 410	2, 5, 6, 7, 8, 14
Copper Oxide (CuO)	302, 400, 410	6, 14
Lead Sulphate ($PbSO_4$)	360, 332, 302, 373, 400, 410, 350	5, 6, 10, 14
Nickel carbonate (Ni_4CO_3)	350i, 341, 360D, 372, 332, H302, 315, 334, 317, 400, 410	4, 5, 6, 7, 10, 11, 13, 14.
Zinc oxide (ZnO)	400, 410	14

For waste to gain a hazardous property, it only needs to exceed the guideline values of one hazard statement. Threshold values are applied to both individual compounds and to compounds with the same hazard statements (e.g. cumulatively).

Of these compounds (Table 8-9), only CaO, CuO, and ZnO are expected to be present in high enough concentrations to pose a risk to human and environmental health under WM3 guidelines. If a waste is classified as hazardous, it influences its waste disposal and future use. Based on the worst-case scenario, a hazardous waste assessment for SSC was conducted and the results are summarised in table 8-10. The compounds ZnO, CuO and $PbSO_4$ are all classified as H400 (very toxic to aquatic life) and H410 (very toxic to aquatic life with long-lasting effects) (Table 8-9). AEM/alkali metal sulphides are also classified as H400, the SSC sulphide concentration is 3,665 mg kg^{-1} or 0.82% expressed as CaS. If Σ [H400-compounds] are <25% wt., the material is not classified as hazardous. $PbSO_4$ is below the threshold values (0.1%) to be considered for assessment. Based on the total concentration of ZnO, CuO and sulphides (expressed as CaS), SSC would contain <1.14% Wt of H400, therefore it is not hazardous by H400.

For H410 assessment, the following equation is used:

$$If: 100\ x\ \Sigma c\ (H410))\ +\ 10\ x\ \Sigma c\ (H411)\ +\ \Sigma c\ (H412)\ \geq\ 25\%,$$
$$the\ material\ is\ hazardous\ in\ accorance\ with\ HP14$$

In accordance with this equation, the potential concentrations of ZnO and CuO will exceed the threshold and the material will be classified as H410 and HP14 (Table 8-10)

Table 8-10: SSC inorganic hazardous waste assessment (worst-case)

Compound	Concentration[1] (% weight)	Individual exceedance	Cumulative exceedance	Hazard Properties
CaO (Total Ca)[2]	14.1%	H314, H318	H314. H318	8, 4
CaO (Est.)[3]	6.3%	H314	H314	8
$Ca(OH)_2$ (Est.)[3]	8.4%	None	None	None
$PbSO_4$	0.04%	Below cut-off value of 0.1% for H400/H410		
CuO	0.11%	-	H410	14
ZnO	0.21%	-		14

[1] Based on SSC-700 elemental concentrations (Table 8-1)

[2] The residual Ca concentration is all assumed to be present as CaO based on the worst-case methodology outlined in WM3.

[3]Estimated CaO or $Ca(OH)_2$ concentration based on the assumption that 60% of SSC-700 phosphate is bound as HAP; metal carbonates are bound as $CaCO_3$; and sulphates are preferentially bound to Ba and Sr and the remaining sulphates are bound to Ca.

All of the calcium in SSC is unlikely to be present as CaO, for example: XANES (X-ray absorption near edge structure) analysis conducted by Robinson et al., (2017) found that SSC phosphate was present as: 60% hydroxyapatite [$Ca_{10}(PO_4)_6(OH)_2$], 20% magnesium pyrophosphate [$Mg_2O_7P_2$] and 19% as iron phosphate [$FePO_4.xH_2O$]. Whilst Kleemann (2015) conducted quantitative XRD experiments and suggested that 70% of the phosphate in SSC was

present as Whitlockite-like compounds [e.g. $Ca_3(PO_4)_2$]. SSC-700 contained 56,903 mg kg^{-1} P, based on 60% of this being fractionated as HAP, approximately 18,000 mg Ca kg^{-1} within SSC is bound as HAP.

In section 8.1.3, XPS analysis was used to calculate the amount of C and S present as metal carbonates and , respectively. Based on the assumption that carbonates are only present as $CaCO_3$, 24,000 mg Ca kg^{-1} are bound in this form rather than CaO. Likewise, assuming all the Ba and Sr within SSC-700 (Table 8-1) are present as sulphates, and the remaining sulphates are all present as $CaSO_4$, approximately 13,450 mg Ca kg^{-1} is bound in this form rather than CaO. Overall, this leaves approximately 45,000 mg Ca kg^{-1} which may be present as either oxides, sulphides, or other aqua-regia extractable forms. Assuming all the leftover Ca is present as CaO, the estimated concentration of CaO in SSC-700 is approximately 63,000 mg kg or 6.3%.

Based on the corrected value of CaO within SSC (6.3% SSC-700 Wt.) the material is expected to be classified as H314 (Causes severe skin burns and eye damage) due to exceedance of the 5% concentration limit therefore the material is corrosive (HP8). For the uncorrected CaO concentration, SSC would also exceed the 10% limit for H318 (Causes serious eye damage) meaning the material is classified as an irritant. Based on the concentrations for CuO and ZnO in SSC-700 in table 8-11, the material will be classified as H410 (very toxic to aquatic life with long-lasting effects) and will be ecotoxic (HP14).

CaO is hygroscopic therefore is absorbs moisture from the air and hydrates forming $Ca(OH)_2$. The estimated quantity of CaO is 6.3% if all of this formed $Ca(OH)_2$ the concentration would increase to approximately 8.4%. However, $Ca(OH)_2$ does not have the H314 hazard code therefore the material would not be classified as corrosive or an irritant. Over-time $Ca(OH)_2$ undergoes carbonation to form $CaCO_3$ does not have hazardous properties and is not classified according to GHS statements. Therefore, although SSC-700 may contain CaO which would render the material corrosive, this hydrates in air or water forming $Ca(OH)_2$ which has hazardous properties but not in the potential concentrations found in SSC. If $Ca(OH)_2$ reacts with CO_2, the Ca in SSC would no longer have any hazardous properties.

8.2.4.1 Inorganic hazards: Most-likely scenario discussion

The aqua-regia extractable concentration of Ca within SSC-700 was approximately 98,500 mg kg^{-1} (Table 8-1). In Table 8-8, the concentration of CaO present within SSC was estimated by deducting the estimated concentration of Ca bound to carbonates, sulphate, and phosphates from the total concentration of Ca. This approach suggested that 45,277 mg kg^{-1} of the Ca was present as an oxide. Calcium oxide is not expected to be present within sludge prior to pyrolysis and is a decomposition product. However, at 700°C neither $CaCO_3$ nor $CaSO_4$ are expected to decompose therefore significant quantities of CaO at this temperature is unlikely.

The remaining Ca (45,277 mg kg^{-1}) may be bound to the following counter-ions:

- Phosphate
- Sulphide
- Aluminosilicates/silicates

Over 60% of the Ca within SSC may be bound to phosphate, and small quantities of CaS may form within SSC at 700ºC, however neither of these fractions is large enough to explain how all the remaining Ca may be bound. A probable explanation is that $CaCO_3$ within sludge reacts with silicates and aluminosilicates, <700ºC. The presence of AEM - silicates and aluminosilicates has been reported in sludge gasification ash (Migliaccio et al., 2021). Some of the mineralogical forms for Ca silicates include wollastonite ($CaSiO_3$), anorthite ($CaAl_2Si_2O_8$) and gehlenite ($Ca_2Al_2SiO_7$) and some of these forms are used as additives within cement (Khan & Ashraf, 2019).

Polettini et al. (2004) found that Wollastonite formed at temperatures higher than 600-700ºC in incineration fly-ash because of the reaction between $CaCO_3$ and SiO_2. The decrease in SSC carbon between 700-750ºC and subsequent stabilisation between 750-1000ºC, is suggestive that the same reaction occurs within SSC, however further XPS analysis is required to validate this. The significance of AEM silicate/aluminosilicate formation, at moderate temperatures 600-750ºC, during pyrolysis, is that the quantity of CaO/MgO and CaS/MgS formed is likely to be suppressed, decreasing the risk posed by these compounds.

During thermogravimetric analysis, metal carbonates are decomposed forming their corresponding oxides, for example, this reaction is complete at 500ºC for $FeCO_3$, 700ºC for $MgCO_3$ and 800ºC for $CaCO_3$ (Attar, 1978). Based on XPS analysis for C presented in section 8.1.3.1, 2.7% of SSC-700 carbon is expected to be present as carbonates which equates to a concentration within SSC-700 of 7167 mg C kg^{-1} or 0.7% weight. Table 7-12 presented the char-C yields, the results were relatively stable between 700-1000ºC (±0.6%) which was suggestive that no further decomposition of carbon occurred between these temperatures. However, above 700ºC all the temperatures (except 950ºC) contained 0.5-0.6% less total carbon than SSC-700. This small decrease may be because of the decomposition of carbonates above 700-750ºC which is supportive of the theory that carbonate reacts with silicates/aluminosilicate. Although because of errors during ultimate analysis (±0.3% absolute wt.) and char collection and weighing (unknown error) this may be coincidental.

Calcium oxide is used within metallurgical processes to scavenge sulphides from metals and convert them into oxides so they can be reduced into their elemental form with a reducing agent (e.g. C, CO, H_2). Metal oxides are easier to reduce than their respective sulphides because oxygen is more electronegative and can accept an electron pair from an incoming nucleophile more easily. Therefore, the formation of calcium oxide during pyrolysis may initiate the reduction and volatilisation of metals. An Ellingham oxide diagram is a plot of the Gibbs free energy (ΔG) versus temperature (Ellingham, 1944) (Tegg (2019), it can predict whether the reduction of a

metal oxide into its elemental form is thermodynamically favourable. However, it does not consider reaction kinetics. Elements with lower (ΔG^o) can reduce metal oxides into their elemental form. Carbon is unique, when forming carbon monoxide its entropy increases therefore its (ΔG^o) decreases with increasing temperature.

This means that with increasing temperature, carbon in the char will become an increasingly effective reducing agent, potentially leading to the formation of elemental metals.

The Ellingham diagram in Tegg (2019) shows that below 1000°C; C, CO and H_2 cannot reduce many of the metal oxides present in SSC, including CaO, MgO, Al_2O_3, Ba_2O_3, SiO_2 and Na_2O. Thermodynamically: Cu_2O and Fe_2O_3 can be reduced to Cu and Fe_3O_4 at low temperatures <300°C by H_2, CO and C. Whilst Fe_3O_4, ZnO, K_2O require higher temperatures and are reduced by C at approximately 750°C, 800°C and 950-1000°C, respectively. In reality, thermodynamic favourability does not guarantee that a specific reaction will proceed because competing reactions may be more favourable, and the reaction kinetics may be unfavourable. The heterogeneity of the system makes predicting which reactions may occur challenging. The reduction of compounds will influence these compounds concentration, toxicity and boiling-point. For example, elemental Zn is volatile >907°C, whilst ZnO is volatile >2360°C.

The worst-case scenario presented in Table 8-10 assumed that Zn/Cu and excess Ca were present as oxides and Pb was present as a sulphate. Metal oxides such as ZnO are expected to undergo sulphidation during pyrolysis, although some compounds may have already undergone sulphidation during anaerobic digestion, for example Samokhvalov & Tatarchuk (2011) state ZnO sulphidation can proceed at room temperature. The absorption of H_2S by metal oxides involves "the dissociation of H_2S into H^+ and HS^-, followed by diffusion of HS^- into the oxide lattice and migration of the oxide and water to the surface". In addition, "the rate of sulfidation is limited by the internal mass-transfer resistance, and only external layers of the grain of the sorbent are sulfide" (Samokhvalov & Tatarchuk, 2011). This suggests that the extent of metal oxide sulphidation may not be driven to completion, although the conversion may be high because metal oxides are likely to be dispersed throughout the material. Also, unlike sorbent materials, the H_2S is generated within the material which may promote contact between the H_2S and oxides within the material.

The sulphidation of compounds will influence their concentration, toxicity, boiling-point, as well as decreasing the likelihood that reduction to elemental forms will occur. For example, the reduction of K_2O at K at 800°C is likely to cause metal volatilisation because K has a boiling point of 760°C however the sulphidation of K_2O makes reduction less likely and is unlikely to volatilise because its boiling point is 912°C. Likewise, the sulphidation of CuO to CuS alters the compound's hazard statement because of the low solubility of many sulphide compounds (Table 9-21). For example, CuO attracts the hazard statement H410, whilst CuS is typically not

classified, or attracts the lesser hazard statement of H413 (may cause long lasting harmful effects to aquatic life).

Since CaO can scavenge sulphide from metal sulphides, its formation between 700-800ºC may cause an increase in metal oxide reduction and potential metal volatilisation.

Although CaO may be more likely to scavenge H_2S from the atmosphere because of the high concentration present (Figure 7-4) and the favourable kinetics of gas-solid over solid-solid reactions. For example, there was a continuous increase in char-S yields between 650ºC and 800ºC from 45.8% to 54.4%, which suggests increased sulphidation between these temperatures.

Wu et al. (2006) investigated the carbothermic reduction of ZnS in the presence of carbon and calcium carbonate between 906-1080ºC in an inert atmosphere. The results suggest that CaO was involved in the carbothermic reduction of ZnS, and scavenged sulphide since ZnO and CaS formed in the solids. ZnO then underwent a reduction reaction forming elemental Zn, which was then volatilised. According to Wu et al. (2006) the following transformations occurred:

- β-Zn(s) → α-Zn (s) → ZnO (s) → Zn (g)
- $CaCO_3$ → CaO → CaS

Tegg (2019) shows that Cu (I) reduction is thermodynamically favourable in ambient conditions therefore, its reduction to elemental form or stabilisation as Cu_2S form may occur prior to pyrolysis. Rao (1987) investigated the reduction of Cu sulphides in the presence of H_2 between 500-1020ºC, the kinetics were relatively slow achieving 20% reduction in 185 minutes at 603ºC and 30 minutes at 970ºC. The elemental Cu formed fibres at low temperatures (<750ºC) which fuse into spongy crusts between 750-850ºC whilst at higher temperatures (894-1020ºC) the copper is entirely composed of sintered crusts. During sludge pyrolysis the presence of sulphide scavengers and more effective reducing agents (C/CO) may increase the likelihood of Cu sulphide reduction to its elemental form although this is offset by the high concentration of H_2S within the atmosphere and the short-retention times.

Metal sulphates within sludge, such as $PbSO_4$ and $ZnSO_4$, are likely to undergo carbothermal reduction, whilst more stable sulphates, such as $CaSO_4$, may not decompose until higher temperatures. The most likely products are assumed to be sulphides because these are more difficult to reduce compared to metal oxides, and the atmosphere contains high concentrations of H_2S which means if any oxides were formed these may rapidly undergo sulphidation reactions. Some of the metal sulphides present in the sludge or formed during pyrolysis may undergo direct carbothermal reduction to their elemental forms, however, although the kinetics of these reactions may limit this conversion. Above 900ºC, the char-S yield declines which may be because of the reduction of metal sulphates, for example:

- $CaSO_4 + 4CO$ → $CaS + 4CO_2$

- $CaSO_4 + CO \rightarrow CaO + CO_2 + SO_2$

The dominant reaction is influenced by the reducing potential of the gas, for example, the partial pressure ratio of CO and CO_2 with more reducing conditions forming CaS (Oh & Wheelock, 1990). Hydrogen can also reduce metal sulphates, for example: Malecki (2015) suggests Pb and Zn sulphate reduction initiates at 550°C and the reduction rate is highly dependent on temperature.

Wet chemical methods can assess metal speciation, for example, Lasheen and Ammar (2009) used sequential extractions to indirectly estimate the quantity of metals bound to the following fractions in sewage sludge: (i) exchangeable; (ii) carbonate bound; (iii) Fe/Mn-oxides (iv) sulphide or organic bound and (v) residual (e.g. secondary minerals). The results indicated Zn was abundant in fractions (i-iii) whilst copper was predominantly found in fractions (iv-v). Gu et al. (2017) investigated metal speciation in char produced from lake sediment (<500°C). A four-step sequential extraction procedure was used based on a method outlined by the European Community Bureau of Reference (BCR). Prior to pyrolysis, Cu and Zn were predominantly bound to fraction (iii), however pyrolysis converted both metals to fraction (iv).

Chen et al. (2015) impregnated sewage sludge with Cu, pyrolysed the material (400-800°C) and investigated the release of heavy metals using a three-step BCR method. Prior to pyrolysis, Zn was predominantly in reducible forms (e.g. oxides), at low pyrolysis temperatures (<500°C) oxidizable forms were dominant (e.g. sulphides), however between 600-800°C Zn was mostly fractionated into the residual fraction. For Cu, the oxidizable fraction was a major species prior to pyrolysis however, Cu fractionation was not analysed post-pyrolysis.

The discussion above suggests:

- Alkali metal carbonates (e.g. $CaCO_3$ or $MgCO_3$) are likely to either: decompose into oxides; react with silicates/aluminosilicates to form alkali-metal silicates; or react with sulphides to form alkali metal sulphides. The decomposition of carbonates into oxides is expected to peak between 750-800°C and will encourage greater retention of sulphides because of the kinetic advantages of oxide sulphidation compared to carbonate sulphidation. Alkali-metal oxides that are formed may initiate carbothermal reduction by scavenging sulphide from other elements. However, oxides may preferentially scavenge H_2S, because of favourable kinetics, limiting the extent of carbothermal reduction.
- Metal sulphates can undergo carbothermal reduction to metal sulphides and oxides, the latter of which may undergo further reduction to elemental forms. However, during Py-G the highly reducing atmosphere and high concentration of H_2S may inhibit the formation of oxides and subsequent reduction to elemental forms. Metal sulphates such

as Pb and Zn are reduced to oxides/sulphides at relatively low temperature whilst $CaSO_4$ may require a temperature of approximately 900°C or higher.

- Zinc compounds within the sludge, such as carbonates and sulphates, are expected to decompose and undergo secondary reactions to form either ZnO or ZnS. The surfaces of ZnO clusters within the sludge are expected to undergo sulphidation to ZnS, however, the ZnO not exposed to the atmosphere is unlikely to react. The fractionation between ZnO and ZnS is not known. Zinc is not expected to undergo reduction to elemental form; therefore, the dominant forms of Zn are expected to ZnS and ZnO.
- Anaerobic digestion may convert CuO, Cu^{2+} and to a lesser extent $CuSO_4$ into CuS. Pyrolysis may facilitate the reduction of CuS into Cu_2S and elemental Cu, although the latter reaction is expected to be limited by kinetics. The presence of metal oxides (e.g. CaO) may facilitate the carbothermal reduction of CuS/Cu_2S into elemental form, however, atmospheric H_2S and char silicates may limit the quantity of oxides available to initiate carbothermal reduction. The dominant forms of Cu expected to be present include Cu_2S and Cu.
- Lead is below the cut-off value of 0.1% cut-off value for hazard assessment, however it's likely to fractionated primarily as PbS and to a lesser extent elemental Pb.

8.2.4.1.1 Inorganic hazards: Most-likely scenario

Based on the discussion above, a conservative hazard assessment was conducted based on the most likely scenario, the results are presented in Table 8-11.

Table 8-11: SSC inorganic hazardous waste assessment: Most likely scenario[1]

Element	Dominant Compounds	Maximum Concentration	Individual Exceedance	Cumulative Exceedance	Hazard Property
Total Sulphide[2]	Unknown	0.82% (expressed as CaS)	n/a	-	-
Ca[3,4]	Silicates/ Aluminosilicates	Unknown	Not classified		
	$Ca(OH)_2$	<8.37-12.79%	(H318)	(H318)	
Pb	PbS	<0.03%	Below cut-off value of 0.1% for H400 and H410		
	Pb	<0.03%			
Cu	Cu_2S	<0.11%	Not Classified		
	Cu	<0.09%	Below cut-off value of 1.0% for H411		
Zn	ZnS	<0.26%	Not classified		
	ZnO	<0.21%	-	-	None

[1]Based on SSC-700 elemental concentration (Table 8-1)

[2]Based on SSC-700 sulphide concentration (Section 8.1.3.3)

[3]Estimated $Ca(OH)_2$ concentration based on the assumption that 60% of SSC-700 phosphate is bound as HAP; metal carbonates are bound as $CaCO_3$; and sulphates are preferentially bound to Ba and Sr and the remaining sulphates are bound to Ca.

[4]The lower and upper bounds are estimates of the maximum concentration before and after carbonate decomposition. These assume that all of the carbonates within SSC-700 are present as $CaCO_3$ (section 8.1.3.1) and above 700°C these decompose entirely into CaO which hydrates to form $Ca(OH)_2$.

Table 8-8 shows that Na_2S, K_2S, BaS, MgS are all classified as H314 (causes severe skin burns and eye damage). If the cumulative sum of these compounds exceeds $\geq 5\%$ or $\geq 1\%$ the material is classified as corrosive or an irritant, respectively. Based on the concentration of Na, K, Ba and Mg (Table 8-1) if these elements were present solely as sulphides the total concentration of H314 compounds would be 3.8% meaning SSC is not corrosive. For WM3 assessment, only compounds that exceed a concentration of 1% would be considered for assessment, therefore only Mg would be assessed, meaning the theoretical maximum concentration of MgS within sludge is 2.7%. However, at 700°C, the total concentration of sulphides within SSC was only 3665 mg kg^{-1}, therefore if all the Mg within SSC formed MgS its total concentration would be just 0.64% meaning SSC is neither corrosive nor an irritant at 700°C according to H314. Therefore, based on the sulphide concentration within SSC-700, none of the sulphide compounds present within SSC are likely to exceed hazard thresholds (Table 8-11). Further XPS analysis is required to assess sulphur speciation at elevated temperatures.

$Ca(OH)_2$ is classified as H318 (causes serious eye damage), if the cumulative sum of H318 compounds within SSC exceeds 10% the material is also classified as an irritant. Table 8-11 shows that at 700°C, if all the Ca not bound to phosphate or sulphate was bound as $Ca(OH)_2$, the material would not be hazardous. However, the conversion of carbonates >700°C could increase the concentration of $Ca(OH)_2$ from 8.37% to 12.79% meaning the SSC would be considered an irritant (H318). These scenarios for MgS and $Ca(OH)_2$ assume that all excess Ca/Mg forms these compounds, however AEMs are expected to undergo reactions with silicates, which are abundant in SSC, therefore the probability of these hazard codes applying to SSC is reduced if AEM silicates are identified within SSC.

Unlike CuO, Cu_2S is not classified, and elemental Cu is classified as H411. The latter falls below the 1% threshold for H411 and under WM3, should not be considered for hazard assessment. In Table 8-10, the cumulative threshold for H410 was only surpassed because of the combined concentrations of CuO and ZnO. If the dominant form of copper is CuS, Cu_2S or elemental Cu, even if all the remaining Zn if present as ZnO the material will not be classified as ecotoxic. Most ZnO at the surface of SSC is expected to undergo sulphidation therefore, SSC is unlikely to ecotoxic.

In contrast to the "worst-case" scenario presented in Table 8-10, the most-likely scenario presented in Table 8-11 suggests SSC may be considered an irritant at high temperatures however, the probability of this is low because of AEM silicate formation. Although unlikely, further testing should be conducted to rule-out the formation of metal cyanides [e.g. $Ca(CN)_2$], metal phosphides (e.g. Ca_3P_2) and metal azides (e.g. NaN_3) do not form as these release very toxic HCN, phosphine (PH_3) and NO_2 gases, respectively. This could be conducted by acidifying the sample and analysing the off-gases with a GC.

8.2.4.2 Inorganic hazards assessment: Conclusions

- In fine-dust form, SSC can produce an explosive atmosphere at the temperatures tested in Table 8-7 and is a Group IIIB non-conductive dust. However, char produced in a screw conveyor retains the structure of the feedstock and is a coarse granule therefore it is not thought to produce an explosive atmosphere.
- H228 will apply to SSC because it is a flammable solid. In addition, SSC may contain small quantities of metal sulphides that are self-heating (H251/H252). Likewise, EUH031 (Contact with acids liberates toxic gas) is likely to apply to SSC because of its content of sulphides. It may be prudent to quench SSC in a mildly acidic to neutral solution to convert readily hydrolysable sulphides to H_2S or soluble HS^- ions.
- Further testing is required to assess whether EUH029/EUH032 apply because of the potential presence of metal cyanides, phosphides or azides.

- The worst-case scenario approach, as specified in WM3, suggests: SSC contains CaO which would render the material an irritant, corrosive and acutely toxic because of H318/H319, H302 and H314 exceedance, respectively.
- The most likely scenario suggests that the Ca within SSC is unlikely to be corrosive or an irritant when carbonates are retained within the material. At elevated temperatures, approximately >750-800^{o}C, if all the carbonates are converted into CaO, which hydrates to form $Ca(OH)_2$, the material may be an irritant. However, the conversion to $Ca(OH)_2$ because it's hypothesised that $CaCO_3$ reacts with silicates/aluminosilicates. Further XPS analysis is required to assess which temperature $CaCO_3$ decomposes, low temperatures would indicate Ca silicate/aluminosilicate formation.
- The most-likely scenario suggests SSC is unlikely to be ecotoxic.

8.2.5 Leaching tests (Landfill)

In the short-term, landfill is the primary route of disposal for sludge char. To dispose of waste at landfill, basic level 1 and 2 characterisation must be conducted.

- Level 1: The EWC code is for SSC is likely to be 19 01 17 (e.g. a pyrolysis waste containing hazardous substances). The materials hazardous properties are likely to include HP12 and HP14.
- Level 2: The "Dispose of Waste to Landfill" guidance says the total concentration of inorganic elements and a BS EN 12457 1-4 leaching test must be conducted for hazardous waste to be accepted into landfill. Copper, zinc, and lead are the main heavy metals present in SSC. For stable non-reactive hazardous waste, the threshold value for a BS EN 12457-3 leaching tests are: 10 mg/kg (Pb) and 50 mg/kg (Cu and Zn). For hazardous waste, the threshold values are: 50 mg/kg (Pb), 100 mg/kg (Cu) and 200 mg/kg (Zn) (ALS Environmental Ltd., 2017).

A BS EN 12457-3 leaching test alongside a NEN 7371 leaching test was conducted for SSC-800. NEN 7371 leaching tests are pH controlled using dilute nitric acid at pH 4 and 7, the test at pH 4 is supposed to replicate extreme leaching behaviour and is a worst-case scenario (Environment Agency, 2005). The results are summarised in Table 8-12.

Table 8-12: EN 12457-3 & NEN 7371 leaching tests for SSC-800

Test	EN 12457-3		NEN 7371 (pH 7)		NEN 7371 (pH 4)	
Parameter	Mean	SD	Mean	SD	Mean	SD
Char pH	9.6	0.2	9.6	0.1	9.86	0.2
Test pH	9.6	0.2	7	0	4	0
Temperature (°C)	26.3	0	26.3	0	26.3	0
Elements[1]	Mean	SD	Mean	SD	Mean	SD
	mg/kg	mg/kg	mg/kg	mg/kg	mg/kg	mg/kg
Al	11.7	1.8	7.0	0.8	17.7	0.5
Ca	2225.4	47.6	2148.8	16.3	2605.6	20.9
K	17.4	4.7	512.4	57.2	286.6	48.3
Na	27.9	0.8	255.9	34.2	457.7	23.9
P	12.3	0.4	10.7	1.1	75.2	3.4
Mg	5.1	0.3	160.5	8.7	293.4	19.6
Sr	5.2	0.1	5.3	0.6	6.8	0.7
Fe	BDL	BDL	BDL	BDL	22.5	4.4

[1]The detection limits for Zn, Cu, Pb and Ni were 6.3, 5.2, 7.0 and 4.5 mg kg^{-1} respectively, which are below the threshold values for waste acceptance.

[2]Ag, B, Ba, Bi, Cd, Co, Cr, Cu, Fe, Ga, In, Li, Mn, Ni, Pb, Tl, and Zn were below the detection limit.

The results suggest SSC does not leach heavy metals even under the extreme conditions required for NEN 7371, therefore the waste can be accepted onto a hazardous waste landfill.

8.2.6 Active waste testing (Landfill)

In 2020 the landfill tax for inactive wastes is £3.00/t, whilst for active waste the tax is £94.15/t, therefore a waste's "activity" is the main factor influencing landfilling costs (HM Revenue & Customs, 2020). To qualify as inactive waste the material must also be classified as non-hazardous. In 2014, the cost of disposing one tonne of non-hazardous SSC by landfill would have been approximately £27.50 (Landfill tax: £2.50, Gate-fee: ~£25). However, the introduction of the loss on ignition (LOI) test in 2015 meant that the cost of landfilling non-hazardous SSC in 2020 is approximately £119.2 t^{-1} (Landfill tax: £94.2, Gate-fee: ~£25). The threshold value for the loss on ignition test has been set to 10% weight loss at 440°C. The main reason for this is to avoid the landfilling of bio-degradable waste since this could be treated more effectively and contribute to long-term landfill management costs. For Py-G SSC produced between 600-1000°C, the mean% C ranged between 24.7-26.8%, whilst LOI tests conducted at 550°C ranged from 25.2-32.0% (across all samples). Therefore, SSC will fail the LOI activity test required by landfills and will be classified as an active waste.

LOI is a suitable method for assessing biodegradability, however this does not extend to char analysis because the materials C content is in a condensed elemental form which is not thought to be biodegradable. Given the high cost of char disposal at landfill, the current regulations could undermine the adoption of pyrolysis. However, treating waste by pyrolysis rather than incineration could be favourable because large quantities of C that would otherwise form CO_2 are stored within the char. The industry may want to lobby the environment agency for an exemption for chars, at least in the short-term whilst more sustainable outlets such as land application are investigated. An alternative landfill test for waste chars (e.g. EWC code 19 01 17 and 19 01 18) could also be introduced. This test could be tailored to ensure the char does not contain solvent extractable or volatile organic compounds which could cause pollution if landfilled. 10-ring PAHs have boiling points <600°C (Achten and Andersson, 2015) and represent some the highest boiling point volatile organic molecules. Based on this, an alternative landfill acceptance test is proposed whereby dry SSC is heated to 700°C in N_2, if the material loses over 5% weight the material will be rejected. A typical SSC produced above 600°C would pass this test, based on results obtained during thermogravimetric analysis. For example, SSC produced at 750°C lost 2.8% of its total mass at 700°C, whilst sewage sludge lost 56.9% of its weight. Alternatively, a LOI based test, such as that proposed by Harvey et al. (2012) could be used and the char could be ranked in accordance with its C-sequestration class. With class A and class B chars being accepted into landfills without being classified as active waste (see table 8-6).

Chapter 9: Char disposal and value recovery options

At present, landfilling SSC is likely to be costly due to its loss on ignition exceeding 10% at 440°C meaning the full landfill tax will be applied to the material (£94.2 t^{-1} in 2020) (Section 8.2.6). In addition, whilst its heavy metal content is not leachable (Table 8-12), SSC may be hazardous (EUH031) due to its content of hydrolysable sulphides (Table 8-8) that may be an issue when landfilling the material. Landfilling SSC is the least desirable disposal route in the waste hierarchy (Figure 2-17) and for SSC should be avoided, especially prior to phosphate extraction due to its high concentration P_2O_5 (~12.8%) (Table 8-1).

So long as SSC is never disposed of by incineration and converted to ash the formation of pyrogenic-carbon within SSC is inherently valuable because the material is a Class B candidate for carbon sequestration and is expected to be resistant to mineralisation over the long-term (Harvey et al., 2012) (Table 8-6). Therefore, unlike other materials, landfilling SSC may be more sustainable to incineration, assuming that P recovery is conducted.

The main viable routes for minimising char disposal costs and recovering additional value from SSC include:

1. Direct application of char to agriculture

2. Phosphorus recovery

3. Adsorbent production

These will be discussed in detail alongside the materials carbon sequestration potential.

9.1 Pyrogenic carbon sequestration

Although SSC is expected to resist mineralisation, in the short-term, the pyrolysis of sewage sludge releases CO_2 into the atmosphere more quickly than biosolids recycling. Renewable electricity can be generated from fuel-gas, however as grid electricity decarbonises, the carbon savings from this generation is likely to decrease. Although, fuel-gas could also be used to produce heat to offset the use of fossil fuels on site. A potential issue for SSC, is that the carbon yields are low and the pay-back period to see a net decline in emissions could be long. For example, the char carbon yields for isothermal Py-G SSC >700°C were only 32.7-33.3%, although this increased to 37.6% for non-isothermal Py-G (Table 7-12). To be sustainable, SSC production must retain more carbon during its production, subsequent reuse, and disposal than biosolids recycling. For comparison, section 9.1.1 presents evidence for biosolids mineralisation rates after land application.

9.1.1 Biosolids carbon

A number of short-term laboratory experiments, long-term field trials, and carbon modelling investigations have been conducted for biosolids and farm-yard manures, these studies have found:

1. Biosolids contain a large labile fraction of organic carbon.

Terry et al. (1979) found that after 336 days of incubation, 46% of sludge C had been mineralised, with rapid decomposition occurring within the first 28 days of application followed by a near constant weight loss over the year. Likewise, Torri et al. (2014) found that soil respiration rates peak in the first 30 days before stabilising at an elevated rate for the remaining 90 days whilst Torri et al. (2007) found 29-45% carbon retention after 1 year of biosolids application. Incubation studies conducted by Mondini et al. (2017) showed respiration rates for sludge peaked within the first few days of application and then stabilised after approximately 4 days with sludge releasing 4.8% of its C content within the first 30 days, higher than biochar (0.2%), animal digestates (4.0%) but much lower than crop residues (10.4%) and animal residues (16.8%). Lignin is concentrated during anaerobic digestion suggesting it is recalcitrant, however Rasse et al. (2006) suggested 92% of lignin was mineralised within 1 year of being added to soils.

2. Biosolids contain and generate recalcitrant organic matter

Torri & Alberti (2012) suggests the recalcitrant fraction within digested sludge may largely comprise cholestane-based sterols, which are produced in animal guts, and these may have a turnover-rate of hundreds of years. The recalcitrance of steroids and structurally similar compounds is because of their hydrophobicity and absence of functional groups. Many of these compounds are natural, including: androgens, oestrogens, progestogens, cholesterol, and bile acids. However, synthetic compounds present in sludge and animal manures such as antibiotics, synthetic hormones and anti-inflammatory drugs also accumulate in the environment and represent a risk to human and environmental health (Olivera & Luengo, 2019).

Sludge application to agricultural land promotes processes that are associated with the formation of recalcitrant SOM, including earthworm activity and humification (Chambers et al., 2007) (Nicholson et al., 2018). Soil humus is made of humic acid, fulvic acids and humins, isotope analysis (^{14}C) suggests these have mean residence times of 143-1740yrs, 213-1690yrs and 293-2173yrs in Taiwanese soils, respectively (Wang & Chang, 2001). Humic acids are “random polycondensates with polyelectrolyte/polyampholite behaviour with a polyphenol or quinone-based aromatic core” (Yang & Antonetti, 2020). These substances can help minimise the mineralisation rates of other organic matter in soil (Spaccini et al., 2002).

Some of the protein content in SAS may also be recalcitrant during digestion. This is mirrored by the mineralisation rate in soils, for example: Weil and Brady (2008) state organic forms of N (e.g. proteins) mineralise at a rate of approximately 1.5-3.5% per annum. This is similar to the long-term degradation rate of biosolids in soils, when applications to soil have been ceased (Tian et al., 2009).

3. Long-term field trials show sludge increases soil organic matter

From 1942 to 1960, Johnston (1975) found 54.2-62% of sludge organic matter was retained within the first eight years, followed by 34.8-36.6% retention over the full 18-year trial. This suggests soils have a finite capacity to retain carbon, with decreased retention over-time. Tian et al. (2009) applied biosolids to soils degraded by strip mining. Forty-one fields were monitored over 34 years and split into four main groups: (i) mine spoil - soil, (ii) mine spoil - fine soil (iii) non-mined soil (vi) non-amended soil. The soils ranged in texture from silt loam to silty-clay loam. On average the mine spoiled soils (i) and (ii) sequestered 29% and 23% of total carbon inputs whilst the non-mined soil (iii) sequestered 27% of total carbon inputs.

Mondini et al. (2017) modified the RothC model to simulate the accumulation of carbon from raw sewage sludge and manure anaerobic digestates. The results, presented in Mondini et al. (2018), showed that at an application rate of 1t C ha yr^{-1}, for 100 years, raw sludge sequestered 14.9% of its C whilst digestates sequestered 26.2% in Italian soils.

4. Soils have a finite capacity to retain carbon

Rothamsted have monitored soil organic C in cultivated soils under different land management regimes continuously since 1843 as part of the Broadbalk experiments. The results show that C accumulation in manure amended soils proceeded rapidly in the early years (1843-1914) (Rothamsted, 2014), however, C accumulation slows as the soil approaches a new equilibrium (Powlson et al., 2011).

5. The retention of carbon is reversible

On fields where biosolid application was stopped for 22 years, Tian et al. (2009) found SOC remained elevated compared to non-amended controls however the level of SOC declined between 2.2-3.3% annually. The Broadbalk experiments (Rothamsted, 2014) corroborate these findings; between 1914-1936, some fields were regularly fallowed rather than cropped with wheat and fertilised with manure. As a result, the quantity of SOC declined from their peak levels.

These studies suggest that most biosolids carbon added to soils is mineralised within the first year, however, sludge contains a recalcitrant fraction and promotes the formation of earth worm activity and humification. The long-term experiments suggest that over a period of several decades to a century biosolids retain 23.0-36.6% of their carbon content, which is not dissimilar to the carbon retention in SSC after production (32.7-37.8%) although most carbon in SSC is expected to be stable for centuries to millennia.

These studies also suggest that soils tested had a limited capacity to retain carbon, suggesting they reach a new equilibrium and when biosolids applications stop, the amount of carbon gradually declines. This suggests that if end-users of biosolids apply the material every year, carbon sequestration may be limited. Continuous applications of biosolids cannot always be conducted because of the potential build-up of nutrients or heavy metals in soils. For example, Assured biosolids Ltd (2020) explain that soils with ADAS P-indexes of 4 can apply biosolids biannually, unless the soil texture is sandy then application can only be conducted every 4-years.

9.1.2 Char carbon

The literature suggests the mineralisation rates of biochar vary, for example: Lutfalla et al. (2017) suggested Py-C generated from biomass burnt in fields had a mean residence times of 116 years (42-214 years) which raised scepticism over the effectiveness chars to sequester C. Gurwick et al. (2012) corroborated, reporting variations in Py-C residence from 8.3 to 3,624 years. However, these variations are likely because of variations in terminology with fire-derived chars, torrefaction chars, slow-pyrolysis chars and pyrolytic-gasification chars all falling under the umbrella of Py-C. Table 8-5 shows that isothermal SSC produced at 500ºC had already undergone aromatisation under both the aromatic index and aromatic fraction, which corroborates with McBeath et al. (2011). At ≥600ºC, the thermal stability (R_{50}) of Py-G SSC suggested the material was a class B candidate for carbon sequestration.

Both the R_{50} and Q_3 indexes suggest the material undergoes a marked increase in stability between 800-900ºC (Table 8-6) which corresponds with increases and stabilisation of the chars C:N index at ≥900ºC (Table 8-5). A similar stabilisation in char-N yields occurred for Py-B SSC ≥850ºC. The stabilisation of N within SSC suggests this element formed stable structures such as graphitic-N. At 900ºC, the R_{50} index of SSC was approximately 0.59-0.60 (Table 8-6) which is similar to the highest R_{50} values presented in the literature for lignocellulosic materials (Harvey et al., 2012) (Gomez et al., 2016). Since Mcbeath et al. (2014) found that most lignocellulosic biochars produced between 500-600ºC had a MRT of 460-1400 years and the R_{50} index of SSC equals (600-800ºC) or is higher (≥900ºC) than those reported for many lignocellulosic biochars. It is assumed that SSC MRT is at least 460 years.

9.1.3 Carbon value

The EU and UK assign a monetary value to CO_2 emissions emitted by power producers, respectively the schemes are called the EU emissions trading scheme (ETS) and carbon price floor (CPF). The ETS originated in 2005, however the UK felt the price was too low and volatile and in 2013 implemented CPF, which from 2016 to 2021 has been set at £18 t CO_2e^{-1}. The CPF price applies when the ETS falls below the CPF, for example, between 2016-2020 the EU ETS price has varied from €4.45-31.47 t CO_2e^{-1}. The Department for Business, Energy, and Industrial Strategy (BEIS. 2018[c]) also publishes carbon values for modelling. Low, central, and high values are given for each year between 2018-2035, according to BEIS (2018[c]) the central value in 2021 was £13.85 tCO2e^{-1} which gradually increases to £42.66 t by 2030-2035. Although, Haw (2017) states that the typical market price the forestry commission generates from carbon sequestration by woodland creation is much lower, ranging between £3-9 tCO_2e^{-1}.

Based on the current UK CPF, the approximate monetary value of the carbon (CO_2e) in XS-B, XS-6 and their respective chars was estimated. In addition, based on the long-term retention of carbon in biosolid-amended soils, as presented in section 9.1.1, the monetary value of biosolid CO_2e in soil was estimated (Table 9-1). The results suggested that over several decades to a century biosolid amended soils retain between £5.3-9.1 CO_2e t digested sludge $^{-1}$ whilst SSC amended soils would retain £7.5-9.1 CO_2e t digested sludge^{-1} (appendix 3). These results suggest that the production of SSC retains more carbon within soil than digested sludge, despite the losses of carbon during its production. As discussed in section 9.1.1, recycled biosolids are expected to undergo rapid initial mineralisation rates, therefore the biosolid carbon value is expected to quickly equalise with SSC. Over the long-term, SSC is then likely to sequester more carbon than biosolids because it is not expected to breakdown.

Table 9-1: Estimated carbon value of digested sludge and SSC, and the long-term retention of this carbon value in soil (expressed as CO_2e per tonne digested sludge)

Material (x)	Material CO_2e value[1] £ t (digested)$^{-1}$	Long-term CO_2e value £ t (digested)$^{-1}$
XS-B	24.8	5.7-9.1[5]
XS-B char	9.1	No Change
XS-6	22.9	5.3-8.4[5]
XS-6-char[3]	7.5	No Change
Non-Iso XS-6 char[4]	8.6	No Change

[1]Calculated from materials percentage of total carbon (i.e. not adjusted for inorganic C)

[2]Py-B to 850°C at 10°C min^{-1} total dwell-time 90 minutes (see table 4-1)

[3]Isothermal Py-G at [850°C, 120s]

[4]Non-isothermal Py-G at [600°C, 600s] then [800°C, 60s]

[5]Correction based on long-term carbon sequestration of between 23-36.6% for biosolid amended soils (section 9.1.1)

9.2 Phosphorus

9.2.1 Background

Globally the P market exhibits low price-elasticity for both supply and demand. Therefore, insufficient rock phosphate supply causes large price increases, and the expansion of production is slow (Horn & Sartorius, 2009). In 2007, large increases in rock phosphate prices occurred and authors predicted imminent peak P, for example Wang et al. (2012) stated economically mineable resources will be depleted by the end of the 21st century based on reserve data published by the US geological survey (Schroder et al., 2010). In 2010, the USGS was the sole source of global phosphate reserve data, with estimates at the time of 16Bn tonnes however, Van Kauwenbergh (2010) questioned the reliability of these figures. In response to criticism the USGS twice revised global reserves for rock-phosphate, first to 60Bn tonnes then to 71Bn tonnes (Ridder et al., 2012) and estimates in 2019 now stand at 69Bn tonnes (USGS, 2020). However, significant non-conventional sources exist, including igneous deposits and marine deposits on continental shelves and seamounts. The USGS (2020) now specifically states that "there are no imminent shortages of rock phosphate" and estimates total world reserves (including non-conventional) at 300 Bn Tonnes. Based on global rock-phosphate consumption in 2019 (0.24 Bn tonnes) there are approximately 287 years of conventional and 1250 years of non-conventional rock phosphate resources available based on current reserves.

Therefore, the concerns about global P scarcity are likely to be overstated, however P security may be a strategic issue for some regions. For example, in the EU (and UK) approximately 88% of rock phosphate is imported and globally there are several regions including; Latin America, the Caribbean, South Asia, Central Europe, Western Europe and Oceania, that have large phosphate trade deficits (FAO, 2015). Increased demand up to 2018 is being driven by India (27%), Brazil (19%) and China (10%).

Given the high financial significance, high reliance on imports and the EUs strategic insecurity of rock phosphate, the material has been classified as a critical raw material (EC, 2017a) and Ridder et al. (2012) recommends that the EU should promote P recovery, reduce demand, and make best use of sewage sludge resources which could provide up to 23% of current P fertiliser demand. Critically however, a trade deficit does not equate to supply insecurity since: Finland (EU) and nearby countries (Morocco, Algeria, Egypt, Jordan, and Syria) and a diverse range of international trading partners (USA, Australia, South Africa, and Brazil) all hold significant reserves (≥ 1 Bn tonnes) which could be further exploited to diversify international supply chains. In 2019, China accounted for over 45% of global rock phosphate production.

Kleemann (2015) expressed concern over diminishing ore quality, which is increasingly contaminated with CaO, lanthanides, heavy metals, and radionuclides. However, Steiner et al. (2015) explains that the ranges of ore qualities have increased, which resulted in Morocco exporting RP-concentrates <29.7 P_2O_5 for the first time in 2013, however average ore-quality actually increased between 1983 and 2013. Steiner (2015) suggests technology-based solutions could be used to upscale poor-quality ores and also reduce P losses during processing.

To conclude, ample reserves of P exist. However, a wider range of ore grades are now being extracted and processed. Despite current supply security, P recovery from SSC may be an attractive proposition, especially if the EWC code for SSC represents a barrier to the direct application of SSC on agricultural land.

9.2.1.1 Phosphate fertilisers

Approximately half of global P inputs to soils are from organic wastes, mostly manure, the other half is from inorganic P_2O_5 fertilisers, which are manufactured from mined rock-phosphate. Fluorapatite [$Ca_5(PO_4)_3F$] and Francolite [$Ca_{10}(PO_4)_{6-x}(CO_3)_x(F,OH)_{2+X}$] are the main phosphate minerals in rock phosphate (RP), the former dominates in igneous deposits whilst the latter dominates in sedimentary deposits (Fertilisers Europe, 2000). Prior to application on soils, RP is processed to concentrate P, increase P availability, and remove impurities. Globally, the most common P fertilisers include super phosphate (SP), triple superphosphate (TSP), mono-ammonium phosphate (MAP) and diammonium phosphate (DAP), see figure 9-1. These fertilisers are used straight or blended with other salts to produce compound fertilisers (e.g. PK fertiliser).

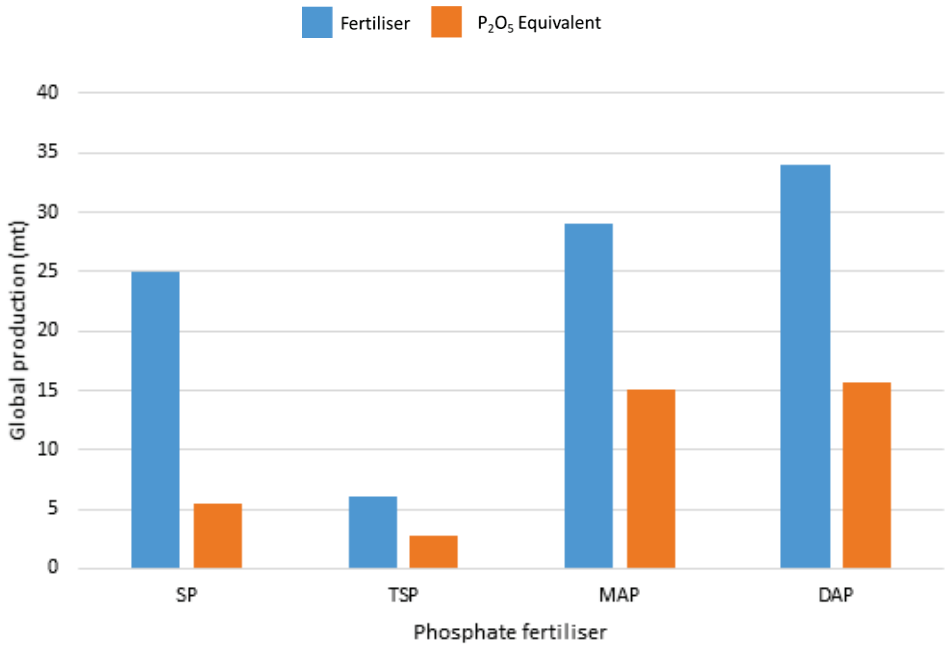


Figure 9-1: The global production of phopshate fertilisers in 2016. Based on estimated P_2O_5 content for SP, TSP, MAP and DAP of 22%, 46%, 52% and 46% respectively (Yara, 2018)

To produce fertilisers, RP minerals are first converted to phosphoric acid (H_3PO_4) by reacting them with mineral acids such as sulphuric (H_2SO_4), nitric (HNO_3) or hydrochloric (HCl). The reactions for $Ca_3(PO_4)_2$ with different mineral acids are summarised below.

$$Ca_3(PO4)_2 + 3H_2SO_4 \rightarrow 2H_3PO_4 + 3CaSO_4 \qquad [H_2SO_4]$$

$$Ca_3(PO_4)_2 + 6HNO_3 \rightarrow 2H_3PO_4 + 3Ca(NO_3)_2 \qquad [HNO_3]$$

$$Ca_3(PO_4)_2 + 6HCl \rightarrow 2H_3PO_4 + 3Ca(Cl)_2 \qquad [HCl]$$

The H_3PO_4 produced may be purified to remove contaminants, it is then neutralised with RP to produce SP and TSP or anhydrous ammonia to produced MAP and DAP. Manufacturing SP is simple and produces very little waste, it involves mixing RP with H_2SO_4 and leaving the mixture to cure. Initially $Ca_3(PO_4)_2$ is converted to H_3PO_4, however during curing, H_3PO_4 reacts with excess $Ca_3(PO_4)_2$ and forms monocalcium phosphate [$Ca(H_2PO_4)$] which is more water soluble. This reaction is shown below:

$$Ca_3(PO_4)_2 + 4H_3PO_4 = 3Ca(H_2PO_4)$$

When RP is leached with H_2SO_4, liberated calcium forms insoluble calcium sulphate (or gypsum). For each tonne of RP leached 1.5t of gypsum is produced however it is impure co-precipitating a range of impurities including: phosphate, fluoride, silica, radionuclides (uranium, thorium, radium, radon), lanthanides and cadmium. Due to its impurities, gypsum produced from RP is typically referred to as phosphogypsum (PG). Since phosphogypsum is not removed during SP manufacture, the final product contains a mixture of $Ca(H_2PO_4)$, phosphogypsum and possibly small amounts of unreacted RP. A phosphate concentration of 15-22% is typical. SP manufacture has a long history and is also produced from animal bones and guano.

Unlike SP, fertilisers like TSP, MAP and DAP do not incorporate phosphogypsum into the final product. Instead of letting the H_3PO_4-RP mixture cure, the H_3PO_4 is separated and filtered to remove phosphogypsum and silicates. Since the formation of phosphogypsum on the RP lowers H_3PO_4 yields, many processes pre-leach the RP multiple times with H_3PO_4 to minimise its formation. The pre-leached RP (containing $Ca(H_2PO_4)$) is then leached with H_2SO_4 to produce further H_3PO_4. Prior to fertiliser production, the H_3PO_4 may be further purified to reduce the concentration of heavy metals and fluoride.

The following processes are used to further purify H_3PO_4:

- Solvent extraction
- Ion exchange
- Precipitation
- Adsorption

During TSP production, purified H_3PO_4 is neutralised with RP to convert $Ca_3(PO_4)_2$ to $Ca(H_2PO_4)$. This produces an enriched fertiliser, with a phosphate content of approximately 46%. MAP/DAP production uses a similar process; however, H_3PO_4 is neutralised with anhydrous ammonia to produce monoammonium phosphate or diammonium phosphate. These contain, approximately 52% and 46% phosphate respectively.

- $H_3PO_4 + NH_3 \rightarrow NH_4H_2PO_4$ [MAP]
- $H_3PO_4 + 2NH_3 \rightarrow (NH_4)_2HPO_4$ [DAP]

The phosphogypsum produced from TSP, MAP and DAP manufacture with H_2SO_4 is a large waste stream and due to the complex range of contaminants is not widely reused as a building material or soil amendment. Currently, only 30% of phosphogypsum produced is reused worldwide, the rest is treated as waste on radiological grounds (IFA, 2020). Counterintuitively, phosphogypsum formation is favoured by many fertiliser manufacturers despite the waste it produces. Firstly, H_2SO_4 is cheaper than HCl and HNO_3 and more widely available.

Also, phosphogypsum co-precipitates a wide range of contaminants including radionuclides and heavy metals which dilutes and immobilises them. Without co-precipitation of these contaminants, process complexity, purification costs and disposal costs would be substantially increased. The main alternative to H_2SO_4 leaching, is the nitro-phosphate process. This involves leaching RP with nitric acid (HNO_3) to produce H_3PO_4 and calcium nitrate. Unlike calcium sulphate, the nitrate salt is not insoluble, however it can be removed from the H_3PO_4 solution by cooling it to 0^oC to promote crystallisation of calcium nitrate tetrahydrate:

- $H_3PO_4 + HNO_3 + Ca(NO_3)_2 + 4H_2O = H_3PO_4 + HNO_3 + Ca(NO_3)_2.4H2O$

These crystals are separated from the H_3PO_4 solution by filtration and either form a final product or are upgraded to ammonium nitrate (AN) in the following reaction:

- $Ca(NO_3)_2 + (NH_4)_2CO_3 \rightarrow CaCO_3 + 2NH_4NO_3$

Ammonium nitrate is a useful agricultural fertiliser, however since it's an oxidiser its frequently converted to calcium ammonium nitrate (CAN). Typically, H_3PO_4 produced from HNO_3 is used to produce MAP or DAP rather than TSP. The phosphate will then be blended with N and K to produce a compound NPK fertiliser. HCl can also be used to produce fertilisers from RP, however unlike H_2SO_4 and HNO_3 it is not currently conducted on a commercial scale.

HCl is very corrosive and may require plastic or plastic lined reactor vessels rather than steel, increasing costs. An advantage of HCl for RP leaching is uranium retention within the silicates reducing purification costs (Habashi et al., 1987).

Habashi et al. (1987) presented a treatment flowsheet for RP with HCl that minimised waste generation. After initial leaching of the RP with HCl the process involved three steps:

1. Phosphoric acid purification

The H_3PO_4 is chemically dosed to remove; fluoride as sodium fluorosilicate and radium as a co-precipitate with barium calcium sulphate. Uranium is removed by solvent extraction with 5% tributyl phosphate in hexane.

2. Phosphoric acid extraction

The H_3PO_4 is removed from the leachate by solvent extraction with 100% tributyl phosphate. The extractant is then scrubbed with water to remove residual contaminants and the H_3PO_4 is stripped from the solvent with ammonia to form ammonium phosphate.

3. Hydrochloric acid regeneration

After solvent extraction with 100% tri-butyl raffinate the solution contains dissolved lanthanides and calcium. The raffinate is dosed with ammonia to remove lanthanides and the solution is then mixed with sulphuric acid to regenerate HCl and precipitate calcium sulphate.

9.2.1.2 Phosphate in soils

Phosphorus (P) is an essential component of genetic and metabolic systems and a requirement for all life on earth. The main forms of phosphate in soil include:

- Ortho-phosphates (Ortho-P)
- Poly-phosphates (Poly-P)
- Immobilised phosphates (Ca/Mg salts in alkaline soils)/(Fe/Al salts in acidic soils)

Ortho-P is the primary form of P taken up by plants and accumulated into biomass. In soil, phosphate availability is often low which limits plant growth. For optimal plant growth, soil solution should contain approximately 0.003 to 0.3 mg ortho-P L^{-1} (McBeath, 2007), however maintaining this concentration whilst minimising leaching and immobilisation is challenging.

The pH of soil influences phosphate availability. In acidic soil, dihydrogen phosphate [$H_2PO_4^-$] is the dominant ion in soil solution, whilst hydrogen phosphate [HPO_4^{2-}] is dominant in alkaline soil solution. Phosphate fertilisers such as SP, TSP, MAP and DAP all contain $H_2PO_4^{-1}$ since this form is more water soluble. Some solubilised phosphate may leach out of soil causing eutrophication of ground or surface waters.

Although this can be minimised by: not over-applying P; timing P additions correctly (not during wet weather); and improving soil structure and organic matter content. Soil contains Al, Fe, Ca and Mg, these metals are capable of immobilising phosphate by fixing it as relatively insoluble metal salts. In highly acidic soils (pH 3-4.5) P fixation is dominated by iron, in moderately-acidic to neutral soils (pH 4.5-7) by aluminium and in alkaline soils (pH 7-9) by calcium. The range of maximum water-soluble P availability occurs between approximately pH 6.0-7.5.

The UK soil observatory publish maps showing the pH of topsoil in Great Britain. Upland regions in Scotland, Wales, northwest England, and southwest England have particularly acidic soils because these regions have large tracts of peatland which are rich in organic acids. In England and Wales, upland in the west is mostly permanent pasture and used for lamb, beef, and grass production. These pastoral soils are also rich in organic matter and typically have a moderately acidic to neutral pH. Lowland Britain has variable soil pH. In Southern and Eastern England, areas such as the South Downs, Lincolnshire and East Anglia have chalk bedrock and the soils in these regions have an alkaline-neutral pH. Whilst in the Southeast, soils tend to be moderately acidic. Most of lowland Britain is arable, producing cereals (e.g. wheat and barley), root crops (e.g. sugar beet and carrots), tubers (e.g. potatoes) and pulses (e.g. peas and beans) alongside horticultural products.

Since soil contains Ca, Mg, Fe and Al and may not be within the pH range of maximum phosphate availability, water soluble ortho-P is extremely prone to immobilisation. Historically, water soluble ortho-P fertilisers were added to the soil without a proper understanding of P immobilisation therefore some soils in the UK now contain relatively high levels of immobilised P. Most UK soils are acidic; therefore, the addition of lime is common to increase the solubility of these immobilised phosphates.

Not all ortho-P fertilisers contain dihydrogen phosphate, both dicalcium phosphate (DCP) ($CaHPO_4$) and struvite (NH_4MgPO_4) contain mono-hydrogen phosphate whose salts are generally much less water soluble. Plant roots have developed strategies to solubilise DCP, struvite and immobilised phosphate. Roots can exude weak organic acids such as citric acid (CA), these solubilise phosphate and chelate metals ions (e.g. Fe^{2+}) preventing immobilisation. However, since the root must be close to the P source, phosphate liberation is limited by the root surface area. Phosphate solubilising bacteria liberate inorganic phosphate using the same mechanisms.

In natural soils, where soluble ortho-phosphate is scarce, most plants form a symbiotic relationship with arbuscular mycorrhizal fungi (AMF). AMF attach to roots and grow hyphae (fine hair-like structures) which increase the volume of soil roots can access. AMF uptake ortho-P, that may have been solubilised by roots or bacteria, and transport it to the plant in exchange for sugars. Most agricultural crops perform better when colonised by AMF due to increased uptake of both phosphate and micronutrients (Nacoon et al., 2020). When agricultural soils

contain high concentrations of water-soluble phosphate it reduces AMF root colonisation, thus making the plant more dependent on artificial P application. AMF also produce glomalin-related soil proteins that have an important function in soil aggregation (Xie et al., 2015) and help regulate soil respiration (Zhang et al., 2016).Therefore, interfering in the natural symbiosis between AMF and roots may be detrimental to soil health. Unlike water-soluble ortho-P fertilisers, DCP and struvite are much less prone to leaching and immobilisation since phosphate is released more gradually. Consequently, they are considered to be sustainable fertiliser options.

Ortho-P consists of a single phosphate molecule; however, phosphate ions can form structural units by sharing oxygen atoms and like carbon can form linear or cyclic ring structures. When phosphate forms these chains, it is referred to as poly-phosphate (poly-P). Poly-phosphates exist as inorganic salts or organic esters with both forms playing an important role in biochemistry. Common poly-P esters include adenosine tri phosphate (ATP), phytic acid and nucleic acid. These organic forms of poly-P typically have short polymeric chain lengths, for example: ATP, the main energy carrier in living cells, is a tri-phosphate. In contrast, inorganic forms are more variable ranging from pyrophosphate (PP) $(P_2O_7)^{4-}$ with a chain length of 2 to Maddrell's salt $(NaPO_3)_n(NaPO_3(OH))_2$ where n can be as great as 2000.

Poly-P is not plant available, however: soil microbes, plant roots, and water can hydrolyse poly-P chains converting them into plant available ortho-P. Microbes and roots use enzymes to convert poly-P more quickly, for example PP hydrolysis is catalysed by pyrophosphatase. Chain length and shape influence the stability of poly-P, for example Torres-Dorante et al. (2005) found that PP was fully hydrolysed in water in just 15 days whilst 30% of cyclic trimetaphosphate was hydrolysed after 90 days. A range of other factors also influence poly-P hydrolysis including soil temperature and acidity (McBeath et al., 2007).

- $H_4P_2O_7 + H_2O \rightarrow 2H_3PO_4$

When exposed to metal-ions ortho-P typically forms immobile precipitates, however poly-P can act as a complexing agent. For example, urine contains small quantities of PP (2-3 mg P L^{-1}) which is sufficient to prevent hydroxyapatite formation in the body even when urine is supersaturated with Ca & P (Fleisch and Bisaz, 1962). Since Poly-P can complex metal cations (e.g. Ca, Al, Fe), in soil it has the ability to inhibit immobilisation and potentially solubilise bound-P however this effect is not permanent due to Poly-P hydrolysis.

Some manufacturers are blending phosphates with different properties, for example: DAP, DCP and PP to produce fertilisers with both instant and slow-release P characteristics (Wardman, 2020) however these are more expensive. Organic fertilisers, for example, manures are rich in Poly-P

esters. Short-chain polyphosphates (e.g. PP) are typically used in fertilisers and are produced by dehydrating ortho-H_3PO_4 which causes polymerisation-condensation reactions. The resulting polyphosphoric acid can then be neutralised to produce salts such as ammonium pyrophosphate alternatively Poly-P can be applied to soil as a liquid fertiliser.

To conclude, globally, there are a range of ores and manufacturing processes used to produce phosphate fertilisers. The products used have a range of properties, with different: solubilities, nutrient contents, purity, contaminants, price, and behaviour within soils. The next sub-section will discuss phosphate fertiliser use within the United Kingdom.

9.2.1.3 Phosphate fertiliser use in the United Kingdom

The UK has 17.5 million hectares of utilised agricultural area, of which: 72% is grassland, 26% is arable, mostly wheat and barley and 1% is used for horticultural crops such as vegetables. In 2019, the total gross output of UK agriculture was £27.3 Bn, the most valuable products include: milk (£4.4 Bn), cattle (£2.8Bn), poultry (£2.6Bn), wheat (£2.4Bn) and fresh vegetables (£1.5Bn) (DEFRA, 2021).

Total phosphate use in the UK has reduced markedly over the past 40 years, from 393-482 kt between 1973-1977 to 194-201 kt between 2013-2017 although over the last decade consumption has stabilised.

This is not isolated to phosphate; the application rates of nitrogen and potassium have also decreased substantially since the 1970s with both stabilising over the last decade. Historically, sulphur (S) addition was largely satisfied by atmospheric deposition. However, the abatement of industrial sulphur dioxide emissions means the use of S fertilisers have, unlike other fertilisers, increased. For example, in 1993 only 3-6% of cereal crops received S addition whilst in 2019 this had increased to between 59-72% (National statistics, 2020)

The mean overall application rate of phosphate fertilisers between 2015-2019 is 8 kg ha^{-1} for grassland and 28 kg ha^{-1} for crops. In 2019, 29% of grasslands and 48% of crops were fertilised with phosphates meaning the actual application rates were 21 and 54 kg ha^{-1} respectively. However, the application rates are crop dependent and vary from 135 kg ha^{-1} for potatoes to <1 kg ha^{-1} for certain mature grasslands. The consumption of phosphate is seasonal, the majority of P fertiliser is applied in the spring (14-31 kg ha^{-1}) and autumn (7-10 kg ha^{-1}) whilst consumption in the summer and winter is limited. The peak consumption of phosphate fertilisers occurs in April (National statistics, 2020)

The main inorganic phosphate fertiliser used in the UK is “PK” (246,000 t), which is a blend of phosphorus, potassium and a wide range of secondary nutrients including S, Mg and Ca. For example, Yara UK limited sell “super PK” which is a blend of SP, TSP, and K_2SO_4. PK is used during early development and helps stimulate germination and root development. Straight TSP (72,000 t) is the second most popular inorganic P fertiliser. The main organic fertilisers used are

cattle manure and cattle slurry, of which 59% and 89% were used on grassland respectively reflecting a trend to use organic fertilisers on the farms where they were produced. Non-farm manures such as biosolids are seldom used on grassland, with the majority being used for "winter-sown crop land" in August and September (National statistics, 2020).

9.3 Phosphorus recovery from Biosolids

Currently sludge is treated mostly by anaerobic digestion and the biosolids produced are applied to land, therefore biosolid-P is recycled. Raw or digested sludge cake can also be pyrolysed to reduce volumes and concentrate the phosphate. XS-char (>600ºC) contains approximately 5.3-5.7% P or 12.1-13.1% P_2O_5 (Table 8-1). There are a number of potential reuse options to valorise char phosphorus (Figure 9-4), including:

- Direct land application
- Char enhancement
- Phosphorus extraction & recovery

Each of these will be discussed in turn and the potential 'phosphate-value' that could be recovered will be assessed. The options for P recovery from digestate presented in Figure 9-4 are not comprehensive because P could be recovered from sludge dewatering liquors (Kleemann, 2015) and other novel processes (e.g. wet oxidation and nano-filtration) (Blocher et al., 2012).

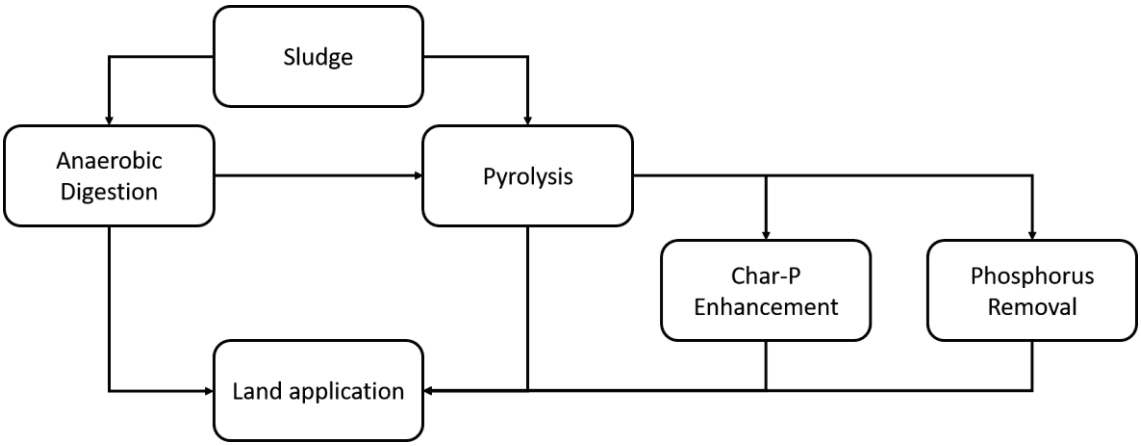


Figure 9-2: Reuse option for sludge phosphorus

9.3.1 Direct land application

Biosolids are currently applied to agricultural land. Recycling biosolids this way has a number of benefits and limitations which were discussed in section 1.2.1. A brief summary of the benefits and limitations is provided in table 9-2:

Table 9-2: Recycling of biosolids to land: Main benefits and limitations

Benefits	Limitations
Sustainable - Recycling sludge to land is beneficial to disposal or incineration and is higher up the waste hierarchy.	Operational expenses - Transport - Testing of metals and pathogen kill to ensure regulatory compliance. - Safe sludge matrix limits where/when the sludge can be amended to agriculture.
Soil conditioner - The organic matter content may improve soil structure, reduce erosion, and increase nutrient cycling. - Provides short-medium term carbon sequestration	Contaminants - Pathogens - Organic contaminants - Inorganic contaminants
Fertiliser - Useful source of macro-nutrients particularly P, S and Ca. - Useful range of micronutrients such as Zn and Mn.	Nutrients - Eutrophication - Odour - Unbalanced nutrient profile, e.g. N and K are undersupplied whilst P is oversupplied.

The application of SSC on land may also be a suitable disposal route, and unlike biosolids its application would not be restricted by pathogens, its available nitrogen content, or organic contaminants because these will be volatilised or transformed into non-available forms during pyrolysis. Charred materials are ubiquitous in soils and the environment because of both natural and anthropogenic incomplete combustion. When char, derived from natural biomass such as lignocellulosic material or manure, is applied to agriculture, it is called biochar. Biochar is used as a soil amendment with the intention to improve soil functions and to reduce emissions from biomass that would otherwise naturally degrade into greenhouse gases (section 2.3.3.4.4). Recently, the STRUBIAS proposals have attempted to formalise the regulatory environment for biochar (section 2.4.2). STRUBIAS suggest biochar has two intrinsic properties that contribute to its value as a soil amendment, these include the materials' carbon and nutrient content (Table 2-8).

The application of SSC to land would be limited by:

1. The rate of heavy metal addition.

The maximum application rates for char were calculated, based on the elemental concentrations outlined in table 8.1 and hypothetically assuming the heavy metal addition rates, outlined in table 2-5 in accordance with the Sludge (Use in Agriculture) Regulations (1989), also apply to char. The results are summarised in table 9-3, for Zn, Cu, Ni and Pb for SSC-900.

Table 9-3: Heavy metals: Char application rates

Element (x)	SSC-900 mg kg^{-1}	Maximum addition[1] kg (x) ha^{-1} yr^{-1}	Maximum application rate t SSC ha^{-1} yr^{-1}
Zinc	1752	15	8.6
Copper	897	7.5	8.4
Nickel	50	3	60.0
Lead	269	15	55.8

[1]Based on sludge (use in agriculture) regulation (1989)

[2]SSC-900 metal concentrations (Table 8-1)

Table 9-3 illustrates that annual application rates of less than 8.4t ha^{-1} would be permissible based on current sludge regulations and the limiting metals in SSC would be Zn and Cu rather than more toxic metals like Pb and Ni. Interestingly, for biosolids application it is the N content of the material rather than the heavy metals contents which typically limits its application rate. For example, the application rate for XS biosolids would be limited to 4.2-5.4 t XS ha^{-1} yr^{-1} based on N concentrations (Table 6-5) of between 4.6-6.0% Wt. and a field limit of 250 kg N ha^{-1} yr^{-1} as outlined in section 1.2.1.4. Therefore, based on a combination of N and heavy metals constraints alone, more SSC could be applied per hectare than the corresponding quantity of biosolids if heavy metal application rates were regulated in the same way as biosolids. Site specific factors such as the heavy metal concentration and soil P index would also need to be accounted for.

For biosolids application, heavy metal limits are based on the soil metal concentration and the addition rate to soils (kg ha^{-1} yr^{-1}). Therefore, the application rate can control the quantity of heavy metals applied to soil. In contrast, STRUBIAS regulates char application based on char heavy metal concentration. Both approaches have limitations since the chemical form, rather than elemental concentration, dictates the toxicity of an element in the environment. In addition, site-specific factors such as land use and soil type also influence the risk of exposure to receptors (e.g. soil organisms, plants, and humans). These factors would typically be accounted for when generating a soil guideline value during contaminated land exposure assessment. Limit values based on char concentration (e.g. STRUBIAS) may promote processing of the amendment prior to application, which utilises resources, without necessarily providing additional protection to receptors. For example, NEN 7371 experimentation (Table 8-12) suggests SSC metals are not

leachable even under extreme conditions not typical of soil. Although chemical leaching tests ignore the biological aspects of metal mobility and metal toxicity in soil.

2. The rate of nutrient addition

The mean application rates of N, P, K and S for different British agricultural products are published by National statistics (2020) and summarised in table 9-4. Although SSC-900 contains P, N, K and S, only P, K and sulphates are expected to be at least partially plant available.

Table 9-4: Crop nutrient requirments and SSC application rates to meet these requirements for selected crops based on total element concentration.[1]

Crop	Fertiliser application rates[2]			SSC-900 application rate	
kg ha^{-1} yr^{-1}	P_2O_5	K_2O	SO_3	P_2O_5	K_2O
Grassland	8	11	5	61.8	2657
Arable crops	26	34	35	201	8213
Winter wheat	24	31	42	186	7488
Spring wheat	17	19	26	131	4589
Potatoes (seed)	144	178	-	1113	42995
Potatoes (maincrop)	89	64		688	15459
Winter oilseed rape	29	27	63	224	6522
Spring oilseed rape	-	-	-	-	-
Brassica vegetables	17	83		131	20048
Other vegetables	36	65	16	278	15700

[1]Char requirement based on total concentration of P not the availability

[2]SSC-900: P_2O_5 and K_2O equal 129.4 and 4.14 (kg t^{-1}) respectively.

The application rate of SSC-900 required to meet crop phosphate demands ranged from approximately 62 kg SSC-900 ha^{-1} for grasslands to 1113 kg SSC-900 ha^{-1} for seed potatoes (Table 9-4). Although this ignores the plant availability of the applied phosphate. The application rates required to meet potassium demands ranged from approximately 2.7 t ha^{-1} for grassland to 43 t ha^{-1} for seed potatoes. Based on the heavy metal limits outlined in Table 2-5, and the maximum char application rates required to comply with these limits outlined in table 9-3 (8.4 t ha^{-1}) SSC-900 is unlikely to be an effective source of K for several crops without supplementation with another K source.

Table 9-3 and 9-4 demonstrate that excessive phosphate loading rather than heavy metal loading may be the limiting factor for char application in agriculture. Although this highly depends on the availability of the applied char-P. Given the small amount of char required to meet agricultural phosphate demands, it may be useful to blend char with another soil amendments, for example compost.

3. Soil sulphide addition and potential odour issues

The total concentration of sulphides within SSC-700 was approximately 3,665 mg kg^{-1} based on S fractionation observed during XPS analysis. The sulphide is expected to be present within a number of forms, including: CaS, MgS, Fe_2S, ZnS, Cu_2S, BaS and PbS. Alkali and AEM sulphides may hydrolyse in the presence of organic acids in soil water. Metal sulphide dissolution leads to sulphide (S^{2-}) formation, a highly basic ion which subsequently binds to protons forming bisulphide (HS^-). The pH dependent speciation of sulphide in aqueous solution is shown in figure 9-5 (Applied analytics, 2020):

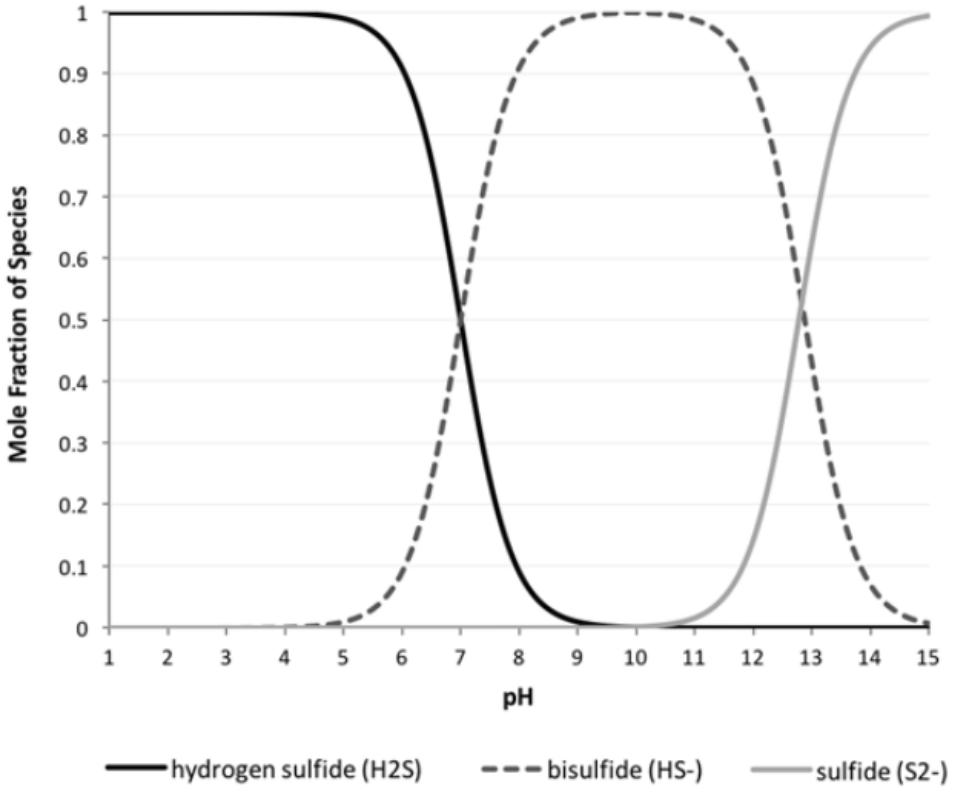


Figure 9-3: The pH dependent speciation of sulphide in aqueous solutions

At approximately pH 9, bisulphide ions begin to protonate forming volatile hydrogen sulphide. Hydrogen sulphide is toxic and odorous. Since most agricultural soils are acidic, SSC amendments could cause hydrogen sulphide related odour issues. The odour threshold for hydrogen sulphide in water is about 0.05 mg L^{-1} whilst a common threshold value for dissolved sulphide, S^{2-}, is 25 mg kg^{-1}, although this is based on dated ICRCL reference values (Environment Agency, 2010).

When SSC was mixed with 0.1M citric acid, a strong rotten-egg odour characteristic of H_2S was immediately noticeable. This shows that odour generation may be an issue when SSC is applied to agricultural land. However, the excess concentration of AEM carbonates or oxides within SSC will provide the material with buffering capacity, which will limit the speed of H_2S generation. Applying char as a granule rather than a powder would help suppress changes in the localised char environment, although this could inhibit nutrient release. Organic amendments such as compost or manure typically have large buffering capacities, due to surface chemistry, organic acids, and carbonate content (Costello and Sullivan, 2013). Blending char with organic amendments may be useful for controlling the rate of sulphide hydrolysis and volatilisation.

The immobilisation of potentially toxic metals as sulphides is an advantage of pyrolysis over incineration, since these compounds are both insoluble and relatively stable, particularly Cu, Pb and to a lesser extent Zn. The addition of char to contaminated soils or effluents containing heavy metals could be advantageous, since both CaS and FeS are used as precipitants within the metallurgic industry to remove heavy metals from solution (Lewis, 2010). Due to the high pH of char and its porous nature, bisulphide ions are likely to exist in small concentrations in solution around the char particle precipitating any solubilised heavy metals.

Iron phosphate has very limited plant availability. However, Likosava et al. (2013) found that sulphide addition to iron phosphate (S:Fe of 2.5) solubilised up to 92% of the bound phosphate at pH 4 and precipitated iron sulphide. Robinson et al. (2017) conducted XANES spectroscopy on digested sewage sludge from Reading STW to investigate phosphate speciation. Prior to pyrolysis, phosphate was bound as P sorbed to Fe oxides (39%), hydroxyapatite (36%), and adenosine triphosphate (ATP). However, in char, it was bound as hydroxyapatite (61%), iron phosphate hydrate (19%) and magnesium pyrophosphate (20%). If sulphide ions help to liberate iron phosphate, some char-P bound this way could solubilise over-time and become plant available whilst iron may precipitate as pyrite. However, this phosphate release will be limited by sulphide availability and requires further assessment.

4. Compliance with Strubias regulations

The Strubias regulations outline limits at component material category (CMC) and product function level (PFC) (Tables 2-8 and 2-9). Under these regulations, SSC would be classified as a nutrient-rich pyrolysis and gasification material (N-PGMs) whilst its product function would be PFC-1, a solid organo-mineral fertiliser. Based on this classification, all the isothermal chars tested exceeded the limit values for four metals: zinc, copper, lead, and nickel (Table 9-5).

Table 9-5: Direct application of char to land: Exceedance of Strubias regulations for PFC 1

Parameter	STRUBIAS: PFC 1 mg kg^{-1}	SSC (600-1000°C) mg kg^{-1}
Zinc	1500	1614-1752
Copper	600	829-897
Lead	120	250-269
Nickel	50	46-57

The Strubias phosphate availability limit for nutrient-rich pyrolysis and gasification materials (N-PGMs) are >25% water availability or >30% neutral ammonium citrate availability or >35% formic acid availability (see table 2-8). The formic acid solubility of sludge (XS-6), char (600-1000°C) and ash were analysed and are summarised in figure 9-6.

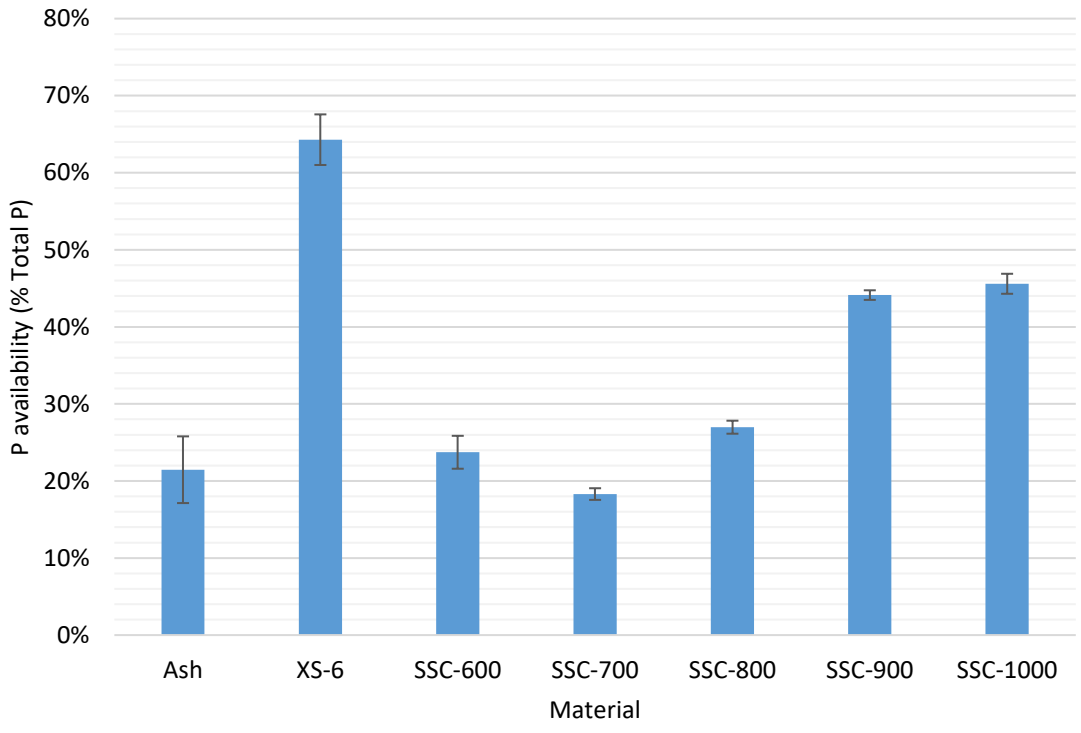


Figure 9-4: P availability for sludge, char, and ash in 2% formic acid

SSC produced below 900ºC does not conform with the formic acid P availability limit for N-PGM materials as outlined in the Strubias regulations. In contrast, char produced at 900ºC or above contained approximately 44-46% of its phosphate in a formic acid available form. Therefore, char produced <900ºC may be a less effective P fertiliser than char produced ≥ 900ºC. A one-way ANOVA and *post hoc* Tukey test ($\alpha = 0.05$) were conducted to test for significant differences between the experimental levels. The results are presented in table 9-6.

Table 9-6: Mean P availability in 2% formic acid with one-way ANOVA and Tukey testing

Material	P Availability	Tukey Group[1]		
XS-6	64.3%	A		
SSC-1000	45.6%		B	
SSC-900	44.1%		B	
SSC-800	27.0%			C
SSC-600	23.7%			C	D
Sludge-ash[2]	21.4%			C	D
SSC-700	18.3%				D

[1]Experimental levels with a different Tukey grouping are significantly different ($\alpha = 0.05$)
[2]Produced from sludge, heated to 550ºC in air for 24 hours.

The reasons for the statistically significant increase in P-availability at high temperatures ≥900ºC could be due to the elimination of heterocyclic-N from the surface of SSC. For example, Table 7-14 shows that char-N yields for Py-G and Py-B appear to stabilise >900ºC and >850ºC, respectively. This may indicate that pyridine/pyrrole structures have been eliminated and only graphitic-N remains. Pyridine contains lone-pairs, when mixed with an acid, these may undergo protonation to form a pyridinium structure (Wan et al., 2015), which may allow it to bind to anions such as phosphate.

Both SSC and sludge-ash have low P solubilities, this suggests that a common mechanism may lower the availability in both materials. One possibility is that the dominant forms of phosphate in SSC/ash are less soluble than in sludge. Calcium phosphate minerals have a wide range of solubility products, for example: HAP (pK_{sp} = 116.8), octacalcium phosphate (pK_{sp} = 96.6), tricalcium phosphate (pK_{sp} = 25.5-28.9) and dicalcium phosphate (pK_{sp} = 6.59-6.90) (Chow, 2009). A possible explanation for decreased availability is the conversion of organic phosphate (e.g. adenosine tri-phosphate) in sludge into relatively insoluble forms, such as HAP or tricalcium phosphate.

9.3.1.1 Direct application summary

In summary, section 9.3.1. suggests:

- SSC does not comply with the heavy metal concentration limits for Zn, Cu, Pb and Ni outlined in the Strubias regulation. When produced below 900ºC, SSC does not comply with Strubias phosphate availability limits.
- Up to 8.2-8.3 t SSC-900 ha^{-1} yr^{-1} could be applied to agricultural soils without exceeding the heavy metal application limits outlined for biosolids in the sludge (use in agriculture) regulation 1989. However based on its phosphate concentration, only 0.06-1.11 t SSC-900 ha^{-1} yr^{1} would be required to meet plant P requirements. Although, when adjusted for P availability (Figure 9-6) this would need to be increased to approximately 0.14-2.3 t SSC-900 ha^{-1} to meet plant P requirements. This suggests that the Strubias heavy metal concentration limits are excessively stringent for phosphate-rich SSC.
- Char contains metal sulphides that undergo decomposition to H_2S when mixed with dilute acids (e.g. 0.1M citric acid). In soil, the presence of organic acids could lead to odour issues.

9.3.2 Agricultural char enhancement

Char enhancement refers to a process that improves the suitability of char for use as an agricultural amendment. The main issues affecting the direct application of char on agricultural land include: the materials safety, in particular its heavy metal content; the materials efficacy, which includes the plant availability of its phosphate content; and the concentration of readily-hydrolysable sulphides (e.g. Alkali/AEM sulphides) because of concerns around hydrogen sulphide generation and odour issues.

Below pH 9, some of the metal sulphides within SSC may decompose into H_2S. Prior to land application, the pH of SSC could be adjusted to decrease the concentration of hydrolysable sulphides in the material and to increase the availability of its phosphate. However, this would generate H_2S which would require treatment.

Manufacturing super phosphate involves mixing rock phosphate with H_2SO_4 and allowing the mixture to cure. This dilutes metal compounds in RP because of the precipitation of gypsum ($CaSO_4$) in the material. It also converts insoluble forms of calcium phosphate into mono-calcium phosphate (MCP), a water-soluble form of phosphate. During SP manufacture, stoichiometric quantities of H_2SO_4 and CaO are mixed, meaning full conversion to MCP and gypsum are achieved. An alternative approach to SP manufacture is partial acidulation (Rajan and Watkinson, 1992), this involves sub-stoichiometric addition to produce partially acidulated rock phosphate. This contains MCP, dicalcium phosphate (DCP) and indigenous forms of calcium phosphate (e.g. HAP), it is more cost effective and produces a fertiliser as effective as SP in the short-term (Mclay et al., 2000) but with the advantages of slow-release P characteristics (Hagin & Harrison, 1993). Char could be processed the same way as RP to produce either super phosphate char or partially acidulated char. The potential advantages, include:

- Increased phosphate availability
- Decreased heavy metal concentration, due to dilution with calcium sulphate.
- Elimination of readily hydrolysable sulphides (mitigation of odour issues)
- The incorporation of sulphur in a plant available form (e.g. sulphates).



Figure 9-5: Sewage sludge char (<5mm) produced at 1000ºC and a dwell-time of 120 seconds. Photograph taken with a Canon G9X with flash please note that when observed with the human eye the char generally appears more black. The silver coloured lump (bottom left) is highly carbonised, low density, fixed carbon thought to originate from tar, these exited the reactor from time to time.



Figure 9-6: Sewage sludge char (<5mm) produced at 700ºC and a dwell-time of 120 seconds. . Photograph taken with a Canon G9X with flash please note that when observed with the human eye the char generally appears more black.

9.3.3 Phosphorus extraction

Prior to conducting experimental work, a MSc project was proposed whereby different extractants would be assessed for their ability to extract P and other elements from SSC. The project was conducted by Koulouri (2018) and the testing schedule is summarised in table 9-7.

Table 9-7: MSc Project: Preliminary screening experiment of SSC extractants (Koulouri, 2018)

Acid/Extractant	Molarity [M]	Liquid: Solid Ratio	Contact (t) Min	Temperature °C
SA NA	0.5 0.8 1.0 2.0	5:1 10:1	30 120	20 50
HA	0.5 1.0		120	20
Acetic Acid	1.0	10:1		
Oxalic Acid				
Citric Acid				
EDTA	0.05 0.1			
Water	-			

Koulouri (2018) found:

- The maximum P extraction efficiencies (EE) for HNO_3, H_2SO_4 and HCl were <84.9%, <49.4% and <74.1%, respectively. For HNO_3 and H_2SO_4, the optimal contact-time and temperature based on the experimentation were 120 minutes and 20°C, respectively.
- Water, acetic acid, oxalic acid and EDTA removed <7.3% P whilst citric acid removed <26% P, therefore these extractants were not effective at removing P nor did they selectively extract heavy metals or other elements.
- A liquid-solid ratio of 5:1 was recommended because it produced a more concentrated P leachate solution.
- The acid load (kg H^+ kg SSC^{-1}) was a better indicator of P extraction than the L:S ratio or acid concentration (M).

The potential use of HCl, HNO_3 and H_2SO_4 to extract elements from SSC was further investigated in a two-level-factorial experiment. The design was generated by Minitab 19 and tested five factors with centre points, except for particle size, which was tested at an upper and lower level only (Table 9-8).

Table 9-8: Factors for P extraction experimentation

Term	Factor	Abbreviation	Lower-level	Mid-point	Upper-level
A	Contact-time	(t)	2hrs	13hrs	24hrs
B	Temperature	T	20°C	30°C	40°C
C	Acid	[N]	0.2N	1.1N	2.0N
D	Stoichiometric ratio	S:R	1	1.25	1.5
E	Particle size	P-size	<0.5mm	n/a	<5mm

A centre-point was not used for particle size, since: (i) Thermogravimetric analysis suggested the inorganic content varied with particle size; (ii) only the upper bound could be controlled; (iii) a consistent particle size reduction was difficult to control.

At first, the char was TEMA milled however the fine powder was prone to compaction and there were issues with filtering, therefore the char was ground by hand and sieved to a maximum particle size of 500μm. The upper level for particle size was unground, however the pyrolysis feed was all sieved to a maximum size of 5.6mm and the char produced passed a 5mm sieve.

Koulouri (2018) found increasing the acid contact-time from 0.5 to 2hrs improved P extraction for all acids, therefore 2hrs was selected as the lower bound whilst 24hrs was selected to test the effect on longer retention times. Koulouri (2018) found 20°C was more effective than 50°C for P extraction, therefore 20°C was selected as the lower bound and 40°C the upper bound so that the whole temperature range between 20-50°C could be explored over both experiments.

Koulouri (2018) recommended future experiments tested acid-loading rather than the L:S ratio or concentration [M]. HAP is expected to be the dominant form of phosphate in char (Robinson et al., 2017) therefore acid loading was selected based on the stoichiometric ratio (S:R) between HAP and the acid used:

H_2SO_4: $Ca_{10}(PO_4)_6(OH)_2 + 10\ H_2SO_4 = 6\ H_3PO_4 + 10\ CaSO_4$

HCl: $Ca_{10}(PO_4)_6(OH)_2 + 20\ HCl = 6\ H_3PO_4 + 10\ CaCl_2$

HNO_3: $Ca_{10}(PO_4)_6(OH)_2 + 20\ HNO_3 = 6\ H_3PO_4 + 10\ Ca(NO_3)_2$

The lower-level for stoichiometric ratio were set at 1, however, since SSC is not HAP and contains an excess of basic metal oxides and sulphides, this was not expected to solubilise all the SSC-P. Therefore, the upper level for the stoichiometric ratio was set to 1.5.

Contrary to the recommendation by Koulouri (2018), the acid concentration was controlled; however, it was measured by normality [N] rather than molarity [M]. The selection of the acid concentration was more complex. During experimentation, the volume of leachate used was kept constant, however, the acid concentration and stoichiometric ratio were varied.

To maintain the correct stoichiometric ratio, at a given acid concentration and set acid volume, the char weight needed to be varied. To ensure adequate mixing, it was considered necessary to maintain an acid-char volume-ratio of over 1. Consequently, the lower boundary for the acid-char volume-ratio was set at 1.5 (e.g. 1.5L of leachate L^{-1} SSC), although this figure was arbitrary. Based on the bulk-density (see section 4.2.1) of the ground (<500μm) and unground char (0.629 and 0.676 kg m^{-3}, respectively) and maintaining an acid-char volume-ratio of at least 1.5, the maximum acid concentration was calculated at 2.0N for all acids. The lower level for acid concentration was set at 0.2N which gave an acid-char volume-ratio of 15-16, depending on the stoichiometric ratio. This elevated acid-char volume-ratio is not expected to be problematic for extraction and is within the normal range of L:S ratios seen in the literature (Kleemann, 2015).

HCl, H_2SO_4 and HNO_3 are all strong acids with pKa values of minus: 6.1, 3.0 and 1.4, respectively (Merck, 2020). In solution, H_3O^+ is completely dissociated from these acids conjugate bases, Cl^-, HSO_4^- and NO_3^-, respectively. H_2SO_4 is diprotic, therefore its conjugate base (HSO_4^+) undergoes further dissociation into SO_4^{2-}, however HSO_4^+ is weak acid and only undergoes partial dissociation. Although it is a relatively strong, weak acid, with a pKa of 1.9. The conjugate bases NO_3^-, HSO_4^- and SO_4^{2-} are all stronger oxidants than H_3O^+ therefore these acids are "oxidising acids". However, because of Le Chatelier's principles, dilute solutions of H_2SO_4 typically act as a "non-oxidising acid". HCl does not contain a stronger oxidant than H^+, since the conjugate base (Cl^-) is in a fully reduced form, consequently HCl is considered a "non-oxidising acid". All the aqua-regia soluble elements presented in Table 8-1 are expected to be soluble in HNO_3, however, several of these elements form compounds with limited solubility in H_2SO_4 and HCl. For example, $PbCl_2$ (pK_{sp} = 4.77) and $CaSO_4$ (pK_{sp} = 4.31) and are only sparingly soluble whilst $PbSO_4$ (pK_{sp} = 7.60) and AEM sulphates are insoluble. These properties will influence the extraction characteristics of these acids when mixed with SSC.

9.3.3.1 P Extraction: Hydrochloric Acid

Figure 9-9 shows that the extraction efficiency ranged widely depending on the extraction parameters used and the elements measured. The P extraction efficiency (P_{EE}) ranged more than other elements, from 35.8% to 96.4%, which shows the sensitivity of extraction to the experimental extraction parameters. High P extraction is consistent with experiments that have conducted leaching of SSC and ISSA with H_2SO_4 (Kleemann, 2015). The elements that achieved extraction of >80% include Ca (<95.4%), Mn (<89.8%), Mg (<85.3%), Sr (<83.9%) and Fe (<81.5%). The group 1 elements, Na and K, were less soluble than expected, with an extraction of <58.2% and <50.9%, respectively. Zn solubility was moderate <59.7%, however, both Cu and Pb were insoluble under the conditions tested.

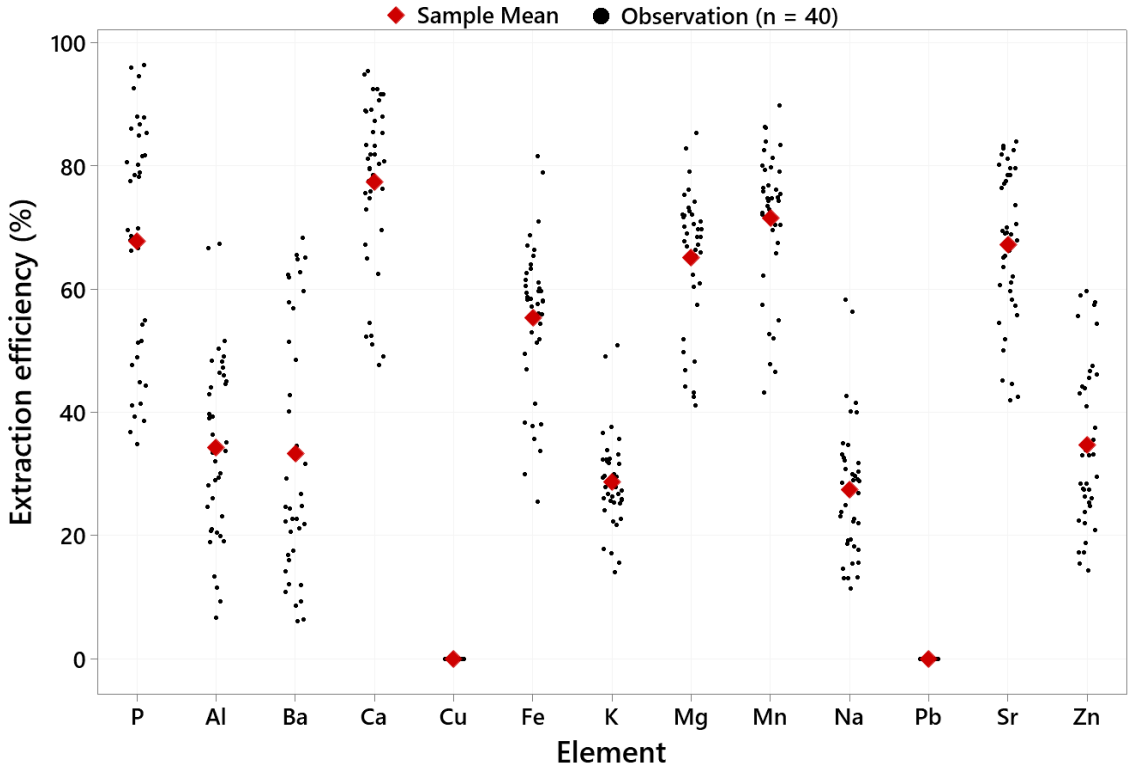


Figure 9-7: HCl leaching: Extraction efficiency distributions for P and other elements (n = 40)

Figure 9-10 summarises the effect of the experimental factors on P extraction. It shows that acid concentration had the strongest effect on P extraction, although most of the increase occurred between the lower level (0.2N) and the centre-point (1.1N). The stoichiometric-ratio (S:R) is interdependent on acid concentration, and its response is similar, although P extraction does not increase above the centre-point of the stoichiometric ratio. When S:R = 1, there is likely to be a deficiency in HCl because, alongside solubilising HAP and other P salts, the HCl will react with bases such as metal oxides and hydrolysable sulphides (e.g. CaS). Therefore, a strong response is seen when the stoichiometric ratio is increased from 1 to 1.25 because the stoichiometric requirements for HCl are met.

Excluding the centre-points, figure 9-10 also shows decreased particle size and reduced contact-time (t) increased P extraction, whilst temperature (T) had a limited influence on P extraction.

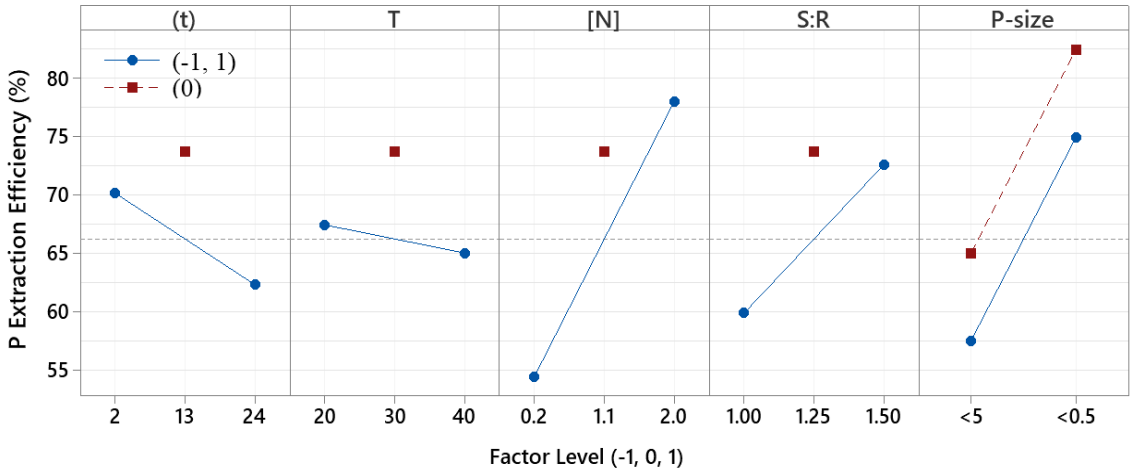


Figure 9-8: The effect of various factors tested at two levels (1 and -1) with centre point (0) on mean P extraction for hydrochloric acid (HCl) leached char

Factorial regression ($\alpha = 0.05$) was conducted to assess the influence of different factors on P extraction. The model was then optimised with stepwise (backwards elimination) regression to remove terms that did not contribute significantly ($\alpha = 0.003$) to the model fit. The model generated had an adjusted R^2 of 97% and statistical analysis presented in Appendix 4 suggests there was no evidence of model over-fit. The residuals of the model were normally distributed (*P = 0.847*). Excluding non-significant factors, the overall equation for this model is shown below:

$$HCl\ P_{EE} = 159.0 - (0.8326A) - (7.23C) - (82.31D) + (17.77E) + (0.4328AC) - (0.4301AE) - (0.3066BC) + (2.890BD) + (19.11CD) - (3.146CE)$$

Where: Variables A-D are uncoded and Variable E is coded as "-1" for a particle-size of <5mm and "+1" for a particle-size of <0.5mm. The code for the variables is defined in Table 9-8.

The relative magnitude and statistical significance of each factor's affect is summarised in figure 9-11. Figure 9-11 shows the first-order factors influenced P extraction significantly, except temperature. The acid concentration, particle size and stoichiometric ratio all had a strong effect on P extraction, which is illustrated in Figure 9-11. Six two-way interactions were identified as significant, interestingly BD (T and S:R) was the strongest two-way interaction, despite temperature alone not being a significant factor. At 20°C, P extraction was independent of the stoichiometric ratio, however, at 40°C, P extraction decreased when this ratio was 1 and increased when the ratio was 1.5. A possible explanation is that increased temperature influences the system's reaction kinetics, which may encourage re-precipitation of solubilised phosphate ions.

For example, when the stoichiometric ratio equals 1, relatively insoluble forms of phosphate may solubilise however, as the system reaches equilibrium, liberation ions may undergo precipitation due to lack of acidity. Temperature changes may influence the kinetics of these reactions. Competing reactions may also consume acidity, for example, the protonation of sulphides or heterocyclic-N groups on the surface of char particles. Temperature may influence the kinetics of these reactions, which could decrease the availability of acidity for P mobilisation when stoichiometric ratio equals 1. When the ratio equals 1.25 or 1.50 the surplus of acidity may retard re-precipitation and limit competition for hydronium ions.

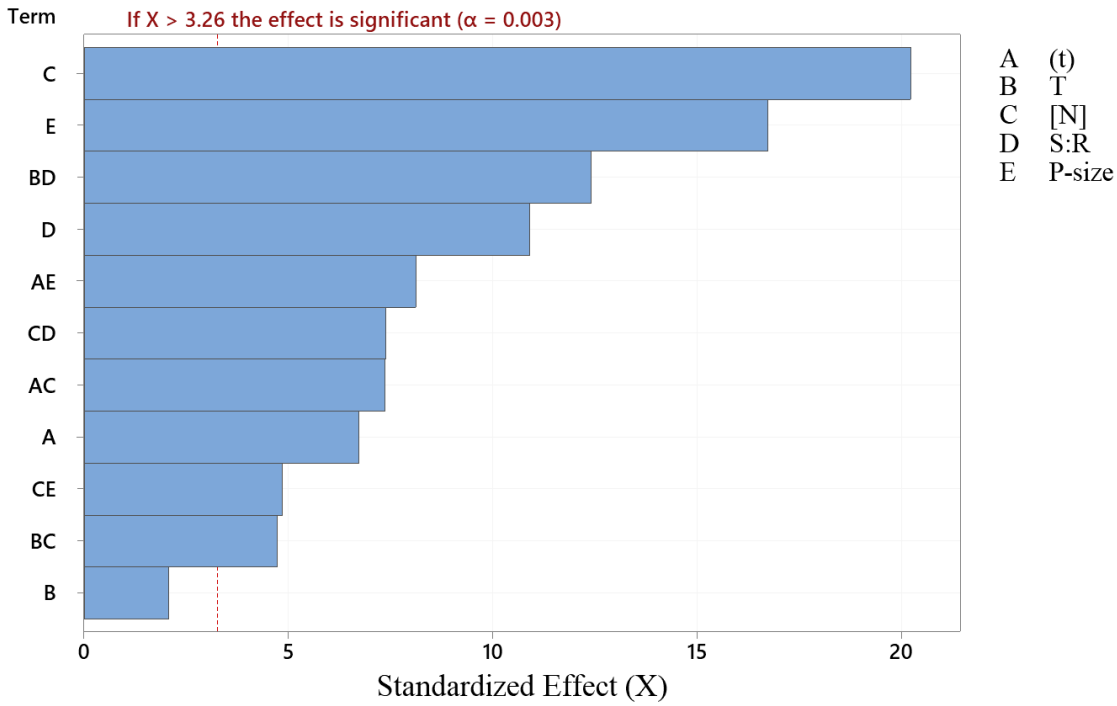


Figure 9-9: Phosphate: The relative effect of extraction parameters

There are five other significant two-way interactions (figure 9-12), including:

AE - For SSC (<5mm), increased contact (t) had a limited influence on P extraction but for SSC (<0.5mm) it decreased P extraction significantly.

CD - P extraction increased with acid-concentration (N), however a disproportional increase occurred when both the stoichiometric ratio and acid concentration were increased.

AC – Increased contact (t) decreased P extraction for 0.2N HCl but extraction with 2N HCl were not influenced by increased contact (t).

CE – Increased acid concentration increased P extraction, however, a disproportionate increase occurred for coarse SSC (<5mm) compared to fine SSC (<0.5mm)

BC – Increased temperature decreased P extraction for 2.0N HCl but increased it for 0.2N solution.

The effect of many of these two-way observations have on P extraction appears to be logical and, because of the experimental design and sample size (n = 40), are considered to be robust from a statistical viewpoint.

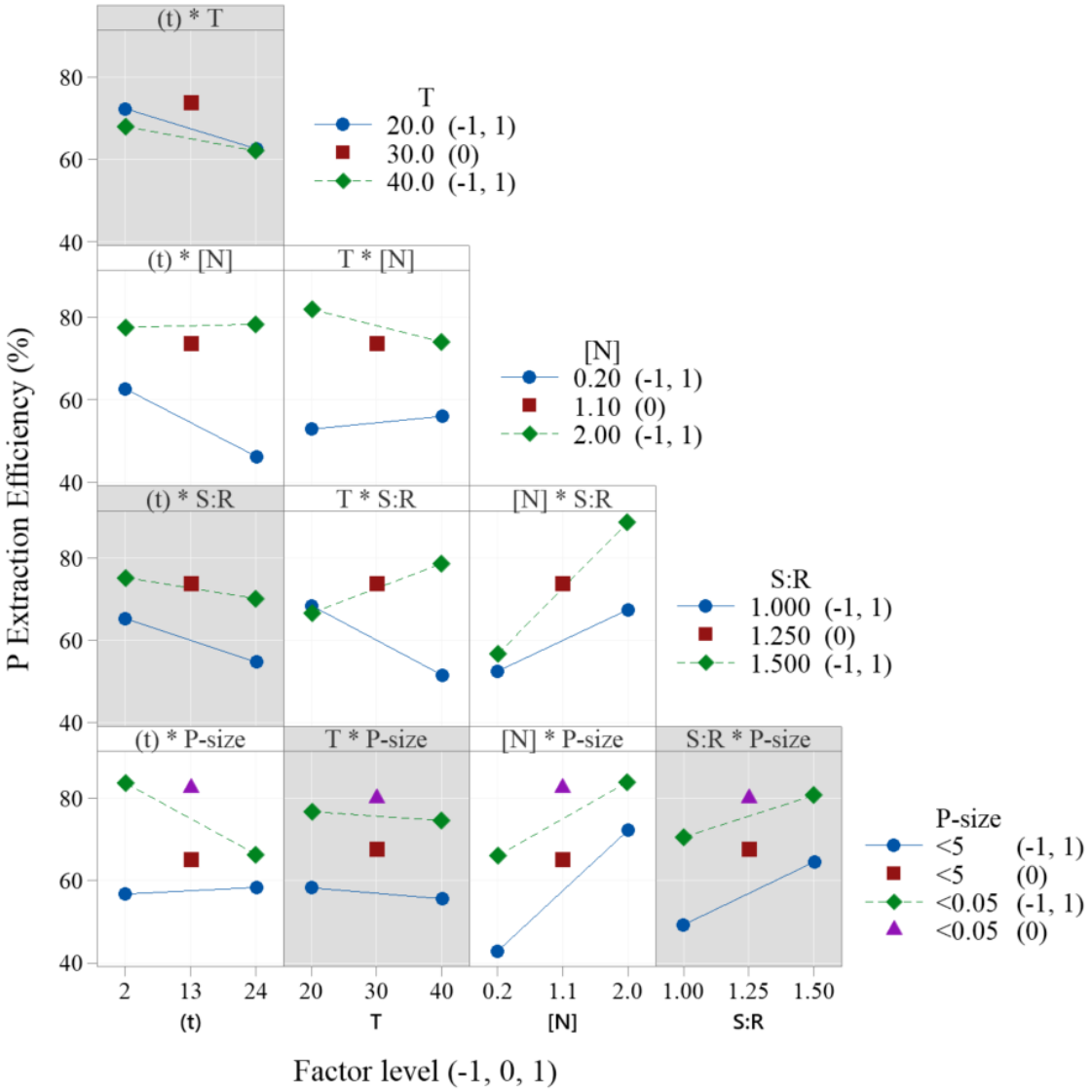


Figure 9-10: P extraction with HCl: Two-way interaction plot for extraction factors. The y-axis shows P_{EE} and the x-axis shows each factors values at levels -1, 0 and 1. The greyed-out plots are non-significant two-interactions that were excluded from the model.

Ignoring the centre-points, figure 9-10 suggested the optimal level for each of the factors were:

Contact (t): 2 hours, Temperature: 20ºC, acid concentration: 2N, stoichiometric ration: 1.5 and particle size: <0.5mm

Figure 9-10 does not include two-way interactions and represents the average of all runs at a given factorial level. This is prone to skew, average extraction for a factorial level may be low but there may be a large standard deviation in the response. The HCl model for P was used to predict the combination of factorial levels that maximised P extraction, and to show which combination of factors should be used when one factor is constrained to its lowest performing level (Table 9-9).

Table 9-9: The optimal combination of experimental factors for P_{EE} according to model 2 during constraint and non-constraint of factorial levels

Constraint	(t) Hours	T ºC	[N] N	S:R Ratio	P-size (mm)	Predicted P_{EE} %	Confidence Interval % (α = 0.05)
None	2	40	2	1.5	<0.5	102.2[1]	98.1, 110.1[1]
T = 20	2	20	2	1.5	<0.5	95.7	87.7-103.6[1]
(t) = 24	24	40	2	1.5	<0.5	93.5	85.6-101.4[1]
P-size = 5	24	40	2	1.5	<5	91.2	87.0, 95.3
[N] = 0.2	2	40	0.2	1.5	<0.05	89.9	81.9-97.8
S:R = 1	t	20	2	1	<0.05	88.8	80.9-96.7

[1]P extraction efficiency (P_{EE}) above 100% is not possible however the model has not been optimised

When unconstrained, the model predicted maximum P extraction of 102.2%, this is not possible and shows the model requires a larger data-set for optimisation. The optimal condition in Table 9-9 were the same as those stated in Figure 9-10. Except temperature, which Table 9-9 suggests 40ºC is optimal. In Table 9-9, when one factor was constrained (e.g. particle size = 5mm), the other factors did not change from the unconstrained optimum except for S:R = 1, which suggested T = 20ºC extracted more P. Including the confidence intervals (α = 0.05), the lowest P extraction in table 9-9 was still 80.9%, which is relatively high. This suggests extraction is relatively resilient to at least one sub-optimal extraction factor.

9.3.3.2 HCl extraction: Potentially toxic metals (PTE)

Figure 9-9 shows that neither Cu nor Pb were solubilised when SSC was extracted with HCl, therefore, only Zn was investigated. Factorial regression with backward elimination (α = 0.003) was used to assess the relative effect of extraction factors on zinc extraction (Figure 9-13). All the first-order factors had a significant effect on Zn extraction, except acid concentration. The particle size of SSC had the largest effect on Zn extraction, followed by the stoichiometric ratio and the two-way interaction between contact (t) and particle size.

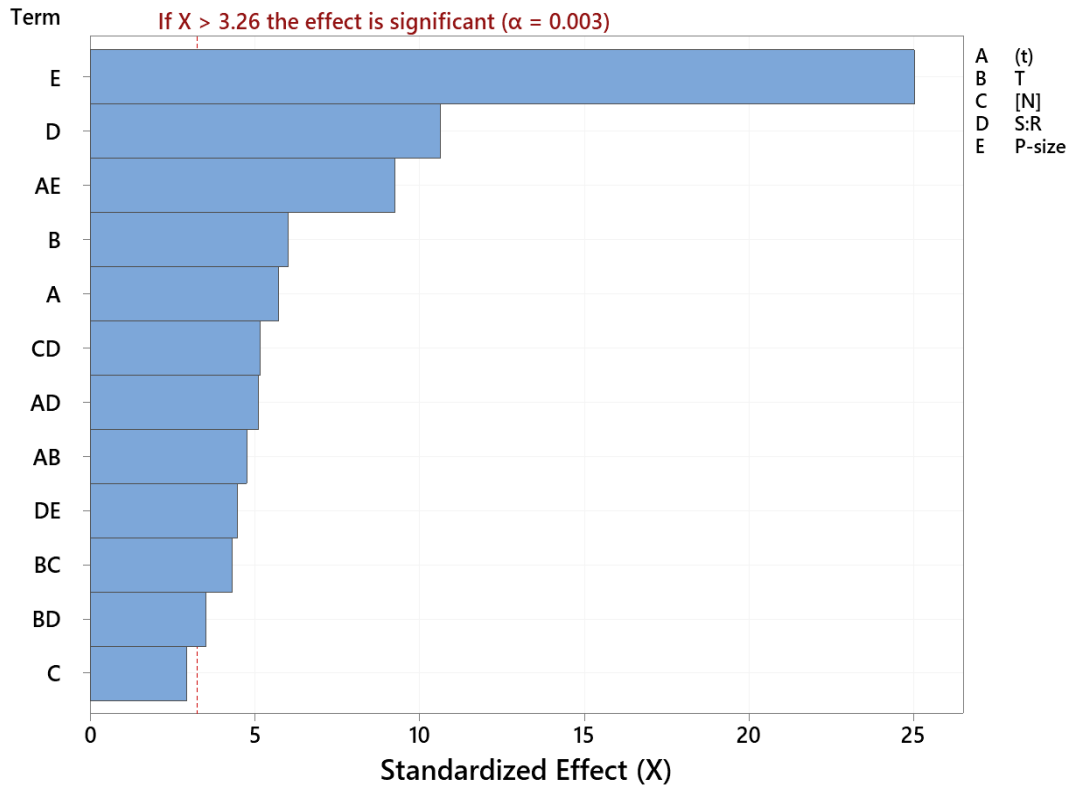


Figure 9-11: Zinc extraction: Pareto chart of standardised effects generated in Minitab (2021) using factorial regression with backwards elimination (α = 0.003). Factors with a standardised effect of >3.26 are statistically significant at a 0.3% significant level.

Response optimisation was used to identify which combination of factors maximised P extraction and minimised Zn extraction. The top solution for this optimisation when P extraction is >80%, 90% and 95% are summarised in Table 9-10. This shows that Zn extraction can be minimised whilst maintaining relatively high P extraction. For example, when the optimisation was constrained to P extraction (>95%), Zn extraction was also high, at 59.4%, respectively. When the constraint for P extraction was reduced to >90% or >80%, the Zn extraction decreased disproportionally to 39.4% and 30.5%, respectively. In practical terms, minimising heavy metal co-extraction could lead to the recovery of a higher purity P product being recovered from the leachate.

Table 9-10: Response optimisation for P and Zn

Condition	(t) hours	T °C	[N] N	S:R Ratio	P-size mm	P_{EE} %	Zn_{EE} %
P_{EE} > 80%	24	20	2	1.5	<5	84.61 (80.5, 88.7)[1]	30.5 (27.2, 33.7)[1]
P_{EE} > 90%	24	40	2	1.5	<5	91.2 (87.0, 95.3)[1]	39.4 (36.1, 42.7)[1]
P_{EE} > 95%	2	20	2	1.5	<5	95.7 (91.6, 99.8)[1]	59.4 (56.1, 62.7)[1]

[1]Confidence intervals (α = 0.05)

9.3.3.3 P Extraction: Sulphuric acid

Figure 9-14 shows that the extraction efficiency ranged widely depending on the extraction parameters used and the elements measured. P extraction ranged more than other elements, from 16.9% to 95.5%, which shows the sensitivity of P to the extraction parameters. The elements that achieved an extraction efficiency of >80% include K (<91.8%), Mn (<89.5%), Fe (<88.1%) and Mg (<86.7%). As expected, Ca was poorly extracted at 13.1% whilst Ba and Sr were insoluble. Zn solubility was moderately high (<75.5% extraction), however, both Cu and Pb were insoluble under the conditions tested.

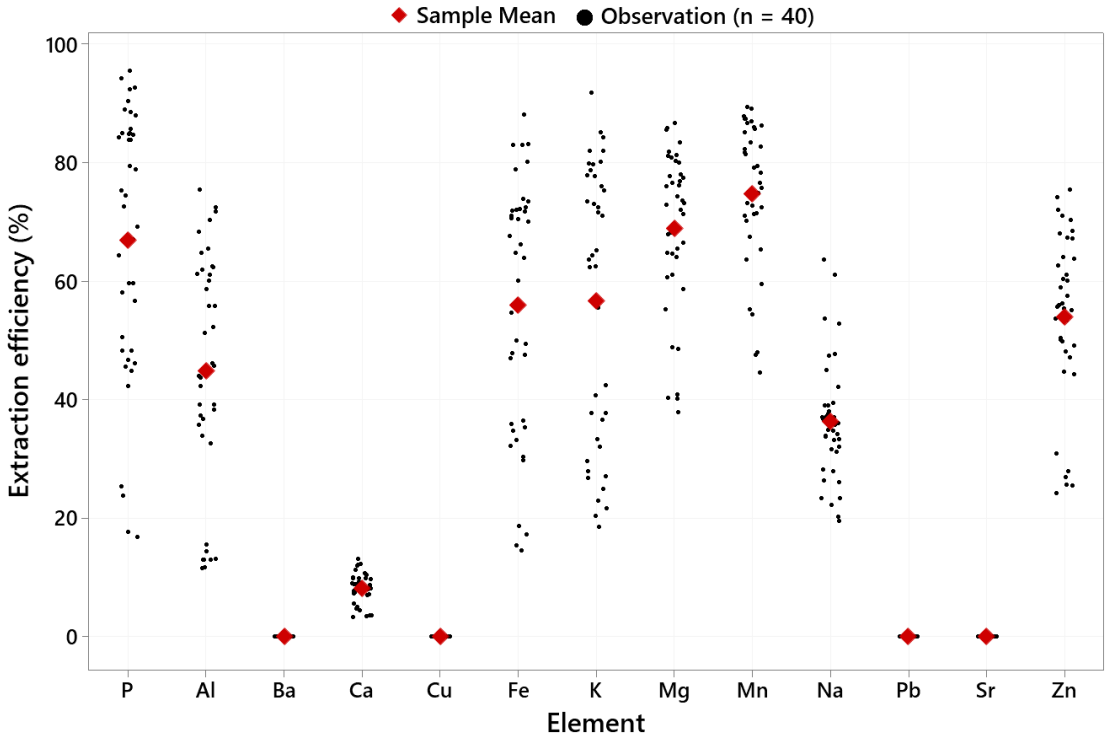


Figure 9-12: H_2SO_4 leaching: Extraction efficiency distributions for P and other elements (n = 40)

Figure 9-15 shows the effect of the experimental factors on P extraction. The upper levels all led to increased P extraction, which differs from the results obtained for HCl. The acid concentration

had the strongest influence on P extraction, which increased from 53.9% at 0.2N to 81% at 2N. For particle size, a mid-point was not measured. Therefore, data series (0) and (1, -1) show the effect of particle size on P when the other experimental factors were tested at their midpoints (0) and upper/lower levels (-1, 1). In both cases, decreased particle size increased P extraction, probably because of the greater accessibility of the acid to the P-salts inside the SSC particles. Unlike HCl, increased contact (t) and temperature led to increased P extraction. A probable explanation is that the formation of insoluble group 2 sulphates by H_2SO_4 blocked the pores in the SSC, decreasing access to phosphate salts inhibiting their extraction.

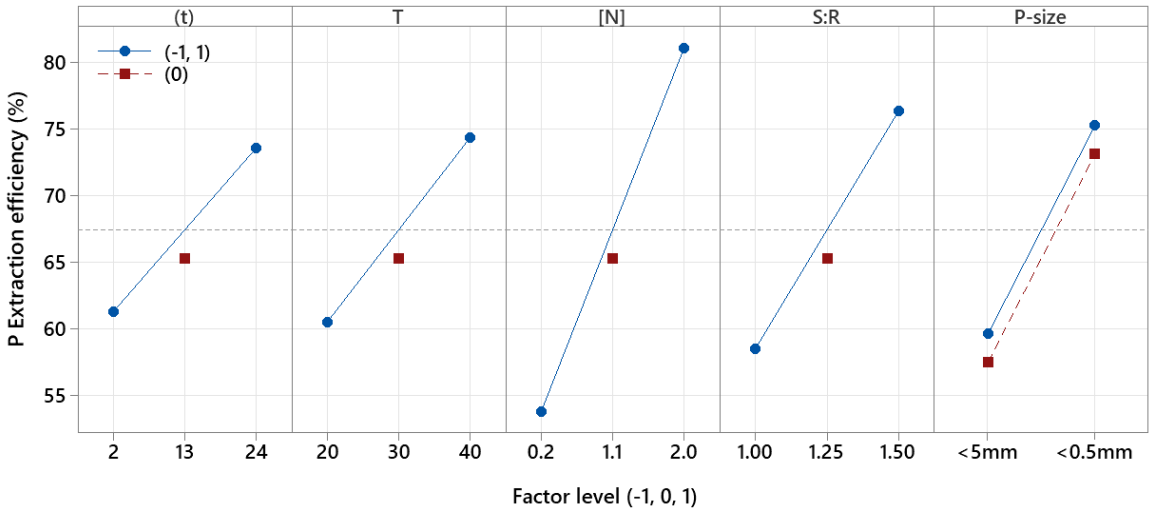


Figure 9-13: The effect of various factors tested at two levels (1 and -1) with centre point (0) on mean phosphate extraction for sulphuric acid leached char

With sufficient contact (t) the H_2SO_4 may dissolve these less accessible P salts, likewise with increased temperature the kinetics of P dissolution may be enhanced. When RP is leached industrially, it is often pre-leached with re-circulated H_3PO_4 to partially remove P salts without the formation of sulphate salts. It is then fully leached with H_2SO_4. The requirement to increase the contact (t) from 2 to 24 hours would have a large impact on the throughput of a plant extracting P from SSC. Therefore, to minimise contact (t), increased temperature alongside pre-washing with H_3PO_4 is recommended.

For HCl, a suggestion was made that increased contact (t) had a negative influence on P extraction because of H_2S formation, which would consume acidity. Decreased acidity could lead to the precipitation of insoluble phosphate salts. Although sulphide protonation will occur for both acids, H_2SO_4 leachate contains far fewer cations. Therefore, in accordance with Le Chatelier's principle, P may be less prone to re-precipitation.

Factorial regression ($\alpha = 0.05$) was conducted to assess the influence of different factors on P extraction (Figure 9-16). The model was optimised with stepwise (backwards elimination) regression to remove terms that did not contribute significantly ($\alpha = 0.05$) to the model fit. The

model generated had an adjusted R^2 of 89.8%, and statistical analysis presented in Appendix 4 suggests there was no evidence of model over-fit. The residuals of the model were normally distributed (*P = 0.990*). Excluding non-significant factors, the overall equation for this model is shown below:

H_2SO_4: P_{EE} = 143.8 – (1.252A) – (4.448B) – (46.47C) + (105.5D) + (28.04E) – (0.633AC) + (0.261AE) - (0.771BC) - (2.327BD) - (18.89DE)

Where: Variables A-D are uncoded and Variable E is coded as "-1" for a particle-size of <5mm and "+1" for a particle-size of <0.5mm. The code for the variables is defined in Table 9-8.

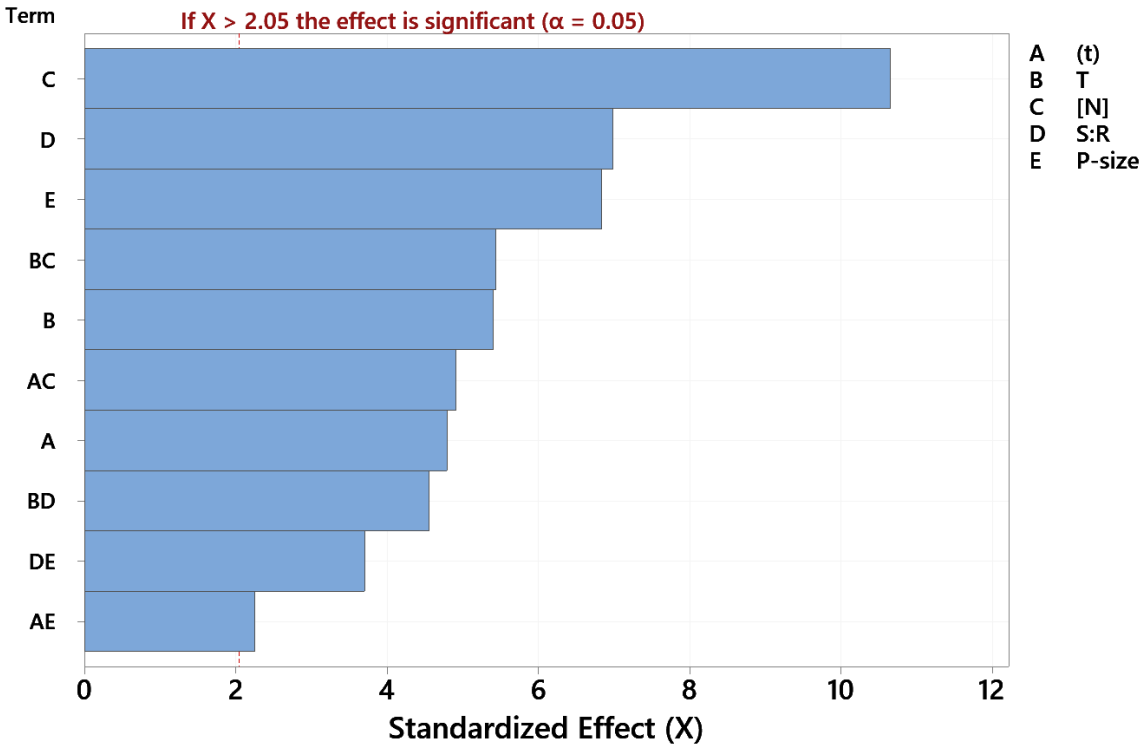


Figure 9-14: Phosphate extraction: The relative effect of extraction parameters

The relative magnitude and statistical significance of these factors are summarised in figure 9-16. All the first-order factors had a significant effect on P extraction, with acid concentration having the strongest effect. Five two-way interactions had a significant effect on P extraction, including BC, AC, BD, DE, and AE. Their influence appears to be logical and, because of the experimental design and sample size (n = 40), are reasonably robust from a statistical viewpoint. All significant two-way interaction, except AE, helped improve P extraction for the lower factorial level (Figure 9-17). For example, the second row of figure 9-17 shows two significant two-way interactions: AC and BC.

For both interactions, when 2N H_2SO_4 was used neither the contact (t) nor temperature effected P extraction. However, with 0.2N H_2SO_4, P extraction is markedly improved with increased

temperature or contact (t). These factors are related to reaction kinetics, since additional contact (t) allows more reactions to occur whilst higher temperature may increase reaction rates. By increasing the reaction rate of P dissolution, the throughput of the P extraction process may be higher, which may be important for its economic viability.

The other significant two-way factors included: BD and DE, these also increase P extraction for the lower factorial level, possibly for the same reason (e.g. the factor at its lower factorial level decreases P extraction which is partially offset when the secondary factor is increased to its upper level). AE was different to the other two-way interactions: an increase in contact (t) increased P extraction for both particle sizes used, however this effect disproportionately benefited ground SSC (<0.5mm).

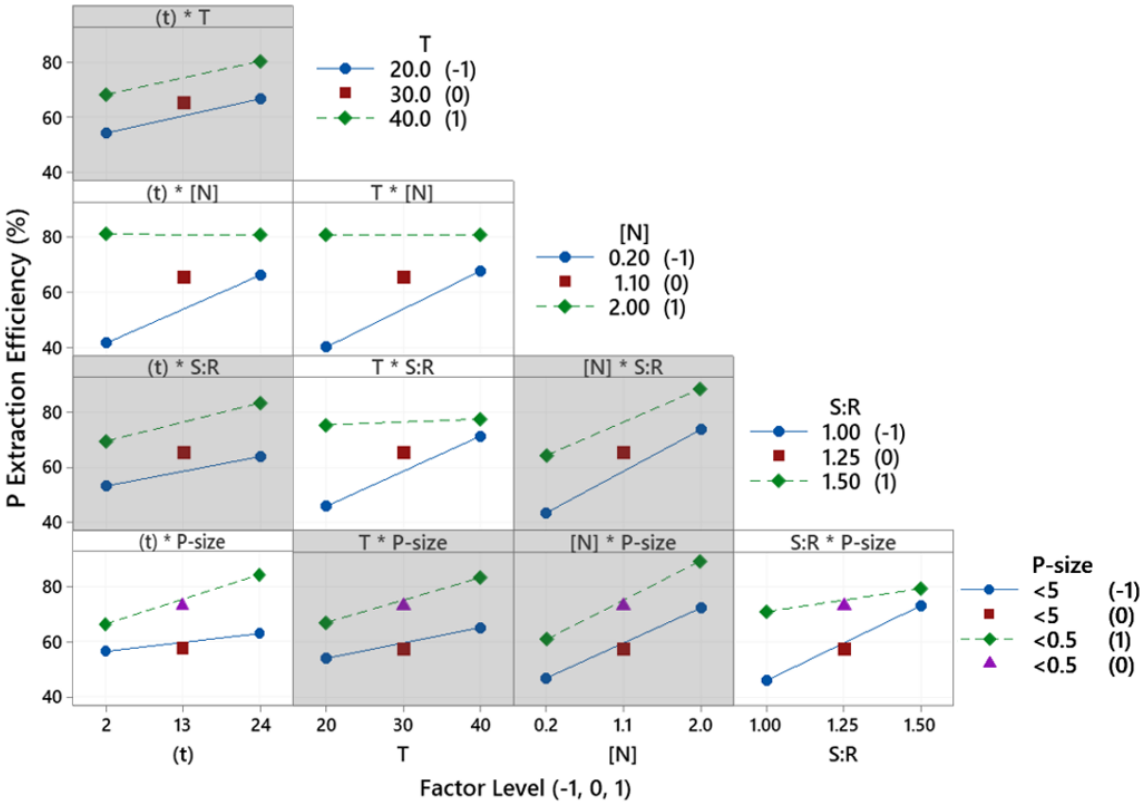


Figure 9-15: P extraction with H_2SO_4: Two-way interaction plot for extraction factors. The y-axis shows P_{EE} and the x-axis shows each factors values at levels -1, 0 and 1. The greyed-out plots are non-significant two-interactions that were excluded from the HCl model

Based on figure 9-15, mean P extraction was maximised when all experimental runs were conducted at their upper level:
(t): 24 hours, T: 40°C, [N]: 2N, S:R: 1.5 and particle size: <0.5mm

However, Figure 9-15 represents the means at each level across all experimental runs and does not account for two-way interaction which may influence P_{EE}. The H_2SO_4 model was used to predict the optimal combination of factorial levels that maximised P extraction. In addition, the optimal combination was also predicted when one factor was constrained to its lowest performing level. The results are summarised in Table 9-11.

Contrary to figure 9-15, the optimal temperature for P extraction was 20°C not 40°C however, the other factorial levels were the same. Including the confidence intervals ($\alpha = 0.05$), the lowest extraction of P in table 9-11 was 83.5%, which is relatively high. This suggests extraction is resilient to at least one sub-optimal factor. Table 9-11 also suggests that the stoichiometric ratio is the most important factor for maintaining optimal P extraction, because when constrained to 1 the extraction decreased the most.

Table 9-11: The optimal combination of experimental factors for P_{EE} according to the H_2SO_4 model when factorial levels are unconstrained or constrained to the lowest performing levels for each factor

Constraint	(t) Hours	T °C	[N] N	S:R Ratio	P-size (mm)	Predicted P_{EE} %	Confidence Interval[1] % ($\alpha = 0.05$)
None	24	20	2	1.5	<0.5	101.2[1]	92.7, 109.7
T = 20	24	40	2	1.0	<0.5	92.7	84.2-101.2
(t) = 24	2	20	2	1.5	<0.5	95.8	87.3-104.3
P-size = 5	2	20	2	1.5	<5	95.3	86.8, 103.8
[N] = 0.2	24	40	0.2	1.0	<0.05	95.5	83.5-100.5
S:R = 1	24	40	2	1	<0.05	92.7	84.2-101.2

[1]P extraction above 100% is not possible however the H_2SO_4 requires optimisation.

9.3.3.4 H_2SO_4 extraction: Potentially toxic metals (PTE)

Factorial regression with backward elimination (α = 0.003) was used to investigate which factors were important for determining Zn extraction, the results are summarised in figure 9-18. All first-order factors had a significant effect, however, contact (t), particle size and the two-interaction between these factors had a disproportionately large influence on Zn extraction.

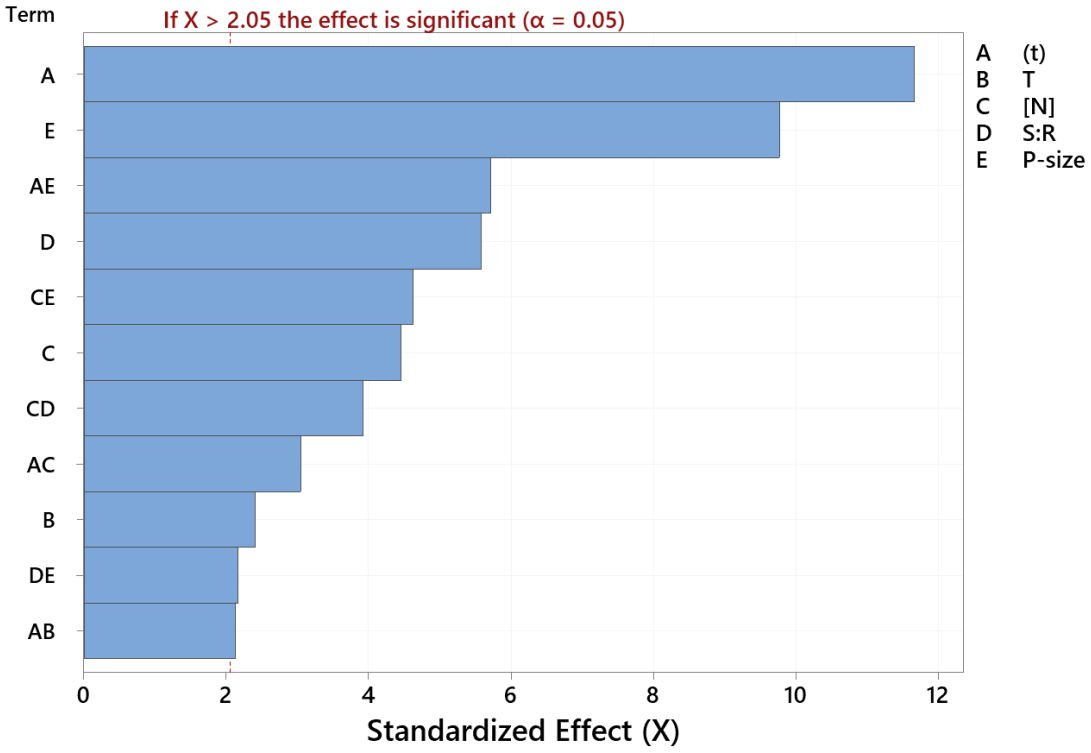


Figure 9-16: Zinc extraction: Pareto chart of standardised effects generated in Minitab (2021) using factorial regression with backwards elimination (α = 0.05). Factors with a standardised effect of >2.05 are statistically significant at a 5% significance level.

Response optimisation was used to identify which combination of factors maximised P extraction but minimised Zn extraction. For each run, an upper bound for Zn extraction was set and the result with the highest P extraction was selected. The results are summarised in Table 9-12.

Table 9-12: Response optimisation for P and Zn

Condition	(t) hours	T °C	[N] N	S:R Ratio	P-size mm	P_{EE} %	Zn_{EE} %
Zn < 30%	2	20	2.0	1.0	<5	56.4 (33.6, 50.6)[1]	29.8 (18.8, 29.6)[1]
Zn < 45%	2	40	2.0	1.0	<5	68.0 (59.5, 76.5)[1]	36.8 (31.3, 42.1)[1]
Zn < 50%	2	20	2.0	1.5	<5	95.3 (86.8, 103.8)[1]	47.7 (42.3, 53.0)[1]

[1]Confidence intervals (α = 0.05)

Unlike HCl, high P and Zn extraction correlated strongly, therefore reductions in Zn led to unacceptably large reductions in P extraction. The condition (Zn < 50%) used coarse SSC (<5mm) and short acid contact (t) and appears to represent the optimal condition for maximising P extraction without mobilising Zn.

9.3.3.5 P Extraction: Nitric acid

Figure 9-19 shows that the extraction efficiency ranged widely depending on the extraction parameters used and the elements measured. P extraction ranged from 35.6% to 97.8%, which shows the sensitivity of P to the experimental extraction parameters. The elements that achieved maximum extraction of >80%, include: Ba (<88.5%), Ca (<98.5%), Fe (<83.2%), Mn (<90.8%), Mg (<86.4%) and Sr (<85.4%) . Zn solubility was moderate <68.2% whilst the solubility of Cu and Pb was relatively low at <11.7% and <24%, respectively.

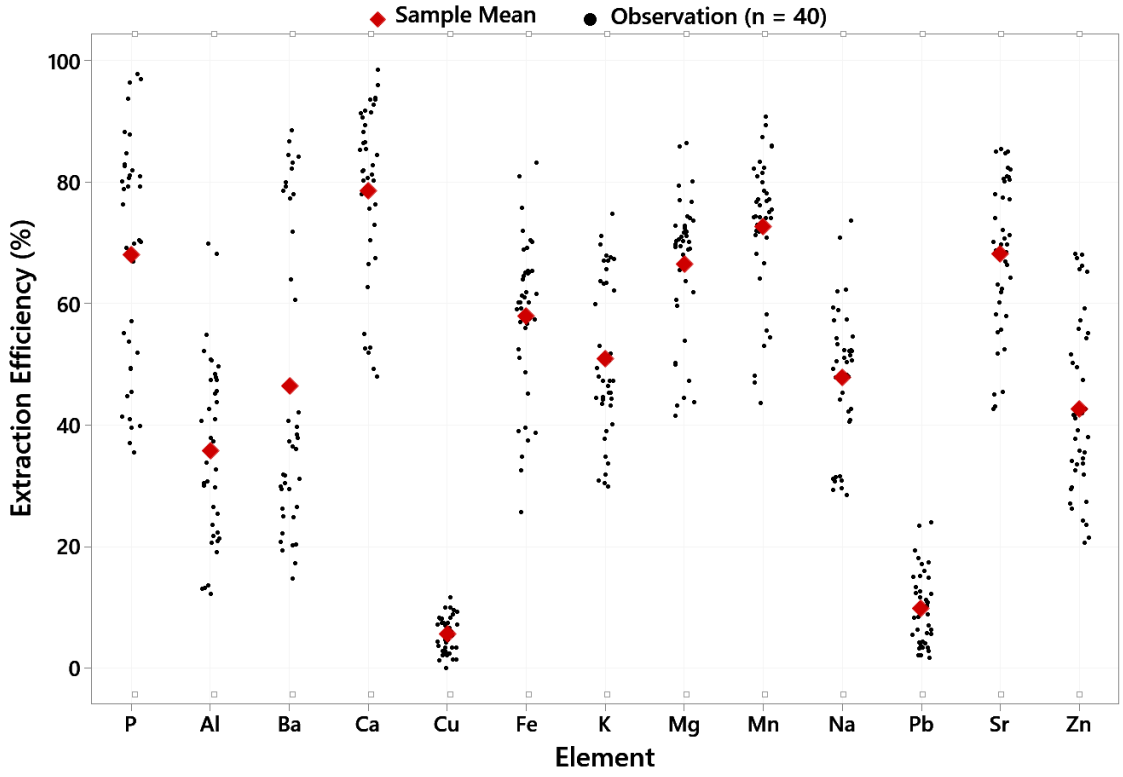


Figure 9-17: HNO_3 leaching: Extraction efficiency distributions for P and other elements (n =

HNO_3 was the only extractant found to solubilise Cu and Pb, this may be because of the oxidising ability of the nitrate ion, which has a standard reduction potential of (+0.96v) higher than elemental Cu and Pb (0.52v and -0.13v, respectively) or sulphide [-0.407v]. The dominant forms of Pb and Cu in SSC are expected to be their elemental form or sulphides, the latter may be particularly immobile because of inherent insolubility. If solubilised, both metals may be prone to reprecipitating as phosphates, although nitrate ions may have inhibited this.

Figure 9-20 summarises the effect of the experimental factors on P extraction. It shows that acid concentration, particle size and to a lesser extent the stoichiometric ratio had a strong positive influence on P extraction whilst contact (t) and temperature decreased extractions slightly. These trends were like those obtained for HCl, suggesting the conjugate bases of these acids (NO_3^-, Cl-) may play a lesser role in P mobilisation. H_2SO_4 might behave differently to HCl/HNO_3 because of the formation of gypsum and other insoluble salts, which are likely to inhibit the kinetics of P mobilisation.

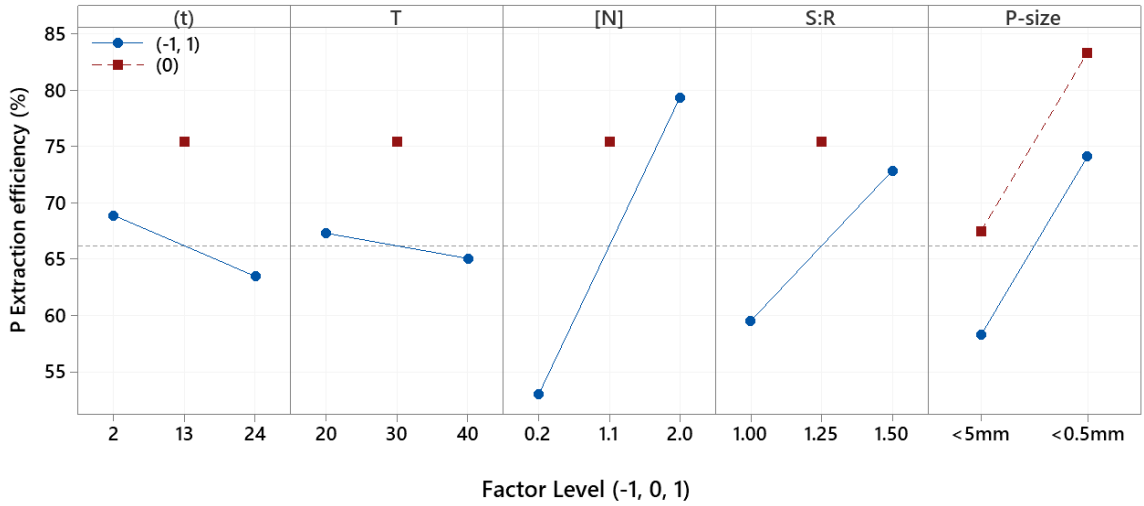


Figure 9-18: The effect of various factors tested at two levels (1 and -1) with centre point (0) on mean P_{EE} for HNO_3 leached char

Factorial regression ($\alpha = 0.05$) was conducted to assess the influence of the different factors on P extraction. The model was then optimised with stepwise (backwards elimination) regression to remove terms that did not contribute significantly ($\alpha = 0.003$) to the model fit. The model generated had an adjusted R^2 of 97.3% and statistical analysis presented in Appendix 4 suggest there was no evidence on model over-fit. The residuals of the model were normally distributed (*P = 0.158*). Excluding non-significant factors, the overall equation for this model is shown below:

$$HNO_3: P_{EE} = 136.38 - (0.6181A) - (2.845B) - (3.90C) - (68.43D) + (14.61E) + (0.3385AC) - (0.3380AE) - (0.3237BC) + (2.471BD) + (19.06CD) - (2.099CE)$$

Where: Variables A-D are uncoded and Variable E is coded as "-1" for a particle-size of <5mm and "+1" for a particle-size of <0.5mm. The code for the variables is defined in Table 9-8.

Figure 9-21 shows the standardised effect of the factors and their two-way interactions on P extraction. The concentration of HNO_3 had by far the strongest effect on P extraction, whilst all the other first-order factors had a significant effect on P, except T. Six two-way interactions were significant, including BD, CD, AE, AC, BC, and CE. The factor BD (temperature and stoichiometric ratio) was the strongest two-way interaction found, which is similar to the results obtained for HCl.

The relationship of all the two-way interactions was similar to those presented in Figure 9-11 for HCl and therefore is not presented.

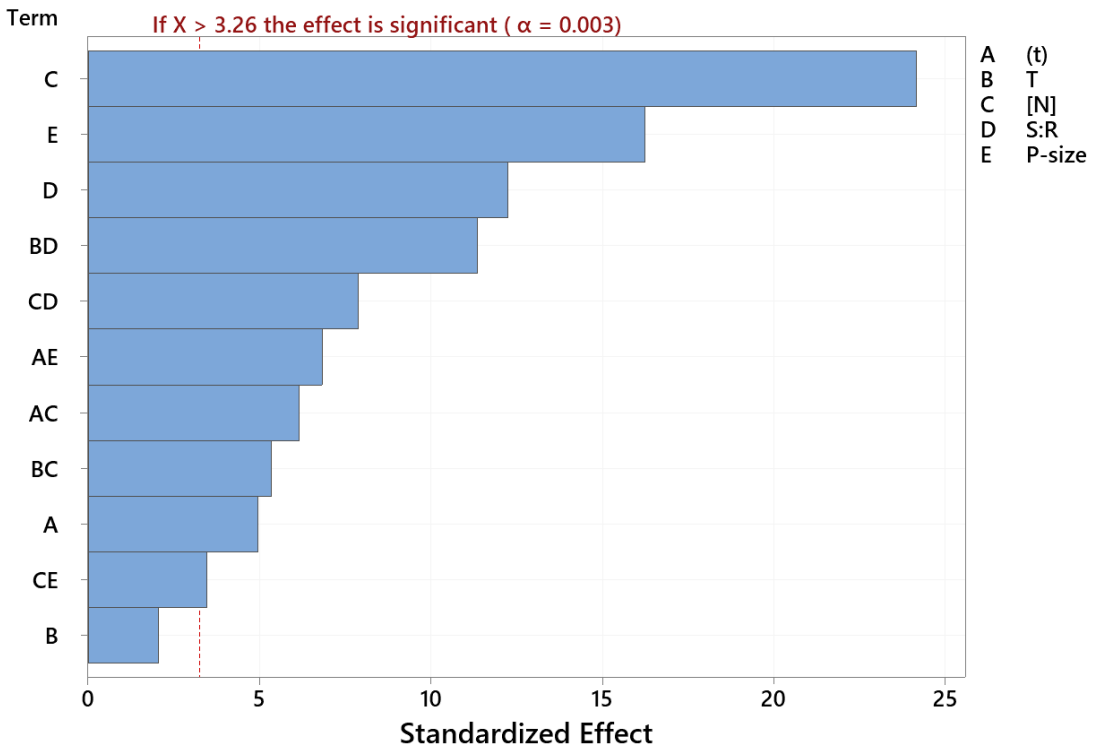


Figure 9-19: Phosphate extraction: Pareto chart of standardised effects generated in Minitab (2021) using factorial regression with backwards elimination (α = 0.003). Factors with a standardised effect of >3.26 are statistically significant at a 0.3% significant level.

Ignoring the centre-points, Figure 9-20 suggested the optimal level for each of the factors were:

Contact (t): 2 hours, Temperature: 20ºC, acid concentration: 2N, stoichiometric ratio: 1.5 and particle size: <0.5mm

Based on figure 9-20, mean P extraction for HNO_3 was maximised when acid concentration, stoichiometric ratio and particle-size are at their upper levels and contact (t) and temperature are at their lower levels. Although this does not include two-way interactions that might influence the lower level differently to the upper level and vice versa. The HNO_3 model was used to predict the optimal combination of factorial levels to maximise P extraction. In addition, the optimal combination was also predicted when one factor was constrained to its lowest performing level. The results are summarised in Table 9-13.

When unconstrained, the model's confidence intervals predicted maximum P extraction of between 97.7-105.4%, which suggests it required further optimisation because extraction >100% is not possible. Contrary to figure 9-20, the optimal temperature for extraction was 40°C, which is similar to the results obtained for HCl. Table 9-13 for HNO_3 and Table 9-9 for HCl share many similarities which suggests these acids behave similarly when extracting P from SSC.

The only difference is that for HCl suboptimal stoichiometric ratio decreased P extraction the most (Table 9-9) whilst Table 9-13 shows suboptimal acid concentration decreased P extraction the most for HNO_3.

Table 9-13: The optimal combination of experimental factors for P extraction during constraint and non-constraint of factorial levels

Constraint	(t) Hours	T °C	[N] N	S:R Ratio	P-size (mm)	Predicted P_{EE} %	Confidence Interval[1] % (α = 0.05)
None	2	40	2	1.5	<0.5	101.6	97.7, 105.4
T = 20	2	20	2	1.5	<0.5	97.3	93.4-101.1
(t) = 24	24	40	2	1.5	<0.5	95.4	91.6-99.3
P-size = 5	24	40	2	1.5	<5	90.8	87.0, 94.7
S:R = 1	2	20	2.0	1	<0.05	87.7	83.9-91.5
[N] = 0.2	2	40	0.2	1.5	<0.5	83.0	79.1-86.8

[1]P extraction above 100% is not possible however the HNO_3 model has not been optimised.

9.3.3.6 HNO_3 Extraction: Potentially toxic elements

Factorial regression with backward elimination (α = 0.003) was used to assess the relative effect of extraction factors on Pb, Cu and Zn extraction. The results are summarised in figures 9-22 to 9-24 and show the standardised effect of each factor on metal extraction.

The particle size was the dominant factor influencing the extraction for Zn, Cu and Pb, with S:R being the second most important factor. This shows that the granular structure of coarse SSC limits the extractability of heavy metals, which is one reason SSC is expected to leach fewer heavy metals than SSA. The particle size was also the dominant factor when leaching Zn from SSC with HCl and H_2SO_4. Tables 9-9, 9-11 and 9-13 all show that although not optimal, high P extraction is feasible when leaching coarse SSC (<5mm) with predicted extraction ranging between 90.8% and 95.3% for HCl, H_2SO_4 and HNO_3.

The strong effect of stoichiometric ratio on Zn, Cu and Pb extraction for HNO_3 was also consistent with Zn extraction for HCl and H_2SO_4. This effect is expected, because when the stoichiometric ratio is equal to 1, the leachate produced will consist primarily of H_3PO_4, limiting the availability of H_3O^+ ions, which may be required to mobilise these metals.

HNO_3 concentration contributed significantly to Zn extraction; however, it was the least important significant factor (Figure 9-22). For Pb and Cu extraction, HNO_3 concentration was not found to be significant and did not contribute to extraction (Figures 9-28 & 9-29). This finding is important because HNO_3 concentration was the most important factor for P extraction. Based on these findings, 2N HNO_3 may be used for P extraction without significantly influencing Cu and Pb extraction, particularly when the stoichiometric ratio is limited to the requirements for P solubilisation.

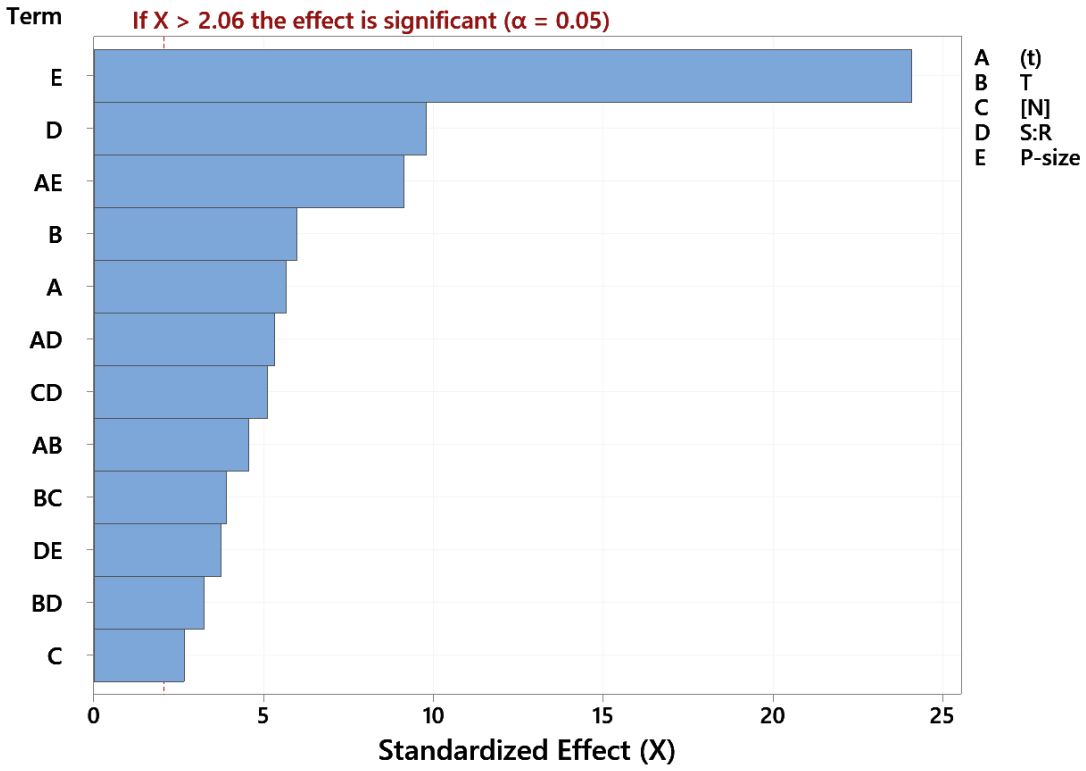


Figure 9-20: Zinc extraction: Pareto chart of standardised effects generated in Minitab (2021) using factorial regression with backwards elimination (α = 0.05). Factors with a standardised effect of >2.05 are statistically significant at a 5% significance level.

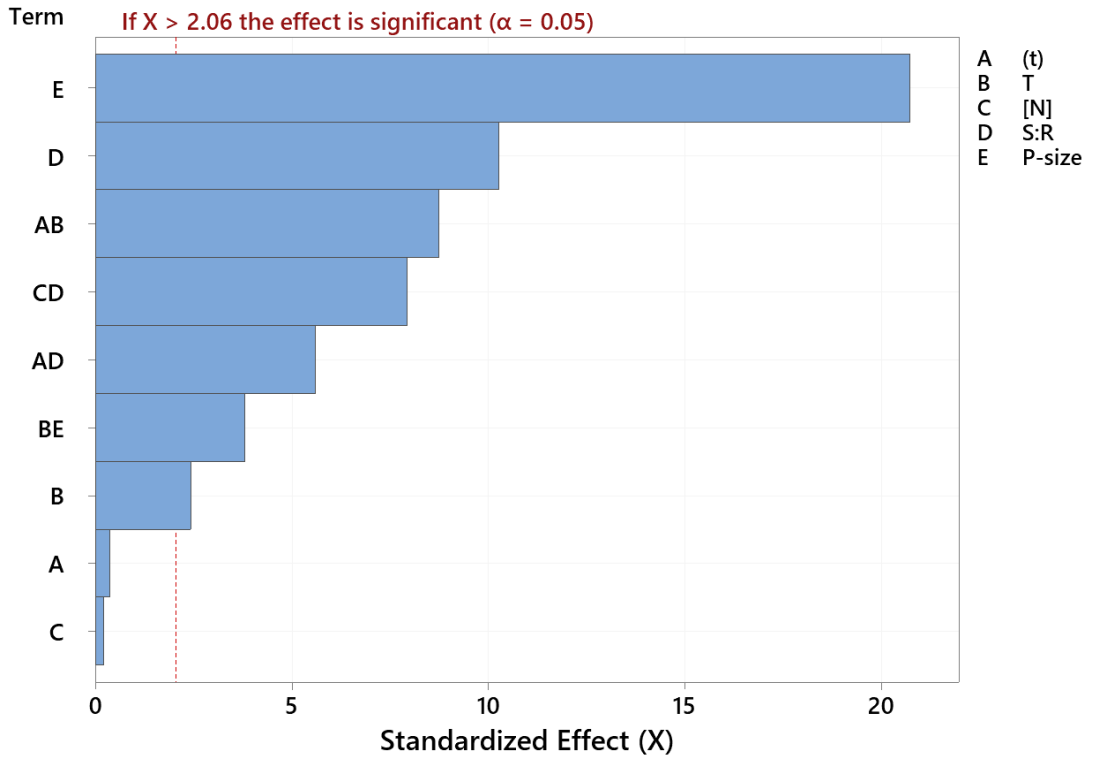


Figure 9-21: Lead extraction: Pareto chart of standardised effects generated in Minitab (2021) using factorial regression with backwards elimination (α = 0.05). Factors with a standardised effect of >2.05 are statistically significant at a 5% significance level.

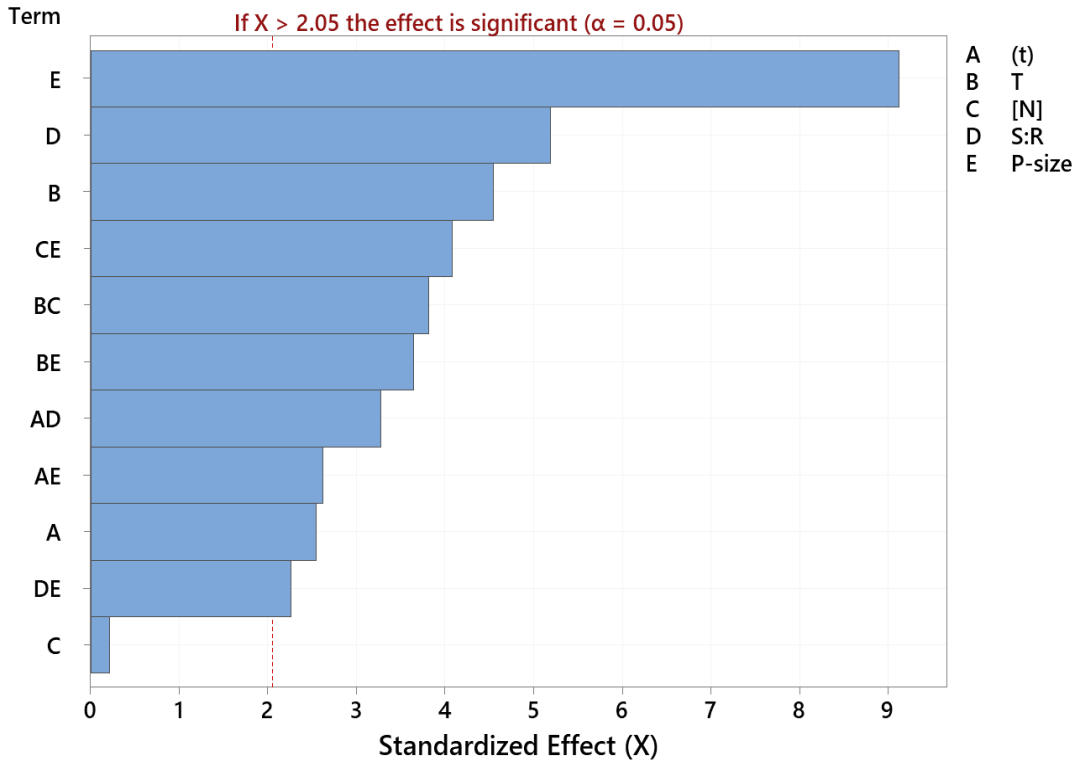


Figure 9-22: Copper extraction: Pareto chart of standardised effects generated in Minitab (2021) using factorial regression with backwards elimination (α = 0.05). Factors with a standardised effect of >2.048 are statistically significant at a 5% significance level.

Response optimisation was used to identify which combination of factors maximised P extraction but minimised the extraction of Zn and Pb. Cu was excluded from the optimisation because unlike Pb it does not pose a risk to human health and unlike Zn is extracted in much smaller concentrations which are not expected to pose a risk to environmental health. The best combination of extraction parameters, when P extraction was constrained to >95%, >90% and >80%, are summarised in Table 9-14. This shows that relatively large reductions in Zn and Pb extraction can be achieved with only small reductions in P extraction. For the conditions P >90% and P >80%, the extraction parameters use an extended contact (t) and coarse particle size to maximise P extraction and minimise Zn/Pb extraction.

Table 9-14: Response optimisation for P and Zn

Condition	(t)	T	[N]	S:R	P-size	P_{EE}	Zn_{EE}	Pb_{EE}
	hours	^oC	N	Ratio	mm	%	%	%
P >95%	2	20	2.0	1.5	<0.5	97.3 (93.4-101[1])	59.3 (52.8-65.9)[1]	16.6 (13.6-19.6)
P > 90%	24	40	2.0	1.5	<5	90.8 (87.0-94.7)[1]	37.8 (31.3-44.3)[1]	9.16 (6.17-12.2)
P >80%	24	20	2.0	1.5	<5	86.5 (82.7-90.4)[1]	31.7 (25.2-38.3)[1]	8.01 (5.02-11.0)

[1]Confidence intervals ($\alpha = 0.05$)

9.3.3.7 Potentially toxic elements: Further discussion

As discussed in section 8.2.4.1 Zn, Cu, and Pb compounds may form sulphides during pyrolysis, whilst Cu and Pb compounds may also undergo reduction into their elemental forms. During these experiments, Zn was soluble in all three acids, whilst Pb and Cu were only soluble in HNO_3. This difference suggests that some of the Cu and Pb present are in their elemental forms and HCl and H_2SO_4 cannot oxidise these metals. For example, the standard reduction potentials ($E°$) for the Cu, Pb, Zn, H_3O^+, chloride, bisulphate, sulphate, and nitrate ions are shown below:

$Cl_2 + 2e^- = 2Cl^-$	[1.36 V]
$NO_3^- + 4H^+ + 2e^- = NO + 2H_2O$	[0.96 V]
$Cu^+ + e^- = Cu$	[0.52 V]
$Cu^{2+} + 2e^- = Cu$	[0.34 V]
$SO_4^{2-} + 4H^+ + 2e^- = SO_3 + 2H_2O$	[0.17 V]
$HSO_4^- + 3H^+ + 2e^- = SO_2 + 2H_2O$	[0.16 V]
$2H_3O^+ + 2e^- = H_2 + 2H_2O$	[0.00 V]
$Pb^{2+} + 2e^- = Pb$	[-0.13 V]
$Zn^{2+} + 2e^- = Zn$	[-0.76 V]

The strongest oxidising ions in HCl and H_2SO_4 are the hydronium and sulphate ions, respectively, therefore these acids cannot oxidise any metallic copper present in SSC. The nitrate ion has a relatively high E^o therefore it can oxidise elemental Cu and form copper nitrate, which is a soluble salt. The E^o for the hydronium, sulphate and nitrate ions are higher than elemental Pb, therefore all the acids tested should be able to oxidise Pb to form their corresponding salt. The reason Pb only solubilised in HNO_3 could be because of the low solubilities of their salts. For example, both $PbCl_2$ (pK_{sp} = 4.77) and $PbSO_4$ (pK_{sp} = 7.60) are only sparingly soluble (Dean, 1999), whilst $Pb(NO_3)_2$ is highly water soluble. When SSC is leached, large quantities of competing ions are also released, therefore whilst H_2SO_4 could oxidise elemental Pb, the sulphate ions are likely to be consumed because of the formation of relatively insoluble AEM sulphates. Likewise, the formation of H_3PO_4 will decrease the quantity of disassociated hydronium ions, minimising the extent of Pb oxidation. In addition, Pb, Cu and Zn phosphate are all relatively insoluble, therefore any liberated ions may be prone to reprecipitating as phosphates (Table 9-15)

The results obtained show that HNO_3 could solubilise some Pb and Cu, the oxidation of their elemental forms may have been a mechanism for their extraction from SSC.

During pyrolysis Cu, Pb and Zn oxides may react with H_2S to form metal sulphides, unlike oxides, sulphides are less likely to be reduced to their elemental forms. Table 9-15 summarises the solubility product constants (pK_{sp}) of Cu, Pb and Zn compounds, including sulphides:

Table 9-15: The pK_{sp} constants for selected Cu, Zn and Pb compounds (Dean, 1999)

Ion	Chloride Cl^-	Carbonate CO_3^{2-}	Hydroxide OH^-	Sulphide S^{2-}	Phosphate PO_4^{3-}
Cu (I)	6.76	-	14.00	47.60	-
Cu (II)	<0	9.86	19.66	35.20	36.85
Pb (II)	4.77	13.13	14.84	27.10	42.10
Zn (II)	<0	9.94	16.50	21.60 - 23.80	32.04

The standard reduction potential for sulphide is shown below:

- $S + 2e^- = S^{2-}$ [-0.407]

Its *E*° is lower than the standard reduction for the hydronium ion, therefore HCl could technically oxidise sulphides into elemental sulphur, and this reaction can occur for oxidising acids. For all the acids, H_2S formation may also occur. For sulphides however, both reactions may be suppressed due to the low solubility of these compounds (Table 9-15) although their solubility is expected to increase with acid concentration for non-oxidising acids (Table 9-16).

The concentration of dissolved Cu^{2+}, Pb^{2+} and Zn^{2+} in a pure 0.2N and 2N non-oxidising acid has been calculated under the following equations and assumptions:

- $[S^{2-}] \approx \frac{K_{a1} * K_{a2} * [H_2S]}{[H^+]^2}$ Where: H_2S: $pK_{s1} \approx 7$, $pK_{s2} \approx 13$, $[H_2S] \approx 0.1$ mol l^{-1},

  $H^+ = 0.2N$ or $2N$.

- $[x^{2+}] \approx \frac{K_{sp}(xS)}{[S^{2-}]}$ Where: (x) = Cu(II), Pb(II) or Zn(II).

Table 9-16: Approximate solubility of metal sulphides in non-oxidising acids

Concentration H^+ mol L^{-1}	Cu(II) sulphide -log mol L^{-1}	Lead (II) sulphide -log mol L^{-1}	Zinc (II) sulphide -log mol L^{-1}
0.2N	17.60	7.49	2.00-4.19
2.0N	15.60	5.49	0.00-2.19

Table 9-16 shows that Pb(II) and Cu(II) sulphide have low solubility in solutions of non-oxidising acids (<2N) where the formation and loss of H_2S is the main route to solubilise the copper ions.

In contrast, Zn(II) sulphide may solubilise in acid concentrations between 0.2-2N. These results indicate how SSC could behave during acidulation since:

- P dissolution will convert HCl/H_2SO_4 to H_3PO_4, a weak acid, therefore the quantity of dissociated H_3O^+ ions will be reduced.
- Any solubilised heavy metals may re-precipitate as phosphates.
- SSC contains a variety of bases (e.g. oxides and sulphides) that will consume the acidity of the initial leaching solution.
- There may be factors that increase the solubility of metal sulphides, for example, the presence of chelating agents (e.g. pyrophosphoric acids). For example, Robinson et al. (2017) suggested <20% of the phosphate in SSC may be present as magnesium pyrophosphate.

9.3.3.8 Zinc, copper, and lead removal from SSC

The presence of toxic elements within SSC may inhibit the materials re-use value. The elemental extraction efficiency when 5M H_2SO_4, HNO_3, aqua-regia or NaOH are added to SSC was investigated. The results showed:

- 5M H_2SO_4, aqua-regia and HNO_3 extracted 95.3%, 91.3% and 101.7% of SSC Zn, respectively. In contrast, 5M NaOH only extracted 12.8% of SSC Zn.
- 5M H_2SO_4, HNO_3 and NaOH did not extract detectable concentrations of Pb, which, except for NaOH, was unexpected. This suggests that Pb is prone to reprecipitating. However, it is not clear why lower acid concentrations facilitated its extraction in HNO_3. Only 5M aqua-regia could remove Pb, with extraction of only 29%. Previous research conducted by Hara (1967) suggested Pb/PbO solubility in HNO_3 peaks at 2.5N and rapidly decreases with increased molarity because of the oxidation of Pb(II) into Pb(IV) and the formation of PbO_2 which is very insoluble. The same process may have occurred when SSC was leached with 5M HNO_3, alternatively solubilised Pb^{2+} ions may have precipitated as $Pb_3(PO_4)_2$.
- Only 5M aqua-regia and HNO_3 were effective at removing Cu from SSC, with extractions of 88.9% and 103.5%, respectively.

A two-stage leaching procedure may be feasible, whereby SSC is leached first to maximise P extraction and minimise toxic metal extraction. Next, the residual SSC could be leached with 5M HNO_3 to remove both Cu and Zn. The P and metals (Cu/Zn) removed during secondary leaching could then be precipitated with a suitable base, for example NaOH or anhydrous NH_3 (e.g. odour) or selectively extracted.

9.3.4 SSC leachate

SSC leaching with HCl and H_2SO_4 extracted Zn, however, neither Cu nor Pb were soluble in these acids (Figure 9-9 and 9-14). Meanwhile, 0.2-2N HNO_3 extracted Zn and relatively small quantities of both Cu and Pb (Figure 9-19). When SSC extraction was conducted with 5N HNO_3, all the Zn and Cu were extracted from SSC, but Pb was insoluble (section 9.3.3.8). Further, the results presented in Table 9-10, 9-12 and 9-14 show that P extracted can be maximised whilst limiting the co-removal of Zn (and Pb, for HNO_3). Cumulatively, these findings suggest that high P extraction efficiency can be achieved, whilst limiting the quantity of Cu, Pb and Zn that are extracted from SSC. In addition, the residual heavy metals in SSC could be removed in a secondary leaching step with 5M HNO_3.

As part of this PhD project, a second masters project was proposed, and supervised, that focused on the precipitation of P from H_2SO_4 leaching solution, with NaOH. The project was conducted by Lee (2019), who found:

- More than 90% of the P in SSC could be removed when leached with H_2SO_4 and that ~80% of the soluble P in the leachate could be precipitated when neutralised with NaOH to a pH of 7.
- Phosphate co-precipitates with Fe, Al, and less abundant metals such as Zn, however these forms of P are not likely to be plant available so must be processed further for use in agriculture.

Secondary analysis of Lee's data suggests that only ~80% of the P in H_2SO_4 leachate precipitated due to the lack of available cations. For example, Figure 9-25 shows that by pH 6: Al, Fe, and to a lesser extent Ca had already precipitated.

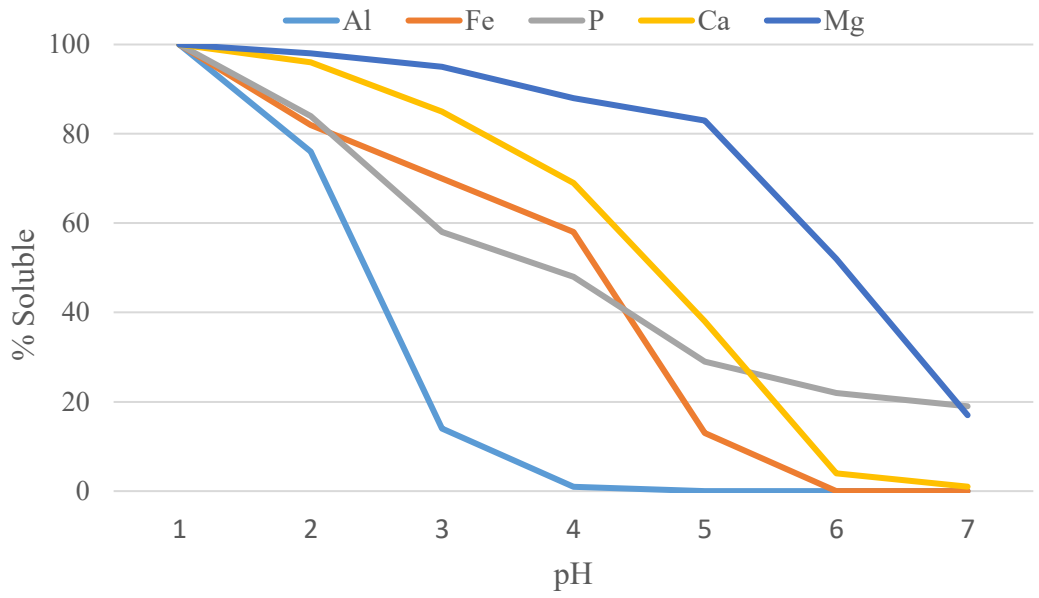


Figure 9-23: Phosphate and metal ion solubility in SSC H_2SO_4 leachate solution neutralised with NaOH between pH 1-7 (Lee, 2019)

Unlike H_2SO_4, both HNO_3 and HCl remove Ca from SSC, therefore cations are available in excess of P. Figure 9-26 shows that when HNO_3 leachate is neutralised with NH_4OH, all the P is precipitated by pH 6.

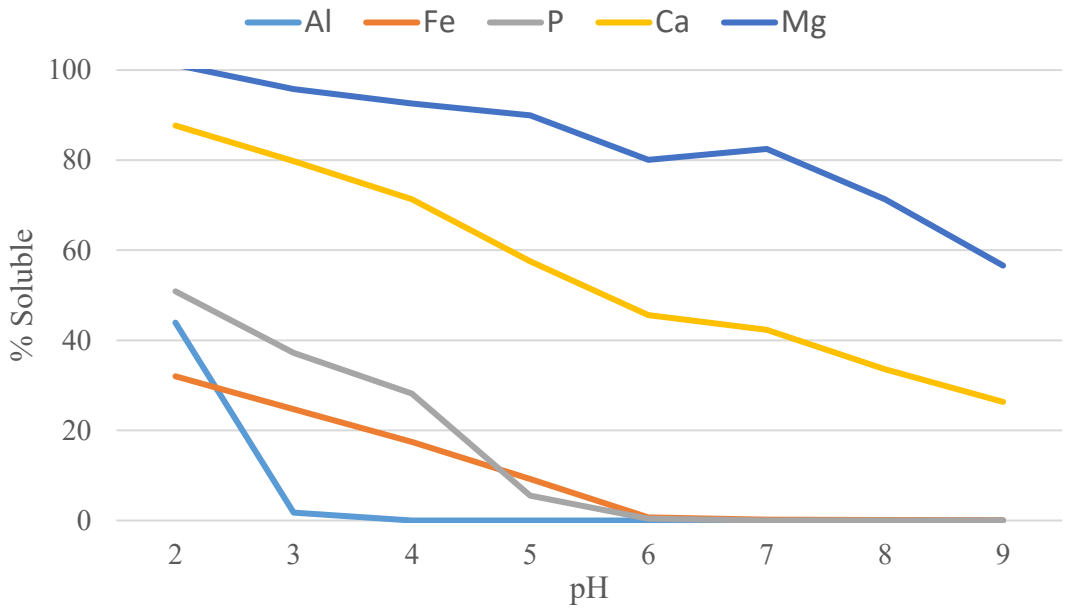


Figure 9-24: Phosphate and metal ion solubility in SSC HNO_3 leachate solution neutralised with NH_4OH between pH 2-9

For agriculture, the recovery of leached P as Al/Fe phosphate is undesirable. Several solutions to this issue have been proposed in the literature for SSA leachate (Takahashi et al. 2001) (Kraus et al., 2018) (Wang et al., 2018). For example, the selective precipitation of leachate-P as $AlPO_4$, which precipitates at very low pH (2-3) (Figures 9-26 & 9-26), thus minimising heavy metal co-precipitation. $AlPO_4$ is amphoteric and could be resolubilised at high pH with a suitable alkali (e.g. NaOH) and converted to sodium phosphate through a gelation process (Takahashi et al. 2001).

The Tetraphos® process leaches SSA with recirculated H_3PO_4 and precipitates leached heavy metals (e.g. Cu) by dosing the solution with CaS to produce insoluble heavy metal salts (e.g. CuS) which are separated. The SSA is then leached with H_2SO_4 to maximise P extraction, and the precipitated gypsum is separated from the H_3PO_4. The solution is then dosed with HCl and undergoes cation exchange and nano-filtration to separate Al/Fe chlorides. The dilute H_3PO_4 is then concentrated to produce technical grade H_3PO_4 (Kraus et al., 2018). The removal of Al/Fe ions from leachate solution through ion exchange has also been proposed by Wang et al. (2018) for the sustainable production of Struvite from SSA leachate. The cation exchange resin used was 732-CR, which has a sulfonic acid functional group and can remove other cations such as Pb (Guo et al., 2013).

Based on the use of CaS within the Tetraphos® process, SSC leachate could also be dosed with CaS to precipitate heavy metals. Figure 9-5 clearly shows that <pH 4 sulphides are almost entirely speciated as H_2S, therefore the CaS will be rapidly transformed into H_2S. This suggests that heavy metal sulphide precipitation is rapid, or the Tetraphos® process uses a system to recirculate H_2S through SSA leachate repeatedly, until the heavy metals are removed to acceptable levels. When SSC is leached with mineral acids, it forms H_2S because of the presence of hydrolysable metal sulphides. This H_2S could be captured and recirculated through SSC leachate to help precipitate heavy metals.

The fertiliser industry typically purifies rock phosphate leachate by extracting the H_3PO_4 with solvents such as tri-butyl phosphate or N-octanol (Ye & Li, 2012) (Habashi et al., 1987). When the leachate contains contaminants such as Fe, Al and SO_4 ions, these are co-extracted alongside the H_3PO_4, diminishing the quality of the resulting H_3PO_4. Several approaches have been used to overcome this issue, for example, Amin et al. (2019) produced rock phosphate leachate containing 2.6% iron. This could be precipitated prior to solvent extraction by reducing the Fe^{3+} to Fe^{2+} and dosing the leachate with oxalic acid to form $FeC_2O_4 \cdot 2H_2O$ (pKsp = 6.5) (Dean, 1999). The iron removal efficiency was 80-91% when the H_3PO_4 concentration was between 10-20%, but rapidly decreased with increased H_3PO_4 concentration. All the iron within SSC leachate is expected to be present as Fe^{2+} because of the highly reducing conditions during pyrolysis therefore the reduction step is unlikely to be required for SSC leachate.

The $FeC_2O_4 \cdot 2H_2O$ can subsequently be dissolved in 5M HCl and the oxalic acid separated by cooling and crystallisation (Liu et al., 2019). Alternatively, $FeC_2O_4 \cdot 2H_2O$ can be mixed with $CaCl_2$ to form $CaC_2O_4 \cdot 2H_2O$ (pKsp = 8.63) and then this can be dissolved in 2.5% H_2SO_4 to precipitate calcium sulphate and regenerate the oxalic acid (Amin et al., 2019).

Rather than, or in addition to, using oxalic acid to remove H_3PO_4, the SSC leachate could be directly extracted with a solvent. Ye & Li (2012) found that when mixed tri-butyl phosphate and N-octanol was saturated with H_3PO_4, it can be stripped of its metal content (e.g. Fe, Mg, Al) with 10% H_3PO_4 or H_2O with minimal H_3PO_4 losses. The stripping liquor can then be treated by ion exchange or simply neutralised to precipitate the unwanted metals. The saturated solvent can also be stripped of its H_3PO_4 with distilled water and the H_3PO_4 can be concentrated through evaporation (Ye & Li, 2012).

Ultimately, the choice of the SSC extractant and downstream leachate upgrading process depends entirely on the desired quality of the H_3PO_4 and the end-use of SSC. A wide range of process exist and much of this is based on mature technology (Binnemans et al., 2015) (Zhang et al., 1989) (Marcata & Giulietti, 1993). Techno-economic and environmental analyses are required to compare the processing costs and sustainability of current phosphate fertiliser production with recovered products.

Chapter 10: Crossness STW: Site energy

10.1 Crossness STW: Energy

Chapter 1 presented a series of gross energy flow diagram for different sludge treatment configurations (Figure 1-2, 1-3, 1-4) based on data obtained from Mills (2015). This chapter presents the energy conversion and flows for Crossness STW (Table 10-4 and Figure 10-1), a THP-digestion site. Based on the results for digested- and raw-sludge pyrolysis presented in Chapter 7 and Appendix 5, respectively. The influence pyrolysis could have on site energy conversion and flows at Crossness STW are explored.

10.1.1 Crossness STW: Present performance data

Data was obtained from Crossness STW (Table 10-1), based upon on-site measurements recorded by Thames Water operations.

Table 10-1: Daily data obtained from Crossness STW between 01.01.2019 and 06.08.2020

	Location	Parameter
Raw-sludge	Digester-feed	Digester-feed volume (m^3) , DS (%)
Digested sludge	Bucher-press feed	Digestate volume (m^3) , DS (%)
Biogas	Digester	Biogas volume (m^3) , methane (%)
Boilers	Thermal hydrolysis	Biogas & Natural gas consumption (m^3)

Sludge mass was estimated from sludge volume and DS (%) using an International Water Association method (Andreoli et al., 2007). The equation to estimate specific gravity (s.g.) is presented below:

Estimating specific gravity of sewage sludge

$$\text{s.g.} = \frac{1}{\left(\frac{\left(\frac{FS}{TS}\right)}{SG\,(FS)}\right) + \left(\frac{\left(\frac{VS}{TS}\right)}{SG(VS)}\right)}$$

FS = Fixed solids, VS = Volatile solids, TS = Total solids, SG = Specific gravity

Where the specific gravity of FS & VS is 2.5 t/m^3 & 1.0 t/m^3 respectively

The water industry refers to the loss on ignition (LOI) at 550^{o}C as volatile solids or matter (VS) (Suez, 2021), therefore FS/TS and VS/TS are simply ash (%) and LOI (%). The specific gravity of the FS and VS can be estimated as 2.5 and 1.0, respectively (Andreoli et al., 2007). The daily measurements of raw and digested sludge VS (%) were used to estimate the specific gravity of the sludge dry solids. The mass of sludge was then back-calculated based on its moisture content.

For example:

1. *Approximate dry solids (volume) = Sludge (volume) – Water (volume)*
2. *Dry solids (mass) = Dry solids (volume) * Dry solids (specific gravity)*

The data over the 583-day data collection period was then annualised, to estimate the annual mass of raw sludge treated and digested sludge produced at Crossness STW. Thames Water operations do not measure sludge HHV. Therefore, the HHV of the raw and digestate was estimated using measured higher heating values on a dry ash-free basis (HHV_{DAF}) (Table 6-1):

3. *Raw sludge (HHV) = Raw sludge VS (%) * XS-raw (HHV_{DAF})*
4. *Digested sludge (HHV)= Digested sludge VS (%)* * XS Mean *(HHV_{DAF})*

The results are summarised in table 10-2:

Table 10-2: Annualised mass & energy balance of Crossness STW between 01.01.2019 and 06.08.2020

	Unit	Raw sludge	Digested sludge	Biogas[1]	Imbalance
DS	tds year^{-1}	47,818	22973	18.84 mcm	-
VS	tds year^{-1}	40712	16,361	-	-
HHV	GWh (HHV) year^{-1}	272.2[3]	114.2	129.8[2]	28.2
VSD	%	59.8	-	-	-

[1]Biogas volume measured in million cubic metres (mcm)
[2]Biogas, annualised methane content - 62.4%
[3]244.0 GWh (HHV) yr^{-1} (if calculated by difference)

Table 10-2 suggests that THP digestion at Crossness STW is achieving a VS destruction (VSD) of approximately 59.8%. This is slightly higher than the generic assumption made by Mills (2015) of 59% for VSD. Table 10-2 also suggests that annually 47.7% of raw sludge (HHV) is converted into biogas (HHV), which is lower than that estimated by Mills (2015) - 57% (LHV). Whilst 41.9% of annual raw (HHV) was retained in the digestate, which is similar to what Mills (2015) estimated – 43% (LHV). Approximately 10.6% of raw sludge (HHV) was unaccounted for. The most likely cause is overestimation of raw sludge (HHV_{DAF}), since this undergoes relatively large seasonal fluctuations. For example, Pullket (2015) found seasonal fluctuations in raw sludge from Little Marlow STW caused 10% variations in raw sludge char ash content. The biogas and digested sludge (HHV_{DAF}) data is expected to be reasonably robust, based on a simple mass balance, the raw sludge energy content was estimated at 244.0 GWh (HHV) year^{-1}. Total THP steam requirements at Crossness STW are unknown, however the natural gas and biogas consumption by the THP boilers are measured by operations.

The consumption data suggests there is currently a large thermal parasitic load:

- 7.0 GWh (LHV) biogas yr^{-1} to THP boilers
- 29.8 GWh (LHV) natural gas yr^{-1} to THP boilers
- Total parasitic heat demand for Crossness THP: 36.8 (LHV) GWh yr^{-1}

This equates to 771 Wh kg raw DS^{-1} (LHV) parasitic heat kg ds^{-1}, which is more than double that predicted by Mills (2015). Ringoot et al (2012) states THP treats sludge with a "typical design dry solids concentration of 16.5%" and "assuming 15°C average raw sludge temperature" this amounts to steam consumption of "895 kg/tonDS" equivalent to "700 kWh_{steam}/tonDS (assuming preheated boiler feed water to 85°C)". Steam consumption is dependent on THP feed temperature and can be reduced to "700 kg/tonDS" if the feed is increased to 35°C with low grade engine heat. A further reduction to "650 kg/tonDS" can be achieved if the sludge is pre-heated to 40°C through dilution with hot water (90°C) (Ringoot et al., 2012).

Previous mass & energy balances of sewage treatment works have shown that steam requirements can exceed these values. THP at Chertsey STW was shown to consume 1.11t steam tds^{-1} with further losses of 0.41t steam tds^{-1} (Pook et al., 2013). There are a range of contributing factors which contribute to the higher-than-expected steam demand (and parasitic thermal load), for example:

- THP-feed DS% and temperature influence steam requirements.
- Not all steam is utilised, for example, some is lost during boiler blowdown.
- High-grade heat to steam conversion in waste heat boilers is dependent on exhaust gas temperature. Engines with high electrical efficiency produce lower temperature exhaust gases. A typical waste heat boiler for biogas CHP may achieve 60-65% recovery efficiency (A, Perrault, personal communication, 2020).
- Variability in steam demand (Garcia-Cascallana et al., 2018).

Approximately 695 kWh of energy is required to produce one tonne of steam at the required pressure and temperature for THP (A, Perrault, personal communication, 2020). Assuming a boiler burner efficiency of 88% and recovery efficiency of 65%, the total steam demand at Crossness STW was estimated:

- 0.39t steam tds^{-1} is produced from high-grade heat recovered from the CHP based on 94% of site biogas energy being consumed by CHP and 18% of fuel (LHV) being converted to high-grade heat.
- 0.98t steam tds^{-1} is produced through the combustion of natural gas and excess biogas.

Total site steam requirements were therefore estimated at 1.36t steam tds^{-1}, which is much higher than the requirements for THP published by Ringoot et al (2012). This value is also similar to the performance of Chertsey STW, when a mass & energy balance of the site was conducted (Pook et al., 2013).

10.1.2 Energy flow diagrams

A series of energy flow diagrams will now be presented based on the data presented in section 10.1.1, and other assumptions summarised in appendix 5. Note:

- The total energy content of raw sludge (HHV) was estimated by difference at 244.0 GWh yr^{-1}, to eliminate the imbalance in table 10-2. Based on estimated raw tds^{-1} at Crossness STW, this is equivalent to 18.4 MJ kg^{-1} and is close to the assumption made by Mills (2015).
- Unlike figures 1-2, 1-3 and 1-4, the energy content of the materials is presented as HHV, since LHV was not measured. However, the conversion of gas to electricity and heat was calculated from gas LHV, under IEA (2004).
- All gas produced was assumed to be consumed by a CHP engine, rather than recirculated for parasitic heating. Any imbalances in the heat balance were assumed to be supplemented by natural gas.
- CHP loading of 100%

10.1.2.1 Thermal hydrolysis (Current site performance)

Based on the data presented in section 10.1.1 and the methodology stated above, the energy flows for sludge treatment at Crossness STW were estimated and are presented in figure 10-1. For a full list of assumptions, see appendix 5.

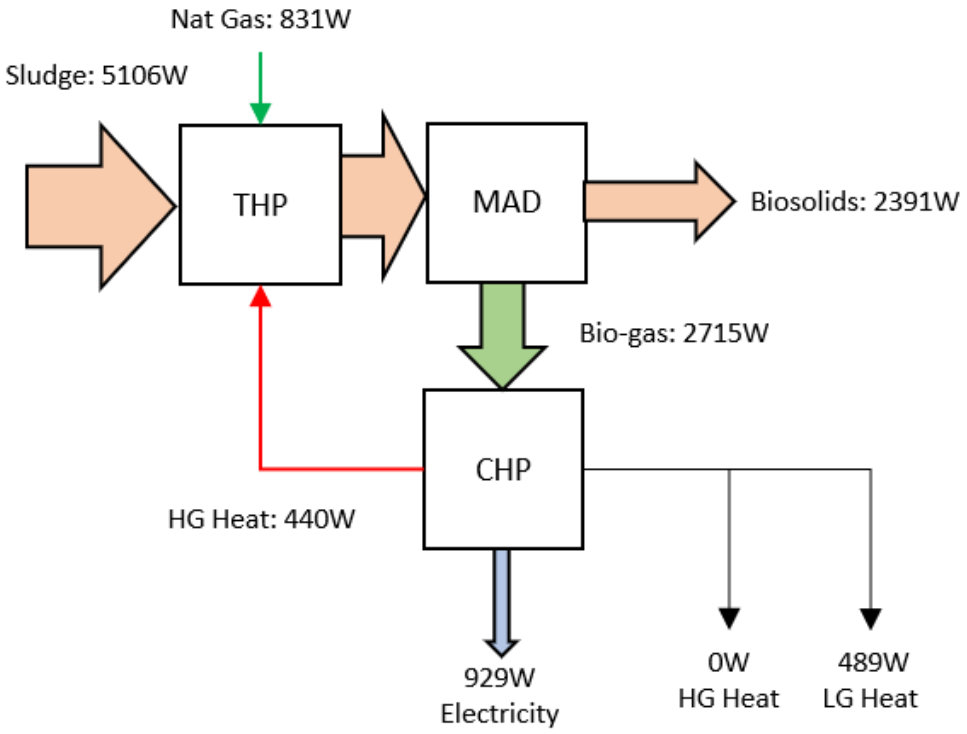


Figure 10-1: Gross energy flows of THP-MAD for 1kg DS^{-1} hr^{-1} based on data obtained from Crossness STW and assumptions from Mills (2015) and personal communication (2021). Units based on feed-rate of 1kg DS $hour^{-1}$.

The estimated parasitic heat demand for Crossness STW - 771 Wh (LHV) (section 10.1.1) is different to the natural gas consumption presented in Figure 10-1 – 831Wh (HHV) because: (1) of the lower and higher heating values being used, respectively; (2) the assumption in Figure 10-1 that all biogas is converted in an engine, rather than some of it being diverted directly to the THP boilers.

At Crossness STW, THP-digestion converts approximately 5106Wh kg^{-1} of raw sludge (HHV) into 929Wh kg^{-1} of electrical energy. Therefore, the GCE from sludge (HHV) to electric energy is approximately 18.2%. The CHP also produces 489Wh kg DS^{-1} of low-grade heat which is unused although it could theoretically be applied for pre-heating the sludge prior to THP thus lowering steam requirements. According to Mills (2015), the parasitic electric load of the process is at least 150Wh kg DS^{-1}, consequently the NCE of the process is 15.3%.

The process also requires a parasitic thermal load of 831Wh (HHV) kg DS^{-1} (figure 10-1), to account for this an adjusted NCE was calculated. An opportunity cost for natural gas consumption was applied, based on the electricity that could have otherwise been produced by the gas. For

example, in a combined-cycle gas turbine (CCGT) power station, the ECE of natural gas would be 50-60%, whilst in a domestic boiler conversion to heat would be >80% efficient. If it were assumed that for each 1000Wh of parasitic natural gas consumed, 500-600Wh of electricity could have otherwise been produced, this would have a significant effect on the perceived efficiency of sludge to energy processes. A penalty for parasitic biogas usage could also be applied because it be converted into biomethane (to offset natural gas) or renewable electricity (to offset grid consumption).

In 2020, the average price of electricity and natural gas to the non-domestic sectors was 13.3 pence kWh^{-1} and 2.3 pence kWh^{-1} respectively (BEIS[a], 2021) therefore there is a strong financial incentive to maximise electricity production rather than minimise natural gas usage. In addition, renewable electricity production receives subsidies either through renewable obligation certificates (ROCs) or the current contracts for difference (CfD) system (Palmer, 2016). Another factor to consider is the CO_2e emission factor. For natural gas and grid electricity these were 0.20297 kg CO_2e kWh^{-1} (LHV) and 0.21233 kg CO_2e kWh^{-1} in 2021 (BEIS[c], 2021), therefore there is also an incentive to produce additional electricity rather than minimise natural gas consumption. However, the emission factor for electricity is decreasing rapidly because of decarbonisation, therefore in the short- to medium-term the situation will reverse and there will be incentives to minimise natural gas usage.

Rather than assume parity with a CCGT power station, a penalty for natural gas consumption was applied based on the ECE of natural gas (or biogas) within a gas engine (ECE: 40%, 5% parasitic load). The opportunity cost for the natural gas consumption illustrated in figure 10-1 was calculated at 285 Wh kg DS^{-1}. To calculate the total parasitic load (e.g. thermal and electrical), the opportunity cost (285 Wh kg DS^{-1}) and electrical parasitic load (150 Wh kg DS^{-1}) were added to get a value of 435Wh kg DS^{-1} . When accounting for the total parasitic load, the adjusted NCE at Crossness STW was reduced to 493Wh tds^{-1} or 9.7%.

If the THP feed DS (%) was optimised and the THP feed temperature was increased from 10°C to 35°C, the THP steam requirement could be reduced to 0.7t tds^{-1}. When factoring in boiler blowdown and other losses, 0.82t steam tds^{-1} may be achievable. Based on this, the natural gas consumption at Crossness STW could be reduced from 831Wh to 347Wh (HHV) kg DS^{-1}. This would also increase the adjusted NCE of the process from 9.7% to 12.1% and would utilise the spare low-grade heat.

10.1.2.2 THP-Pyrolysis (Current THP performance)

The digested sludge samples XS-6 and XS-9 have different properties and behaved differently during pyrolysis, for example:

- XS-6 had a higher HHV_{DAF} than XS-9 which means its organics were more energy dense.
- XS-9 had a greater LOI and C (%) meaning its organic fraction was larger than XS-6

- The gas yields for XS-9 were higher than XS-6

At first, the reasons for this were unclear, however, analysis of site data show that there is a drop in VSD (%) between 2019 and 2020. The reasons for this are unclear, however, XS-9 had higher VS and produced higher gas yields without a corresponding increase in condensable liquid yields. An energy balance for combined THP-pyrolysis was produced based on Crossness STW data and laboratory-scale observations. Since XS-6 and XS-9 performed differently, a separate energy flow diagram was produced for each sludge (figure 10-2). This highlights the sensitivity of pyrolysis to upstream processes. Based on the current performance of Crossness STW, the combination of THP and pyrolysis could convert sludge HHV (5106 Wh kg DS^{-1}) into 1,457-1,548 Wh kg DS^{-1} of electrical energy (or a GCE of 28.5-30.3%). The pyrolysis parasitic load was estimated based on:

- The laboratory scale parasitic load for pyrolysis at 850ºC which equalled 387 Wh kg digested DS^{-1} (Table 7-10). This value may be an over-estimate compared to a commercial pyrolysis process; however it does not include any ancillary equipment.
- Dryer parasitic load of 80Wh t $water^{-1}$. Based on dried solids destruction of 52.1% (Table 10-2) and DS (%) =30.9%.
- The opportunity cost for natural gas consumption based on conversion in a gas engine.

The electric parasitic load for THP-digestion, pyrolysis and drying were estimated at 150Wh, 185Wh and 80Wh kg raw DS^{-1}, respectively. The thermal parasitic loads for XS-6 and XS-9 were 810 and 717Wh (HHV) kg raw DS^{-1}, respectively, which corresponded to an electrical opportunity cost of 277Wh and 245Wh, respectively. The NCE of the overall process was therefore reduced to 763 and 886Wh tds^{-1} or between 14.9% and 17.3% of the raw sludge. Based on current performance, THP-pyrolysis could not eliminate natural gas usage at Crossness STW because of high steam consumption and low digested cake DS%. However, if the DS (%) of the digested cake was increased from just 30.9% to 34.6% for XS-6 and 33.4% for XS-9. The dryer would no longer require support fuel, increasing NCE to 16.4% and 18.4%, respectively.

For THP-pyrolysis, there is no spare engine heat available, therefore heat cannot be recycled to the THP-feed to increase sludge temperature. The dryer condensate and char cooling water could be used to dilute the THP feed. Realistically, however, these heat sources are likely too small and diffuse to increase THP-feed temperature significantly.

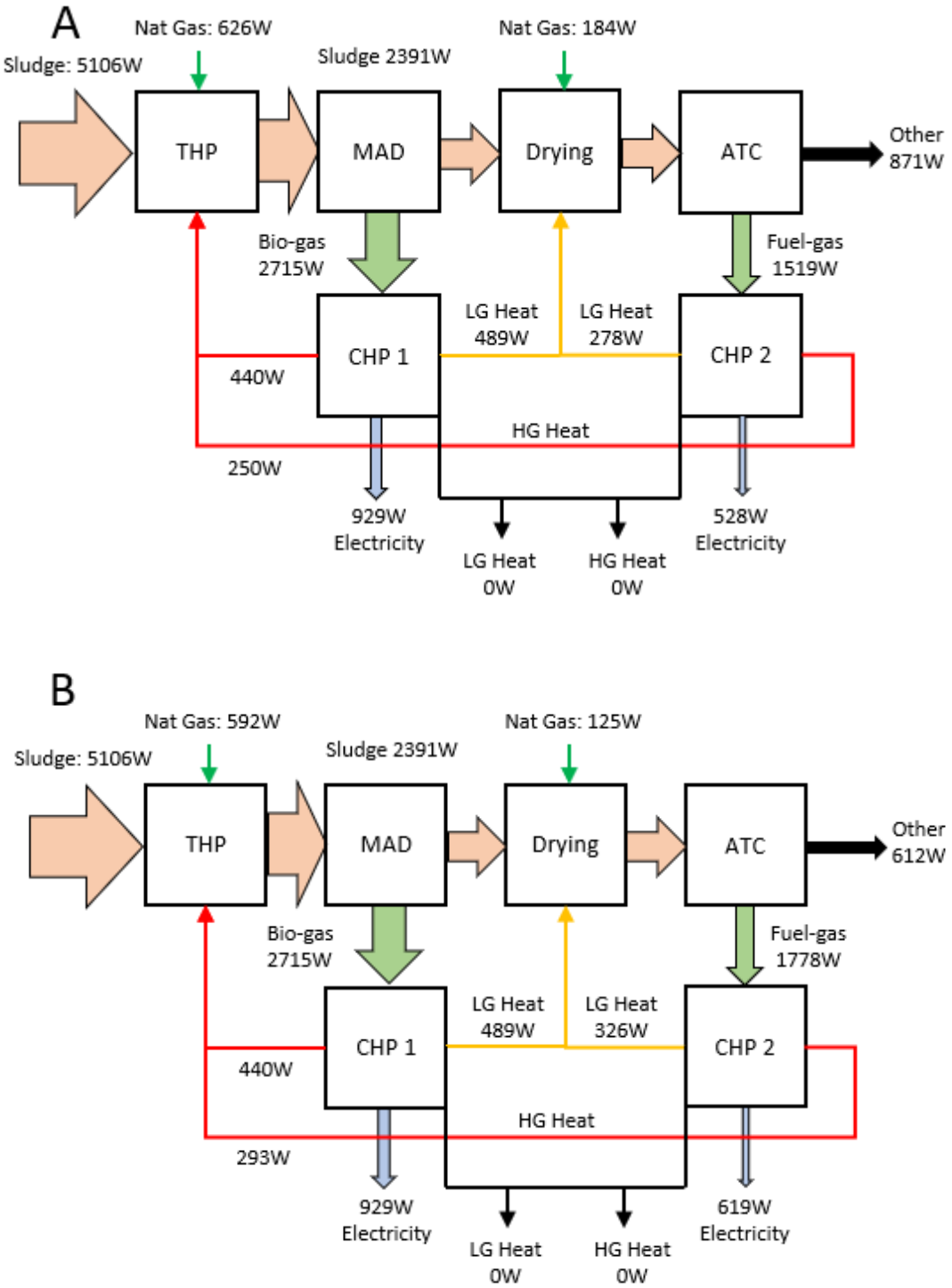


Figure 10-2: Gross energy flows of THP-pyrolysis at 850ºC for A) XS-6 and B) XS-9 biosolids. Based on data obtained from Crossness STW, laboratory-scale pyrolysis and assumptions from Mills (2015) and personal communication (2021). Units based on feed-rate of 1kg DS hour^{-1}.

Given the large requirement for steam at Crossness STW, pyrolysis could be used solely for heat generation. For example, the volatiles (fuel-gas, tar, and contaminants) could be oxidised through combustion to produce high-grade heat for steam production in a boiler. Alternatively, a non-condensing steam turbine could produce small quantities of power and low-pressure steam. The low-pressure steam could then be used directly for THP. Excess heat could also be used for drying purposes. From an operational perspective, there are many advantages to this approach, the complexity of gas treatment would be minimised, and contaminants eliminated. In addition, the natural gas requirements could be reduced or eliminated.

To calculate the conversion efficiency from volatiles to heat, following combustion, fuel-gas (LHV) and condensable liquids (LHV) must be known. The LHV of the liquids fraction was estimated from its elemental composition (table 7-16) using a method outlined by Cooper et al. (1999). The measured HHV of the liquids at 850ºC was 23.5 MJ kg^{-1} whilst its estimated LHV was 20.0 MJ kg^{-1}. When adjusted for mass yield, the LHV of the liquid fraction was 414 Wh kg ds^{-1}. Together, the volatiles have an energy content (LHV) of approximately 66.7% of XS-6 (Table 10-3)

Table 10-3: Energy content of XS-6 fuel-gas and liquids

	SSC	Liquid	Fuel-gas
HHV (kWh tds^{-1})[1]	1263	487	3197
XS-6 (HHV)	25.4%	9.8%	64.3%
LHV (kWh tds^{-1})	-	414[2]	2906
XS-6 (HHV)	-	8.3%	58.4%

[1]Based on laboratory measurements, mass balance of char, liquid, and fuel-gas (HHV) equals 99.5%. See figure 7-5 for more information.

[2]Estimate based on elemental composition and method outlined by Cooper (1999)

The values presented in table 10-3 were used to estimate the energy balance based on 1kg DS^{-1} $hour^{-1}$ of raw sludge at Crossness STW (Figure 10-3). The experimental data presented within table 10-3 had an imbalance of 0.5% of feedstock (HHV), this was assumed to reside in the non-volatile fraction. Unlike figure 10-2, the efficiency of the waste heat boiler was increased to 80% because of the high temperature of the gases produced during combustion. This may be an underestimate and values up to 90% may be feasible, however it is consistent with the approach used by Mills (2015) for sewage sludge incineration.

Figure 10-3 demonstrates that the steam requirements for THP could easily be met with up to 384Wh of spare steam capacity. A small quantity of heat was required to balance site drying requirements.

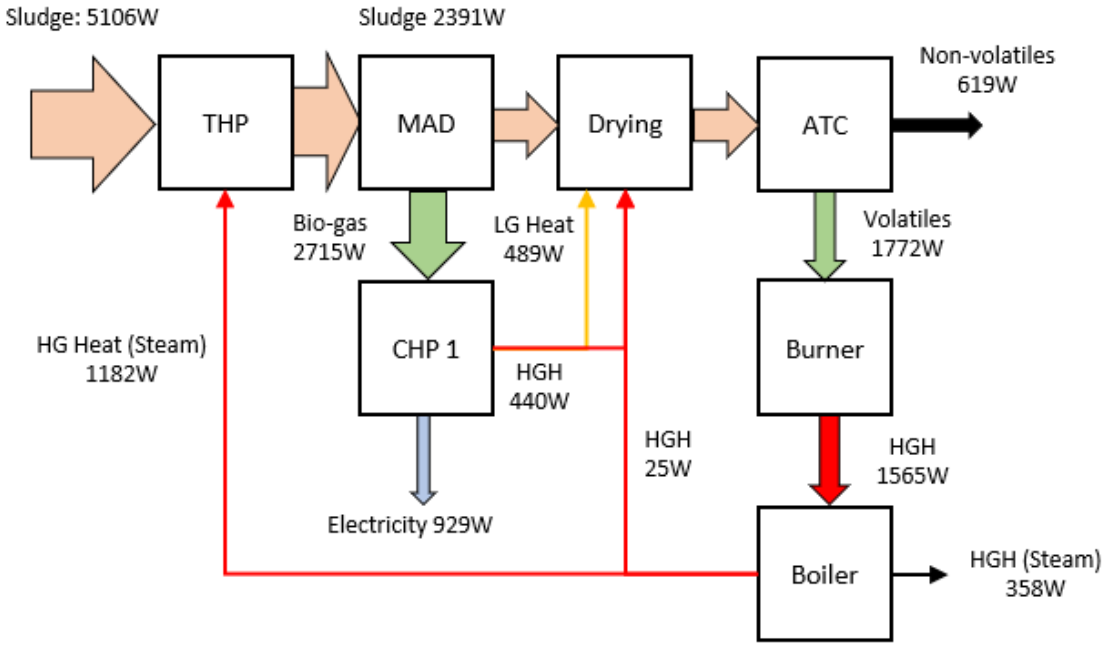


Figure 10-3: Gross energy flows of THP-pyrolysis at 850ºC for XS-6 biosolids. Based on data obtained from Crossness STW, laboratory-scale pyrolysis and assumptions from Mills (2015) and personal communication (2021). Units based on feed-rate of 1 kg DS hour^{-1}.

From an electrical perspective, this configuration only achieves a GCE of 929Wh kg DS^{-1} or 18.2%, whilst the NCE is 512Wh kg DS^{-1} (10%). As the CO_2e emissions factor for electricity drops below natural gas, this configuration may provide a viable method for reducing the consumption of natural gas. The pyrolysis unit could be sized solely to meet site heat requirements, with excess biosolids being recycled to land. Immediate combustion of the volatiles could also facilitate the co-disposal of other wastes, for example FOG and screenings. Although a bespoke permit would be required and to avoid contamination of the SSC, a separate waste screenings pyrolyser would be required. Since this configuration produces an excess of thermal energy, it also facilitates alternative methods of converting biogas to energy. Biogas is a relatively clean fuel, containing small quantities of H_2S and siloxanes which are typically removed with an activated carbon filter. Once clean, biogas may be suitable for conversion into electricity and heat in a solid oxide fuel-cell (SOFC) which have ECEs of approximately 50-60% (Saadabadi et al., 2019). Several pilot-scale and demo-scale fuel-cell plants have been operated in recent years, including: the Biocell project (Barcelona, Spain) the SOFCOM demonstration project (Torino, Italy) the BioZEG pilot plant (Saadabadi et al., 2019). Since SOFC utilises H_2 and CO as fuels, the CH_4 in biogas would require reforming to prevent carbon deposition within the cell.

For biogas, the conversion of CH_4 to H_2 and CO would most likely be conducted using catalytic dry reforming possibly supplemented with steam reforming or POX. A comprehensive review of the reforming steps is detailed by Saadabadi et al., (2019). At present, SOFC's for biogas

conversion are unlikely to be reliable or financially feasible because of carbon deposition issues during reforming, sensitivity to contaminants and the high cost of the catalysts used. However, the development of novel low costs catalysts and technological development could change this in the future. SOFC could also convert contaminants present on STW into additional energy, for example ammoniacal-N (Xu et al., 2017).

10.1.2.3 Raw pyrolysis

A central premise of the work conducted by Mills (2015) is that the combination of different technologies (e.g. THP, MAD, dryers, and pyrolysis) could achieve a higher overall NCE because all the waste heat generated could be utilised and higher DS (%) could be achieved. However, this creates a relatively complex process stream. ATC technologies could be used in place of digestion. Raw sludge pyrolysis was conducted at 850ºC with a dwell time of 120 seconds and feed-rate of 2.6 kg DS hour^{-1}. The results are summarised in Appendix 4.

10.1.3 Summary

Table 10-4 summarises the GCE, NCE, and the NCE (Adjusted) for the different process configurations presented in section 10.1.2. The Adjusted NCE was calculated by applying an opportunity cost for natural gas consumption, this was calculated by assuming that natural gas (LHV) could be converted into electricity in a CHP engine with an efficiency of 40% of gas (+5% parasitic load).

Table 10-4: Gross and net conversion efficiencies for different sludge treament configurations based on the HHV of Crossness sludge[1]

Process	ATC energy Conversion	GCE	NCE	NCE (adjusted)
THP	-	18.2%	15.3%	9.7%
THP-Pyrolysis	*Gas engine (CHP)*	28.5-30.3%	20.4-22.2%	14.9-17.3%
Raw-Pyrolysis		30.3%	19.4%	15.9%
THP-Pyrolysis	*Thermal oxidiser and waste heat boiler*[2]	18.2%	10.0%	10.0%
Improved DS (%)				
THP-Pyrolysis[3]	*Gas engine (CHP)*	28.5-30.3%	20.6-22.3%	16.4-18.3%
Raw-Pyrolysis[4]		30.3%	20.1%	20.1%

[1]Based on the average Crossness raw (HHV) of 18.4 MJ kg^{-1} (see section 10.1.2)
[2]Thermal oxidiser for steam production only
[3]Improved DS (%) to 33.4% for XS-9 and 34.6% for XS-6, the minimum requirements to operate the process without dryer support-fuel.
[4]Improved DS (%) to 36.2% for XS-Raw, the minimum requirement to operate the process without dryer support-fuel.

Table 10-4 shows that GCE, NCE and adjusted NCE of the configurations presented vary widely because of differences in the electrical and thermal parasitic load. Based on the current performance of Crossness STW, the highest GCE was achieved for THP-pyrolysis and raw-pyrolysis, which similar GCEs. The performance of the processes that utilise pyrolysis are dependent on the DS (%) of the raw or digested cake. To eliminate supplementary fuels for drying the pyrolysis feedstock, a minimum DS (%) for digested and raw cake of 33.4-34.6% and 36.2% are recommended, respectively. Once these thresholds are reached, THP-pyrolysis achieved a NCE of between 20.6-22.3%, however, because of high natural gas consumption for the THP step, the adjusted NCE was reduced to 16.4-18.3%. In contrast, raw-pyrolysis could achieve a NCE and adjusted NCE of 20.1%. At present, there are likely significant technical challenges associated with fuel-gas cleaning, therefore the most feasible process at present would be THP-pyrolysis with oxidation of the fuel-gas in a burner and the production of steam for THP in a waste heat boiler. However, this achieved a NCE similar to THP, albeit without fossil fuel consumption.

Chapter 11: Discussion, Conclusions & Future Work

11.1 Discussion

11.1.1 Introduction

The overall goal of this research was to explore the potential for pyrolysis to dispose of digested sludge and convert it into value-added products, including fuel-gas and char. This involved the design, construction, and operation of a laboratory-scale pyrolytic gasification plant, in order to explore its practical application. A key-driver of this research is the dependence of the water industry on land recycling to dispose of digested sludge. The conversion of digested sludge to fuel-gas and char provides alternative value recovery and disposal options to conventional biosolids recycling.

11.1.2 Feedstock

Raw sludge contains a variety of macromolecules, including: fibre, protein, lipids, sugars, and starch whose digestibility varies. Because of its high concentration in surplus activated sludge and its poor digestibility, protein is expected to be dominant in digestate. Char formation is macromolecule dependent, with lignin expected to contribute most significantly, and other macromolecules contribute comparatively little. The devolatilisation of sludge is approximately 85% complete at ≤568^{o}C (Figure 6-1) because of macromolecular dehydration and depolymerisation reactions. This suggests that pyrolysis alone can achieve high conversion of sludge to volatiles without the requirement for oxidants. A unique feature of sludge pyrolysis is the material's high concentration of both N and S compared to other feedstocks. Their presence influences the properties of the gas, liquids and char produced.

11.1.3 Sludge pyrolysis

The feed-screw, screw-auger and heating systems on the laboratory-scale pyrolytic gasification plant all performed reliably. A minor issue was friction between the auger-shaft and mineral-based packing materials, which caused a high-pitched squealing noise in operation. Future development may opt for graphite to reduce friction. The process critical issues were chocking of the gas-outlet pipework (Figure 5-8) and the blockage of downstream pipework with soot-tar composites. These issues can be resolved by routinely or continuously gasifying build-ups. Design features can also reduce the incidence of blockages, including: ascension pipework design and sealed collecting mains (Figure 5-13 and 2-7). Alternatively, tar condensation can be avoided by immediately oxidising the hot-gas to produce heat (e.g. Clinipower Ltd.) or tar concentrations could be minimised by reforming the hot volatiles at high temperatures in a secondary treatment step. The combination of soot and refractory tars is thought to lead to the formation of particularly challenging blockages; therefore, the deposition of these products together should be avoided. Alongside product minimisation through gasification/reforming, early condensation of vapour can be minimised through temperature control of downstream pipework.

Approximately 50ppm of Ni (Table 8-1) was detected in Py-G SSC, it is not clear whether this was present within the feedstock or accumulated because of attrition between the stainless-steel reactor and char during conveyance. This warrant future investigation.

11.1.4 Char

11.1.4.1 Char and mass and elemental yields

Char yield quantification was an objective of this research and is important because post-pyrolysis char must be disposed of or recycled. For Py-G, once char carbon stabilised at ≥700°C the yield only varied slightly (43.2-46.0% Wt.). Approximately one-third of sludge-C stabilised in char (Table 7-12), although the slower heating-rates for Py-B and non-isothermal Py-G increased this slightly. XPS analysis of char produced at 700°C showed >98% of char carbon was organic and consisted of graphitic (C=C) and heterocyclic organic structures (e.g. C=N) (section 8.1.3.1).

Py-B was expected to enhance char yields compared to Py-G because of the slower heating rates used and longer retention times. Both processes char yields were similar because char carbon retention was similar, however there were particularly large differences in N and S retention. For example, at 700°C and 850°C, Py-B:

- Increased char-C retention modestly, by 6% and 3.8%, respectively (Table 7-12);
- Increased char-N retention by 15.5% and 6.9%, respectively (Table 7-14);
- Decreased char-S retention by 26.3% and 35.4%, respectively (Table 7-15);

Increased N retention is thought to be because of greater amine condensation. XPS analysis of Py-G char produced at 700°C identified condensed heterocyclic structures within SSC, including pyridinic-N and pyrrolic-N (Figure 8-3), which likely originate from proteins. These structures exhibited relatively low stability because the char-N yields decreased with increased temperature for both Py-B and Py-G (Table 7-14). Heterocyclic-N will influence the surface chemistry of char, therefore, the heating rate and temperature could modify the properties of the char.

Char-S retention was lower for Py-B than Py-G. The mechanisms for this are unclear, however XPS analysis of Py-G char showed S is retained predominately as sulphates, condensed heterocyclic-S structures (e.g. thiophene) (Figure 8-5) and small quantities of sulphides. Unlike heterocyclic-N, condensed thiophene is expected to be extremely stable because of the structure's high resonance energy per hydrogen atom (Louden & Parise, 2015) (Bruinsma et al., 1988). Char-S retention is a major advantage of Py-G because it suppresses the generation of contaminants, including: H_2S and SO_2.

N and S electronegativity means their presence within condensed carbon rings will create charge imbalances across the char structure. For example, the dipole moment (D) and relative permittivity (ε) of pyridine, pyrrole and thiophene compounds are: ε = 12.3, D = 2.215; ε =8.00,

D = 1.74; and ε = 2.74, D = 0.55 respectively (Dean, 1999). The presence of polar surface groups within SSC means the material will have an affinity for charged cations (e.g. NH_4^+, Zn^{2+}, K^+) or polar organic compounds (e.g. phenol). Aprotic heterocyclic structures such as pyridine and thiophene have a lone-pair of electrons that are available for donation. These lone-pairs may undergo protonation or oxidation. For example, if the pyridine structure in SSC is protonated it may form a pyridinium structure, allowing it to bind to anions such as phosphate. Carbonaceous materials containing surface pyridine/pyrrole groups are currently being investigated for their potential applications in catalysis, particularly the oxygen reduction reaction to form hydrogen peroxide (Zhang et al., 2020). Many of these studies suggest surface heterocyclic groups undergo protonation in acidic media (Wan et al., 2015).

At ≥900ºC, char-N is expected to stabilise at graphitic-N because its yield stops decreasing with increased temperate. If pyridinium structures with anion exchange capacity are formed within acidulated char, the elimination of pyridine from char may explain why SSC produced ≥900ºC had greater formic-acid P availability (Table 9-6). Although further experimentation is required to validate this.

11.1.4.2 Char carbon

Aromatic condensation and ring-size help determine the long-term stability of char. The ring-size can be directly determined by NMR, however less complex measurements correlate with NMR, including: the molar H:C ratio and thermal stability of the material. The molar H:C of SSC decreased up to 700ºC because of devolatilisation. It then undergoes further reductions above 800ºC, which is thought to because of the elimination of pyrrolic-N and further condensation. Thermal stability analyses corroborate, the R_{50} and Q_3 indexes both show a sharp increase in char stability above 800ºC. Chemically, condensed heterocyclic-N structures may be less stable than heterocyclic-S or graphitic structures because of their lower resonance energy. Supporting this Santin et al., (2017) also found that char Q_3 values increased with temperature for biomass samples which could be due to elimination of O-heterocyclic groups. Py-G char (≥600ºC) is a Class B candidate for C sequestration in soils which is equivalent to many of the biomass derived chars presented in the literature (see section 8.1.5.2). The mean residence time of SSC in the environment is uncertain, however it's expected to range between several hundred to thousands of years (section 2.3.3.2).

The addition of biosolids to soil is also a form a carbon sequestration because the material undergoes stabilisation processes such as humification and aggregate formation that increase the materials long-term stability (section 9.1.1). Pyrolysis processes emit C as soon as the gas is combusted, however the heat released through oxidation facilitates energy recovery. In contrast, when sludge is recycled to land, it will undergo rapid initial rates of mineralisation (up to 46% - Section 9.1.1) and then decompose more slowly over-time. The CO_2e value for XS-6 and XS-9 biosolids was estimated at between £22.9-24.8 t^{-1}. Based on the findings of a Roth-C carbon model

(Mondini et al., 2017) and long-term field trials (Johnston, 1975) (Tian et al., 2009) the long-term retention (26-100 years) of biosolid-C within soil was estimated at between 26.2-36.6% (section 9.1.1). If XS-6 and XS-9 behave similarly to the biosolids in these studies, the long-term CO_2e value of these materials may range between £5.3-9.4 t^{-1} (Table 9-1). Whilst the chars of XS-6 and XS-9 are likely to retain a CO_2e value of between £7.5-9.1 t^{-1} over the long-term, assuming they do not undergo long-term mineralisation. Unlike SSC, the degradation of sludge will depend on a complex range of factors, such as field management, agronomic activity, field-C stocks, climate, and many others. Over the medium-term (26-100 years) and long-term (<millennia) there is a high probability SSC will retain more carbon than biosolids and this difference will likely increase with time. The main issues for carbon-sequestration using biosolids are (see section 9.1.1 for further explanation):

- The finite capacity of soils to retain carbon
- The reversibility of the stored carbon
- Site specific issues

11.1.4.3 Char hazard assessment

Char hazard assessment (chapter 8.2) suggested:

- Char is flammable (H228); however, ignition may be difficult because of its high ash-content and absence of volatile organic matter. Char dust can produce an explosive atmosphere (Table 8-7) and is classified as a combustible non-conductive dust (Group IIIB). However, char retains the feedstocks structure during pyrolysis, therefore the risks of it forming an explosive atmosphere are minimised and could likely be managed.
- AEM sulphides and other metal sulphides are classified within WM3 as EUH031 (releases toxic gases in contact with acid releases flammable gases) (Table 8-8) and SSC was found to release H_2S in contact with dilute citric acid or mineral acids (Section 9.3.1). Therefore, SSC will be classified as EUH031.
- Metal sulphides may also be ecotoxic (H400). Mild acid washing of SSC to <pH 9.0 may be effective at converting acid-hydrolysable sulphides into H_2S (Figure 9-5), eliminating the risk posed by these compounds. Mild leaching with sulphuric acid may also convert relatively insoluble forms of P such as TCP/HAP into more soluble forms (e.g. MCP/DCP), whilst any released calcium will precipitate as gypsum (section 9.3.2). If used for agriculture, it may be preferable to adjust the pH of SSC to the zone of maximum phosphorus availability (~pH 6-7) and this would not cause any heavy metal leaching (Table 8-12).
- Based on the worst-case scenario (as outlined in WM3), char would have the following hazard codes: H302, H314, H318, H319, H400 and H410, which means the material is

also ecotoxic, acutely toxic and corrosive. However, this scenario is unlikely to represent char metal speciation because of reduction and sulphidation reactions. The main heavy metals present within char were not leachable in dilute HNO_3 at pH 4 (NEN 7371) (Table 8-12), which is supposed to replicate the most extreme leaching conditions in the environment. This is likely because of their inherent insolubility or subsequent re-precipitation as phosphates (Table 9-15). Neither Zn/Cu sulphide are classified as ecotoxic by the European chemical's agency. Lead sulphide is classified as ecotoxic; however, the highest concentration of Pb within SSC was 270 mg kg^{-1} (PbS = 312 mg kg^{-1}), and this does not exceed the threshold value for H400 of 1000 mg kg^{-1}. If Cu and Pb are reduced during pyrolysis to their elemental forms, neither of these metals would exceed hazardous waste thresholds.

To conclude, fresh SSC may be hazardous because of its EUH031 classification, however these could be removed by pH adjustment. The worst-case WM3 classification for SSC is unlikely to representative. The heavy metals in SSC are unlikely to be hazardous (e.g. ecotoxic) in the concentrations present because of their expected chemical form.

11.1.5 Char phosphorus

11.1.5.1 Introduction

Our agricultural systems depend on the addition of P to soil to maintain high yields and its value in this respect cannot be understated. However, there are 287 years of conventional and 1250 years of non-conventional rock phosphate resources available, therefore the current concerns about global P scarcity are possibly over-stated (section 9.2.1). Nonetheless, phosphate supply and demand are inelastic, meaning that the market price is sensitive to supply disruptions. Most P fertilisers contain water-soluble salts; however there is growing awareness that slow-release P fertilisers containing water insoluble, but organic-acid soluble salts, such as DCP, TCP and struvite may be more efficient fertilises because they are not prone to immobilisation. Water-soluble P salts may also lower arbuscular mycorrhizal fungi root colonisation, which reduces the soil volume roots access and may make plants more dependent on P additions rather than diffuse sources.

11.1.5.2 Phosphorus: Utilisation

Crossness contains approximately 2.6% P by weight (Table 6-8) and two-thirds is in a plant available form (Figure 9-6). Therefore, biosolids recycling helps minimise the reliance on external P sources. Biosolids recycling has several limitations, for example; the presence of emerging contaminants, public perception, odour, competition with other bio-wastes and nitrate vulnerable zones (sections 1.2.1.3 & 1.2.1.4). Moreover, sludge is produced throughout the year, whilst the demand for both N and P is seasonal.

Pyrolysis concentrates P in the char (5.6% Wt) (Table 8-1). However, its availability was reduced (Figure 9-6), only surpassing the minimum requirements outlined in the STRUBIAS proposals when pyrolysed at ≥900°C (section 9.3.1). Suppressed P availability is likely because of:

- Increased alkalinity.
- Conversion of organic P into insoluble salts, for example: ATP into HAP.
- The potential formation of anion exchange capacity when char is exposed to acids (e.g. pyridinium structures). Further work is required to assess whether this capacity is exchangeable.

11.1.5.2.1 Phosphorus: Extraction

The P content within char is almost entirely extractable with mineral acids (section 9.3.3). Leaching char with HCl or H_2SO_4 may be advantageous because Cu and Pb are not solubilised. The inability of these acids to oxidise elemental Cu (section 9.3.3.7) and the relative insolubility of Cu/Pb sulphides (Table 9-15), chlorides and sulphates helps explain this phenomena.

All the mineral acids solubilised moderate quantities of Zn, although tables 9-10, 9-12 and 9-14 demonstrate that its extraction can be minimised. For example, decreased char particle size and increased stoichiometric ratio had a strong positive effect on Zn extraction (Figure 9-13) (Figure 9-18) (Figure 9-22). Controlling these factors limits co-extraction and when optimised >90% P extraction and <40% Zn extraction is achievable.

The co-extraction of Al, Fe and Zn makes P recovery through neutralisation challenging. However, oxalate precipitation and solvent extraction could be used to purify the leachate and facilitate the successful recovery of P fertiliser (section 9.3.4). Techno-economic analysis is required to assess whether char leaching, and leachate purification are viable and how it compares to less intensive P recovery (e.g. application of unaltered or upgraded SSC to land – section 9.3.2). Techno-economic analysis should include novel non-agricultural applications for recovered phosphate, for example – the production of lithium iron-phosphate batteries since the recovery as iron phosphate would be technically less complex and may offset potentially unsustainable high demand from the power sector (Spears et al., 2022)

11.1.5.2.2 Phosphorus: Land application

Char application to agricultural land is an alternative method of phosphate recycling. It would minimise resource use and be less technically complex. Enhancement of char properties could be achieved through partial acidulation with H_2SO_4. This would convert insoluble P salts (e.g. hydroxyapatite) into more soluble forms (e.g. dicalcium phosphate), eliminate acid-hydrolysable sulphides, incorporate plant available S, and lower heavy metals concentrations. This approach

has been proposed before for rock phosphate because it is simple, cost effective and produces a fertiliser with both rapid- and slow- P release characteristics (Rajan and Watkinson, 1992).

The STRUBIAS proposals would consider SSC a solid organo-mineral phosphate fertiliser (PFC-1). However, human-derived waste streams are excluded from the positive input list because of the broad-range of emerging contaminants that may be present. The main difference between sludge and "natural" feedstocks is that sludge may contain small concentrations of organic contaminants. Of these, only halogenated organic contaminants (e.g. flame retardants, pesticides, PCBs and PFOA) would be expected to form contaminants significantly different to those produced by lignocellulosic biomass or manure. For example, chlorine may form chlorinated organic contaminants such as polychlorinated dibenzo-p-dioxins (PCDD) and polychlorinated dibenzofurans (PCDFs) which are mutagenic and toxic. Wakefield (2010) reports that these contaminants typically form between 500-700ºC and are only destroyed after heating to 800ºC for prolonged periods. PFAS compounds may also be present within sludge, including Perfluorooctane sulfonate (PFOS) and perfluorooctanoic acid (PFOA) which are persistent organic contaminants. However their respective boiling points are just 260ºC and 192ºC meaning they will volatilise during pyrolysis. Xiao et al. (2020) investigated the thermal stability of a range of PFAS compounds, PFOA decomposed at temperatures as low as 200ºC, whilst PFOS required temperatures as high as 450ºC to decompose. Once decomposed, these compounds formed volatile organofluorine tars, however by 700ºC, >99.9% of the PFOA and PFOS compounds and their tars had been eliminated. Lignocellulosic biomass, manures and sludge all have the potential to form contaminated char. For example, amines form aromatic amines above 150ºC which are toxic, mutagenic, and carcinogenic (section 2.3.3.2). The pyrolysis conditions and reactor design proposed during this project are likely to minimise the retention of extractable organics. For example, organics are likely to volatilise at high temperatures. The highest heating temperature of char does not guarantee the full removal of extractable organic compounds. For example, carbon black is produced between 1320-1540ºC, however it has been shown to contain solvent extractable PAHs, although these adhere strongly to the carbon and are not bio-available (section 2.3.3.1). The residence times used during carbon black manufacture are typically very short (e.g. <1s) and the carbon is rapidly quenched with water to limit carbon particle growth, which is not desirable for the materials applications (Witt, 1968). The char in this project was produced with a residence time of <120s, which will favour the devolatilisation of residual organics. In addition, bulk devolatilisation will occur in furnace 2 (Figure 5-3), meaning in furnace 3 char will be heated in the presence of limited amounts of volatiles limiting the potential for contamination further.

The requirements outlined in the STRUBIAS proposals allow materials to be processed at low temperatures (>180ºC) and for as little as 2-seconds (Table 2-7). The formation of carcinogenic heterocyclic compounds occurs at temperatures as low as 150ºC (section 2.3.3.2). The premise of excluding SSC from the STRUBIAS proposals because of trace organic contaminants in the

feedstock, but allowing char production from other wastes, under conditions that facilitate the production of carcinogens, without the required temperatures and residence times to facilitate their full volatilisation and decomposition may be inconsistent. Rather than exclude SSC from land application; it is recommended that STRUBIAS could include a test that measures the solvent extractable organics within chars (For example - Mckenna et al., 2021). If extractable organics are present in concentrations that pose a health or environment risk, these organics may be qualified and quantified by the producer. However, if they are not present, the material may be safe, pending agronomic trials with sensitive soil biota (e.g. earthworms).

Annex 1B of Council Directive 86/278/EEC lists the limit values for heavy metal concentrations in sludge for agriculture. These values are far higher than the limit values outlined by STRUBIAS. For example, the limit value for Cu in Annex 1B ranges between 1,500-1,750 mg kg^{-1} (European Commission, 1986), whilst the limit set for PFC 1 chars is only 600 mg kg^{-1} (Table 9-5). SSC contained between 829-897 mg Cu kg^{-1}, therefore it narrowly exceeds the concentration limit for STRUBIAS but not for sludge. Individual countries can set stricter limits; however, both the UK and Ireland have never done this for sludge. The Sludge (Use in Agriculture) Regulations (1989) outline the maximum addition rate of heavy metals to soil. Based on these values, Table 9-3 showed that the limiting metal in SSC was Cu, with a maximum annual application rate of up to 8,400 kg SSC ha^{-1} yr^{-1}. However, to meet the crop phosphate requirements for selected grassland, arable and horticultural crops, only 62-1113 kg ha^{-1} yr^{-1} of the material would be required. This is strongly indicative that the heavy metal concentration in char does not pose a risk when applied in agriculture.

Further:

- Table 8-11 suggests SSC is non-hazardous and the concentration of heavy metals in the material are below the concentration required for hazard waste assessment or far below the relevant cut-off points.
- Table 8-12 shows that the worst-case leaching test, NEN 7371, did not solubilise detectable concentrations of heavy metals from SSC.

The STRUBIAS heavy metal limits maybe amended in line with those in sewage sludge applied to land so that a more consistent approach is used. In addition, the chemical form of these elements could be considered, which is common practice for contaminated land or hazard assessment, as described in WM3, published for hazardous waste assessment.

11.1.6 Pyrolysis: Energy

11.1.6.1 Digested sludge

The objectives of this research included:

- Mass yield quantification

- The characterisation of the gas produced and the identification of the optimal conditions for energy recovery

The gas mass yield for Py-G increased with temperature, primarily between 600-800ºC, from 28.5% to 47.7% (Table 7-3) with a further increase between 950-1000ºC to 50.4%. Heating char and volatiles above 700ºC and 800ºC, respectively, may be unnecessary because carbon, the main energy carrier, stabilised in char and liquids above these temperatures. At 800ºC:

- The conversion of sludge (HHV) to gas (LHV) was 58.7% efficient. The relatively energy dense gas (19.7 MJ LHV m^{-3}) had high concentrations of CH_4 (19.6% v/v), C_2H_4 (8.3% v/v) and H_2 (30.9% v/v) (Table 7-5 and 7-6).

At 1000ºC, H and C were released from the liquids as syngas. The volume of H_2 increased disproportionally compared to CO, suggesting non-organic hydrogen sources (e.g. NH_3 and steam) may contribute significantly. At 1000ºC:

- The conversion of sludge (HHV) to gas (LHV) was 59.3% efficient. The gases energy density was lower (16.7 MJ LHV m^{-3}) because of its high concentrations of H_2 (38.7% v/v), CO (28.5 v/v) and CH_4 (13.2% v/v).

The parasitic electrical load at 1000ºC was 47% higher (Table 7-10), therefore operation at 800ºC was optimal from a net energy perspective (Table 7-11).

11.1.6.2 Raw sludge

Although not the focus of this research, pyrolysis could treat raw rather than digested sludge. XS-raw was pyrolysed at 850ºC, the gas composition was similar to that obtained from digested sludge, however the concentration of H_2 (23.3% v/v) was lower and C_2H_4 (13.4 v/v) higher (Table 12-2 – Appendix 4). The overall conversion of XS-raw (HHV) to fuel-gas (LHV) was 79.7% which is higher than the results obtained for digested sludge because of the high gas yields (69.4%) and energy density (LHV = 22.8 MJ m^{-3}). Lipids undergo a 60-65% reduction during digestion (Table 6-2) and unsaturated fatty-acid chains are less stable that saturated fatty-acid chains because the C=C bonds cause bends in the chain's structure. Unsaturated fatty-acids may be preferentially decomposed during digestion, resulting in lower ethylene concentrations in fuel-gas produced from digested sludge compared to raw sludge. For XS-raw, the liquids yield (12.8%) was higher than digested sludge. Reduced volatile retention times (because of high gas yields) and the low concentration of ash within the feedstock may have contributed to lower tar conversion. The relatively high residual liquid yield suggested the conversion of sludge to gas could be increased further at higher temperatures. Raw sludge pyrolysis should be explored further because it offers great potential to simplify the treatment process on sewage treatment works.

11.1.7 STW: Site energy balance

An objective of this research was to assess how pyrolysis could influence the overall site energy flows and performance at Crossness STW. Based on the current performance of conventional THP at Crossness STW, the results of this project suggest that if pyrolysis was conducted at 850^{o}C after digestion it could increase: GCE by 57-66%, NCE by 33-45% and adjusted NCE by 54-78% (Table 10-4). Previous research suggested that THP-pyrolysis with gas conversion in engines could eliminate parasitic gas consumption. However, section 10.1.2.2 and figure 10-2 suggest that at Crossness STW this is not the cause because:

- Steam consumption was elevated
- Digested cake DS % is lower
- Gas engines produce comparatively low temperature gases, therefore high-grade heat recovery is less efficient than suggested
- Pyrolysis achieved lower energy conversion of sludge to fuel-gas than previously suggested.

The parasitic thermal load for sludge drying could be eliminated if the cake was increased from 30.9% to between 33.4-34.6%. This is likely achievable if dewatering was optimised since other sites have achieved higher DS% cake, for example Oxford and Chertsey STW (Fountain et al., 2013). An alternative approach is raw-sludge pyrolysis, which could increase GCE, NCE and adjusted NCE by 66.5%, 26.7% and 63.9% respectively. Figure 12-1 showed that raw-pyrolysis had a high parasitic thermal load, because of drying requirements, however, these could be eliminated if a raw cake DS (%) of just 36.2% was achieved. Therefore, an adjusted NCE of up to 20.1% could be achieved for raw sludge in a single treatment step, which is more than double the current performance of THP at Crossness STW.

Crossness STW currently has a thermal parasitic load of approximately 831Wh kg ds^{-1} because it utilises THP to pre-treat sludge prior to digestion (Figure 10-1). Rather than convert fuel-gas to combined heat and power in a gas engine, immediate oxidation of the volatiles (e.g. gas and liquid) and conversion of the heat to steam in a boiler could eliminate this parasitic load. In addition, this process would not release additional carbon because carbon released during combustion would have been released from biosolids when applied to agriculture. Compared to the current performance of THP-pyrolysis at Crossness STW, this process would reduce NCE by 34.6% but there would be a marginal increase in adjusted NCE. From an energy perspective, this is not a strong case, however, it could help divert sludge from land and replace the use of parasitic fuel (e.g. natural gas or biogas).

11.1.8 Pyrolysis: Gas treatment

An aim of this project was to determine the pyrolysis conditions that minimised process contaminants and to explore the operational challenges associated with these contaminants within the reactor and during subsequent gas clean-up. The main contaminants formed during pyrolysis include:

- Soot
- Tar
- Nitrogen gases (e.g. HCN/NH_3
- Sulphur gases (e.g. H_2S)

11.1.8.1 Soot removal

The co-deposition of soot and tar must be avoided to avoid blockages. To minimise tar condensation, the outlet pipes and cyclone may need to operate above the tar dew-point. Alternatively, there must be a mechanism to routinely gasify any deposited build-ups. In addition, the ascension pipework should be simplified to minimise the risks of tar deposition (Figure 5-13).

11.1.8.2 Tar removal

Oil scrubbers paired with demister technology are currently proposed for condensable liquids extraction. These technologies use a combination of cooling, condensation, and coalescence to remove entrained vapours. From 800-1000^{o}C, the yield of condensable liquids ranged between 3.7-8.1% Wt. (Table 7-3) which equates to 57-151 g m^{-3}. To achieve "syngas" EOW status, the gas must contain <1.45 and <1.20 mg m^{-3} of aromatic hydrocarbons at 800^{o}C and 1000^{o}C respectively (Table 7-20). Therefore, a 99.999% decrease in vapour-phase aromatics is required. The coal-gas industry previously identified that only electrostatic precipitators could eliminate entrained vapours (section 2.2.1.3) although demister technology may be effective at promoting coalescence. Using packing material is high-risk however, and a method of cleaning the packing is required to prevent tar build-ups.

Failure to remove entrained vapour has environmental and human health risks. For example, tars could contaminate scrubbing liquors. If HCN is removed with chlorinated oxidising agents, tar carry-over could form secondary pollutants. Like dissolves like, therefore polar phenolics and partially polar heterocyclic compounds represent the largest process risks. For example, phenolics are toxic and can promote tumours (section 2.3.3.2). The low C:N ratio of the liquids at 800^{o}C (C:N = 3.8) suggests heterocyclic-N compounds are concentrated at this temperature. The C:N ratio increased at higher temperatures (e.g. 950^{o}C = 9.4, 1000^{o}C = 18.4) suggesting extreme temperatures eliminate heterocyclic-N (Table 7-17) and may minimise the risk of liquor contamination. However, at 1000^{o}C the H:C ratio of the liquids decreased to 0.55, which is equivalent to large multi-ring PAHs such as anthanthrene ($C_{22}H_{12}$). If similar compounds are formed during Py-G, these may be prone to condensing at high temperature and causing blockages.

Previous work suggested tar elimination required temperatures as high as 1300°C (section 2.3.2.1). The main alternative are reforming reactions using sub-stoichiometric oxygen, steam, and CO_2. Since gasification reactions may be required to eliminate carbon deposits anyway, the conversion of both carbon-deposits and tars may be preferable. Because of the extreme temperatures required to rapidly eliminate tars, it may be cost effective to raise the gas temperature through electric heating and POX reactions. The injection of O_2 into the reactor will consume gas, however the high reactivity of O_2 would improve decomposition kinetics. In recent years, multi-stage processes have been developed that combine medium temperature gasifiers and secondary reformers. Several technologies have been explored for the reforming step, for example: swirl flow reformers operated at 1300°C (Pei et al., 2018) and direct-current plasma arcs operated at 1200°C (Materazzi et al., 2016). The reformer used by Pei et al. (2018) reduced tar from 18.9-33 g m^{-3} to approximately 10 mg m^{-3}. Another advantage of high-temperature processes is that the Boudouard reaction would help reduce the concentration of CO_2 in the gas, which may be beneficial for subsequent H_2S removal if caustic scrubbers are used (section 7.6.1.)

11.1.8.3 Acid-gas removal

11.1.8.3.1 Sulphur gases

The estimated H_2S volume underwent a large increase above 900°C for Py-G (Figure 7-4) because of temperature induced S release from char (Figure 7-7). Likewise, increased heating rates (Py-G > non-isothermal Py-G > Py-B) also increased char-S retention (Table 7-15). Therefore, rapid heating rates to a maximum temperature of 900°C are recommended. The current proposals opt to remove acidic gases (H_2S, SO_2, HCN & HCl) through neutralisation with caustic. However, the fuel-gas CO_2:H_2S ratio exceeds 5, which will compromise the selectivity of the system, leading to CO_2 precipitation and excessive caustic consumption (section 7.6.1). The "syngas" EOW requirements for H_2S are just 0.19-0.22 mg m^{-3} (table 7-20), to achieve this the caustic system will probably need to operate at elevated pH, further compromising selectivity.

For fuel-gas produced at 800°C, at least 20kg of NaOH and 73kg of NaClO would be required to convert the expected concentration of H_2S into Na_2SO_4 tds^{-1} (Table 7-22). Therefore, the current proposals do not appear cost-effective or sustainable. The conversion of H_2S to NaHS is a preferable end-product due to lower overall chemical consumption (9.85 kg NaOH tds^{-1}) and could be resold to paper manufacturers or used as a heavy metal precipitant in a phosphate recovery process. However, low scrubber selectivity will diminish its resale value and without HCN oxidation will be contaminated with NaCN.

To achieve fuel-gas EOW status, hot-gas desulphurisation with regenerative sorbents could be a sustainable approach for achieving bulk H_2S removal. In addition, heavy metal oxides such as ZnO have used to polish liquors and gases to extremely low sulphide concentrations. Regenerative solvents could also be used, but not in the presence of HCN.

11.1.8.3.2 Nitrogen gases

When the amines in sludge proteins are heated, evidence in the literature suggests they form HAAs. These may undergo further decomposition before preferentially condensing within the SSC or volatilising. With increased temperatures, HAAs are expected to decompose into heterocyclics-N (e.g. pyridine), then breakdown into HCN/NH_3, and finally N_2. Figure 7-8 shows that the N within Py-G liquids was highly recalcitrant to decomposition undergoing no yield decreases between 600-750^{o}C. The rapid decomposition of N in Py-G liquids above 750^{o}C will likely cause a sharp increase in fuel-gas HCN and NH_3 concentrations.

Treating NH_3/HCN by in-situ conversion to N_2 may be more sustainable than attempting to remove these gases with chemicals. Section 2.3.2.3 presents evidence from the literature that showed conversion was enhanced by passing the gas through hot chars but increased in the presence of steam. If a screw-conveyer was used for pyrolysis, the pitch of the flights could be adjusted to increase bed thickness after initial devolatilisation, thereby passing hot NH_3/HCN through the char bed and promoting decomposition to N_2. If a secondary reforming step was used to eliminate tars, the high temperatures used and increased presence of both oxidants and radicals may help eliminate HCN/NH_3. This warrants further investigation because it could simplify the gas clean-up.

11.1.8.4 Gas treatment: concluding remarks

For sludge, a novel process design is likely required that draws upon a multitude of successful designs that have been implemented in the past for gas manufacture and treatment. Carbon deposition, tar blockages, cost effective removal of gaseous contaminants and avoidance of problematic secondary waste streams are all issues to be overcome. A secondary reforming zone may resolve many of these issues and this requires further research. In addition, the use of regenerative H_2S sorbents should be explored so that non-regenerative sorbents, such as caustic can be minimised.

11.1.9 Pyrolysis: Regulatory challenges

There are several regulatory challenges that may hinder the adoption of pyrolysis for sludge treatment, for example:

- The full landfill tax is applied to active wastes. Activity is tested by LOI at 440^{o}C (HM Revenue & Customs, 2020), and the aim of this analysis is to identify bio-degradable organic carbon. Char carbon gradually decomposes when heated in air, consequently, char is classified as active waste and landfill disposal is expensive. If properly stabilised, char is not expected to be bio-degradable because it contains condensed aromatic carbon. Observations of charred materials in the environment (e.g. Terra Preta) and NMR studies of biochar suggest condensed carbon may have mean residence times in the environment of thousands of years. On a technical and scientific basis, char should be exempt from the LOI test; however, an alternative test could be introduced to ensure the material has been

sufficiently stabilised. A suggestion is that pyrogenic materials could be tested for "activity" using an alternative test. For example: (i) the recalcitrance index, achieving a class B or higher (section 4.2.3.2) or (ii) thermogravimetric analysis with a suitable retention time, temperature, atmosphere, and weight loss threshold (e.g. 1 hour at 600ºC in a N_2 atmosphere with a weight loss threshold of less than <1%) to ensure volatile removal. The latter may need to be conducted below the temperature where condensed heterocyclic groups are eliminated from the carbon structure. For N this occurred at approximately >700ºC (Table 7-14) for Py-B char.

- Fuel-gas is considered waste; therefore, its oxidation is waste incineration. Consequently, the whole pyrolysis process must comply with the control of emissions; monitoring of emissions; required operating conditions; and reporting requirements outlined for waste incinerators in chapter IV of the IED. These requirements were developed for incinerators, not pyrolysis processes, therefore some requirements may not be suitable. For example, the IED requires the solid by-products to contain - <3% TOC or <5% LOI, which char exceeds. Likewise, the gas must be heated to 850ºC to eliminate dioxins, however these are typically formed during oxidative processes, not pyrolysis. A special provision for ATC technologies is available, however this requires pyrolysis gas to be "purified to such an extent they are no longer a waste' and cause 'emissions no higher than'… 'burning natural gas'. In practice, these requirements require fuel-gas to achieve higher standards than other waste to energy processes. Based on standardised SO_2 emissions, Table 7-21 demonstrates that the limits for fuel-gas are 12x stricter than biomethane and >1000x stricter to biogas combustion on a STW. An alternative mechanism for fuel-gas EOW may be required and biogas rather than natural gas may be a more suitable comparator material.
- The STRUBIAS regulations, explained in detail in section 11.1.5.2.

11.2 Contributions to knowledge

- Pyrolysis has not yet been widely adopted for sewage sludge treatment and there is a scarcity of published data that provides detailed information on the effect of operating conditions on mass and energy conversion and gas composition at a large enough scale for the process to be representative of a demonstration or full-scale process. Chapter 7 presents mass (Figure 7-1) and elemental mass conversion (Figure 7-7 and 7-8) data for pyrolysis. It also presents detailed energy conversion (Figure 7-5) and gas composition data (Figure 7-2) for pyrolytic gasification. Much of this data is unique, providing key information and the foundations to those interested in developing the process further at laboratory and larger scale (e.g. pilot- or full-scale).
- This research provides operational experiences at a large enough scale for the process to be representative of a demonstration-scale process. It shows that ascension pipework choking, and tar blockages are relevant for sludge pyrolysis, providing visual evidence (Figure 5-7 to 5-11) and data on their thermal stability (Table 5-3) to aid their management. It also presents unique safety information that may be valuable for plant commissioning, for example: the fuel-gas flammability range (Table 7-8) and the minimum ignition temperature of sewage sludge char dust (Table 8-7).
- An in-depth hazard assessment of sewage sludge char was presented, which included novel data. For example, XPS quantification of total char sulphides (section 8.1.3.3) and the potential classification of the material as EUH031 (section 8.2.3). In addition, heavy metal leachability was examined using NEN 7371 (Table 8-12) and acid-extraction experiments (Figures 9-9, 9-14, 9-19), which alongside theoretical and literature led to the conclusion that Pb, Cu and Zn in char are likely to be non-hazardous (Table 8-11) because of their expected chemical form.
- The temperature dependence of formic-acid P availability (Figure 9-6) combined with the elemental balance for N and S (Figure 7-7) and XPS identification of heterocyclic-N and -S structures (Figure 8-3 and 8-5) led to the novel suggestion that surface group protonation inhibits char P availability at low pyrolysis temperatures because of the development of anion exchange capacity.
- Extensive char P extraction data was presented in section 9.3.3 which built upon previous work in ash. The novel aspects of this work included the material used and the identification of conditions that maximised P extraction whilst minimising the extraction of Zn.

11.3 Conclusions

11.3.1 Process

- A laboratory-scale pyrolytic gasification plant was built and tested as part of this project. Its operation highlighted that carbon deposition, and the formation of soot-tar composites represent an operational challenge.
- Sludge pyrolysis produced an energy-rich fuel-gas containing hydrocarbons (CH_4, C_2H_2, C_2H_4, C_2H_6), syngas (CO, H_2), CO_2, N_2 and contaminants. The gas may be suitable for conversion in a gas engine once its contaminants have been eliminated. Despite the presence of acetylene, the results of flammability testing suggest the overall gas mixture has flammability limits ranging between 7.5-41.0%.
- The CO_2:H_2S ratio of fuel-gas was approximately 13.7 at 800°C and 5.5 at 1000°C. Short contact-time caustic scrubbers are typically designed for a ratio of <5, therefore the removal of H_2S with caustic will operate at sub-optimal selectivity because of CO_2 removal. A high temperature reforming process after pyrolysis could help consume CO_2 via the Boudouard reaction thus increasing the selectivity of the caustic scrubbers.
- Heating SSC with rapid-heating rates and to highest heating temperatures ≤900°C helps minimise gaseous-S emissions.
- The conversion of sludge HHV to fuel-gas LHV peaked at 800°C and 1000°C at 58.7% and 59.3%, respectively. From an energy perspective, the production of fuel-gas at 800°C is preferable because the parasitic load was 47% lower.
- Based on the current performance of conventional THP at Crossness STW – coupling THP-digest with pyrolysis could increase the sites adjusted net conversion efficiency by <54-78%. Preliminary results suggest raw-pyrolysis could increase adjusted net conversion efficiency >63.9%. Pyrolysis of raw sludge cake represents a far simpler process stream than THP-digestion and pyrolysis and should be considered as an alternative to digestion.
- The EOW requirements for “syngas” are based on a statement within the IED that states syngas must be as clean as natural gas. In practice, this means that the limits for “syngas” EOW status are far stricter than comparable waste to energy processes. A case could be made to regulatory bodies to align these limits with other waste to energy processes.

11.3.2 Char

- At ≥600°C, sludge formed SSC that met Class B requirements for pyrogenic-C sequestration. The formation of char is expected to retain more C than biosolids recycled to agriculture, and once formed is expected to be stable for millennia. The H:C ratio of the SSC is closely related to degree of condensation, ring-size and long-term stability. The H:C ratio of SSC began to stabilise at 550°C and then increased with temperature.
- The retention of N and S within SSC is dependent on the highest heating temperature and heating rate. XPS suggests N forms heterocyclic-N structures (e.g. pyridinic-N), although these may have limited stability at higher temperatures. At ≥900°C, graphitic-N may be the dominant form of N within SSC. XPS analysis suggests the S within SSC is mostly present as sulphates and organic S such as thiophene-S, whilst small quantities of sulphides are also present. Heterocyclic-S is expected to be thermally stable. The presence of heterocyclic structures means SSC will have an affinity for charged cations (e.g. NH_4^+, Zn^{2+}, K^+) and polar organic compounds (e.g. phenol). Whilst protonation of these structures may give the SSC an affinity for charged anions. Some structures, such as pyridinic-N may have lone-pairs of electrons available for donation, and thus may be able to influence redox reactions.
- Pyrolysis concentrates P within SSC, and the material may be suitable for agricultural land application. The availability of P within SSC exceeds the minimum requirements outlined by the STRUBIAS proposals. However, the material origin and its heavy metal concentration would exclude it from being a STRUBIAS material. Because of the materials high concentration of P, if used within agriculture the heavy metal application rate would be far below the limits typically used for sludge. Therefore, land recycling is likely to be a viable route provided bespoke permits are in place. To show that the material does not contain organic compounds that represent a risk to human or environmental health, solvent extraction should be conducted.
- A low-cost P fertiliser with slow-release characteristics would be valuable for agriculture. The organic-acid availability of the P within SSC could be improved through partial acidulation with H_2SO_4, this would also incorporate S into the product which is increasingly deficient in UK soils because of lower industrial emissions.
- P can be extracted from SSC with high efficiency and the co-extraction of heavy metals is limited or does not occur. However, the co-extraction of Fe/Al complicates the recovery process meaning solvent extraction or oxalate precipitation may be necessary to recover the P in a plant available form.
- Although SSC contains heavy metals these are not leachable and are unlikely to be hazardous because of their chemical form. However, the presence of AEM sulphides is likely to render the material hazardous because of the potential for the material to form

toxic gases (e.g. H_2S) when mixed with acids. The removal of AEM sulphides is likely to be straightforward, requiring pH adjustment to below approximately pH 9.

11.4 Future Work

- NMR spectrometry (^{13}C) has been used by others to estimate the ring-size and mean residence time of condensed C in chars. This analysis could be conducted for SSC to directly illustrate the materials long-term stability. Accelerated aging tests (section 8.1.5.2) could also be conducted to provide an indication of long-term stability.

- XPS analysis was conducted in the latter stages of this research, therefore, only SSC produced at 700ºC was analysed, however the information gained was extremely informative. An extensive study of the effect of temperature and other factors on SSC surface chemistry using XPS analysis should be conducted.

- This research included an elemental mass balance for H, C, N and S which highlighted the sensitivity of these elements within char and liquids to temperature. A focused study is required that investigates the effect of temperature on the gas-phase speciation of these elements. The behaviour of N during pyrolysis and high-temperature reforming should be prioritised because the conversion of NH_3/CHN and other N compounds to N_2 could decrease the complexity, costs, and viability of cleaning fuel-gas.

- Total gasification is not required for sludge because the material has a natural tendency to form volatiles rather than char. However, valorisation of the fuel-gas is expected to be complex because of the presence of a multitude of contaminants. The viability of a two-stage ATC process that couple's moderate temperature pyrolytic gasification (700-900ºC) and high-temperature reforming should be explored so contaminants within the fuel-gas can be minimised prior to clean-up.

- The formation of heterocyclic structures within SSC will give the material an affinity for charged ions and polar compounds. The potential use of the material for pollutant adsorption should be further explored. In addition, heterocyclic structures within SSC have potential applications in catalysis and this should be explored further.

- Although unlikely, further testing is required to assess whether EUH029/EUH032 apply because of the potential presence of metal cyanides, phosphides or azides within SSC.

- The viability of hot-gas desulphurisation with regenerative sorbents should be explored to minimise the use of non-regenerable chemicals (e.g. caustic).

- Fat, oil, and greases recovered at sewage treatment works or from wastewater networks is energy rich and expected to predominately form hydrocarbon gases when pyrolysed. Pyrolysis could be used to dispose of this waste, and this warrants further research.

- Future techno-economic analysis should be conducted that compares the whole lifecycle costs of THP-digestion, THP-pyrolysis, and raw-sludge pyrolysis. Ideally this work needs to be full costed, including: product revenue, OpEx, carbon, asset lifespan, asset depreciation and CapEx (from reliable cost-curves or fully-costed design work).

References

Abatzoglou, N. and Boivin, S., 2009. A review of biogas purification processes. *Biofuels, Bioproducts and Biorefining*, 3(1), pp.42-71.

Achten, C. and Andersson, J., 2015. Overview of Polycyclic Aromatic Compounds (PAC). *Polycyclic Aromatic Compounds*, 35(2-4), pp.177-186.

Agegnehu, G., Srivastava, A. and Bird, M., 2017. The role of biochar and biochar-compost in improving soil quality and crop performance: A review. *Applied Soil Ecology*, 119, pp.156-170.

AHDB, 2020. *Organic Materials*. Nutrient Management Guide (RB209). [online] Kenilworth: AHDB, pp.pp.27-30. Available at: <https://projectblue.blob.core.windows.net/media/Default/Imported%20Publication%20Docs/RB209/RB209_Section2_2020_200116_WEB.pdf> [Accessed 28 April 2020].

Akhtar, A., Krepl, V. and Ivanova, T., 2018. A Combined Overview of Combustion, Pyrolysis, and Gasification of Biomass. *Energy & Fuels*, 32(7), pp.7294-7318.

ALS Environmental Ltd., 2017. *Technical Datasheet - Waste acceptance criteria*. [online] Coventry: ALS Environmental Ltd. Available at: <https://www.alsenvironmental.co.uk/media-uk/pdf/datasheets/waste-management/als_wm_waste-acceptance-criteria_td_uk_2017.pdf> [Accessed 12 May 2020].

Andreoli, C., Sperling, M. and Fernandes, F., 2007. *Sludge treatment and disposal*. London: IWA Publishing, pp.13-14.

Applied Analytics, 2020. *pH-Independent Measurement of Hydrogen Sulfide in Liquids*. [online] Aai.solutions. Available at: <https://aai.solutions/news/ph-independent-measurement-of-hydrogen-sulfide-in-liquids/> [Accessed 8 January 2021].

Anis, S. and Zainal, Z. (2011). Tar reduction in biomass producer gas via mechanical, catalytic and thermal methods: A review. *Renewable and Sustainable Energy Reviews*, 15(5), pp.2355-2377.

Aravind, P. and de Jong, W., 2012. Evaluation of high temperature gas cleaning options for biomass gasification product gas for Solid Oxide Fuel Cells. *Progress in Energy and Combustion Science*, 38(6), pp.737-764.

Arisoy, A. and Beamish, B., 2015. Mutual effects of pyrite and moisture on coal self-heating

rates and reaction rate data for pyrite oxidation. *Fuel*, 139, pp.107-114.

Assured Biosolids Limited, 2020. *The BAS Standard*. [online] Huntingdon: Assured Biosolids Limited. Available at: <https://assuredbiosolids.co.uk/wp-content/uploads/2020/07/BAS-Standard-Issue-5-10th-July-2020.pdf> [Accessed 7 March 2021].

Assured Biosolids Ltd., 2021. *About Us*. [online] Assuredbiosolids.co.uk. Available at: <https://assuredbiosolids.co.uk/> [Accessed 16 July 2021].

Atkins Ltd., 2019. *Rapid evidence assessment: Evidence review on the effect of pyrolysis and/or gasification of biosolids on antimicrobial resistance in the environment*. London: Department for environment, food and rural affairs, p.25.

ATSDR,. Toxicological Profile for Phenol. Atlanta: Agency for Toxic Substances and Disease Registry, 2008. Print.

Attar, A., 1978. Chemistry, thermodynamics, and kinetics of reactions of sulphur in coal-gas reactions: A review. *Fuel*, 57(4), pp.201-212.

Ayiania, M., Smith, M., Hensley, A., Scudiero, L., McEwen, J. and Garcia-Perez, M., 2020. Deconvoluting the XPS spectra for nitrogen-doped chars: An analysis from first principles. *Carbon*, 162, pp.528-544.

Babich, H. and Davis, D., 1981. Phenol: A review of environmental and health risks. *Regulatory Toxicology and Pharmacology*, 1(1), pp.90-109.

Baker, E. and Mudge, L., 1984. Mechanisms of catalytic biomass gasification. *Journal of Analytical and Applied Pyrolysis*, 6(3), pp.285-297.

Baker, E., Brown, M., Moore, R., Mudge, L. and Elliott, D., 1986. *Engineering analysis of biomass gasifier product gas cleaning technology*. [online] Richland: U.S. Department of Energy. Available at: <https://www.osti.gov/servlets/purl/5452542> [Accessed 11 May 2021].

Bakshi, S., Banik, C. and Laird, D., 2020. Estimating the organic oxygen content of biochar. *Scientific Reports*, 10(1).

Bandosz, T., 2006. *Activated Carbon Surfaces in Environmental Remediation*. Amsterdam: Elsevier, p.4.

Barber, W., 2016. Thermal hydrolysis for sewage treatment: A critical review. *Water Research*, 104, pp.53-71.

Bargiacchi, E., Candelaresi, D., Valente, A., Spazzafumo, G. and Frigo, S., 2021. Life Cycle Assessment of Substitute Natural Gas production from biomass and electrolytic hydrogen. *International Journal of Hydrogen Energy*,.

Barker, C., 2020. *Europe caustic soda Q1 price falls 10% as market readjusts*. [online] ICIS.com. Available at: <https://www.icis.com/explore/resources/news/2020/01/28/10461663/europe-caustic-soda-q1-price-falls-10-as-market-readjusts> [Accessed 12 April 2021].

Barzegar, F., Kamankesh, M. and Mohammadi, A., 2019. Heterocyclic aromatic amines in cooked food: A review on formation, health risk-toxicology and their analytical techniques. *Food Chemistry*, 280, pp.240-254.

Beer, M., Maree, J., Liebenberg, L. and Doucet, F., 2014. Conversion of calcium sulphide to calcium carbonate during the process of recovery of elemental sulphur from gypsum waste. *Waste Management*, 34(11), pp.2373-2381.

BEIS, 2017. *Boiler Plus*. Heat in Buildings. London: Department for Business, Energy, & Industrial Strategy, p.8. Available at:

BEIS, 2018. *Digest of United Kingdom Energy Statistics 2018*. London: Department for Business, Energy & Industrial Stategy, pp.52-57.

BEIS, 2012. *Greenhouse gas reporting: conversion factors 2012*. London: Department for Business, Energy, and Industrial strategy.

BEIS, 2020. *Greenhouse gas reporting: conversion factors 2020*. London: Department for Business, Energy, and Industrial strategy.

BEIS[b], 2018. *Updated short-term traded carbon values used for UK public policy appraisal*. [online] London: Department for Business, Energy & Industrial Strategy. Available at: <https://assets.publishing.service.gov.uk/government/uploads/system/uploads/attachment_data/file/794186/2018-short-term-traded-carbon-values-for-appraisal-purposes.pdf> [Accessed 1 March 2021].

BEIS[a], 2021. *Quarterly energy prices, United Kingdom, Quarter 4 (October - December) 2020*. London: Department for Business, Energy and Industrial strategy.

BEIS[b], 2021. *A detailed guide for CHP developers - Part 2*. Combined Heat and Power - Technologies. London: Department for Business, Energy, and Industrial strategy.

BEIS[c], 2021. *Greenhouse gas reporting: conversion factors 2021*. London: Department for Business, Energy, and Industrial strategy.

BEIS[d], 2021. *Historical gas data: gas production and consumption and fuel input 1920 to 2020*. London: Department for Business, Energy & Industrial Strategy.

Bevan, E., Fu, J. and Zheng, Y., 2020. Challenges and opportunities of hydrothermal carbonisation in the UK; case study in Chirnside. *RSC Advances*, 10(52), pp.31586-31610.

Bhaskar, T., Bhavya, B., Singh, R., Naik, D., Kumar, A. and Goyal, H., 2011. *Biofuels*. 1st ed. Amsterdam: Elsevier, pp.56-59.

Biffiger, H. and Soltic, P., 2015. Effects of split port/direct injection of methane and hydrogen in a spark ignition engine. *International Journal of Hydrogen Energy*, 40(4), pp.1994-2003.

Binnemans, K., Jones, P., Blanpain, B., Van Gerven, T. and Pontikes, Y., 2015. Towards zero-waste valorisation of rare-earth-containing industrial process residues: a critical review. *Journal of Cleaner Production*, 99, pp.17-38.

Bioenergy International, 2017. *CPL plans UK's first commercial-scale hydrothermal carbonisation (HTC) plant | Bioenergy International*. [online] Bioenergy International. Available at:<https://bioenergyinternational.com/pellets-solid-fuels/cpl-plans-uks-first-commercial%E2%80%90scale-hydrothermal-carbonisation-htc-plant> [Accessed 13 March 2022].

Bird, M., Wynn, J., Saiz, G., Wurster, C. and McBeath, A., 2015. The Pyrogenic Carbon Cycle. *Annual Review of Earth and Planetary Sciences*, 43(1), pp.273-298.

Blöcher, C., Niewersch, C. and Melin, T., 2012. Phosphorus recovery from sewage sludge with a hybrid process of low pressure wet oxidation and nanofiltration. *Water Research*, 46(6), pp.2009-2019.

Blyth, R., Buqa, H., Netzer, F., Ramsey, M., Besenhard, J., Golob, P. and Winter, M., 2000. XPS studies of graphite electrode materials for lithium ion batteries. *Applied Surface Science*, 167(1-2), pp.99-106.

BP, 1965. *Gasmaking*. 2nd ed. London: British Petroleum, p.29.

Brady, N. and Weil, R., 2008. *Elements of the nature and properties of soils*. 14th ed. New Jersey: Pearson Education inc., p.510.

Brendel, S., Polleichtner, C., Behnke, A., Jessel, S., Hassold, E., Jennemann, C., Einhenkel-Arle, D. and Seidel, A., 2018. Four selected high molecular weight heterocyclic aromatic hydrocarbons: Ecotoxicological hazard assessment, environmental relevance and regulatory needs under REACH. *Ecotoxicology and Environmental Safety*, 163, pp.340-348.

Bridgewater, A. (2012). Review of fast pyrolysis of biomass and product upgrading. Biomass

and Bioenergy, 38, pp.68-94.

British Gas, 2021. *History of British Gas | British Gas business*. [online] Britishgas.co.uk. Available at: <https://www.britishgas.co.uk/business/history> [Accessed 26 March 2021].

Bruinsma, O., Tromp, P., de Sauvage Nolting, H. and Moulijn, J., 1988. Gas phase pyrolysis of coal-related aromatic compounds in a coiled tube flow reactor. *Fuel*, 67(3), pp.334-340.

Burrell, L., Zehetner, F., Rampazzo, N., Wimmer, B. and Soja, G., 2016. Long-term effects of biochar on soil physical properties. *Geoderma*, 282, pp.96-102.

Cambi, 2020. *THP before anaerobic digestion - Cambi - world leader in thermal hydrolysis*. [online] Cambi.com. Available at: <https://www.cambi.com/what-we-do/thp-solutions/thp-before-anaerobic-digestion/> [Accessed 2 April 2020].

Campo, J. and Merino, A., 2016. Variations in soil carbon sequestration and their determinants along a precipitation gradient in seasonally dry tropical forest ecosystems. *Global Change Biology*, 22(5), pp.1942-1956.

Campos-M, M. and Campos-C, R., 2017. Applications of quartering method in soils and foods. *International Journal of Engineering Research and Applications*, 7(1), pp.35-39.

Campuzano, F., Brown, R. and Martínez, J., 2019. Auger reactors for pyrolysis of biomass and wastes. *Renewable and Sustainable Energy Reviews*, 102, pp.372-409.

CARBON8, 2020. *Using carbon dioxide to give waste value*. [online] C8s.co.uk. Available at: <http://c8s.co.uk/> [Accessed 17 April 2020].

Carbon Gold, 2015. *Processing biomass into biochar with Carbon Gold's pyrolysis kilns*. [online] Youtube.com. Available at: <https://www.youtube.com/watch?v=CqKPNvaapGs> [Accessed 25 March 2021].

Carrier, M., Hardie, A., Uras, Ü., Görgens, J. and Knoetze, J., 2012. Production of char from vacuum pyrolysis of South-African sugar cane bagasse and its characterization as activated carbon and biochar. *Journal of Analytical and Applied Pyrolysis*, 96, pp.24-32.

Carrizo, D., Domeño, C., Nerín, I., Alfaro, P. and Nerín, C., 2015. Atmospheric pressure solid analysis probe coupled to quadrupole-time of flight mass spectrometry as a tool for screening and semi-quantitative approach of polycyclic aromatic hydrocarbons, nitro-polycyclic aromatic hydrocarbons and oxo-polycyclic aromatic hydrocarbons in complex matrices. *Talanta*, 131, pp.175-184.

Chakrabarty, A., Mannan, S. and Cagin, T., 2016. *Multiscale modeling for process safety applications*. Amsterdam: Elsevier/Butterworth-Heinemann.

Chambers, B., Nicholson, F., Cartmell, E. and Rowlands, C., 2007. Benefits of biosolids to soil

quality and fertility. *Water and Environmental Journal*, [online] 17(3). Available at: <https://onlinelibrary.wiley.com/doi/abs/10.1111/j.1747-6593.2003.tb00455.x> [Accessed 7 April 2020].

Casa Software Ltd., 2008. *Basic Quantification of XPS Spectra*. [online] Teignmouth: Casa Software Ltd. Available at: <http://www.casaxps.com/help_manual/manual_updates/Basics_Quantification_of_XPS_Spectra.pdf> [Accessed 20 May 2021].

ChEBI, 2021. *coprostanol (CHEBI:89519)*. [online] Ebi.ac.uk. Available at: <https://www.ebi.ac.uk/chebi/searchId.do?chebiId=89519> [Accessed 2 March 2021].

Chen, D., Gao, A., Cen, K., Zhang, J., Cao, X. and Ma, Z., 2018. Investigation of biomass torrefaction based on three major components: Hemicellulose, cellulose, and lignin. *Energy Conversion and Management*, 169, pp.228-237.

Chen, F., Hu, Y., Dou, X., Chen, D. and Dai, X., 2015. Chemical forms of heavy metals in pyrolytic char of heavy metal-implanted sewage sludge and their impacts on leaching behaviors. *Journal of Analytical and Applied Pyrolysis*, 116, pp.152-160.

Chen, P. and Faust, S., 1974. The Solubility Product of Ferrous Phosphate. *Environmental Letters*, 6(4), pp.287-296.

Cho, S., Yun, Y., Lee, S., Jang, D., Park, K., Kim, J., Kim, B., Kang, K., Kaplan, D. and Jin, H., 2015. Carbonization of a stable β-sheet-rich silk protein into a pseudographitic pyroprotein. *Nature Communications*, 6(1).

Chow, C. L., 2009. Next generation calcium phosphate-based biomaterials. *Dental Materials Journal*, 28(1), pp.1-10.

Chuang, H., Lin, C. and Chen, H., 2008. Carbothermic reduction of zinc sulfide in the presence of sodium carbonate. *Journal of the Chinese Institute of Chemical Engineers*, 39(5), pp.457-465.

Clergé, A., Le Goff, J., Lopez, C., Ledauphin, J. and Delépée, R., 2019. Oxy-PAHs: occurrence in the environment and potential genotoxic/mutagenic risk assessment for human health. *Critical Reviews in Toxicology*, 49(4), pp.302-328.

Clinipower Ltd., 2019. *Pyrolysis - Clinipower*. [online] Clinipower.net. Available at: <https://clinipower.net/technologies/pyrolysis/> [Accessed 25 October 2019].

Coleman, K. and Jenkinson, D., 1996. RothC-26.3 - A Model for the turnover of carbon in soil. *Evaluation of Soil Organic Matter Models*, pp.237-246.

Coltters, R., 1985. Thermodynamics of binary metallic carbides: A review. *Materials Science and Engineering*, 76, pp.1-50.

Compact Power, n.d. *Compact Power puts pyrolysis and gasification to work for sustainable solutions*. [online] Chilledfood.org. Available at: <https://www.chilledfood.org/wp-content/uploads/2015/07/Gasification-and-Pyrolosis.pdf> [Accessed 9 April 2020].

Cooper, C., Kim, B. and MacDonald, J., 1999. Estimating the Lower Heating Values of Hazardous and Solid Wastes. *Journal of the Air & Waste Management Association*, 49(4), pp.471-476.

Costello, R. and Sullivan, D., 2013. Determining the pH Buffering Capacity of Compost Via Titration with Dilute Sulfuric Acid. *Waste and Biomass Valorization*, 5(3), pp.505-513.

Costigan, M., 2003. Hydrogen sulfide: UK occupational exposure limits. *Occupational and Environmental Medicine*, 60(4), pp.308-312.

Coward, H. and Jones, G., 1952. *Limits of flammability of gases and vapors*. 4th ed. Springfield, Va.: U.S. Govt. Print. Off.

Craig, B. (1993). Sour-gas design considerations. Richardson, TX: Henry L. Doherty Memorial Fund of AIME.

Cross, A. and Sohi, S., 2012. A method for screening the relative long-term stability of biochar. *GCB Bioenergy*, 5(2), pp.215-220.

Cyr, M., Coutand, M. and Clastres, P., 2007. Technological and environmental behavior of sewage sludge ash (SSA) in cement-based materials. *Cement and Concrete Research*, 37(8), pp.1278-1289.

Dakota Gas, n.d. *Synthetic Natural Gas - Dakota Gasification Company*. [online] Dakotagas.com. Available at: <https://www.dakotagas.com/products/pipeline-and-liquefied-gases/synthetic-natural-gas> [Accessed 25 April 2020].

Danzi, E., Marmo, L. and Riccio, D., 2015. Minimum Ignition Temperature of layer and cloud dust mixtures. *Journal of Loss Prevention in the Process Industries*, 36, pp.326-334.

Davidson, D., Kohse-Höinghaus, K., Chang, A. and Hanson, R., 1990. A pyrolysis mechanism for ammonia. *International Journal of Chemical Kinetics*, 22(5), pp.513-535.

Davies, N., Laughlin, K. and Hayhurst, A., 1994. The oxidation of calcium sulphide at the temperatures of fluidised-bed combustors. *Symposium (International) on Combustion*, 25(1), pp.211-218.

De Andrés, J., Roche, E., Narros, A. and Rodríguez, M., 2016. Characterisation of tar from

sewage sludge gasification. Influence of gasifying conditions: Temperature, throughput, steam and use of primary catalysts. *Fuel*, 180, pp.116-126.

Dean, A., Chou, M. and Stern, D., 1984. Kinetics of rich ammonia flames. *International Journal of Chemical Kinetics*, 16(6), pp.633-653.

Dean, J., 1999. *Lange's Handbook of Chemistry*. 15th ed. New York, USA: McGraw-Hill Inc.

DEFRA, 2011. *Guidance on applying the waste hierarchy*. London: The Department for Environment, Food and Rural Affairs, p.3.

DEFRA, 2021. *Agriculture in the United Kingdom 2019*. London: Department of Environmental, Food and Rural affairs.

Demirbas, A., 2017. Higher heating values of lignin types from wood and non-wood lignocellulosic biomasses. *Energy Sources, Part A: Recovery, Utilization, and Environmental Effects*, 39(6).

Devi, P. and Saroha, A., 2017. Utilization of sludge based adsorbents for the removal of various pollutants: A review. *Science of The Total Environment*, 578, pp.16-33.

Dewil, R., Baeyens, J., Roels, J. and Steene, B., 2008. Distribution of Sulphur Compounds in Sewage Sludge Treatment. *Environmental Engineering Science*, 25(6), pp.879-886.

Díaz-Cruz, M., García-Galán, M., Guerra, P., Jelic, A., Postigo, C., Eljarrat, E., Farré, M., López de Alda, M., Petrovic, M. and Barceló, D., 2009. Analysis of selected emerging contaminants in sewage sludge. *TrAC Trends in Analytical Chemistry*, 28(11), pp.1263-1275.

Doerr, S., Santín, C., Merino, A., Belcher, C. and Baxter, G., 2018. Fire as a Removal Mechanism of Pyrogenic Carbon From the Environment: Effects of Fire and Pyrogenic Carbon Characteristics. *Frontiers in Earth Science*, 6.

Dou, B., Gao, J., Sha, X. and Baek, S., 2003. Catalytic cracking of tar component from high-temperature fuel gas. *Applied Thermal Engineering*, 23(17), pp.2229-2239.

Dudziak, T., Jura, K., Dudek, P., Boroń, L. and Rutkowska, J., 2019. Sulphidation of Low-Alloyed Steels Used in Power Industry. *Oxidation of Metals*, 92(5-6), pp.379-399.

Dumfort, S., Huemer, M., Hofmann, A., Huber, M. and Kruegar, J. (2015). Tar Decomposition at low Temperatures within staged Gasification Reactors-first Approach towards Mechanisms and Background. *Journal of Engineering Technology*, 3(3).

DuPont, n.d. *Hydrogen sulfide scrubbing for refinery flare gas system*. Dynawave® Case Study No. 55. Wilmington: Dupont.

EBC, 2022. *The European Biochar Certificate (EBC)*. [online] European-biochar.org. Available

at: <https://www.european-biochar.org/en/home> [Accessed 3 April 2022].

EBC (2012-2022) 'European Biochar Certificate - Guidelines for a Sustainable Production of Biochar.' European Biochar Foundation (EBC), Arbaz, Switzerland. (http://european-biochar.org). Version 10.1 from 10th Jan 2022.

EBRI, 2015. *Biomass and Waste Pyrolysis: A Guide to UK Capabilities*. [online] Pyne.co.uk. Available at: <http://www.pyne.co.uk/Resources/user/UK%20Biomass%20and%20Waste%20Pyrolysis%20Guide%202015%20081015.pdf> [Accessed 17 February 2021].

European Council (2008) Directive 2008/98/EC on waste and repealing certain Directives Office Journal of the European Communities, L312, 3-30.

ECHA, 2020. *Table of harmonised entries in Annex VI to CLP - ECHA*. [online] Echa.europa.eu. Available at: <https://echa.europa.eu/information-on-chemicals/annex-vi-to-clp> [Accessed 25 April 2021].

Ecofys, 2018. *Innovation needs assessment for biomass heat*. [online] Utrecht: UK Department for Business, Energy, and Industrial Strategy. Available at: <https://assets.publishing.service.gov.uk/government/uploads/system/uploads/attachment_data/file/699669/BE2_Innovation_Needs_Final_report_Jan18.pdf> [Accessed 19 July 2021].

Eliquo-tech.com. 2020. *PYREG® - ELIQUO Technologies*. [online] Available at: <https://www.eliquo-tech.com/en/pyreg.html> [Accessed 25 March 2021].

Ellingham, H., 1944. Reducibility of oxides and sulphides in metallurgical processes. *Journal of the Society of Chemical Industry*, [online] 63(5), pp.125-160. Available at: <https://onlinelibrary.wiley.com/doi/abs/10.1002/jctb.5000630501> [Accessed 8 May 2020].

Elliott, D.C. 1988. “Relation of Reaction Time and Temperature to Chemical Composition of Pyrolysis Oils,” ACS Symposium Series 376, Pyrolysis Oils from Biomass. Edited by E.J. Soltes and T.A. Milne. Denver, CO. April 1987.

Environment Agency, 2005. *EA NEN 7371:2004 - Leaching characteristics of granular building and waste materials - The maximum lavailability leaching test*. The determination of the availability of inorganic components for leaching. [online] Bristol: Environment Agency. Available at: <https://webarchive.nationalarchives.gov.uk/20140328113735/http://www.environment-agency.gov.uk/static/documents/Business/ea_nen_7371_2004_1026067.pdf> [Accessed 12 May 2020].

Environment Agency, 2010. *Guidance on gas treatment technologies for landfill gas engines*. Bristol: Environment Agency, p.13.

Environment Agency, 2010. *The determination of easily liberated sulphide in soils and similar matrices*. Methods for the Examination of Waters and Associated Materials. Bristol: Environment Agency, p.6.

Environment Agency, 2013. *Biomethane from waste: End of waste criteria for the production and use of biomethane from landfill gas and anaerobic digestion (AD) biogases*. Banbury: Environment Agency, p.12.

Environment Agency, 2014. *End-of-waste and by-product hazard and risk assessment*. Bristol: Environment Agency, pp.44-45.

Environment Agency, 2016. *Material comparators for end-of-waste decisions*. Report: SC130040/R15 (ShARE 25). [online] Bristol: Environment Agency, p.3. Available at: <https://assets.publishing.service.gov.uk/government/uploads/system/uploads/attachment_data/file/545567/Material_comparators_for_fuels_-_natural_gas.pdf> [Accessed 9 June 2020].

Environment Agency[a], 2018. *Standard rules SR2009 No 4 – Combustion of biogas in new Medium Combustion Plant engines at a sewage treatment works*. Bristol: Environment Agency.

Environment Agency[b], 2018. *Waste Classification*. Guidance on the classification and assessment of waste v1.1. [online] Bristol: Environment Agency. Available at: <https://assets.publishing.service.gov.uk/government/uploads/system/uploads/attachment_data/file/719394/Waste-classification-technical-guidance-WM3.pdf> [Accessed 6 May 2020].

Environment Agency, 2019. *The state of the environment: soil*. [online] Bristol. Available at: <https://assets.publishing.service.gov.uk/government/uploads/system/uploads/attachment_data/file/805926/State_of_the_environment_soil_report.pdf> [Accessed 16 April 2020].

ETIA Ecotechnologies, 2020. *Spirajoule: Electrically heated screw conveyor – Spirajoule*. [online] ETIA Group. Available at: <https://etia-group.com/our-products/spirajoule/> [Accessed 23 April 2020].

European Commission, 2020. *Study on the EU's list of Critical Raw Materials*. Luxembourg: European Commission.

Eurostat, 2019. *Energy balance guide*. Methodology guide for the construction of energy balances. [online] Brussels: European Commission. Available at: <https://ec.europa.eu/eurostat/documents/38154/4956218/ENERGY-BALANCE-GUIDE-DRAFT-31JANUARY2019.pdf/cf121393-919f-4b84-9059-cdf0f69ec045> [Accessed 6 October 2020].

EUROSTAT, 2020. *Sewage sludge production and disposal - Eurostat*. [online] Ec.europa.eu. Available at: <https://ec.europa.eu/eurostat/web/products-datasets/product?code=env_ww_spd> [Accessed 29 February 2020].

FAO, 2015. *World fertilizer trends and outlook to 2018*. [online] Rome: Food and Agriculture Organisation of the United Nations. Available at: <http://www.fao.org/3/i4324e/i4324e.pdf> [Accessed 25 April 2019].

Feng, Y., Mi, J., Wu, M., Shangguan, J. and Fan, H., 2016. In Situ Preparation and Regeneration Behaviors of Zinc Oxide/Red Clay Desulfurization Sorbents. *Energy & Fuels*, 31(1), pp.1015-1022.

Fertilisers Europe, 2000. *Booklet No. 4 of 8: Production of phosphoric acid*. Best Available Techniques for Pollution Prevention and Control in the European Fertilizer Industry. [online] Brussels: Fertilisers Europe. Available at: <https://www.fertilizerseurope.com/wp-content/uploads/2019/08/Booklet_4_final.pdf> [Accessed 24 December 2020].

Fijalkowski, K., Rorat, A., Grobelak, A. and Kacprzak, M., 2017. The presence of contaminations in sewage sludge – The current situation. *Journal of Environmental Management*, 203, pp.1126-1136.

Fitzer, E., Kochling, K., Boehm, H. and Marsh, H., 1995. Recommended terminology for the description of carbon as a solid (IUPAC Recommendations 1995). *Pure and Applied Chemistry*, 67(3), pp.473-506.

Fleisch, H. and Bisaz, S., 1962. Isolation from urine of pyrophosphate, a calcification inhibitor. *American Journal of Physiology-Legacy Content*, 203(4), pp.671-675.

Fountain, P., Lee, K., Kellari, S. and Webb, I., 2013. High Dry Solids Dewatering - From pilot scale through to full scale implementation comparing performance. In: *18th European Biosolids & Organic Resources Conference & Exhibition*. Aqua Enviro Technology Transfer.

Frigge, L., Ströhle, J. and Epple, B., 2017. Release of sulfur and chlorine gas species during coal combustion and pyrolysis in an entrained flow reactor. *Fuel*, 201, pp.105-110.

Gale, P., 2005. Land application of treated sewage sludge: quantifying pathogen risks from consumption of crops. *Journal of Applied Microbiology*, 98(2), pp.380-396.

Gao, N., Kamran, K., Quan, C. and Williams, P., 2020. Thermochemical conversion of sewage sludge: A critical review. *Progress in Energy and Combustion Science*, 79, p.100843.

García-Cascallana, J., Borge-Díez, D. and Gómez, X., 2018. Enhancing the efficiency of thermal hydrolysis process in wastewater treatment plants by the use of steam accumulation. *International Journal of Environmental Science and Technology*, 16(7), pp.3403-3418.

García-Labiano, F., Hampartsoumian, E. and Williams, A., 1995. Determination of sulfur release and its kinetics in rapid pyrolysis of coal. *Fuel*, 74(7), pp.1072-1079.

Garcia-Nunez, J., Pelaez-Samaniego, M., Garcia-Perez, M., Fonts, I., Abrego, J., Westerhof, R.

and Garcia-Perez, M., 2017. Historical Developments of Pyrolysis Reactors: A Review. *Energy & Fuels*, 31(6), pp.5751-5775.

Gee, I. (1997). *Production and application of activated carbons derived from waste*. PhD. Imperial College London.

Giacalone, S., 2018. *Optimising the anaerobic digestion process through improved understanding of the fundamental operational parameters.* PhD. Imperial College London.

Glaser, B., 2006. Prehistorically modified soils of central Amazonia: a model for sustainable agriculture in the twenty-first century. *Philosophical Transactions of the Royal Society B: Biological Sciences*, 362(1478), pp.187-196.

Gomez-Eyles, J., Sizmur, T., Collins, C. and Hodson, M., 2011. Effects of biochar and the earthworm Eisenia fetida on the bioavailability of polycyclic aromatic hydrocarbons and potentially toxic elements. *Environmental Pollution*, 159(2), pp.616-622.

Gómez, N., Rosas, J., Singh, S., Ross, A., Sánchez, M. and Cara, J., 2016. Development of a gained stability index for describing biochar stability: Relation of high recalcitrance index (R50) with accelerated ageing tests. *Journal of Analytical and Applied Pyrolysis*, 120, pp.37-44.

Gu, Z., Wu, M., Li, K. and Ning, P., 2017. Variation of heavy metal speciation during the pyrolysis of sediment collected from the Dianchi Lake, China. *Arabian Journal of Chemistry*, 10, pp.S2196-S2204.

Guo, H., Ren, Y., Sun, X., Xu, Y., Li, X., Zhang, T., Kang, J. and Liu, D., 2013. Removal of Pb2+ from aqueous solutions by a high-efficiency resin. *Applied Surface Science*, 283, pp.660-667.

Guo, L. and Gifford, R., 2002. Soil carbon stocks and land use change: a meta analysis. *Global Change Biology*, 8(4), pp.345-360.

Gurwick, N., Kelly, C. and Elias, P., 2012. *The Scientific Basis for Biochar as a Climate Change Mitigation Strategy: Does it Measure Up?*. Cambridge, MA: Union of concerned scientists, p.11.

Habashi, F., Awadalla, F. and Yao, X., 1987. The hydrochloric acid route for phosphate rock. *Journal of Chemical Technology & Biotechnology*, 38(2), pp.115-126.

Hagin, J. and Harrison, R., 1993. Phosphate rocks and partially-acidulated phosphate rocks as controlled release P fertilizers. *Fertilizer Research*, 35(1-2), pp.25-31.

Hajaligol, M., Howard, J., Longwell, J. and Peters, W., 1982. Product compositions and kinetics for rapid pyrolysis of cellulose. *Industrial & Engineering Chemistry Process Design and Development*, 21(3), pp.457-465.

Hammond, J., Shackley, S., Prendergast-Miller, M., Cook, J., Buckingham, S. and Pappa, V., 2013. Biochar field testing in the UK: outcomes and implications for use. *Carbon Management*, 4(2), pp.159-170.

Hansson, K., Samuelsson, J., Tullin, C. and Åmand, L., 2004. Formation of HNCO, HCN, and NH3 from the pyrolysis of bark and nitrogen-containing model compounds. *Combustion and Flame*, 137(3), pp.265-277.

Harris, E., 1942. Activated Carbon in Sugar Refining. *Industrial & Engineering Chemistry*, 34(9), pp.1057-1060.

Harvey, O., Kuo, L., Zimmerman, A., Louchouarn, P., Amonette, J. and Herbert, B., 2012. An Index-Based Approach to Assessing Recalcitrance and Soil Carbon Sequestration Potential of Engineered Black Carbons (Biochars). *Environmental Science & Technology*, 46(3), pp.1415-1421.

Haw, R., 2017. *Assessing the investment returns from timber and carbon in woodland creation projects*. Bristol: Forestry Commission.

Hennebert, P., Samaali, I. and Molina, P., 2016. A proposal for a test method for assessment of hazard property HP 12 ("Release of an acute toxic gas") in hazardous waste classification – Experience from 49 waste. *Waste Management*, 58, pp.25-33.

Higgins & Hewins Ltd., n.d. *Sulfatreat now well established for odour control - WWT*. [online] Wwtonline.co.uk. Available at: <https://wwtonline.co.uk/65787/PressRelease/sulfatreat-now-well-established-for-odour-control/33461> [Accessed 12 April 2021].

Higman, C. and Van der Burgt, M., 2008. *Gasification*. 2nd ed. Burlington: Elsevier Science, p.232.

HM Revenue & Customs, 2020. *Excise Notice LFT1: a general guide to Landfill Tax*. [online] gov.uk. Available at: <https://www.gov.uk/government/publications/excise-notice-lft1-a-general-guide-to-landfill-tax/excise-notice-lft1-a-general-guide-to-landfill-tax> [Accessed 28 July 2020].

Hodges, J., Geary, W., Graham, S., Hooker, P. and Goff, R., 2015. *Injecting hydrogen into the gas network – a literature search*. Buxton: Health & Safety Executive, p.6.

Hollis, P., 2014. *Energy from Waste & Biomass Fuels*. 1st ed. Bloomington, USA: AuthorHouse.

Horn, J.V, Sartorius, C. (2009). Impact of supply and demand on the price development of phosphate (fertiliser). IWA Publishing, London, United Kingdom

Houben, M.P. "Analysis of tar removal in a partial oxidation burner", Technical University of

Eindhoven, 2004.

Houser, T., Hull, M., Alway, R. and Biftu, T., 1980. Kinetics of formation of HCN during pyridine pyrolysis. *International Journal of Chemical Kinetics*, 12(8), pp.569-574.

Huff, W., 1926. The Origin of Carbon Disulfide in the Carbonization of Coal. *Industrial & Engineering Chemistry*, 18(4), pp.357-361.

Huygens, D., Saveyn, H., Tonini, D., Eder, P. and Sancho Delgado, L., 2019. *Technical proposals for selected new fertilising materials under the Fertilising Products Regulation (Regulation (EU) 2019/1009) Process and quality criteria, and assessment of environmental and market impacts for precipitated phosphate salts & derivates, thermal oxidation materials & derivates and pyrolysis & gasification materials*. EUR 29841 EN. Luxembourg: Publications Office of the European Union.

Hydrogen Europe, 2020. *Fuel cells | Hydrogen*. [online] Hydrogeneurope.eu. Available at: <https://hydrogeneurope.eu/fuel-cells> [Accessed 30 March 2020].

IARC, 2010. *IARC Monographs on the Evaluation of Carcinogenic Risks to Humans: Carbon black, titanium dioxide, and talc*. 93rd ed. Lyon: International Agency for Research on Cancer.

IARC, 2012. *IARC monographs on the evaluation of carcinogenic risks to humans: Soot, as found in occupational exposure of chimney-sweeps*. 100th ed. Lyon: International Agency for Research on Cancer.

IARC, 2013. *Bitumens and Bitumen emissions, and some N- and S- heterocyclic polycyclic aromatic hydrocarbons*. Volume 103. Lyon: International Agency for Research on Cancer.

IEA, 2004. *Energy Statistics manual*. Paris: International Energy Agency, p.20.

IFA, 2020. *Phosphogysum*. [online] Fertilizer.org. Available at: <https://www.fertilizer.org/Public/About_Fertilizers/Fertilizer_Topics/Phosphogypsum.aspx> [Accessed 24 December 2020].

ILO, 2021. *International Chemical Safety Cards (ICSCs)*. [online] ilo.org. Available at: <https://www.ilo.org/dyn/icsc/showcard.home> [Accessed 8 May 2021].

International Biochar Initiative (IBI), 2015. *Standardized Product Definition and Product Testing Guidelines for Biochar That Is Used in Soil*. Product Definition and Specification Standards V2.1. [online] Available at: <https://biochar-international.org/wp-content/uploads/2020/06/IBI_Biochar_Standards_V2.1_Final2.pdf> [Accessed 27 June 2020].

Jagtap, S. and Wheelock, T., 1996. Regeneration of Sulfided Calcium-Based Sorbents by a Cyclic Process. *Energy & Fuels*, 10(3), pp.821-827.

Jansen, R. and van Bekkum, H., 1995. XPS of nitrogen-containing functional groups on activated carbon. *Carbon*, 33(8), pp.1021-1027.

Jess, A. (1996). Mechanisms and kinetics of thermal reactions of aromatic hydrocarbons from pyrolysis of solid fuels. Fuel, 75(12), pp.1441-1448.

Jiang, F., Zhang, L., Jiang, Z., Li, C., Cang, D., Liu, X., Xuan, Y. and Ding, Y., 2019. Diatomite-based porous ceramics with high apparent porosity: Pore structure modification using calcium carbonate. *Ceramics International*, 45(5), pp.6085-6092.

John, K. and Beedanagari, S., 2014. *Encyclopedia of toxicology*. Amsterdam: Elsevier, pp.855-863.

Johnston, A., 1975. The Woburn Market Garden Experiment, 1942,69 II. The effects of the treatments on soil pH, soil carbon, nitrogen, phosphorus and potassium. *Rothamsted Experimental Station Report For 1974 Part 2*, pp.102-131.

Johnston, R., 2013. World's slowest-moving drop caught on camera at last. *Nature*,.

Keiluweit, M., Kleber, M., Sparrow, M., Simoneit, B. and Prahl, F., 2012. Solvent-Extractable Polycyclic Aromatic Hydrocarbons in Biochar: Influence of Pyrolysis Temperature and Feedstock. *Environmental Science & Technology*, 46(17), pp.9333-9341.

Kew Projects Ltd., 2019. *Kew H_2: Zero-carbon bulk supply*. BEIS Hydrogen supply competition - Phase one report: Feasibility study. [online] Tamworth: Kew Projects Ltd. Available at: <https://assets.publishing.service.gov.uk/government/uploads/system/uploads/attachment_data/file/873885/kew-zero-carbon-bulk-hydrogen-supply.pdf> [Accessed 19 July 2021].

Khan, R. and Ashraf, W., 2019. Effects of ground wollastonite on cement hydration kinetics and strength development. *Construction and Building Materials*, 218, pp.150-161.

Kim, J., Ok, Y., Choi, G. and Park, B., 2015. Residual perfluorochemicals in the biochar from sewage sludge. *Chemosphere*, 134, pp.435-437.

Kleemann, R. (2015). Sustainable Phosphorus Recovery from Waste. PhD. University of Surrey.

Koch, B. and Dittmar, T., 2006. From mass to structure: an aromaticity index for high-resolution mass data of natural organic matter. *Rapid Communications in Mass Spectrometry*, 20(5), pp.926-932.

Koulouri, M., 2018. *Phosphorus recovery from sewage sludge char*. MSc. Imperial College London.

Kraus F., Zamzow M., Conzelmann L., Remy C., Kleyböcker A., Seis W., Kabbe C., Miehe U., Hermann L., Hermann R. (2018). Report in German: Ökobilanzieller Vergleich der P-

Rückgewinnung aus dem Abwasserstrom mit der Düngemittelproduktion aus Rohphosphaten unter Einbeziehung von Umweltfolgeschäden und deren Vermeidung, on behalf of Umweltbundesamt (German EPA), FKZ 3716 31 330 0

Krueger, B.C., Fowler, G.D., Templeton, M.R., Septien, S. (in press) Faecal sludge pyrolysis: understanding the relationships between organic composition and thermal decomposition. Journal of Environmental Management.

Krygowski, T., Szatylowicz, H. and Zachara, J., 2006. How H-Bonding Modifies Molecular Structure and π-Electron Delocalization in the Ring of Pyridine/Pyridinium Derivatives Involved in H-Bond Complexation. *ChemInform*, 37(4).

Krylova, V. and Andrulevičius, M., 2009. Optical, XPS and XRD Studies of Semiconducting Copper Sulfide Layers on a Polyamide Film. *International Journal of Photoenergy*, 2009, pp.1-8.

Kuusik, R., Salkkonen, P. and Niinistö, L., 1985. Thermal decomposition of calcium sulphate in carbon monoxide. *Journal of Thermal Analysis*, 30(1), pp.187-193.

Lamers, L., Govers, L., Janssen, I., Geurts, J., Van der Welle, M., Van Katwijk, M., Van der Heide, T., Roelofs, J. and Smolders, A., 2013. Sulfide as a soil phytotoxin—a review. *Frontiers in Plant Science*, 4.

Lawrence-Jones, C., 2019. *Londoners used to be able to ski on a toxic-sludge heap known as Beckton Alps*. [online] MyLondon.news. Available at: <https://www.mylondon.news/news/east-london-news/londoners-used-able-ski-toxic-16897746> [Accessed 2 May 2020].

Lasheen, M. and Ammar, N., 2009. Assessment of metals speciation in sewage sludge and stabilized sludge from different Wastewater Treatment Plants, Greater Cairo, Egypt. *Journal of Hazardous Materials*, 164(2-3), pp.740-749.

Le Chatelier, H., 1891. Estimation of firedamp by flammability limits. *Ann. Mines*, 19(8), pp.388-395.

Lee, A., Parlett, C. and Wilson, K., 2017. *Contemporary catalysis: X-Ray Photoelectron Spectroscopy*. 1st ed. London: Royal Society of Chemistry, pp.513-525.

Lefers, J., Koetsier, W. and Van Swaaij, W., 1978. The oxidation of sulphide in aqueous solutions. *The Chemical Engineering Journal*, 15(2), pp.111-120.

Lehmann, J. and Joseph, S. (2015). *Biochar for environmental management*. Abingdon: Routledge.

Leichtnam, J., Schwartz, D. and Gadiou, R., 2000. The behaviour of fuel-nitrogen during fast

pyrolysis of polyamide at high temperature. *Journal of Analytical and Applied Pyrolysis*, 55(2), pp.255-268.

Leng, L., Yang, L., Chen, J., Leng, S., Li, H., Li, H., Yuan, X., Zhou, W. and Huang, H., 2020. A review on pyrolysis of protein-rich biomass: Nitrogen transformation. *Bioresource Technology*, 315, p.123801.

Lewes, V., 1912. *Royal Society of Arts: Cantor Lectures on The Carbonisation of Coal*. 1st ed. London: WM. Clowes and Sons Ltd., Duke Street, Stamford Street, SE.

Lewis, A., 2010. Review of metal sulphide precipitation. *Hydrometallurgy*, 104(2), pp.222-234.

Li, C. and Suzuki, K., 2009. Tar property, analysis, reforming mechanism, and model for biomass gasification—An overview. *Renewable and Sustainable Energy Reviews*, 13(3), pp.594-604.

Li, C. and Tan, L., 2000. Formation of NOx and SOx precursors during the pyrolysis of coal and biomass. Part III. Further discussion on the formation of HCN and NH3 during pyrolysis. *Fuel*, 79(15), pp.1899-1906.

Li, X., Lv, Y., Ma, B., Wang, W. and Jian, S., 2017. Decomposition kinetic characteristics of calcium carbonate containing organic acids by TGA. *Arabian Journal of Chemistry*, 10, pp.S2534-S2538.

Li, Y., Xing, B., Wang, X., Wang, K., Zhu, L. and Wang, S., 2019. Nitrogen-Doped Hierarchical Porous Biochar Derived from Corn Stalks for Phenol-Enhanced Adsorption. *Energy & Fuels*, 33(12), pp.12459-12468.

Likosova, E.M., Keller, J., Rozendal, R., Poussade, Y. and Freguia, S., 2013. Understanding colloidal FeSx formation from iron phosphate precipitation sludge for optimal phosphorus recovery. *Journal of Colloid and Interface Science*, 403, pp.16-21.

Lindberg, B., Hamrin, K., Johansson, G., Gelius, U., Fahlman, A., Nordling, C. and Siegbahn, K., 1970. Molecular Spectroscopy by Means of ESCA II.Sulfur compounds. Correlation of electron binding energy with structure. *Physica Scripta*, 1(5-6), pp.286-298.

Liu, D., Wang, Q., Wu, J. and Liu, Y., 2018. A review of sorbents for high-temperature hydrogen sulfide removal from hot coal gas. *Environmental Chemistry Letters*, 17(1), pp.259-276.

Liu, F., Peng, C., Wilson, B. and Lundström, M., 2019. Oxalic Acid Recovery from High Iron Oxalate Waste Solution by a Combination of Ultrasound-Assisted Conversion and Cooling Crystallization. *ACS Sustainable Chemistry & Engineering*, 7(20), pp.17372-17378.

Loudon, G. and Parise, J., 2015. *Organic chemistry*. 6th ed. Colorado: Roberts and Co, p.1223.

Lu, G., Ikeya, K. and Watanabe, A., 2016. Size distribution of carbon layer planes in biochar from different plant type of feedstock with different heating temperatures. *Chemosphere*, 163, pp.252-258.

Luo, Q., Park, C., Raju, A. and Norbeck, J., 2014. Experimental Study of Gaseous Sulfur Species Formation during the Steam Hydrogasification of Coal. *Energy & Fuels*, 28(5), pp.3399-3402.

Lutfalla, S., Abiven, S., Barré, P., Wiedemeier, D., Christensen, B., Houot, S., Kätterer, T., Macdonald, A., van Oort, F. and Chenu, C., 2017. Pyrogenic Carbon Lacks Long-Term Persistence in Temperate Arable Soils. *Frontiers in Earth Science*, 5.

Macedo, F., Fountain, P., Huppert, M., Pinnow, D. and Webb, I., 2015. One Year of Bucher Press operational experience at Oxford Sewage Treatment Works. [online] Available at: <http://www.aquaenviro.co.uk/wp-content/uploads/2016/05/Flavia-Macedo-paper.pdf> [Accessed 6 April 2020].

Machado, M., Caramão, E. and Zini, C., 2011. Investigation of sulphur compounds in coal tar using monodimensional and comprehensive two-dimensional gas chromatography. *Journal of Chromatography A*, 1218(21), pp.3200-3207.

Mackie, J., Colket, M., Nelson, P. and Esler, M., 1991. Shock tube pyrolysis of pyrrole and kinetic modeling. *International Journal of Chemical Kinetics*, 23(8), pp.733-760.

Maillard, É. and Angers, D., 2013. Animal manure application and soil organic carbon stocks: a meta-analysis. *Global Change Biology*, 20(2), pp.666-679.

Major, G., Fairley, N., Sherwood, P., Linford, M., Terry, J., Fernandez, V. and Artyushkova, K., 2020. Practical guide for curve fitting in x-ray photoelectron spectroscopy. *Journal of Vacuum Science & Technology A*, 38(6), p.061203.

Makeswari, M. and Santhi, T., 2013. Optimization of Preparation of Activated Carbon from Ricinus communis leaves by Microwave-Assisted Zinc Chloride Chemical Activation: Competitive Adsorption of Ni2+Ions from Aqueous Solution. *Journal of Chemistry*, 2013, pp.1-12.

Małecki, S., 2015. Reduction of lead and zinc sulphates by hydrogen. *Journal of Thermal Analysis and Calorimetry*, 121(2), pp.861-866.

Mamvura, T. and Danha, G., 2020. Biomass torrefaction as an emerging technology to aid in energy production. *Heliyon*, 6(3), p.e03531.

Mantovani, G., Anker, S., Fanelli, F., Inui, A., Morley, J., Scevola, D., Schuster, M. and Yeh, S., 2006. *Cachexia and Wasting*. Milano: Springer, p.48.

Marques, R., Stüber, F., Smith, K., Fabregat, A., Bengoa, C., Font, J., Fortuny, A., Pullket, S., Fowler, G. and Graham, N., 2011. Sewage sludge based catalysts for catalytic wet air oxidation of phenol: Preparation, characterisation and catalytic performance. *Applied Catalysis B: Environmental*, 101(3-4), pp.306-316.

Marsh, H. and Rodríguez-Reinoso, F., 2006. *Activated carbon*. Amsterdam: Elsevier.

Marsh, N., Ledesma, E., Sandrowitz, A. and Wornat, M., 2004. Yields of Polycyclic Aromatic Hydrocarbons from the Pyrolysis of Catechol [ortho-Dihydroxybenzene]: Temperature and Residence Time Effects. *Energy & Fuels*, 18(1), pp.209-217.

Mashuga, C. and Crowl, D., 2000. Derivation of Le Chatelier's mixing rule for flammable limits. *Process Safety Progress*, 19(2), pp.112-117.

Materazzi, M., Lettieri, P., Taylor, R. and Chapman, C., 2016. Performance analysis of RDF gasification in a two stage fluidized bed–plasma process. *Waste Management*, 47, pp.256-266.

Matinde, E., Sasaki, Y. and Hino, M., 2008. Phosphorus Gasification from Sewage Sludge during Carbothermic Reduction. *ISIJ International*, 48(7), pp.912-917.

McBeath, A., Smernik, R., Krull, E. and Lehmann, J., 2014. The influence of feedstock and production temperature on biochar carbon chemistry: A solid-state 13C NMR study. *Biomass and Bioenergy*, 60, pp.121-129.

McBeath, A., Smernik, R., Schneider, M., Schmidt, M. and Plant, E., 2011. Determination of the aromaticity and the degree of aromatic condensation of a thermosequence of wood charcoal using NMR. *Organic Geochemistry*, 42(10), pp.1194-1202.

McBeath, T., Lombi, E., McLaughlin, M. and Bünemann, E., 2007. Polyphosphate-fertilizer solution stability with time, temperature, and pH. *Journal of Plant Nutrition and Soil Science*, 170(3), pp.387-391.

McKenna, A., Chacón-Patiño, M., Chen, H., Blakney, G., Mentink-Vigier, F., Young, R., Ippolito, J. and Borch, T., 2021. Expanding the Analytical Window for Biochar Speciation: Molecular Comparison of Solvent Extraction and Water-Soluble Fractions of Biochar by FT-ICR Mass Spectrometry. *Analytical Chemistry*, 93(46), pp.15365-15372.

McLay, C., Rajan, S. and Liu, Q., 2000. Agronomic effectiveness of partially acidulated phosphate rock fertilizers in an allophanic soil at near-neutral pH. *Communications in Soil Science and Plant Analysis*, 31(3-4), pp.423-435.

McNeil, D., 1975. *Coal carbonization products*. 2nd ed. Oxford: Pergamon press.

Meade, A., 1921. *Modern Gasworks Practice*. 2nd ed. London: Benn Brothers Limited.

Medalia, A., Rivin, D. and Sanders, D., 1983. A comparison of carbon black with soot. *Science*

of The Total Environment, 31(1), pp.1-22.

Merck, 2020. *Relative Strength of Acids & Bases*. [online] sigmaaldrich.com. Available at: <https://www.sigmaaldrich.com/chemistry/stockroom-reagents/learning-center/technical-library/acid-base-chart.html> [Accessed 9 February 2021].

Meyer, S., Genesio, L., Vogel, I., Schmidt, H., Soja, G., Someus, E., Shackley, S., Verheijen, F. and Glaser, B., 2017. Biochar standardization and legislation harmonization. *Journal of Environmental Engineering and Landscape Management*, 25(2), pp.175-191.

Migliaccio, R., Brachi, P., Montagnaro, F., Papa, S., Tavano, A., Montesarchio, P., Ruoppolo, G. and Urciuolo, M., 2021. Sewage Sludge Gasification in a Fluidized Bed: Experimental Investigation and Modeling. *Industrial & Engineering Chemistry Research*, 60(13), pp.5034-5047.

Mills, N. (2015). *Unlocking the full energy potential of sewage sludge*. EngD. University of Surrey.

Milne, T., Evans, R. and Abatzoglou, N. (1998). *Biomass Gasifier "Tars": Their Nature, Formation and Conversion*. Golden, Colorado: National Renewable Energy Laboratory.

Minitab, 2021. *Minitab 20 Support - Minitab*. [online] Support.minitab.com. Available at: <https://support.minitab.com/en-us/minitab/20/> [Accessed 2 Jan 2021].

Mulder, M., Appeldoorn, K., Weij, P. and Kempen, R. (2017). Full Scale Optimisation of Sludge Dewatering and Phosphate Removal at Harnaschpolder wwtp (The Hague, NL). In: *IWA Specialist Conference on Sludge Management - SludgeTech 2017*. The Netherlands.

Munera-Echeverri, J., Martinsen, V., Strand, L., Zivanovic, V., Cornelissen, G. and Mulder, J., (2018). Cation exchange capacity of biochar: An urgent method modification. *Science of The Total Environment*, 642, pp.190-197.

Mohan, D., Pittman, C. and Steele, P., 2006. Pyrolysis of Wood/Biomass for Bio-oil: A Critical Review. *Energy & Fuels*, 20(3), pp.848-889.

Mondini, C., Cayuela, M., Sinicco, T., Fornasier, F., Galvez, A. and Sánchez-Monedero, M., 2017. Modification of the RothC model to simulate soil C mineralization of exogenous organic matter. *Biogeosciences*, 14(13), pp.3253-3274.

Mondini, C., Cayuela, M., Sinicco, T., Fornasier, F., Galvez, A. and Sánchez-Monedero, M., 2018. Soil C Storage Potential of Exogenous Organic Matter at Regional Level (Italy) Under Climate Change Simulated by RothC Model Modified for Amended Soils. *Frontiers in Environmental Science*, 6.

Mood, S., Ayiania, M., Jefferson-Milan, Y. and Garcia-Perez, M., 2020. Nitrogen doped char from anaerobically digested fiber for phosphate removal in aqueous solutions. *Chemosphere*, 240, p.124889.

MosayebNezhad, M., Mehr, A., Gandiglio, M., Lanzini, A. and Santarelli, M., 2018. Techno-economic assessment of biogas-fed CHP hybrid systems in a real wastewater treatment plant. *Applied Thermal Engineering*, 129, pp.1263-1280.

Munir, M., Mansouri, S., Udugama, I., Baroutian, S., Gernaey, K. and Young, B., 2018. Resource recovery from organic solid waste using hydrothermal processing: Opportunities and challenges. *Renewable and Sustainable Energy Reviews*, 96, pp.64-75.

MWM Energy, 2019. *MWM TCG 3016 V16 S Gasmotor / Gas Engine*. [online] www.flickr.com. Available at: <https://www.flickr.com/photos/67106931@N06/46282759494> [Accessed 2 August 2021].

Nacoon, S., Jogloy, S., Riddech, N., Mongkolthanaruk, W., Kuyper, T. and Boonlue, S., 2020. Interaction between Phosphate Solubilizing Bacteria and Arbuscular Mycorrhizal Fungi on Growth Promotion and Tuber Inulin Content of Helianthus tuberosus L. *Scientific Reports*, 10(1).

Nasrollahzadeh, M., 2021. Biopolymer-based metal nanoparticle chemistry for sustainable applications. Volume 1: Classification, properties, and synthesis. 1st ed. Amsterdam: Elsevier.,

National statistics, 2020. *Fertiliser use on farm crops for crop year 2019*. The British Survey of Fertiliser Practice. Newbury: National Statistics.

Navarro, I., Sanz, P. and Martínez, M., 2011. Analysis of perfluorinated alkyl substances in Spanish sewage sludge by liquid chromatography–tandem mass spectrometry. *Analytical and Bioanalytical Chemistry*, 400(5), pp.1277-1286.

NETL, n.d. *British Gas/Lurgi Gasifier*. [online] netl.doe.gov. Available at: <https://www.netl.doe.gov/research/coal/energy-systems/gasification/gasifipedia/bgl> [Accessed 22 April 2020].

Nicholson, F., Bhogal, A., Taylor, M., McGrath, S. and Withers, P., 2018. Long-term Effects of Biosolids on Soil Quality and Fertility. *Soil Science*, 183(3), pp.89-98.

Odongo, A. (2015). *Tar removal in hot gas streams*. Ph.D. Imperial College London.

Ofwat, 2015. *Appendix 1: Sludge treatment, transport and disposal - supporting evidence and design options*. Water 2020: Regulatory framework for whole markets and the 2019 price

review. [online] Birmingham: Ofwat, p.5. Available at: <https://www.ofwat.gov.uk/wp-content/uploads/2015/12/pap_tec20151210water2020app1.pdf> [Accessed 16 July 2021].

O'Haver, 2018. *Pragmatic Introduction to Signal Processing*. 1st ed. Baltimore: Self-published.

Oh, J. and Wheelock, T., 1990. Reductive decomposition of calcium sulfate with carbon monoxide: reaction mechanism. *Industrial & Engineering Chemistry Research*, 29(4), pp.544-550.

Olivera, E. and Luengo, J., 2019. Steroids as Environmental Compounds Recalcitrant to Degradation: Genetic Mechanisms of Bacterial Biodegradation Pathways. *Genes*, 10(7), p.512.

Palmer, S., 2016. Leveraging the Value of Sludge for sustainable minimum TOTEX: winners and losers in a sludge market. In: *Sludgetech*. University of Surrey.

Palmer, S., Ord, J., Maclaren, J. and Nair, A., 2013. The prospects for replacing sludge incineration with advanced energy recovery systems and the potential benefits to U.K. water and sewage companies. In: *18th European Biosolids & Organic Resources Conference & Exhibition*. Aqua Enviro Technology Transfer.

Paneque, M., De la Rosa, J., Kern, J., Reza, M. and Knicker, H., 2017. Hydrothermal carbonization and pyrolysis of sewage sludges: What happen to carbon and nitrogen?. Journal of Analytical and Applied Pyrolysis, 128, pp.314-323.

Panter, K., 2008. Mass and energy balances in high solids digestion following thermal hydrolysis pre-treatment. In: *13th European Biosolids & Organic Resources Conference & Workshop*. Aqua Enviro technology transfer.

Park, Y., Kim, Y., Chang, H., Won, S., Kim, H. and Kwon, W., 2020. Correction: Biocompatible nitrogen-doped carbon dots: synthesis, characterization, and application. *Journal of Materials Chemistry B*, 8(42), pp.9812-9812.

Paterson, N., Zhuo, Y., Dugwell, D. and Kandiyoti, R., 2005. Formation of Hydrogen Cyanide and Ammonia during the Gasification of Sewage Sludge and Bituminous Coal. *Energy & Fuels*, 19(3), pp.1016-1022.

Pei, H., Wang, X., Dai, X., Jin, B. and Huang, Y., 2018. A novel two-stage biomass gasification concept: Design and operation of a 1.5 MWth demonstration plant. *Bioresource Technology*, 267, pp.102-109.

Peltre, C., Christensen, B., Dragon, S., Icard, C., Kätterer, T. and Houot, S., 2012. RothC simulation of carbon accumulation in soil after repeated application of widely different organic amendments. *Soil Biology and Biochemistry*, 52, pp.49-60.

Perkins, T., 2019. *Biosolids: mix human waste with toxic chemicals, then spread on crops*.

[online] the Guardian. Available at: <https://www.theguardian.com/environment/2019/oct/05/biosolids-toxic-chemicals-pollution> [Accessed 25 April 2021].

Plewa, J. and Steindor, J., 1989. Investigation of basic zinc sulfate thermal decomposition under nitrogen and carbon monoxide atmosphere. *Thermochimica Acta*, 137(2), pp.281-291.

Polettini, A., Pomi, R., Trinci, L., Muntoni, A. and Lo Mastro, S., 2004. Engineering and environmental properties of thermally treated mixtures containing MSWI fly ash and low-cost additives. *Chemosphere*, 56(10), pp.901-910.

Ponthus, J. and Riches, E., 2013. Evaluating the multiple benefits offered by ion mobility-mass spectrometry in oil and petroleum analysis. *International Journal for Ion Mobility Spectrometry*, 16(2), pp.95-103.

Pook, M., Mills, N., Heitmann, M., Panter, K. and Walley, P., 2013. Exploring the upper limits of thermal hydrolysis at Chertsey STW. In: *18th European Biosolids & Organic Resources Conference & Exhibiti*. [online] Manchester: Aqua Enviro. Available at: <https://conferences.aquaenviro.co.uk/wp-content/uploads/sites/7/2015/06/Pook-M.-Thames-Water-Utilities.pdf> [Accessed 22 March 2020].

Pott, P., 1775. *Cancer Scroti*. Chirurgical observations relative to the cataract, the polypus of the nose, the cancer of the scrotum, the different kinds of ruptures, and the mortification of the toes and feet. London: T.J.Carnegy, pp.63-68.

Powlson, D., Bhogal, A., Chambers, B., Coleman, K., Macdonald, A., Goulding, K. and Whitmore, A., 2012. The potential to increase soil carbon stocks through reduced tillage or organic material additions in England and Wales: A case study. *Agriculture, Ecosystems & Environment*, 146(1), pp.23-33.

Powlson, D., Whitmore, A. and Goulding, K., 2011. Soil carbon sequestration to mitigate climate change: a critical re-examination to identify the true and the false. *European Journal of Soil Science*, 62(1), pp.42-55.

Prévoteau, A., Ronsse, F., Cid, I., Boeckx, P. and Rabaey, K., 2016. The electron donating capacity of biochar is dramatically underestimated. *Scientific Reports*, 6(1).

Prasertcharoensuk, P., Bull, S. and Phan, A., 2019. Gasification of waste biomass for hydrogen production: Effects of pyrolysis parameters. *Renewable Energy*, 143, pp.112-120.

Pullket, S. (2015). Sewage sludge as source of activated carbon for the removal of endocrine disrupting chemicals in wastewater. PhD. Imperial College London.

Pyreg, 2021. *Carbonization - Our Technology Our Solutions | PYREG*. [online] Pyreg.com. Available at: <https://pyreg.com/our-technology/> [Accessed 25 March 2021].

Pyreg, n.d. *Sewage Sludge*. [online] Pyreg. Available at: <https://www.pyreg.de/wp-content/uploads/2020_pyreg_brochure_sludge_EN.pdf> [Accessed 7 July 2020].

Rahinov, I., Ditzian, N., Goldman, A. and Cheskis, S., 2003. NH2 radical formation by ammonia pyrolysis in a temperature range of 800-1000K. *Applied Physics B: Lasers and Optics*, 77(5), pp.541-546.

Rajapaksha, A., Chen, S., Tsang, D., Zhang, M., Vithanage, M., Mandal, S., Gao, B., Bolan, N. and Ok, Y., 2016. Engineered/designer biochar for contaminant removal/immobilization from soil and water: Potential and implication of biochar modification. *Chemosphere*, 148, pp.276-291.

Rajan, S. S. S. and J. H. Watkinson. "Unacidulated And Partially Acidulated Phosphate Rock: Agronomic Effectiveness And The Rates Of Dissolution Of Phosphate Rock". Fertilizer Research 33.3 (1992): 267-277. Web.

Rao, Y. and Bagheri, H., 1988. Reduction of copper(I) sulfide with hydrogen and the morphology of Cu(s) product. *Reactivity of Solids*, 5(1), pp.29-51.

Rasse, D., Dignac, M., Bahri, H., Rumpel, C., Mariotti, A. and Chenu, C., 2006. Lignin turnover in an agricultural field: from plant residues to soil-protected fractions. *European Journal of Soil Science*, 57(4), pp.530-538.

Reed, P., 2013. *Galligu: An environmental legacy of the Leblanc alkali industry, 1814-1920*. [online] Environmental chemistry group. Available at: <https://www.envchemgroup.com/galligu-an-environmental-legacy-of-the-leblanc-alkali-industry-1814-1920.html> [Accessed 7 January 2021].

Reed, T., 1971. *Free energy of formation of binary compounds*. Cambridge, Mass.: MIT Press.

Ren, Q., Wu, Z., Hu, S., He, L., Su, S., Wang, Y., Jiang, L. and Xiang, J., 2020. Sulfur self-doped char with high specific capacitance derived from waste tire: Effects of pyrolysis temperature. *Science of The Total Environment*, 741, p.140193.

Ren, Q., Zhao, C., Chen, X., Duan, L., Li, Y. and Ma, C., 2011. NOx and N_2O precursors (NH3 and HCN) from biomass pyrolysis: Co-pyrolysis of amino acids and cellulose, hemicellulose and lignin. *Proceedings of the Combustion Institute*, 33(2), pp.1715-1722.

Ridder, M., Jong, S., Polchar, J. and Lingemann, S. Risks and Opportunities in The Global Phosphate Rock Market. The Hague: The Hague Centre for Strategic Studies, 2012. Print. Robust Strategies in Times of Uncertainty.

Ringoot, D., Kleiven, H. and Panter, K., 2012. Energy efficient thermal hydrolysis with steam explosion. In: *European Biosolids and Organic Resources Conference*. [online] Wakefield:

Aqua Enviro. Available at: <https://conferences.aquaenviro.co.uk/wp-content/uploads/sites/7/2015/07/28-Panter-K.-Ebcor-Ltd-UK.pdf> [Accessed 24 March 2021].

Robinson, J., Baumann, K., Hu, Y., Hagemann, P., Kebelmann, L. and Leinweber, P., 2017. Phosphorus transformations in plant-based and bio-waste materials induced by pyrolysis. *Ambio*, 47(S1), pp.73-82.

Rodríguez, C., Flores, M., Sandoval-Paz, M., Delplancke, M., Cabello–Guzmán, G. and Carrasco, C., 2018. Study of the early growth stages of chemically deposited ZnS thin films from a non-toxic solution. *Materials Research Express*, 5(7), p.076404.

Rodríguez-Vila, A., Selwyn-Smith, H., Enunwa, L., Smail, I., Covelo, E. and Sizmur, T., 2017. Predicting Cu and Zn sorption capacity of biochar from feedstock C/N ratio and pyrolysis temperature. *Environmental Science and Pollution Research*, 25(8), pp.7730-7739.

Rosa, J. and Knicker, H., 2011. Bioavailability of N released from N-rich pyrogenic organic matter: An incubation study. *Soil Biology and Biochemistry*, 43(12), pp.2368-2373.

Roskill, 2017. *Activated Carbon*. Global Industry, Markets and Outlook, 9th edition. London: Roskill.

Rosso, I., Galletti, C., Bizzi, M., Saracco, G. and Specchia, V., 2003. Zinc Oxide Sorbents for the Removal of Hydrogen Sulfide from Syngas. *Industrial & Engineering Chemistry Research*, 42(8), pp.1688-1697.

Rothampsted, 2014. *RothC - A model for the turnover of carbon in soil*. Harpenden: Rothampsted Research.

Rus, E., Fountain, P., Mills, N., Achame, S., Obinna, M. and Manocher, A., 2017. The role of soluble P & EPS on dewatering performance. *Proceedings of the Water Environment Federation*, 2017(1), pp.1007-1024.

Rus, E., Mills, N., Shana, A., Perrault, A., Fountain, P., Thorpe, R., Ouki, S. and Nilsen, P., 2017. The intermediate thermal hydrolysis process: results from pilot testing and techno-economic assessment. *Water Practice and Technology*, 12(2), pp.406-422.

Rus, E., Perrault, A., Mills, N., Shana, A., Nilsen, J. and Thorpe, R., 2015. Optimizing THP – The Intermediate Thermal Hydrolysis Process. [online] Available at: <http://www.sludgetech.com/wp-content/uploads/2015/07/9.-Rus-et-al_SludgeTech2015.pdf> [Accessed 2 April 2020].

Rus, E., Winter, P., Smith, S.R., 2013. Optimum anaerobic digestion organic loading rates. In: *18th European Biosolids & Organic Resources Conference & Exhibition*. Aqua Enviro Technology Transfer.

Saadabadi, S., Thallam Thattai, A., Fan, L., Lindeboom, R., Spanjers, H. and Aravind, P., 2019. Solid Oxide Fuel Cells fuelled with biogas: Potential and constraints. *Renewable Energy*, 134, pp.194-214.

Sadrameli, S., 2015. Thermal/catalytic cracking of hydrocarbons for the production of olefins: A state-of-the-art review I: Thermal cracking review. *Fuel*, 140, pp.102-115.

Samokhvalov, A. and Tatarchuk, B., 2011. Characterization of active sites, determination of mechanisms of H2S, COS and CS2 sorption and regeneration of ZnO low-temperature sorbents: past, current and perspectives. *Physical Chemistry Chemical Physics*, 13(8), p.3197.

Sing, K., 1991. Characterization Of Porous Solids: An Introductory Survey. *Characterization of Porous Solids II, Proceedings of the IUPAC Symposium (COPS 11)*, pp.1-9.

S.I: No. 2349 - The Nitrate Pollution Prevention Regulations 2008. 3 - Limiting the application of organic manure.

Santín, C., Doerr, S., Merino, A., Bucheli, T., Bryant, R., Ascough, P., Gao, X. and Masiello, C., 2017. Carbon sequestration potential and physicochemical properties differ between wildfire charcoals and slow-pyrolysis biochars. *Scientific Reports*, 7(1).

Schachtman, D., Reid, R. and Ayling, S., 1998. Phosphorus Uptake by Plants: From Soil to Cell. *Plant Physiology*, 116(2), pp.447-453.

Schmidt, H., Anca-Couce, A., Hagemann, N., Werner, C., Gerten, D., Lucht, W. and Kammann, C., 2018. Pyrogenic carbon capture and storage. *GCB Bioenergy*, 11(4), pp.573-591.

Schnell, M., Horst, T. and Quicker, P., 2020. Thermal treatment of sewage sludge in Germany: A review. *Journal of Environmental Management*, 263, p.110367.

Schroder, J., Cordell, D., Smit, A. and Rosemarin, A. (2010). Sustainable use of phosphorus: EU tender ENV.B1/ETU/2009/0025. Wageningen: Plant Research International.

Shana, A., Fountain, P., Mills, N. and Hunt, P., 2013. SAS only THP with series digestion - more options for energy recovery. In: *Aqua Enviro Technology Transfer*. [online] Manchester: Aqua Enviro. Available at: <https://conferences.aquaenviro.co.uk/proceedings/sas-only-thp-with-series-digestion-more-options-for-energy-recovery/>.

Shen, D., Xiao, R., Gu, S. and Zhang, H., 2013. The Overview of Thermal Decomposition of Cellulose in Lignocellulosic Biomass. *Cellulose - Biomass Conversion*.

Sherwood, T. and Maak, R., 1962. The Reaction of Ammonia with Carbon at Elevated Temperatures. *Industrial & Engineering Chemistry Fundamentals*, 1(2), pp.111-115.

Shudo, T., Shimamura, K. and Nakajima, Y. (2000). Combustion and emissions in a methane DI stratified charge engine with hydrogen pre-mixing. *JSAE Review*, 21(1), pp.3-7.

Smith, K., Fowler, G., Pullket, S. and Graham, N., 2009. Sewage sludge-based adsorbents: A review of their production, properties and use in water treatment applications. *Water Research*, 43(10), pp.2569-2594.

Smith, K., Fowler, G., Pullket, S. and Graham, N., 2012. The production of attrition resistant, sewage–sludge derived, granular activated carbon. *Separation and Purification Technology*, 98, pp.240-248.

Smith, S., 2009. Organic contaminants in sewage sludge (biosolids) and their significance for agricultural recycling. *Philosophical Transactions of the Royal Society A: Mathematical, Physical and Engineering Sciences*, 367(1904), pp.4005-4041.

Sönnichsen, N., 2020. *Anaerobic digestion supply to the UK 2008-2017 | Statista*. [online] Statista. Available at: <https://www.statista.com/statistics/962653/anaerobic-digestion-supply-to-united-kingdom-uk/> [Accessed 17 April 2020].

Spaccini, R., Piccolo, A., Haberhauer, G. and Gerzabek, M., 2002. Increased soil organic carbon sequestration through hydrophobic protection by humic substances. *Soil Biology and Biochemistry*, 34(12), pp.1839-1851.

Spears, B., Brownlie, W., Cordell, D., Hermann, L. and Mogollón, J., 2022. Concerns about global phosphorus demand for lithium-iron-phosphate batteries in the light electric vehicle sector. *Communications Materials*, 3(1).

Speight, J., 2011. Hydrocarbons from Coal. *Handbook of Industrial Hydrocarbon Processes*, pp.163-202.

Stein, R., 2016. *Advanced Plasma Power: BioSNG - Thermal production of biomethane*.

Steiner, G., Geissler, B., Watson, I. and Mew, M., 2015. Efficiency developments in phosphate rock mining over the last three decades. *Resources, Conservation and Recycling*, 105, pp.235-245.

Subramanian, S., Yan, S., Tyagi, R. and Surampalli, R. (2010). Extracellular polymeric substances (EPS) producing bacterial strains of municipal wastewater sludge: Isolation, molecular identification, EPS characterization and performance for sludge settling and dewatering. *Water Research*, 44(7), pp.2253-2266.

Su, C., Guo, Y., Chen, H., Zou, J., Zeng, Z. and Li, L., 2020. VOCs adsorption of resin-based activated carbon and bamboo char: Porous characterization and nitrogen-doped effect. *Colloids and Surfaces A: Physicochemical and Engineering Aspects*, 601, p.124983.

Susmozas, A., Iribarren, D. and Dufour, J., 2013. Life-cycle performance of indirect biomass gasification as a green alternative to steam methane reforming for hydrogen production. *International Journal of Hydrogen Energy*, 38(24), pp.9961-9972.

Sylvis, 2009. *The biosolids emissions assessment model (BEAM): A method for determining greenhouse gas emissions from Canadian biosolids management practices*. New Westminster: Sylvis, p.66.

Takaishi, T., Numata, A., Nakano, R. and Sakaguchi, K., 2008. *Approach to High Efficiency Diesel and Gas Engines*. [online] Mitsubishi Heavy Industries Ltd, p.21. Available at: <https://pdfs.semanticscholar.org/3b35/8426f86e2ae7c667878f7c3c1de1b6747e12.pdf> [Accessed 3 April 2020].

Talus, K., 2016. *Introduction to EU energy law*. S.L.: Oxford Univ Press, p.163.

Tang, J., Zhu, W., Kookana, R. and Katayama, A., 2013. Characteristics of biochar and its application in remediation of contaminated soil. *Journal of Bioscience and Bioengineering*, 116(6), pp.653-659.

Tang, L., Wang, S., Zhu, X., Guan, Y., Chen, S., Tao, X. and He, H., 2018. Feasibility study of reduction removal of thiophene sulfur in coal. *Fuel*, 234, pp.1367-1372.

Tegg, L., 2019. *A Python script to generate Ellingham diagrams from energy of formation for binary compounds.*. [online] github.com. Available at: <https://github.com/ltegg/ellingham> [Accessed 31 March 2021].

Terry, R., Nelson, D. and Sommers, L., 1979. Carbon Cycling During Sewage Sludge Decomposition in Soils. *Soil Science Society of America Journal*, 43(3), pp.494-499.

Thames Water, 2019. *Bioresources Market Information Tables (2018-2019)*. [online] Thames Water. Available at: <https://corporate.thameswater.co.uk/About-us/Protecting-our-environment/Managing-our-impact/Managing-sewage-sludge> [Accessed 26 March 2020].

The Sludge (Use in Agriculture) Regulations 1989. (c1). [online] London: Public Health England. Available at: <https://www.legislation.gov.uk/uksi/1989/1263/made> [Accessed 11 January 2020].

Thevenot, M., Dignac, M. and Rumpel, C., 2010. Fate of lignins in soils: A review. *Soil Biology and Biochemistry*, 42(8), pp.1200-1211.

Tian, F., Yu, J., McKenzie, L., Hayashi, J. and Li, C., 2007. Conversion of Fuel-N into HCN and NH3During the Pyrolysis and Gasification in Steam: A Comparative Study of Coal and Biomass†. *Energy & Fuels*, 21(2), pp.517-521.

Tian, G., Granato, T., Cox, A., Pietz, R., Carlson, C. and Abedin, Z., 2009. Soil Carbon

Sequestration Resulting from Long-Term Application of Biosolids for Land Reclamation. *Journal of Environmental Quality*, 38(1), pp.61-74.

Tomczyk, A., Sokołowska, Z. and Boguta, P., 2020. Biochar physicochemical properties: pyrolysis temperature and feedstock kind effects. *Reviews in Environmental Science and Bio/Technology*, 19(1), pp.191-215.

Torres-Dorante, L., Claassen, N., Steingrobe, B. and Olfs, H., 2005. Hydrolysis rates of inorganic polyphosphates in aqueous solution as well as in soils and effects on P availability. *Journal of Plant Nutrition and Soil Science*, 168(3), pp.352-358.

Torri, S. and Alberti, C., 2012. Characterization of organic compounds from biosolids of Buenos Aires city. *Journal of soil science and plant nutrition*, 12(1), pp.143-152.

Torri, S., Alvarez, R. and Lavado, R., 2003. Mineralization of Carbon from Sewage Sludge in Three Soils of the Argentine Pampas. *Communications in Soil Science and Plant Analysis*, 34(13-14), pp.2035-2043.

Torri, S., Corrêa, R. and Renella, G., 2014. Soil Carbon Sequestration Resulting from Biosolids Application. *Applied and Environmental Soil Science*, 2014, pp.1-9.

Trimeric Corporation, n.d. *Caustic scrubber designs for H2S removal from refinery gas streams*. [online] Buda, Texas: Trimeric Corporation. Available at: <http://trimeric.com/assets/caustic-scrubber-designs-for-h2s-removal-from-refinery-gas-streams---afpm-2014.pdf> [Accessed 12 April 2021].

Tumuluru, J., Sokhansanj, S., Hess, J., Wright, C. and Boardman, R., 2011. REVIEW: A review on biomass torrefaction process and product properties for energy applications. *Industrial Biotechnology*, 7(5), pp.384-401.

Turpin, H., 2021. *Interview with tenant sheep farmer Henry Turpin on what influences his decision to apply biosolids to land*.

UKSO, 2020. *UKSO Map Viewer*. [online] http://www.ukso.org/. Available at: <http://mapapps2.bgs.ac.uk/ukso/home.html> [Accessed 15 June 2021].

USGS, 2019. *Method 36: Aqua Regia Digestion Method*. [online] Reston: United States Geological Survey. Available at: <https://www.usgs.gov/media/files/aqua-regia-digestion-method> [Accessed 28 April 2021].

USGS, 2020. *Phosphate Rock - 2020*. Annual Publications. [online] Reston: United States Geological Survey. Available at: <https://www.usgs.gov/centers/nmic/phosphate-rock-statistics-and-information> [Accessed 25 April 2021].

USP Technologies, n.d. *Cyanide Treatment with Hydrogen Peroxide*. [online] H2o2.com.

Available at: <https://www.h2o2.com/industrial/applications.aspx?pid=106&name=Cyanide-Treatment> [Accessed 13 April 2021].

Van Dyk, J., Keyser, M. and Coertzen, M., 2006. Syngas production from South African coal sources using Sasol–Lurgi gasifiers. *International Journal of Coal Geology*, 65(3-4), pp.243-253.

Van Kauwenbergh, S.J. World Phosphate Rock Reserves and Resources. Muscle Shoals: International Fertiliser Development Centre (IFDC), 2010. Print.

Vassilatos, V., Taralas, G., Sjöström, K. and Björnbom, E., 1992. Catalytic cracking of tar in biomass pyrolysis gas in the presence of calcined dolomite. *The Canadian Journal of Chemical Engineering*, 70(5), pp.1008-1013.

Vreugdenhill, B. and Zwart, R. (2009). *Tar formation in pyrolysis and gasification*. ECN (energy research centre of the Netherlands).

Waldheim, L. and Nilsson, T., 2001. *Heating value of gases from biomass gasification*. Nyköping: TPS Termiska Processer AB, p.3.

Wan, K., Yu, Z., Li, X., Liu, M., Yang, G., Piao, J. and Liang, Z., 2015. pH Effect on Electrochemistry of Nitrogen-Doped Carbon Catalyst for Oxygen Reduction Reaction. *ACS Catalysis*, 5(7), pp.4325-4332.

Wang, J., Odinga, E., Zhang, W., Zhou, X., Yang, B., Waigi, M. and Gao, Y., 2019. Polyaromatic hydrocarbons in biochars and human health risks of food crops grown in biochar-amended soils: A synthesis study. *Environment International*, 130, p.104899.

Wang, J., Xia, K., Waigi, M., Gao, Y., Odinga, E., Ling, W. and Liu, J., 2018. Application of biochar to soils may result in plant contamination and human cancer risk due to exposure of polycyclic aromatic hydrocarbons. *Environment International*, 121, pp.169-177.

Wang, M. and Chang, S., 2001. Mean residence times and characteristics of humic substances extracted from a Taiwan soil. *Canadian Journal of Soil Science*, 81(3), pp.299-307.

Wang, S., Fan, X., Zheng, A., Wang, Y., Dou, Y., Wei, X., Zhao, Y., Wang, R., Zong, Z. and Zhao, W., 2014. Evaluation of atmospheric solids analysis probe mass spectrometry for the analysis of coal-related model compounds. *Fuel*, 117, pp.556-563.

Wang, S., Wei, X., Wang, Y., Li, Z., Chen, Y., Xu, D., Teng, Q., Li, W., Liu, X., Zhou, M. and Zong, Z., 2016. Compositional features of extracts from Shenmu char powder. *Journal of Fuel Chemistry and Technology*, 44(1), pp.1-6.

Wang, T., Camps-Arbestain, M., Hedley, M. and Bishop, P. (2012). Predicting phosphorus bioavailability from high-ash biochars. Plant Soil, 357(1-2), pp.173-187.

Wang, T.; Camps Arbestain, M.; Hedley, M.; Bishop, P., (2012). Chemical, and bioassay characterisation of nitrogen availability in biochar produced from dairy manure and biosolids. Org. Geochem. 51, pp.45–54.

Wardman, J., 2020. *Agronomy Advice | Why di-ammonium phosphate is not the best choice of phosphate fertiliser*. [online] Yara.co.uk. Available at: <https://www.yara.co.uk/crop-nutrition/agronomy-advice/why-di-ammonium-phpsphate-is-not-the-best-choice-of-phosphate/> [Accessed 2 January 2021].

Warnock, D., Lehmann, J., Kuyper, T. and Rillig, M., 2007. Mycorrhizal responses to biochar in soil – concepts and mechanisms. *Plant and Soil*, 300(1-2), pp.9-20.

The Waste Framework Directive (2008). (article 18). [online] London: Public Health England. Available at: <https://www.legislation.gov.uk/uksi/1989/1263/made> [Accessed 11 January 2020].

Water UK, 2020. *Net Zero 2030 Routemap - Summary for Policymakers*. [online] London: Water UK. Available at: <https://www.water.org.uk/routemap2030/wp-content/uploads/2021/03/Water-UK-Net-Zero-2030-Routemap-Summary-updated.pdf> [Accessed 2 May 2022].

Watson, A. and Valberg, P., 2001. Carbon Black and Soot: Two Different Substances. *AIHAJ - American Industrial Hygiene Association*, 62(2), pp.218-228.

Webb, J., 2014. *Tedium, tragedy and tar: The slowest drops in science*. [online] BBC News. Available at: <https://www.bbc.co.uk/news/science-environment-28402709> [Accessed 22 February 2021].

Weil, R. and Brady, N., 2008. *Elements of the nature and properties of soils*. 14th ed. New Jersey: Pearson Education inc., p.510.

Wiedemeier, D., Abiven, S., Hockaday, W., Keiluweit, M., Kleber, M., Masiello, C., McBeath, A., Nico, P., Pyle, L., Schneider, M., Smernik, R., Wiesenberg, G. and Schmidt, M., 2015. Aromaticity and degree of aromatic condensation of char. *Organic Geochemistry*, 78, pp.135-143.

Williams, T. and Burrowes, P., 2016. Thermal Hydrolysis Offerings and Performance. In: *European Biosolids and Organic Resources Conference*. [online] Aqua Enviro. Available at: <https://www.aquaenviro.co.uk/wp-content/uploads/2017/03/Todd-Williams.pdf>.

Wu, C., Lin, C. and Chen, H., 2006. Carbothermic reduction of zinc sulfide in the presence of calcium carbonate. *Metallurgical and Materials Transactions B*, 37(3), pp.339-347.

WWT, 2016. *Breaking new ground in biogas production*. [online] Wwtonline.co.uk. Available at: <https://wwtonline.co.uk/features/breaking-new-ground-in-biogas-production> [Accessed 2

April 2020].

Xiao, F., Sasi, P., Yao, B., Kubátová, A., Golovko, S., Golovko, M. and Soli, D., 2020. Thermal Stability and Decomposition of Perfluoroalkyl Substances on Spent Granular Activated Carbon. *Environmental Science & Technology Letters*, 7, pp.343-350.

Xiao, K., Guan, R., Yang, J., Li, H., Yu, Z., Liang, S., Yu, W., Hu, J., Hou, H. and Liu, B., 2019. Effects of red mud on emission control of NOx precursors during sludge pyrolysis: A protein model compound study. *Waste Management*, 85, pp.452-463.

Xiao, X., Chen, Z. and Chen, B., 2016. H/C atomic ratio as a smart linkage between pyrolytic temperatures, aromatic clusters and sorption properties of biochars derived from diverse precursory materials. *Scientific Reports*, 6(1).

Xu, L., Dong, F., Zhuang, H., He, W., Ni, M., Feng, S. and Lee, P., 2017. Energy upcycle in anaerobic treatment: Ammonium, methane, and carbon dioxide reformation through a hybrid electrodeionization–solid oxide fuel cell system. *Energy Conversion and Management*, 140, pp.157-166.

Yan, Z., Wang, Z., Liu, H., Tu, Y., Yang, W., Zeng, H. and Qiu, J., 2015. Decomposition and solid reactions of calcium sulfate doped with SiO2, Fe2O3 and Al2O3. *Journal of Analytical and Applied Pyrolysis*, 113, pp.491-498.

Yang, F. and Antonietti, M., 2020. Artificial Humic Acids: Sustainable Materials against Climate Change. *Advanced Science*, 7(5), p.1902992.

Yao, Y., 2014. *Use of Carbohydrate, Protein and Fat to Characterise Wastewater in Terms of its Major Elemental Constituents and Energy*. PhD Thesis. University of Manchester: Faculty of Engineering and Physical Sciences.

Yara, 2018. *Yara fertiliser industry handbook*. [online] Oslo: Yara International ASA, p.86. Available at: <https://www.yara.com/siteassets/investors/057-reports-and-presentations/other/2018/fertilizer-industry-handbook-2018-with-notes.pdf/> [Accessed 24 December 2020].

Yaws, C. and Braker, W., 2001. *Matheson gas data book*. Parsippany, NJ: Matheson Tri-Gas.

Ye, C. and Li, J., 2013. Wet process phosphoric acid purification by solvent extraction using N-octanol and tributylphosphate mixtures. *Journal of Chemical Technology & Biotechnology*, 88(9), pp.1715-1720.

Yorkshire Water, 2019. *Appendix 17b - Bioresources Technical Appendix*. PR 19 appendices. [online] Bradford: Yorkshire Water. Available at: <https://www.yorkshirewater.com/media/jizfjwhv/appendix-17b-bioresource-technical-appendix.pdf> [Accessed 16 July 2021].

Zglobisz, N., Castillo-Castillo, A., Grimes, S. and Jones, P., 2010. Influence of UK energy policy on the deployment of anaerobic digestion. *Energy Policy*, 38(10), pp.5988-5999.

Zhang, B., Xu, W., Lu, Z. and Sun, J., 2020. Recent Progress on Carbonaceous Material Engineering for Electrochemical Hydrogen Peroxide Generation. *Transactions of Tianjin University*, 26(3), pp.188-196.

Zhang, J., Liu, J. and Liu, R., 2015. Effects of pyrolysis temperature and heating time on biochar obtained from the pyrolysis of straw and lignosulfonate. *Bioresource Technology*, 176, pp.288-291.

Zhang, L., Xiao, B., Hu, Z., Liu, S., Cheng, G., He, P. and Sun, L., 2014. Tar-free fuel gas production from high temperature pyrolysis of sewage sludge. *Waste Management*, 34(1), pp.180-184.

Zhang, Y., Xu, X., Zhang, P., Zhao, L., Qiu, H. and Cao, X., 2019. Pyrolysis-temperature depended quinone and carbonyl groups as the electron accepting sites in barley grass derived biochar. *Chemosphere*, 232, pp.273-280.

Chapter 12: Appendices

12.1 Appendix 1 - Health and safety considerations

12.1.1 Motor control panel

Table 12-1: Health & Safety control measures for the motor control panel.

Hazard Description	Control Measure	Consequences if faulty/disregarded by operator.
Solid Particle Ingress	- Components are IP2X rated, this prevents ingress of solid particles (>12.5mm) e.g. fingers. - Enclose motor control panel to prevent dust ingress.	-Electric shock -Death - Overheating - Fire
Liquid Ingress	- Enclose motor control panel to prevent liquid ingress. - Erect physical barrier to provide spatial barrier between other lab users and the rig.	- Electric shock - Death
Excessive Current A mechanical (e.g. blockage) or electrical fault may lead to the inverters/motors drawing excessive current.	- 6A circuit breaker and adjustable overloads prevent the inverters drawing excessive current. - The adjustable overloads should be set to the minimum value wherein the motors run reliably.	- Overheating - Fire
Electric fault The panel & rig becomes electrically live. To receive a shock the circuit operators must touch the rig whilst touching a surrounding metallic object (e.g. light fixture/fume cupboard)	- Equipotential bonding conductors have been installed onto the pyrolysis rig and surrounding metallic objects (including high level pipework, the fume cupboards, air ducts, light fixtures and cable trays). This will prevent an electric shock, even if an electrical fault occurs and the rig becomes live. - A type-C RCD was installed however it was subsequently removed because it is incompatible with the frequency inverters due to high earth leakage. The earth leakage for each inverter was 11.5 milliamps. Frequency inverters are generally incompatible with RCDs.	- Electric shock - Death

12.1.2 Heating Equipment

Table 12-2: Health & Safety control measures for the heating equipment

Hazard Description	Control Measure	Consequences if faulty/disregarded by operator
High Temperature The furnaces operate at (<1000ºC) and infrared testing shows that the insulated and exposed pipework is extremely hot (<300ºC).	- Wear suitable PPE. - Erect physical barrier to provide spatial barrier between other lab users and the rig. - Never open furnaces or reach inside furnaces when operational and/or hot.	Severe burns
Controller Fault The furnace controller experiences a fault and heats in excess of the design/desired temperature	- The digital over-temperature protection has been set to 1005ºC - Each furnace has three zones, which can deviate +/- 25ºC from one another. If the operator suspects a zone is heating excessively or the thermocouple temperature reading is incorrect the furnace must not be operated, and a competent person should replace/repair the damaged components.	Mechanical failure of the rig.
Design Temperature The furnaces have a maximum operating temperature of 1200ºC, however the pyrolysis rig has been designed for operation at 1000ºC.	- The digital over-temperature protection has been set to 1005ºC - Operators must not operate the machinery above 1000ºC without conducting an additional risk assessment.	Mechanical failure of the rig

12.1.3 Mechanical Equipment

There are several moving parts, these include: the agitator, the feed screw, conveyor screw A and conveyor screw B. The agitator and feedscrew are located in the feed hopper, to ensure safety never operate these whilst the feed hopper lid is removed. The screw for conveyors A and B is fully enclosed within the pipework, and their drive shafts have dedicated enclosures.

12.1.4 Flammable gases and materials

Pyrolysis produces flammable gases, for a fire or explosion to occur three ingredient are required: (i) Fuel (ii) Ignition source (e.g. heat) (iii) Oxygen.

Hazard Description	Control Measure	Consequences if ignored
Pyrolysis Reactor The pyrolysis reactor will produce a range of flammable gases at high temperatures.	**Oxygen –** The reactor will be purged with nitrogen prior to operation. **Oxygen -** The pyrolysis rig is gas tight. The feed hopper and char outlet can be opened however each can be isolated with a gas tight ball valve.	Fire Explosion

Gas Outlet Hot flammable gases will be vented to a fume cupboard (via a glass condensation system).	**Ignition Source - Heat** The outlet gases were cooled prior to discharge into the fume cupboard. Acetylene has the lowest auto-ignition temperature of the main fuel-gases produced (305^{o}C). The gases were cooled by the condensers and vented to the fume cupboard at approximately 35^{o}C. The temperature of the outlet gases was continuously measured using a K-type thermocouple and digital thermometer. If a blockage in the condensation system occurs or gas temperature exceed the threshold temperature. The feeding system will be immediately isolated. The primary condenser has a long Cynder column acting as a failsafe for a downstream blockage or pressure build-up within the condensers. **Ignition Source – Sparks** The fume cupboards are spark free environments. All electrical supplies, switches and lights are physically isolated from the atmosphere within the fume cupboard. However, two electrical items will be placed within the fume cupboard: (i) A chiller (ii) digital thermometer. Two factors will ensure minimal contact of the flammable gases with the electrical items: (i) The pyrolysis gases will be vented directly towards the fume cupboard outlet and away from the electrical items (ii) The gas flow rate will quickly dilute the gases to below the lower explosion limit.	Fire Explosion
Hot Char The hot char will be collected in a gas tight borosilicate trap. During removal, the char will be exposed to oxygen and could combust. Evidence from thermogravimetric analysis suggests char will combust at temperatures between 335-380^{o}C	**Ignition Source – Heat** The char was left to cool prior to exposure to oxygen.	Fire

12.1.5 Chemical safety

To mitigate hazards associated with sewage sludge, pyrolysis outputs and chemicals used during the operation of the reactor a suitable COSHH assessment should be conducted, and suitable PPE should be worn. In addition, a suitable training course should be attended to operate compressed gases.

12.2 Appendix 2 – Mass balance results

12.2.1 Slow batch-pyrolysis (Py-B)

Table 12-3: Batch pyrolysis of Crossness Sludge (supplementary data for Table 7-1)

	Char Yield (% Wt.)			Liquid Yield (% Wt.)			Gas Yield (% Wt.)[1]		
Run	1	2	3	1	2	3	1	2	3
450ºC	56.2	57.3	57.8	20.6	19.2	20.5	23.2	23.5	21.7
500ºC	52.0	49.9	51.0	22.8	23.4	23.0	25.1	26.7	26.0
550ºC	50.4	51.3	51.3	24.9	23.8	25.4	24.7	24.9	23.3
600ºC	46.5	46.7	46.1	23.4	22.4	23.1	30.1	30.9	30.8
650ºC	50.1	48.2	48.6	19.4	19.4	22.0	30.5	32.5	29.5
700ºC	46.9	46.0	46.5	22.8	22.7	22.9	30.3	31.4	30.6
750ºC	45.8	44.3	45.0	22.3	22.7	24.0	31.8	33.0	31.1
800ºC	41.1	40.6	38.6	23.0	23.0	23.2	35.9	36.3	38.2
850ºC	42.7	42.7	40.7	21.2	21.8	21.7	36.1	35.6	37.5
900ºC	43.2	42.3	45.1	19.5	21.1	20.4	37.3	36.5	34.5

[1]The mass yield for gas was calculated by difference

12.2.2 Continuously-fed pyrolytic gasification

Table 12-4: Mass yields during isothermal pyrolysis (supplementary data for Table 7-3)

	Char Yield (% Wt.)					Liquid Yield (% Wt.)			Gas Yield (% Wt.)[1]		
Run	1	2	3	4	5	1	2	3	1	2	3
500ºC	79.6	82.1	78.0	78.1	79.8						
550ºC	64.0	60.1	62.0	60.8	62.4						
600ºC	52.0	53.3	52.9	49.9	54.4	18.5	18.2	19.3	29.5	28.5	27.8
650ºC	48.4	48.5	48.1	47.7	46.2	17.8	19.0	18.5	33.8	32.5	33.4
700ºC	43.7	43.0	42.0	44.6	42.6	16.5	16.9	16.3	39.8	40.1	41.7
750ºC	45.9	43.5	42.3	43.9	42.4	13.2	12.5	14.1	40.9	44.0	43.6
800ºC	44.6	45.9	45.2	44.8	46.8	8.1	8.0	7.8	47.4	46.1	46.9
850ºC	45.0	45.0	45.1	46.0	46.2	7.3	7.6	7.4	47.7	47.4	47.5
900ºC	44.1	46.2	42.6	45.4	46.1	7.2	7.0	7.4	48.7	46.8	50.0
950ºC	45.1	46.0	45.7	46.3	46.4	6.0	6.5	6.1	48.9	47.5	48.2
1000ºC	46.2	45.9	45.8	46.4	45.0	3.4	4.0	3.6	50.4	50.1	50.6

[1]The mass yield for gas was calculated by difference

12.3 Appendix 3 – Carbon Values

The material CO_2e values in Table 9-1 were calculated as follows:

Material CO_2e value = $((Mass\ yield\ \cdot Total\ C) \cdot CO_2\ mass\ correction\ factor)\ \cdot UK\ CPF$

- *Mass yield as a percentage of digested sludge (Table 7-1)*
- *Total C (Sludge – Table 6-5, Char – Table 8-2)*
- *Carbon to CO_2 mass correction factor equals 3.666*
- *UK CPF = £18 tCO_2e^{-1}*

Long-term CO_2e value (sludge only) = $(Material\ CO_2e\ value\ \cdot\ correction\ factor)$

- *Correction factor:23-36.6% for biosolid amended soils (section 9.1.1)*

12.4 Appendix 4 – P extraction

Sections 9.3.3.1, 9.3.3.3, and 9.3.3.5 presented P extraction models from SSC for H_2SO_4, HCl and HNO_3, respectively. The models were selected based on their high R^2 values; however, precautions were taken to avoid over fit.

- Differences between adjusted R^2 and predicted R^2 were minimised because large differences are indicative of model over fit.
- The Modified Akaike Information Criterion (AICc) assesses overfit in small sample sets and penalises models with excessive factors. Lower AICc scores were considered desirable.

The summary statistics for these models are presented below.

Table 12-5: P-extraction summary statistics

Model Output	Hydrochloric Acid	Sulphuric Acid	Nitric Acid
Adjusted R^2	97.0%	89.8%	97.3%
Predicted R^2	95.3%	88.2%	95.6%
Regression Standard error	3.3%	7.2%	3.1%
Prediction sum of squares	660.7	2355.1	602.4%
Modified Akaike Information Criterion	238.0	294.4	232.6

12.5 Appendix 5 – Energy balance assumptions

Table 12-6: Main process assumptions for Crossness STW energy balances

Parameter	Unit	Value	Source
Thermal hydrolysis (THP)			
Energy for THP steam	Wh kg^{-1}	695	A, Perrault, personal communication, 2020
CHP waste heat boiler efficiency	%	65	
Boiler burner efficiency	%	88	
Crossness STW steam requirement	t tds^{-1}	1.36	Calculated
Thermal hydrolysis MAD (THP-MAD)			
Dried solids destruction	%	52.1	Calculated
Conversion: Biosolids to biogas (HHV)	%	53.2	Calculated
Crossness STW biosolids dried solids	%	30.9	(Thames Water, 2019)
Dryer			
Parasitic electrical load	Wh kg DS^{-1}	80	(Mills, 2015)
Target dried solids (DS)	%	90	A, Perrault, personal communication, 2020
Low-grade heat for water removal	Wh kg^{-1}	900	(Mills, 2015)
High-grade heat for water removal	Wh kg^{-1}	980	(Mills, 2015)
Natural gas to high-grade heat conversion	%	98%	Estimate
Pyrolysis (AER)			
Parasitic load (@ 850ºC)	Wh kg DS^{-1}	387	Measured (Table 7-10)
XS-9 (Feed HHV to Fuel-gas HHV)	%	74.4	Mass balance and quantification of the gas components by gas chromatography (GC). The contribution of H_2S is excluded because it will be removed prior to energy conversion.
XS-9 (Feed HHV to Fuel-gas LHV)	%	68.1	
XS-6 (Feed HHV to Fuel-gas HHV)	%	63.6	
XS-6 (Feed HHV to Fuel-gas HHV)	%	58.1	
XS-Raw (Feed HHV to Fuel-gas HHV)	%	86.3	
XS-Raw (Feed HHV to Fuel-gas HHV)	%	79.7	
Engine - Combined heat and power (CHP)			
Spark-ignition gas engine electrical conversion efficiency[1]	%	40	(Mills, 2015)
Spark-ignition gas engine parasitic electrical load[2]	%	5	(Mills, 2015)
High-grade heat recovery	%[1]	18	(Personal communication, 2020)
Low-grade heat recovery	%[1]	20	(Mills, 2015)
Fuel-gas oxidiser			
Volatiles (LHV) to high-grade heat	%	98	Estimate
High-grade heat to steam boiler efficiency	%	80	Estimate

[1]As a percentage of fuel (LHV), [2]As a percentage of gross electrical output

12.6 Appendix 6: Raw sludge pyrolysis

The key-results for XS-raw pyrolysis are summarised in Table 12-2.

Table 12-7: Key results for XS-raw isothermal pyrolysis at 850ºC [120s dwell (t)]

Parameter	Unit	Value
Gas yield	% Wt.	69.4%
Tar yield	% Wt.	12.8%
Char yield	% Wt.	17.8%
Specific gas production	$m^3\ tds^{-1}$	716.2
H_2	$m^3\ tds^{-1}$	166.6
CO	$m^3\ tds^{-1}$	150.6
CH_4	$m^3\ tds^{-1}$	136.4
CO_2	$m^3\ tds^{-1}$	89.7
C_2H_2	$m^3\ tds^{-1}$	26.9
C_2H_4	$m^3\ tds^{-1}$	96.1
C_2H_6	$m^3\ tds^{-1}$	8.8
N_2	$m^3\ tds^{-1}$	33.8
H_2S	$m^3\ tds^{-1}$	7.2
Fuel gas (HHV)	MJ m^3	24.7
Fuel-gas (LHV)	MJ m^3	22.8
GCE of feedstock HHV to fuel gas LHV	%	79.7%
GCE of feedstock HHV to fuel gas HHV	%	86.3%

By mass, 69.4% of XS-raw was converted to fuel-gas, 12.8% to condensable liquids, and 17.8% to char. This shows that the material had a much higher volatility than biosolids. Most of the additional C (%) present within SSC formed volatiles, with only 12.1% of feedstock C present within the SSC. The energy content of the fuel-gas (HHV) and SSC were measured and equalled 24.7 MJ m^{-3} and 11MJ kg^{-1}, respectively. Unfortunately, measurement of pyrolysis liquids (HHV) was problematic because it had a high moisture content and ignition during bomb calorimetry was an issue. Overall, 86.3% of feedstock (HHV) was converted into fuel-gas (HHV) and 79.7% to fuel-gas (LHV). Based on this conversion efficiency, the potential for raw pyrolysis at Crossness STW is presented in figure 12-1.

Standalone pyrolysis converted 5106Wh of raw-cake into 1724 Wh of fuel-gas, a GCE of 30.3%, which is identical to XS-9. This is an extremely interesting result because it suggests that raw pyrolysis converted the same energy as the combined processes of THP-pyrolysis. Both XS-9 and XS-raw were sampled together. The process utilised all high-grade heat and low-grade heat produced by the CHP engine for drying and it required a natural gas support fuel to achieve dry feedstock. The DS (%) for raw cake was assumed to be the same as digested cake (30.9%). Historically, Crossness STW dewatered raw-cake with legacy plate presses which achieved a DS of approximately 30-32% (Personal communication (b), 2021). Beckton STW, a nearby incineration site, currently achieves a raw-cake DS of 35.1% based on Bucher Press dewatering (Thames Water, 2019).

Therefore, achieving raw-cake DS% above 30.9% is likely to be viable. Based on the energy balance presented, a raw cake DS (%) of only 36.2% would be required to eliminate the use of natural gas.

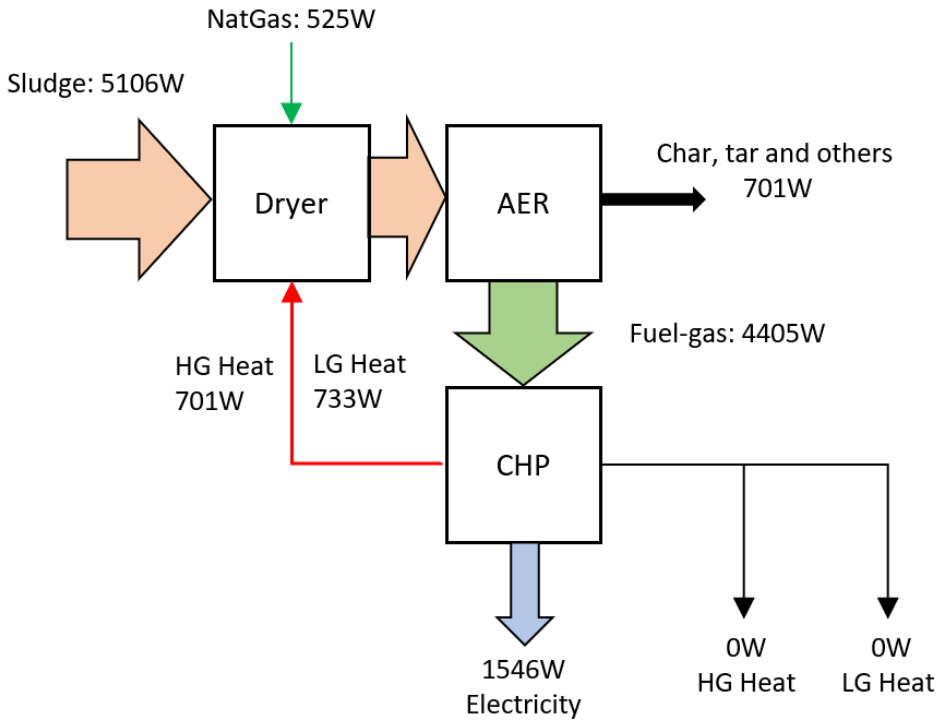


Figure 12-1- Gross energy flows for standalone pyrolysis at 850°C. Based on data obtained from Crossness STW, laboratory-scale pyrolysis and assumptions from Mills (2015). Units based on feed-rate of 1kg DS hour^{-1}.

The investigation of raw-cake pyrolysis was outside of the scope for this project and was only conducted at 850°C for comparison. At 850°C, the pyrolysis liquids contained a large aqueous phase which is likely released during primary macromolecule depolymerisation. If the temperature of the process was increased to 1000°C, whereby steam reforming reactions are expected to occur, it may be possible to achieve greater tar elimination compared to biosolid pyrolysis. Raw pyrolysis warrants further investigation as an alternative to digestion-based processes. The parasitic load during raw pyrolysis was not measured, therefore the NCE cannot be calculated.